ISSN 2071-4726
2071-0305

Инженерно-строительный журнал

НАУЧНОЕ ИЗДАНИЕ

№7(83) 2018

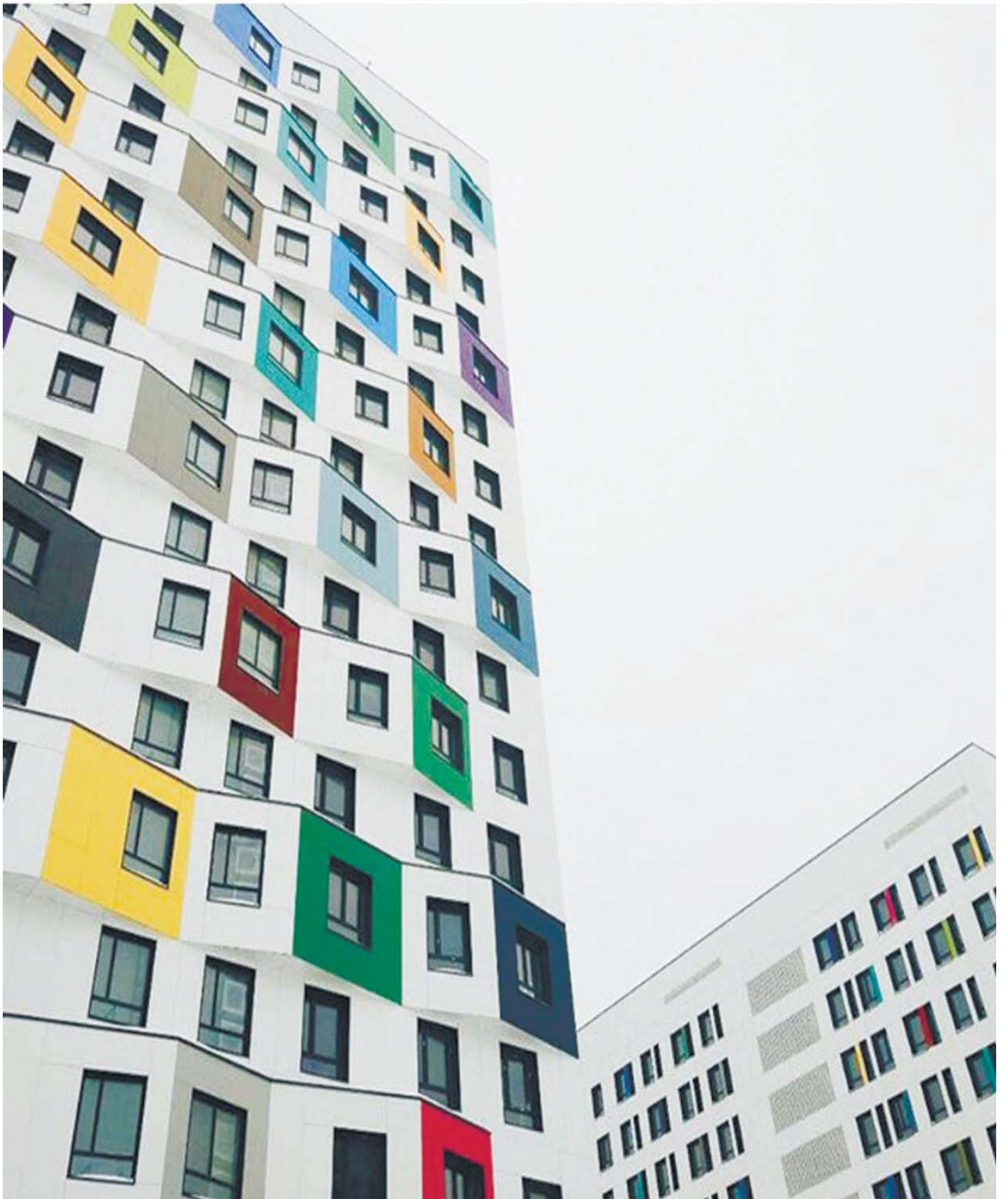

Федеральное государственное автономное образовательное учреждение высшего образования
Санкт-Петербургский политехнический университет Петра Великого

ПОЛИТЕХ
Санкт-Петербургский политехнический университет Петра Великого

Инженерно-строительный институт
Центр дополнительных профессиональных программ

195251, г. Санкт-Петербург, Политехническая ул., 29,
тел/факс: 552-94-60, www.stroikursi.spbstu.ru,
stroikursi@mail.ru

Приглашает специалистов организаций, вступающих в СРО, на курсы повышения квалификации (72 часа)

Код	Наименование программы	Виды работ*
	Курсы по строительству	
БС-01-04	«Безопасность и качество выполнения общестроительных работ»	п.1,2, 3, 5, 6, 7, 9, 10, 11, 12, 13, 14
БС-01	«Безопасность и качество выполнения геодезических, подготовительных и земляных работ, устройства оснований и фундаментов»	1,2,3,5
БС-02	«Безопасность и качество возведения бетонных и железобетонных конструкций»	6,7
БС-03	«Безопасность и качество возведения металлических, каменных и деревянных конструкций»	9,10,11
БС-04	«Безопасность и качество выполнения фасадных работ, устройства кровель, защиты строительных конструкций, трубопроводов и оборудования»	12,13,14
БС-05	«Безопасность и качество устройства инженерных сетей и систем»	15,16,17,18,19
БС-06	«Безопасность и качество устройства электрических сетей и линий связи»	20,21
БС-08	«Безопасность и качество выполнения монтажных и пусконаладочных работ»	23,24
БС-12	«Безопасность и качество устройства мостов, эстакад и путепроводов»	29
БС-13	«Безопасность и качество выполнения гидротехнических, водолазных работ»	30
БС-14	«Безопасность и качество устройства промышленных печей и дымовых труб»	31
БС-15	«Осуществление строительного контроля»	32
БС-16	«Организация строительства, реконструкции и капитального ремонта. Выполнение функций технического заказчика и генерального подрядчика»	33
	Курсы по проектированию	
БП-01	«Разработка схемы планировочной организации земельного участка, архитектурных решений, мероприятий по обеспечению доступа маломобильных групп населения»	1,2,11
БП-02	«Разработка конструктивных и объемно-планировочных решений зданий и сооружений»	3
БП-03	«Проектирование внутренних сетей инженерно-технического обеспечения»	4
БП-04	«Проектирование наружных сетей инженерно-технического обеспечения»	5
БП-05	«Разработка технологических решений при проектировании зданий и сооружений»	6
БП-06	«Разработка специальных разделов проектной документации»	7
БП-07	«Разработка проектов организации строительства»	8
БП-08	«Проектные решения по охране окружающей среды»	9
БП-09	«Проектные решения по обеспечению пожарной безопасности»	10
БП-10	«Обследование строительных конструкций и грунтов основания зданий и сооружений»	12
БП-11	«Организация проектных работ. Выполнение функций генерального проектировщика»	13
Э-01	«Проведение энергетических обследований с целью повышения энергетической эффективности и энергосбережения»	
	Курсы по инженерным изысканиям	
И-01	«Инженерно-геодезические изыскания в строительстве»	1
И-02	«Инженерно-геологические изыскания в строительстве»	2,5
И-03	«Инженерно-гидрометеорологические изыскания в строительстве»	3
И-04	«Инженерно-экологические изыскания в строительстве»	4
И-05	«Организация работ по инженерным изысканиям»	7

***(согласно приказам Минрегионразвития РФ N 624 от 30 декабря 2009 г.)**

По окончании курса слушателю выдается удостоверение о краткосрочном повышении квалификации установленного образца (72 ак. часа)

Для регистрации на курс необходимо выслать заявку на участие, и копию диплома об образовании по телефону/факсу: 8(812) 552-94-60, 535-79-92, , e-mail: stroikursi@mail.ru.

Инженерно-строительный журнал
НАУЧНОЕ ИЗДАНИЕ

ISSN 2071-4726, 2071-0305

Свидетельство о государственной регистрации: ПИ №ФС77-38070, выдано Роскомнадзором

Специализированный научный журнал. Выходит с 09.2008.

Включен в Перечень ведущих периодических изданий ВАК РФ

Периодичность: 8 раз в год

Учредитель и издатель:

Санкт-Петербургский политехнический университет Петра Великого

Адрес редакции:

195251, СПб, ул. Политехническая, д. 29, Гидрокорпус-2, ауд. 245

Дата выхода: 27.02.2019

Содержание

Контакты:
E-mail: mce@spbstu.ru
Web: http://www.engstroy.spbstu.ru

Magazine of Civil Engineering
SCHOLAR JOURNAL

ISSN 2071-4726, 2071-0305
Peer-reviewed scientific journal
Start date: 2008/09
8 issues per year

Publisher:
Peter the Great St. Petersburg Polytechnic University

Indexing:
Scopus, Russian Science Citation Index (WoS), Compendex, DOAJ, EBSCO, Google Academia, Index Copernicus, ProQuest, Ulrich's Serials Analysis System

Corresponding address:
245 Hydro Building, 29 Polytechnicheskaya st., Saint-Petersburg, 195251, Russia

Date of issue: 27.02.2019

Contents

E-mail: mce@spbstu.ru
Web: http://www.engstroy.spbstu.ru/eng/index.html

doi: 10.18720/MCE.83.1

Laminar polymer composites for wooden structures

Слоистые полимерные композиты для деревянных конструкций

A.S. Gribanov*,
S.I. Roshchina,
M.V. Popova,
M.S. Sergeev,
Vladimir State University named after Alexander and Nikolay Stoletovs, Vladimir, Russia

Ассистент А.С. Грибанов*,
д-р техн. наук, заведующий кафедры С.И. Рощина,
канд. техн. наук, доцент М.В. Попова,
канд. техн. наук, доцент М.С. Сергеев,
Владимирский государственный университет имени Александра Григорьевича и Николая Григорьевича Столетовых, г. Владимир, Россия

Key words: polymer composites; glass fiber reinforced polymer (GFRP); fiber glass composites; curing matrix; elastic modulus; contact molding; vacuum infusion; compressed-flexural elements; wood

Ключевые слова: слоистые полимерные композиты; стеклоткань; стеклопластик; отверждающая матрица; клеевая композиция; деревянные конструкции; сжато-изгибаемые элементы; контактное формование; вакуумная инфузия

Abstract. The lack of a clear regulatory framework governing the use of polymer composites to strengthen wooden structures, stimulates the conduct of numerous studies in this area. An important task is to obtain reinforcing materials with the best physico-mechanical and operational parameters. The choice of the type of curing adhesive has a great influence to characteristics of polymer composites such as viscoelastic parameters of the material, adhesion properties on the contact surfaces, the presence of internal defects, etc. The paper describes a method for determining the physicomechanical characteristics of a composite material based on experimental studies. The stand, test samples and the pattern array of tensometric sensors for testing according to Russian State Standard GOST R 56800-2015 "Polymer composites. Determination of tensile properties of unreinforced and reinforced materials have been presented. Dependences of stress-strain, modulus of elasticity, Poisson's ratio, tensile strength for laminate polymer composite have been obtained. Comparative analysis of the obtained results for various adhesive compositions has been performed. According to the results of experimental studies, it was found that the physicomechanical characteristics of polymer composites based on epoxy matrix are higher than those of polyurethane matrix composites due to uniform filling of the filler volume, as well as better wettability of the reinforcing fibers. In conclusion, the article draws conclusions about the effect of the adhesive composition on the mechanical characteristics of the obtained composites have been made, relevance and applied significance of the investigation for strengthening the compressed-flexural elements of wooden structures has been justified.

Аннотация. Отсутствие четкой нормативно-правовой базы, регулирующей возможность применения полимерных композитов для усиления деревянных конструкций, стимулирует проведение многочисленных исследований в данной области. Важной задачей является получение армирующих материалов с наилучшими физико-механическими и эксплуатационными параметрами. Большое влияние на характеристики полимерных композитов оказывает выбор типа отверждающей клеевой матрицы, от которого зависят вязкоупругие параметры материала, адгезионные свойства по контактным поверхностям, наличие внутренних дефектов. В работе описана методика определения физико-механических характеристик композитного материала на основе экспериментальных исследований. Представлен стенд, испытательные образцы и схема расстановки тензометрических датчиков для проведения испытаний по ГОСТ Р 56800-2015. Получены зависимости «напряжения – деформации», значения модуля упругости, коэффициента Пуассона, прочности при растяжении для слоистых полимерных композитов. Выполнен сравнительный анализ полученных результатов для различных клеевых композиций. По результатам экспериментальных исследований установлено, что физико-механические характеристики полимерных композитов на основе эпоксидной матрицы выше, чем у композитов на

основе полиуретановой за счет равномерного заполнения объема наполнителя, а также лучшей смачиваемости армирующих волокон. В заключении сделаны выводы о влиянии клеевой композиции на механические характеристики полученных композитов, обоснована актуальность и прикладное значение исследований для усиления сжато-изгибаемых элементов деревянных конструкций.

1. Introduction

Development of the building science at present and in the foreseeable future is inseparably linked with the trends towards the efficient use of resources, the reduction of the material consumption of structures, elements and units, increasing their operational reliability while reducing labor costs for production and installation. Dynamic development of non-traditional structural materials based on glass, carbon and aramid fabrics, improvement and cheapening of technology for their production opens up a wide range of applications of strengthening for wooden elements of building structures. Combination of high mechanical and performance characteristics, low weight of composite materials in comparison with traditional ones, such as steel and concrete, simplicity of erecting in the construction conditions, mainstreams the use of composites in large reinforcement volumes for different purposes [1–5]. At the micro level, composite polymeric materials consist of two or more components. A continuous component is called a matrix, and the reinforcing is called a filler. The mechanical characteristics of the composite are largely determined by the reinforcing material, and the role of the matrix is reduced to a uniform transfer of forces between the filler fibers, so it must have some specific characteristics: to have low viscosity and high wettability of the filler surface, to create strong adhesion bonds with the reinforcing material at the interface, provide a continuous environment without pores, shells, voids, acting as stress concentrators.

A large amount of research is devoted to the strengthening of wood bent elements with canvases, fabrics, lamellae and laminates [6–21]. The use of reinforcing material in the stretched zone of elements allows reducing the effect of wood flaws, making full use of its strength characteristics. Carbon fiber-based fillers have the best physicomechanical characteristics, but the widespread use of this material is constrained by its high cost. The cheapest replacement of the latter is fiberglass. Composite material based on it (GFRP) has a tensile strength comparable to the tensile strength of pure wood, which will maximize the use of its physico-mechanical characteristics when reinforcing wooden bending elements in the stretched zone. The following reinforcement schemes for wooden elements are possible depending on the type of the material used:

1. The use of laminate composites obtained by impregnating glass, carbon or aramid fabrics under construction site conditions (GFRP, CFRP, AFRP).

2. The use of laminate material – half-finished composite materials presenting a fabric or tape made of fibrous material, pre-impregnated and cured by polymer compositions at the factory.

The advantage of the first scheme is the reinforcement cost reduction due to a more flexible approach in the selection of reinforcing material and polymer compounds for solving specific engineering problems. Materials obtained at the factory have higher performance due to the advanced production technology.

The technological process of impregnation and gluing the laminate polymer composites to the surface of reinforced elements has a significant effect on the mechanical characteristics of the resulting composite materials. The simplest method of preparation is contact molding. The method consists in lamination of the curative composition and reinforcing fibrous material with further impregnation to achieve the required reinforcement coefficient of the structure. In this case, each layer is compacted, leveled, the air bubbles are removed, the non-glued areas are eliminated. The disadvantage of the technology lies in the uncontrolled increase in the volumetric weight of the curative polymer in the composite that significantly degrades its mechanical and performance characteristics.

The resin content of this technology can significantly exceed the reinforcing material volume content that has adverse effects on the actual work of the reinforcement elements and leads to a significant overconsumption of materials.

The second method of producing laminated polymeric composites is the method of vacuum infusion (vacuum bag). The technology is based on the creation of a leak-proof working space with reinforced material embedded in it internally, by which a polymer curing compound is injected by means of preliminary atmospheric desaturation. Mechanization of the working process is provided, the negative influence of the human factor is reduced, the labor intensity and the duration of work are reduced significantly, and the release of harmful substances into the environment is reduced in comparison with the contact method. In turn, the content of the curative glue mould is minimal (it is up to 40 % of the volume of the reinforcing

material in industrial methods), which allows to achieve high physical-mechanical and operational properties of the laminate polymer composite.

The question of determining the mechanical characteristics of polymer composites and the effect of the curing matrix has been taken up since the beginning of their mass introduction, occurring in the second half of the 40s of the 20th century. The main field of application of structural composite materials for a long time remained the space and aviation industries, and the molding of composites was carried out in the factory with the proven technology of obtaining them. Since the 80s, thanks to the accumulated experience in design, calculation, and a large volume of experimental studies, a wide application of polymer composites in the construction industry has begun. An important advantage along with high specific modulus of elasticity and specific strength of composite materials is the possibility of their application "locally", directly on the construction site, which reduces the laboriousness of the work, reduces the weight of the reinforcement elements.

Evaluation of the strength of polymer composites is a multifaceted task L.J. Broutman, C.C. Chamis, A. Kelly, J.O. Outwater, P.I. Zubov, S.L. Shreiner, L.I. Lepilkina, studied the effect of adhesion properties on the matrix-filler interface etc. The works devoted to the theory of viscoelastic operation of polymer composite materials were published by B.W. Rosen, G.K. Shmitz, K.H. Boller, A.Ya. Malkin, G.M. Bartenev, A.V. Zakharenko etc. At present, a large volume of research of composite materials is devoted to viscoelastic operation of multilayer plates based on matrix equations using the theory of hereditary damage accumulation [22–29]. Matrix and filler are paid special attention to joint work of the matrix and filler, and the use of new materials leads to the need for updating and refining existing knowledge on the example of specific engineering problems.

The lack of normative documentation in the field of using composite materials to strengthen wooden structures, in contrast to reinforced concrete, where a large number of inter-industry standards and the main document in the person of JV 164.1325800.2014 "Strengthening of reinforced concrete structures with composite materials", actualizes further studies and generalization of existing experience in this issue. In addition, the joint work of composite materials and wood is a difficult task both because of the anisotropy of the wood and due to the presence of pronounced rheological properties of the materials.

The study of the stress-strain state of compressed-bent elements reinforced with composite materials is a complex task, the solution of which must be done step-by-step. The aim of the presented study is to determine the physical and mechanical properties of glass-fiber laminate composites, as well as to study the degree of influence on the temporary strength and modulus of elasticity of the curing matrix of widely used polyurethane and epoxy adhesives in contact molding of the composite. To achieve this purpose, it is necessary to solve a number of tasks:

1. Perform short-term tests of samples according to Russian State Standard GOST 56800-2015 "Polymer composites. Determination of tensile properties of unreinforced and reinforced materials" on the basis of glass fiber cloth T-13, matrix of epoxy glue "ED-20" and polyurethane adhesive "Laprol PP-3152"

2. Carry out the processing of the results and plot the stress-strain curves for the samples obtained.

2. Methods

To simulate the real behavior of wooden structures reinforced with composite materials, it is necessary to carry out a complex of numerical and laboratory investigations. The actual values of the mechanical characteristics of the laminated polymer composites are obtained after tensile tests of the check samples in accordance with GOST 56800-2015 "Polymer composites. Determination of tensile properties of unreinforced and reinforced materials" or GOST 25.601-80 "Design calculation and strength testings. Methods of Mechanical testing of Polymeric Composite Materials Test for Tensile Properties on Plane Specimens at Normal, Elevated and Low Temperatures". Elastic modulus, Poisson's ratio, ultimate tensile strength are determined, stress-strain diagrams are constructed.

The article is devoted to the influence of curative glue mould type and the molding method on the mechanical characteristics of the laminate polymer composite. The structural fiberglass T-13 in the amount of 15 layers has been used as a reinforcing material and a two-component epoxy ED-20 resin with polyethylene polyamine hardener and a one-component polyurethane adhesive Laprol PP-3152 as a glue mould. Samples are carried out by the contact molding according to GOST 56800-2015. The mould type based on the epoxy resin ED-20 meets the manufacturability requirements, preparation simplicity and cheapness. In turn, performance factors can be increased by adding dibutyl phathalate plasticizing agent or slate modifier slamor to the composition. The second is a surperficially active substance that increases the wetting properties of epoxy compositions, reduces the cost of the hardener by 15–20 %, significantly

reduces the initial viscosity thus improving the composition penetrating properties, herewith being more affordable and cheaper than its counterpart. One-component polyurethane adhesive Laprol PP-3152 does not require preparatory work, the introduction of additional plasticizers and additives. The composition is cured by moisture from air and wood. However, when forming the prepregs on this glue basis, the mould curing occurs unevenly, an airtight layer of the cured resin and glass fabric is formed in the edge zones making further polymerization of the sample difficult. Among other things, the volume of the adhesive composition increases significantly due to "swelling" during curing, microbubbles of air appear in the adhesive seam disrupting the prepreg homogeneous structure, thereby reducing its strength and deformation characteristics. Two series of 5 samples in the form of rectangular cross section blades in each have been mold as part of the investigation. The blades dimensions are shown in Figure 1. Holes in which steel short shoots have been installed during the tests have been made at the end sections of the sample-blades, preventing reduction in the cross section during compression of the locking grips and further destruction of the sample. Resistive strain sensors have been installed in two mutually perpendicular directions to determine the relative deformations in the middle part of the sample (Figure 2). Strain sensors with a base of 20 mm, transverse sensors with a base of 5 mm have been used to measure the relative longitudinal strain. Before beginning the test, the samples are labeled, the thickness and width of the sample working part are measured at three points: at the edges and in the middle to an approximation of 0.025 mm, then the average value of each parameter is calculated and used in the calculations.

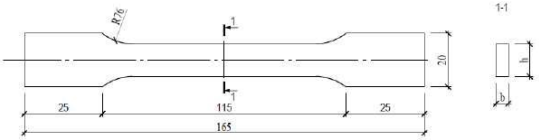

Figure 1. Flat sample for tensile tests in accordance with GOST 56800-2015

As a bench testing the REM-100 tensile machine has been used. Loading speed has been 5 ± 25 % mm/min. The following mechanical characteristics of the laminate polymeric composites have been determined during the tests: elasticity modulus, tensile strength, strain yield or conditional strain yield, breaking extension, yield point elongation, Poisson's ratio.

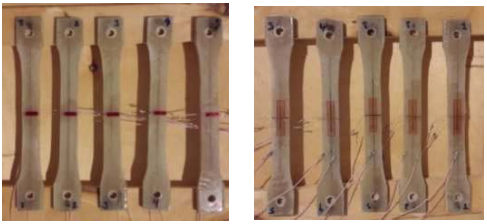

Figure 2. General view of the blades samples for tensile tests with installed strain sensors

The Poisson's ratio ν has been determined by the formula:

$$\nu = \frac{\Delta\varepsilon_{II}}{\Delta\varepsilon_{II}}, \quad (1)$$

where $\Delta\varepsilon_{II}$ is the change of the relative transverse strain of the sample when the voltage is changed by $\Delta\sigma$, $\Delta\ \varepsilon_I$ is the change in the relative longitudinal strain of the sample when the voltage is changed by $\Delta\sigma$. The values, in turn, have been determined by the strain sensors indications [30].

3. Results and Discussion

The initial data and test results of two series of samples on the laminate curative mould from epoxy resin ED-20 and polyurethane adhesive Laprol PP-3152 have been presented respectively in Tables 1 and 2.

Table 1. The initial data and test results of series of samples on the laminate curative mould from epoxy resin ED-20

Woven fiberglass T13 – 15 layers, mould – two-component epoxy resin ED-20							
Sample number	Section width b, mm	Cross-sectional hight h, mm	Working zone cross sectional area, mm^2	Tensile strength yield $\sigma_в$, MPa	Conditional strain yield ε_p,%	Elasticity modulus E, GPa	Poisson's ratio ν
I	13.4	5.7	76.38	225.86	16.45	15.30	0.1
II	13.1	6.1	79.91	216.94	16.15	15.86	0.1
III	13.5	5.7	76.95	227.91	16.41	14.11	0.1
IV	13.3	5.9	78.47	203.99	16.42	13.49	0.1
V	13.1	5.8	75.98	215.63	16.90	12.91	0.1

Table 2. The initial data and test results of series of samples on the laminate curative mould from polyurethane adhesive Laprol PP-3152

Woven fiberglass T13 – 15 layers, polyurethane adhesive Laprol PP-3152							
Sample number	Section width b, mm	Cross-sectional hight h, mm	Working zone cross sectional area, mm^2	Tensile strength yield $\sigma_в$, MPa	Conditional strain yield ε_p,%	Elasticity modulus E, GPa	Poisson's ratio ν
I	13.3	6.3	83.79	125.75	19.80	8.11	0.2
II	13.3	6.8	90.44	125.94	23.26	6.13	0.2
III	13.3	6.7	89.11	1143.0	17.62	8.41	0.2
IV	13.2	7.3	95.92	86.26	14.71	5.72	0.2
V	12.9	7.1	91.59	114.64	21.68	5.99	0.2

The destruction of the samples was brittle and occurred in the calculation zone. The integrity of the prepregs in the grips was ensured until the destruction.

The fragile nature of fracture with matrix shift, according to the studies of F.M. Ernsberger, points at weak adhesion of the matrix of polyurethane glue "Laprol PP-3152" and filler made of glass fabric T-13 and destruction along the interface, which significantly reduces the strength of the composite as a whole. In turn, the samples of the first series collapsed brittle with pulling out of the fibers, which is preferable from the point of view of the working conditions of the composite material.

The nature of the destruction of the samples is shown in Figure 3.

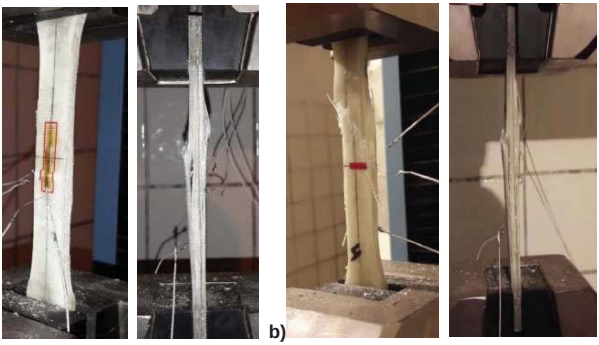

a) **b)**

Figure 3. Brittle fracture patterns: a – the first series with pulling out the fibers, b – the second series with shear failure of the matrix

Diagram of the stress-strain relationship for two series of blade patterns is shown in Figure 4. To achieve the correct values of mechanical characteristics, the section must be corrected to obtain a zero point, with allowance for the strain axis or the elongation axis. The point of intersection N is a point of zero

strains with a fulfilled correction, from which all elongations or strains, including plastic yield of NQ_1, NQ_2, are to be calculated. The longitudinal elastic modulus can be calculated by dividing the stress at any point on the straight line Q_1D_1, Q_2Q_2 by the strain at the same point (measured from point N) [30]. According to the test results, it has been found that the elasticity modulus and the tensile strength of a series of samples on the epoxy resin ED-20 curative mould is twice as high as that of samples on a polyurethane adhesive Laprol PP-3152. Point D2 characterizes the onset of shear deformation in the matrix for the second series of samples. The relative conditional strain yield of the samples before destruction is 16–20 %. On-line tests of samples by standards allow to obtain the true values of the composite materials mechanical characteristics, however from the point of view of trial design they are quite laborious, long and, in the case of expensive materials, economically impractical. In this case, the following formulas have been used for the preliminarily evaluation of the materials elasticity modulus:

$$\begin{aligned} \mathrm{E} &= \mathrm{E_f V_f} \cdot \mathrm{E_m V_m} \\ \mathrm{V_f} + \mathrm{V_m} &= 1, \end{aligned} \tag{2}$$

Where E_f, V_f are the modulus of elasticity respectively, the tensile strength yield, and the volume ratio in the reinforcing fiber composite, E_m, V_m is the same for the curative polymer.

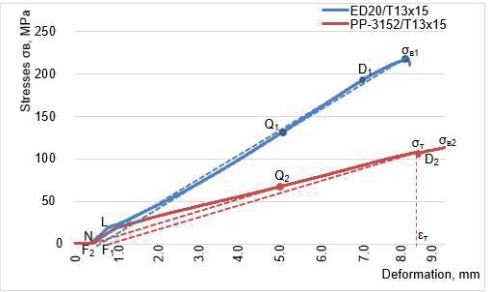

Figure 4. Diagram of the stress-strain relationship for two series of blade patterns

To evaluate the obtained results and to confirm the analytical system formulas (2), mathematical calculations of mechanical characteristics have been carried out. Recognized – Russian State Standard, technical conditions, material certificates allow to mark out all the initial data for calculation sufficiently. Glass fibre of E glass type with elasticity modulus of 76–78 GPa, intertwined with each other in larger fibres (rovings) have been used in the structural glass fabric T-13 for warp threads. Fiberglass has a linen weaving with 16 pieces of warp threads per 1 cm. The number of warp threads per sample width of 13.9 mm is:

$$(16/10) \cdot 13.9 = 22 \text{ pcs.}$$

15 layers of the sample fiber glass contain:

$$22 \cdot 15 = 330 \text{ warps.}$$

The trade mark of the warp yarn is EC7 54x2, where 54 denotes the linear density of the yarn in tex. Tex is a non-system unit of linear density, used in the textile industry because of the difficulty in determining the rovings diameter, denotes the weight of 1 g of warp 1 km in length. Sections of the operating area 50 mm long have been cut out and weighed after testing the samples. The average mass of the operating area has been 5.95 g for the first batch of samples and 6.3 g for the second. The weight of all warps has been determined within the operating area of 50 mm in length:

$$0.000054 \text{ g / mm} \cdot 50 \text{ mm} \cdot 330 \text{ pts} = 0.891 \text{ g.}$$

At the final stage, we have determined the volume content of the reinforcing material and mould in the prepreg:

$$\mathrm{V_f} = 0.891/5.95 = 0.149,$$

for the curative mould respectively

$$\mathrm{V_m} = 1 - 0.149 = 0.850.$$

The elastic modulus of the epoxy resin ED-20 has been obtained by the compressive test of the samples adhesive composition and is 2.54 GPa. Then the modulus of elasticity of the laminate polymer composite is

$$E = 78 \cdot 0.149 + 2.54 \cdot 0.850 = 14.23\ \text{GPa}.$$

The discrepancy between the results and in-place tests is:

$$(14.33 - 14.23) \cdot 100\% / 14.33 = 0.69\%.$$

The high convergence of the theoretical data with the experimental results shows the adequacy of the model of viscoelastic deformation of glass-fiber composites proposed by Rosen. The results obtained may indicate a significant effect of the type and amount of the adhesive curing matrix in the layered polymer composite on its mechanical characteristics. In turn, the method of forming prepregs is often not taken into account when simulating the actual operation of reinforced wooden structures. The value of the modulus of elasticity of a layered polymer composite in numerical studies is taken without taking into account the effect of the type and amount of the curing matrix, which leads to a discrepancy between the calculation results and experimental studies. Further research should be aimed at improving the technology of producing layered polymer composites in structural conditions. The production of composites with high physical and mechanical characteristics opens the possibility of significantly reducing the material consumption of building structures with a low weight of the reinforcement elements. In turn, the workability of the work actualizes the use of composite materials at large volumes of reconstruction of buildings.

4. Conclusions

Based on the tests results the following conclusions and recommendations can be made:

1. The laminate polymer composites on the base of woven fibre glass obtained by the contact molding method have insufficient mechanical characteristics for use as wooden structures reinforcement with considerable reinforcement ratio. The prepregs elasticity modulus in tension (14.33 GPa) is commensurate with the analoguos value for the 2nd grade of wood (10 GPa) that is not enough to achieve high rigidity indicators in the work of wooden structures flexural and compressed-flexural elements. In turn, the low value of the laminated polymeric composites elasticity modulus is conditioned by the uncontrolled increase in the bulk density of the polymer curative composition. This disadvantage is leveled out by the transition to a more advanced production technology to the method of vacuum infusion.

2. Low values of mechanical characteristics for the second series of samples on the base of the polyurethane adhesive Laprol PP-3152 curative mould are associated with the irragulation of the molding technology, problems with the adhesive polymerization and its increase in volume as a result of "bloating" during curing. It is necessary to carry out molding by the narrow width 200 mm tape tools because of the negative influence of the above mentioned factors, therewith it is necessary to load the samples upper plane by pressure similar to the analogous glued wooden structures technologies (0.3-0.5 MPa). In this case, the excess of the adhesive composition as a result of the volume increase during the polymerization process does not lead to a significant increase in the bulk density of the curative mould.

3. The samples destruction is of a fragile nature without a significant strain increase in (relative elongation 16.47–19.41 %), the composite material strain character is elastic, the plastic deformation zone is either absent (1 series) or slightly expressed (2 series).

4. The analytical method for determining the elasticity modulus is sufficiently precise for the materials preliminary analysis for the production of the laminate polymer composites.

References

1. Shokhin, P.B. Povysheniye ekspluatatsionnoy nadezhnosti derevokompozitnykh balochnykh konstruktsiy: dissertatsiya na soiskaniye uchenoy stepeni kandidata tekhnicheskikh nauk: 05.21.05.05 [Improvement of operational reliability of wood-composite beam structures: dissertation for obtaining a scientific degree of a candidate of technical sciences: 05.21.05]. Arkhangelsk: SAFU, 2012. 157p. (rus)
2. Lisyatnikov, M.S. Sovershenstvovaniye tekhnologii izgotovleniya derevokleyenykh konstruktsiy s usileniyem priopornykh zon: dissertatsiya na soiskaniye uchenoy stepeni kandidata tekhnicheskikh nauk: 05.21.05. Arkhangelsk: SAFU, 2015. 179 p. (rus)
3. Lisyatnikov, M.S., Popova, M.V., Sergeyeva, A.N., Sidorov, S.A. Chislennyye issledovaniya vysokikh derevokleyenykh balok s usileniyem priopornykh zon [Numerical studies of high-girdered beams with reinforcement of bearing zones]. BST: Byulleten stroitelnoy tekhniki. 2016. No. 5(981). Pp. 35–37. (rus)

Литература

1. Шохин П.Б. Повышение эксплуатационной надежности деревокомпозитных балочных конструкций: диссертация на соискание ученой степени кандидата технических наук: 05.21.05. Архангельск : САФУ, 2012. 157с.
2. Лисятников М.С. Совершенствование технологии изготовления деревоклееных конструкций с усилением приопорных зон: диссертация на соискание ученой степени кандидата технических наук: 05.21.05. Архангельск : САФУ, 2015. 179 с.
3. Лисятников М.С., Попова М.В., Сергеева А.Н., Сидоров С.А. Численные исследования высоких деревоклееных балок с усилением приопорных зон // БСТ: Бюллетень строительной техники. 2016. № 5(981). С. 35–37.
4. Шохин П.Б., Лукин М.В., Сергеева А.Н., Глебова Т.О. Technological solutions of manufacture of composite wood joist construction // БСТ: Бюллетень строительной техники. 2016. № 8(984). С. 54–55.
5. Рощина С.И., Лисятников М.С.,Мелехов В.И., Лабудин Б.В., Лукин М.В., Применение высоких деревоклееных

Грибанов А.С., Рощина С.И., Попова М.В., Сергеев М.С. Слоистые полимерные композиты для деревянных конструкций // Инженерно-строительный журнал. 2018. № 7(83). С. 3–11.

4. Shokhin, P.B., Lukin, M.V., Sergeyeva, A.N., Glebova, T.O. Technological solutions of manufacture of composite wood joist construction. BST: Byulleten stroitelnoy tekhniki. 2016. No. 8(984). Pp. 54–55.
5. Roshchina, S.I., Lisyatnikov, M.S., Melekhov, V.I., Labudin, B.V., Lukin, M.V. Primeneniye vysokikh derevokleyenykh balok v pokrytii zdaniy tekstilnykh tsekhov [The use of high decorated beams in the cover of the buildings of textile shops]. Izvestiya vysshikh uchebnykh zavedeniy. Tekhnologiya tekstilnoy promyshlennosti. 2016. No. 5(365). Pp. 267–271. (rus)
6. Roshchina, S.I., Lukin, M.V., Luckina, A.V., Sergeyev, M.S., Lisyatnikov, M.S. Experimental research on pressed-bending reinforced timberwork. International Journal of Applied Engineering Research. 2015. Vol. 10. No. 24 Pp. 45307–45312.
7. Tikhonov, A.V., Lobov, D.M. Issledovaniye voprosov usileniya derevyannykh konstruktsiy kompozitnymi materialami [Investigation of issues of reinforcement of wooden structures with composite materials]. VI Vserossiyskiy festival nauki Sbornik dokladov v 2-kh tomakh. Nizhegorodskiy gosudarstvennyy arkhitekturno-stroitelnyy universitet. 2016. Pp. 87–90. (rus)
8. Lobov, D.M. Usileniye derevyannykh konstruktsiy uglerodnym voloknom [Strengthening wooden structures with carbon fiber]. Sbornik: Velikiye reki 2013 Trudy kongressa 15-ogo Mezhdunarodnogo nauchno-promyshlennogo foruma: v 3-kh tomakh. Nizhegorodskiy gosudarstvennyy arkhitekturno-stroitelnyy universitet. 2013. Pp. 184–187. (rus)
9. Lobov, D.M., Kritsin, A.V., Tikhonov, A.V. Osobennosti armirovaniya derevyannykh elementov, usilennykh uglerodnym voloknom, pri staticheskom izgibe [Features of reinforcement of wooden elements reinforced with carbon fiber, with static bending]. Izvestiya Kazanskogo gosudarstvennogo arkhitekturno-stroitelnogo universiteta. 2013. No. 2(24). Pp. 132–138. (rus)
10. Labudin, B.V. K obosnovaniyu raschetnoy modeli kleyenoy drevesiny kak ortogonalnogo transversalno-izotropnogo materiala [To substantiation of the calculated model of laminated wood as an orthogonal transversally-isotropic material]. Izvestiya vysshikh uchebnykh zavedeniy. Lesnoy zhurnal. 2006. No. 6. Pp. 136–139. (rus)
11. Kritsin, A.V., Likhacheva, S.Yu., Lobov, D.M., Tikhonov, A.V. Eksperimentalnyye issledovaniya derevyannykh balok, usilennykh uglerodnoy lentoy [Experimental studies of wooden beams reinforced with carbon tape]. Privolzhskiy nauchnyy zhurnal. 2015. No. 3(35). Pp. 103–109. (rus)
12. Yahyaei-Moayyed, M., Taheri, F. Experimental and computational investigations into creep response of AFRP reinforced timber beams. Composite Structures. 2011. No. 93. Pp. 616–628.
13. Kim, Y.J., Harries, K.A. Modeling of timber beams strengthened with various CFRP composites. Engineering Structures. 2010. No. 10. Pp. 3225–3234.
14. D'Ambrisi, A., Focacci, F., Luciano, R. Experimental investigation on flexural behavior of timber beams repaired with CFRP plates. Composite Structures. 2014. No. 108. Pp. 720–728.
15. Nadir, Y., Nagarajan, P., Ameen, M., Arif, M.M. Flexural stiffness and strength enhancement of horizontally glued laminated wood beams with GFRP and CFRP composite sheets. Construction and Building Materials. 2016. No. 112. Pp. 547–555.
16. Basterra, L.A., Balmori, J.A., Morillas, L., Acuna, L., Casado, M. Internal reinforcement of laminated duo beams of low-grade timber with GFRP sheets. Construction and Building Materials. 2017. No. 154. Pp. 914–920.
17. Fossetti, M., Minafт, G., Papia, M. Flexural behaviour of glulam timber beams reinforced with FRP cords. Construction and Building Materials. 2015. No. 95. Pp. 54–64.

балок в покрытии зданий текстильных цехов // Известия высших учебных заведений. Технология текстильной промышленности. 2016. № 5(365). С. 267–271.

6. Roshchina S.I., Lukin M.V., Luckina A.V., Sergeyev M.S., Lisyatnikov M.S. Experimental research on pressed-bending reinforced timberwork // International Journal of Applied Engineering Research. 2015. Vol. 10. № 24. Pp. 45307–45312
7. Тихонов А.В., Лобов Д.М. Исследование вопросов усиления деревянных конструкций композитными материалами // VI Всероссийский фестиваль науки Сборник докладов в 2-х томах. Нижегородский государственный архитектурно-строительный университет. 2016. С. 87–90.
8. Лобов Д.М. Усиление деревянных конструкций углеродным волокном // В сборнике: Великие реки 2013 Труды конгресса 15-ого Международного научно-промышленного форума: в 3-х томах. Нижегородский государственный архитектурно-строительный университет. 2013. С. 184–187.
9. Лобов Д.М., Крицин А.В., Тихонов А.В. Особенности армирования деревянных элементов, усиленных углеродным волокном, при статическом изгибе // Известия Казанского государственного архитектурно-строительного университета. 2013. № 2(24). С. 132–138.
10. Лабудин Б.В. К обоснованию расчетной модели клееной древесины как ортогонального трансверсально-изотропного материала // Известия высших учебных заведений. Лесной журнал. 2006. № 6. С. 136–139.
11. Крицин А.В., Лихачева С.Ю., Лобов Д.М., Тихонов А.В. Экспериментальные исследования деревянных балок, усиленных углеродной лентой // Приволжский научный журнал. 2015. № 3(35). С. 103–109.
12. Yahyaei-Moayyed M., Taheri F. Experimental and computational investigations into creep response of AFRP reinforced timber beams // Composite Structures. 2011. № 93. Pp. 616–628.
13. Kim Y.J., Harries K.A. Modeling of timber beams strengthened with various CFRP composites // Engineering Structures. 2010. № 10. Pp. 3225–3234.
14. D'Ambrisi A., Focacci F., Luciano R. Experimental investigation on flexural behavior of timber beams repaired with CFRP plates // Composite Structures. 2014. № 108. Pp. 720–728.
15. Nadir Y., Nagarajan P., Ameen M., Arif M.M. Flexural stiffness and strength enhancement of horizontally glued laminated wood beams with GFRP and CFRP composite sheets // Construction and Building Materials. 2016. № 112. Pp. 547–555.
16. Basterra L.A., Balmori J.A., Morillas L., Acuña L., Casado M. Internal reinforcement of laminated duo beams of low-grade timber with GFRP sheets // Construction and Building Materials. 2017. № 154. Pp. 914–920.
17. Fossetti M., Minafт G., Papia M. Flexural behaviour of glulam timber beams reinforced with FRP cords // Construction and Building Materials. 2015. № 95. Pp. 54–64.
18. Григолюк Э.И., Чулков П.П. Статика упругих слоистых оболочек. М.: НИИ Механики МГУ, 1999. 215 с.
19. Chen W. A selective review on recent development of displacementbased laminated plate theories // Recent patents on mechanical engineering. 2008. Vol. 1. Pp. 29–44.
20. Ruslantsev A.N., Portnova Ya.M., Tairova L.P., Dumansky A.M. Analisys of mechanical properties anisotropy of nanomodified carbon fiber-reinforced woven composites // IOP Conference Series: Material Science and Engineering (MSE). 2016. Vol. 153. DOI: 10.1088/1757–899.
21. Yao Z., Wua D., Chen C., Zhang M. Creep behavior of polyurethane nanocomposites with carbon nanotubes // Composites: Part A. 2013. № 50. P. 65.

Gribanov, A.S., Roshchina, S.I., Popova, M.V., Sergeev, M.S. Laminar polymer composites for wooden structures. *Magazine of Civil Engineering*. 2018. 83(7). Pp. 3–11. doi: 10.18720/MCE.83.1.

18. Grigolyuk, E.I., Chulkov, P.P. Statika uprugikh sloistykh obolochek [Static of elastic layered shells]. Moscow: NII Mekhaniki MGU, 1999. 215 p. (rus)
19. Chen, W. A selective review on recent development of displacementbased laminated plate theories. Recent patents on mechanical engineering. 2008. Vol. 1. Pp. 29–44.
20. Ruslantsev, A.N., Portnova, Ya.M., Tairova, L.P., Dumansky, A.M. Analisys of mechanical properties anisotropy of nanomodified carbon fiber-reinforced woven composites. IOP Conference Series: Material Science and Engineering (MSE). 2016. Vol. 153. DOI: 10.1088/1757–899.
21. Yao, Z., Wua, D., Chen, C., Zhang, M. Creep behavior of polyurethane nanocomposites with carbon nanotubes. Composites: Part A. 2013. No. 50. P. 65.
22. Ponomarev, A.N., Rassokhin, A.S. Hybrid wood-polymer composites in civil engineering. Magazine of Civil Engineering. 2016. 68(8). Pp. 45–57.
23. Kliger, I.R., Haghani, R., Brunner, M., Harte, A.M., Schober, K.U. Wood-based beams strengthened with FRP laminates: improved performance with pre-stressed systems. European Journal of Wood and Wood Products. 2016. Vol. 74. No. 3. Pp. 319–330.
24. Sprenger, S. Epoxy resins modified with elastomers and surface-modified silica nanoparticles. Polymer. 2013. Vol. 54. No. 18. Pp. 4790–4797.
25. Rassokhin, A.S., Ponomarev, A.N., Figovsky, O.L. Ultra-light hybrid composite wood-polymer structural materials in construction. Magazine of Civil Engineering. 2018. 79(3). Pp. 132–139.
26. Nekliudova, E.A., Semenov, A.S., Melnikov, B.E., Semenov, S.G.. Experimental research and finite element analysis of elastic and strength properties of fiberglass composite material. Magazine of Civil Engineering. 2014. 47(3). Pp. 25–39.
27. Barreto, A.M.J.P., Campilho, R.D.S.G, De Moura, M.F.S.F, Morais, J.J.L., Santos, C.L. Repair of wood trusses loaded in tension with adhesively bonded carbon-epoxy patches. The Journal of Adhesion. 2010. Vol. 86. No. 5–6. Pp. 630–648.
28. Brandner, R., Flatscher, G., Ringhofer, A., Schickhofer, G., Thiel, A. Cross laminated timber (CLT): overview and development. European Journal of Wood and Wood Products. 2016. No. 3. Pp. 331–351.
29. Kalamkarov, A.L., Challagulla, K.S. Effective properties of composite materials, reinforced structures with matrix voids using unit cells at multi-scales. Polimer International. 2013. No. 62. Pp. 1029–1037.
30. Russian State Standard 56800-2015 Kompozity polimernyye. Opredeleniye mekhanicheskikh svoystv pri rastyazhenii nearmirovannykh i armirovannykh materialov [Composites polymeric. Determination of mechanical properties when tensile non-reinforced and reinforced materials]. Moscow: Standartinform. 2016. (rus)

22. Пономарев А.Н., Рассохин А.С. Гибридные древесно-полимерные композиты в строительстве // Инженерно-строительный журнал. 2016. № 8(68). С. 45–57.
23. Kliger I.R., Haghani R., Brunner M., Harte A.M., Schober K.U. Wood-based beams strengthened with FRP laminates: improved performance with pre-stressed systems // European Journal of Wood and Wood Products. 2016. Vol. 74. № 3. Pp. 319–330.
24. Sprenger S. Epoxy resins modified with elastomers and surface-modified silica nanoparticles. Polymer. 2013. № 18(54). Pp. 4790–4797.
25. Рассохин А.С., Пономарев А.Н., Фиговский О.Л. Сверхлегкие гибридные композитные древесно-полимерные конструкционные элементы в строительстве // Инженерно-строительный журнал. 2018. № 3(79). С. 132–139.
26. Неклюдова Е.А., Семенов А.С., Мельников Б.Е., Семенов С.Г. Экспериментальное исследование и конечно-элементный анализ упругих и прочностных свойств стекловолоконного композиционного материала // Инженерно-строительный журнал. 2014. № 3(47). С. 25–39.
27. Barreto A.M.J.P., Campilho R.D.S.G, De Moura M.F.S.F, Morais J.J.L., Santos C.L. Repair of wood trusses loaded in tension with adhesively bonded carbon-epoxy patches. The Journal of Adhesion. 2010. Vol. 86. № 5–6. Pp. 630–648.
28. Brandner R., Flatscher G., Ringhofer A., Schickhofer G., Thiel A. Cross laminated timber (CLT): overview and development // European Journal of Wood and Wood Products. 2016. № 3. Pp. 331–351.
29. Kalamkarov A.L., Challagulla K.S. Effective ptoperties of composite materials, reinforced structures with matrix voids using unit cells at multi-scales // Polimer International. 2013. № 62. Pp. 1029–1037.
30. ГОСТ Р 56800-2015 Композиты полимерные. Определение механических свойств при растяжении неармированных и армированных материалов // М.: Стандартинформ. 2016.

Aleksei Gribanov,*
+7(930)740-07-83; panecito@bk.ru

Svetlana Roshchina,
+7(4922)47-98-04; rsi3@mail.ru

Marina Popova,
+7(4922)47-76-63; popovamv@bk.ru

Michael Sergeev,
+7(4922)47-98-10; sergeevmichael@inbox.ru

Алексей Сергеевич Грибанов,*
+7(930)740-07-83; эл. почта: panecito@bk.ru

Светлана Ивановна Рощина,
+7(4922)47-98-04; эл. почта: rsi3@mail.ru

Марина Владиславовна Попова,
+7(4922)47-76-63; эл. почта: popovamv@bk.ru

Михаил Сергеевич Сергеев,
+7(4922)47-98-10;
эл. почта: sergeevmichael@inbox.ru

Грибанов А.С., Рощина С.И., Попова М.В., Сергеев М.С. Слоистые полимерные композиты для деревянных конструкций // Инженерно-строительный журнал. 2018. № 7(83). С. 3–11.

doi: 10.18720/MCE.83.2

Stress-strain state of a steel-reinforced concrete slab under long-term

Напряженно-деформированное состояние сталежелезобетонной плиты при длительных нагружениях

F.S. Zamaliev*,
M.A. Zakirov,
Kazan State University of Architecture and Engineering, Kazan, Russia

Канд. техн. наук, доцент Ф.С. Замалиев*,
аспирант М.А. Закиров,
Казанский государственный архитектурно-строительный университет, г. Казань, Россия

Key words: steel reinforced concreteslab; numerical experiments; full-scale tests; stresses; deflections; comparisons

Ключевые слова: сталежелезобетонная плита; численные эксперименты; натурные испытания; напряжения; прогибы; сравнения

Abstract. This article explores the evaluation of the stress-strain state of steel reinforced concrete slabs under the action of long-term loads. The technique of computer simulation for the performance evaluation of steel reinforced concrete slabs under short-term and long-term loads and the results of numerical studies are shown. A unit for long-term tests has been prepared based upon the numerical studies. The mounting locations of instruments for measuring vertical displacements, the label diagram of sensors of strains in steel reinforced concrete test structures are given. The measurement results are summarized in tables and graphs. The analysis of the results of full-scale tests is given as are comparisons with numerical experiments' data. Analytical expressions for the calculation of steel reinforced concrete slabs for long-term loads taking into account the creep of concrete are given.

Аннотация. Оценке напряженно-деформированного состояния сталежелезобетонной плиты при действии длительных нагрузок посвящена данная статья. Приведены методика компьютерного моделирования оценки работы составной плиты при кратковременных и длительных нагружениях, результаты численных исследований. На основе численных исследований подготовлена установка для длительных испытаний. Приведены места установки приборов для замера вертикальных перемещений схема наклейки датчиков деформаций бетона и стали на испытуемой конструкции. Результаты измерений сведены в таблицы и графики. Дан анализ результатов натурных испытаний и сравнения с данными численных экспериментов. Приведены также аналитические выражения для расчета сталежелезобетонных плит на длительные нагружения с учетом ползучести бетона.

1. Introduction

In recent years, the construction practice has exhibited a tendency of expanding the application of steel reinforced concrete structures which renders their further study more relevant. However, the studies of steel reinforced concrete flexible elements are mainly dedicated to the identification of the stress-strain state by short-term external impacts [1–18] or to the identification of their preoperational stress-strain state [19–20]. To study the stress-strain state of steel reinforced concrete structures both analytical [1–8] and experimental methods – that is numerical experiments [14–18], or full-scale tests [19–20] are employed. The article deals with studies of steel reinforced concrete slabs for the action of long-term loads. The applicable Eurocode in European countries and the Russian design and construction specifications SP 266.1325800.2016 mainly view steel reinforced concrete structures under the action of short-term loads.

In order to identify the stress-strain state of steel reinforced concrete structures, different mathematical models and experimental studies on large-scale field models are employed. Experimental studies on full-scale models require considerable time, human and physical costs. Therefore, it is quite often that mathematical models which lead to faster results are selected. Many researchers while in search of effective mathematical models come to use numerical experiments based on application software. However, the accuracy of the data in large part depends on the proper choice of the numerical experiment model that would correspond to the physical operational essence of the nature structure by all the

Замалиев Ф.С., Закиров М.А. Напряженно-деформированное состояние сталежелезобетонной плиты при длительных нагружениях // Инженерно-строительный журнал. 2018. № 7(83). С. 12–23.

parameters. There are many PC software systems (SCAD, Microfe, LIRA, ANSYS, etc.) used by researchers to model the elements of building structures. When choosing a PC, the question arises as to how close they are to the actual operation of the structures and how accurately they can assess the behavior of the structural element from its zero load up to the point of its destruction as well as taking into account the stress-strain state in various modes of load (short-term, long-term, repeated-static loads).

Studies of steel reinforced concrete structures on the basis of a mathematical model using application programs with further verification of the calculation results is an actual task. In this connection, the following tasks are set:

– The choice of the settlement complex, most fully reflect the actual work of the composite slab under operating loads.

– Analysis of the stress-strain state of the slab under the operational load (stresses in the ribs and plate, deflections, shear at the "steel-concrete" boundary)

– Carrying out full-scale tests of the model of composite slab on a scale of 1: 2.

– Comparison of results of full-scale tests with analogous data of numerical studies.

– Record analytical expressions for the evaluation of strength for the case of prolonged loading and comparison of calculation results by analytical formulas with the data of numerical and on-line experiments.

2. Methods and Results

The third stage (post-processing) is the analysis of calculation results. The calculated physical quantities (displacements, strains, stress, temperature and others) are represented in the ANSYS graphic window as pictures, tables, diagrams, animations.

The following structural solution was studied:

The steel part of the steel-concrete composite slab is the 3 000 mm rolled I-beams #14 per; the dimensions of the heavy B25 concrete slab part are as follows: length is 3 000 mm, width is 3 000 mm, height is 45 mm (Figure 1).

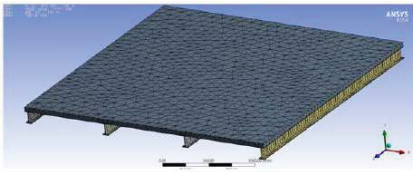

Figure 1. Finite-element mesh generation of the steel-concrete composite slab

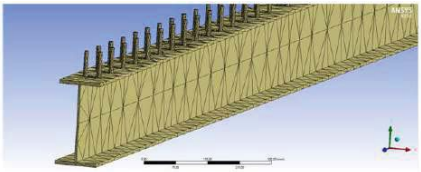

Figure 2. Finite-element mesh generation of the I- beam

The anchors are made from steel reinforcement in the form of two rows of 60 mm tall vertical bars (2ø8 S245), welded throughout the entire length to the upper flange of steel beams spaced at intervals of 150 mm in the middle of the stairwell and of 100 mm on the ends (Figure 2). Height of the full construction is 190 mm.

The next stage of modelling is to select materials for the created bodies and to specify their properties.

For these purposes, there is a separate material management unit in Workbench, which deals with the analysis unit and is represented by the Engineering Data unit. For this particular slab, two materials from the library of General Materials – the library of the general use materials – were used; however, some characteristics were altered.

Metal ductility is calculated via a non-linear material model. In this particular case, Bilinear Isotropic Hardening was selected from the plasticity models.

For obtaining the numerical solution, it is necessary to split the geometric models by the finite-element grid. This procedure is carried out in the Modelling unit “Mechanical”. The grid on solid bodies is created with the aid of the tetrahedral or hexahedral solid-state members. For this particular slab, the Medium grid – from 75° to 24° – was used in the Relevance center. There also exists a Fine grid – from 36° to 12° and a coarse grid – form 91° to 60°.

The slab was modelled according to the diagram of the free-supported structure distributed along the surface area by the load. The bearing distance of the slab is 2900 mm.

The load was applied for 3 steps. The boundary conditions were applied by means of the Remote Displacement.

The contact between the anchors and the reinforced concrete slab was assigned through Rough – this particular case corresponds to the infinite friction coefficient between the connected bodies; however, with the possible detachment along the surface the absence of friction is implied.

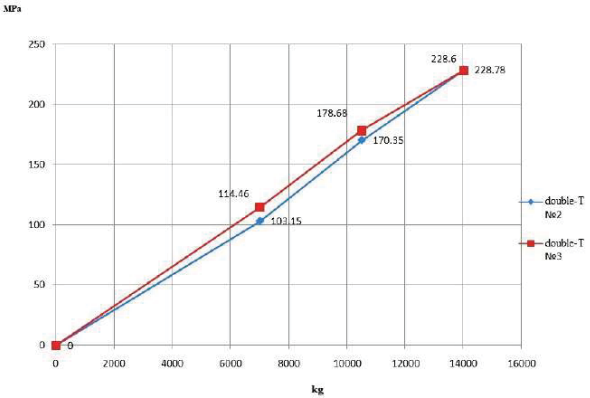

Figure. 3 Graphs showing the development of loads in the lower flange of the I-beams of a steel reinforced concrete slab

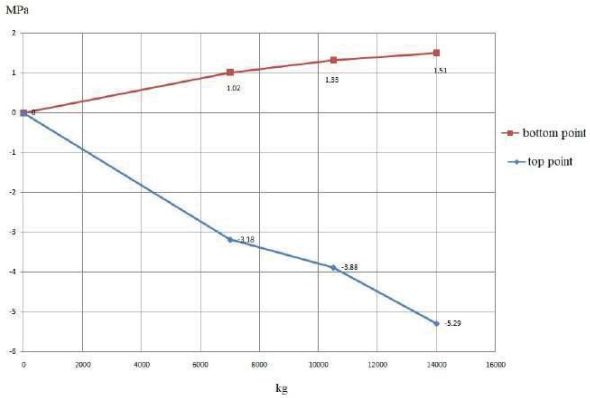

Figure 4. Graphs showing the development of loads in a reinforced concrete slab

A calculation of a steel reinforced concrete slab performed on the ANSYS software serves to reveal the situation of a stress-strain state, stages of development of plastic strains in a steel beam and in a concrete slab.

The findings of the studies show a sequence of development of loads and strains in the steel I-beam and in the reinforced concrete slab as strains develop from a more stressed zone to a less stressed one; from the middle to the ends. In a steel beam, strains develop at a more intense pace as the load increases than in a steel reinforced concrete slab which can be explained by a smaller cross-section of the tension flange than a compressed reinforced concrete shelf. Graphs showing the distribution of loads in beams and in a slab

Figures 3–4 and graphs showing changes in deflections (Figure 5) have been formed.

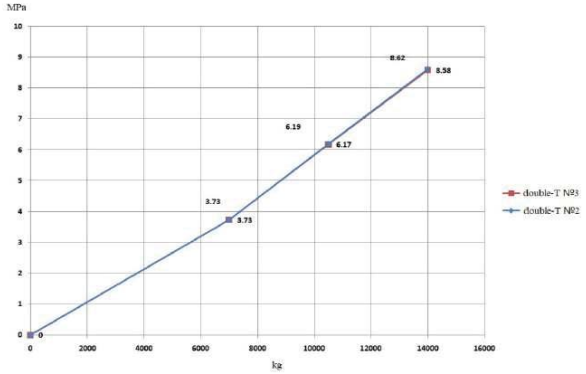

Figure 5. A graph depicting deflections per stage of load

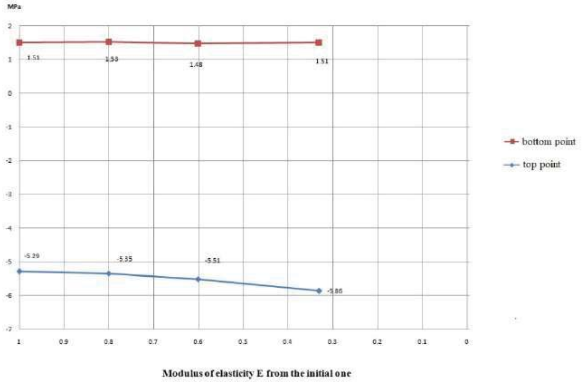

Figure 6. A graph showing the development of loads in the case of a long-term load

Modulus of elasticity E from the initial one.

The attained results of calculations clearly show the development of a stress-strain state in the anchor rods: strains and stresses in them increase as the distance from the middle of a beam grows, stresses increase along the height of rods as they approach the contact zone "steel and concrete"; the surface of the top flange of the steel profile has clearly visible zones of tension using which it is possible to judge about the size of crushed zones or where the concrete in the shelf of a composite beam has split.

The results of the numerical study confirm the theoretical foundation and methodology of calculations of steel reinforced concrete slabs for long-term loads. The creep in the concrete part of the structure confirms the change in the stress-strain state over time. An increase of stresses in the steel part of the structure as the creep accounts for up to 19 %, an increase in deflections up to 39 % in comparison with calculations at short-term loads (Figures 6–8).

To ensure the combined action of metal beams with a slab, various anchoring devices are welded to their upper flange to prevent shifts in the layers. In this study, cylindrical rods have been selected as anchors.

In order to study the peculiarities behind the action of a steel reinforced concrete slab under long-term loads, its large-scale model in the scale 1:2 with the following geometric parameters and components was tested: A reinforced concrete slab with a width of 3 000 mm, a length of 3 000 mm and a height of 45 mm, supported by four steel beams from an I-beam No. 14 GOST (Russian State Standard) 8239-89, with a length of 3 000 mm located at a distance of 1 000 mm from each other. The combined action of steel ribs and the reinforced concrete slab was achieved through two rows of vertical anchor rods (2ø6 A400) with a height of 40 mm welded along the entire length to the upper flange of steel I-beams with a step of 150 mm on the ends

at a quarter of the span and with a step of 250 mm in the middle in half span. The concrete slab model was reinforced by reinforcement grids from a wire ø4 B500 with a step of 200 mm by the classical scheme for ribbed uncut reinforced concrete slabs. The B25-class concrete was used. The slab under the experiment rested against rolling and stationary rollers by means of steel ribs with a working span of 2 900 mm. Rolling and stationary rollers were installed on reinforced concrete blocks on the ends of steel I-beams.

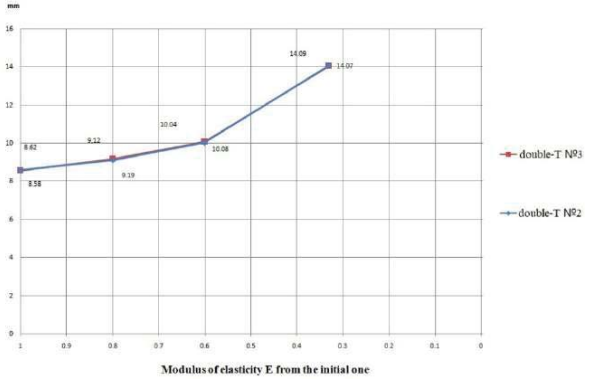

Figure 7. Graphs of the development of deformations in the edges of the plate under prolonged loading

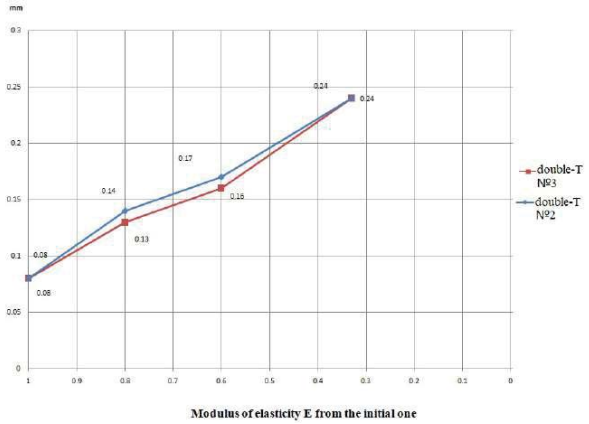

Figure 8. Graph of development of shear at the steel-concrete border

Figure 9. A general view of the slab under load

Figure 10. Dial gauges to record the shift at the border of steel and concrete and settlement of the supports

Замалиев Ф.С., Закиров М.А. Напряженно-деформированное состояние сталежелезобетонной плиты при длительных нагружениях // Инженерно-строительный журнал. 2018. № 7(83). С. 12–23.

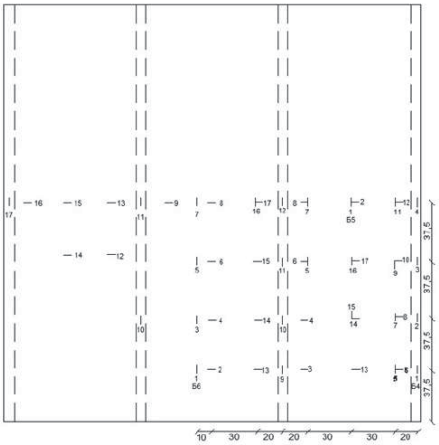

Figure 11. A diagram showing the stickers of strain sensors on the bottom surface of the slab

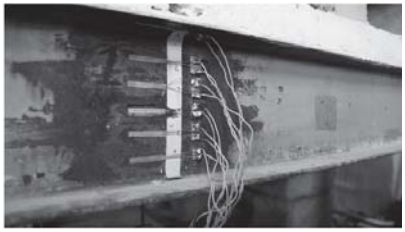

Figure12. Strain sensors on the ribs of the slab

Vertical strains (deflections) of the slab were measured on the centers of the middle and marginal steel beams by means of beam compasses firmly fixed on a tripod with a dial gage installed under the middle beam. A dial gage (Figure 10) was also installed to measure the settlement of supports in the roller support zone. In order to measure strains (stresses) on the upper and lower surfaces of the concrete slab (Figure 11), resistive-strain sensors with a base of 20 mm (for steel) (Figure 12) and 50 mm (for concrete) were glued onto the walls and shelves of the steel I-beams. A total of 120 resistive-strain sensors were glued. The moment when cracks formed and the manner of their propagation were determined visually; a 24-times magnification MBP-2 microscope was used to measure the values of cracks openings.

The slab fragment model was tested in a laboratory on the premises of the Kazan State University of Architecture and Engineering under static short-term and long-term loads. The static load was transferred to the slab in 48 points in the zone above the steel ribs.

The static evenly distributed load was supplied step-by-step: The distribution layer consisted of 48 reinforced concrete cubes 100 x 100 x 100 in size; the subsequent stages of loads were generated from foundation blocks 400 x 600 x 1200 in size with a weight of 580–590 kg. The second and third layers of the foundation blocks were placed through the wooden gaskets along the ends to provide a static pattern of load transfer from the blocks. A total of 24 blocks were used (Figure 9).

At each stage, the readings of the resistive-strain sensors were taken through AID, deflections in the middle of the beams and the settlement of the supports of the slab were measured and crack formation was observed in the reinforced concrete slab. Strains of the steel ribs were measured as well as those of the I-beams of the reinforced concrete slab and vertical strains of the slab and deflections; based on the readings of resistive-strain sensors and strain indicators, first graphs were formed on the day when the test slab was loaded, i.e. short-term load results. The readings were taken every day during the first week, then once a week. Figures 13–15 show graphs of stress development in the upper and lower flanges of the ribs and in the slab whereas Figure 16 shows a "steel and concrete" shift development at the junction of the ribs with the slab.

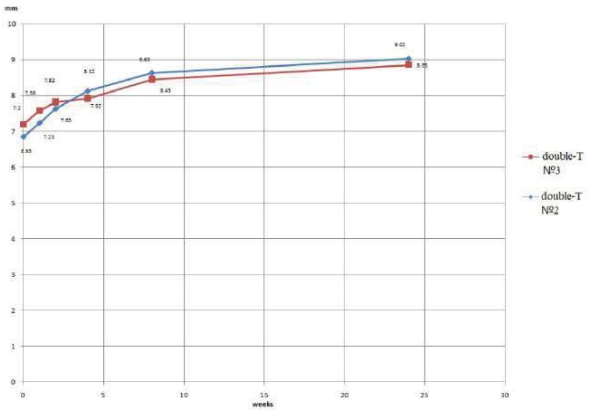

Figure 13. Graphs showing the development of strains in the case of a long-term load

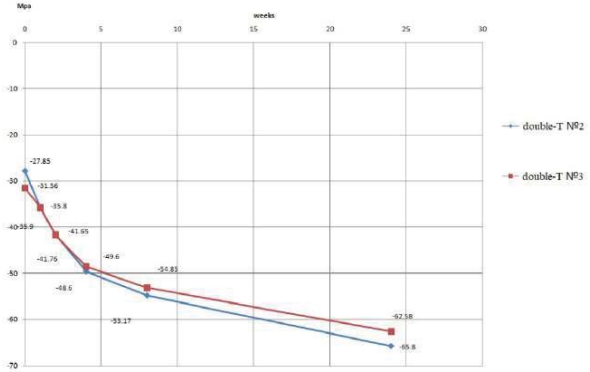

Figure 14. Graphs showing the development of loads in the upper flange of I-beams in the case of a long-term load

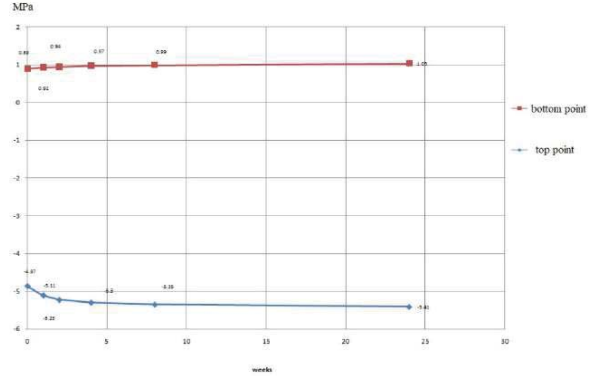

Figure 15. Graphs showing the development of stresses in the case of a long-term load

Замалиев Ф.С., Закиров М.А. Напряженно-деформированное состояние сталежелезобетонной плиты при длительных нагружениях // Инженерно-строительный журнал. 2018. № 7(83). С. 12–23.

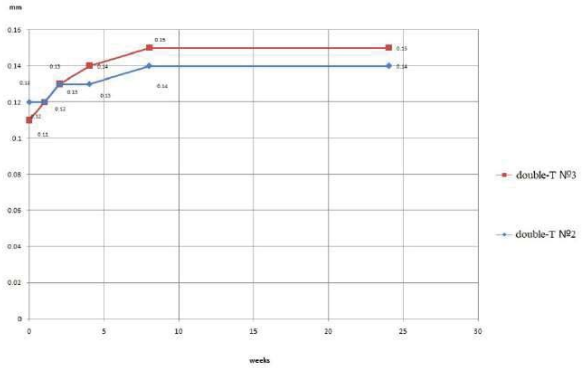

Figure 16. Graphs showing the development of a shift at the border of steel and concrete

An analytical description of the stress-strain state of the steel reinforced concrete slab under long-term loads.

The calculation of the strength of normal cross-sections is performed based on the following prerequisites:

– cross-sections normal to the longitudinal axis of the steel reinforced concrete element are considered;

– normal stresses in the monolithic reinforced concrete slab and a steel beam are taken as calculation data;

– the connection between the main stresses and the relative strains of concrete and steel is presented in the form of corresponding diagrams "$\sigma - \varepsilon$ ".

– the hypothesis of flat cross-sections is considered fair for the average strains of the concrete of the monolithic slab and beams' steel;

– the ductility of the connecting seam (conjunction) of the reinforced concrete part and the steel part of the steel reinforced concrete bending element is not taken into account; the condition of compatibility of strains of concrete and steel along the plane of the contact "steel and concrete" is accepted.

Based on the hypothesis of flat cross-sections and analytical or actual diagrams of concrete "$\sigma_b - \varepsilon_b$ "and steel" $\sigma_s - \varepsilon_s$ " function, the stresses in the concrete of the monolithic slab and in the steel beam are determined by the corresponding strains. Thus, the internal stress forces in the concrete σ_b, in the slab reinforcement σ_a and in the steel of the beam σ_s are defined in the cross-section for any considered load level caused by the action of operational loads.

In this case, there are two equations of equilibrium [1, 2]:

$$N_x = \int_0^{h_n^{'}} \sigma_b\left[\varepsilon_b(x)\right] \cdot b_n^{'} \cdot dx + \sigma_s^{'}\left(\varepsilon_s^{'}\right) \cdot A_s^{'} - \sigma_s\left(\varepsilon_s\right) \cdot A_s + \sigma_a^{'}\left(\varepsilon_a^{'}\right) \cdot A_a^{'} + \sigma_a\left(\varepsilon_a\right) \cdot A_a = 0 \qquad (1)$$

$$M_z = \int_0^{h_n^{'}} \sigma_b\left[\varepsilon_b(x)\right] \cdot b_n^{'} \cdot z_1(x_i) \cdot dx + \sigma_s^{'}\left(\varepsilon_s^{'}\right) \cdot A_s^{'} \cdot z_2 + \sigma_s\left(\varepsilon_s\right) \cdot A_s \cdot z_3 + \sigma_a^{'}\left(\varepsilon_a^{'}\right) \cdot A_a^{'} \cdot z_4 + \sigma_a\left(\varepsilon_a\right) \cdot A_a \cdot z_5 \qquad (2)$$

where is $\sigma_b(\varepsilon_b), \sigma_s^{'}(\varepsilon_s^{'}), \sigma_s(\varepsilon_s), \sigma_a^{'}(\varepsilon_a^{'}), \sigma_a(\varepsilon_a)$ " the dependence of the stress-strain of concrete, steel and reinforcements;

$\varepsilon_b(x)$ – the law of variation of strains along the height of the cross-section of the steel reinforced concrete element;

$b_n^{'}$ – the width of the reinforced concrete monolithic shelf is entered into the calculation;

x_i – the height of the compressed zone;

z_1 – the distance from the center of gravity of the curve of normal stresses in monolithic concrete to the neutral axis;

z_2 – the distance from the center of gravity of the curve of normal stresses of the compressed part of the steel beam to the neutral axis;

z_3 – the distance from the center of gravity of the curve of normal stresses of the stretched area of the steel beam to the neutral axis;

z_4 – the distance from the center of gravity of the top reinforcement of the concrete shelf to the neutral axis;

z_5 – the distance from the center of gravity of the bottom reinforcement of the concrete shelf to the neutral axis.

Until the condition $\left|\Delta N_x\right| \le \delta$ () (-δ the specified accuracy of executions) is fulfilled, the consecutive approximations method is used to calculate the desired height of the compressed zone x_i of the steel reinforced concrete built-up section according to the formula (1).

For long-term loads, the strength is expressed as

$$M_i + \Delta M_b + \Delta M_{sr} \le M_z \qquad (3)$$

where M_i is the bending moment of the action of the external load.

$\Delta M_b = 0.5\left[\sigma_{b(t)}^{\partial on} + \sigma_{b(t)}^{'\partial on}\right] b_n h_n z_1 + \sigma_a^{'} A_a^{'} z_4 + \sigma_a A_a z_5$ – an additional bending moment due to the occurrence and accumulation of residual stresses in the concrete of the slab.

$\Delta M_{sr} = \sigma_{sr}^{'}(t) A_{sr}^{'} z_2 + \sigma_{sr}(t) A_{sr} z_3$ – an additional bending moment due to the development of residual stresses in the upper and lower parts of the steel rib's cross-section.

3. Discussion

An analysis of the existing literature, rules and regulations pertaining to the design and calculation of steel structures and reinforced concrete structures as well as of instructions and recommendations [12, 13] lead to the conclusion that obtaining theoretical calculations closest to full-scale studies by modeling in the ANSYS software is possible if changes in the stress-strain modulus of the concrete part of the structure and creep are taken into account. Moreover, factors such as temperature, shrinkage and relaxation have less impact on the stress-strain modulus of the structure compared to creep in long-term loads calculations. In this regard, calculations were performed taking into account the changes in the stress-strain modulus of concrete over time taking into consideration the creep coefficient with results attained (A value of E_b = 30000 MPa for concrete B25 was taken as the initial modulus of elasticity). Stresses were also observed which are reflected in the graphs.

The attained results of calculations in ANSYS clearly show the development of a stress-strain state in the anchor rods: strains and stresses in them increase as the distance from the middle of a beam grows, stresses increase along the height of rods as they approach the contact zone "steel and concrete"; the surface of the top flange of the steel profile has clearly visible zones of tension using which it is possible to judge about the size of crushed zones or where the concrete in the shelf of a composite beam has split.

The calculation model used to calculate the durability of normal cross-sections of steel reinforced concrete bending elements is accepted based on analytical diagrams of strains of concrete and steel [1.2]. This approach allows for calculating the structural elements for durability from one position taking into account the non-linear properties of materials at different loads at any moment of time.

– The full-scale tests made it possible to record longitudinal strains of concrete and steel, transverse strains of the concrete of a reinforced concrete slab, strains of the shift at the contact point "steel and concrete" as well as the width of the crack opening and deflections in the structure

– The results of experimental studies allowed for constructing curves of longitudinal and transverse stresses of the steel reinforced concrete slab in the middle zone of the span of the built-up section.

– An analysis of the attained results revealed that due to the creep of concrete caused by long-acting loads in the beams combined with the slab and due to plastic deformations, the share of force endured by the slab goes down which accordingly leads to an additional load on the beam. This said, the greatest additional stress caused by the impact of concrete creep occurs in the top flange of the metal beam connected with the slab by means of anchors.

4. Conclusions

A comparison of the results of stresses according to numerical and full-scale experiments has been made as well as according to analytical formulas.

1) The results of experimental stresses with data obtained by the ANSYS software differ;

– up to 11 % on average for short-term loads.

– up to 19 % for long-term loads.

2) The results of the experiment differ with the analytical method of calculation:

– up to 14 % for long-term loads.

– up to 24 % for long-term loads.

3) The results of the experiment and those of numerical calculations for the shift in the contact plane of steel and concrete presents a good convergence of up to 7 %.

Summarizing the conclusions, it should be noted that numerical methods based on software complexes can be used to investigate the stress-strain state of steel slabs under the action of long loads in the initial period, however, the work material diagrams, changes in their strength properties, must be corrected with experimental data.

For further research, it is necessary to use analytical expressions that most fully reflect the actual work of steel-reinforced concrete structures and to shift them into program complexes in order to accelerate the calculation processes.

References

1. Pekin, D. Plitnaya stalezhelezobetonnaya konstruksia [Slab steel reinforced concrete structure]. Moscow, 2010. 440 p.
2. Zamaliyev, F. Uchet nelineinih svoistv materialov i podatlivosti sloev pri raschete prochnosti stalezhelezobetonnih perekritii [Accounting for the non-linear properties of materials and ductility of layers in calculating the durability of steel reinforced concrete floor slabs]. Industrial and civil construction. 2013. No. 5. Pp. 38–41.
3. Zamaliyev, F., Kayumov, R. K raschetu stalezhelezobetonnogo perekritiya kak ortotropnoy pliti [Calculating a steel reinforced concrete floor slab as an orthotropic bridge]. News of the Kazan State University of Architecture and Engineering. 2014. No. 1(27). Pp. 94–99.
4. Tusnin, A. Perekritiya mnogoetashnih zdaniy so stalnim karkasom [Floor slabs in multi-storied buildings with a steel frame]. Industrial and civil construction. 2015. No. 8. Pp. 10–14.
5. Ayrumyan, E., Kamensikov, N., Rumiyantseva, I. Osobennosti rascheta monolitnih plit stalezhelezobetonnih pokritii po profilirovannomu stalnomu nastilu [The peculiarities associated with calculations of monolithic slabs of steel reinforced concrete floor slabs by the steel sheet] // Industrial and civil construction. 2015. No. 9. Pp. 21–26.
6. Tusnin, A., Kolyago, A. Konstruksia i rabota stalezhelezobetonnogo perekritiya s ispolzovaniem sbornih pustotnih shelezobetonnih plit [Construction and function of steel reinforced concrete floor slabs using precast hollow-core concrete slabs]. Modern science and innovation. 2016. No. 3. Pp. 141–147.
7. Astakhov, I., Kuznetsov, A., Morozova, D. Issledovanie raboti stalezhelezobetonnih konstruksii [Studies of the

Литература

1. Пекин Д.А. Плитная сталежелезобетонная конструкция. М.: Издательство Ассоциация строительных вузов, 2010. 440 с.
2. Замалиев Ф.С. Учет нелинейных свойств материалов и податливости слоев при расчете прочности сталежелезобетонных перекрытий // Промышленное и гражданское строительство. 2013. № 5. С. 38–41.
3. Замалиев Ф.С., Каюмов Р.А. К расчету сталежелезобетонного перекрытия как ортотропной плиты // Известия КазГАСУ. 2014. № 1(27). С. 94–99.
4. Туснин А.Р. Перекрытия многоэтажных зданий со стальным каркасом // Промышленное и гражданское строительство. 2015. № 8. С. 10–14.
5. Айрумян Э.Л., Каменщиков Н.И., Румянцева И.А. особенности расчета монолитных плит сталежелезобетонных покрытий по профилированному стальному настилу // Промышленное и гражданское строительство. 2015. № 9. С. 21–26.
6. Туснин А.Р., Коляго А.А. Конструкция и работа сталежелезобетонного перекрытия с использованием сборных пустотных железобетонных плит // Современная наука и инновации. 2016. № 3. С. 141–147.
7. Астахов И.В., Кузнецов А. Ю., Морозова Д. В. Исследование работы сталежелезобетонных конструкций // Вестник гражданских инженеров. 2017. № 3(62)
8. Замалиев Ф.С. Выявление доэксплуатационных напряжений и деформаций стальных балок-ребер сталежелезобетонные перекрытия // Вестник МГСУ. 2013. № 7. С. 33–39
9. Замалиев Ф.С., Биккинин Э.Г. Экспериментальные исследования начального напряженно-деформированного состояния сталежелезобетонных

Zamaliev, F.S., Zakirov, M.A. Stress-strain state of a steel-reinforced concrete slab under long-term. *Magazine of Civil Engineering*. 2018. 83(7). Pp. 12–23. doi: 10.18720/MCE.83.2.

function of steel reinforced concrete structures]. The herald of civil engineers. 2017. No. 3(62).

8. Zamaliyev, F. Viyavlenie doekspluatasionnih napryashenii i deformasii stalnih stalnih balok-reber stalezhelezobetonnie perekritiya [Identifying the preoperational stresses and strains in steel beam ribs of steel reinforced concrete floor slabs]. The herald of the Moscow State University of Civil Engineering. 2013. No. 7. Pp. 33–39.
9. Zamaliyev, F., Bikkinin, E. Experimentalnih issledovaniya nachalnogo napyashenno-deformirovannogo sostoyania stalezhelezobetonnih balok i plit [Experimental studies of the initial stressed-deformed state of composite steel beams and slabs]. News of the Kazan State University of Architecture and Engineering. 2014. No. 2(32). Pp. 139–143.
10. Zamaliyev, F., Filippov, V. Raschetno-experimentalnie issledovaniya stalezhelezobetonnih konstruksii [Calculation and experimental studies of composite structures]. Industrial and civil construction. 2015. No. 7. Pp. 29–36.
11. Zamaliyev, F., Mirsayapov, I. Raschet prochnosti stalezhelezobetonnih izgibaemih konstruksii na osnove analiticheskih diagramm [A strength calculation of steel reinforced concrete flexible structures based upon analytical programs]. Development and studies of metal and wooden structures: a collection of scientific works. 1999. Pp. 142–149.
12. BSI (2010) BS 5950-3.1. A1. Structural use of steelwork in buildings. Design in composite construction. Code of practice for design of simple and continuous composite beams. BSI, London.
13. Roger, P. Jonson Designers' guide to Eurocode 4: design of composite steel and concrete structures EN 1994-1-1. 2011. 412 p.
14. Vasdravellis, G., Uy, B., Tan, E.L., Kirkland, B. Behaviour and design of composite beams subjected to sagging bending and axial compression Original Research. Journal of Constructional Steel Research. 2015. No. 110. Pp. 29–39.
15. Hadzalic, E., Barucija, K. Concrete shrinkage effects in composite beam. Construction of Unique Buildings and Structures. 2014. No. 11(26). Pp. 85–93.
16. Champenoy, D., Corfdir, A., Corfdir, P. Calculating the critical buckling force in compressed bottom flanges of steel-concrete composite bridges. European Journal of Environmental and Civil Engineering. 2014. 18(3). Pp. 271–292.
17. Gholamhoseini, A., Khanlou, A., MacRae, G., Scott, A., Hicks, S., Leon, R. An experimental study on strength and serviceability of reinforced and steel fibre reinforced concrete (SFRC) continuous composite slabs. Engineering Structures. 2016. 114(1). Pp. 171–180.
18. Ye, J.H., Chen, W. Elastic restrained distortional bucking of steel-concrete method. International Journal of Structural Stability and Dynamics. 2013. 13(1). Pp.1–29.
19. Beck, A.T., DaRosa, E. Structural Reliability Analysis Using Deterministic Finite Element Programs. Latin American Journal of Solids and Structures. 2006. No. 3. Pp. 197–222.
20. Padmarajaiah, S.K., Ramaswamy, A.A. Finite element assessment of flexural strength of prestressed concrete beams with fiber reinforcement. Cement and Concrete Composites. 2002. No. 24. Pp. 229–241.
21. Kim, S., Lee, U. Effects of delamination on guided waves in a symmetric laminated composite beam. Mathematical Problems in Engineering. 2014. No. 14. Pp. 12.
22. Karpov, V.V., Ignat'ev, O.V., Semenov, A.A. The stress-strain state of ribbed shell structures. Magazine of Civil

балок и плит // Известия КазГАСУ. 2015. № 2(32). С. 139–143.

10. Замалиев Ф.С., Филлипов В.В. Расчетно-экспериментальные исследования сталежелезобетонных конструкций // Промышленное и гражданское строительство. 2015. № 7. С. 29–36.
11. Замалиев Ф.С., Мирсаяпов И.Т. Расчет прочности сталежелезобетонных изгибаемых конструкций на основе аналитических диаграмм // Разработка и исследование металлических и деревянных конструкций: сборник научных трудов. 1999. С. 142–149.
12. BSI (2010) BS 5950-3.1. A1. Structural use of steelwork in buildings. Design in composite construction. Code of practice for design of simple and continuous composite beams. BSI, London.
13. Roger P. Jonson Designers' guide to eurocode 4: design of composite steel and concrete structures EN 1994-1-1. 2011. pp. 412.
14. Vasdravellis G., Uy B., Tan E.L., Kirkland B. Behaviour and design of composite beams subjected to sagging bending and axial compression Original Research // Journal of Constructional Steel Research. 2015. № 110. Pp. 29–39.
15. Hadzalic E., Barucija K. Concrete shrinkage effects in composite beam// Construction of unique buildings and structures. 2014. № 11(26). Pp. 85–93.
16. Champenoy D., Corfdir A., Corfdir P. Calculating the critical buckling force in compressed bottom flanges of steel-concrete composite bridges // European Journal of Environmental and Civil Engineering. 2014. № 3(18). Pp. 271–292.
17. Gholamhoseini A., Khanlou A., MacRae G., Scott A., Hicks S., Leon R. An experimental study on strength and serviceability of reinforced and steel fibre reinforced concrete (SFRC) continuous composite slabs // Engineering Structures. 2016. № 1(114). Pp. 171–180.
18. Ye J.H., Chen W. Elastic restrained distortional bucking of steel-concrete method // International Journal of Structural Stability and Dynamics. 2013. № 1(13). Pp. 1–29.
19. Beck A.T., DaRosa E. Structural Reliability Analysis Using Deterministic Finite Element Programs // Latin American Journal of Solids and Structures. 2006. № 3. Pp. 197–222.
20. Padmarajaiah S.K., Ramaswamy A.A. Finite element assessment of flexural strength of prestressed concrete beams with fiber reinforcement // Cement and Concrete Composites. 2002. № 24. Pp. 229–241.
21. Kim S., Lee U. Effects of delamination on guided waves in a symmetric laminated composite beam // Mathematical Problems in Engineering. 2014. № 14. Pp. 12.
22. Карпов В.В., Игнатьев О.В., Семенов А.А. Напряженно-деформированное состояние ребристых оболочечных конструкций // Инженерно-строительный журнал. 2017. № 6(74). С. 147–160.
23. Назмеева Т.В., Ватин Н.И. Численные исследования сжатых элементов из холодногнутого просечного С-профиля с учетом начальных несовершенств // Инженерно-строительный журнал. 2016. № 2(62). С. 92–101.
24. Черняев А.А. Вариантное проектирование стальных балочных клеток геометрическими методами// Инженерно-строительный журнал. 2018. № 2(78). С. 3–15.

Замалиев Ф.С., Закиров М.А. Напряженно-деформированное состояние сталежелезобетонной плиты при длительных нагружениях // Инженерно-строительный журнал. 2018. № 7(83). С. 12–23.

Engineering. 2017. 74(6). Pp. 147–160. doi: 10.18720/MCE.74.12

23. Nazmeeva, T.V., Vatin, N.I. Numerical Investigations of Notched C-Profile Compressed Members with Initial Imperfections. Magazine of Civil Engineering. 2016. 62(2). Pp. 92–101. doi: 10.5862/MCE.62.9
24. Chernyaev A.A. Alternative engineering of steel girder cages by geometrical methods. Magazine of Civil Engineering. 2018. 78(2). Pp. 3–15. doi: 10.18720/MCE.78.1.

Farit Zamaliev,*
+7(987)296-09-49; zamaliev49@mail.ru

Marat Zakirov,
+7(917)294-59-23; z_marat_a@mail.ru

Фарит Сахапович Замалиев,*
+7(987)296-09-49;
эл. почта: zamaliev49@mail.ru

Марат Азатович Закиров,
+7(917)294-59-23;
эл. почта: z_marat_a@mail.ru

Zamaliev, F.S., Zakirov, M.A. Stress-strain state of a steel-reinforced concrete slab under long-term. *Magazine of Civil Engineering*. 2018. 83(7). Pp. 12–23. doi: 10.18720/MCE.83.2.

doi: 10.18720/MCE.83.3

Reliability estimation of industrial building structures

Оценка надежности конструкций промышленных зданий

S.F. Pichugin,
Poltava National Technical Yuri Kondratiuk University, Poltava, Ukraine

Д-р техн. наук, заведующий кафедрой С.Ф. Пичугин,
Полтавский национальный технический университет имени Юрия Кондратюка, г. Полтава, Украина

Key words: construction; building; structure; reliability; failure; probabilistic method; load; redundant system

Ключевые слова: сооружение; здание; конструкция; надежность; отказ; вероятностный метод; нагрузка; статически неопределимая система

Abstract. The article is devoted to solving the problem of the reliability of industrial building structures: crane and roof beams, columns, redundant building systems. For this aim, the probabilistic method of structural reliability estimation is developed after the criterion of bearing strength, in which the main component of structure reliability is faultlessness. The method takes account of the random loads and material strength, loads joint action, the specific character of work and failure elements, nodes and the whole structure as well. For the ground of method, the large amount of statistic results on crane load is examined for the bridge cranes of the different types. A large amount of wind and snow meteorological data is collected for the territory of Ukraine. Stationary probabilistic model of crane load and quasi-stationary model of the snow and mean wind load are substantiated. The most widely spread probabilistic presentations of random loads are observed. They are as follows: stationary random process and its absolute maxima, random sequence of independent and correlated loads, discrete presentation and extreme model. It was deduced that the redundant structure reliability estimation is a very complicated problem as depends upon the system complexity. The method of states, a probabilistic method of ultimate equilibrium and logic and probabilistic method are developed for solving this problem. On the base of the determined method, the numerical reliability computations of a wide range of industrial building structures are realized. It is shown that the structures have quite different levels of reliability. In particular, the light roof structures are not reliable enough being under the great influence of snow load. At the same time, the Design Code allows over-estimation of reliability for industrial columns. The estimation of industrial redundant structures with a different degree of redundancy is obtained on the base of developed approach. It gave the possibility to evaluate the high safety level of redundant structures in comparison with separate members and statically determined structures. With regard to mentioned results, it is recommended to correct some load factors, a combination factor and a factor for model uncertainties of the Design Codes of structures and loads.

Аннотация. В статье рассмотрены вопросы оценки надежности конструкций промышленных зданий: подкрановых и стропильных балок, колонн, статически неопределимых конструктивных систем. Для этого разработан вероятностный метод оценки надежности конструкций по критерию несущей способности, основой которого является безотказность конструкции. Метод учитывает случайные нагрузки и прочность материалов, совместное действие нагрузок, специфический характер работы и отказов элементов, узлов и сооружений в целом. Для обоснования метода был сформирован обширный объем статистических данных по нагрузкам мостовых кранов различных типов. Большое количество метеорологических данных по ветру и снегу было собрано для территории Украины. Обоснованы стационарная вероятностная модель для крановой нагрузки и квазистационарная модель для снеговой и ветровой нагрузок. Рассмотрены наиболее распространенные вероятностные представления случайных нагрузок: стационарный случайный процесс и его абсолютные максимумы, случайная последовательность независимых и коррелированных нагрузок, дискретное представление и экстремальная модель. Было подтверждено, что оценка надежности статически неопределимых систем – достаточно сложная проблема, поскольку она зависит от сложности таких систем. Для решения данной проблемы разработаны метод состояний, вероятностный метод предельного равновесия, логико-вероятностный метод. На основе разработанного метода выполнены численные расчеты надежности широкого круга строительных конструкций. Показано, что различные конструкции

Пичугин С.Ф. Оценка надежности конструкций промышленных зданий // Инженерно-строительный журнал. 2018. № 7(83). С. 24–37.

имеют разный уровень надежности. В частности, недостаточно надежными могут быть легкие стропильные конструкции при действии значительных снеговых нагрузок. В то же время нормы проектирования закладывают в колонны промышленных зданий излишний запас надежности. На основе разработанного подхода выполнены расчеты надежности статически неопределимых систем разной степени сложности, которые дали возможность оценить повышенный уровень надежности таких систем по сравнению с отдельными элементами и статически неопределимыми системами. В результате были обоснованы коэффициенты норм проектирования, такие как коэффициенты надежности по нагрузке, коэффициент сочетания нагрузок, коэффициент условий работы.

1. Introduction

The building structure reliability is the problem of a high priority today. It can be treated as a scientific trend, which does not need both material and financial expenses.

The eminent scientists created the classic works in building reliability [1–3], numerous foreign and native scientists were involved in the study of this problem [4–12]. The general probabilistic models of wind, snow and crane loads can be considered as a statistic basis of reliability estimation of industrial building structures. Loads of bridge cranes were considered in [13], the description of the wind load was summarized in [14]. Active researches of the wind load proceed the last years [15–17]. The analysis of snow load was resulted in [18], the influence of global temperature rise on the snow load is analyzed in work [19]. In different countries, systematic researches of climatic influences are conducted with the purpose of Codes correcting [20]. The perspective model is a correlated casual sequence of loads (based on the method of the generalized covariance, developed by A.P. Kudzis [21]). The linearizing of the functions of random parameters worked out in work [22]. However, these approaches lack both systematic analysis and model comparison, which can cause different results in structure reliability design.

The probabilistic computation of structures has not been developed with regard to joint loads application, their real distributions, and frequency characteristics. At the same time, active studies of probabilistic models for concrete elements proceed the last years [23], in particular, the initial reliability of reinforce-concrete elements was defined [24]. However, the estimation of reliability is yet absent for many buildings and structures. The problem of reliability continues to be probed [25–30] and expects further investigations and solutions. The exploitation experience demonstrated the existence of quite different reliability of various structures. The reliability of existing structures has to be examined together with the reliability of elements (sections) as well as nodes [31–33]. The assessment of a redundant structure safety is rather a difficult task. In spite of many studies that have been done the problem of reliability analysis of these structures has not been solved yet.

As follows from the preceding, the evolution of reliability computation theory and design Codes of building structures are still of interest because of the complexity of a problem on the one hand and on the other of the ignoring the random loads.

The article is devoted to solving the problem related to the assessment of the reliability of industrial building structures: crane and roof beams, columns, redundant building systems. This task deals with the developing of the general method of reliability estimation of industrial building structures after the criterion of bearing strength, in which the main component of structure reliability is faultlessness. At such interpretation the estimation of structure reliability includes the decision of the following questions: probabilistic description of loads; mechanical descriptions of materials, joints and other random parameters; reliability estimation of elements of building structures; calculation of reliability of the structural systems taking into account the possible character of their failure; quantitative estimation of reliability of buildings and structures of the different setting.

2. Methods

It was put and decided the complicated and difficult task of formation of the generalized probabilistic models of crane and atmospheric loads. The decision was based on sufficient statistical material, took into account the specific features of the different loads, type of their distributions and frequency structure.

The stochastic model of the crane loads was built as a result of experimentally statistical researches. The vertical and horizontal loads were investigated for bridge cranes with rigid and flexible hanged cargo of different carrying capacity and regimes which were exploited in the conditions of metallurgical and machine-building shops from 10 to 30 years of service. The generalized numerical and frequency descriptions of the crane loads were grounded and the possibility of application for them of normal low was substantiated (Figure 1, d). The special attention in model experiments was spared lateral forces of bridge cranes.

The systematic information about the wind velocity measurements done with ten minutes average at 70 Ukrainian meteorological stations were used as an initial data. The mean value of wind load is of quasi-stationary origin with the constant frequent parameters and normalized distribution. For the description of ordinate density of wind mean value Veibull's law was used, for wind dynamic value the normal distribution was based. Having integrated some initial data all necessary mean parameters of probabilistic wind models were determined for territory of Ukraine.

The results of regular snow measurements for 15–40 years at 62 Ukrainian meteorological stations have been taken as the reference statistic material for the snow probabilistic model. It is substantiated that the ground snow load is of a quasi-stationary origin. Its mathematical expectation and standard have a seasonal trend. At the same time snow frequent characteristics and normalised ordinate distribution remain constant during the season. For its description it was first applied polinomo-exponential distributing (Figure 1, b). In future in PoltNTU there were executed the researches of deposits of snow on coverages with the overfalls of heights, the estimation of influence of roofs heating descriptions on the value of the snow load, the calculation of the snow load on the cold roofs of buildings with the positive internal temperatures of air.

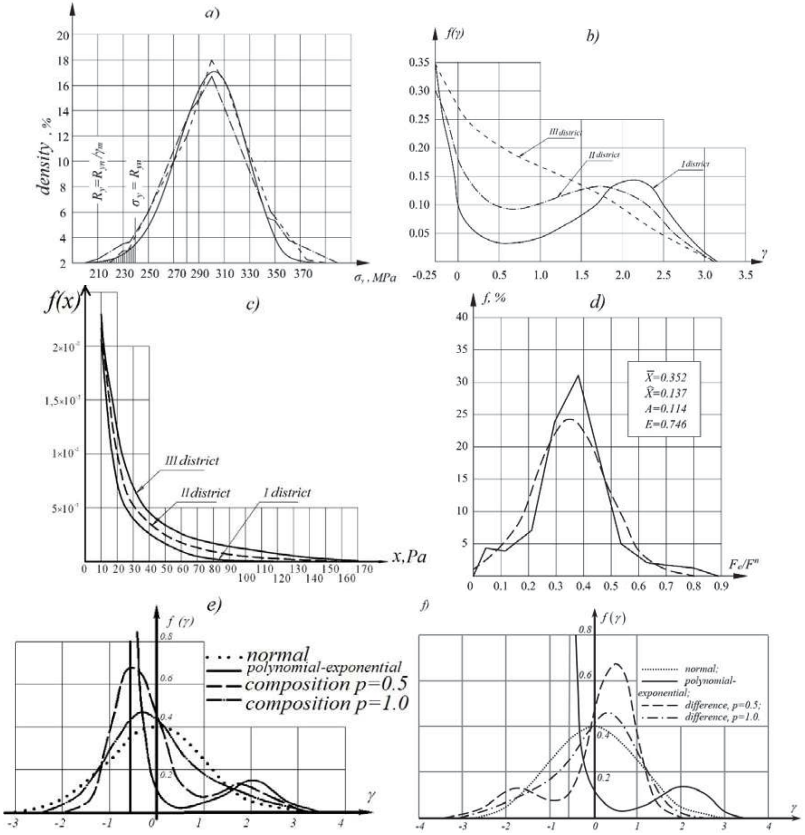

Пичугин С.Ф. Оценка надежности конструкций промышленных зданий // Инженерно-строительный журнал. 2018. № 7(83). С. 24–37.

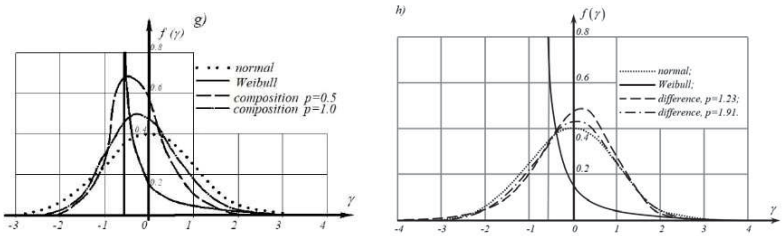

Figure 1. Distributions of random arguments:
a – durability of steel; b – snow load; c – wind load; d – crane load; e – composition of polinomo-exponential and normal distributions; f – difference of polinomo-exponential and normal distributions; g – composition of Veibull's and normal distributions;
h – difference of Veibull's and normal distributions

The systematic analysis of random loads was realized for the six most commonly used probabilistic models. The main one is presented in the form of a stationary (crane load) or quasi-stationary (wind and snow loads) random processes (Figure 2, a, pos.1); their parameters are an effective frequency ω and the coefficient of trend K_{tr} which accounts the atmospheric load season change.

The absolute maxima of random process are one of simpler model; they are determined by the tail part of the distribution of outliers and are higher then characteristical maximum level γ_0. The letter is a solution of the following equation $N_+(\gamma_0; 0 \le \tau \le t) = 1$, where $N_+(\cdot)$ – the number of outliers of random process.

The model in the form of a random sequence of independent random loads with the intensity λ is widely spread (λ – the number of loads in per-unit time t_λ). For discrete presentation of loads (Figure 2,a, pos. 2) the frequent parameter of which is the mean duration of overloading $\overline{\Delta}$ connected with the intensity by the ratio $\overline{\Delta} = t_\lambda / \lambda$.

The analysis of the problem has demonstrated that the load values sampling can be classified as the exponential type. That's why their maximum values can be presented correctly by the extreme double exponential Gumbel distributions of a normalized type:

$$y = \alpha_n(\gamma - u_n), \tag{1}$$

where u_n – characteristic extremum; α_n – extreme intensity; $y = -\ln[-\ln F(t)]$ – Gumbel distribution argument.

The normalised load level was taken into account $\gamma = (x - \overline{x})/x$, where *x* – the load ordinate, $\overline{x}$ – mathematical expectation, $\hat{x}$ – standard deviation.

The choice of models of loads depends on a specific of solving probabilistic problems: the more complicated ones are solved in the manner of random processes which, however, are difficult for description and take much more computation time. More accessible and simple models, mentioned earlier, are based on the random values and corresponding frequent characteristics and provide not less exact solution if they are proper grounded. In particular, all the examined models are close to its sense of the following evaluation:

$$Q(t) = \frac{\omega f(\gamma) t}{\sqrt{2\pi}} = \frac{f(\gamma)}{f(\gamma_0)} = \lambda t[1 - F(\gamma)] = \frac{t[1 - F(\gamma)]}{\overline{\Delta}} = [r(1-\rho) + \rho][1 - F(\gamma)], \tag{2}$$

where $Q(t)$ – probability of exceeding γ – level during t; $F(t)$ and $f(\gamma)$ – accordingly integral and differential functions of load distribution; r – amount of calculation cuts of casual sequence of loads; ρ – generalized coefficient of correlation of sequence.

Load probabilistic comparison can be well performed at the extreme scale which is illustrated in Figure 2, b. On the axis of ordinate of a scale the standardized load is laid off, on the axis of abscissa the

Gumbel's distribution argument y is laid of which is connected with the load return period T. Gumbel's distribution (1) is described on the scale in the form of straight lines. The models of a random process, a random sequence of independent loads and discrete presentation are introduced as different curves. The main advantage of this scale is its visual effect of the tail parts of the load distributions which have rather small distinctions in the usual form of presentation. It enables to present the visual comparison and correspondence of parameters of different load models.

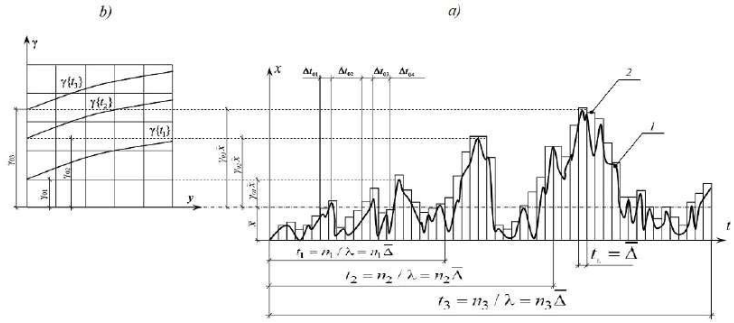

Figure 2. Presentation of random load:
a – realization of random process: 1 – model of continuous process; 2 – discrete model;
b – general form of load presentation

A model of random processes, without regard to its relative complication, is for today most studied, the model of absolute maximums of random processes also enabled to get interesting scientific results. It should be noted that other perspective models, the especially random sequences of independent and correlated overloads, and also discrete presentation of loads, are less studied and recommended for the use in subsequent researches of loads.

The worked out random parameters give possibility to develop the reliability estimation of building structures.

3. Results and Discussion

3.1. Reliability estimation of building structures in the technique of random values

The failure of an element takes place when a stochastic stress under the joint applied loads $S(t)$ (t-time) exceeds the resistance of an element $R(t)$. The failure of the element is defined by the equation

$$\widetilde{Y}(t) = \widetilde{R}(t) - \widetilde{S}(t) < 0, \tag{3}$$

where $Y(t)$ – margin function of load carrying capacity.

The probabilistic technique of random values without the account of time factor is applied in this section. The technique is grounded at the action of loads with little change in time (dead and some technological loads) or those which have non-permanent character. Then the margin function will be written down as

$$\widetilde{Y} = \widetilde{R} - \widetilde{S} < 0. \tag{4}$$

Mathematical expectation and standard mean deviation of margin function are determined as for a linear function:

$$\overline{Y} = \overline{R} - \overline{S}\ ;\ \hat{Y} = \sqrt{\hat{R}^2 + \hat{S}^2}\ . \tag{5}$$

The safety characteristic is of great importance and is derived from equation

$$\beta = \overline{Y} / \hat{Y} = (\overline{R} - \overline{S}) / (\hat{R}^2 + \hat{S}^2)^{1/2}, \tag{6}$$

where $\overline{Y},\overline{R},\overline{S}$ – the corresponding mathematical expectations, $\hat{Y},\hat{R},\hat{S}$ – the corresponding standard mean deviations.

This characteristic determines probability of structural failure

$$Q(Y \le 0) = F_Y(0) = F_Y\left(\overline{Y} - \beta\hat{Y}\right), \tag{7}$$

where $F_Y(.)$ – an integral function of margin function distributing.

In the case of normal distribution $f(Y)$ the safety characteristic is very convenient:

$$Q(Y < 0) = 0.5 - \Phi(\beta),\ P(Y \ge 0) = 0.5 + \Phi(\beta). \tag{8}$$

Here $\Phi(\beta)$ – the well-known function of Laplace contained in widespread statistical tables.

The element resistance and margin function of the load carrying capacity (3) are generalized by the function of a few arguments:

$$Y = f(X_1, X_2, ..., X_n).$$

In general case this function can be nonlinear, and for simplification of calculations, its linearizing is often executed with replacement of initial expression the linear function:

$$Y = f(\overline{X}_1, \overline{X}_2, ..., \overline{X}_n) + \sum_{i=1}^{n} \frac{\partial Y}{\partial X_i}(\overline{X}_1, \overline{X}_2, .., \overline{X}_n)(X_i - \overline{X}_i) = \overline{Y} + \sum_{i=1}^{n} D_i(X_i - \overline{X}_i), \tag{9}$$

In the calculations of reliability the linearizing is executed near the mathematical expectation of function, here the angular coefficient of entered line is determined by the partial differentiation of initial function on the proper argument. Error in determination of $\overline{Y}$ as a result of linearizing for (8) it is possible to estimate the following expression:

$$\Delta\overline{Y} = \frac{1}{2}\sum_{i=1}^{n} \frac{\partial^2 Y}{\partial X_i^2}(\overline{X}_1, \overline{X}_2, ...\overline{X}_n)\hat{X}_i.$$

Here $\hat{X}_i$ – dispersion of *i* - argument.

At insignificance of this error a formula for determination of mathematical expectation (9) is simplified and taken to the substitution of mathematical expectations of arguments in an initial function:

$$\overline{Y}(X_1, X_2, ..., X_n) = f(\overline{X}_i, \overline{X}_2, ..., \overline{X}_n). \tag{10}$$

Standard deviation of the margin function is determined, in the case of independence of arguments, from equation:

$$\hat{Y} = \sqrt{\hat{Y}} = \sqrt{\sum_{i=1}^{n}\left[\frac{\partial Y}{\partial X_i}(\overline{X}_1, \overline{X}_2, ..., \overline{X}_n)\right]^2 \hat{X}_i^2} = \sqrt{\sum_{i=1}^{n} D_i^2 \hat{X}_i^2}. \tag{11}$$

Error of this expression as a result of linearizing is estimated as follows

$$\Delta\hat{Y} = \Delta\left(\hat{Y}^2\right) = \frac{1}{2}\sum_{i=1}^{n}\left[\frac{\partial^2 Y}{\partial X_i^2}(\overline{X}_1, \overline{X}_2, ..., \overline{X}_n)\right]^2 \hat{X}_i^2 + \sum_{i>j}\left[\frac{\partial^2 Y}{\partial X_i \partial X_j}(\overline{X}_1, \overline{X}_2, ..., \overline{X}_n)\right]^2 \hat{X}_i \hat{X}_j. \tag{12}$$

3.2. Practical reliability estimation of structure elements

In quality an example we will consider the reliability calculation of reinforced concrete beams with carbon-plastic external strengthening. For the receipt of reliability estimations we will use the worked out reception with the substitution of probabilistic parameters in the deterministic decisions of durability of reinforced concrete beams. Taken into account thus, that most random arguments of the margin function of load carrying capacity of reinforced concrete beams can be reasonably described by a normal law, in particular, durability of concrete, armature, carbon-plastic, and also row of loads (dead, technological, crane etc.).

Random value of maximum bend moment which is perceived by a beam with a double armature:

$$\tilde{M}_{ult} = f\left(\tilde{\sigma}_b, \tilde{\sigma}_s, \tilde{\sigma}_{sc}\right) = \tilde{\sigma}_s A_s \left(h_0 - 0.5\tilde{x}\right) + \tilde{\sigma}_{sc} A'_s \left(0.5\tilde{x} - a'\right), \quad (13)$$

where: $\tilde{\sigma}_b$ – random value of concrete resistance to the compression for the limit states of the first group; $\tilde{\sigma}_s$ – random value of the armature durability to tension; A_s – section area of the stretched armature; $\tilde{\sigma}_{sc}$ –random value of concrete resistance to tension; A'_s – section area of the compressed armature; a' – distance from resultant effort in the compressed armature to the compressed verge of element; h_0 – calculation height of section; x – height of the compressed zone of concrete, equal

$$\tilde{x} = \left(\tilde{\sigma}_s A_s - \tilde{\sigma}_{sc} A'_s\right) / \tilde{\sigma}_b b,$$

where: b – width of section.

We put expression for x in a formula (13):

$$\tilde{M}_{ult} = \tilde{\sigma}_s A_s h_0 - \tilde{\sigma}_{sc} A'_s a' - \frac{0.5}{\tilde{\sigma}_b b}\left(\tilde{\sigma}_s A_s - \tilde{\sigma}_{sc} A'_s\right)^2. \quad (14)$$

We have the mathematical expectation of limit moment putting the expected values of casual arguments in this common expression.

We will define coefficients for the calculation of standard of limit moment:

$$D_{sc} = \frac{\partial M_{ult}}{\partial \sigma_{sc}} = \frac{A'_s}{\sigma_b b}\left[-\sigma_b b a' + \left(\sigma_s A_s - \sigma_{sc} A'_s\right)\right]; \quad (15)$$

$$D_s = \frac{\partial M_{ult}}{\partial \sigma_s} = \frac{A_s}{\sigma_b b}\left[\sigma_b h_0 b - \left(\sigma_s A_s - \sigma_{sc} A'_{sc}\right)\right]; \quad (16)$$

$$D_b = \frac{\partial M_{ult}}{\partial \sigma_b} = \frac{0.5}{\sigma_b^2 b}\left(\sigma_s A_s - \sigma_{sc} A'_s\right)^2. \quad (17)$$

The numerical values of coefficients we get, putting the expected values of random arguments in these expressions.

The standard of limit bend moment is determined as

$$\hat{M}_{ult} = \sqrt{\left(D_b \hat{\sigma}_b\right)^2 + \left(D_s \hat{\sigma}_s\right)^2 + \left(D_{sc} \hat{\sigma}_{sc}\right)^2}. \quad (18)$$

For the reliability estimation of beams we determine a safety characteristic, having in this case next kind:

$$\beta = \left(\overline{M}_{ult} - M_{cal}\right) / \hat{M}_{ult}, \quad (19)$$

where: M_{cal} – calculation value of external bend moment in a beam.

Farther we will consider a beam strengthened by carbon-plastic (FAP). Random value of the limit bend moment, perceived by an increased beam:

$$\tilde{M}_{ult} = f\left(\tilde{\sigma}_b, \tilde{\sigma}_s, \tilde{\sigma}_{sc}, \tilde{\sigma}_{fu}\right) = \tilde{\sigma}_{fu} A_f \left(h - 0.5\tilde{x}\right) + \tilde{\sigma}_s A_s \left(h_0 - 0.5\tilde{x}\right) + \sigma_{sc} A'_s \left(0.5\tilde{x} - a'\right), \quad (20)$$

where: $\tilde{\sigma}_{fu}$ – random value of durability on tension of FAP; A_f – area of section of carbon-plastic armature; h – height of section; x – height of the compressed zone of concrete, equal

$$\tilde{x} = \left(\tilde{\sigma}_{fu} A_f + \tilde{\sigma}_s A_s - \tilde{\sigma}_{sc} A'_s\right) / \tilde{\sigma}_b b.$$

We put expression for x in a formula (20):

$$\tilde{M}_{ult} = \tilde{\sigma}_{fu} A_f h + \tilde{\sigma}_s A_s h_0 - \tilde{\sigma}_{sc} A'_s a' - \frac{0.5}{\tilde{\sigma}_b b}\left(\tilde{\sigma}_{fu} A_f + \tilde{\sigma}_s A_s - \tilde{\sigma}_{sc} A'_s\right)^2. \quad (21)$$

Mathematical expectation of limit moment we get, putting the expected values of random arguments in this expression.

We will define coefficients for the calculation of standard of limit moment:

$$D_{fu} = \frac{\partial M_{ult}}{\partial \sigma_{fu}} = \frac{A_f}{\sigma_b b}\left[\sigma_b hb - \left(\sigma_{fu} A_f + \sigma_s A_s - \tilde{\sigma}_{sc} A'_{sc}\right)\right]; \quad (22)$$

$$D_{sc} = \frac{\partial M_{ult}}{\partial \sigma_{sc}} = \frac{A'_s}{\sigma_b b}\left[-\sigma_b ba' + \left(\sigma_{fu} A_f + \sigma_s A_s - \sigma_{sc} A'_s\right)\right]; \quad (23)$$

$$D_s = \frac{\partial M_{ult}}{\partial \sigma_s} = \frac{A_s}{\sigma_b b}\left[\sigma_b h_0 b - \left(\sigma_{fu} A_f + \sigma_s A_s - \sigma_{sc} A'_{sc}\right)\right]; \quad (24)$$

$$D_b = \frac{\partial M_{ult}}{\partial \sigma_b} = \frac{0.5}{\sigma_b^2 b}\left[\left(\sigma_{fu} A_f + \sigma_s A_s - \sigma_{sc} A'_s\right)\right]^2. \quad (25)$$

The numerical values of coefficients we get, putting the expected values of random arguments in these expressions.

The standard of limit bend moment is determined as

$$\hat{M}_{ult} = \sqrt{\left(D_{fu}\hat{\sigma}_{fu}\right)^2 + \left(D_b\hat{\sigma}_b\right)^2 + \left(D_s\hat{\sigma}_s\right)^2 + \left(D_{sc}\hat{\sigma}_{sc}\right)^2}. \quad (26)$$

For the reliability estimation of beams, we determine a safety characteristic utilizing formulae (8), (19) and the function of Laplace.

Application of the got results is illustrated on a numerical example with a reinforce-concrete beam. A beam has section sizes b = 300 mm, h = 700 mm, external calculation bend moment is M_{cal} = 500 kNm. After the above-mentioned formulae, numerical descriptions of maximum moment of beam are $\bar{M}_{ult}$ = 762.7 kNm, $\hat{M}_{ult}$ = 29.92 kNm. The safety characteristic in relation to the calculation value of external bend moment in a beam makes β = (762.7 – 500) / 29.92 = 8.78, that answers the low probability of beam failure $Q(\beta) = 4.0 \cdot 10^{-19}$. Farther on the terms of example, a beam is loaded with the increase of calculation moment to M'_{cal} = 750 kNm. The safety characteristic here is diminished substantially β = (762.7 – 750) / 29.92 = 0.42, the probability of failure $Q(\beta)$ = 0.337 becomes too high, that testifies to the accident rate of beam and necessity of its strengthening.

The strengthening of the beam is one layer of carbon-plastic fibre with width 250 mm, thickness 1.4 mm, area section of strengthening A_f = 350 mm² =3.5 cm². Calculated durability of carbon-plastic fibre is R_{fu} = 1071 MPa. Numerical descriptions of maximum moment of beam are increased – $\bar{M}_{ult}$ = 991.0 kNm, $\hat{M}_{ult}$ = 35.5 kNm. The safety characteristic in relation to the calculation value of heightened external bend moment in a beam makes β = (991.0 – 750) / 35 / 5 = 6 / 79, the probability of failure of the increased beam $Q(\beta) = 1.3 \cdot 10^{-11}$ is substantially below than failure probability of beam without strengthening. The got estimation of failure probability testifies to sufficient reliability of beam and efficiency of its strengthening of carbon-plastic fibre.

The analysis of results of reliability calculation of the increased beam confirmed the validity of application for this purpose the described higher linearized probabilistic model, as an insignificant error is here assumed: - 0.12 % for the mathematical expectation of maximum moment and 0.43 % for its standard.

For elements which perceive a multicomponent dead load a stochastic model as a sum of random values allows to enter the reducing coefficient of combination ψ = 0.90…0.95. It allowed also estimating the reliability of linear part of main pipeline and faultlessness of bearings and non-load-bearing structures from steel of the thin-walled types.

The compositions of sums and differences of loads and strength should be done for several loads and for design of margin of carrying capacity (4). Convolution formulae are used for this purpose.

$$Y = X_1 + X_2, \quad f(Y) = \int_0^Y f_1(X_1) f_2(Y - X_1) dX_1;$$

$$Y = X_1 - X_2, \quad f(Y) = \int_{-\infty}^{\infty} f_1(X_1) f_2(X_1 - Y) dX_1 . \tag{27}$$

They cannot be determined in a closed form for the mentioned distributions and therefore numerical integration is adopted. The convolutions are transformed (presented in an unified comparable form) for the design simplification and their parameters are combined. From 13 received analytical expressions of convolutions, only the formula for difference of normal and arbitrary $f_2(z)$ density distributions is suggested

$$f(\gamma) = \frac{D}{\sqrt{2\pi}} \int_{z_1}^{z_2} \exp\left(-0.5E^2\right) f_2(z)\, dz , \tag{28}$$

where: $\gamma = \left(Y - \overline{Y}\right)/\hat{Y}$ – standardised variable; $E = D \cdot \gamma + z/p$; $D = \sqrt{1+p^2}$; $p = \hat{x}_n / \hat{x}_a$; $v_n = \hat{x}_n / \overline{x}_n$; $\overline{x}_n$; $\hat{x}_n$ – parameters of the normal distribution, $\hat{x}_a$ – standard deviation of arbitrary distribution, $z_1 = \gamma\sqrt{1+p^2} - p/v_n$ – lower limit of integration, z_2 – upper limit of integration which is determined with the account of necessary calculation accuracy.

The examples of joint distributions based on the proposed formulae are presented on the Figure 1, d–g. They can be non-symmetrical and differ considerably from the normal distribution in solutions of structural reliability problems. Without the account of this factor the estimation of structure reliability can have noticeable inaccuracy.

3.3. Reliability estimation of structure elements with the account of time factor

The loads are presented in the form of stationary and quasistationary random processes. Hence the $\tilde{Y}(t)$-function is a random process as well. Therefore the element failure is a projection of random process of the load carrying capacity margin (3) into the negative region. In this case the probability of failure Q(t) is estimated as follows

$$Q(t) = \omega_q f_Y(\beta) t \Big/ \left(\beta_\omega \sqrt{2\pi}\right), \tag{29}$$

where: ω_q and $f_Y(\beta)$ – the effective frequency and density of the distribution of the random process $\tilde{Y}(t)$ ordinate; β_ω – the coefficient of structural complexity of the random process $\tilde{Y}(t)$ which takes into account the spectrum of frequencies of the real loads; t – the work time of element (different from his term of service).

The solving of the problem (29) demands the presentation of the frequency characteristics of summary random processes of loads and $\tilde{Y}(t)$. Frequency description of load connection, presented in the form of quasistationary random processes is determined as

$$\omega_{12} = \frac{1}{\sqrt{1+K^2}} \left[\left(\omega_1 \cdot K_{tr1}\right)^2 + \left(\omega_2 \cdot K \cdot K_{tr2}\right)^2 \right]^{\frac{1}{2}} , \tag{30}$$

where: $\omega_1, \omega_2, \omega_{12}$ – effective frequencies of separate random processes and their sum; $K = \hat{x}_2 / \hat{x}_1$ – a relation of standards of loads which are composed; K_{tr1}, K_{tr2} – trend coefficients that take into account the slow seasonal changes of the atmospheric loads.

The frequency analysis of the composition of the random loads are constantly investigated by scientists [34, 35].

It is necessary to underline that the investigated random loads are substantially differed on frequency, it is evidently shown their realization (Figure 3, a,b) and also substantially different spectral densities (Figure 3, d). Effective frequencies of random processes of various loads are differed considerably: for crane loads ω_c = 1700 – 5160 1/day, for wind ones ω_w = 5.4 – 6.6 1/day, for snow

loads $\omega_s = 0.073 - 0/141$ 1/day. Therefore the joint action of several loads becomes multifrequent (Figure 3, c).

This peculiarity can be defined in the formula (29) by the coefficient of structural complexity of the random process β_ω which equals the ratio of mean frequency on maximum ω_m to the effective frequency on zero ω_q:

$$\beta_\omega = \frac{\omega_m}{\omega_q} = \frac{\left[K^{IV}(0)\cdot K(0)\right]^{1/2}}{\left[-\ddot{K}(0)\right]} = \frac{\beta_i \cdot \left[(1+k^2\cdot\Theta^4)(1+k^2)\right]^{1/2}}{(1+k^2\cdot\Theta^2)}, \quad (31)$$

where: $K(0)$, $\ddot{K}(0)$, $K^{IV}(0)$ – random process correlation function and its derivatives with zero argument; β_i – structure complexity coefficient of separate loads; $k = \hat{x}_2 / \hat{x}_1$; $\Theta = \omega_2 / \omega_1$ – standard deviations and effective frequency proportion of summed up random loads.

In accordance with equation (31) the frequency composition analysis can be realised if the load random process is differentiated sufficiently many times. For the atmospheric and crane loads the coefficient of structure complexity differs negligibly from $\beta_i = 3$. As a result of substantial difference of frequencies of loads, this coefficient of their composition can be considerable.

If the effective frequency of one of the loads prevails and ω is large, then formula (31) is simplified as follows:

$$\beta_\omega = \beta_i (1+k^2)^{1/2} / k, \quad (32)$$

Crane beams as well as crane trestle structures can be treated like elements under only crane load. We will examine general stress of these elements without local effects and fatigue. In this case the probability of structure failure $Q(t)$ depends on the ratio of a load stress of one bridge crane X_{M1} to the load stress of two bridge cranes X_{M2}, then on the ratio of a load carrying capacity of cranes to their mass and it also depends on crane work condition. The analysis showed that elements have a deficient reliability in the case of the one crane loads dominance. In the rest cases the elements reliability under crane loads is sufficient. In some cases the design crane load on structures can be decreased: if the approach of a loaded crane trolley to a crane track is limited or if the structure service term T is also limited.

The reliability of structures (beams, trusses) under snow load was estimated by a developed method. The calculation demonstrated the lack of reliability of these structures. That justifies the idea of understating of existing snow loads in the norms of SNiP, which operated on territory of Ukraine to 2006 year. Besides this fact validates the causes of steel truss failures. It applies to steel structures with lightweight roofs in the southern districts of Ukraine when there is much snow in winter. The increasing of snow design load for 1.5–2 times for our region can solve the reliability problem of steel structures under snow load. It was executed in national Code in Ukraine DBN V.1.2:2-2006 "Loads and influences". The reliability of steel roofs under snow load is constantly probed by the specialists of different countries [36].

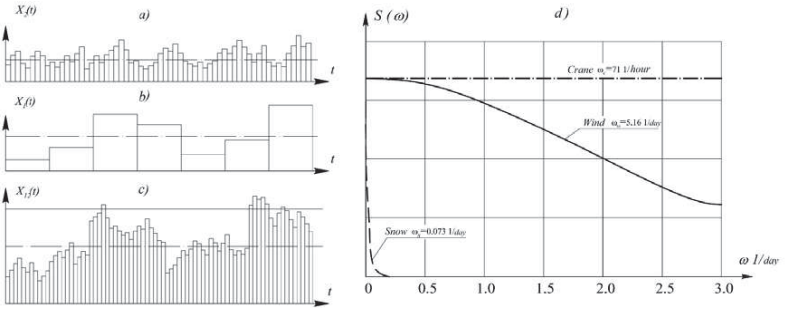

Figure 3. To the estimation of frequency of load composition
a – high-frequency component; b – low-frequency component; c – total randoml process;
d – comparison of the load spectral densities

Pichugin, S.F. Reliability estimation of industrial building structures. Magazine of Civil Engineering. 2018. 83(7). Pp. 24–37. doi: 10.18720/MCE.83.3.

Structure elements under wind load designed in accordance with the existing code (glass elements, wind protection screens etc.) are of sufficient reliability. So if the service term of these elements will be limited it is possible to introduce the temporary coefficient $\gamma_T \leq 1$ for the design wind load. It is recommended to introduce the increasing coefficients of combination $\psi = 0.7 - 0.9$into the structure design under snow, wind and crane loads.

The special attention was spared the evaluation of reliability of steel beam-column structures. Time factor, existing loads, random steel strength were taken into account during computation process of these elements. Existing steel columns of industrial buildings in a broad range of parameters were examined. The general conclusion is as follows: the reliability of steel columns of industrial buildings is quite sufficient. In quality tasks for subsequent researches it is possible to name the search of direct probabilistic decisions of tasks of compressed elements and subsequent development of probabilistic version of method of finite elements.

3.4. Reliability analysis of structure nodes and redundant systems

It was founded out that reliability of typical structure nodes could be compared with the schemes of successive connections of correlated elements. Thus, the node reliability depends upon the number of engaged independent load carrying elements.

Some beams and simple frames, as well as multi-storey and multi-span structures of industrial and residential buildings present the redundant structures. Redundant structure failures occur after some member failures in the form of transmission to different workable states. Thus, the redundant structure failure estimation is a very complicated problem as depends upon the system complexity. Illustration of it is a multibranch graph of the states of twice statically indefinite system (Figure 4, a). The complete estimation of the failure probability of elastic-plastic redundant systems with random durability and loading was got as a result of application of probabilistic method of limit equilibrium. A method allows, walking around the transient states of system, directly to examine the reliability of the last (true) mechanism of failure of the system (Figure 4, b). Corresponding formulae are derived; the algorithms and computing programs are developed. The estimation of a wide range of industrial redundant structures with different degree of redundancy was obtained on the base of this approach. It gave possibility to evaluate the safety level of redundant structures in comparison with separate members and statically determined structures. This level can be taken into account introducing the additional coefficient of work condition $\gamma_c = 1.1 - 1.4$.

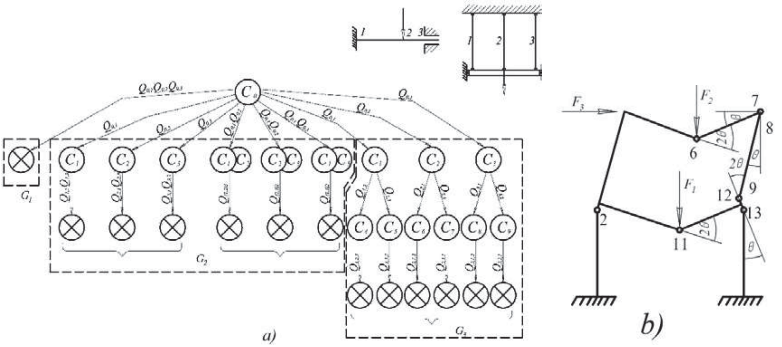

Figure 4. To the reliability estimation of redundant structures:
a – graph of the states of twice statically indefinite system; b – true mechanism of frame failure

Among questions, connected with the estimation of reliability of redundant systems, which remained unsolved, it follows to name formalization and translation on personal computer of method of the states and logic-probabilistic method, and also classification of redundant system elements, after the criterion of reliability. This direction becomes especially actual in connection with development of scenarios of failures, questions of vitality and progressive failure of buildings [37–39].

Пичугин С.Ф. Оценка надежности конструкций промышленных зданий // Инженерно-строительный журнал. 2018. № 7(83). С. 24–37.

4. Conclusions

1. The reliability analysis of wide range of structures designed in accordance with existing Design Codes is examined in the article. Considered structures of industrial buildings are as follows: crane and roof beams, columns, redundant building systems.

2. This analysis exposes that the structures have quite different levels of reliability. It is shown that the light roof structures are not reliable enough being under the great influence of snow load. At the same time, the Design Code allows over-estimation of reliability for steel columns and redundant structures.

3. For the achievement of the put aim, the practical method of reliability analysis of structural elements is worked out. This method takes into account real load distributions and frequency characteristics.

4. The general probabilistic models of wind, snow and crane loads were designed and taken as a statistic basis of reliability estimation. These models are as follows: stationary and quasi-stationary random processes, its absolute maxima, random sequences of independent and correlated loads, discrete presentation and extreme model.

5. The simplest method of structure reliability estimation is realized in the technique of random values. Reliability estimation of reinforced concrete beams with carbon-plastic external strengthening is presented as an example.

6. Substantial results are got in the probabilistic techniques of random processes. It is important to notice that correlation functions and effective frequencies of random processes of various loads differ considerably. Therefore the joint action of several loads becomes multi-frequent. This peculiarity can be defined by the structure complexity coefficient β_ω which equals the ratio of mean frequency on maximum to the effective frequency on zero.

7. There is confirmed that redundant structure failure estimation is a very complicated problem as depends upon the system complexity. The method of states, a probabilistic method of ultimate equilibrium and logic, as well as a probabilistic method is developed for solving this problem.

8. With regard to mentioned above, it is recommended to correct some load factors, a combination factor and a factor for model uncertainties of the Design Codes of steel structures and loads.

References

1. Streletskiy N.S. Osnovyi statisticheskogo ucheta koeffitsienta zapasa prochnosti sooruzheniy [Bases of the statistical account of constructions safety factor]. Moscow: Stroyizdat. 1947. 92 p. (rus)
2. Rzhanitsyin, A.R. Teoriya rascheta stroitelnyih konstruktsiy na nadezhnost [The theory of calculation of building structures reliability]. Moscow: Stroyizdat. 1978. 239 p. (rus)
3. Bolotin, V.V. Statistical methods in structural mechanics. San Francisco: Holden Day. 1969. 276 p.
4. Freudenthal, A.M. The Safety of Structures. Proc. ASCE. 1947. Vol. 112. No. 1. Pp. 125–180.
5. Benjamin, J.R. Cornell, C.A. Probability, Statistics and Decision for Civil Engineers. New York: McGraw-Hill. 1970. 684 p.
6. Thoft-Christensen, P., Baker, M.J. Structural reliability theory and its applications. Berlin: Springer. 1982. 267 p.
7. Augusti, G., Baratta, A., Casciati, F. Probabilistic methods in structural engineering. London: Chapman & Hall.1984. 583 p.
8. Ditlevsen, O., Madsen, H. Structural reliability methods. Chichester: John Wiley. 1996. 372 p.
9. Elishakoff, I. Probabilistic Theory of Structures. New York: Dover Publications,1999. 502 p
10. Raizer, V. Reliability of Structures. Analysis and Application. USA: BACKBONE Publishing Company. 2009. 146 p.
11. Perelmuter, A.V. Izbrannyie problemyi nadezhnosti i bezopasnosti stroitelnyih konstruktsiy [The selected problems of building structures reliability and safety]. Moscow: Izdatelstvo ASV, 2007. 256 p. (rus)

Литература

1. Стрелецкий Н.С. Основы статистического учета коэффициента запаса прочности сооружений. М.: Стройиздат, 1947. 92 с.
2. Ржаницын А.Р. Теория расчета строительных конструкций на надежность. М.: Стройиздат, 1978. 239 с.
3. Bolotin V.V. Statistical methods in structural mechanics. San Francisco: Holden Day.1969. 276 p.
4. Freudenthal A.M. The Safety of Structures // Proc. ASCE, 1947. Vol. 112. № 1. Pp. 125–180.
5. Benjamin J.R. Cornell C.A. Probability, Statistics and Decision for Civil Engineers. New York: McGraw-Hill. 1970. 684 p.
6. Thoft-Christensen P., Baker M.J. Structural reliability theory and its applications. Berlin: Springer. 1982. 267 p.
7. Augusti G., Baratta A., Casciati F. Probabilistic methods in structural engineering. London: Chapman & Hall.1984. 583 p.
8. Ditlevsen O., Madsen H. Structural reliability methods. Chichester: John Wiley. 1996. 372 p.
9. Elishakoff I. Probabilistic Theory of Structures. New York: Dover Publications.1999. 502 p.
10. Raizer V. Reliability of Structures. Analysis and Application. USA: BACKBONE Publishing Company. 2009. 146 p.
11. Перельмутер А.В. Избранные проблемы надежности и безопасности строительных конструкций. 3-е изд., перераб. и доп. М.: Изд-во АСВ, 2007. 256 с.
12. Пичугин С.Ф. Надежность стальных конструкций производственных зданий. М: Изд-во АСВ, 2011. 456 с.

Pichugin, S.F. Reliability estimation of industrial building structures. Magazine of Civil Engineering. 2018. 83(7). Pp. 24–37. doi: 10.18720/MCE.83.3.

12. Pichugin, S.F. Nadezhnost stalnyih konstruktsiy proizvodstvennyih zdaniy [Reliability of industrial building steel structures]. Moscow: Izdatelstvo ASV, 2011. 456 p. (rus)
13. Pichugin, S. Analysis of bridge crane loads on industrial buildings. XLIV Konferencja Naukowa KILiW PAN i KN PZITB. Tom VII. Poznan-Krynica, 1998. Pp. 171–178.
14. Pichugin, S. Probabilistic analysis on wind Load and reliability of structures. Proc. of the 2 EACWE. Vol. 2. Genova. Italy. 1997. Pp. 1883–1890.
15. Kinash, R.I.; Huk, J.S. Geographical altitude coefficient utilisation for wind gust loading determination in the mountainous terrain of the Transcarpathian region. Technical Transactions, Civil Engineering. 2015. No. 2. B/2015. Politechnika Krakowska: Krakow. Poland. Pp. 83–89.
16. Kwon, D.K., Kareem, A., Stansel, R., Ellington, B.R. Wind load factors for dynamically sensitive structures with uncertainties. Engineering Structures. 2016. Vol. 103. Pp. 53–62.
17. Baravalle, M., Köhler, J. On the probabilistic representation of the wind climate for calibration of structural design standards. Structural Safety. 2018. Vol. 70. Pp. 115–127.
18. Pichugin, S. Probabilistic description of ground snow loads for Ukraine. Snow Engineering. Recent Advanced and Developments. Rotterdam: A.A.Balkema. 2000. Pp. 251–256.
19. Ledovskoy, I.V. Trend snegovyih nagruzok na grunt pod vliyaniem globalnogo potepleniya klimata [Trend of the snow loading on ground under influence of the global warming of climate] Stroitelnaya mehanika i raschet sooruzheniy. 2012. No. 4. Pp. 71–76.
20. Fikke, S.M., Nygaard, B.E.K. Assessing environmental actions from modern meteorology. Technical Transactions. Civil Engineering. 2015. No. 2. B/2015. Politechnika Kracowska: Krakow. Poland. Pp. 405–415.
21. Kudzys, A.P. Otsenka nadezhnosti zhelezobetonnyih konstruktsiy [Reliability estimation of reinforced concrete structures]. Vilnius: “Mokslas”. 1985. 156 p.
22. Cornell, C.A. Bounds on the reliability of structural systems. Journal of the Structural Division. ASCE. 1967. Vol. 93. No. ST. Pp. 171–200.
23. Liang, J., Ding, Z., Li, J. A probabilistic analyzed method for concrete fatigue life. Probabilistic Engineering Mechanics. 2017. Vol. 49. Pp. 1–32.
24. Moiseenko, R.P. Nachalnaya nadezhnost zhelezobetonnyih elementov [Initial reliability of reinforce-concrete elements] Stroitelnaya mehanika i raschet sooruzheniy. 2016. No. 2(265). Pp. 66–70.
25. Gromatskiy, V.A. O nekotoryih metodah veroyatnostnogo rascheta nadezhnosti konstruktsiy [About some methods of probabilistic calculation of reliability of constructions] Stroitelnaya mehanika i raschet sooruzheniy. 2016. No. 2(265). Pp. 61–65.
26. Krakovskiy, M.B. Povyishenie nadezhnosti zhelezobetonnyih konstruktsiy pri raschetah po neskolkim programmnyim kompleksam [Increase of reliability of reinforce-concrete constructions at calculations on a few programmatic complexes]. Stroitelnaya mehanika i raschet sooruzheniy. 2016. No. 5(268). Pp. 45–49.
27. Rayzer, V.D. Analiz nadezhnosti konstruktsiy pri iznose nesuschih konstruktsiy [Analysis of structure reliability at the wear of load carrying structures]. Stroitelnaya mehanika i raschet sooruzheniy. 2013. No. 6(251). Pp. 16–20.
28. Perelmuter, A.V., Pichugin, S.F. Ob otsenke uyazvimosti stroitelnyih konstruktsiy [About an estimation of building structures vulnerability]. Magazine of Civil Engineering. 2014. No. 5(49). Pp. 5–14. doi: 10.5862/MCE.49.1
13. Pichugin S. Analysis of bridge crane loads on industrial buildings // XLIV Konferencja Naukowa KILiW PAN i KN PZITB. Tom VII. Poznan-Krynica. 1998. Pp. 171–178
14. Pichugin S. Probabilistic analysis on wind load and reliability of structures // Proc. of the 2 EACWE. Vol. 2. Genova. Italy. 1997. Pp. 1883–1890.
15. Kinash R.I., Huk J.S. Geographical altitude coefficient utilisation for wind gust loading determination in the mountainous terrain of the Transcarpathian region // Technical Transactions, Civil Engineering. 2015. № 2. B/2015. Politechnika Krakowska: Krakow. Poland. Pp. 83–89.
16. Kwon D.K., Kareem A., Stansel R., Ellington B.R. Wind load factors for dynamically sensitive structures with uncertainties // Engineering Structures. 2016. Vol. 103. Pp. 53–62.
17. Baravalle M., Köhler J. On the probabilistic representation of the wind climate for calibration of structural design standards // Structural Safety. 2018. Vol. 70. Pp. 115–127.
18. Pichugin S. Probabilistic description of ground snow loads for Ukraine // Snow Engineering. Recent Advanced and Developments. Rotterdam: A.A.Balkema., 2000. Pp. 251–256.
19. Ледовской И.В. Тренд снеговых нагрузок на грунт под влиянием глобального потепления климата // Стр. мех и расчет сооруж. 2012. № 4. С. 71–76.
20. Fikke S.M., Nygaard B.E.K. Assessing environmental actions from modern meteorology // Technical Transactions. Civil Engineering. 2015. № 2. B/2015. Politechnika Kracowska: Krakow. Poland. Pp. 405–415.
21. Кудзис А.П. Оценка надежности железобетонных конструкций. Вильнюс: Мокслас, 1985. 156 с.
22. Cornell C.A. Bounds on the reliability of structural systems // Journal of the Structural Division, ASCE. 1967. Vol. 93, № ST. Pp. 171–200.
23. Liang J., Ding Z., Li J. A probabilistic analyzed method for concrete fatigue life // Probabilistic Engineering Mechanics. 2017. Vol. 49. Pp. 1–32.
24. Моисеенко Р.П. Начальная надежность железобетонных элементов // Стр. мех и расчет сооруж. 2016. № 2(265). С. 66–70.
25. Громацкий В.А. О некоторых методах вероятностного расчета надежности конструкций // Стр. мех и расчет сооруж. 2016. № 2(265). С. 61–65.
26. Краковский М.Б. Повышение надежности железобетонных конструкций при расчетах по нескольким программным комплексам // Стр. мех и расчет сооруж. 2016. № 5(268). С. 45–49.
27. Райзер В.Д. Анализ надежности конструкций при износе несущих конструкций // Стр. мех и расчет сооруж. 2013. № 6(251). С. 16–20.
28. Перельмутер А.В., Пичугин С.Ф. Об оценке уязвимости строительных конструкций // Инженерно-строительный журнал. 2014. № 5(49). С. 5–14.
29. Климович В.Н., Парьев К.В.Надежность конструкции защиты от размывов дна вблизи платформы «Приречная» // Инженерно-строительный журнал. 2017. № 7(75). С. 52–65.
30. Индейкин А.В., Чижов С.В., Шестакова Е.Б., Антонюк А.А., Кулагин Н.И., Смирнов В.Н., Карпов В.В., Голицынский Д.М. Приближенные методы оценки надежности балочных пролетных строений железнодорожных мостов // Инженерно-строительный журнал. 2017. № 7(75). С. 150–160.
31. Исхаков Ш.Ш., Ковалев Ф.Е., Васкевич В.М., Рыжиков В.Ю. Оценка надёжности эксплуатации зданий и сооружений по методикам возникновения риска их неработоспособных состояний // Инженерно-строительный журнал. 2012. № 7(33). С. 76–88.

Пичугин С.Ф. Оценка надежности конструкций промышленных зданий // Инженерно-строительный журнал. 2018. № 7(83). С. 24–37.

29. Klimovich, V.I. Pariev, K.V. Reliability of scour protection design near the platform «Prirazlomnaja». Magazine of Civil Engineering. 2017. No. 7(75). Pp. 52–65. doi: 10.18720/MCE.75.5
30. Indeykin, A.V., Chizhov, S.V., Shestakova, E.B., Antonyuk, A.A., Kulagin, N.J., Smirnov, N.V., Karpov, V.V., Golitsynsky, D.M. Approximated method of estimation of the reliability of framed railway structures of railway bridges. Magazine of Civil Engineering. 2017. No. 7(75). Pp.150–160. doi: 10.18720/MCE.75.15.
31. Ishakov, Sh.Sh., Kovalev, F.E., Vaskevich, V.M., Ryizhikov, V.Yu. Otsenka nadezhnosti ekspluatatsii zdaniy i sooruzheniy po metodikam vozniknoveniya riska ih nerabotosposobnyih sostoyaniy [Estimatiing reliability of buildings and structures according to the methods of the risk of unserviceability]. Magazine of Civil Engineering. 2012. No. 7(33). Pp. 76–88.
32. Pryadko, Yu.N., Muschanov, V.F., Bartolo, H., Vatin, N.I., Rudneva, I.N. Improved numerical methods in reliability analysis of suspension roof joints. Magazine of Civil Engineering. 2016. No. 5(65). Pp. 27–41. doi: 10.5862/MCE.65.3
33. Kowal, Z. Influence of the bearing capacity and reliability of connections and nodes on the bearing capacity and reliability of complex bar structures. Proc. of the XIII Int. Conf. on Metal Structures (ICMS2016). Rotterdam: Balkema. Pp. 202–203.
34. Mori, Y., Kato, T., Murai, K. Probabilistic models of combinations of stochastic loads for limit state design. Structural Safety. 2003. Vol. 25. No. 1. Pp. 69–97.
35. Dimitrov, N. Probabilistic model for multi-axial dynamic load for wind turbines. Engineering Structures. 2016. Vol. 117. Pp. 239–249.
36. Derek, L., Kozak, A.B.L. Reliability of steel roof structures under snow load. Structural Safety. 2015. Vol. 54. Pp. 46–56.
37. Thai, H.T., Uy, B., Kang, W.H., Hikc, S. System reliability evaluation of steel frames with semi-rigid connections. Journal of Constructional Steel Research. 2016. Vol. 121. Pp. 29–39.
38. Tao, Y.R., Cao, L., Cheng, G.Q., Huang, Zh.H. Safety analysis of structures with probability and evidence theory. International Journal of Steel Structures. 2016. Vol. 16. No. 2. Pp. 289–298.
39. Dehtyar, A.S. O vozmozhnosti progressiruyuschego razrusheniya [About possibility of progressive failure]. Stroitelnaya mehanika i raschet sooruzheniy. 2017. No. 6 (275). Pp. 2–6.
32. Прядко Ю.Н., Мущанов В.Ф., Бартоло Х., Ватин Н.И., Руднева И.Н. Усовершенствование числовых методов и расчета узлов висячих конструкций // Инженерно-строительный журнал. 2016. № 5(65). С. 27–41.
33. Kowal Z. Influence of the bearing capacity and reliability of connections and nodes on the bearing capacity and reliability of complex bar structures // Proc. of the XIII Int. Conf. on Metal Structures (ICMS2016). Rotterdam: Balkema. Pp. 202–203.
34. Mori Y., Kato T., Murai K. Probabilistic models of combinations of stochastic loads for limit state design // Structural Safety. 2003. Vol. 25. № 1. Pp. 69–97.
35. Dimitrov N. Probabilistic model for multi-axial dynamic load for wind turbines // Engineering Structures. 2016. Vol. 117. Pp. 239–249.
36. Derek L., Kozak A.B.L. Reliability of steel roof structures under snow load // Structural Safety. 2015. Vol. 54. Pp. 46–56.
37. Thai H.T., Uy B., Kang W.H., Hikc S. System reliability evaluation of steel frames with semi-rigid connections // Journal of Constructional Steel Research. 2016. Vol. 121. Pp. 29–39.
38. Tao Y.R., Cao L., Cheng G.Q., Huang Zh. H. Safety analysis of structures with probability and evidence theory // International Journal of Steel Structures. 2016. Vol. 16. № 2. Pp. 289–298.
39. Дехтярь А.С. О возможности прогрессирующего разрушения // Стр. мех и расчет сооруж. 2017. № 6 (275). С. 2–6.

Sergii Pichugin,
+3(8050)591-77-28; pichugin.sf@gmail.com

Сергей Федорович Пичугин,
+3(8050)591-77-28;
эл. почта: pichugin.sf@gmail.com

Pichugin, S.F. Reliability estimation of industrial building structures. Magazine of Civil Engineering. 2018. 83(7). Pp. 24–37. doi: 10.18720/MCE.83.3.

doi: 10.18720/MCE.83.4

Structure and mineral composition of soil-cement with complex additive

Структура и минеральный состав цементогрунта с комплексной добавкой

P.E. Bulanov*,
JSC "Alekseevskdorstroy", Alekseevskoe, Republic of Tatarstan, Russia
E.U. Ermilova,
L.F. Mavliev,
Kazan State University of Architecture and Engineering, Kazan, Russia

Канд. техн. наук, гл. технолог
П.Е. Буланов*,
ОАО «Алексеевскдорстрой», Алексеевское, Республика Татарстан, Россия
канд. техн. наук, ассистент
Е.Ю. Ермилова,
канд. техн. наук, доцент Л.Ф. Мавлиев,
Казанский государственный архитектурно-строительный университет, г. Казань, Россия

Key words: soil-cement; polycarboxylate ether; octyltriethoxysilane; X-ray diffraction pattern; differential scanning calorimetry; ettringite; low-basic hydrated calcium silicate; structure

Ключевые слова: цементогрунт; эфир поликарбоксилата; октилтриэтоксисилан; рентгенофазовый анализ; сканирующая дифференциальная калориметрия; эттрингит; низкоосновные гидросиликаты кальция; структура

Abstract. The effect of the polycarboxylate ether and the complex hydrophobic-plasticizing additive on the structure, phase and mineral composition of cement based on polymineral clay with content of relict minerals more than 85 % (52.49 % of quartz) was studied. As research methods chosen X-ray diffraction pattern, differential scanning calorimetry and scanning electron microscopy. The regularities of the effect of the complex hydrophobic-plasticizing additive based on polycarboxylate ether and octyltriethoxysilane on the formation of cement hydration products in a strengthened clayey soil are established. Changes in structure and composition include the following: the formation of a strong skeleton of the crystallization phase due to the increase in the number of hydrated new formation in the form of low-basic hydrated calcium silicate and ettringite, decrease in portlandite content, as well as an increase in the amount of amorphous phase (up to 16 %) in the form of tobermorite gel filling intercrystalline spaces. In soil-cement hydrated silicate calcium are formed in an amount of more than 4 % and ettringite in an amount of more than 7 %, the amount of portlandite reduced by 46 %. The result of modification of the complex hydrophobic-plasticizing admixture of soil-cement, a denser and homogeneous structure with a pronounced "overgrowth" of the pores formed by gel-like hydrated calcium silicate is formed, which are deposited in a large amount on the minerals of the strengthened soil.

Аннотация. Проведены исследования влияния эфира поликарбоксилата и комплексной гидрофобно-пластифицирующей добавки на структуру, фазовый и минеральный состав цементогрунта на основе полиминеральной глины содержанием реликтовых минералов более 85 % (52,49 % кварца). В качестве методов исследования выбраны рентгенофазовый анализ, дифференциально-сканирующая калориметрии и электронно-растровая микроскопия. Установлены закономерности влияния комплексной гидрофобно-пластифицирующей добавки на основе эфира поликарбоксилата и октилтриэтоксисилана на процессы образования продуктов гидратации цемента в укрепленном глинистом грунте, заключающиеся в следующих структурных изменениях: создание прочного каркаса кристаллизационной фазы за счет повышения количества гидратных новообразований в виде низкоосновных гидросиликатов кальция и эттрингита, уменьшения содержания портландита, а также увеличение количества аморфной фазы (до 16 %) в виде тоберморитового геля, заполняющего межкристаллическое пространство. В цементогрунте происходит образование гидросиликатов кальция в количестве более 4 % и эттрингита в количестве более 7 %, уменьшается количество портландита на 46 %. В результате модификации комплексной гидрофобно-пластифицирующей добавкой цементогрунта формируется более плотная и однородная структура с ярко выраженным «зарастанием» пор, образованными гелевидными

гидросиликатами кальция, которые в большом количестве осаждаются (плотно формируются) на минералах укрепляемого грунта.

1. Introduction

Clay minerals are class of phyllosilicates, which are usually formed as a result of chemical weathering of other silicate minerals on the crustal surface [1, 2].

Since the time of prehistoric civilization, mankind has used layered clay minerals in various fields of activity because of their wide distribution and diversity in nature [2–4]. Depending on the structure and properties, such as high specific surface area, ion exchange capacity or hydration of clays are widely used in ceramics, paper industry, in oil drilling, in pharmaceutical preparations, as adsorbents, etc. [1, 5, 6].

Clay soils, strengthened by Portland cement (soil-cement), are used in the construction of road clothes as bases and road surfaces [7]. However, the use of clay soils strengthened by Portland cement is ineffective due to the high costs of binder (more than 12 % of the mass of the soil) to achieve the required grades in strength and frost resistance. The solution to this problem is the modification of soil-cement with various chemical additives [8].

The history of the development binders using for improving the exploitative properties of soil in construction goes back to the distant past. Strengthened soil roads existed in Ancient Mesopotamia, Egypt, Greece and Rome [9].

Lime and cement were widely spread in road construction. A significant contribution to the development of strengthened soils, inorganic binders, in particular cement and lime, in construction was made by V.M. Bezruk, V.M. Mogilevich, Yu. M. Vasiliev, L.V. Goncharova, O.V. Tyumentseva, G.A. Levchanovsky, L.A. Markov, V.M. Knatko, V.A. Kelman, V.V. Okhotin, M.M. Filatov, C.W. Correns, C.S. Dunn, J. Hashimoto, J.K. Mitchell, A. Herzod, G.H. Hilt, D.T. Davidson, J.G. Laguros, T.W. Lambe, R.C. Mainfort and others.

Increasing the strength of soil-cement occurs as a result of physical and chemical reactions between the soil and the binder, i.e. in the interaction of substances present in ground minerals and products of hydration of Portland cement [10]. At the same time, a higher density and strength are achieved by reducing the voids, binding the ground particles and aggregating them, preserving the flocculation structure and soil swelling [11, 12].

According to D.T. Bergado, L.R. Anderson, N. Miura, A.S. Balasubramaniam [13], there are two main chemical reactions that regulate the physical and mechanical properties of soil-cement. Primary hydration reaction between cement and water, and the secondary – pozzolanic reaction between portlandite, resulting from the cement hydration and clay minerals. The hydration reaction leads to the formation of primary products of cement hydration, which proves the relatively high strength and frost resistance of soil-cement. A secondary pozzolanic reaction occurs when the $Ca(OH)_2$ concentration reaches a certain limit in the pore water. According to the data [13–15], the pozzolanic reaction occurs between the silicon and aluminum oxides present in the clay with calcium ions in the cement with the formation of calcium aluminate hydrates, calcium silicate hydrates and calcium aluminosilicate hydrates.

It was established earlier that in order to increase the soil-cement and soil strength, it is expedient to use polycarboxylate superplasticizers [16, 17], and for increasing the freeze-thaw resistance – organosilicon compound octyltriethoxysilane [8]. Earlier, we found the influence of a complex hydrophobic-plasticizing additive based on the polycarboxylate ether and octyltriethoxysilane on the basic physical and technical properties of soil-cement [18]. However, the influence of polycarboxylate superplasticizers and complex hydrophobic-plasticizing additive on the structure, phase and mineral composition of the soil-cement remains uninvestigated.

In this connection, the aim of the work was to determine the effect of a complex hydrophobic-plasticizing additive on the composition and structure of soil-cement based on polymineral clay to identify the reasons for increasing its physical and technical properties.

To achieve this aim, the following tasks are formulated:

1. to study the effect of the complex hydrophobic-plasticizing additive on the phase and mineral composition of soil-cement;
2. to investigate the structure of the soil-cement modified with the complex hydrophobic-plasticizing additive.

2. Materials and methods of research

For research, clay soil was used with the mineral composition (Table 1) in accordance with Russian State Standard GOST 9169-75 refers to polymineral clay, and according to Russian State Standard GOST 25100-2011 in accordance with the number of ductility and the content of sand particles to loam light silty. The content of relict minerals is more than 85 % (52.49 % quartz). The selected clayey soil satisfies the requirements of Russian State Standard GOST 23558-94 in terms of the plasticity number, according to which for strengthening of inorganic binders in the construction of bases and road surfaces, it should not exceed 12. This soil is the most widespread polymineral clayey soil in the Republic of Tatarstan and the Volga Region, according to the granulometric composition.

The mineral composition of the investigated clay soil is presented in Table 1, the X-ray diffraction pattern in Figure 1. The particle-size distribution, physical and technical properties of clay soil are presented in Tables 2 and 3.

For the batching of cement mortars, portland cement CEM I 42.5N was used. To obtain more clear results on the determination of the mineral composition of the hardening products, the dosage of cement in the samples of the cement mortar was 50 %.

Table 1. Mineral composition of polymineral clay

No.	The name of the mineral	Content,%
1	Quartz	52.49
2	Montmorillonite	2.44
3	Kaolinite	1.00
4	Hydromica	8.80
5	Potash feldspar	15.05
6	Peach-stone	1.86
7	Albite	16.03
8	Pyrite	0.33
9	Dolomite	0.66
10	Calcite	1.34

Table 2. Particle-size distribution of clay soil

Size of fraction, mm	1.00	0.50	0.25	0.10	0.05	<0.05
Partial remains, %	-	0.01	0.11	0.76	8.26	90.86
Full remains, %	-	0.01	0.12	0.88	9.14	100.00

Table 3. Physical and technical properties of clay soil

No	The name of properties	Values of properties
1	Liquid limit, %	30.04
2	Plastic limit, %	18.42
3	Plasticity index, %	11.62
4	pH aqueous extract	8.70
5	Organic matter contents, in mass, %	-

The following additives as surface-active agent are used: polycarboxylate ether and octyltriethoxysilane.

Polycarboxylate ether – polycarboxylate superplasticizer Pantarhit PC 160 Plv is a light gray powder obtained by spray drying from a polymer solution. The active substance is polyacrylic acid.

1. Octyltriethoxysilane ($C_8H_{17}Si(OC_2H_5)_3$) is a colorless, low-viscosity, low-volatile liquid with a density of 0.875 g/cm³.

2. The additives were introduced in the following dosages from the weight of the soil-cement: ether polycarboxylate 0.1 %; octyltriethoxysilane – 0.02 %.

To research and identify the processes of hydration hardening soil-cement at the age of 28 days was used and the method of X-ray diffraction pattern of the combined thermogravimetry, differential thermogravimetry and differential scanning calorimetry.

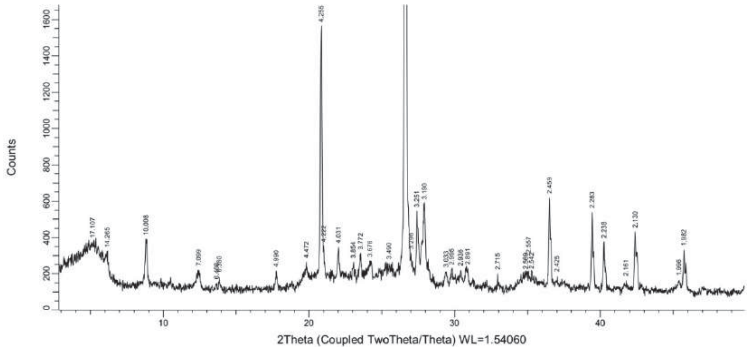

Figure 1. X-ray diffraction pattern polymineral clay

A study of the structure and composition was carried out on the following samples, soil-cement at the age of 28 days hardening of the following compositions.

Composition No 1 is a soil-cement.

Composition No 2 is a soil-cement modified by polycarboxylate ether.

Composition No 3 is a soil-cement modified by complex hydrophobic-plasticizing additive based on polycarboxylate ether and octyltriethoxysilane.

X-ray diffraction pattern analysis was chosen to determine the mineralogical composition, change and identification of products of new formation during hardening of strengthened soils with polycarboxylate ether. The experiment was carried out on an automatic X-ray diffractometer Bruker D8 Advance, equipped with a Vario attachment and a linear coordinate detector Vantec. CuKα radiation monochromatized (λ(Cu-K) = 1.54184 Å) is used with a germanium curved monochromator of Johanson, the operating mode of the X-ray tube is 40 kV, 40 mA. The experiments were performed at room temperature in the Bragg-Brentano geometry with a flat sample. The construction and analysis of the diffractograms were performed using the Bruker Diffrac Eva program. This method is one of the most effective way of determining the mineral composition in cement and clay soils.

The thermal analysis of the samples was carried out by the method of combined thermogravimetry and differential scanning calorimetry using a NETZSCH STA 449C thermal analyzer under continuous heating (40 to 1000 °C) of samples weighing 35–40 mg at a flow rate of 10 °C/min (50 ml/min) of air in crucibles from alundum with mass-spectrometric control of the gas phase. This method was chosen to identify the features of cement hydration products in strengthened soils with polycarboxylate ether and complex hydrophobic-plasticizing additive at the 28-day age.

To study the structure of clay soils strengthened with cement, the morphology of the hydrate new formation and the surface of the investigated soil-cement compositions, electron microscopic studies of the samples were carried out using a scanning electron microscope REM-100U.

3. Results and Discussion

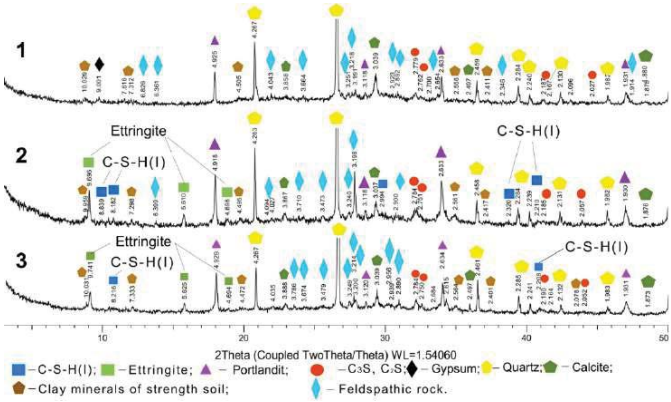

Figure 2 – X-ray diffraction pattern of soil-cement:
1 – control composition; 2 – composition modified by polycarboxylate ether;
3 – composition modified with a complex hydrophobic-plasticizing additive

Figure 2 is shows an X-ray diffraction pattern control composition (composition No 1), which is characterized by large peaks unreacted clinker minerals – alite and belite (d = (2.779; 2.752; 2.700; 2.187; 2.027)·Å). Diffraction peaks with basal spacings d = (4.925; 3.118; 2.633; 1.931)·Å correspond to reflections new formation portlandite and unreacted gypsum d = (9.002)·Å. The remaining peaks in the X-ray diffraction pattern correspond diffraction maxima with basal spacings relict d = (6.826; 6.361; 4.267; 4.043; 3.858; 3.664; 3.347; 3.251; 3.218; 3.191; 3.039; 2.972; 2.923; 2.892; 2.654; 2.497; 2.459; 2.346; 2.284; 2.240; 2.167; 2.130; 2.096; 1.982; 1.914; 1.880; 1.875)·Å clay and d = (10.029; 7.616; 7.312; 4.505; 2.556; 2.411)·Å minerals present in strengthens clayey soil. The content of the amorphous phase is 38.1 % of the sample weight.

The composition No 2 is an appearance of new formations in the form of ettringite (d = (9.696; 5.610; 4.696)·Å) and low-basic hydrated calcium silicate of the type C–S–H(I) (d = (8.839; 8.182; 2.994 2.320; 2.210)·Å. Diffraction maxima with interplanar distances d = (4.918; 3.118; 2.633; 1.930)·Å correspond to new formations of portlandite. The addition of polycarboxylate ether leds to decrease the formed portlandite in comparison with the composition No 1. In comparison with the composition No 1 decreases the amount of unhydrated remaining clinker minerals, as evidenced by diffraction peaks with interplanar spacings d = (2.784; 2.751; 2.185; 2.057) · Å, characteristic of the alite and belite. The intensity of peaks characterizing the presence of relict (d = (6.399; 4.263; 4.094; 4.027; 3.867; 3.710; 3.473; 3.348; 3.240; 3.198; 3.037; 2.900; 2.458; 2.284;2.239; 2.131; 1.982; 1.876)·Å) and clay (d = (9.959; 7.298; 4.495; 3.474; 2.561; 2.417; 2.210)·Å) minerals present in clay soil. Most of the new formations are in the form of amorphous compounds, which is confirmed by an increase in the amorphous phase to 46.0 %, which is 7.9 % higher in comparison with the composition No 1.

Composition No 3 shows slightly more unreacted clinker minerals d = (2.784; 2.750; 2.190; 2.052)·Å in comparison with composition No 2, but less with composition No 1. There are traces of formed ettringite (d = (9.741; 5.625; 4.694)·Å), low-basic hydrated calcium silicate of type C–S–H(I) (d = (8.216; 2.208)·Å and portlandite (d = (4.929; 3.120; 2.634; 1..931)·Å, in a smaller amount in comparison with composition No 2. However, the diagram shows the presence of relict (d = (4.267; 4.035; 3.888; 3.786; 3.674; 3.479; 3.353; 3.249; 3.200; 3.039; 2.956; 2.939; 2.890; 2.497; 2.461; 2.285; 2.241; 2.164;2.132; 1.983; 1.931; 1.873)·Å) and clay (d = (10.031; 7.333; 4.472; 2.564; 2.401; 2.078)·Å) minerals of the clay soil to be consolidated. The amorphous phase of composition No 3 amounted to 44.2 %, which is 6.1 % higher than for composition No 1, and 1.8 % lower than for No 2.

Figure 3 shows the thermogram of the control composition (composition No 1) sample. It can be seen from figure 3 that when the sample is heated, a continuous mass decrease is observed, reaching up to 13.27 % at 1000 °C. In this case, the rate of change in the mass of differential thermogravimetry has three expressed maxima at temperatures of 110, 448 and 693 °C, coinciding with peaks of endothermic effects on the differential scanning calorimetry heat flux line.

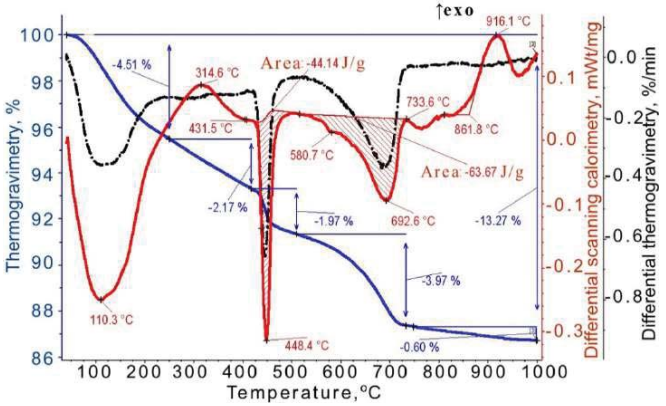

Figure 3. Curves of thermogravimetry, differential thermogravimetry and differential scanning calorimetry upon heating of a control sample (composition No 1)

The differential scanning calorimetry curve shows the most pronounced endothermic effects with the temperature at the beginning of the maximum at 40/110, 432/448 and 500/693 °C, as well as the exothermic effect at 862/916 °C. In the low-temperature region (up to 250 °C), a combined endothermic effect with a temperature maximum at 110.3 °C is observed, which is related to the loss of free and adsorption water present in the control sample. Also on the differential scanning calorimetry curve, two more endothermic peaks are seen in the temperature range at 140 and 170 °C, related to the presence of unreacted gypsum. The total weight loss in the temperature range 0–250 ºC is 4.51 %. The loss of mass in the temperature range of 250–430 ºC is equal to 2.17 %.

The endothermic effect with the maximum at 448 °C, followed in the temperature range 431–505 °C by a mass loss of 1.97 %, is associated with the decomposition of portlandite. The magnitude of the thermal effect is 44.14 J/g. In the temperature interval 505–734 °C the high temperature endotherm maximum at 692.6 °C is observed with characterized decompounding of calcium carbonate. Also, the following endothermic effects are seen on differential scanning calorimetry: at 548 °C, associated with the removal of hydroxyl water from hydromica, at 580.7 °C – with removal of hydroxyl water from kaolinite and at 624 °C – destruction of the brucite chlorite layer and loss of water from the montmorillonite lattice. The total mass loss in the temperature range 505.0–733.6 ºC is 3.97 %, and the magnitude of the thermal effect is 63.67 J/g.

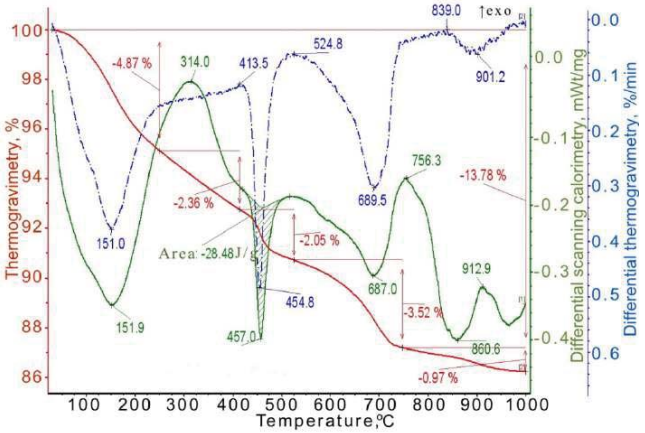

Figure 4. Curves of thermogravimetry, differential thermogravimetry and differential scanning calorimetry upon heating of a sample modified by polycarboxylate ether (composition No 2)

Bulanov, P.E., Ermilova, E.U., Mavliev, L.F. Structure and mineral composition of soil-cement with complex additive. Magazine of Civil Engineering. 2018. 83(7). Pp. 38–48. doi: 10.18720/MCE.83.4.

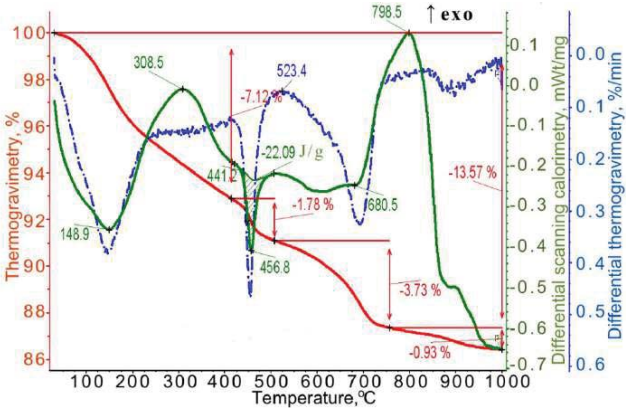

Figure 5. Curves of thermogravimetry, differential thermogravimetry and differential scanning calorimetry upon heating of a sample modified by complex hydrophobic-plasticizing additive (composition No 3)

In the temperature range 733.6–1000.0 ºC, in which the total weight loss was 0.60 %, there are small endothermic effects with the maximum at 769 ºC and 800 ºC, related to the decomposition of relict calcium carbonate and dehydration of the mica layer in chlorite, respectively. The exothermic effect at 916.1 ºC is due to the formation of spinel from the clay minerals present in the polymineral clay.

Thermal analysis of composition No 2 (figure 4) on the differential scanning calorimetry curve showed an endotherm at 151.9 °C, inherent dehydration of ettringite and low-basic hydrated calcium silicate. The total mass loss when sample No 2 is heated up to 250 °C is 4.87 %, and the mass loss in the temperature range 250–421 °C is 2.36 %. The endothermic effect on differential scanning calorimetry with the temperature maximum of 457.0 ºC and a loss of mass of 2.05 % in the temperature range 421–519 °C characterizes, basically, the decomposition of portlandite. The magnitude of the thermal effect is 28.48 J/g, which is 35.48 % less than the control composition No 1.

In the temperature range 519.0–756.3 ºC, the high endothermic effect with the maximum at 687 ºC is observed, characterized by the decomposition of calcium carbonate (composition No 2). Also on the differential scanning calorimetry with this temperature range, there are weak endothermic depressions associated with the removal of hydroxyl water from hydromica and hydroxyl water from kaolinite, the destruction of the brucite chlorite layer, and the loss of water from the montmorillonite lattice. The total weight loss in the temperature range 519.0–756.3 ºC was 3.5 %.

In the temperature range of 756.3–1000.0 ºC, in which the total weight loss was 0.97 %, an exothermic effect with the maximum at 847 ºC is observed, which is associated with the transition of a tobermorite gel of the type C-S-H(I) to ß-wollastonite. The exothermic effect at 916.1 ºC is associated with the formation of spinel. In general, when the sample is heated up to 1000 °C, the total weight loss is 13.78 %.

Figure 5 shows a thermogram of a sample modified by complex hydrophobic-plasticizing additive (composition No 3), the significant endothermic depression is observed at 148.9 °C, typical for the dehydration of ettringite and low-basic hydrated calcium silicate. The total weight loss in the temperature range 0–250 ºC is 4.78 %. The mass loss in the temperature range 250.0–421.0 ºC is equal to 2.34 %.

The endothermic effect with the temperature maximum of 456.8 ºC and a weight loss of 1.78 % in the temperature range 421–505 ºC is characterized mainly by the decompounding of portlandite. The magnitude of the thermal effect was 22.09 J/g, which is 49.95 % less compared to the control composition No 1 and 22.44 % less compared to sample No 2.

In the temperature range of 505.0–763.0 ºC, the endothermic effect characterizing the decompounding of calcium carbonate is observed. The total weight loss in the temperature range 505–763 ºC is 3.73 %.

In the range 763.0–1000.0 ºC, in which the total mass loss is 0.93 %, an exothermic effect at 901 ºC is observed, associated with the formation of spinel from the clay minerals present in the polymineral clay. In general, when the sample is heated up to 1000 °C, the total weight loss is 13.57 %.

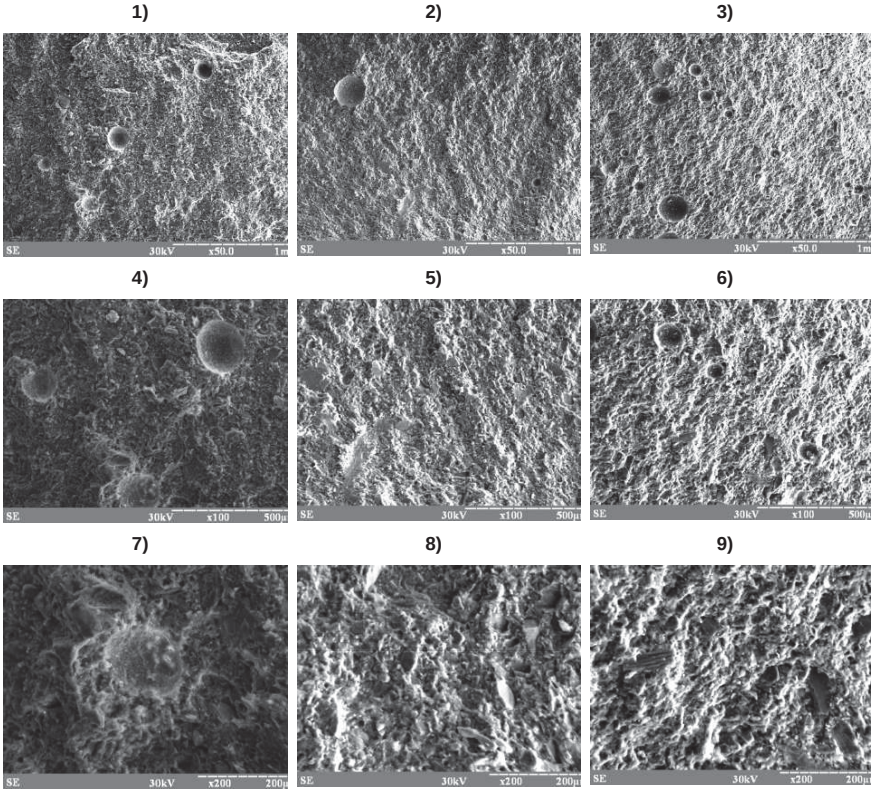

Figure 6 – Microstructure of the chips of soil-cement samples modified with polycarboxylate ether and complex hydrophobic-plasticizing additive: 1, 4, 7) control composition; 2, 5, 8) modified polycarboxylate ether; 3, 6, 9) modified complex hydrophobic-plasticizing additive; 1, 2, 3) increase in x50; 4, 5, 6) increase in x100; 7, 8, 9) an increase in x200

As can be seen from table 4, for all samples, unreacted minerals of clinker alite and belite are observed. At the same time, the introduction of polycarboxylate ether or complex hydrophobic-plasticizing additive leads to a decrease in the intensity of the peaks corresponding to the non-hydrated phases of the alite and the belite, which indicates an increase in the degree of hydration of the clinker minerals.

The content of portlandite is reduced in all compositions in comparison with the no-additive composition. Especially noticeable decrease in the amount of calcium hydroxide up to 2 times in composition No 3, that is, with complex hydrophobic-plasticizing additive. According to studies [19–21], polycarboxylate ether molecules are able to form metastable complexes with Ca^{2+} ions, which leads to a decrease in the basicity of hydrated silicate. On the other hand, when interacting with C_3A, they are able to be incorporated into the structure of hydrates formed with the formation of stable organomineral phases [22]. On the basis of which it can be concluded that Ca^{2+} ions of portlandite and calcium carbonate participate in the reaction with polycarboxylate ether to form other compounds that are not identified by X-ray diffraction pattern and differential scanning calorimetry.

The changes that occurred during the modification of the soil-cement from polycarboxylate ether or complex hydrophobic-plasticizing additive were confirmed in the analysis of the microstructure. Studies of

the microstructure of clayey soils strengthened with cement were carried out on samples aged 28 days. Figure 6 shows the results of the fracturing of clay soil samples strengthened with cement.

Table 4. Semiquantitative X-ray diffraction pattern analysis of soil-cement samples modified with polycarboxylate ether and complex hydrophobic-plasticizing additive

Name of mineral/phase	Amount of mineral/phase in the control composition, %	Amount of mineral/phase in composition with polycarboxylate ether, %	Amount of mineral/phase in the composition with the complex hydrophobic-plasticizing additive, %
Ettringite	-	8.90	7.70
C-S-H (I)	-	8.00	4.64
Alite, belite	10.43	6.68	7.62
Minerals of polymineral clay	71.79	68.96	73.02
Portlandite	13.01	7.46	7.02
Gypsum	4.77	-	-
Amorphous phase	38.10	46.00	44.20

In the control sample of soil-cement, a number of pronounced chaotic defects are mainly observed: in the form of separate particles, shells, strata, which break the solidity of the material, which reduces strength and increases drainage capacity. With the introduction of polycarboxylate ether or complex hydrophobic-plasticizing additive, a change in the microsurface is observed: a decrease in the number and size of shells and caverns, a transition to a more ordered dense structure.

In general, it can be noted that the cement grout with polycarboxylate ether or complex hydrophobic-plasticizing additive formed a dense structure with a pronounced overgrowth of the pores formed by gel-like hydrated calcium silicate, which in large quantities are densely formed on the minerals of the strengthened soil.

Thus, by means of electron-raster microscopy it was established that during the hydration of soil-cement, modified polycarboxylate ether or complex hydrophobic-plasticizing additive, a uniform distribution of hydration products in the volume of the composite is observed, which provides enhanced physical and technical properties.

4. Conclusions

1. The regularities of the effect of the complex hydrophobic-plasticizing additive based on polycarboxylate ether and octyltriethoxysilane on the formation of cement hydration products in a strengthened clayey soil are established. Changes in structure and composition include the following: the formation of a strong skeleton of the crystallization phase due to the increase in the number of hydrated new formation in the form of low-basic hydrated calcium silicate and ettringite, decrease in portlandite content, as well as an increase in the amount of amorphous phase (up to 16 %) in the form of tobermorite gel filling intercrystalline spaces. In soil-cement hydrated silicate calcium are formed in an amount of more than 4 % and ettringite in an amount of more than 7 %, the amount of portlandite reduced by 46 %.

2. It is established that as a result of modification of the complex hydrophobic-plasticizing admixture of soil-cement, a denser and homogeneous structure with a pronounced "overgrowth" of the pores formed by gel-like hydrated calcium silicate is formed, which are deposited in a large amount on the minerals of the strengthened soil.

3. The established changes in the composition and structure of soil-cement based on polymineral clay when introducing the complex hydrophobic-plasticizing additive studied explain the increase in its physical and technical properties.

References

1. Zhang, D., Zhou, C.-H., Lin, C.-X., Tong, D.-S., Yu, W.-H. Synthesis of clay minerals. Applied Clay Science. 2010. No. 50. Pp. 1–10.
2. Martin, R.T., Bailey, S.W., Eberl, D.D., Fanning, D.S., Guggenheim, S., Kodama, H., Pevear, D.R., Srodon, J., Wicks, F.J. Report of the clay minerals society

Литература

1. Zhang D., Zhou C.-H., Lin C.-X., Tong D.-S., Yu W.-H. Synthesis of clay minerals // Applied Clay Science. 2010. № 50. Pp. 1–10.
2. Martin R.T., Bailey S.W., Eberl D.D., Fanning D.S., Guggenheim S., Kodama H., Pevear D.R., Srodon J., Wicks F.J. Report of the clay minerals society

Буланов П.Е., Ермилова Е.Ю., Мавлиев Л.Ф. Структура и минеральный состав цементогрунта с комплексной добавкой // Инженерно-строительный журнал. 2018. № 7(83). С. 38–48.

nomenclature committee: revised classification of clay materials. Clays Clay Miner. 1991. 39(3). Pp. 333–335.

3. Vaccari, A. Preparation and catalytic properties of cationic and anionic clays. Applied Clay Science. 1998. 41(1-3). Pp. 53–71.
4. Carretero, M.I., Lagaly, G. Clays and health: an introduction. Applied Clay Science. 2007. No. 36. Pp. 1–3.
5. Choy, J.-H., Choi, S.-J., Oh, J.-M., Park, T. Clay minerals and layered double hydroxides for novel biological applications. Applied Clay Science. 2007. No. 36. Pp. 122–132.
6. Carretero, M.I. Clay minerals and their beneficial effects upon human health. A review. Applied Clay Science. 2002. Pp. 155–163.
7. Venkatarama Reddy, B.V., Latha, M.S. Retrieving clay minerals from stabilised soil compacts. Applied Clay Science. 2014. No. 101. Pp. 362–368.
8. Mavliev, L., Bulanov, P., Vdovin, E., Zaharov, V., Gimazov, A. Road soil cement with complex additives based on organosilicon compounds and electrolytes. ZKG: ZEMENT-KALK-GIPS INTERNATIONAL. 2016. Vol. 69. No 9. Pp. 49–54.
9. McDowell, C. Stabilization of soils with lime, lime/fly ash and other lime reactive materials. Highway Research Board. 1959. No. 231. Pp. 60–66.
10. Chen, H., Wang, Q. The behavior of organic matter in the process of soft soil stabilization using cement. Bulletin of Engineering Geology and The Environment. 2006. 65(4). Pp. 445–448.
11. Sokolov, V.N., Osipov, V.I., Rumyantseva, N.A. Regularities of structure formation in clay sediments. Global view of Engineering Geology and the Environment – Proceedings of the International Symposium and 9th Asian Regional Conference of IAEG. London: CRC PRESS-TAYLOR & FRANCIS GROUP. 2013. Pp. 739–742.
12. Knatko, V.M., Shcherbakova, E.V., Knatko, M.V. Elementy nanotekhnologiy v kompleksnykh metodakh ukrepleniya glinistykh gruntov i proizvodstve alyumosilikatnykh gidroizolyatsionnykh materialov [Elements of nanotechnologies in complex methods of clay ground consolidation and production of alum silicate hydroisolating material]. Vestnik Sankt-Peterburgskogo Universiteta. 2008. Vol. 7. No. 4. Pp. 82–85. (rus)
13. Balasubramaniam, A.S., Buessucesco, B., Yan–Nam Erwin Oh, Bolton, M.W., Bergado, D.T., Lorenzo, G.A. Strength degradation and critical state seeking behaviour of lime treated soft clay. Deep Mixing. 2005. No. 5. Pp. 35–40.
14. Bergado, D.T., Anderson, L.R., Miura, N., Balasubramaniam, A.S. Improvement of soft ground in lowland and other environments. ASCE Reston. 1996. 427 p.
15. Xiao, H.W., Lee, F.H. Curing time effect on behavior of cement treated marine clay. Proceedings of The National Academy of Sciences. 2008. No. 33. Pp. 71–78.
16. Bulanov, P.E., Vdovin, Ye.A., Mavliyev, L.F. Vliyaniye plastifitsiruyushchikh dobavok na fiziko-mekhanicheskiye svoystva tsementogrunta dorozhnogo naznacheniya [Influence of plasticizers on physical and mechanical properties of soil-cement for road purpose]. Izvestiya KGASU. 2015. No. 1(31). Pp. 160–164. (rus)
17. Bulanov, P.E., Mavliev, L.F., Vdovin, E.A., Yagund, E.M. The interaction between the kaolinite or bentonite clay and plasticizing surface-active agents. Magazine of Civil Engineering. 2017. 75(7). Pp. 173–181. doi: 10.18720/MCE.75.17
18. Bulanov, P.E., Vdovin, E.A., Mavliev, L.F., Stroganov, V.F. Optimizatsiya sostava i issledovaniye vliyaniya kompleksnoy gidrofobno-plastifitsiruyushchey dobavki na fiziko-tekhnicheskiye svoystva, ukreplennykh

nomenclature committee: revised classification of clay materials // Clays Clay Miner. 1991. № 3(39). Pp. 333–335.

3. Vaccari A. Preparation and catalytic properties of cationic and anionic clays // Applied Clay Science. 1998. № 1-3(41). Pp. 53–71.
4. Carretero M.I., Lagaly G. Clays and health: an introduction // Applied Clay Science. 2007. № 36. Pp. 1–3.
5. Choy. J.-H., Choi. S.-J., Oh. J.-M., Park. T. Clay minerals and layered double hydroxides for novel biological applications // Applied Clay Science. 2007. № 36. Pp. 122–132.
6. Carretero. M.I. Clay minerals and their beneficial effects upon human health. A review // Applied Clay Science. 2002. № 21. Pp. 155–163.
7. Venkatarama Reddy B.V., Latha M.S. Retrieving clay minerals from stabilised soil compacts // Applied Clay Science. 2014. № 101. Pp. 362–368.
8. Mavliev L., Bulanov P., Vdovin E., Zaharov V., Gimazov A. Road soil cement with complex additives based on organosilicon compounds and electrolytes // ZKG: ZEMENT-KALK-GIPS INTERNATIONAL. 2016. Vol. 69. № 9. Pp. 49–54.
9. McDowell C. Stabilization of soils with lime, lime/fly ash and other lime reactive materials // Highway Research Board. 1959. № 231. Pp. 60–66.
10. Chen H., Wang Q. The behavior of organic matter in the process of soft soil stabilization using cement // Bulletin of Engineering Geology and The Environment. 2006. № 4(65). Pp. 445–448.
11. Sokolov V.N., Osipov V.I., Rumyantseva N.A. Regularities of structure formation in clay sediments // Global view of Engineering Geology and the Environment – Proceedings of the International Symposium and 9th Asian Regional Conference of IAEG. London: CRC PRESS-TAYLOR & FRANCIS GROUP, 2013. Pp. 739–742.
12. Кнатько В.М., Щербакова Е.В., Кнатько М.В. Элементы нанотехнологий в комплексных методах укрепления глинистых грунтов и производстве алюмосиликатных гидроизоляционных материалов // Вестник Санкт-Петербургского университета. 2008. Сер. 7. № 4. С. 82–85.
13. Balasubramaniam A.S., Buessucesco B., Yan–Nam Erwin Oh, Bolton M.W., Bergado D.T., Lorenzo G.A. Strength degradation and critical state seeking behaviour of lime treated soft clay // Deep Mixing. 2005. № 5. Pp. 35–40.
14. Bergado D.T., Anderson L.R., Miura N., Balasubramaniam A.S. Improvement of soft ground in lowland and other environments // ASCE Reston. 1996. 427 p.
15. Xiao H.W., Lee F.H. Curing time effect on behavior of cement treated marine clay // Proceedings of The National Academy of Sciences. 2008. № 33. Pp. 71–78.
16. Буланов П.Е., Мавлиев Л.Ф., Вдовин Е.А., Строганов В.Ф., Асадуллина А.Р., Сафин Д.Р. Влияние пластифицирующих добавок различной химической основы на физико-технические свойства глинистых грунтов, укрепленных портландцементом // Известия КГАСУ. 2017. № 4(42). С. 384–391.
17. Буланов П.Е., Мавлиев Л.Ф., Вдовин Е.А., Ягунд Э.М. Взаимодействие каолиновой и бентонитовой глин с пластифицирующими поверхностно-активными веществами // Инженерно-строительный журнал. 2017. № 7(75). С. 171–179.
18. Буланов П.Е., Вдовин Е.А., Мавлиев Л.Ф., Строганов В.Ф. Оптимизация состава и исследование влияния комплексной гидрофобно-пластифицирующей добавки на физико-технические свойства, укрепленных портландцементом, глинистых грунтов // Известия КГАСУ. 2017. № 4(42). С. 376–383.
19. Koizumi K., Umemura Y., Tsuyuki N. Effects of Chemical Admixtures on the Silicate Structure of Hydrated Portland

Bulanov, P.E., Ermilova, E.U., Mavliev, L.F. Structure and mineral composition of soil-cement with complex additive. Magazine of Civil Engineering. 2018. 83(7). Pp. 38–48. doi: 10.18720/MCE.83.4.

portlandtsementom, glinistykh gruntov [Optimization of the composition of a complex hydrophobic-plasticizing additive and investigation of its effect on the physical and technical properties of clay soils reinforced with Portland cement]. Izvestiya KGASU. 2017. No. 4(42). Pp. 376–383. (rus)

19. Koizumi, K., Umemura, Y., Tsuyuki, N. Effects of Chemical Admixtures on the Silicate Structure of Hydrated Portland Cement. Proceedings of the 12th International Congress on the Chemistry of Cement. Montreal. 2007. Pp. 64–71.
20. Plank, J., Keller, H., Andres, P. Novel organo-mineral phases obtained by Interaction of maleicanhydrite-allyl ether copolymers into layered calcium aluminum hydrates. Inorganic Chemical Acta. 2006. No. 359. Pp. 4901–4908.
21. Plank, J., Sakai, E., Miao, C.W., Yu, C., Hong, J.X. Chemical admixtures – chemistry, applications and their impact on concrete microstructure and durability. Cement and Concrete Research. 2015. Vol. 78. Pp. 81–99.
22. Gubaydullina, A.M., Lygina, T.Z., Khalitova, A.N., Panina, A.A. Issledovaniye protsessov gidratatsii i tverdeniya portlandtsementa metodami termicheskogo analiza [Investigation of hydration and hardening of Portland cement using thermal analysis methods]. Vestnik Kazanskogo tekhnologicheskogo universiteta. 2012. No. 15. Pp. 15–17. (rus)

Cement // Proceedings of the 12th International Congress on the Chemistry of Cement. Montreal. 2007. Pp. 64–71.

20. Plank J., Keller H., Andres P. Novel organo-mineral phases obtained by Interaction of maleicanhydrite-allyl ether copolymers into layered calcium aluminum hydrates // Inorganic Chemical Acta. 2006. № 359. Pp. 4901–4908.
21. Plank J., Sakai E., Miao C.W., Yu C., Hong J.X. Chemical admixtures – chemistry, applications and their impact on concrete microstructure and durability // Cement and Concrete Research. 2015. Vol. 78. Pp. 81–99.
22. Губайдуллина А.М., Лыгина Т.З., Халитова А.Н., Панина А.А. Исследование процессов гидратации и твердения портландцемента методами термического анализа // Вестник Казанского технологического университета. 2012. № 15. С. 15–17.

Pavel Bulanov,*
+7(952)044-43-48;
pavel.bulanov1991@yandex.ru

Elizaveta Ermilova,
+7(953)482-33-39; lizabeta_91@list.ru

Lenar Mavliev,
+7(904)668-76-64; lenarmavliev@yandex.ru

Павел Ефимович Буланов,*
+7(952)044-43-48;
эл. почта: pavel.bulanov1991@yandex.ru

Елизавета Юрьевна Ермилова,
+7(953)482-33-39;
эл. почта: lizabeta_91@list.ru

Ленар Фидаесович Мавлиев,
+7(904)668-76-64;
эл. почта: lenarmavliev@yandex.ru

Буланов П.Е., Ермилова Е.Ю., Мавлиев Л.Ф. Структура и минеральный состав цементогрунта с комплексной добавкой // Инженерно-строительный журнал. 2018. № 7(83). С. 38–48.

doi: 10.18720/MCE.83.5

The stress state of a tank shell in the group under wind load

Напряжения от ветровой нагрузки в стенке резервуара, находящегося в группе

V.P. Mushchanov*,
H.V. Zubenko,
M.N. Tsepliaev,
Donbas National Academy of Civil Engineering and Architecture, Makiyivka, Donetsk region, Ukraine

Д-р техн. наук, проректор по научной рабооте, заведующий кафедрой В.Ф. Мущанов*,
ассистент А.В. Зубенко,
аспирант М.Н. Цепляев,
Донбасская национальная академия строительства и архитектуры, Макеевка, Донецкая область, Украина

Key words: wind tunnel; aerodynamic coefficient; vertical cylindrical tank

Ключевые слова: аэродинамическая труба; аэродинамический коэффициент; вертикальный цилиндрический резервуар

Abstract. The distribution of the wind flow has been studied and its effect on the stressed state of the shell of a steel vertical cylindrical tank. Variants of wind pressure were considered for one tank and for a group of tanks. Aerodynamic coefficients are obtained for the considered variants in the SolidWorks software package. A physical experiment on a reduced tank model in a wind tunnel was conducted to verify the coefficients obtained. The stresses in the tank shell were determined by the finite element method using the SCADOffice calculation complex. The result revealed differences normative distribution of wind pressure from the pilot for single tank and located in the band. The most unfavorable version of the distribution of wind pressure for the tank located in the group was determined. The stress-strain state of the tank shell is compared under the normative and experimental wind load for the most unfavorable variant.

Аннотация. Изучено распределение ветрового потока и его влияние на напряженное состояние стенки стального вертикального цилиндрического резервуара. Рассматривались варианты ветрового давления на один резервуар и на группу резервуаров. Аэродинамические коэффициенты для рассматриваемых вариантов получены в программном комплексе SolidWorks. Для верификации полученных коэффициентов был проведён физический эксперимент на уменьшенной модели резервуара в аэродинамической трубе. Напряжения в стенке резервуара определялись методом конечных элементов при помощи расчётного комплекса SCADOffice. В результате выявлены отличия нормативного распределения ветрового давления от экспериментального для одиночного резервуара и находящегося в группе. Определён наиболее неблагоприятный вариант распределения ветрового давления для резервуара, находящегося в группе. Проведено сравнение напряженно-деформированного состояния стенки резервуара при нормативной и экспериментальной ветровой нагрузке для наиболее невыгодного варианта.

1. Introduction

To calculate wind loading on buildings there are several ways of defining aerodynamic characteristics with the use of analytical and experimental data. Accurate analytical decisions in the constructional aerodynamics embrace very limited tasking, because it is very difficult to obtain a clear mathematical model for aerodynamic processes, and that is why in most cases for new and complicated structures the research is conducted in the wind tube. This research is a reliable remedy for the process study of airflow of buildings, structures and their complexes. The computer simulation of airflow and defining basic aerodynamic characteristics for buildings and structures must be mentioned as one of the developing methods.

The existing methods of wind load simulation on buildings and structures with the use of aerodynamic formulae were developed in the early 70-s in CNIISK named after Kucherenko on the base of works of A. Davenport and A. Vaisand realized in the SNiP II-6-74 [1]. In 1985 at publishing SNiP 2.01.07-85 [2] there were simplified the expressions describing the dynamic reaction of structures at wind effect.

Мущанов В.Ф., Зубенко А.В., Цепляев М.Н. Напряжения от ветровой нагрузки в стенке резервуара, находящегося в группе // Инженерно-строительный журнал. 2018. № 7(83). С. 49–62.

The basic theoretical information on architectural-building aerodynamics, methods of defining wind loads on buildings and structures are represented in the works of J. D. Holmes, O. I. Poddaeva, A.S. Kubenin [3, 4]. The works of Ye. V. Gorokhov, M. A. Berezin [5, 6], are devoted to defining wind effects on buildings and structures in the wind tube. The works of R.I. Kinash, Yasushi Uematsu, Y.Zhao, Y.Zhang [7–12] describe the experimental simulation of interaction between the wind flow and engineering structures in the wind tube.

The results of model experimental investigations of wind and snow loads on technically sophisticated large-span coverings with complex geometry are represented in the books of Ye.V. Gorokhov [13] and P.G. Eremeev [14]. Verification results and methods of computer simulation of wind influence on high-rise buildings are presented in the publications of S.A. Isaev, P.A. Vatin, P.A. Baranov [15–17].

The investigations of Ya. Jumpei, A. Moshida, Y. Tominaga, T. Shirasava [18–21] and others are devoted to the numerical simulation of wind effects.

In spite of numerous works in the field of design, construction and exploitation of tanks some problems connected with the estimation and tank efficiency are still unsolved. Among them it is necessary to mention the following ones:

- loads and effects on vertical cylindrical tanks for new types of roof coverings including slack membranous coverings have been understudied;
- loads and effects on vertical cylindrical tanks within a group, in spite of the fact, that in most oil storage tanks such composition is predominant, have been understudied.

2. Methods

General methods used in the performance of all problems given in the report are:

- calculus of approximations of constructional mechanics (method of finite-elements – MFE) with the use of universal program complexes “SCAD Office”;
- method of physical simulation with the use of the similarity theory;
- methods of mathematical statistics (while processing the results of experimental and numerical simulation).

Additionally used calculus of approximations of finite volumes (MFV) of simulation of turbulent flows with the use of program complex “SolidWorks Flow Simulation”.

3. Results and Discussion

Taking into account the complexity, multi-faceted essence and volatility of results of numerical simulation in the environment of SolidWorks Flow Simulation of flow-around of the wind flow of the 4 tanks group, it has been performed the experiment in the wind tube of the Donbass National Academy of Civil Engineering and Architecture MAT-1.

To define Reynolds number that is a similarity criterion during aerodynamic experiments, the test experiment has been conducted in the wind tube for the model of tank with a flat roof.

To meet the requirements of the surface area of the projection of the experimental model to the surface area of the cross section of a work part of the aerodynamic tube ratio it must not exceed 3 % [5]. To take into account the actual size of building (according to the requirements of VBN the distance between tanks must be 0.5D, so, while composing the group of 4 tanks with the volume of 20 000m³ the total length is 100 m (see Figure) and peculiarities of the work part arrangement of the wind tube MAT- 1 DonNACEA with the width 1 м, it has been chosen the model scale M = 1:320.

According to the research plan of the wind tube MAT-1 DonNACEA the provision has been made for defining coefficients of the wind pressure (C_{pi}) in 49 supporting points on the model of the tank (Figures 1, 2). During investigations it has been defined the dependence $C_{pi}=f(\beta)$ within the limits β = 0…360˚ in increments of $\Delta\beta$ = 10˚. The results have been represented by 6 areas of activity (β = 0˚, 45˚, 90˚, 150˚, 180˚, 270˚).

Figure 1 and Figure 4 demonstrate a physical model of a tank with a rounded spherical roof for which the investigation has been performed.

In basic data of high-speed wind flow characteristics the value of Reynolds number is defined as:

$$\mathrm{Re} = \frac{L \cdot U(z_e)}{\nu}, \quad (1)$$

where L is a diameter;

ν is a kinematic air viscosity, ν = 1.5·10^{-5} m^2/s;

$U(z_e)$ is a peack height of the wind speed, $U(z_e)$ = 14.9 m/s.

$Re \approx 1.28 \cdot 10^5$. is a Reynolds number

To estimate the drag of high-speed flow of wind it has been done the expulsion: 1) a model with a flat roof for a physical model with drain ports (Figure 2a); 2) for a model fixed on the triple-component aerodynamic tensometric balance (Figure 2b, 2c [22]); 3) the numerical simulation in SolidWorks Flow Simulation (Figure 2d).

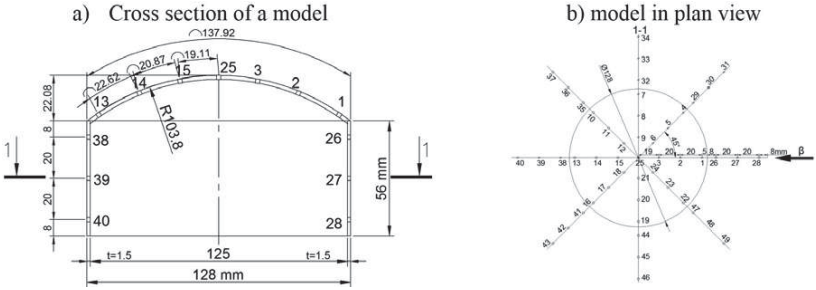

Figure 1. Scheme of the Tested Model of VCT with the Arrangements of the Horizontal Points

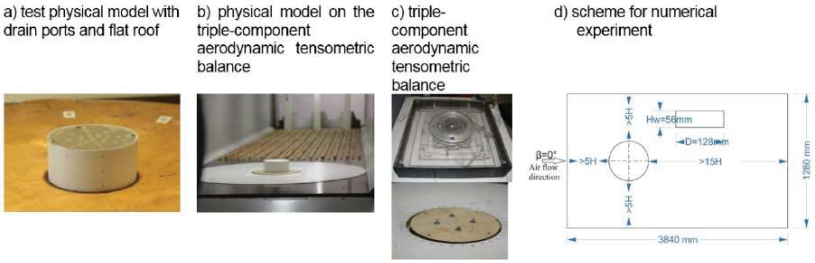

Figure 2. Scheme of a Test Physical Model of VCT with a Flat Roof at Determining the Drag Coefficient

Based on the research results for the model with a flat roof according to three techniques a graph of variation of drag coefficient with Reynolds number is made.

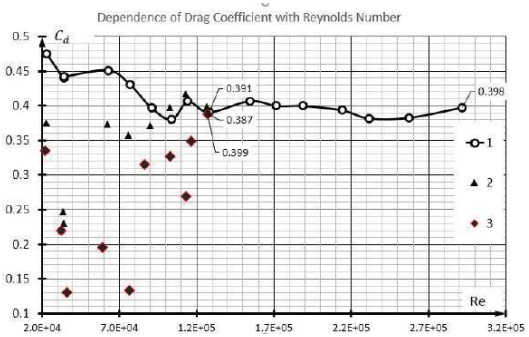

Figure 3. Dependence of Drag Coefficient with Reynolds Number

Мущанов В.Ф., Зубенко А.В., Цепляев М.Н. Напряжения от ветровой нагрузки в стенке резервуара, находящегося в группе // Инженерно-строительный журнал. 2018. № 7(83). С. 49–62.

Based on the results obtained by 3 techniques it was decided to conduct further experiment at Reynolds numbers ($Re \approx 1.28 \cdot 10^5$)

where 1is a graph made on the values obtained in numerical simulation.

2 is a graph made on the values obtained in experimental simulation in wind tunnel for the test drained model with a flat roof

3 is a graph made on the values obtained in experimental simulations in wind tunnel for the test model with a flat roof set on the aerodynamic tensometric balance.

In Figure 4 the scheme with sizes of arrangement and models installations on turntable with calibration is shown.

Each cycle of the experimental purge (the given angle of attack, speed of wind flow) consisted of the following stages: start of wind wheel with the sixty-second normalization of speed of wind flow, measurement of static air pressure, its transformation to an electric signal, processing and display of the received results with the use of automatic highly productive information technology system “SCADA”. It consists of a pneumatic commutator with pressure units, the high-performance computer with the system of transformation of an analog signal in digital and also the corresponding switching equipment and electrical power supply. One polling cycle takes 1sec. During the cycle of measurements each of drainage points was read twelve times. In further processing the corresponding primary signals on each drainage point were averaged. After each turn of the examined model on $\Delta\beta = 10$ ° the inquiry of the signal from each drainage point at zero speed of airflow was made, the so-called "0" was maintained, then the wind tunnel was started, and the speed of air was brought up to speed about 15 m/s, then speed was maintained not less than 60 s and drainage points were also read.

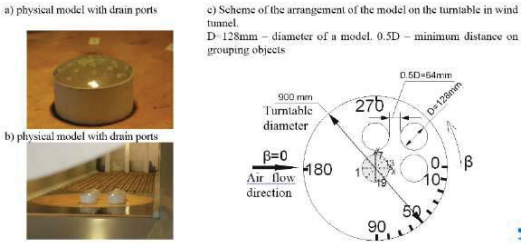

Figure 4. Arrangement of the Group of Vertical Cylindrical Tanks

Distribution of the aerodynamic coefficients on the shell of the VCT model for a single VCT with a spherical convex up roof, consisting of the group of 4 objects. The values for the 25 mm mark from the bottom of the model are given.

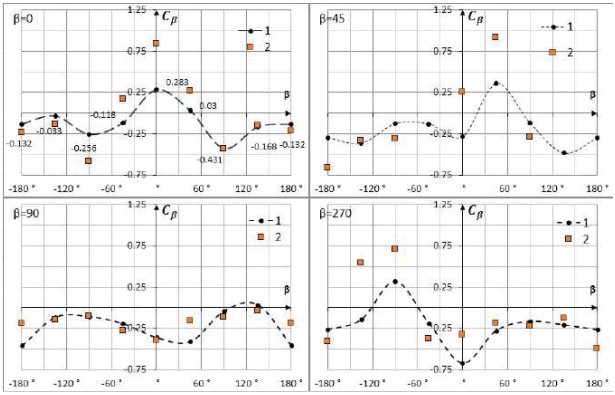

Figure 5. Comparison of Distribution of Aerodynamic Coefficients on the Tank Shell in the Group with a Convex up Roof (an angle of attack of wind flow β=0-270 °)

Mushchanov, V.P., Zubenko, H.V., Tsepliaev, M.N. The stress state of a tank shell in the group under wind load. Magazine of Civil Engineering. 2018. 83(7). Pp. 49–62. doi: 10.18720/MCE.83.5.

where 1– the values obtained during the experiment in wind tunnel;

2 – the values obtained in numerical simulation in SolidWorks Flow Simulation.

Analyzing the obtained values we can conclude that the obtained results are qualitatively convergent.

According to the obtained data of the comparative analysis of experimental, analytical and normative data the analytical model for calculation for single and VTC groups in Solid Works Flow Simulation for numerical simulation of aerodynamic processes was created. The main feature of this procedure was the determination of the size of the computer simulation of the component. A methodical approach providing a correct display of the physical processes of flow around the tank shell by wind flow (comparison of the results of experimental data and numerical studies ensure convergence within 15% for the main design cross-sections) is proposed.

3.1. Statement of a Problem of Numerical Experiment:

- to obtain the values of the aerodynamic coefficients for the separately standing vertical cylindrical tank represented as a circular cylinder with given initial geometric and thermodynamic parameters on a scale of 1:1 and compare it with the current normative documents, namely Eurocode [23];
- according to the obtained results in the form of coefficients of wind pressure on the shell of the vertical cylindrical tank to compare with the experimental data given in [22];
- to make final element model in the program complex SCAD Office c and to analyze stressed state for the isolated tank at wind load determined by a technique Eurocodes [23] and the load received as a result of numerical simulation in the program complex SolidWorks Flow Simulation
- providing admissible convergence within 10-15% to execute calculation for the group of 4 vertical cylindrical tanks, to analyze stressed state for the tank which is affected by the most adverse load in the group.

To solve the problems formulated above, verification calculation for a VCT model in the SolidWorks Flow Simulations software package was performed, the results of which are given in the article.

Before determining the wind effect by means of computer simulation it is necessary to define all the variables which satisfy the purposes of this calculation which can be compared with the experiment.

3.2. The Size of the Computational Domain

From the experience of the research in wind tunnels it is considered that a structure with height H affects the distance to almost 10H. And as the test calculations of the Japanese Institute of Architecture show [18, 20, 24, 25], the size of the computational vertical area for isolated structures should be at least 5H. When examining a group of objects, it is recommended to use a factor blocking, which is equal to the cross-sectional area ratio of the structure to the cross-sectional area of the computational area, the coefficient should not exceed 3 %. In our case, for the group with building height of 24.89 m ≈ 25 the percentage of blocking is 2.09 %. Width of the calculated area must also be set so that the blocking factor is less than 3 %. The distance along the flow to the structure must be at least 5H. And the distance behind the structure should be ≥ 15H. The following figure shows the domain scheme.

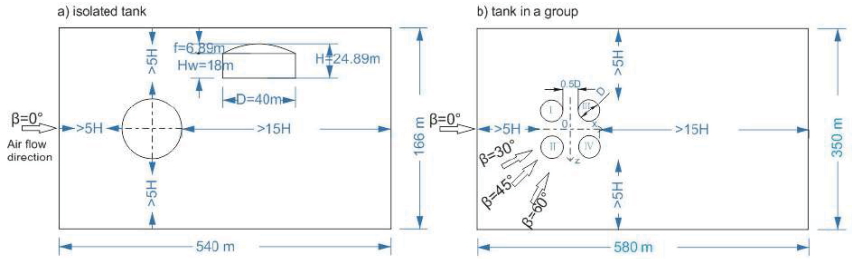

Figure 6. Size of the Calculated Area for the Isolated Tank and in the Group of 4 Objects

3.3. The Choice of Boundary and Initial Conditions

The profile of the average speed on the input is usually obtained in accordance with the requirements of normative documents. For our research, we took the profile of the average velocity $v_m(z)$, the turbulence intensity $I_v(z)$, the integral turbulence scale $L(z)$ according to formulas (8, 7, 12) according to Eurocode standards, because of the norms of Ukraine [26] and Russia [27], the energy of velocity pulsations is described by the Davenport spectrum, which does not take into account the dependence of the energy of turbulent wind pulsations on height and the integral longitudinal scale of turbulence assumes a constant value $L_u(z)$ = 1200 m, the intensity does not appear explicitly in turbulence.

We have followed the recommendations of A. Moshida, Y. Tominaga [18] from the Japanese Institute of Architecture when specifying the sizes of the finite elements mesh to solve the CFD tasks. The FE mesh resolution should be 1/10 from the lower structure in the group (approximately 0.5- 5m).

The FE meshes ratio for sequential mesh systems should not exceed 3.4 [28].

The verification analysis in three-dimensional view of a test model (Figure 1) for Reynolds number based on the wind-tunnel testing has been made to determine the mesh size in CFD.

Figures 7 and 8 illustrate the comparison graphs of aerodynamic factors for the shell of both an isolated tank and a tank in the group.

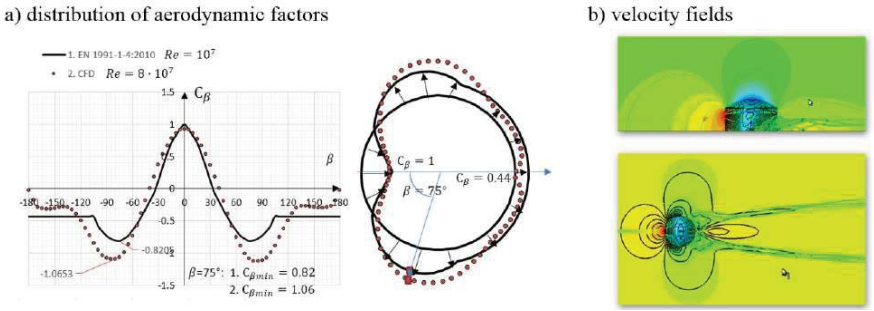

Figure 7. Comparison of Aerodynamic Factors Graphs for an Isolated Tank

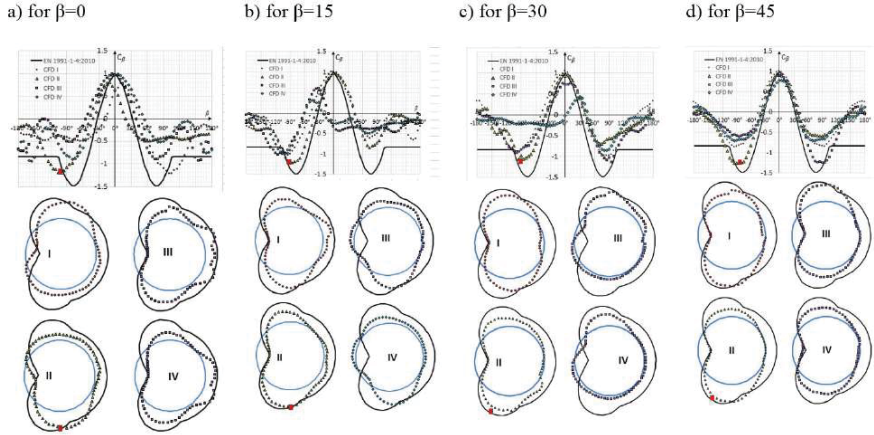

Figure 8. Comparison of Aerodynamic Factors Graphs for a Tank in the Group

The comparison of the obtained values of aerodynamic factors for an isolated vertical cylindrical tank presented in the form of a circular cylinder with preset initial geometrical and thermal properties in full scale (Eurocodes norms) has shown that they differ greatly in negative pressure environment by 50 %.

The analysis of the obtained aerodynamic factors for a tank in the group has revealed the most negative effect of the wind flow at the angle of attack of 45° for tank number II (see Figure 6).

3.4. Simulation of Finite Elements Model of a Tank in SCAD Office

The values of the wind load on the isolated tank and the tanks in the group are determined by means of SolidWorks Flow Simulation. Nevertheless, it is not available to assess the strain-stress state of the tanks resulting from the wind load by means of this program. It is a good practice to apply the finite elements method to assess the strain-stress state of the tanks. So far as there is little scope for a designer to use some program, this paper presents the setting of an actual wind load distribution by means of SCAD Office, the most available software system in CIS states.

We shall consider the wind load distribution on the shell of a vertical cylindrical tank in the following instances:

- the actual wind load distribution profile according to Eurocodes [23];
- the wind load on the isolated tank and the tanks in group based on the results of numerical simulation.

3.5. Parameters of a Tank FE Model

In numerical simulation in SolidWorks Flow Simulation the dimensions of tanks have been assumed according to the type design No. 704-1-70 in the volume of 20 000 m^3 [29]. Therefore, the finite element model of a tank conforming to the type design dimensions has been made. The bottom is fixed rigidly in the entire area, the shell of the tank is hinged to the bottom, the support ring of the roof is assigned in parameters in the form of a rod having computed characteristics, the elements of a ribbed and circular dome are also assigned by the rods. The thickness of rings of the shells, bottom and plate are preset according to the type design [29]. The size of the finite element is set to 250 x 250 mm. With the further size reduction of FE the accuracy increases insignificantly, whereas both the complexity of designing and load setting increase greatly. Thus, the shell of a tank is to consist of 36072 finite elements.

It is impossible to set non-linear load variations on a curved surface by means of the known quantity of load values for different points in SCAD system. It means that in order to set the wind load on tank's curved surface, we have to calculate manually and set the load on each finite element separately. So far as the tank model consists of more than 96000 FE, it could take a few days to specify the wind load. The method of load specifying by means of a text file can be used as an alternative. The procedure for specifying the actual profile of wind load on the similar tank is described in the paper [30], for this reason we shall use the excerpts from it in the given paper, the process will not be detailed.

3.6. Determining the Design Load Based on the Results of Numerical Simulation

Profiles of wind load on the isolated tank and the tank within the group obtained by means of SolidWorks Flow Simulation have a complicated form. To transfer the given load on each FE, the table of load values on vertical cylindrical tank shells depending on design point location over the height and length of the circle has been formed. The vertical pitch equals 1m, the circumference pitch is 2° (0.696 m). Intermediate values are determined by double linear interpolation in MS Office Excel by means of macros. An example of the table for an isolated tank is given below (Table 1).

Table 1. Values of Wind Load on the Shell of an Isolated Tank

		Height of the Design Point, m							
		0.01	**1**	**2**	**…**	**15**	**16**	**17**	**17.9**
Circumference Pitch 2° =0.696 м	**0**	−336.985	602.378	554.547	…	847.6	791	628.4	−824
	0.696	−256.211	602.428	552.147	⋯	853.8	798.3	636.5	−820
	1.392	−266.838	602.342	544.477	⋯	847.6	792.9	644.5	−815
	…	…	…	…	…	…	…	…	…
	123.17	123.86	−537.288	602.8	⋯	834.11	779.53	632.56	−811.146
	123.86	124.56	−442.437	602.8	⋯	847.756	793.048	644.333	−815.617
	124.56	125.54	−336.985	602.4	⋯	853.772	798.247	636.201	−820.177
	125.35	123.86	−537.288	602.8	…	847.609	790.968	628.39	−823.84

Мущанов В.Ф., Зубенко А.В., Цепляев М.Н. Напряжения от ветровой нагрузки в стенке резервуара, находящегося в группе // Инженерно-строительный журнал. 2018. № 7(83). С. 49–62.

Similar tables have been made for either of four tanks in the group at different angles of attack. For further strain-stress state analysis of tanks in the group the vertical cylindrical tank No. 2 (Figure 6) at the angles of attack of 0 and 45 degrees has been chosen based on comparison results of the tables. At these angles the wall of the vertical cylindrical tank No. 2 is affected by the most distinct wind load profile in comparison to that one affecting the isolated tank.

Further on, three tables for determining the wind load on each finite element are made in MS Office Excel for the next task in SCAD:

- the wind load on the isolated tank;
- the wind load on tank No. 2 in the group (angle of attack is 0°);
- the wind load on tank No. 2 in the group (angle of attack is 45°).

Since the concept for such tables is absolutely identical, below is given an example of a table segment for one of the cases – the wind load on the isolated tank (Table 2).

Table 2. Determining the Wind Load on each FE of the Shell of the Isolated VCT

No. of element	z, m	$C_{e(z)}$	Arc length, m	W_e, kN/m^2	W_e* $C_{e(z)}$, kN/m^2	Type of load	Direction		Load value: No. of element		
1	2	3	4	5	6	7	8	9	10	11	12
1	0.25	0.974	0.125	−0.207	−0.201	6	3		−0.201:1		/
2	0.25	0.974	0.376	−1.813	−0.177	6	3		−0.177:2		/
…	…	…	…	…	…	…	…	…	…	…	…
36071	17.88	3.32	125.29	−0.783	−2.598	6	3		−2.598:36071		/
36072	17.88	3.32	125.54	−0.784	−2.6	6	3		−2.6:36072		/

Notes to the Table:

column 4 – the length of an arc from the 1-st FE till the design one over the circle length, m;

column 5 – the value of wind load regardless of $C_{e(z)}$ factor, being defined by means of double interpolation according to Table 5inMSOfficeExcel;

column 6 – the design value of wind load.

3.7. Specifying the Load by Means of a Text File

Wind loading procedure by means of a text file is described in full detail in the paper [30]. The principle of method consists in editing the file of a tank model, created in SCAD and saved in the form of a text. In a text file the designation of the load is entered manually, the parameters and values of the load for each element are copied. Thus, columns 7-12 and lines 1-36072 of Table 3 are used for the wind load on the isolated tank. To display the results of specifying the actual wind load profile, below are given two typical cross-sections of the wall (stacked to the bottom and the roof) made transversely (in the middle of the wall height) and length wise for four design diagrams under consideration (Figure 9–12):

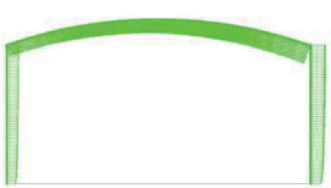

a) longitudinal cross-section along the height of the vertical steel tank

b) transverse cross-section along the height of the vertical steel tank

Figure 9. Wind Load in SCAD – Wind Load according to Eurocodes

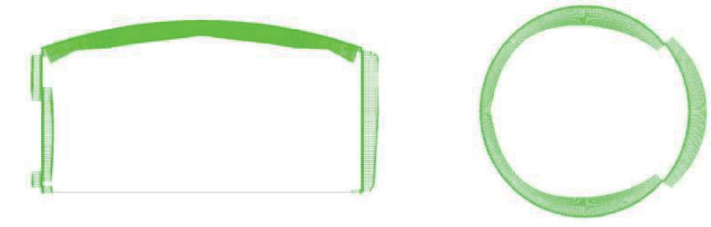

a) longitudinal cross-section along the height of the vertical steel tank

b) transverse cross-section along the height of the vertical steel tank

Figure 10. Wind Load in SCAD – Experimental Wind Load on Isolated Tank

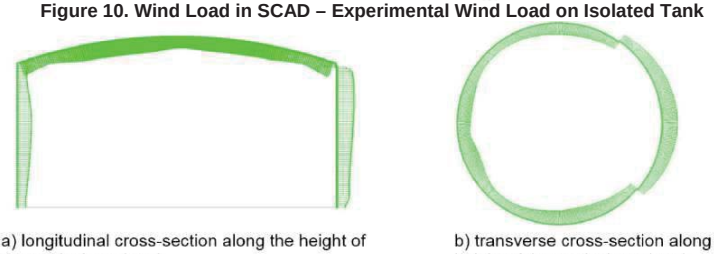

a) longitudinal cross-section along the height of the vertical steel tank

b) transverse cross-section along the height of the vertical steel tank

Figure 11. Wind Load in SCAD – Experimental Wind Load on Tank No. 2 in the Group (Wind 0°)

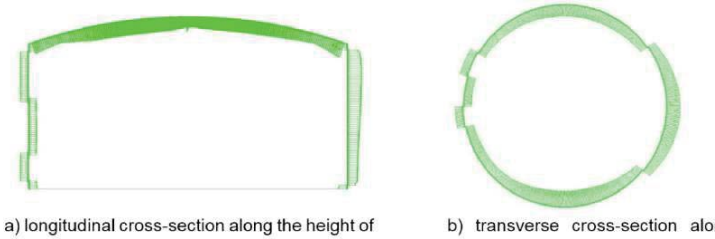

a) longitudinal cross-section along the height of the vertical steel tank

b) transverse cross-section along the height of the vertical steel tank

Figure 12. Wind Load in SCAD – Experimental Wind Load on Tank No. 2 in the Group (Wind 45°)

So far as the wind load on the vertical cylindrical tank in the group has less peak values at the angle of attack of 0° than at the angle of 45° and coincides greatly with the wind load on the isolated tank, we shall use three design situations to make a strain-stress state analysis of the tanks:

- the wind load according to Eurocodes [23];
- the wind load on the isolated tank based on the results of numerical simulation;
- the wind load on tank No. 2 from the group of four tanks at the angle of 45°.

3.8. Finite Element Analysis of the Shell Strain-Stress State at the Wind Load on Isolated Vertical Cylindrical Tank According to Eurocodes and Numerical Simulation Results

The combination of the wind load and own weight with unity combination factors (1 x Wind + 1 x Own Weight) has been used to compare the strain-stress state of the tank at the wind load obtained according to Eurocodes and the load obtained by numerical simulation results. To give an outline of the strain-stress state of the vertical cylindrical tank's shell resulting from the given loads, below is given the distribution of equivalent stresses in the tank's shell according to maximum distortion energy theory (Figures 13, 14):

a) distribution of stresses

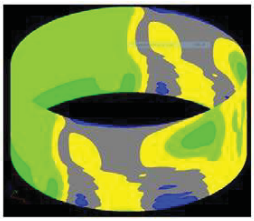

b) values of stresses

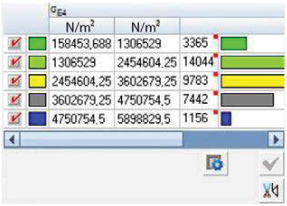

Figure 13. Equivalent Stresses in the Tank's Shell at Wind Load according to Maximum Distortion Energy Theory Computed by Eurocodes

a) distribution of stresses

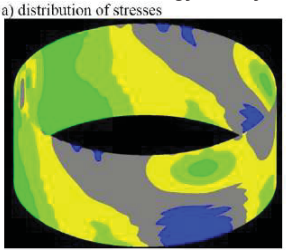

b) values of stresses

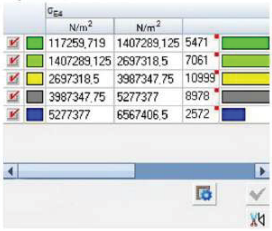

Figure 14. Equivalent Stresses in the Isolated Tank's Shell at Wind Load according to Maximum Distortion Energy Theory Computed by SolidWorks Flow

For strain-stress state analysis two rings of vertical cylindrical tank No. 5 (half the height of the wall) and No. 8 (2/3 of the wall height) have been singled out. Since edge effects have little influence on the strain values in these rings, heavy wind loads are brought about. It is more relevant to present the comparison results in the form of a table (Table 3).

Table3. The Strain-Stress State of the Isolated Vertical Cylindrical Tank

No. of Tank Rings	Design Load	Ny= σ_1 (+), MPa	Ny= σ_1 (−), MPa	Nx=σ_2 (+), MPa	Nx=σ_2 (−), MPa	σ_{e4}(maximum distortion energy theory), MPa
5	According to Eurocodes	1.872	2.863	4.400	2.947	3.967
	Numerical Simulation	2.166	3.173	5.138	3.149	4.148
Variation%		15.74	10.84	16.79	6.86	4.57
8	According to Eurocodes	2.086	2.744	4.690	3.000	4.322
	Numerical Simulation	3.385	5.104	5.695	5.000	5.154
Variation %		62.23	86.02	21.42	66.65	19.2

Thus, according to the results of numerical simulation the largest deviation had been recorded in the upper ring of VCT of the shell. Minimum deviation is 21 %, maximum one is 108 %, in both cases stresses were great because of the wind load obtained by numerical simulation in Solid Works Flow. Considerable difference in upper rings can be explained by the disarrangement of wind flow in the area of roof joint with the shell, thus some part of the upper ring is under the influence of "breaking off wind load".

3.9. Finite Element Analysis of Strain-Stress State of the Shell at Unfavorable Wind Load on VCT, Consisting of a Group of 4 Objects

As it was mentioned earlier, VCT No. 2 will be examined at the angle of wind of 45° as the most unfavorable one. As a whole the distribution of equivalent stresses according to the 4th maximum distortion energy theory is given in figure 15.

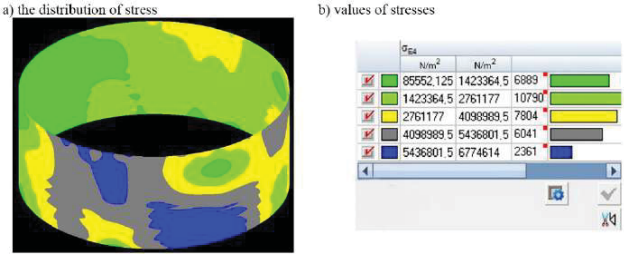

Figure 15 Equivalent Stresses according to the 4th Maximum Distortion Energy Theory on the Shell of VCT in the Group of Tanks Depending on the Load Obtained in SolidWorks Flow

Below are given the values of occurring stresses in the 5th and 8th rings of the tank and the percentage-based comparison of these stresses deviations from the wind load according to the codes of the European Union and stresses occurring in an isolated tank under the influence of wind pressure obtained as a result of numerical simulation (Table 5).

Table 5.Stress and Strain State of VCT Shell in the Group

No. of tank ring	Design load	Ny= σ_1 (+), MPa	Ny= σ_1 (−), MPa	Nx=σ_2 (+), MPa	Nx=σ_2 (−), MPa	σ_{e4}(The 4th maximum distoration energy theory), MPa
5	VCT in group	1.922	1.026	5.705	4.147	5.870
	Difference from European code, %	2.67	179.04	29.67	40.73	47.97
	Difference from wind on 1 VCT, %	12.73	209.27	11.02	31.69	41.51
8	VCT in group	2.485	1.120	6.082	5.024	6.199
	Difference from European code, %	19.11	145.05	29.68	67.46	43.41
	Difference from wind on 1 VCT, %	36.20	355.83	6.8	0.49	20.27

The analysis of comparative table shows, that stress and strain state of the shell of tank which is in the group differs greatly from stress and strain state of the shell of an isolated VCT. Thus maximum deviation of stresses makes 356%. In this case maximum stresses occur exactly in the case of wind load on VCT in group, though most part of the shell undergoes less stress than in two other examined cases.

3.10. Discussion

In this work, new results were obtained on the distribution of wind loads on the wall of a tank that is in a group of 4 reservoirs, which is not taken into account by the current design standards. The need for such an account is confirmed by the data of subsection 3.9.

At the same time, these data are subject to discussion and can be considered as primary, to be clarified before introduction into the relevant regulatory documents, due to the following reasons, in our opinion:

- the need to conduct a physical experiment on large models,
- the need to conduct a numerical experiment with a larger range of tanks, ranging from 100 to 30 000 m³;
- the need to obtain generalized expressions for rationing the wind load on a group of tanks with varying parameters of the geometrical dimensions of the tanks, the shape of the roof, the distance between the tanks.

4. Conclusion

1. In the shell of an isolated tank affected by the wind load according to the results of numerical simulation, in the middle and low rings the equivalent stresses differ not more than by 5 % from those according to Eurocode, in the upper tanks – by 20 %. The difference of upper ring stress and strain state has been caused by the fact that diagram of wind pressure according to the Eurocode for examined standard size of the tank because of the small values of occurring stresses, did not take into account break up lifting wind pressure in the area of roof and shell joint.

2. Maximum values of stresses in the shell all of VCT in all examined cases of loadings, occur in tank No. 2 at wind attack angle of 45°.

3. Stress and strain state of the shell under the effect of unfavorable wind load on VCT, which is in the group of 4 objects differs greatly from the stresses occurring in the shell of isolated VCT. On the whole peace loads of equivalent stresses differ by 48 % as compared to isolated VCT according to the Eurocode and by more than 41 % in comparison with isolated VCT according to the results of numerical simulation. Thus objects situated nearby influence greatly stress and strain state of the shell of VCT and it requires the development of the technique taking this fact into account.

References

1. SNiP II-6-74. Nagruzki i vozdeystviya [SNiP II-6-74. Loads and effects]. Moscow : Stroyizdat, 1976. 58 p. (rus)
2. SNiP 2.01.07-85*. Nagruzki i vozdeystviya [SNiP 2.01.07-85*. Loads and effects]. Moscow : FGUP TsPP, 2005. 44 p. (rus)
3. Holmes, J.D. Wind loading of structures. Boca Raton, FL : CRC press, 2015. 412 p.
4. Lawson, T. Building aerodynamics. London: Imperial College Press, 2001. 286 p.
5. Gorokhov, Ye.V., Kuznetsov, S.G. Eksperimentalnye metody opredeleniya vetrovykh nagruzok na zdaniya i sooruzheniya [Experimental methods of determination of wind load on buildings and constructions]. Donetsk: Nord-Press, 2009. 169 p. (rus)
6. Berezin, M.A., Katyushin, V.V. Atlas aerodinamicheskikh kharakteristik stroitelnykh konstruktsiy [Aerodynamic characteristics atlas of engineering constructions]. Novosibirsk : Oldenpoligrafiya, 2003. 140 p. (rus)
7. Kinash, R.I., Kopylov, A.Ye. Bulletin of Lviv Polytechnic National University. Series: Theory and Practice in Construction. 2004. No. 495. Pp. 88–92. (rus)
8. Kinash, R.I., Kopylov, A.Ye. Proceeding of the Donbas National Academy of Civil Engineering and Architecture. 2007. No. 2007-6(68). Pp. 32–40. (rus)
9. Uematsu, Y., Koo, C., Kondo, K. Wind loads on open-topped oil storage tanks. BBAA VI International Colloquium on Bluff Bodies Aerodynamics and Applications, Milano, Italy, July, 20-24 2008. Milano, 2008. Pp. 1–15.
10. Zha, Y., Lin, Y., Shen, Y.-B. Wind loads on large cylindrical open-topped tanks in group. Thin-Walled Structures. 2014. No. 78. Pp. 108–120.
11. Zhang, Y. Study of microburst-like wind and its loading effects on structures using impinging-jet and cooling-source approaches. Ames, Iowa: Iowa State University, 2013. 235 p.
12. Zhang, Y., Hu, H., Sarkar, P.P. Comparison of microburst-wind loads on low-rise structures of various geometric shapes. Journal of Wind Engineering and Industrial Aerodynamics. 2014. No. 133. Pp. 181–190.
13. Gorokhov, Ye.V., Mushchanov, V.F., Kinash, R.I., Shimanovskiy, A.V., Lebedich, I.N. Konstruktsiyi statsionarnykh pokrytiy nad tribunami stadionov [Construction of fixed-site coverings over terraces]. Makeyevka : RIO DonNASEA, 2008. 405 p. (rus)
14. Yeremeyev, P.G. Sovremennye stalnye konstruktsiyi bolsheproletnykh pokrytiy unikalnykh zdaniy i sooruzheniy [Current steel constructions of large-span shell of one-off buildings and constructions]. Moscow: ASV, 2009. 336 p. (rus)

Литература

1. СНиП II-6-74. Нагрузки и воздействия. – Взамен СНиП II-А.11-62; СН 318-65; СН 355-66 ; вед. 01.09.1974. М: Стройиздат, 1976. 58 с.
2. СНиП 2.01.07-85*. Нагрузки и воздействия. – Взамен главы СНиП II-6-74 ; введ. 01-01-1987. М: ФГУП ЦПП, 2005. 44 с. (Строительные нормы и правила).
3. Holmes J.D. Wind loading of structures. Boca Raton, FL : CRC press, 2015. 412 p.
4. Lawson T. Building aerodynamics. London: Imperial College Press, 2001. 286 p.
5. Горохов Е.В., Кузнецов С.Г. Экспериментальные методы определения ветровых нагрузок на здания и сооружения. Донецк : Норд-Пресс, 2009. 169 с.
6. Березин М.А., Катюшин В.В. Атлас аэродинамических характеристик строительных конструкций. Новосибирск : Олденполиграфия, 2003. 140 с.
7. Кинаш Р.И., Копылов А.Е. Аэродинамические исследования четырех круглых цилиндров // Вісник Національного університету “Львівська політехніка”. Серія: Теорія і практика будівництва. 2004. № 495. С. 88–92.
8. Кинаш Р.И., Копылов А.Е. Исследование аэродинамических параметров системы из двух круговых цилиндров // Вестник Донбасской национальной академия строительства и архитектуры. 2007. №. 2007-6(68). С. 32–40.
9. Uematsu Y., Koo C., Kondo K. Wind loads on open-topped oil storage tanks // BBAA VI International Colloquium on Bluff Bodies Aerodynamics and Applications, Milano, Italy, July, 20-24 2008. Milano, 2008. Pp. 1–15.
10. Zhao Y., Lin Y., Shen Y.-B. Wind loads on large cylindrical open-topped tanks in group // Thin-Walled Structures. 2014. № 78. Pp. 108–120.
11. Zhang Y. Study of microburst-like wind and its loading effects on structures using impinging-jet and cooling-source approaches. Ames, Iowa : Iowa State University, 2013. 235 p.
12. Zhang Y., Hu H., Sarkar P.P. Comparison of microburst-wind loads on low-rise structures of various geometric shapes // Journal of Wind Engineering and Industrial Aerodynamics. 2014. No. 133. Pp. 181–190.
13. Горохов Е.В., Мущанов В.Ф., Кинаш Р.И. [и др.]. Конструкции стационарных покрытий над трибунами стадионов. Макеевка : РИО ДонНАСА, 2008. 405 с.
14. Еремеев П.Г. Современные стальные конструкции большепролетных покрытий уникальных зданий и сооружений: монография. М: АСВ, 2009. 336 с.
15. Исаев С.А., Ватин Н.И., Баранов П.А., Судаков А.Г., Усачов А.Е., Егоров В.В. Разработка и верификация

Mushchanov, V.P., Zubenko, H.V., Tsepliaev, M.N. The stress state of a tank shell in the group under wind load. Magazine of Civil Engineering. 2018. 83(7). Pp. 49–62. doi: 10.18720/MCE.83.5.

15. Isaev, S.A., Vatin, N.I., Baranov, P.A., Sudakov, A.G., Usachov, A.Ye., Yegorov, V.V. Development and verification of multiblock computational technologies for solution of unsteady problems of high building aerodynamics in the framework of URANS approach. Magazine of Civil Engineering. 2013. 36(1). Pp. 103–109.
16. Isaev, S.A., Baranov, P.A., Vatin, N.I., Zhukova, Y.V., Sudakov, A.G. Suppression of the Karman vortex street and reduction in the frontal drag of a circular cylinder with two vortex cells. Technical Physics Letters. 2014. No. 40(8). Pp. 653–656.
17. Isaev, S.A., Vatin, N.I., Lebiga, V.A., Zinoviev, V.N., Chang, K.-C., Miau, J.-J. Problems and methods of numerical and experimental investigation of high rise constructions' aerodynamics in the coastal region "sea-land". Magazine of Civil Engineering. 2013. 37(2). Pp. 54–61; Pp. 118-120.
18. Mochida, A., Tominaga, Y., Murakami, S., Yoshie, R., Ishihara, T., Ooka, R. Comparison of various k-ε models and DSM applied to flow around a high-rise building — Report on AIJ cooperative project for CFD prediction of wind environment. Wind and Structures. 2002. No. 5 (2–4). Pp. 227–244.
19. Tominaga, Y., Mochida, A., Yoshie, R., Kataoka, H., Nozu, T., Yoshikawa, M., Shirasawa, T. AIJ guidelines for practical applications of CFD to pedestrian wind environment around buildings. Journal of Wind Engineering and Industrial Aerodynamics. 2008. No. 96(10). Pp. 1749–1761.
20. Shirasawa, T., Tominaga, T., Yoshie, R. Mochida, A., Yoshino, H., Kataoka, H., Nozu, T. Development of CFD Method for Predicting Wind Environment around a High-Rise Building: Part 2: The cross comparison of CFD results using various k-ε models for the flowfield around a building model with 4:4:1 shape (Environmental Engineering). AIJ Journal of Technology and Design. 2003. Vol. 9. No. 18. Pp. 169–174.
21. Yasunaga, J., Koo, C., Uematsu, Y. Kondo, K., Yamamoto, M. Wind loads on two or three open-topped oil-storage tanks in various arrangements. Proceedings of the 2012 World Congress on Advances in Civil, Environmental, and Materials Research (ACEM'12). Seoul. 2012. Pp. 2339–2352.
22. Zubenko, H., Drozdov, A. Model'nyye ispytaniya vertikal'nykh uglovykh rezervuarov [Model tests of vertical cylindrical tanks and verification of numerical studies]. Metal Constructions. 2016. Vol. 22. No. 2. Pp. 91–97. (rus)
23. DSTU-N B EN 1991-1-4:2010. Yevrokod 1. Dii na konstruktsii. Chastyna 1-4. Zagalni dii. Vitrovi navantazhennya (EN 1991-1-4:2005, IDT) [Eurocode 1. Actions on structures – Part 1-4. General actions – Wind actions (EN 1991-1-4:2005, IDT)]. Kyiv : Ministry of Regional Development of Ukraine, 2012. 165 p. (ukr)
24. Tominaga, Y., Mochida, A., Shirasawa, T., Yoshie, R., Kataoka, H., Harimoto, K., Nozu, T. Cross comparisons of CFD results of wind environment at pedestrian level around a high-rise building and within a building complex. Journal of Asian Architecture and Building Engineering. 2004. Vol. 3. Pp. 63–70.
25. DBN V.1.2-2:2006. Derzhavni budivelni normy. Systema zabezpechennya nadiynosti ta bezpeky budivelnikh obyektiv. Navantazhennya i vplyvy. Normy proektuvannya [National Structural Rules and Regulations. The system of reliability and safety provision of constructional projects. Loads and effects]. Kyiv: Ministry of Regional Development of Ukraine, 2006. 61 p. (ukr)
26. SP 20.13330.2011. Nagruzki i vozdeystviya. Aktualizirovannaya redaktsiya SNiP 2.01.07-85* [Loads and effects. Updated reaction. SNiP 2.01.07-85*]. многоблочных вычислительных технологий для решения нестационарных задач строительной аэродинамики высотных зданий в рамках подхода URANS // Инженерно-строительный журнал. 2013. № 1(36). С. 103–109.
16. Isaev S.A., Baranov P.A., Vatin N.I. [et al.] Suppression of the Karman vortex street and reduction in the frontal drag of a circular cylinder with two vortex cells // Technical Physics Letters. 2014. № 40(8). Pp. 653–656.
17. Исаев С.А., Ватин Н.И., Лебига В.А., Зиновьев В.Н., Кэ-Чин Чан, Цзюн-Цзи Мяу. Задачи и методы численного и физического исследования аэродинамики высотных зданий в прибрежной зоне «море-суша» // Инженерно-строительный журнал. 2013. №2(37). С. 54–61.
18. Mochida A., Tominaga Y., Murakami S. [et al.] Comparison of various k-ε models and DSM applied to flow around a high-rise building — Report on AIJ cooperative project for CFD prediction of wind environment // Wind and Structures. 2002. № 5(2-4). Pp. 227-244.
19. Tominaga Y., Mochida A., Yoshie R. [et al.] AIJ guidelines for practical applications of CFD to pedestrian wind environment around buildings // Journal of Wind Engineering and Industrial Aerodynamics. 2008. № 96(10). Pp. 1749–1761.
20. Shirasawa T., Tominaga T., Yoshie R. [et al.] Development of CFD Method for Predicting Wind Environment around a High-Rise Building : Part 2 : The cross comparison of CFD results using various k-ε models for the flowfield around a building model with 4:4:1 shape (Environmental Engineering) // AIJ Journal of Technology and Design. 2003. Vol. 9. № 18. Pp. 169–174.
21. Yasunaga J., Koo C., Uematsu Y. [et al.] Wind loads on two or three open-topped oil-storage tanks in various arrangements // Proceedings of the 2012 World Congress on Advances in Civil, Environmental, and Materials Research (ACEM'12). Seoul, 2012. Pp. 2339–2352.
22. Зубенко А.В., Дроздов А.А. Модельные испытания вертикальных цилиндрических резервуаров и верификация численных исследований // Металлические конструкции. 2016. Т. 22. № 2. С. 91–97.
23. ДСТУ-Н Б EN 1991-1-4:2010. Єврокод 1. Дії на конструкції [Text]. Частина 1-4. Загальні дії. Вітрові навантаження (EN 1991-1-4:2005, IDT). – Уведено вперше ; чинні 01.07.2013. К. : Мінрегіон України, 2013. 165 с. (Національний стандарт України).
24. Tominaga Y., Mochida A., Shirasawa T. [et al.] Cross comparisons of CFD results of wind environment at pedestrian level around a high-rise building and within a building complex // Journal of Asian Architecture and Building Engineering. 2004. Vol. 3. Pp. 63–70.
25. ДБН В.1.2-2:2006. Державні будівельні норми. Система забезпечення надійності та безпеки будівельних об'єктів. Навантаження і впливи. Норми проектування [Text]. – Замість СНиП 2.01.07-85 ; надано чинності 2007-01-01. К. : Мінбуд України, 2006. 61 с.
26. СП 20.13330.2011. Нагрузки и воздействия. Актуализированная редакция СНиП 2.01.07-85* [Text]. – Введ. 20-05-2011. М. : Госстандарт, 2011. 80 с. (Свод правил).
27. Franke J., Hirsch C., Jensen A.G. [et al.] Recommendations on the Use of CFD in Wind Engineering // Proceedings of the International Conference on Urban Wind Engineering and Building Aerodynamics: COST C14 – Impact of Wind and Storm on City life and Built Environment. Rhode-Saint-Genèse . 2004. Pp. 1.1–1.11.
28. Типовой проект 704-1-70. Стальной вертикальный цилиндрический резервуар для нефти и нефтепродуктов емкостью 20000 куб. м [Text]. Альбом I. Рабочие чертежи КМ резервуара. – М. :

Мущанов В.Ф., Зубенко А.В., Цепляев М.Н. Напряжения от ветровой нагрузки в стенке резервуара, находящегося в группе // Инженерно-строительный журнал. 2018. № 7(83). С. 49–62.

Moscow: Ministry of Regional Development of Russia, 2011. 80 p. (rus)

27. Franke, J., Hirsch, C., Jensen, A.G., Krüs, H.W., Schatzmann, M., Westbury, P.S., Miles, S.D., Wisse, J.A., Wright, N.G. Recommendations on the Use of CFD in Wind Engineering. Proceedings of the International Conference on Urban Wind Engineering and Building Aerodynamics: COST C14 – Impact of Wind and Storm on City life and Built Environment, Rhode-Saint-Genèse / J.P.A.J. van Beek (Ed.). Rhode-Saint-Genèse : Von Karman Institute for Fluid Dynamics, 2004. Pp. 1.1–1.11.
28. Tipovoy proyekt 704-1-70. Stalnoy vertikalnyy tsilindricheskiy rezervuar dlya nefti i nefteproduktov yemkostyu 20000 kub. m. Albom I. Rabochiye chertezhi KM rezervuara [Type design 704-1-70. Steel vertical cylindrical tank of 20000 volume for crude oil and refined products. Album I. Drawing design of tank]. Moscow: Research and Development Establishment Projectsteelconstructions of State Committee for Construction of the USSR, 1972. 46 p. (rus)
29. Tcepliaev, M. Modelirovaniye real'noy epyury vetrovogo davleniya na tsilindricheskiy rezervuar v srede SCAD [Simulation of real epure of wind pressure on a cylindrical tank in SCAD environment]. Metal Constructions. 2016. Vol. 22. No. 4. Pp. 183–192. (rus)

ЦНИИпроектстальконструкция Госстроя СССР, 1972. – 46 с.

29. Цепляев М.Н. Моделирование реальной эпюры ветрового давления на цилиндрический резервуар в среде SCAD // Металлические конструкции. 2016. Т. 22. № 4. С. 83–192.

Volodymyr Mushchanov,*
+380(50)368-08-04;
volodymyr.mushchanov@mail.ru

Hanna Zubenko,
+380(50)815-93-47; zubienko_anna@mail.ru

Maxim Tsepliaev,
+380(71)319-82-29; m.s.sepliaev@donnasa.ru

Владимир Филиппович Мущанов,*
+380(50)368-08-04;
эл. почта: volodymyr.mushchanov@mail.ru

Анна Васильевна Зубенко,
+380(50)815-93-47;
эл. почта: zubienko_anna@mail.ru

Максим Николаевич Цепляев,
+380(71)319-82-29;
эл. почта: m.s.sepliaev@donnasa.ru

Mushchanov, V.P., Zubenko, H.V., Tsepliaev, M.N. The stress state of a tank shell in the group under wind load. Magazine of Civil Engineering. 2018. 83(7). Pp. 49–62. doi: 10.18720/MCE.83.5.

doi: 10.18720/MCE.83.6

Strength and phase composition of autoclaved material: an approximation

Взаимосвязь прочности и фазового состава автоклавированного материала

G.I. Ovcharenko*,
D.I. Gilmiyarov,
Polzunov Altai State Technical University, Barnaul, Russia

Д-р техн. наук, заведующий кафедрой Г.И. Овчаренко*,
канд. техн. наук, начальник лаборатории Д.И. Гильмияров,
Алтайский государственный технический университет им. И.И.Ползунова, Барнаул, Россия

Key words: autoclaved building materials; lime-fly ash mixtures; Na_2SO_4 addition; phase composition; strength of the stone; interrelationships

Ключевые слова: автоклавные строительные материалы; известково-зольные смеси; добавка Na_2SO_4; фазовый состав; прочность камня; взаимосвязи

Abstract. The purpose of this work was to identify the relationship between the phase composition and strength of autoclaved pressed stone from a mixture of lime and ash of CHP in the presence of Na_2SO_4. From these mixtures are made such building materials as silicate brick and blocks from autoclaved cellular concrete. The phase analysis of the autoclaved samples was carried out by X-ray and thermal methods. It was found that the mixtures studied after autoclaving for 8; 50 and 100 hours at 0.8 MPa isotherm with no addition or with 1 and 2% Na_2SO_4 is represented by gel-like phase C-A-S-H, aluminum substituted tobermorite, hydrogarnet katoite. Adding of 1 and 2% Na_2SO_4 makes no qualitative change in phase composition, but significantly redistribute the phase composition and increase the rate of phase formation. Thus 2 % Na_2SO_4 contributes to a substantial increase in the synthesis of Al-tobermorite, but reduces the C-A-S-H phase formation. Katoite hydrogarnet content remains unchanged. The degree of hydration of the composition with 2% Na_2SO_4 for 8 hours of autoclaving is the same as for 100 hours of treatment without an additive. This increases the strength of the material by 1.65 times with the same 8 hour steaming time. Strength of the stone is always directly proportional to the content of a gel C-A-S-H phase. Its content is proportional to the number of Al-tobermorite in non-additional mixtures, but does not correspond to the content of tobermorite in compositions with addition of 2 % Na_2SO_4. Keywords: autoclaved building materials, lime-fly ash mixtures, Na_2SO_4 addition, phase composition, strength of the stone, interrelationships.

Аннотация. Целью данной работы было выявить связь между фазовым составом и прочностью автоклавного прессованного камня из смеси извести и золы ТЭЦ в присутствии Na_2SO_4. Из подобных смесей изготавливаются такие строительные материалы как силикатный кирпич и блоки из автоклавного ячеистого бетона. Фазовый анализ автоклавированных образцов проводили рентгенофазовым и термическими методами. Было обнаружено, что смеси, изученные после автоклавирования при 8; 50 и 100 часов при изотерме 0,8 МПа без добавления или с 1 и 2% Na_2SO_4 содержат гелевидную фазу C-A-S-H, алюминий замещенный тоберморит, гидрогранат катоит. Добавление 1 и 2% Na_2SO_4 не приводит к качественному изменению фазового состава, но значительно перераспределяют фазовый состав и увеличивает скорость фазообразования. Таким образом, 2% Na_2SO_4 способствует существенному увеличению содержания Al-тоберморита, но уменьшает образование фазы C-A-S-H. Содержание гидрограната остается неизменным. Степень гидратации композиции с 2% Na_2SO_4 за 8 часов автоклавирования такая же как за 100 часов обработки без добавки. Это увеличивает прочность материала в 1,65 раза при одинаковом 8 часовом времени запаривания. Прочность камня всегда прямо пропорциональна содержанию гелевидной фазы C-A-S-H. Её содержание пропорционально содержанию Al-тоберморита в смесях без добавки, но не соответствует содержанию тоберморита в композициях с добавлением 2% Na_2SO_4. Ключевые слова: автоклавные строительные материалы, известково-зольные смеси, добавка Na_2SO_4, фазовый состав, прочность камня, взаимосвязи.

Овчаренко Г.И., Гильмияров Д.И. Взаимосвязь прочности и фазового состава автоклавированного материала // Инженерно-строительный журнал. 2018. № 7(83). С. 63–72.

1. Introduction

The object of research in this paper is to reveal the relationship between the strength of autoclaved stone based on the lime-ash mixture and its phase composition.

The phase composition of hydrates of autoclave stone on the basis of lime and aluminosilicate raw materials still provokes discussions, not to mention the interrelation between the components of the phase composition and its strength. At the same time, numerous silicate brick plants are used as the main component or as an additive to the ash class F of the CHP.

The main law of the strength formation of silicate autoclaved materials have been discussed since the beginning of the 50s of the 20th century, when G.L. Kalouzek had found its direct dependence on the quantity of generated 11.3 angstrom tobermorite [1]. Then H.F.W. Taylor objected Kalouzek, noting that the strength of any material is a function of its density, and, for autoclaved materials, it also depends on presence of gel phase in them. The effect of a gel phase on the strength had been previously mentioned in the works of P.I. Bozhenov for whom Taylor referred. However, both P.I. Bozhenov, and Taylor have not reported quantitative relationships in those years. It was only 1977, when Taylor published the article [2] proving a direct link of strength of lime-silica material with a number of C-S-H gel being formed. Taylor stated a brief review of these issues in the last lifetime edition of "Chemistry of cement" [3], also specifying differences in opinion on this issue, particularly in the extent beneficial to crystallize a gel phase.

When using various aluminosilicate materials, including it in the form of CHP ash of the aluminosilicate composition, as well as Portland cements the silica component, phase formation of autoclave materials becomes more complicated. Even the qualitative composition of the phases had caused discussions. It was only in the 2000s, when the publications of A.S. Ray in conjunction with D.S. Klimesch [4] were issued, and as well of Japanese researchers [5] and others [6, 7], which allowed to interpret and quantify unambiguously the phases being formed in such systems. The issue of the interrelation of the phase composition and strength of autoclave stone composed of lime-aluminosilicate raw materials remained open. Because synthetic tobermorites and their Al- and Fe-substituted forms easily synthesized under saturated steam or in hydrothermal conditions at temperatures from 80 to 225 °C from a wide range starting materials, including various following mixtures: lime, zeolites, quartz, gibbsite, cement, clays, sodium silicate, ashes, cullet, trachyte and others [1, 8–19]. And the presence of a gel-like phase of the C-A-S-H type in these syntheses was often not paid attention. At the same time, publications on the features of the structure of the tobermorites and their analogs, the synthesis of minerals and their ion-exchange properties, do not give an answer to the question of the regularities in the formation of the strength of the stone on their basis [20–28].

Therefore, the purpose of this study was to establish such a relationship between the phase composition and strength for such an aluminosilicate raw material as ash.

For this, it was necessary to establish a reliable quantitative composition of phases of autoclave stone composed of alumino-silicate raw materials on the basis of the CHP ash, to use an addition that promotes redistribution of the main phases in order to disclose interrelations between the phase composition and strength of stone.

It follows from [5, 26] that the addition of Al_2O_3 or SO_3 in lime-silica autoclave composition accelerates crystallization of C-S-H gel phase and formation of larger amount of tobermorite. Furthermore, it is known that the presence of alkali in autoclave synthesis significantly accelerates the hydrate formation [29]. By definition, alumina is present in the aluminosilicate raw material. Therefore, $Na_2SO_4$was selected as an activator additive. Sodium sulphate contains the required group of SO_3, and alkaline, released in hydrothermal reactions, will accelerate the synthesis and crystallization of hydrated phases. The possibility of such processes due to the high real defectness tobermorite structure [20, 30–37].

The relevance of this study is that, for aluminosilicate raw materials, the relationship between strength and phase composition for autoclave materials has not yet been established. At the same time, such aluminosilicate materials as CHP ashes are widely used in the technology of autoclave materials.

The purpose of this study is to establish a relationship between the strength and phase composition of autoclave material based on lime and aluminosilicate ash from CHP.

To achieve the goal it is necessary to solve the following tasks:

– investigate the strength and phase composition of lime-ash material in a wide range of phase composition changes;

– to increase the range of changes in the phase composition and strength of the stone, apply the method of prolonged autoclave treatment and intensification of the processes by the Na_2SO_4 additive-activator;
– to establish the relationship between the phase composition of lime-ash and its strength.

2. Materials and Methods

In experiment, was used electrostatic precipitator ash provided by burning coal (coal ash – CA) of Kuznetsk Basin brand G at Novosibirsk CHP-5 with the composition of unburned coal of 3.29 % (Table 1, recalculated on ignited product). Ash particles range from 1.5 to 250 μm with an average diameter of 70.5 μm (determined in an equipmentSALD-2101 Laser Diffraction Particle Size Analyzer – SHIMADZU, Japan). Calcium lime contained about 92 % of active CaO and MgO and, by main indicators, was consistent with first grade lime according to Russian standards. In some mixtures, it was used curing activator of Na_2SO_4 with 98 % content of the main substance.

Table1. Chemical composition of ash provided by Novosibirsk CHP-5

Material	SiO_2	Al_2O_3	Fe_2O_3	CaO	MgO	SO_3	Total
CHP-5 ash	61.87	23.73	5.0	4.38	1.29	0.33	99.98

The ash was mixed with powdered lime with Blaine specific surface area of about 6.000 cm^2/g with a ratio of 20 % basing on active CaO and MgO. In some mixtures with tempering water, Na_2SO_4 was added as hardening activator in an amount of 1 or 2% by weight. The raw material mixture was moistened, sealed in plastic containers and ensilaged at 60 ^{0}C for 2 hours to full lime hydration. After that, from that mass, it was formed cylinder samples of diameter and height of 50 mm at specific pressing pressure of 20 MPa, which were treated in an autoclave at 0.8 MPa with isothermal exposure of 8, 50 and 100 hours correspondingly. Samples strength tests were produced after their drying at 100 ^{0}C to constant mass. Six samples for test was chosen to ensure measurement error of not more than 3-5%. Some samples were taken out of those ones for analysis by methods of X-ray diffraction (XRD) and thermal analysis, including differential and thermal analysis (DTA), differential thermogravimetric analysis (DTG), and thermogravimetric analysis (TG).The X-ray diffraction analysis was performed on a DRON-3 (Russia) with CuKα radiation at tube voltage of 40 kV and current of 25 A. The thermal analysis at rate of 10 deg/min was conducted using an equipment Netzsch STA 449C (Germany) in a closed crucible and helium flow to create not-oxidative environment and eliminate the effects of burning coal residues in the ash.

3. Results and Discussions

Figure 1 shows that with increasing isothermal hold up time from 8 to 100 hours, strength of lime-ash compositions without additional of $Na_2SO_4$is steadily increasing from 20 to 45.5 MPa. When injected with 1 and 2% Na_2SO_4, there is an inflection in strength at 50 hours of autoclaving, or composition strength decrease in proportion to additions at isotherm of 100 hours. At this, the samples with the addition of 2% sodium sulphate gain the main strength after the first 8 hours of heat treatment in the autoclave and then there is no substantial increase observed. Compared with the addition-free composition, the addition of 1 and 2% of sodium sulfate increases strength by 1.3 and 1.6 times respectively at isotherm autoclaving of 8 hours.

These data require an interpretation. For this it is necessary to determine the phase composition of stone.

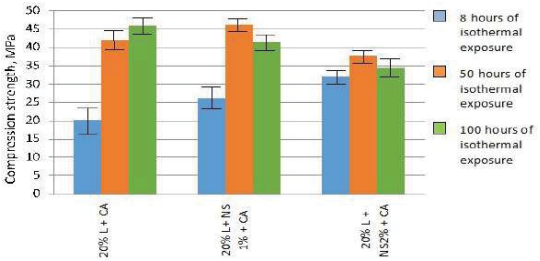

Figure 1. Strength of lime-ash samples autoclaved at pressure of 0.8 MPA depending on time of isothermal exposure and addition of Na_2SO_4. Notice: L – lime, NS – Na_2SO_4, CA – coal ash

Овчаренко Г.И., Гильмияров Д.И. Взаимосвязь прочности и фазового состава автоклавированного материала // Инженерно-строительный журнал. 2018. № 7(83). С. 63–72.

The composition of the formed hydrothermal synthesis products in the addition-free mixture according to XRF (Figure 2) is presented by the following main phases: 8 hours isotherm (X-ray pattern1) - residual portlandite $Ca(OH)_2$ (4.91; 2.63; 1.80),the residual quartz ash of SiO_2 (4.27; 3.35; 2.28; 1.80), synthesized tobermorite (11.48; 5.41; 3.08; 2.98; 2.79), calcite (3 04; 2.28; 1.93).In addition to these phases, there are reflections of hydrogarnets: katoite – 5.10; 2.79; 2.28; 1.67, and ferrous hydrogarnet – 3.08; 2.74; 1.62. Probably, the presence of C-S-H phases (I and II) - peaks are 3.07 and 2.80, but reflections for these phases are absent at small angles (12.5 and $9.80\times10\text{-}^{10}$ m). Increasing the isotherm up to 100 hours in the addition-free composition (X-ray pattern2), we observe portlandite disappearance, the proportion of silica is reduced, the proportion of tobermorite is increased, but not all peak intensities of tobermorite change proportionally - the peak of 5.41 decreases, the one of 2.98 remains unchanged, and the peaks of 11.60 and 3.08 increase. Instead of the 2.79 peak, the peak of 2.76 appears. The significant deviation of 11-angstrem peak of 11.30 to 11.60×10^{-10}m should be noted. The peaks of katoite transform to reflections of ferrous hydrogarnet – 5.045; 3.08; 2.755; 1.62-1.63, although certain sources attribute the peak of 2.76 as well to katoite. Besidesof 1.1 nm of tobermorite and perhaps xonotlite (3.07-3.08; 2.83; 2.70), there are no peaks of other calcium hydrosilicates.

In the presence of 1 % Na_2SO_4 activator for 8 hours of treatment (X-ray pattern3), there is an intermediate phase composition reached compared with 8 and 100 hours without additive composition except of a significant increase in the peak of 2.76.It can be referred to katoite or ferrous hydrogarnet. 100 hour exposure in the presence of 2% Na_2SO_4 (X-ray pattern4) differs only slightly from the 100 hour exposure in a system without the activator, except of even larger decrease of quartz proportion and outlined supplements.

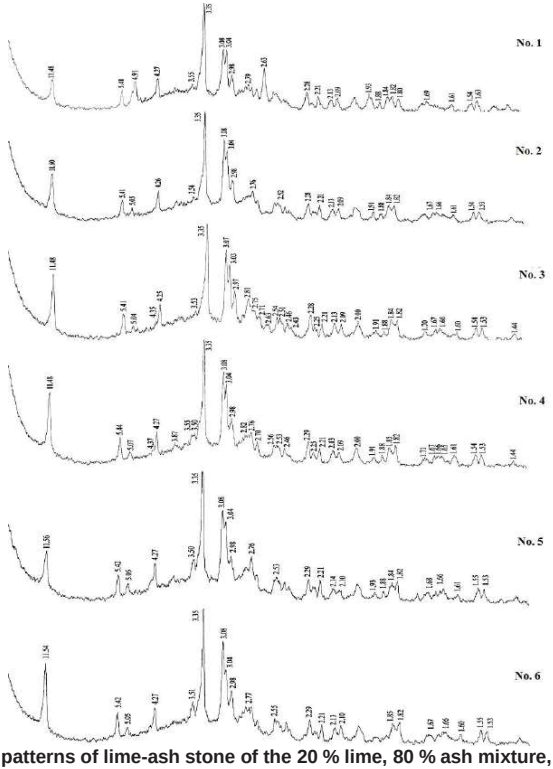

Figure 2. X-ray patterns of lime-ash stone of the 20 % lime, 80 % ash mixture, at: No. 1 – 8 h of isothermal exposure; No. 2 – at 100 h of isothermal exposure; No. 3 – 8 h of isothermal exposure with additive injection of 1% Na_2SO_4; No. 4 – 100 h of isothermal exposure with additive injection of 1% Na_2SO_4; No. 5 – 8 h of isothermal exposure with additive injection of 2 % Na_2SO_4; No. 6 – 100 h of isothermal exposure with additive injection of 2% Na_2SO_4.

Ovcharenko, G.I., Gilmiyarov, D.I. Strength and phase composition of autoclaved material: an approximation. Magazine of Civil Engineering. 2018. 83(7). Pp. 63–72. doi: 10.18720/MCE.83.6.

Analysis of the mixture thermogram based on the ash of Novosibirsk CHP-5 at 8 hours of isothermal exposure (Figure 3) shows the effect of weight loss (DTG curve at approximately 95 °C, which is associated with removal of moisture adsorption. There we see presence of hydrogarnets that are noted with little effect at 373 °C. A large weight loss at 447 °C corresponds to residual portlandite $Ca(OH)_2$. In the 700–780 °C interval, there occurs decomposition of calcium hydrosilicates, calcite, and probably, of C-A-S-H phase, dehydration of which is accompanied by a pronounced effect at 741 °C.H.F.W. Taylor also attributed this effect to amorphous hydrosilicate phase [2]. Tobermorite phase having significant deviations of XRD reflections from 11.3, represents aluminum substituted tobermorite with other impurities and thus loses weight at 180 ^{0}C, being much smaller than 240 ^{0}C [4].

At increasing the isothermal exposure to 100 hours, a differential curve of weight loss, DTG (Figure 4), represents a significant increase in endothermic effect at 86 °C and the disappearance of residual portlandite $Ca(OH)_2$because of the formation of hydrate phases large number being a result of hydrothermal synthesis. For this, as additional evidence, the large weight loss may serve as evidence which is associated with the removal of moisture adsorption and with loss of water by the gel phase. Weight loss effect by hydrogarnet at 381 °C is registered. The weight loss at effects of 185 and 727 °C increases up to 2.4 %.

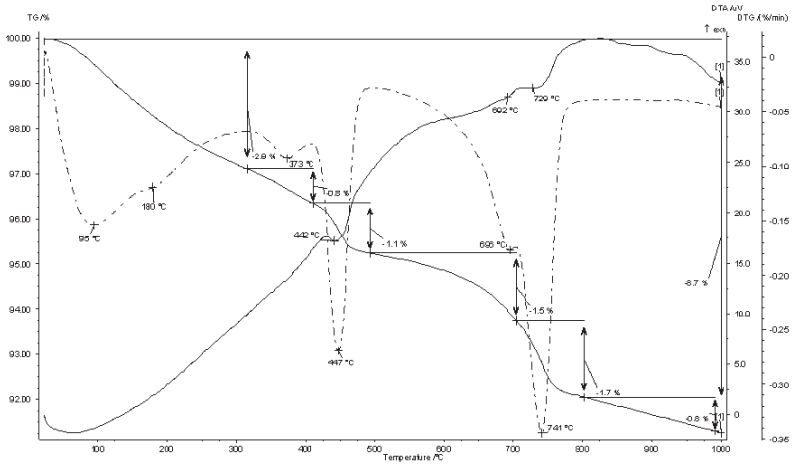

Figure 3. Thermogram of products of autoclave treatment basing on Novosibirsk CHP-5 ash at 20 % of lime at 8 hours of isothermal exposure

The thermogram of samples hydration products on the basis of Novosibirsk CHP-5 ash at 20 % of lime, with 8 hours of isothermal exposure with additional injection of 2% Na_2SO_4 (Figure 5) differs only slightly from the thermogram being addition-free of lime-ash mixture at 100 hours of isothermal exposure that indicates the activation of hydrothermal synthesis in the presence of sodium sulfate. However, with the activator additive, the proportion of C-A-S-H phase gets reduced, if judging by the weight loss at 727 °C endothermic effect.

Estimation of interrelation between strength of the stone with its composition of hydrate phases variety (Table 2) shows that it increases in proportion to the main XRD reflection of Al-tobermorite (11.5×10^{-10}m), to increase in weight loss both at the temperature range 180 °C (tobermorite) and at 730 °C (gel C-A-S-H) that indicates the correct classifying of that effects to hydrated phases. This pattern holds true for both addition-free and Na_2SO_4-activator systems.

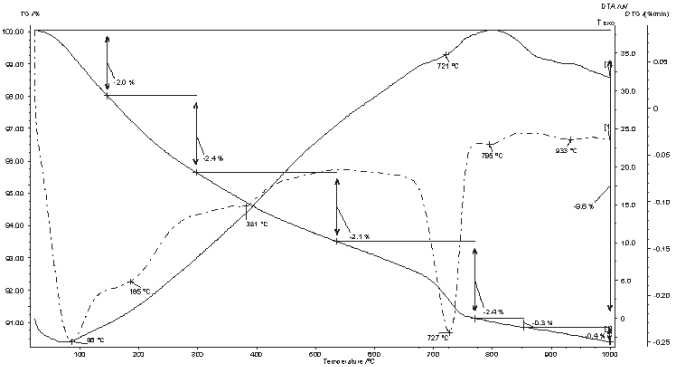

Figure 4. Thermogram of hydration products samples basing on Novosibirsk CHP-5 ash with 20 % of lime at 100 hours of isothermal exposure

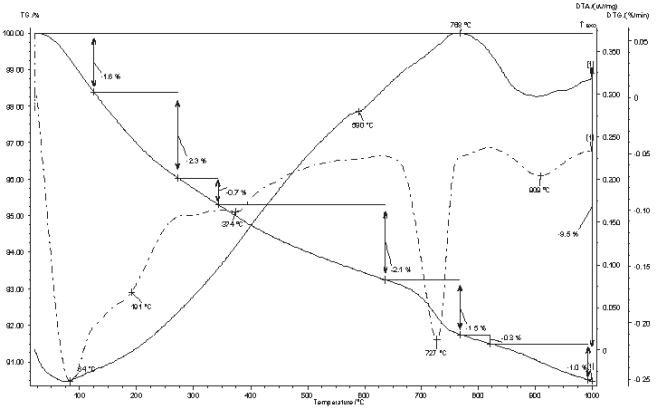

Figure 5. Thermogram of hydration products samples basing on Novosibirsk CHP-5 ash with 20 % of lime at 8 hours of isothermal exposure with additional injection of 2% Na_2SO_4.

Table 2 Strength and quantitative characteristics of phase contents in stone

Mass composition	Isotherm of autoclaving, h	Stone strength, MPa	Peak intensity $11.5x10^{-10}$ mtobermorite (XRD) length, mm	Weight loss DTG at 165-190, ^{0}C, % tobermorite	Weight loss DTG at 373-381, ^{0}C, % hydrogarnet katoite	Weight loss DTG at439-447, ^{0}C, % $CA(OH)_2$	Weight loss DTG at725-735 ^{0}C, % gel C-A-S-H
Base composition	8	20	48	1.5	0.8	1.1	1.7
Base composition	100	46	77	2.4	1.0	--	2.4
Base composition + 1% Na_2SO_4	8	26	96	2.3	0.8	0.4	2.0
Base composition + 1% Na_2SO_4	100	41	107	2.7	1.0	--	2.6
Base composition + 2% Na_2SO_4	8	31	60	2.3	0.9	--	1.5
Base composition + 2% Na_2SO_4	100	34	112	2.9	1.0	--	1.5

Note: base composition – 20% of lime + 80% of coal ash

Ovcharenko, G.I., Gilmiyarov, D.I. Strength and phase composition of autoclaved material: an approximation. Magazine of Civil Engineering. 2018. 83(7). Pp. 63–72. doi: 10.18720/MCE.83.6.

Quantitative phase composition of autoclave stone, after its recalculation on corresponding compounds, is shown in Figure 6.

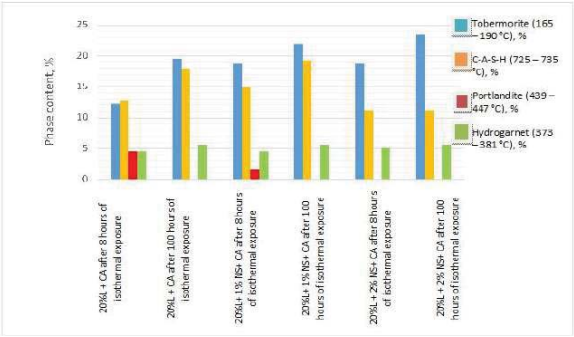

Figure 6. Quantitative phase composition of autoclave stone made of lime and ash. Notice: L – lime, NS – Na_2SO_4, CA – coal ash

The interrelation between strength and phase composition of the stone of the studied compositions is shown in Figures 7–9 from which is obvious that the strength of Na_2SO_4-free compositions is directly proportional to the content of both the Al-tobermorite and gel phase of C-A-S-H (Figure 7). This interrelation becomes less pronounced, but still maintained at 1% of sodium sulfate (Figure 8). However, with addition of 2% Na_2SO_4(Figure 9), this relationship is not observed anymore. At this, a considerable increase in Al-tobermorite in this composition according to both the data of XRD and DTG does not correspond completely to a slight increase in stone's strength. However, a small amount of C-A-S-H phase here fully agrees with the same slight increase in strength.

Thus, the strength of the autoclave stone made of lime-ash mixtures always proportional to the content of gel C-A-S-H phase. At the same time, the content of the latter can be or can be absolutely not proportional to the amount of Al-tobermorite. It is typical that initiating the synthesis of Al-tobermorite with the Na_2SO_4-addition, its crystallization is carried out at the expense of C-A-S-H phase. The content of katoite hydrogarnet remains practically unchanged at the 5–6% level.

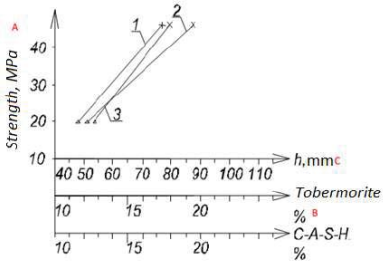

Figure 7. Correlation of lime-ash stone strength with its phase composition. 1 – Change in the intensity of the peak of aluminum substituted tobermorite according to the X-ray data; 2 – Change in content of aluminum substituted tobermorite according to the DTG data; 3 –Change in content of C-A-S-H according to the DTG data.

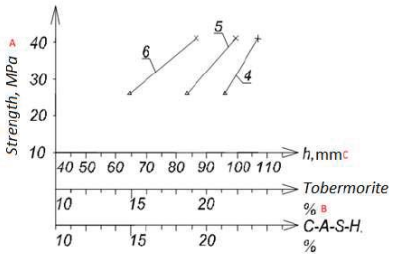

Figure 8. Correlation of lime-ash stone strength with its phase composition at addition of 1% Na_2SO_4. 4 – Change in the intensity of the peak of aluminum substituted tobermorite according to the X-ray data; 5 – change in content of aluminum substituted tobermorite according to the DTG data; 6 – change in content of C-A-S-H according to the DTG data. Note: ∆ – 8 hours of isothermal exposure; x – 100 hours of isothermal exposure

Овчаренко Г.И., Гильмияров Д.И. Взаимосвязь прочности и фазового состава автоклавированного материала // Инженерно-строительный журнал. 2018. № 7(83). С. 63–72.

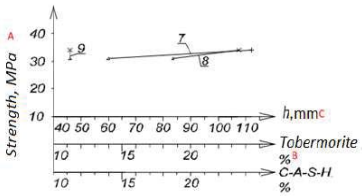

Figure 9. Correlation of lime-ash stone strength with its phase composition at addition of 2% Na_2SO_4. 7 – Change in the intensity of the peak of aluminum substituted tobermorite according to the X-ray data; 8 – change in content of aluminum substituted tobermorite according to the DTG data; 9 – change in content of C-A-S-H according to the DTG data

The results obtained conforms with the most recent publications [5–7] reporting the formation of the phase composition in the autoclave stone basing on lime-quartz and cement-aluminosilicate compositions with additions of alumina or sulphate-containing materials.

Thus, the results obtained on the strength of the stone (Figure 1) are well explained by the findings of its phase composition. When there is no addition of sodium sulfate, the strength is proportional to the content of Al-tobermorite and gel C-A-S-H content. By adding of sodium sulfate, the rate crystallization of Al-tobermorite is increased and it replaces C-A-S-H phase. The more complete this substitution occurs, the less the strength of the stone. This can be explained by the high specific surface area of the particles of the solid phase of the C-A-S-H gel, which "glue" the composite. It is known that the specific surface area phase C-S-H is 250–300 m^2/g.

However, the same rock strength is proportional to its density. Therefore, the larger the hydration products, the higher the density of the stone and greater its strength. For this reason, the strength of the stone through autoclaving 8 hours with admixture of sodium sulfate higher than without additives. Total weight loss of the composition without additives, after 8 hours of autoclaving was 8.7 % (Figure 3), and with the addition of sodium sulfate – 9.5% (Figure 5).

4. Conclusions

1. The strength of autoclaved stone based on lime and aluminosilicate ash of CHP increases in proportion to the duration of hydrothermal treatment. The amount of Al-tobomorite and the gel phase of C-A-S-H in the stone also increases in proportion. The hydrogarnet katoite plays a subordinate role and its quantity in the stone remains constant – 4–6 %.

2. Activation of hydrothermal synthesis in stone with the addition of Na_2SO_4 substantially redistributes the phase composition. The gel phase of C-A-S-H is significantly reduced by the crystallization of Al- tobermorite. The content of katoite remains constant. At the same time, it should be taken into account that when the hydration process is carried out, the C-A-S-H phase in tobermorite is activated, injected with alkaline sulphates, the total amount of hydrates is increased, which leads to the compaction of the stone increase its strength.

3. The strength of autoclave stone basing on aluminosilicate fly ash and lime is always proportional to the content of the C-A-S-H phase irrespectively to the content of tobermorite.

References

1. Kalousek, G.L., Adams, M. Tobermorite formation and strength of autoclave materials. Journal of the America concrete institute. 1951. No. 48. Pp. 77-81.
2. Crennan, G.M., El-Hemaly, S.A., Taylor, H.F.W. Autoclaved lime-quartz materials. Cement and Concrete Research. 1977. Vol. 7. Pp. 493–502.
3. Taylor, H.F.W. Cement Chemistry. Academic Press. London, 1990. 490 p.
4. Ray, A. Hydrothermally treated cement-based building materials. Past, present, and future. Pure Appl. Chem. 2002. Vol. 74. No. 11. Pp. 2131–2135.
5. Matsui, K., Kikuma, J., Tsunashima, M. In situ time-resolved X-ray diffraction of tobermorite formation in autoclaved aerated concrete: Influence of silica source reactivity and Al addition. Cement and Concrete Research. 2011. Vol. 41. No. I 5. Pp. 510–519.

Литература

1. Kalousek G.L., Adams M. Tobermorite formation and strength of autoclave materials // Journal of the America concrete institute. 1951. № 48. Pp. 77–81.
2. Crennan G.M., El-Hemaly S.A., Taylor H.F.W. Autoclaved lime-quartz materials // Cement and Concrete Research. 1977. Vol. 7. Pp. 493–502.
3. Taylor H.F.W. Cement Chemistry. Academic Press. London, 1990. 490 p.
4. Ray A. Hydrothermally treated cement-based building materials. Past, present, and future // Pure Appl. Chem. 2002. Vol. 74. № 11. Pp. 2131–2135.
5. Matsui K., Kikuma J., Tsunashima M. In situ time-resolved X-ray diffraction of tobermorite formation in autoclaved aerated concrete: Influence of silica source reactivity and Al addition // Cement and Concrete Research. 2011. Vol. 41. № I 5. Pp. 510–519.

Ovcharenko, G.I., Gilmiyarov, D.I. Strength and phase composition of autoclaved material: an approximation. Magazine of Civil Engineering. 2018. 83(7). Pp. 63–72. doi: 10.18720/MCE.83.6.

6. Ríos, C.A., Williams, C.D., Fullen, M.A. Hydrothermal synthesis of hydrogarnet and tobermorite at 175 °C from kaolinite and metakaolinite in the $CaO–Al_2O_3–SiO_2–H_2O$ system: A comparative study. Applied Clay Science. 2009. Vol. 43. Pp. 228–237.
7. Galvánková, L., Másilko, J., Solný, T., Štepánková, E. Tobermorite synthesis under hydrothermal conditions. Procedia Engineering. 2016. Vol. 151. Pp.100–107.
8. Komarneni, S., Roy, D.M. New tobermorite cation exchangers. Journal of material science. 1985. No. 20. Pp. 2930–2936.
9. Diamond, S., White, J.L., Dolch, W.L. Effects of isomorphous substitution in hydrothermally-synthesized tobermorite. American mineralogist. 1966. No. 51. Pp. 388–401.
10. Coleman, N.J., Brassington, D.S. Synthesis of Al-substituted 11A tobermorite from newsprint recycling residue: A feasibility study. Material research bulletin. 2003. No. 38. Pp. 485–497.
11. Coleman, N.J. Synthesis, structure and ion exchange properties of 11 Å tobermorities from newsprint recycling residue. Material research bulletin. 2005. No. 40. Pp. 2000–2013.
12. Volodchenko, A.N., Vorontsov, V.M., Golikov, G.G. Vliyanie paragenezisa kvarts – glinistyie mineralyi na svoystva avtoklavnyih silikatnyih materialov [Influence of paragenesis of quartz - clay minerals on the properties of autoclave silicate materials]. Izvestiya vuzov. Stroitelstvo. 2000. No. 10. Pp. 57–60. (rus)
13. Loganina, V.I., Pyshkina, I.S., Martyashin, G.V. Influence of the additive on the basis of calcium hydrosilicates on the resistance of calcareous coatings Magazine of Civil Engineering. 2017. 72(4). Pp. 20–27.
14. Sirotyuk, V.V., Lunyov, A.A. Strength and deformation characteristics of the ash and slag mixture. Magazine of Civil Engineering. 2017. 74(6). Pp. 3–16.
15. Volodchenko, A.N., Lesovik, V.S. Silikatnyie avtoklavnyie materialyi s ispolzovaniem nanodispersnogo syirya [Silicate autoclave materials using nanodisperse raw materials]. Stroitelnyie materialyi. 2008. No. 11. Pp. 42–43. (rus)
16. Yamb, E., Chemu, Zh. Lesovik, V.S. Stroitelnyie materialyi na osnove lateritnyih porod Kameruna i tsementa [Construction materials based on lateritic rocks of Cameroon and cement]. Vestnik BGTU im. V.G. Shuhova. 2010. No. 1. Pp. 27–33. (rus)
17. Volodchenko, A.N. Osobennosti vzaimodeystviya magnezialnoy glinyi s gidroksidom kaltsiya pri sinteze novoobrazovaniy i formirovanie mikrostrukturyi [Features of the interaction of magnesian clay with calcium hydroxide in the synthesis of hydrates and the formation of a microstructure]. Vestnik BGTU im. V.G. Shuhova. 2011. No. 2. Pp. 51–55. (rus)
18. Volodchenko, A.N., Lesovik, V.S. Avtoklavnyie yacheistyie betonyi na osnove magnezialnyih glin [Autoclaved cellular concrete based on magnesian clays]. Izvestiya vuzov. Stroitelstvo. 2012. No. 5. Pp. 14–21. (rus)
19. Strokova, V.V., Nelyubova, V.V., Altyinnik, N.I., Zhernovskiy, I.V. Fazoobrazovanie v sisteme tsement-izvest-kremnezem v gidrotermalnyih usloviyah s ispolzovaniem nanostrukturirovannogo modifikatora [Phase formation in the cement-lime-silica system under hydrothermal conditions using a nanostructured modifier] Stroitelnyie materialyi. 2013. No. 9. Pp. 30–32. (rus)
20. Tunega, D., Zaoui, A. Understanding of bonding and mechanical characteristics of cementious mineral tobermorite from first principles. Journal of the European Ceramic Societ. 2012. Vol. 32. Pp. 306–314.
21. Richardson, I.G. The calcium silicate hydrates. Cement Concrete Res. 2008. Vol. 38. Pp. 137–158.

6. Ríos C.A., Williams C.D., Fullen M.A. Hydrothermal synthesis of hydrogarnet and tobermorite at 175 °C from kaolinite and metakaolinite in the $CaO–Al_2O_3–SiO_2–H_2O$ system: A comparative study // Applied Clay Science. 2009. Vol. 43. Pp. 228–237.
7. Galvánková L., Másilko J., Solný T., Štepánková E. Tobermorite synthesis under hydrothermal conditions // Procedia Engineering. 2016. Vol. 151. Pp.100–107.
8. Komarneni S., Roy D.M. New tobermorite cation exchangers // Journal of material science. 1985. № 20. Pp. 2930–2936.
9. Diamond S., White J.L., Dolch W.L. Effects of isomorphous substitution in hydrothermally-synthesized tobermorite // American mineralogist. 1966. № 51. Pp. 388-401.
10. Coleman N.J., Brassington D.S. Synthesis of Al-substituted 11A tobermorite from newsprint recycling residue: A feasibility study // Material research bulletin. 2003. № 38. Pp.485–497.
11. Coleman N.J. Synthesis, structure and ion exchange properties of 11 Å tobermorities from newsprint recycling residue // Material research bulletin. 2005. № 40. Pp. 2000–2013.
12. Володченко А.Н., Воронцов В.М., Голиков Г.Г. Влияние парагенезиса «кварц-глинистые минералы» на свойства автоклавных силикатных материалов // Известия ВУЗов. Строительство. 2000. № 10. С. 57–60.
13. Логанина В.И., Пышкина И.С., Мартяшин Г.В. Влияние добавки на основе гидросиликатов кальция на стойкость известковых покрытий // Инженерно-строительный журнал. 2017. № 4(72). С. 20–27.
14. Сиротюк В.В., Лунёв А.А. Прочностные и деформационные характеристики золошлаковой смеси // Инженерно-строительный журнал. 2017. № 6(74). С. 3–16.
15. Володченко А.Н., Лесовик В.С. Силикатные автоклавные материалы с использованием нанодисперсного сырья // Строительные материалы. 2008. № 11. С. 42–43.
16. Ямб Э., Чему Ж., Лесовик В.С., Володченко А.Н. Строительные материалы на основе латеритных пород Камеруна и цемента // Вестник БГТУ им. В.Г. Шухова. 2010. № 1. С. 27–33.
17. Володченко А.Н. Особенности взаимодействия магнезиальной глины с гидроксидом кальция при синтезе новообразований иформирование микроструктуры // Вестник БГТУ им. В.Г. Шухова. 2011. № 2. С. 51–55.
18. Володченко А.Н., Лесовик В.С. Автоклавные ячеистые бетоны на основе магнезиальных глин // Известия ВУЗов. Строительство. 2012. № 5. Pp. 14–21.
19. Строкова В.В., Нелюбова В.В., Алтынник Н.И., Осадчий Е.Г. Фазообразование в системе цемент-известь-кремнезем в гидротер мальных условиях с использованием наноструктурированного модификатора // Строительные материа лы. 2013. № 9. С. 30–32.
20. Tunega D., Zaoui A. Understanding of bonding and mechanical characteristics of cementious mineral tobermorite from first principles // Journal of the European Ceramic Societ. 2012. Vol. 32. Pp. 306–314.
21. Richardson I.G. The calcium silicate hydrates // Cement Concrete Res. 2008. Vol. 38. Pp. 137–158.
22. Biagioni C., Merlino S., Bonaccorsi E., The tobermorite supergroup: a new nomenclature // Mineral. Mag. 2015. Vol. 79. Pp. 485–495.
23. Maeda H., Abe K., Ishida E.H. Hydrothermal synthesis of aluminium substituted tobermorite by using various crystal phases of alumina // J. Ceram. Soc. Jpn. 2011. Vol. 119 Pp. 375–377.

Овчаренко Г.И., Гильмияров Д.И. Взаимосвязь прочности и фазового состава автоклавированного материала // Инженерно-строительный журнал. 2018. № 7(83). С. 63–72.

22. Biagioni, C., Merlino, S., Bonaccorsi, E. The tobermorite supergroup: a new No.menclature. Mineral. Mag. 2015. Vol. 79. Pp. 485–495.
23. Maeda, H., Abe, K., Ishida, E.H. Hydrothermal synthesis of aluminium substituted tobermorite by using various crystal phases of alumina. J. Ceram. Soc. Jpn. 2011. Vol. 119. Pp. 375–377.
24. Coleman, N.J., Trice, C.J., Nicholson, J.W. 11 Å tobermorite from cement bypass dust and waste container glass: A feasibility study. Int. J. Miner. Process. 2009. Vol. 93. Pp. 73–78.
25. Tsutsumi, T., Nishimoto, S., Kameschima, Y. Hydrothermal preparation of tobermorite from blast furnace slag for Cs+ anr Sr2+ sorption. J. Hazard. Mater. 2014. Vol. 266. Pp. 174–181.
26. Mostafa, N.Y., Shaltout, A.A., Omar, H. Hydrothermal synthesis and characterization of aluminium and sulfate susbstituted 1.1 nm tobermorities. J. Alloys Compd. 2009. Vol. 467. Pp. 332–337.
27. Kikuma, J., Tsunashima, M., Ishikawa, T. Effect of quartz particle size and water-to-solid ratio on hydrothermal synthesis of tobermorite studied by in-situ time-resolved X-ray diffraction. J. Solid State Chem. 2011. Vol. 184. Pp. 2066–2074.
28. Jackson, M.D., Moon, J., Gotti, E. Material and Elastic Properties of Al-Tobermorite in Ancient Roman Seawater Concrete. Journal of the American Ceramic Society. 2013, Vol. 96. No. 8. Pp. 2598
29. Ilyukhin, V.V., Kuznetsov, V.A., Lobachev, A.N. Gidrosilikaty kalciya. Sintez monokristallov I kristallohimiya. [Calcium hydrosilicates. Synthesis of single crystals and crystal chemistry]. Moscow: Nauka, 1979. 184 p. (rus).
30. Churakov, S.V. Structural position of H_2O molecules and hydrogen bonding in anomalous 11 Å tobermorite. American Mineralogist. 2009. Vol. 94. Pp. 156–165.
31. Grangeon, S., Claret, F., Lerouge, C. On the nature of structural disorder in calcium silicate hydrates with a calcium/silicon ratio similar to tobermorite. Cement and Concrete Research. 2013. Vol. 52. Pp. 31–37.
32. Youssef, H., Ibrahim, D., Komarneni, S. Synthesis of 11 A Al-substituted tobermorite from trachyte rock by hydrothermal treatment. Ceramics International. 2010. No. 36. Pp. 203–209.
33. Miyake, M., Komarneni, S., Roy, R. Kinetics, Equilibria and Thermodynamics of Ion Exchange in Substituted Tobermorites. Material research bulletin. 1989. No. 24. Pp. 311–320.
34. Nocun-Wezelik, W. Effect of Na and Al on the phase composition and morphology of autoclaved calcium silicate hydrates. Cement Concrete Res. 1999. Vol. 29. Pp. 1759–1767.
35. Reinik, J., Heinmaa, I., Mikkola, J.-P. Hydrothermal alkaline treatment of oil shale ash for synthesis of Tobermorites. Fuel. 2007. No. 86. Pp. 669–676.
36. Huang, X., Jiang, Tan S. Tobermorites synthesiz from newsprint recycling residue. Journal of the European Ceramic Societ. 2003. No. 23. Pp. 123–126.
37. Komarneni, S., Komarneni, J.S., Newalkar, B. Microwave-hidrothermal synthesis of Al-substituted tobermorite from zeolites. Material research bulletin. 2002. Vol. 37. No. 6. Pp. 1025.

22. Biagioni, C., Merlino, S., Bonaccorsi, E. The tobermorite supergroup: a new No.menclature. Mineral. Mag. 2015. Vol. 79. Pp. 485–495.
23. Maeda, H., Abe, K., Ishida, E.H. Hydrothermal synthesis of aluminium substituted tobermorite by using various crystal phases of alumina. J. Ceram. Soc. Jpn. 2011. Vol. 119. Pp. 375–377.
24. Coleman, N.J., Trice, C.J., Nicholson, J.W. 11 Å tobermorite from cement bypass dust and waste container glass: A feasibility study. Int. J. Miner. Process. 2009. Vol. 93. Pp. 73–78.
25. Tsutsumi, T., Nishimoto, S., Kameschima, Y. Hydrothermal preparation of tobermorite from blast furnace slag for Cs+ anr Sr2+ sorption. J. Hazard. Mater. 2014. Vol. 266. Pp. 174–181.
26. Mostafa, N.Y., Shaltout, A.A., Omar, H. Hydrothermal synthesis and characterization of aluminium and sulfate susbstituted 1.1 nm tobermorities. J. Alloys Compd. 2009. Vol. 467. Pp. 332–337.
27. Kikuma, J., Tsunashima, M., Ishikawa, T. Effect of quartz particle size and water-to-solid ratio on hydrothermal synthesis of tobermorite studied by in-situ time-resolved X-ray diffraction. J. Solid State Chem. 2011. Vol. 184. Pp. 2066–2074.
28. Jackson, M.D., Moon, J., Gotti, E. Material and Elastic Properties of Al-Tobermorite in Ancient Roman Seawater Concrete. Journal of the American Ceramic Society. 2013, Vol. 96. No. 8. Pp. 2598
29. Ilyukhin, V.V., Kuznetsov, V.A., Lobachev, A.N. Gidrosilikaty kalciya. Sintez monokristallov I kristallohimiya. [Calcium hydrosilicates. Synthesis of single crystals and crystal chemistry]. Moscow: Nauka, 1979. 184 p. (rus).
30. Churakov, S.V. Structural position of H_2O molecules and hydrogen bonding in anomalous 11 Å tobermorite. American Mineralogist. 2009. Vol. 94. Pp. 156–165.
31. Grangeon, S., Claret, F., Lerouge, C. On the nature of structural disorder in calcium silicate hydrates with a calcium/silicon ratio similar to tobermorite. Cement and Concrete Research. 2013. Vol. 52. Pp. 31–37.
32. Youssef, H., Ibrahim, D., Komarneni, S. Synthesis of 11 A Al-substituted tobermorite from trachyte rock by hydrothermal treatment. Ceramics International. 2010. No. 36. Pp. 203–209.
33. Miyake, M., Komarneni, S., Roy, R. Kinetics, Equilibria and Thermodynamics of Ion Exchange in Substituted Tobermorites. Material research bulletin. 1989. No. 24. Pp. 311–320.
34. Nocun-Wezelik, W. Effect of Na and Al on the phase composition and morphology of autoclaved calcium silicate hydrates. Cement Concrete Res. 1999. Vol. 29. Pp. 1759–1767.
35. Reinik, J., Heinmaa, I., Mikkola, J.-P. Hydrothermal alkaline treatment of oil shale ash for synthesis of Tobermorites. Fuel. 2007. No. 86. Pp. 669–676.
36. Huang, X., Jiang, Tan S. Tobermorites synthesiz from newsprint recycling residue. Journal of the European Ceramic Societ. 2003. No. 23. Pp. 123–126.
37. Komarneni, S., Komarneni, J.S., Newalkar, B. Microwave-hidrothermal synthesis of Al-substituted tobermorite from zeolites. Material research bulletin. 2002. Vol. 37. No. 6. Pp. 1025.

Gennady Ovcharenko,*
+7(905)928-11-90; egogo1980@mail.ru

Danil Gilmiyarov,
+7(905)928-11-90; egogo1980@mail.ru

Геннадий Иванович Овчаренко,*
+7(905)928-11-90;
эл. почта: egogo1980@mail.ru

Данил Игоревич Гильмияров,
+7(905)928-11-90;
эл. почта: egogo1980@mail.ru

Ovcharenko, G.I., Gilmiyarov, D.I. Strength and phase composition of autoclaved material: an approximation. Magazine of Civil Engineering. 2018. 83(7). Pp. 63–72. doi: 10.18720/MCE.83.6.

doi: 10.18720/MCE.83.7

The nonlinear stress-strain state of the concrete-filled steel tube structures

Нелинейное напряженно-деформированное состояние трубобетонных конструкций

V.A. Snigireva*,
G.L. Gorynin,
Surgut State University, Surgut, Russia

Преподаватель В.А. Снигирева*,
д-р физ.-мат. наук, заведующий кафедрой Г.Л. Горынин,
Сургутский государственный университет, Сургут, Россия

Key words: concrete-filled steel tube structures; nonlinear concrete deformation diagram; concrete column in a steel cage

Ключевые слова: трубобетонные конструкции; нелинейная диаграмма деформирования бетона; бетонная стойка в стальной обойме

Abstract. The article is devoted to the mathematical modeling of the nonlinear stress-strain state of the concrete core in the concrete-filled steel tube structures. The paper uses a nonlinear diagram of concrete deformation under compression, which consists of two straight sections. In addition, the increase in the Poisson's ratio with increasing longitudinal deformations is taken into account. The article discusses two types of concrete-filled steel tube structures: the traditional concrete-filled steel tube column and the concrete column in steel tube cage. It is established that when the traditional concrete-filled steel tube column is loaded, the steel tube break contact with concrete core. This is the latent defect in such structures. The concrete column in steel tube cage does not have this defect. Concrete is acted to the three-dimensional compression here. It is concluded that taking into account the nonlinear behavior of concrete leads to the increasing of the calculated load-bearing capacity of the concrete column in the steel tube cage. In addition, change in the Poisson's ratio of concrete leads to the increasing of the load-bearing capacity too.

Аннотация. Статья посвящена математическому моделированию нелинейного напряженно-деформированного состояния бетонного ядра трубобетонных конструкций. В работе используется нелинейная диаграмма деформирования бетона при сжатии, которая состоит из двух прямолинейных участков. Кроме того, учитывается эффект возрастания величины коэффициента Пуассона при росте продольных деформаций. В статье рассматриваются два типа конструкций трубобетонных стоек: традиционная трубобетонная стойка и бетонная стойка в стальной обойме. Установлено, что при загружении традиционной стойки происходит отрыв стальной трубы от бетонного ядра, что является скрытым дефектом таких конструкций. Бетонная стойка в стальной обойме лишена этого недостатка, бетон в составе таких конструкций находится в состоянии трехосного сжатия. Сделан вывод, что учет нелинейного поведения бетона приводит к существенному увеличению расчетной несущей способности бетонной стойки в стальной обойме. Кроме того, учет эффекта изменения коэффициента Пуассона также приводит к дополнительному увеличению несущей способности стойки.

1. Introduction

The concrete-filled steel tube structures are composite structures, consisting of tube (often steel) and concrete filling, they are widely used as piles, columns or elements of trusses [1]. The stress-strain state of concrete-filled steel tube structures is complicated, since concrete and tube interact with each other in all directions. One of the variants of the cross section of concrete-filled steel tube structures is rectangular section [2], but the most rational form of the cross-section of such structures is the circle [3]. The object of our research is the stress-strain state of the concrete-filled steel tube column with circular cross-section.

According to many authors, the main advantage of concrete-filled steel tube structures is an increase of the load-bearing capacity of concrete. This fact is due to the reactive lateral pressure from the concrete to the tube side [4, 5]. The active use of concrete-filled steel tube structures is restricted due to the lack of a universal methodology for their calculation. Analytical calculation of such structures in accordance with the existing European standard EN1994-1-1 is based on empirical determination of the coefficients, these recommendations and formulas have a limited scope and can not be taken into account for the whole

Снигирева В.А., Горынин Г.Л. Нелинейное напряженно-деформированное состояние трубобетонных конструкций // Инженерно-строительный журнал. 2018. № 7(83). С. 73–82.

variety of building materials and structures [6]. The problem of calculating concrete-filled steel tube structures with a metal tube has been widely discussed since the first half of the 20th century. There are another point of view concerning the stress-strain state of concrete-filled steel tube columns under load presented by N. Skvortsov in 1953 [7]. In this work N. Skvortsov questions the availability of concrete compression by the steel tube. His argument is that the Poisson's ratio of concrete can never be greater than the Poisson's ratio of steel, and therefore the transverse deformation of concrete is always smaller than the transverse deformations of the steel tube, so concrete does not get compression by the steel tube. N. Skvortsov explains that the carrying capacity of compressible element, as observed from experiments, is increased due to the influence of frictional forces arising over the contact surface of the support plates of testing machines and the ends of the test specimens. Indeed, according to experimental studies of long samples, the steel tube is separated from the concrete core. The same effect was observed with the exploitation of the concrete-filled steel tube bridge across the Iset river [8]. The arguments advanced by N. Skvortsov were not supported by the majority of authors and in 1991, the book of L. Storozhenko "Calculation of concrete-filled steel tube structures" was published. The book describes an attempt to consider the problem of compression of a concrete-filled steel tube column as a spatial problem in the theory of elasticity [9]. However, in our opinion, the author did not take into account the fact that the normal longitudinal stresses in the concrete-filled steel tube element are negative (on page 49). As a result of that he made an incorrect conclusion that the difference in the Poisson's coefficients of concrete and steel "irrespective of the sign increases the rigidity of the composite bar brings the concrete core closer to the conditions of all-round compression". Many of the leading researchers refer to the works of L. Storozhenko [8, 10], but due to the presence of the error this work does not help clarify the question of the spatial work of the concrete-filled steel tube structures.

Thus, the topic of our research is actual, since the existing methods do not take into account the thickness of the tube wall and the forces of interaction between concrete and steel.

In connection with relevance of the above-described problem, the purpose of our research is to create the calculating method for the spatial stress-strain state of concrete-filled steel tube structures. To achieve the research purpose, it is necessary to fulfill the objectives: to derive formulas for simulating the spatial stress-strain state of concrete, taking into account the nonlinearity of the deformation; to analyze the interaction of concrete and steel tube in the structure; to suggest an improvement in concrete-filled steel tube structures; to derive formulas for the simulating the spatial stress-strain state of the proposed structure and analyze it.

Our research motivation is the desire to contribute to the effective application of the hidden advantages of concrete-filled steel tube structures, especially as they are widely used in construction.

2. Methods

2.1. Modelling of the stress-strain state of concrete in the nonlinear case

Modelling of the stress-strain state of concrete in the general case is a complex and unsolved problem because concrete has non-linearity of deformation [11]. In addition, the complex spatial stress-strain state is characteristic for concrete, which is part of concrete-filled steel tube structures due to interaction with the steel tube. We suppose that the concrete-filled steel tube column is under the action of the axial compressive force P. It is assumed that the stress-strain state of the structure has axial symmetry and the longitudinal displacements *W* depend only on the coordinate *z*, and the radial displacements *U* - on *r*, where "*z, θ, r*" is the cylindrical coordinate system (Figure 1). In this case, normal stresses $\sigma_{rr}, \sigma_{\theta\theta}, \sigma_{zz}$, arise, and tangential stresses do not arise.

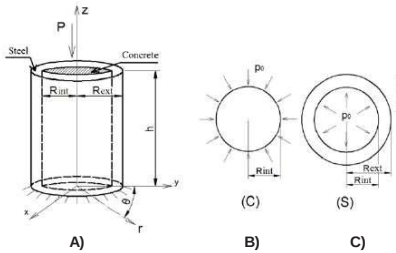

Figure 1. The design model; A) a concrete-filled steel tube column; B) the concrete core cross section of the column; C) the steel tube cross section of the column

To take into account the non-linearity of concrete deformation as state diagram determining the relationship between stresses and deformations, we use the three-line diagram (Figure 2) describing the uniaxial stress-strain state, according to the Russian Construction Norms and Regulations 63.13330.2012 "Concrete and reinforced concrete structures". There are no recommendations for taking into account the spatial stress-strain state of concrete in the Construction Norms and Regulations. We consider the proposed three-line diagram of uniaxial compression of concrete (Figure 2): when $\sigma < \sigma^* = 0.6R_b : \sigma = E\varepsilon$ (section 0-1); when $0.6R_b \le \sigma < R_b : \sigma = \sigma^* + \Delta\sigma$ (section 1-2), $\Delta\sigma$ – stress difference, R_b – design resistance of concrete under uniaxial compression. Many authors suggest a design model that takes into account the non-linearity of concrete deformation but the methods vary, because they are based on empirical dependencies [12].

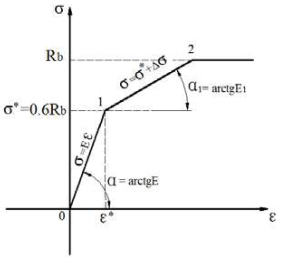

Figure 2. Three-line diagram of concrete deformation in uniaxial compression (Stresses and deformations are used without taking into account the sign)

Let us make natural assumption that the stresses in the radial and tangential directions of the concrete core of the concrete-filled steel tube column are much less than the axial stresses. Therefore, uniaxial stress-strain states, when radial and tangential stresses act separately, always correspond to section 0-1 of the diagram $(\sigma < 0.6R_b)$ (Figure2). But in the direction of the z-axis, two cases of the uniaxial stress-strain state are possible. Case 1: $\sigma_{zz} < 0.6R_b$ (section 0-1); or case 2: $0.6R_b \le \sigma_{zz} < R_b$ (section 1-2). At the initial stage (case 1), all components of the stress tensor $\sigma_{rr}, \sigma_{\theta\theta}\ \sigma_{zz}$ linearly depend on deformations, i.e. Hooke's law is valid (Figure 2):

$$\begin{cases} \sigma_{rr} = \dfrac{E}{(1-2\nu)(1+\nu)}\left((1-\nu)\cdot\varepsilon_{rr} + \nu\varepsilon_{zz} + \nu\varepsilon_{\theta\theta}\right); \\ \sigma_{zz} = \dfrac{E}{(1-2\nu)(1+\nu)}\left((1-\nu)\cdot\varepsilon_{zz} + \nu\varepsilon_{rr} + \nu\varepsilon_{\theta\theta}\right); \\ \sigma_{\theta\theta} = \dfrac{E}{(1-2\nu)(1+\nu)}\left((1-\nu)\cdot\varepsilon_{\theta\theta} + \nu\varepsilon_{rr} + \nu\varepsilon_{zz}\right), \end{cases} \quad (1)$$

where E, ν – the Young's modulus and the Poisson's ratio of concrete.

Let us consider case 2. In this state, the stresses and deformations in concrete are determined by the dependences:

$$\sigma_{rr} = \sigma^*_{rr} + \Delta\sigma_{rr};\ \sigma_{\theta\theta} = \sigma^*_{\theta\theta} + \Delta\sigma_{\theta\theta};\ \sigma_{zz} = \sigma^*_{zz} + \Delta\sigma_{zz}$$
$$\varepsilon_{rr} = \varepsilon^*_{rr} + \Delta\varepsilon_{rr};\ \varepsilon_{\theta\theta} = \varepsilon^*_{\theta\theta} + \Delta\varepsilon_{\theta\theta};\ \varepsilon_{zz} = \varepsilon^*_{zz} + \Delta\varepsilon_{zz}, \quad (2)$$

where $\sigma^*_{rr}, \sigma^*_{\theta\theta}, \sigma^*_{zz}, \varepsilon^*_{rr}, \varepsilon^*_{\theta\theta}, \varepsilon^*_{zz}$ – values of stresses and deformations, when $\sigma_{zz} = 0.6R_b$; $\Delta\sigma_{rr}, \Delta\sigma_{\theta\theta}, \Delta\sigma_{zz}, \Delta\varepsilon_{rr}, \Delta\varepsilon_{\theta\theta}, \Delta\varepsilon_{zz}$ – increments of stresses and deformations respectively.

We set that the deformation increments caused by the simultaneous action of radial, tangential and axial stress increments are the sum of the deformation increments caused by the action of these stress increments separately. Thus the generalized relations of the deformation increments have the form:

$$\begin{cases} \Delta\varepsilon_{rr} = \dfrac{\Delta\sigma_{rr}}{E} - \nu\dfrac{\Delta\sigma_{\theta\theta}}{E} - \nu_1\dfrac{\Delta\sigma_{zz}}{E_1}; \\ \Delta\varepsilon_{\theta\theta} = -\nu\dfrac{\Delta\sigma_{rr}}{E} + \dfrac{\Delta\sigma_{\theta\theta}}{E} - \nu_1\dfrac{\Delta\sigma_{zz}}{E_1}; \\ \Delta\varepsilon_{zz} = -\nu_2\dfrac{\Delta\sigma_{rr}}{E} - \nu_2\dfrac{\Delta\sigma_{\theta\theta}}{E} + \dfrac{\Delta\sigma_{zz}}{E_1}, \end{cases} \quad (3)$$

where E,ν and E_1,ν_1 – the Young's modulus and the Poisson's ratio of concrete, when the stress values correspond to sections 0-1 or 0-2 of the diagram, respectively.

Relations (3) are analogous to the Hooke's law for an orthotropic elastic body, the symmetry of the matrices of elastic constants implies the fulfillment of the relation :

$$\frac{\nu_1}{E_1} = \frac{\nu_2}{E} \quad (4)$$

Express the stress increments through the deformation increments from formulas (3), (4). Then equalities (2) and (5) are the spatial law of the stress-strain state of the concrete core of the concrete-filled steel tube column when $\sigma_{zz} \geq 0.6R_b$ (case 2).

$$\begin{cases} \Delta\sigma_{rr} = \Delta\varepsilon_{rr}\left(\dfrac{E}{1-\nu^2} + \dfrac{E^2\nu_1^2}{(1-\nu)(E_1(1-\nu)-2\nu_1^2E)}\right) + \Delta\varepsilon_{\theta\theta}\left(\dfrac{E\nu}{1-\nu^2} + \dfrac{E^2\nu_1^2}{(1-\nu)(E_1(1-\nu)-2\nu_1^2E)}\right) + \Delta\varepsilon_{zz}\dfrac{EE_1\nu_1}{E_1(1-\nu)-2\nu_1^2E}; \\ \Delta\sigma_{\theta\theta} = \Delta\varepsilon_{\theta\theta}\left(\dfrac{E}{1-\nu^2} + \dfrac{E^2\nu_1^2}{(1-\nu)(E_1(1-\nu)-2\nu_1^2E)}\right) + \Delta\varepsilon_{rr}\left(\dfrac{E\nu}{1-\nu^2} + \dfrac{E^2\nu_1^2}{(1-\nu)(E_1(1-\nu)-2\nu_1^2E)}\right) + \Delta\varepsilon_{zz}\dfrac{EE_1\nu_1}{E_1(1-\nu)-2\nu_1^2E}; \\ \Delta\sigma_{zz} = \dfrac{E_1^2(1-\nu)}{E_1(1-\nu)-2\nu_1^2E}\left(\Delta\varepsilon_{zz} + \dfrac{E\nu_1}{E_1(1-\nu)}\left(\Delta\varepsilon_{rr}+\Delta\varepsilon_{\theta\theta}\right)\right) \end{cases} \quad (5)$$

2.2. The traditional concrete-filled steel tube structures

We represent the solution of the problem of compressing the traditional concrete-filled steel tube structures.

Because of the axisymmetry of the problem, one of the equilibrium equations holds identically, while the remaining two simplify and have the form:

$$\frac{\partial\sigma_{rr}}{\partial r} + \frac{\sigma_{rr}-\sigma_{\theta\theta}}{r} = 0, \ \frac{\partial\sigma_{zz}}{\partial z} = 0. \quad (6)$$

In the future to indicate the physical characteristics related to the steel tube, we will use the superscript "S", to the concrete - the superscript "C".

The load P is acting on the entire cross-section, but the nature of load distribution on the steel shell the concrete core is not known. There are no longitudinal displacements of the points on the lower end of the column, this is due to an anchorage of the end (Figure 1), so the boundary conditions at the ends of the column have the form:

$$W = 0 \ \textit{(when z=0)}; \ \int_F \sigma_{zz}dF = -P \ \textit{(when z=h)}. \quad (7)$$

We assume that there is no lateral pressure on the outer cylindrical surface of the steel tube. Then the boundary condition on the lateral surface is valid (Figure 1):

$$\sigma_{rr}^S = 0 \ \textit{(when r=}R_{ext}\textit{)} \quad (8)$$

To ensure the joint operation of the steel tube-shell and the concrete cylinder, it is necessary to fulfill the conditions of layer interfacing (Figure1):

$$\sigma_{rr}^C = \sigma_{rr}^S \ \textit{(when r=}R_{int}\textit{) (Figure1)}, \ U^C = U^S, W^C = W^S. \quad (9)$$

We introduce the following notation:

p_0 – radial pressure at the contact of the layers, then $\sigma_{rr}^C = \sigma_{rr}^S = -p_0$ *(when r=R_{int})*, p^C, p^S – longitudinal (along the z-axis) compressive pressures to the concrete core and steel tube, respectively.

The stress-strain state of the tube material corresponds to the generalized the Hooke's law (1).

Let us consider the operation of the structure when the stress-strain state of concrete corresponds to case 1. The problem (1), (6) – (9) is the problem of the spatial theory of elasticity in the formulation of Saint-Venant, the solution of problems of this type is considered in the paper [12]. The solutions of the problems (1), (6) – (8) for the steel tube and the concrete core, separately taking into account the first equation for the stresses (9) and without taking into account the second and the third equalities has the form:

$$\begin{cases} \sigma_{rr}^S = \dfrac{p_0 \cdot R_{\text{int}}^2 \cdot (r^2 - R_{ext}^2)}{(R_{ext}^2 - R_{\text{int}}^2) \cdot r^2}; \\ \sigma_{zz}^S = -p^S; \\ \sigma_{\theta\theta}^S = \dfrac{p_0 \cdot R_{\text{int}}^2 \cdot (r^2 + R_{ext}^2)}{(R_{ext}^2 - R_{\text{int}}^2) \cdot r^2}. \end{cases} \quad \begin{cases} \sigma_{rr}^C = -p_0; \\ \sigma_{zz}^C = -p^C; \\ \sigma_{\theta\theta}^C = -p_0. \end{cases} \tag{10}$$

Taking into account the second and the third equalities of the conditions of layer interfacing (9) and the equalities (7), we obtain the solution of problem (1), (6) – (9):

$$p^C = p_0 \cdot \left(\frac{(1-2\nu^C)\cdot(1+\nu^C)}{(\nu^C - \nu^S)} + 2\nu^C + \frac{E^C}{E^S} \cdot \frac{R_{\text{int}}^2 (1-2\nu^S)\cdot(1+\nu^S) + R_{ext}^2 (1+\nu^S)}{(\nu^C - \nu^S)\cdot(R_{ext}^2 - R_{\text{int}}^2)} \right),$$

$$p^S = p_0 \cdot \left(\frac{E^S}{E^C} \frac{(1-2\nu^C)\cdot(1+\nu^C)}{(\nu^C - \nu^S)} + \frac{R_{\text{int}}^2 (1-\nu^S) + R_{ext}^2 (1+\nu^S) - 2R_{\text{int}}^2 \nu^S \nu^C}{(\nu^C - \nu^S)\cdot(R_{ext}^2 - R_{\text{int}}^2)} \right), \tag{11}$$

$$p_0 = P \cdot \frac{E^C E^S (\nu^C - \nu^S)(R_{ext}^2 - R_{\text{int}}^2)}{\alpha},$$

where
$$\alpha = \pi R_{\text{int}}^2 E^C \left(E^S (1 - \nu^C - 2\nu^C \nu^S)(R_{ext}^2 - R_{\text{int}}^2) + E^C (1+\nu^S)(R_{\text{int}}^2 (1-2\nu^S) + R_{ext}^2) \right)$$
$$+ \pi (R_{ext}^2 - R_{\text{int}}^2) E^S \left(E^S (1-2\nu^C)(1+\nu^C)(R_{ext}^2 - R_{\text{int}}^2) + E^C \left(R_{\text{int}}^2 (1 - \nu^S - 2\nu^S \nu^C) + R_{ext}^2 (1+\nu^S) \right) \right).$$

Let us analyze the obtained dependences and draw the main conclusions:

According to formula (11), the compression pressure sign p_0 is completely determined by the difference in Poisson's coefficients of concrete and steel $(\nu^C - \nu^S)$.

The Poisson's ratio of concrete is $\nu^C = 0.2$, the Poisson's ratio of steel is $\nu^S = 0.3$ (according to the Construction Norms and Regulations 63.13330.2012 “Concrete and reinforced concrete structures” and Construction Norms and Regulations 16.13330.2011 "Steel Structures"), therefore, the compression pressure p_0,<0 and the radial stresses in the concrete core are tensile (10), which leads to break of contact between the concrete core and the steel tube, and therefore, the joint work of concrete and steel is not realized. This is the latent defect of traditional the concrete-filled steel tube structures. This fact is also confirmed when calculating the traditional structures taking into account the nonlinear deformation of concrete.

2.3. The concrete column in steel tube cage

Since the traditional concrete-filled steel tube structures have the latent defect, as mentioned above, in [13] the authors proposed different concrete-filled steel tube structure - the concrete column in steel tube cage. When using this structure, the external load is applied only to the concrete core, and the tube is used as a cage, while the joint work of the concrete core and the steel tube in the longitudinal direction is excluded.

Let us consider the operation of the structure when the stressed state of concrete corresponds to case 1. The equations of equilibrium (6) and the Hooke's law (1) for concrete and steel and the boundary

condition on the lateral surface (8) remain in effect in the formulation of this problem, but the boundary conditions at the ends of (7) vary and have the form:

$$W = 0 \ \textit{(when z=0)}; \ \int_{F^C} \sigma_{zz} dF = -P \ \textit{(when z=h)}. \tag{12}$$

In this design, there is no joint work of the concrete core and the steel tube in the longitudinal direction, and the interaction in the transverse direction is performed according to the following conditions of layer interfacing:

$$\sigma_{rr}^C = \sigma_{rr}^S, \ U^C = U^S. \textit{(when } r=R_{int}\textit{)} \tag{13}$$

The boundary problem (1), (6), (8), (12), (13) is the problem of the spatial theory of elasticity in the formulation of Saint-Venant. We obtain the solution of problems (1), (6), (8), (12) for a steel tube and a concrete core separately, taking into account the fact that the longitudinal pressure acts only on concrete, and there is no joint work of the layers (13):

$$\begin{cases} \sigma_{rr}^S = \dfrac{p_0 \cdot R_{\text{int}}^2 \cdot (r^2 - R_{ext}^2)}{(R_{ext}^2 - R_{\text{int}}^2) \cdot r^2}; \\ \sigma_{zz}^S = -p^S = 0; \\ \sigma_{\theta\theta}^S = \dfrac{p_0 \cdot R_{\text{int}}^2 \cdot (r^2 + R_{ext}^2)}{(R_{ext}^2 - R_{\text{int}}^2) \cdot r^2}. \end{cases} \quad \begin{cases} \sigma_{rr}^C = -p_0; \\ \sigma_{zz}^C = -p^C = -\dfrac{P}{F^C}. \\ \sigma_{\theta\theta}^C = -p_0. \end{cases} \tag{14}$$

The equations (14) are obtained only with the use of equilibrium equations and do not depend on the linearity or nonlinearity of the concrete deformation law. The magnitude of the interaction pressure of the layers p_0 depends on the nature of the material deformation.

Taking into account the conditions of layer interfacing (13) and the equalities (12), we obtain the solution of the problem (1), (6), (8), (12), (13), in which the stress-strain state of concrete corresponds to the law (1) (case 1):

$$p_0 = \frac{P}{\pi R_{\text{int}}^2} \cdot \frac{E^S \nu^C \left(R_{ext}^2 - R_{\text{int}}^2\right)}{E^C \left(R_{\text{int}}^2 \left(1-\nu^S\right) + R_{ext}^2 \left(1+\nu^S\right)\right) + E^S \left(R_{ext}^2 - R_{\text{int}}^2\right)\left(1-\nu^C\right)}. \tag{15}$$

It follows from formula (15) that the compression pressure p_0 is always a positive value, hence the radial stresses in the concrete core are compressive, the concrete is in a state of triaxial compression (according to formula (14)). This fact has a positive effect on increasing the strength of the concrete core, as shown by the experiments of the researchers [15, 16].

We consider the operation of the structure when the stress state of concrete corresponds to case 2, that is, taking into account the nonlinearity of the concrete deformation diagram.

In the future, to denote the values related to the solution of the problem, taking into account the nonlinearity of the concrete deformation diagram, we will use the superscript "n", and when considering the deformation of concrete according to Hooke's linear law, the superscript "l".

Taking into account the conditions of layer interfacing (13) and the solutions obtained for the independently operating steel tube cage and the concrete cylinder (14), we obtain the solution of the non-linear problem (1), (2), (5), (6), (8), (12), (13), in which the stress-strain state of concrete obeys the law (2), (5) (case 2):

$$p^n{}_0 = \left(\frac{P}{\pi R_{\text{int}}^2} \cdot \frac{\nu_1^C}{E_1^C} + \frac{E^C \nu_1^C - E_1^C \nu^C}{E_1^C \left(1-2\nu^C\right)\left(1+\nu^C\right)} \cdot \left(\nu^C \varepsilon_{rr}^* + \nu^C \varepsilon_{\theta\theta}^* + \left(1-\nu^C\right)\varepsilon_{zz}^* \right) \right) \cdot$$
$$\cdot \frac{E^C E^S \left(R_{ext}^2 - R_{\text{int}}^2\right)}{E^S \left(1-\nu^C\right)\left(R_{ext}^2 - R_{\text{int}}^2\right) + E^C \left(\left(1-\nu^S\right) R_{вн}^2 R_{\text{int}}^2 + \left(1+\nu^S\right) R_{ext}^2\right)} \tag{16}$$

3. Results and Discussion

3.1. The increasing the load-bearing capacity of concrete under comprehensive compression

Let us analyze the increase in the load-bearing capacity of the concrete column in steel tube cage due to strengthening of the concrete core. The most common form of presenting the strength of concrete under a three-axis contraction is the formula proposed by F. Richard, A. Brown and A. Brandraeg [15]:

$$R_{b,3} = R_b + K \cdot p_0 \ ,$$

where $R_{b,3}$ – the design resistance of concrete under three-axial compression, K – the concrete strengthening coefficient $K \approx 4$.

Thus the formula for determining the strength of concrete under triaxial compression has the form:

$$R_{b,3} = R_b + 4 \cdot p_0$$

In order to further increase the load-carrying capacity of concrete-filled steel tube structures, in cases where vibration is impossible it is more preferable to apply self-compacting concrete mixtures [17].

3.2. An example

Let us consider an example of calculation of the concrete-filled steel tube column. We compare two different approaches: the nonlinear model of the concrete deformation diagram (case 2) and the linear model (case 1). We take different thickness of the tube wall and R_{int} = 0.210 m. We assume the deformation-strength characteristics of materials: E^C = 30000 MPa, $E_1{}^C$ = 8571.4 MPa, ν^C = 0.2, ν_1^C = 0.2, R_b = 14.5 MPa (concrete B 25) and E_S = 206000 MPa, ν^S = 0.3. The results are presented in Table 1, where Δ is the increment of pressure. For example, when the wall thickness is 4 mm, we have the maximum value P_3^n = 2.56 MN, P_3^i = 2.2 MN, and the values of the design resistance of concrete under three-axial $R_{b,3}^n$ = 18.56 MPa, $R_{b,3}^l$ = 15.95 MPa(Figure 3).

Table 1. Results of calculations when ν^C = 0.2, ν_1^C = 0.2

Tube wall thickness, mm	$\frac{\Delta p_0^l}{\Delta p^C}$	$\frac{\Delta p_0^n}{\Delta p^C}$	$\frac{\max p_0^n}{\max p_0^l}$	$\frac{R_{b,3}^l}{R_b}$	$\frac{R_{b,3}^n}{R_b}$	$\frac{R_{b,3}^n}{R_{b,3}^l}$
4	0.02	0.08	2.69	1.10	1.28	1.16
4.5	0.03	0.09	2.81	1.12	1.33	1.19
5	0.03	0.10	2.96	1.13	1.38	1.22
10	0.05	0.18	5.41	1.25	2.36	1.89

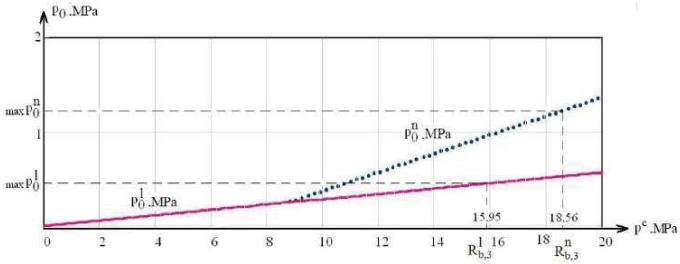

Figure 3. Dependence of the radial compression pressure on the axial compressive pressure on concrete when ν^C = 0.2, ν_1^C = 0.2, and the wall thickness of the pipe is 4 mm.

Снигирева В.А., Горынин Г.Л. Нелинейное напряженно-деформированное состояние трубобетонных конструкций // Инженерно-строительный журнал. 2018. № 7(83). С. 73–82.

According to the results (Table 2) and the presented graph (Figure 3), the calculated compression pressure of concrete is underestimated. Thus the design load-bearing capacity of the structure is also underestimated as the result of calculation by the linear model.

It is known that the Poisson's ratio of concrete is the variable that increases with increasing of load on concrete [18]. We perform calculations with the initial data presented above but the Poisson's ratio of concrete is different ν_1^C = 0.25. The results are presented in Table 2.

Table 2. Results of calculations when ν^C = 0.2, ν_1^C = 0.25

Tube wall thickness, mm	$\frac{\Delta p_0^l}{\Delta p^C}$	$\frac{\Delta p_0^n}{\Delta p^C}$	$\frac{\max p_0^n}{\max p_0^l}$	$\frac{R_{b,3}^l}{R_b}$	$\frac{R_{b,3}^n}{R_b}$	$\frac{R_{b,3}^n}{R_{b,3}^l}$
4	0.02	0.10	3.60	1.10	1.37	1.24
4.5	0.03	0.11	3.86	1.12	1.45	1.30
5	0.03	0.12	4.15	1.13	1.53	1.36
10	0.05	0.22	15.67	1.25	4.95	3.95

Comparison of the results presented in Tables 1 and 2 shows that in the case when we taking into account the increase in the Poisson's ratio of concrete, the value of the calculated bearing capacity of the concrete core is higher than this value when the calculation is made with an unchanged coefficient.

3.3. Discussion

According to the calculation of the formulas obtained by us (10-11), when loading traditional concrete-filled steel tube structures, contact between the concrete core and the steel tube breaks, these results confirm the position of N. Skvortsov [7].However, a universal calculation model for concrete-filled steel tube structures was not developed by him.

Different approaches to calculate concrete-filled steel tube structures are mainly based on the calculation of the uniaxial stress-strain state. In this case the load-bearing capacity of the centrally compressed concrete-filled steel tube element is determined by the formula [3, 6, 19]:

$$N = (c \cdot R_b + d) \cdot F_b + \alpha \cdot F_s \cdot R_s, \quad (17)$$

where R_b and R_s – the design resistances to the axial compression of concrete and steel respectavly; F_b and F_s - the cross-sectional area of the concrete core and the steel tube; c, d, α – the constant coefficients determined experimentally.

The limits of the coefficients *c, d* and *α* for various geometric and mechanical characteristics of steel and concrete have been determined as a result of numerous experiments and thus it possible to formulate practical recommendations on their calculation. However, since this calculation method (17) is based on empirical determination of the coefficients, these recommendations and formulas have limited scope and can not be taken into account for the whole variety of building materials and structures [19–21]. The refinement of the empirical coefficients requires new extensive and time-consuming experiments. This is due to the fact that the empirical dependence (17) does not take into account the spatial work of the concrete-filled steel tube structures. In this article, we presented formulas for three-dimensional calculating the concrete-filled steel tube structures taking into account the non-linearity of spatial deformation of concrete, the interaction of steel tube and concrete, the characteristics of materials, and the structure dimensions.

4. Conclusions

1. The model for three-dimensional the stress-strain state of concrete taking into account the non-linear concrete behavior (2)-(3) are presented.

2. We present the derivation of analytical solution for the three-dimensional model of the concrete column in steel tube cage taking into account the non-linear model.

3. Taking into account the nonlinear behavior of concrete leads to the increasing of the calculated load-bearing capacity of the concrete column in the steel tube cage by 16–89 %, depending on the tube wall thickness.

4. Change in the Poisson's ratio of concrete leads to the increasing of the load-bearing capacity of the concrete column in the steel tube cage by 7–109 % too, depending on the tube wall thickness.

5. Acknowledgement

The reported study was funded by RFBR according to the research project No. 18-07-01326.

References

1. Prachasaree, W., Piriyakootorn, S., Sangsrijun, A., Limkatanyu, S. Behavior and Performance of GFRP Reinforced Concrete Columns with Various Types of Stirrups. International Journal of Polymer Science. 2015. Article ID 237231.
2. Kanishchev, R.A. Analysis of local stability of the rectangular tubes filled with concrete. Magazine of Civil Engineering. 2016. No. 4. Pp. 59–68.
3. Krishan, A.L., Chernyshova, E.P., Sabirov, R.R. Calculating the Strength of Concrete Filled Steel Tube Columns of Solid and Ring Cross-section. Procedia Engineering. 2016. No. 150. Pp. 1878–1884.
4. Ma, J., Liu, Y., Gao, Q., Hou, K. Investigating the Hysteretic Behavior of Concrete-Filled Steel Tube Arch by Using a Fiber Beam Element. Mathematical Problems in Engineering. 2015. Vol. 2015. Article number 409530.
5. Liang, Q.Q. Numerical simulation of high strength circular double-skin concrete-filled steel tubular slender columns. Engineering Structures. 2018. Vol. 168. Pp. 205–217.
6. Eurocode 4. Common Unified Rules for Composite Steel and concrete Structures European Committee for Standardization. (CEN) ENV. 1994. 180 p.
7. Skvorcov, N.F. Prochnost' staletrubobetona [Strength of concrete-filled steel tube structures] The DSc dissertation of Tech.Sci. Moscow. 1953. 453 p. (rus)
8. Krishan, A.L., Troshkina, E.A., Chernyshova, E.P. Efficient Design of Concrete Filled Steel Tube Columns. Procedia Engineering. 2016. No. 150. Pp. 1709-1714.
9. Stosozhenko, L.I., Plahotniy, P.I., Cherniy, A.Ya. Raschet trubobetonnyh konstrukciy [Calculation of concrete-filled steel tube structures]. Kiev: Budivel'nik, 1991. 120 p. (rus)
10. Lapenko, O.I., Shevchenko, O.V., Masud, N.N. Compression Work of Steel Reinforced Concrete Columns. International Journal of Engineering & Technology. 2018. No. 7(3.2). Pp. 229–231.
11. Benin, A.V., Semenov, A.S., Semenov, S.G., Beliaev, M.O., Modestov, V.S. Methods of identification of concrete elastic-plastic-damage models. Magazine of Civil Engineering. 2017. No. 8. Pp. 279–297.
12. Patel, V.I., Liang, Q.Q., Hadi, M.N.S. Nonlinear analysis of biaxially loaded rectangular concrete-filled stainless steel tubular slender beam-columns. Engineering Structures. 2017. No. 140. Pp. 120–133
13. Gorynin, G.L., Snigireva, V.A. Non-linear simulation of load-bearing capacity for steel-encased concrete piles. Advances in Engineering Research. 2017. Vol. 133. Pp. 816–822.
14. Gorynin, G.L., Nemirovskii, Yu.V. Deformation of laminated anisotropic bars in the three-dimensional statement 1.Transverse-longitudinal bending and edge compatibility condition. Mechanics of Composite Materials. 2009. Vol. 45. No. 3. Pp. 257–280.
15. Richart, F., Brown, A., Brandraeg, A. A study of failure of concrete under combined compressive stresses. University Illinois, Eng. Exper. Station. Bull. No. 185. 1928. 105 p.
16. Thermou, G. E., Papanikolaou, V.K., Kappos, A. J. Flexural behaviour of reinforced concrete jacketed columns under reversed cyclic loading. Engineering Structures. 2014. No. 76. Pp. 270–282.

Литература

1. Prachasaree W., Piriyakootorn S., Sangsrijun A., Limkatanyu S. Behavior and Performance of GFRP Reinforced Concrete Columns with Various Types of Stirrups // International Journal of Polymer Science. 2015. Article ID 237231.
2. Каницщев Р.А. Анализ местной устойчивости трубобетонных конструкций прямоугольного сечения // Инженерно-строительный журнал. 2016. № 4(64). С. 59–68.
3. Krishan A.L., Chernyshova E.P., Sabirov R.R. Calculating the Strength of Concrete Filled Steel Tube Columns of Solid and Ring Cross-section // Procedia Engineering. 2016. № 150. Pp. 1878–1884.
4. Ma J., Liu Y., Gao Q., Hou K. Investigating the hysteretic behavior of concrete-filled steel tube arch by using a fiber beam element // Mathematical Problems in Engineering. 2015. Vol. 2015. Article number 409530.
5. Liang Q.Q. Numerical simulation of high strength circular double-skin concrete-filled steel tubular slender columns // Engineering Structures. 2018. Vol. 168. Pp. 205–217.
6. Eurocode 4. Common Unified Rules for Composite Steel and concrete Structures European Committee for Standardization. (CEN) ENV. 1994. 180 p.
7. Скворцов Н.Ф. Прочность сталетрубобетона: Дисс. . докт. техн. наук.-М, 1953.- 453с.
8. Krishan A.L., Troshkina E.A., Chernyshova E.P. Efficient Design of Concrete Filled Steel Tube Columns // Procedia Engineering. 2016. № 150. Pp. 1709–1714.
9. Стороженко Л.И., Плахотный П.И., Черный А.Я. Расчет трубобетонных конструкций. Киев: Будивельник, 1991. 120 с.
10. Lapenko O.I., Shevchenko O.V., Masud N.N. Compression Work of Steel Reinforced Concrete Columns // International Journal of Engineering & Technology. 2018. № 7(3.2). Pp. 229–231.
11. Бенин А.В., Семенов А.С., Семенов С.Г., Беляев М.О., Модестов В.С. Методы идентификации упругопластических моделей бетона с учетом накопления повреждений // Инженерно-строительный журнал. 2017. № 8(76). С. 279–297.
12. Patel V.I., Liang Q.Q., Hadi M.N.S. Nonlinear analysis of biaxially loaded rectangular concrete-filled stainless steel tubular slender beam-columns // Engineering Structures. 2017. № 140. Pp. 120–133.
13. Gorynin G.L., Snigireva V.A. Non-linear simulation of load-bearing capacity for steel-encased concrete piles // Advances in Engineering Research. 2017. Vol. 133. Pp. 816–822.
14. Gorynin G.L., Nemirovskii Yu.V. Deformation of laminated anisotropic bars in the three-dimensional statement 1.Transverse-longitudinal bending and edge compatibility condition // Mechanics of Composite Materials. 2009. Vol. 45. № 3. Pp. 257–280.
15. Richart F., Brown A., Brandraeg A. A study of failure of concrete under combined compressive stresses. University Illinois, Eng. Exper. Station. Bull. № 185. 1928. 105 p.
16. Thermou G. E., Papanikolaou V.K., Kappos, A. J. Flexural behaviour of reinforced concrete jacketed columns under reversed cyclic loading // Engineering Structures. 2014. № 76. Pp. 270–282

Снигирева В.А., Горынин Г.Л. Нелинейное напряженно-деформированное состояние трубобетонных конструкций // Инженерно-строительный журнал. 2018. № 7(83). С. 73–82.

17. Larsen, L.O., Naruts, V.V. Self-compacting concrete with limestone powder for transport infrastructure. Magazine of Civil Engineering. 2016. No. 8. Pp. 76–85.
18. Zhang, J., Jiang, S., Chen, B., Li, Ch., Qin, H. Numerical Study of Damage Modes and Damage Assessment of CFST Columns under Blast Loading. Shock and Vibration. 2016. Vol. 2016. Article number 3972791.
19. Deng, J., Zheng, Y., Wang, Y., Liu, T., Li, H. Study on axial compressive capacity of frp-confined concrete-filled steel tubes and its comparisons with other composite structural systems. International Journal of Polymer Science. 2017. Vol. 2017. Article number 6272754.
20. Teng, J.G., Xiao, Q.G, Yu, T. Three-dimensional finite element analysis of reinforced concrete columns with FRP and/or steel confinement. Engineering Structures. 2015. Vol. 97. Pp. 15–28.
21. Hassanein, M.F., Patel, V.I., Bock, M. Behaviour and design of hexagonal concrete-filled steel tubular short columns under axial compression. Engineering Structures. 2017. No. 153. Pp. 732–748.

Vera Snigireva,*
+7(982)416-44-14; snow-vera@mail.ru

Gleb Gorynin,
+7(904)872-84-76; ggorynin@list.ru

17. Ларсен О.А., Наруть В.В. Самоуплотняющийся бетон с карбонатным наполнителем для объектов транспортной инфраструктуры // Инженерно-строительный журнал. 2016. № 8(68). С. 76–85.
18. Zhang J., Jiang S., Chen B., Li Ch., Qin H. Numerical Study of Damage Modes and Damage Assessment of CFST Columns under Blast Loading // Shock and Vibration. 2016. Vol. 2016. Article number 3972791.
19. Deng J., Zheng Y., Wang Y., Liu T., Li H. Study on axial compressive capacity of frp-confined concrete-filled steel tubes and its comparisons with other composite structural systems // International Journal of Polymer Science. 2017. Vol. 2017. Article number 6272754.
20. Teng J.G., Xiao Q.G., Yu T. Three-dimensional finite element analysis of reinforced concrete columns with FRP and/or steel confinement // Engineering Structures. 2015. Vol. 97. Pp. 15–28.
21. Hassanein M.F., Patel V.I., Bock M. Behaviour and design of hexagonal concrete-filled steel tubular short columns under axial compression // Engineering Structures. 2017. № 153. Pp. 732–748.

Вера Алексеевна Снигирева,*
+7(982)416-44-14;
эл. почта: snow-vera@mail.ru

Глеб Леонидович Горынин,
+7(904)872-84-76; эл. почта: ggorynin@list.ru

Snigireva, V.A., Gorynin, G.L. The nonlinear stress-strain state of the concrete-filled steel tube structures. Magazine of Civil Engineering. 2018. 83(7). Pp. 73–82. doi: 10.18720/MCE.83.7.

doi: 10.18720/MCE.83.8

Filled epoxy composites based on polyfraction microcalcite

Наполненные эпоксидные композиты на основе полифракционного микрокальцита

T.A. Nizina*,
Ogarev Mordovia State University, Saransk, Russia
J.A. Sokolova,
National Research Moscow State University of Civil Engineering, Moscow, Russia
A.N. Chernov,
D.R. Nizin,
A.I. Popova,
N.S. Kanaeva,
Ogarev Mordovia State University, Saransk, Russia

Д-р техн. наук, профессор Т.А. Низина*,
Мордовский государственный университет им. Н.П. Огарёва, Саранск, Россия
д-р техн. наук, профессор Ю.А. Соколова,
Национальный исследовательский Московский государственный строительный университет, Москва, Россия
аспирант А.Н. Чернов,
канд. техн. наук, младший научный сотрудник Д.Р. Низин,
магистрант А.И. Попова,
аспирант Н.С. Канаева,
Мордовский государственный университет им. Н.П. Огарёва, Саранск, Россия

Key words: epoxy composites; filler; micromarble; degree of filling; ultimate strength at compression; ultimate bending tensile strength; isolines; triangular Gibbs-Roseboom diagrams

Ключевые слова: эпоксидные композиты; наполнитель; микромрамор; степень наполнения; предел прочности при сжатии; предел прочности на растяжение при изгибе; изолинии; треугольные диаграммы Гиббса-Розебома

Abstract. The effect of the polyfractional micromarble introduction on the change in the physical and mechanical characteristics of polymer composites based on low-viscosity epoxy binders has been studied. Evaluation of changes in compressive strength and tensile strength in bending of epoxy composites samples containing micromarble of three different fractions, depending on the degree of filling, was carried out. Using the method of least squares, mathematical dependences of the epoxy composites strength characteristics on the type of used micromarble and the degree of filling have been obtained. The analysis of isolines and Gibbs-Rosebom triangular diagrams allowed to determine the composition of the polyfractional filler, the composites on the basis of which have the greatest strength characteristics. Polymer composite containing a mixture of micromarble of different fractions in the amount of 80 % of the maximum filling level and having an increased compressive strength (up to 40 %) and close to the limit tensile strength during bending (decrease by no more than 10 %) compared to the unfilled composition epoxy polymer was obtained. The mechanical properties and the high filling degree of the obtained composite indicate the possibility of using micromarble as an effective filler for epoxy polymers, which is also confirmed by the achieved substantial economic effect.

Аннотация. Исследовано влияние введения полифракционного микромрамора на изменение физико-механических характеристик полимерных композитов на основе низковязких эпоксидных связующих. Проведена оценка изменения предела прочности при сжатии и на растяжение при изгибе образцов эпоксидных композитов, содержащих микромрамор трех различных фракций, в зависимости от степени наполнения. С использованием метода наименьших квадратов получены математические зависимости прочностных характеристик эпоксидных композитов от вида используемого микромрамора и степени наполнения. Анализ изолиний и треугольных диаграмм Гиббса-Розебома позволил определить состав полифракционного наполнителя, композиты на основе которого, обладают наибольшими прочностными характеристиками. Получен полимерный композит, содержащий смесь микромрамора различных фракций в количестве 80 % от предельного уровня наполнения и обладающий повышенным пределом прочности при сжатии (до 40 %) и близким по значению пределом прочности на растяжение при изгибе (снижение не более 10 %) по

Низина Т.А., Соколова Ю.А., Чернов А.Н., Низин Д.Р., Попова А.И., Канаева Н.С. Наполненные эпоксидные композиты на основе полифракционного микрокальцита // Инженерно-строительный журнал. 2018. № 7(83). С. 83–91.

сравнению с ненаполненным составом эпоксидного полимера. Механические свойства и высокая степень наполнения полученного композита свидетельствуют о возможности использования микромрамора в качестве эффективного наполнителя для эпоксидных полимеров, что также подтверждается достигаемым существенным экономическим эффектом.

1. Introduction

Nowadays, polymeric materials are widely applied in various industries, which is caused by a set of unique properties and continuously extending product range [1–6]. In the building industry, thermoset polymers on the basis of low-molecular epoxy and diane resins with the average molecular weight of 350-600 are the most widespread [7–11]. High resistance to the majority of corrosive media allows to apply them as protective coats and impregnations almost anywhere [12–16]. However, wider application is significantly restricted by high cost and insufficient preservation of properties under the influence of solar radiation [17–22]. To date, the main way of reducing the cost price of protective coats is reduction of binders consumption by supplementing their composition with various disperse fillers [23–29].

It is considered that fillers were initially added to rubbers for increase of their durability in dozen times [27]. Then fillers were added to thermoset materials too. Today numerous kinds of fillers of various purposes are used in different industries and enable to modify mechanical, technological, and decorative characteristics of composites. Marshallit, chalk, portland cement, diatomite, and dolomite [11–13, 27–29] are applied as fillers at manufacture of polymeric composites of building purposes. However, scientists and manufacturers are searching for new effective fillers with controllable chemical and fractional composition. In the recent years, microcalcite (calcium carbonate, micromarble) is widely applied for manufacture of polymeric composites. This material is obtained by mechanical crushing of waste left after processing of white marble with further separation [27]. Constant physical and chemical properties, granulometric composition, and high degree of whiteness made microcalcite very widespread in manufacture of plastic, building materials, and papers [27, 30]. These properties combined with high resistance to corrosive media, atmospheric factors, and ultra-violet radiation make microcalcite very promising filler for building polymeric protective and decorative coats.

From one hand, increase of disperse filler share in polymer coat composition leads to considerable reduction of its cost price due to smaller consumption of binder. On the other hand, this results in significant worsening of mixture workability [30–32]. As a result, the optimal filler content for ensuring the best possible economic effect should be researched and determined. As a rule, application of plasticizers and solvents for obtaining a better plasticity of the filled mixtures is not expedient, as it leads to significant reduction of crack resistance, worsening of strength and adhesive properties of polymeric coats [16, 23, 28]. Considering constantly growing range of low-molecular epoxy and diane resins, authors believe this problem can be solved by application of low-viscosity binders, which, in its turn, requires conducting additional researches for analyzing the principles of their interaction with various fillers.

There are ways for obtaining filled coats of building products and structures, which properties are distributed according to functional requirements by control of polymeric binder of viscosity, as well as filling degree and fraction composition of the filler [26, 33]. Approach applied fir forming non-uniform distribution of polymeric coat properties by cross section height based on theoretical and experimental researches of restricted sedimentation processes with the help of multispeed continuum mechanics has shown obviously promising outlook for development of filled composite compositions.

The purpose of carried out researches was the development of structures filled with epoxy composites on the basis of low-viscosity binders and polyfractional microcalcite featuring high physical and mechanical properties. The following tasks have been solved for achieving the set objective: 1) influence of fractional composition of microcalcite and filling degrees on the change of mechanical properties of polymeric composites was defined; 2) polynomial equation ratios were determined with the help of planning methods and mathematical analysis of experimental researches and the graphic dependences reflecting the influence of filling degree and fractional composition of microcalcite on filled composite properties were built; 3) compositions on the basis of which the composites feature the best complex of properties were determined.

2. Materials and Methods

Surface properties of composites based on two-component epoxy compound of cold setting Etal-27NT/12NT which composition was supplemented with microcalcite of various fractions were researched within the scope of experiment:

1) MKM1 (V_1) – coarse fraction (0.5÷1 mm);

2) MKM2 (V_2) – medium fraction (0.2÷0.5 mm);

3) MKM3 (V_3) – fine fraction (less than 0.2 mm).

Degree of composite filling varied in the range from 40 to 80% of the limit filler content (Table 1). $V_1 + V_2 + V_3 = 1$ condition was observed for all compositions at experiment planning. Experimental research plan in coded values is presented in Table 2.

Change of ultimate compression and tensile strength when bending bar samples having the size of 20×20×70 mm was determined at the experiment. Samples filled with epoxy composites were produced by casting a mix of filler and Etal-27NT/12NT compound (manufacturer - JSC “ENPC EPITAL”). Samples solidified on air within 24 hours with further additional solidification within 6 hours at temperature of 80 ℃.

Table 1. Level of variable factor varying

In 100 mass fractions of epoxy binder					
Mass content of fillers			Maximal content of fillersin a mix, gram		
–1	0	+1	MKM1 (V_1)	MKM2 (V_2)	MKM3 (V_3)
40 %	60 %	80 %	300	250	200

Table 2. Experiment plan in coded values

Test number	Values of factors under study			
	fraction in filler mix			Degree of filling (X)
	MKM1 (V_1)	MKM2 (V_2)	MKM3 (V_3)	
1	1	0	0	-1
2	0	1	0	-1
3	0	0	1	-1
4	0.5	0.5	0	-1
5	0.5	0	0.5	-1
6	0	0.5	0.5	-1
7	1	0	0	0
8	0	1	0	0
9	0	0	1	0
10	0.5	0.5	0	0
11	0.5	0	0.5	0
12	0	0.5	0.5	0
13	1	0	0	+1
14	0	1	0	+1
15	0	0	1	+1
16	0.5	0.5	0	+1
17	0.5	0	0.5	+1
18	0	0.5	0.5	+1

Polynomial dependence of the following kind was used for description of experimental research results:

$$Y = b_1 \cdot V_1 + b_2 \cdot V_2 + b_3 \cdot V_3 + b_{12} \cdot V_1 \cdot V_2 + b_{13} \cdot V_1 \cdot V_3 + b_{23} \cdot V_2 \cdot V_3 + d_1 \cdot V_1 \cdot X + d_2 \cdot V_2 \cdot X + d_3 \cdot V_3 \cdot X + d_{12} \cdot V_1 \cdot V_2 \cdot X + d_{13} \cdot V_1 \cdot V_3 \cdot X + d_{23} \cdot V_2 \cdot V_3 \cdot X + k_1 \cdot V_1 \cdot X^2 + k_2 \cdot V_2 \cdot X^2 + k_3 \cdot V_3 \cdot X^2 + k_{12} \cdot V_1 \cdot V_2 \cdot X^2 + k_{13} \cdot V_1 \cdot V_3 \cdot X^2 + k_{23} \cdot V_2 \cdot V_3 \cdot X^2 \quad (1)$$

Polynomial equation ratios were defined using the method of the least squares, which consists in the selection of the equation coefficients, for which the squares of deviations sum of the calculated values from the experimental ones is minimal [34]. According to the experiment plan, the plan matrix $[X]$ and the outputs column vector $[Y]$ were compiled. Using matrix operations, unknown coefficients column vector $[B]$ was found from the solutions of linear algebraic expressions system:

$$[B] = ([X^T] \cdot [X])^{-1} \cdot [X^T] \cdot [Y]. \quad (2)$$

Adequacy of mathematical models was verified with Fisher criterion. Numerical values of polynomial equation ratios are specified in Table 3.

Table 3. Ratios of polynomial equation describing the change of ultimate compression and bending strength depending on varied factors

Polynomial equation ratios (1)																	
b_1	b_2	b_3	b_{12}	b_{13}	b_{23}	d_1	d_2	d_3	d_{12}	d_{13}	d_{23}	k_1	k_2	k_3	k_{12}	k_{13}	k_{23}
Ultimate compression strength, MPa																	
56.6	62.3	67.4	-5.16	3.72	8.06	0.87	1.33	2.74	-0.99	6.62	5.08	-1.36	-3.58	-0.20	21.01	8.48	2.28
Ultimate bending tensile strength, MPa																	
46.8	59.2	48.9	-3.77	80.1	40.9	-20.0	-19.9	-5.32	19.4	41.8	28.0	8.05	0.76	0.81	-7.97	-31.5	-4.39

3. Results and Discussion

Isolines of ultimate compression and tensile strength change in bending (Figures 1, 2) depending on ratio of two fractions in micromarble at various degrees of filling were formed on the basis of obtained polynomial equations.

All studied compositions feature increased strength at compression with the increase of degree of filling, which is caused by two factors, one of which underlies the principle of filling and consists in greater strength at compression of mineral filler compared to polymer's strength. The second factor relates to composition changes in the polymeric matrix on the border between filler and binder. During sedimentation, filler particles aim to reduce their surface energy and are grouped as cluster formations that have new quality properties. Structural order of polymeric matrix can be observed inside the cluster, in a polymer layer adjoining filler particles' surface. As a result, higher density leads to significant strengthening of the boundary layer [27, 31, 32]. Binder in the cluster is in a film state, and beyond the cluster - in a bulk state. Increase in the degree of filling leads to greater amount of clusters, which raises film phase content in a composite.

On the basis of results of the carried out research, it was found out that the greatest compression strength values (Figure 1, c) are observed in composites filled with a combination of medium and fine fractions of micromarble (MKM2+MKM3) in the ratio of 0.2:0.8 at maximum degree of filling. Similar values were obtained for combination of MKM1+MKM3 (Figure 1, b). Thus, increase of fine fraction micromarble share in the composition of binary filler leads to significant increase of strength, which we believe is caused by greater density of a structure and greater total area of the boundary layer between the filler particles and the binder and, as consequence, greater volume content of film phase in a composite. The obtained data can be compared to results of researches presented in works [31, 32, 35, 36] and describing polymer property change depending on filler's degree of filling and degree of dispersion.

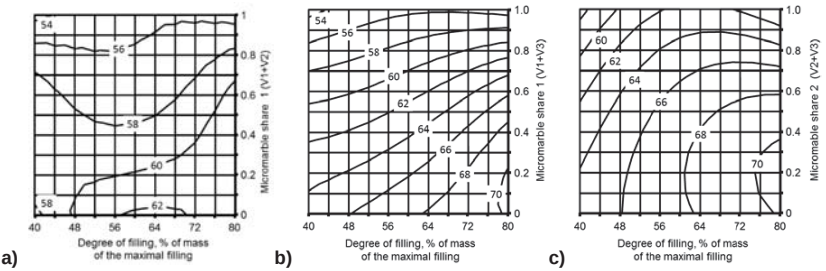

Figure 1. Isolines of epoxy composite ultimate strength change at compression (MPa) depending on degree of filling and micromarble fractions ratio: a) coarse (MKM1) and medium (MKM2); b) coarse (MKM1) and fine (MKM3); c) medium (MKM2) and fine (MKM3)

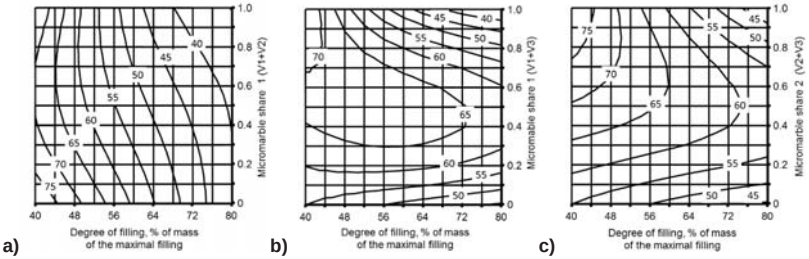

Figure 2. Isolines of epoxy composite ultimate bending tensile strength change depending on degree of filling and micromarble fractions ratio: a) coarse (MKM1) and medium (MKM2); b) coarse (MKM1) and fine (MKM3); c) medium (MKM2) and fine (MKM3)

It is known [31, 32] that increase of the total filler surface area leads to strengthening of the composite at compressing load impact only to a certain extent. This effect is caused by increase in polymer consumption for wetting of filler's grains, which results in formation of unit from them that are not wetted with the binder and are encapsulated in it. Compounds obtained from combination of micromarble of fine fraction and insignificant (up to 20 % of the total filler's mass) content of medium and coarse fractions at the maximal degree of filling feature higher compression strength than the composites that are filled only with micromarble of MKM3. Increase of strength when a polyfractional filler is used is also caused by the fact that with the greater density of a structure packing, where fine fraction micromarble particles fill the space between grains of the coarse filler ejecting binder's volume phase.

From the analysis of isolines of bending tensile strength, presented in Figure 2, it has been found out that composites containing micromarble of medium (MKM2) and coarse fractions (MKM1) features essential reduction of bending tensile strength – from 77 to 38 MPa at increase of the filling degree (Figure 2,a). High bending tensile strength obtained for these compounds with 40% degree of filling can be explained, first of all, by lack of filler's particles in the stretched section zone due to their complete setting in the process of sedimentation. In compounds having fine fraction micromarble (MKM3) of more than 80 % in MKM1+MKM3 combination, bending tensile strength with increased degree of filling almost does not change, which is proved by almost horizontal arrangement of isolines (Figure 2,b). In this case, the highest tensile strength at the maximal degree of filling was observed at equal shares of coarse and fine fillers (63 MPa).

According to [36], internal stresses do not depend on filler's dispersion; though, deformation energy caused by residual stresses is higher around coarse particles, which results in the fact that composites filled with micromarble of coarse (MKM1) and medium (MKM2) fractions have smaller strength at high degrees of filling than compounds containing micromarble of fine fraction (MKM3). Tests of composites filled with micromarble of fine fraction together with coarse or medium fractions led to a wide range of tensile strength values in bending, varying values depending on the share of each fraction (Figure 2,b,c). The best results were observed at equal ratio of shares; in this case, bending tensile strength does not exceed 10 % for the degree of filling from 40 to 80 %.

Three-component Gibbs-Roseboom diagrams based on simplexes in a form of regular triangles were used for a visual presentation of change in properties of filled epoxy composite materials at varying ratio of three micromarble fractions (MKM1, MKM2, MKM3). Figures 3 and 4 present triangular Gibbs-Roseboom diagrams of compression and tensile strength changes in bending plotted with Statistica 10.0.1011 software.

On the basis of triangular diagrams presented in Figure 3 it can be seen that the greatest compression strength values for all degrees of filling is observed with maximal content of MKM3 micromarble and combination of MKM2+MKM3 fillers, while MKM2 share does not exceed 25–40 %. Samples containing micromarble of coarse and medium fractions show that the optimal content of MKM2 makes about 60 % with the degree of filling of 40 and 80 % (Figure 3, a, c). The maximal compression strength has been observed in the compound filled with a combination of MKM2+MKM3 fillers in the ratio of 0.2:0.8 with the degree of filling of 80 %. Increase of micromarble coarse fraction in all investigated compounds led to considerable decrease of compression strength. The most obvious change of compression strength has been observed at variation of fine and coarse fractions of microcalcite, while

change of micromarble medium share in polyfractional filler has essentially smaller impact, especially when the degree of filling makes 60 % (Figure 3,b).

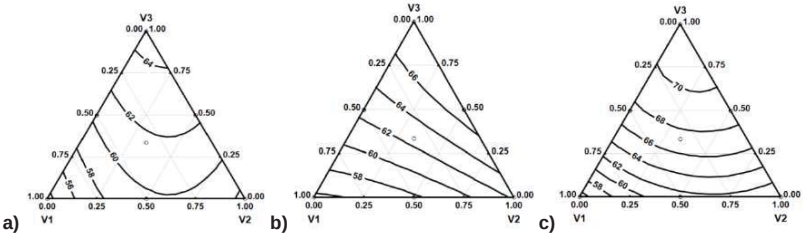

Figure 3. Triangular Gibbs-Roseboom diagrams of compression strength of filled epoxy composite materials (MPa) with degree of filling: a) 40%; b) 60%; c) 80% (MKM1 (V1) – coarse fraction (0.5÷1 mm); MKM2 (V2) – medium fraction (0.2÷0.5 mm); MKM3 (V3) – fine fraction (less than 0.2 mm))

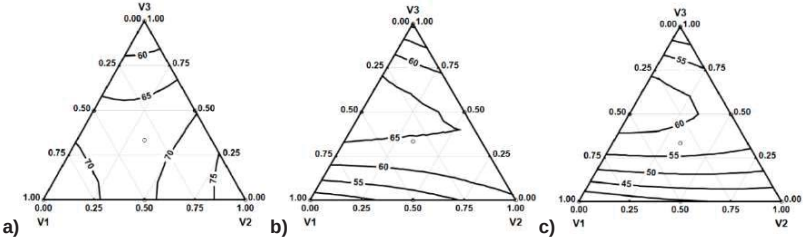

Figure 4. Triangular Gibbs-Roseboom diagrams of tensile strength of filled epoxy composite materials(MPa) with degree of filling: a) 40%; b) 60%; c) 80% (MKM1 (V1) – coarse fraction (0.5÷1 mm); MKM2 (V2) – medium fraction (0.2÷0.5 mm); MKM3 (V3) – fine fraction (less than0.2 mm))

The greatest bending tensile strength value has been observed in a compound with maximal share of micromarble of medium fraction at 40% degrees of filling (Figure 4,a). Generally, increase of degree of filling to 60 and 80% leads to reduction of bending tensile strength; thus, the optimal combination of strength and economic indicators is observed in composites filled with a combination of MKM1 + MKM3 micromarble. With these degrees of filling, medium fraction micromarble in polyfractional filler has minimal impact on strength properties.

4. Conclusions

Analysis of research results allowed us to draw the following conclusions:

1. Ultimate compression strength properties of epoxy composites can be enhanced from 10 to 40 % depending on dispersion and fractional composition of the added micromarble, as well as on the filling degree. The greatest ultimate strength reaching 70 MPa can be attained with application of the binary filler with increased calcium carbonate content of MSM3 fraction; the composite filled with microcalcite of fine and average fraction with 0.8:0.2 ratio and filling degree of 80 % features the optimal properties.

2. It has been determined that compounds with the filling degree of 40 % containing microcalcite of coarse or average fraction feature the greatest ultimate tensile strength, which is caused by forming a layer consisting mainly from unfilled epoxy polymer in a stretched area of the composite. Generally, increase of the filling degree leads to reduction of ultimate tensile bending strength. When polyfractional combinations of fillers containing micromarble with the fraction size of less than 0.2 mm and 0.5÷1 mm or 0.2÷0.5 mm tensile bending strength decreases does not exceed 10% for compounds with the filling degree of 80 % compared to unfilled compound (64 MPa), which proves economic feasibility of highly filled composite application.

3. Analysis of mathematical models of filled composite properties change depending on dispersion and fractional composition of the filler and filling degree presented in the form of isolines and triangular Gibbs-Rosenboom diagrams enabled us to reveal a compound featuring the best combination of economic and performance properties. Obtained composite contains a combination of MKM1+MKM3 fillers in the

ratio of 0.2:0.8 and has almost maximal compression and tensile strength in bending with the filling degree of 80 %.

References

1. Khozin, V.G. Osnovnyye oblasti primeneniya epoksidnykh materialov v tekhnike [Main applications of epoxy materials in technology]. All materials. Encyclopedic reference book. 2008. No. 11. Pp. 12–16. (rus)
2. Govariker, V.R., Visvanatkhan, N.V., Shridkhar, Dzh. Polimery. [Polymers]. Scientific publication. Moscow: Science, 1990. 396 p. (rus)
3. Ponomarev, A.N., Rassokhin, A.S. Hybrid wood–polymer composites in civil engineering. Magazine of Civil Engineering. 2016. 68(8). Pp. 45–57.
4. Neilsen, L. Mechanical Properties of Polymers and Composites. NY: Marcel Dekker, inc. 1974. 556 p.
5. Azeez, A.A., Rhee, K.Y., Park, S.J., Hui, D. Epoxy clay nanocomposites – processing, properties and applications: a review. Compos. Part B Eng. 2013. No. 45. Pp. 308–320.
6. Kurlapov, D.V., Kuvayev, A.S., Rodionov, A.V., Valeyev, R.M. Usileniye zhelezobetonnykh konstruktsiy s primeneniyem polimernykh kompozitov [Strengthening of Reinforced Concrete Structures Using Polymer Composite Materials]. Magazine of Civil Engineering. 2009. 5(3). Pp. 22–24. (rus)
7. Alam, M.A., Sherif, E.-S.M., Al-Zahrani, S.M. Fabrication of various epoxy coatings for offshore applications and evaluating their mechanical properties and corrosion behavior. International Journal of Electrochemical Science. 2013. Vol 8. No. 3. Pp. 3121–3131.
8. Pascault, J. P. Epoxy Polymers. New Materials and Innovations. Weinheim, 2010. 390 p.
9. Paranicheva, N.V., Nazmeyeva, T.V. Usileniye stroitelnykh konstruktsiy s pomoshchyu uglerodnykh kompozitsionnykh materialov [Strengthening of building structures using carbon composite materials]. Magazine of Civil Engineering. 2010. 12(2). Pp.19–22. (rus)
10. Shvets, G., Korsun, V. Protective coatings of reinforced cooling towers. Construction of Unique Buildings and Structures. 2018. No. 3(66). Pp. 30–40.
11. Pakharenko, V.A., Pakharenko, V.V., Yakovleva, R.A. Plastmassy v stroitelstve [Plastics in Construction]. SaintPetersburg: Nauchnyye osnovy i tekhnologii. 2010. 350 p. (rus)
12. Startsev, V.O., Lebedev, M.P., Khrulev, K.A., Molokov, M.V., Frolov, A.S., Nizina, T.A. Effect of outdoor exposure on the moisture diffusion and mechanical properties of epoxy polymers. Polymer Testing. 2018. Vol. 65. Pp. 281–296.
13. Mostafaei, A., Nasirpouri, F. Epoxy/polyaniline–zno nanorods hybrid nanocomposite coatings: synthesis, characterization and corrosion protection performance of conducting paints. Progress in Organic Coatings. 2014. Vol. 77. No. 1. Pp. 146–159.
14. Nishimura, T., Raman, V. Epoxy polymer coating to prevent the corrosion of aluminum nanoparticles. Polymers for Advanced Technologies. 2016. Vol. 27. No. 6. Pp. 712–717.
15. Singh-Beemat, J., Iroh, J.O. Characterization of corrosion resistant clay/epoxy ester composite coatings and thin films. Progress in Organic Coatings. 2012. Vol. 74. No. 1. Pp. 173–180.
16. Vakulenko, D.A., Turusov, R.A. Water resistance of polymer compounds. Magazine of Civil Engineering. 2017. No. 7. Pp. 106–113.
17. Viana, G., Costa, M., Banea, M.D., da Silva, L.F.M. A review on the temperature and moisture degradation of

Литература

1. Хозин В. Г. Основные области применения эпоксидных материалов в технике // Все материалы. Энциклопедический справочник. 2008. № 11. С. 12–16.
2. Говарикер В.Р., Висванатхан Н.В., Шридхар Дж. Полимеры: Научное издание. М.: Наука, 1990. 396 с.
3. Пономарев А.Н., Рассохин А.С. Гибридные древесно-полимерные композиты в строительстве // Инженерно-строительный журнал. 2016. № 8(68). С. 45–57
4. Neilsen L. Mechanical Properties of Polymers and Composites. NY: Marcel Dekker, inc. 1974. 556 p.
5. Azeez A.A., Rhee K.Y., Park S. J., Hui D. Epoxy clay nanocomposites - processing, properties and applications: a review // Compos. Part B Eng. 2013. No. 45. Pp. 308–320.
6. Курлапов Д.В., Куваев А.С., Родионов А.В., Валеев Р.М. Усиление железобетонных конструкций с применением полимерных композитов // Инженерно-строительный журнал. 2009. № 3(5). С. 22–24.
7. Alam M.A., Sherif E.-S.M., Al-Zahrani S.M. Fabrication of various epoxy coatings for offshore applications and evaluating their mechanical properties and corrosion behavior // International Journal of Electrochemical Science. 2013. Vol. 8. No. 3. Pp. 3121–3131.
8. Pascault J.P. Epoxy Polymers. New Materials and Innovations. Weinheim, 2010. 390 p.
9. Параничева Н.В., Назмеева Т.В. Усиление строительных конструкций с помощью углеродных композиционных материалов // Инженерно-строительный журнал. 2010. № 2(12). С. 19–22.
10. Швец Г.А., Корсун В.И., Устройство защитных покрытий железобетонных башенных градирен // Строительство уникальных зданий и сооружений. 2018. № 3(66). С. 30–40.
11. Пахаренко В.А., Пахаренко В.В., Яковлева Р.А. Пластмассы в строительстве. СПб.: Научные основы и технологии, 2010. 350 с.
12. Startsev V.O., Lebedev M.P., Khrulev K.A., Molokov M.V., Frolov A.S., Nizina T.A. Effect of outdoor exposure on the moisture diffusion and mechanical properties of epoxy polymers // Polymer Testing. 2018. Vol. 65. Pp. 281–296.
13. Mostafaei A., Nasirpouri F. Epoxy/polyaniline-zno nanorods hybrid nanocomposite coatings: synthesis, characterization and corrosion protection performance of conducting paints // Progress in Organic Coatings. 2014. Vol. 77. No. 1. Pp. 146–159.
14. Nishimura T., Raman V. Epoxy polymer coating to prevent the corrosion of aluminum nanoparticles // Polymers for Advanced Technologies. 2016. Vol. 27. No. 6. Pp. 712-717.
15. Singh-Beemat J., Iroh J.O. Characterization of corrosion resistant clay/epoxy ester composite coatings and thin films // Progress in Organic Coatings. 2012. Vol. 74. No. 1. Pp. 173–180.
16. Вакуленко Д.А., Турусов Р.А. Водостойкость полимерных компаундов // Инженерно-строительный журнал. 2017. № 7(75). С. 106–113.
17. Viana G., Costa M., Banea M.D., da Silva L.F.M., A review on the temperature and moisture degradation of adhesive joints // Proc. Inst. Mech. Eng. Part L J. Mater. Des. Appl. 2017. Pp. 488–501.
18. Afshar A., Alkhader M., Korach C.S., Fu-Pen C., Effect of long-term exposure to marine environments on the flexural

Низина Т.А., Соколова Ю.А., Чернов А.Н., Низин Д.Р., Попова А.И., Канаева Н.С. Наполненные эпоксидные композиты на основе полифракционного микрокальцита // Инженерно-строительный журнал. 2018. № 7(83). С. 83–91.

adhesive joints. Proc. Inst. Mech. Eng. Part L J. Mater. Des. Appl. 2017. Pp. 488–501.

18. Afshar, A., Alkhader, M., Korach, C.S., Fu-Pen C., Effect of long–term exposure to marine environments on the flexural properties of carbon fiber vinylester composites. Compos. Struct. 2015. No. 126. Pp. 72–77.
19. Startsev, V.O., Nizina, T.A., Startsev, O.V. A colour criterion of the climatic ageing of an epoxy polymer. International Polymer Science and Technology. 2016. Vol. 43. No. 8. Pp. 45–49.
20. Agubra, V.A., Mahesh, H.V. Environmental degradation of E–glass/nanocomposite under the combined effect of UV radiation, moisture, and rain. Polym. Sci., Part B: Polym. Phys. 2014. Vol. 52. Pp.1024–1029.
21. Thinius, K. Stabilisirung und Alterung von Plastwerkstoffen. Bd 2. Alterung der Plastwerkstoffe. Berlin, 1970. 498 p.
22. Startsev, V.O., Lebedev, M.P., Khrulev, K.A., Molokov, M.V., Frolov, A.S., Nizina, T.A. Effect of outdoor exposure on the moisture diffusion and mechanical properties of epoxy polymers. Polymer Testing. 2018. Vol. 65. Pp. 281–296.
23. Mascia, L. The Role of Additives in Plastics. London: Edward Arnold, 1974. 172 p.
24. Kothmann, M., Ziadeh, M., Bakis, G., Rios de Anda, A., Breu, J, Altstädt, V. Analyzing the influence of particle size and stiffness state of the nanofiller on the mechanical properties of epoxy/clay nanocomposites using a novel shear–stiff nano-mica. Journal of Materials Science. 2015. Pp. 4845–4859.
25. Solomatov, V.I., Bobryshev, A.N., Proshin, A.P. Effect of dimensional factors of a disperse filler on the strength of epoxy composites. Mechanics of Composite Materials. 1983. Vol. 18. No. 6. Pp. 674–679.
26. Selyayev, V.P. Funktsionalno–gradiyentnyye pokrytiya na osnove polimernykh svyazuyushchikh [Functional gradient coatings based on polymeric binders].Proceedings of higher educational institutions. Construction. 2007. No. 7. Pp. 36–40. (rus)
27. Xanthos, M. Functional Fillers for Plastics. Second, updated and enlarged edition. Weinheim, 2010. 507 p.
28. Khozin, V.G., Murafa, A.V., Cherevatskii, A.M. Principles of strengthening of epoxy binders. Mechanics of Composite Materials. 1987. Vol. 23. No. 1. Pp. 116–122.
29. Astruc, A., Joliff, E., Chailan, J.F., Aragon, E., Petter, C.O., Sampaio, C.H. Incorporation of kaolin fillers into an epoxy/polyamidoamine matrix for coatings. Progress in Organic Coatings. 2009. Vol. 65. No. 1. Pp. 158–168.
30. Novoselova, S.N., Tatarintseva, O.S., Uglova, T.K. The influence of the degree of filling of epoxy composites with microcalcite of different degree of dispersion on their rheological properties. International Polymer Science and Technology. 2015. Vol. 42. No. 1. Pp. 35–39.
31. Kozlov, G.V., Lipatov, Y.S. Change in the structure of polymer matrix of particulate–filled composites: the fractal treatment. Mechanics of Composite Materials. 2004. Vol. 40. No. 6. Pp. 545–550.
32. Lipatov, Y.S, Babich, V.F. Viscoelastic properties of interphase layers and laws governing their effect on the mechanical properties of composite materials. Mechanics of Composite Materials. 1987. Vol. 23. No. 1, Pp. 15–21.
33. Amirova, L.M., Andrianova, K.A. Gradient polymeric materials based on poorly compatible epoxy oligomers. Journal of Applied Polymer Science. 2006. Vol. 102. No. 1. Pp. 96–103.
34. Selyayev, V.P., Nizina, T.A., Lankina, Yu.A., Lazarev, A.L. Teoriya eksperimenta i statisticheskiye metody issledovaniya stroitelnykh materialov [The theory of experiment and statistical methods of building materials, products and structures research]. Saransk: Izd-vo Mord. Un-ta, 2010. 156 p. (rus)

properties of carbon fiber vinylester composites // Compos. Struct. 2015. No. 126. Pp. 72–77.

19. Startsev V.O., Nizina T.A., Startsev O.V. A colour criterion of the climatic ageing of an epoxy polymer. International Polymer Science and Technology. 2016. Vol. 43. No. 8. Pp. 45–49.
20. Agubra V.A., Mahesh H.V. Environmental degradation of E-glass/nanocomposite under the combined effect of UV radiation, moisture, and rain // Polym. Sci., Part B: Polym. Phys. 2014. Vol. 52. Pp. 1024–1029.
21. Thinius K. Stabilisirung und Alterung von Plastwerkstoffen. Bd 2. Alterung der Plastwerkstoffe. Berlin, 1970. 498 p.
22. Startsev V.O., Lebedev M.P., Khrulev K.A., Molokov M.V., Frolov A.S., Nizina T.A. Effect of outdoor exposure on the moisture diffusion and mechanical properties of epoxy polymers // Polymer Testing. 2018. Vol. 65. Pp. 281–296.
23. Mascia, L. The Role of Additives in Plastics. London: Edward Arnold, 1974. 172 p.
24. Kothmann M., Ziadeh M., Bakis G., Rios de Anda A., Breu J, Altstädt V. Analyzing the influence of particle size and stiffness state of the nanofiller on the mechanical properties of epoxy/clay nanocomposites using a novel shear-stiff nano-mica // Journal of Materials Science. 2015. Pp. 4845–4859.
25. Solomatov V.I., Bobryshev A.N., Proshin A.P. Effect of dimensional factors of a disperse filler on the strength of epoxy composites // Mechanics of Composite Materials. 1983. Vol. 18. No. 6. Pp. 674–679.
26. Селяев В.П., Низина Т.А., Лазарев А.Л., Ланкина Ю.А., Цыганов В.В. Функционально-градиентные покрытия на основе полимерных связующих // Известия ВУЗов. Строительство. 2007. № 7. С. 36–40.
27. Xanthos M. Functional Fillers for Plastics. Second, updated and enlarged edition. Weinheim, 2010. 507 p.
28. Khozin V.G., Murafa A.V., Cherevatskii A.M. Principles of strengthening of epoxy binders // Mechanics of Composite Materials. 1987. Vol. 23. No. 1. Pp. 116–122.
29. Astruc A., Joliff E., Chailan J.F., Aragon E., Petter C.O., Sampaio C.H. Incorporation of kaolin fillers into an epoxy/polyamidoamine matrix for coatings // Progress in Organic Coatings. 2009. Vol. 65. No. 1. Pp. 158–168.
30. Novoselova S.N., Tatarintseva O.S., Uglova T.K. The influence of the degree of filling of epoxy composites with microcalcite of different degree of dispersion on their rheological properties // International Polymer Science and Technology. 2015. Vol. 42. No. 1. Pp. 35–39.
31. Kozlov G.V., Lipatov Y.S. Change in the structure of polymer matrix of particulate-filled composites: the fractal treatment // Mechanics of Composite Materials. 2004. Vol. 40. No. 6. Pp. 545–550.
32. Lipatov Y. S, Babich V. F. Viscoelastic properties of interphase layers and laws governing their effect on the mechanical properties of composite materials || Mechanics of Composite Materials. 1987. Vol. 23. No. 1. Pp. 15–21.
33. Amirova L.M., Andrianova K.A. Gradient polymeric materials based on poorly compatible epoxy oligomers. Journal of Applied Polymer Science. 2006. Vol. 102. No. 1. Pp. 96–103.
34. Селяев В.П., Низина Т.А., Ланкина Ю.А., Лазарев А.Л. Теория эксперимента и статистические методы исследования строительных материалов, изделий, конструкций. Саранск: Изд-во Морд. ун-та, 2010. 156 с.
35. Низина Т.А., Чернов А.Н., Морозов М.А., Низин Д.Р., Попова А.И. Влияние гранулометрического состава микромрамора на физико-механические характеристики наполненных эпоксидных композитов // Вестник МГСУ. 2016. №9. С. 98–107.
36. Бобрышев А.Н., Козоматов В.Н., Бабин Л.О., Соломатов В.И. Синергетика композитных материалов. Липецк: РПГФ «Юлис», 2006. 170 с.

Nizina, T.A., Sokolova, J.A., Chernov, A.N., Nizin, D.R., Popova, A.I., Kanaeva, N.S. Filled epoxy composites based on polyfraction microcalcite. Magazine of Civil Engineering. 2018. 83(7). Pp. 83–91. doi: 10.18720/MCE.83.8.

35. Nizina, T.A., Chernov, A.N., Morozov, M.A., Nizin, D.R., Popova, A.I. Vliyaniye granulometricheskogo sostava mikromramora na fiziko–mekhanicheskiye kharakteristiki napolnennykh epoksidnykh kompozitov [Influence of micromarble granulometric composition on the physical and mechanical characteristics of filled epoxy composites]. Bulletin of MGSU. 2016. No. 9. Pp. 98–107. (rus)
36. Bobryshev, A.N., Kozomatov, V.N., Babin, L.O., Solomatov, V.I. Sinergetika kompozitnykh materialov [Synergetics of composite materials]. Lipetsk: RPGF "Yulis", 2006. 170 p. (rus)

Tatyana Nizina,*
+7(917)993-63-89; nizinata@yandex.ru

Julia Sokolova,
+7(916)626-23-20; inep_s@mail.ru

Alexey Chernov,
+7(951)056-06-47; lhms13@yandex.ru

Dmitrii Nizin,
+7(927)184-84-22; nizindi@yandex.ru

Anastasya Popova,
+7(906)379-51-22; popova_nastya2013@mail.ru

Nadegda Kanaeva,
+7(987)691-96-20; aniknadya@yandex.ru

Татьяна Анатольевна Низина,*
+7(917)993-63-89;
эл. почта: nizinata@yandex.ru

Юлия Андреевна Соколова,
+7(916)626-23-20; эл. почта: inep_s@mail.ru

Алексей Николаевич Чернов,
+7(951)056-06-47;
эл. почта: lhms13@yandex.ru

Дмитрий Рудольфович Низин,
+7(927)184-84-22; эл. почта: nizindi@yandex.ru

Анастасия Ивановна Попова,
+7(906)379-51-22;
эл. почта: popova_nastya2013@mail.ru

Надежда Сергеевна Канаева,
+7(987)691-96-20;
эл. почта: aniknadya@yandex.ru

Низина Т.А., Соколова Ю.А., Чернов А.Н., Низин Д.Р., Попова А.И., Канаева Н.С. Наполненные эпоксидные композиты на основе полифракционного микрокальцита // Инженерно-строительный журнал. 2018. № 7(83). С. 83–91.

doi: 10.18720/MCE.83.9

Parameter of thermal resistance of bamboo multilayer wall

Показатели теплотехнического сопротивления бамбуковой стены

J. Bonivento Bruges*,
G.B. Vieira,
D. Revelo Orellana,
I. Togo,
Peter the Great St. Petersburg Polytechnic University, St. Petersburg, Russia

Магистрант Х. Бонивенто Брюгес*,
магистрант Г.Б. Виейра,
д-р архитектуры Д. Ревело Орельяна,
канд. техн. наук, заведующий кафедрой И. Того,
Санкт-Петербургский политехнический университет Петра Великого, г. Санкт-Петербург, Россия

Key words: bamboo; guadua; thermal resistance; thermal transmittance (U-Value)

Ключевые слова: бамбук; гуадуа; тепловое сопротивление; коэффициент теплопередачи (U-Value)

Abstract. With the increasing of problems related to air pollution and rising of the mean temperature around the globe, new solutions must be investigated in order to diminish the magnitude of such environmental issues. Therefore, the appliance of bamboo in the construction can be one of the solutions. Even though, this grass does not present mechanical or thermal homogeneity, its high sustainability (CO_2 reducer, highness and fast speed of growth), strength and hollowed cylindrical morphology make it an option in the construction sector. As an energy-efficient material, this woody grass can have a positive thermal performance due to the presence of air cavities, however, its rounded nature influence to a non-homogeneous performances in the surface and interior. The literature about the thermal performance of this element as building envelopment is reduced. Thus, the aim of this research is to analyse the thermal performance of a one, two and three bamboo layers, placing them in a way to mitigate the heat leaking and improving the thermal resistance. It is analysed numerically and through a simulation developed in THERM 7.5 Finite Element Simulator. As a result, two line of bamboo is convenient as a material construction with U-Value of 1.4 W/m².K, but three layers is recommended to mitigate the presence of thermal bridges. The results obtained leads to a different approach and suggests further analysis for different parameters.

Аннотация. Ввиду роста проблем, связанных с загрязнением воздуха и повышением средней температуры на планете, необходимы альтернативные решения, которые смогут снизить вред, наносимый окружающей среде. Применение бамбука как строительного материала может стать одним из таких решений. Несмотря на то, что он механически или теплотехнический неоднороден, его высокая экологическая устойчивость (снижает уровень CO_2, обладает высокой скоростью роста), прочность и полая цилиндрическая структура позволяют рассматривать бамбук в одном ряду с другими строительными материалами. Бамбук имеет хорошие теплотехнические характеристики благодаря наличию пустот, однако его цилиндрическое строение становится причиной неоднородного поведения внешней и внутренней частей материала. Недостаточное количество литературы, описывающей теплотехнические свойства бамбука как ограждающей конструкции, стало причиной для проведения анализа одного, двух и трех слоев бамбука путем, размещенных способом, уменьшающим теплопотери и повышающим тепловое сопротивление. Анализ был проведен численно и с помощью симуляции, разработанной в THERM 7.5 Finite Element Simulator. Результаты исследования показали, что достаточно двух слоев бамбука, чтобы получить строительный материал с U-value 1,4 W/m²K, но использование трех слоев рекомендуется для уменьшения мостиков холода. Полученные результаты позволяют рассматривать использование нового подхода и могут стать основой для дальнейшего исследования других параметров.

1. Introduction

The construction industry is one of the major source of pollution in the air -around 4% of particulate emission-, water, noise and soil [1]. Therefore, the use of sustainable materials in construction is a decisive factor to reduce this negative environmental impact. The bamboo is a renewable material, well known as

Бонивенто Брюгес Х., Виейра Г.Б., Ревело Орельяна Д., Того И. Показатели теплотехнического сопротивления бамбуковой стены // Инженерно-строительный журнал. 2018. № 7(83). С. 92–101.

a giant grass, belongs to the family Graminace (Poaceae) and is spread around the world according to Figure 1.

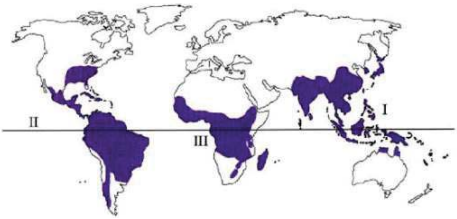

Figure 1. Distribution of Bamboo around the world. I – Asia-Pacific region, II – America region and III – African region (INBAR 2010 [2])

Some remarkable benefits of this vegetal are the capability of CO2 sequestration (Bamboo – Guadua fixing capacity of 76 t CO2/ha) [3], rapidly rate growth, 6 months to have its height and 4 – 6 years [4] and high mechanical performances along its fibres [5, 6]. International standardizations and codifications from China, Colombia, Ecuador, India, Peru and USA promote this sustainable material for construction of complex projects [7]. Moreover, it has high resistant in seismic events [8].

A cylindrical and hollowed shape governs the morphology of the bamboo stick. Normally, the separation of internodes varies between 10 cm and 40 cm (Figure 2). Depending on the specimens the culm can reach height upper 18m with diameters from 5 cm to 25 cm and wall thickness from 0.9 to 1.3 cm [9].

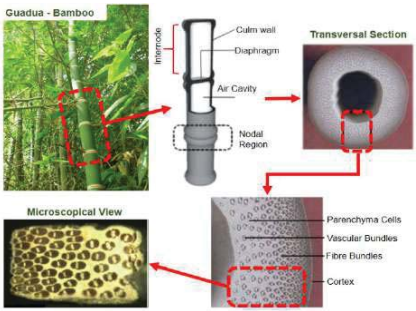

Figure 2. Morphology of Bamboo [9]

Regarding its thermal characteristic, it has a cavity filled with air entrapped, low thermal-conductor element, enveloped by a porous woody material with fibre and vascular bundles. However, the bamboo stick as an insulation material presents two noticeable withdraws: firstly, due to its vegetable nature, its physical, mechanical and geometrical properties change between species, moreover, [10, 11] demonstrated that in the wall of Guadua-Bamboo, after 15 % of its thickness measured from the cortex the aggrupation of vascular bundles are more separated (Figure 2), changing its properties. Thus, it is considered a heterogeneous material with physical, mechanical and thermal variations, making this raw product difficult for being industrialized in mass, like industrial woods panels or commercial wood elements [5, 12]. Because of this variability, many researches about bamboo are focused on making glued or pressed composites or mixing its fibres with another elements in order to improve the resistance of the bamboo and generate mechanical and thermal properties predictable for calculation [12, 13].

The second withdraw is related to its cylindrical geometry, Huang, P [10] researched the thermal properties of a stick (culm) of Asian family “Moso-Bamboo” (Phyllostachys edulis) and found that the thermo-diffusivity and thermo-resistance of this specimen vary in different transversal points, due to its rounded shape and heterogeneous density in its wall. He registered an average thermo-conductivity of 0.226 W/m*K. Mata, M [14] obtained values of 0.158 W/m*K for Bamboo-Guadua.

Even though the process of industrial lamination of bamboo is a feasible exportation technique, it demands unnecessary costs for infrastructures surrounded by this vegetal. The Colombian Standard NSR 10 [8] establishes parameters of constructability of raw bamboo walls for the specimen Bamboo-Guadua

addressing suitable techniques for not losing its mechanical properties, however, a thermal performance section is not included in the chapter for bamboo. Construction of wall with this rounded material, as shown in Figure 3, creates joins which drive thermal bridges, giving the chance to of heat leaking due to the reduced contact area [15].

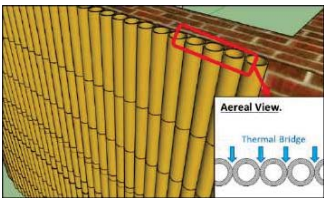

Figure 3. Thermal Bridges in Bamboo Wall

Nevertheless, the lack of studies related to Bamboo's thermal performance and its discrepancy of values still an issue, making unclear its properties, which leads for a reduced use of this material as insulation layer. Likewise, usually the studies linked to this material are about its mechanical characteristics. Due to this fact, this paper aims the study of bamboo as insulation material, and not, as a structural one.

Therefore, the objectives of this paper are:

- Numerical analysis of the thermal resistance of the non-homogenous surface of the Bamboo;
- Software thermal analysis by modelling in a finite element simulator THERM 7.5;
- Formulate a feasible solution to mitigate the presence of thermal bridges;
- Compare the result obtained both numerically and by Software Analysis.

The analysis is done in a residential house located in the city of Guayaquil, Ecuador.

2. Methods

This research include a numerical and a simulation method of thermal parameters of thermal resistance and heat lost through a theoretical wall, built of vertical sticks of bamboo in its natural state.

The bamboo model is located in Guayaquil, Ecuador with the adopted information:

- Outside Temperature: 37.2 ºC;
- Inside Design Temperature: 22.0 ºC;
- Relative Humidity: 79%;
- The wall length which underwent through thermal simulation has 1.00 m;
- The interior part of the bamboo was considered as a Frame Cavity – CEN Simplified;
- The thermal characteristics of the bamboo was set as Table 1.

Table 1. Thermal-physics Parameters: Thermal Conductivity (λ), Thermal Effusivity (e), Thermal Diffusivity (α), density (ρ) and Specific Heat (c) of Guadua According to Gordillo, F. [16].

λ	e	α	ρ	c
$Wm^{-1}K^{-1}$	$Ws^{1/2}m^{-2}K^{-1}$	$10^{-6}m^2s^{-1}$	10^3kgm^{-3}	$Jkg^{-1}K^{-1}$
0.157	1000 ± 20	0.11±0.01	0.6±0.07	1491

One of the facts of the thermodynamic law is the transference of the energy by the interaction (work and heat) of a system with its surrounding. The transfer used in this document is heat transfer, which is the thermal energy in transit due to a spatial temperature difference [17]. There are three modes of heat transfer: Conduction, Convection and Radiation.

This article pays more attention on the heat transfer that will occur through a medium (solid or stationary fluid), in this case, this medium is the bamboo layers. Therefore, it is necessary to calculate the capacity of the materials to conduct heat, in other words, the thermal resistance, which is estimated primarily by the Fourier Law.

$$q = \lambda * \frac{T1 - T2}{\delta} * A * t \quad (1)$$

where: λ – Coefficient of thermal conductivity (W/m K);

δ – Thickness of the material (m);

T1 and T2 – Indoor and outdoor temperature respectively (or outdoor if it is hotter that indoor);

A – Area of the surface of layer (m2);

t – Time (s).

In order to analyse the thermal resistance of the Bamboo layers, it will be calculated according to [18–21], which give the formulas (2) (3):

$$\mathrm{R} = \frac{1}{\propto_{\mathrm{int}}} + \sum_{i=1}^{j} \frac{\delta_i}{\lambda_i} + \frac{1}{\propto_{\mathrm{ext}}} \quad (2)$$

where: R – Thermal resistance (m² K/ W);

$\propto_{int}$ – inner surface heat transfer coefficient, 25 W/m2 K according to IRAM 11601;

$\propto_{ext}$ – outer surface heat transfer coefficient, 7.69 W/m2 K according to IRAM 11601.

A typical section of 2-layers bamboo wall was considered (Figure 4). The axis or sections 1, 2 and 3 represents different performances of the partial thermal-resistance located along each horizontal axis (A-O), moreover, the contact between sticks is studied as a perfect and constant contact along the elements and the air gaps formed, thanks to the union of each stick, is not considered, their small area is not representative for calculations.

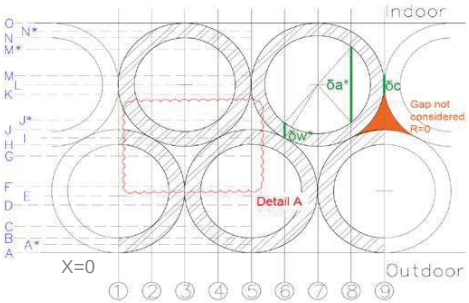

Figure 4. Cross-section of 2-layers bamboo wall

The one-dimensional tendency of the thermal resistances evaluated in the sections 1, 2 and 3 for "n" number of layers are described in the Table 2 and generalized in the equations 4 and 5 and 6.

Table 2. Thermal Resistance along the sections for n number of layers.

n Layers	Section 1	Section 2	Section 3
2	$\frac{\delta c}{\lambda b} + \frac{2\delta w}{\lambda b} + \frac{\delta a}{\lambda a}$	$\frac{4\delta w^*}{\lambda b} + \frac{2\delta a^*}{\lambda a}$	$\frac{\delta c}{\lambda b} + \frac{2\delta w}{\lambda b} + \frac{\delta a}{\lambda a}$
3	$\frac{\delta c}{\lambda b} + \frac{4\delta w}{\lambda b} + \frac{2\delta a}{\lambda a}$	$\frac{6\delta w^*}{\lambda b} + \frac{3\delta a^*}{\lambda a}$	$\frac{2\delta c}{\lambda b} + \frac{2\delta w}{\lambda b} + \frac{\delta a}{\lambda a}$
4	$\frac{2\delta c}{\lambda b} + \frac{4\delta w}{\lambda b} + \frac{2\delta a}{\lambda a}$	$\frac{8\delta w^*}{\lambda b} + \frac{4\delta a^*}{\lambda a}$	$\frac{2\delta c}{\lambda b} + \frac{4\delta w}{\lambda b} + \frac{2\delta a}{\lambda a}$
5	$\frac{2\delta c}{\lambda b} + \frac{6\delta w}{\lambda b} + \frac{3\delta a}{\lambda a}$	$\frac{10\delta w^*}{\lambda b} + \frac{5\delta a^*}{\lambda a}$	$\frac{3\delta c}{\lambda b} + \frac{4\delta w}{\lambda b} + \frac{2\delta a}{\lambda a}$

For the restriction.

$$\delta w < \frac{\delta a}{2}$$

Then,

$$R_1 = \frac{1}{\alpha in} + \left\lfloor \frac{n}{2} \right\rfloor \frac{\delta c}{\lambda b} + 2\left(n - \left\lfloor \frac{n}{2} \right\rfloor\right)\frac{\delta w}{\lambda b} + \left(n - \left\lfloor \frac{n}{2} \right\rfloor\right)\frac{\delta a}{\lambda a} + \frac{1}{\alpha ext} \quad (3)$$

$$R_2 = \frac{1}{\alpha in} + \frac{n}{2\lambda b}\left(\sqrt{3}\delta b - \sqrt{4\delta a^2 - \delta b^2}\right) + \frac{n}{2\lambda a}\sqrt{4\delta a^2 - \delta b^2} + \frac{1}{\alpha ext} \quad (4)$$

$$R_3 = \frac{1}{\alpha in} + \left\lfloor \frac{n}{2} \right\rfloor \frac{\delta c}{\lambda b} + 2\left(n - \left\lfloor \frac{n}{2} \right\rfloor\right)\frac{\delta w}{\lambda b} + \left(n - \left\lfloor \frac{n}{2} \right\rfloor\right)\frac{\delta a}{\lambda a} + \frac{1}{\alpha ext} \quad (5)$$

$$\delta a^* = \frac{\sqrt{4\delta a^2 - \delta b^2}}{2} \quad (6)$$

$$\delta w^* = \frac{\sqrt{3}}{4}\delta b - \frac{\sqrt{4\delta a^2 - \delta b^2}}{4} \quad (7)$$

where n = Number of bamboo layers in the wall;

δa = Diameter of the air cavity (δb- δw) (m);

δw = Thickness of the Bamboo (m);

δc = Distance of contact between bamboos –contact zone- (assumed as 0.15 δb) (m);

δb = External diameter of the bamboo stick (m);

λb = Conductivity of the bamboo woody material (W/mK);

λa = Conductivity of the air (W/mK).

Acknowledging the vertical Axis of the Figure 4 as the axis “X” of a Cartesian diagram and the result of every thermal resistance as the axis “Y”, it is possible to represent graphically the performance of every section for n number of layers, Figure 6. Nevertheless, in order to find an average performance of thermal resistance, it is assumed a hypothetical homogeneous wall, Figure 5, with similar tendency to the three sections aforementioned and following the next criteria:

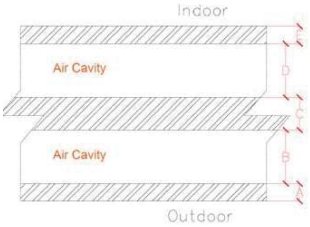

Figure 5. Wall Equivalent for 2 layers bamboo wall. A, C and E is a hypothetical solid material with the same thermal properties as the Bamboo-Moso and B and D are air cavities

- Thickness of A and E are assumed similar.
- In the Figure 4 is observed that the proportion of air in the steam of bamboo from the sections 1-9 are similar between both layers. The air in the first layer section 1, 5 and 9 is δa, but in sections 2, 4 and 8 is δa*, as seen in the Figure. Thus, the average air in the first layer is measured as ¾ δa*, so it is assumed that B = D = ¾ δa*.
- For the first layer, it is shown in the Figure 4 that the section 1 and 3 show the minimum and maximum respectively in the first increase, so the first resistance purposed is by the means of section A and Section B, thus:

$$A = E = \frac{\delta w + 0.15\delta b}{2}\ (Thickness) \quad (8)$$

$$A = E = \frac{\delta w + 0.15\delta b}{2\lambda b} \ (Thermal\ Resistance) \tag{9}$$

- C is a variable and depends on A, B, D and E.
- The total resistance is leaded by the section 2 (Figure 4) and the section 1 and 3 have the minimum value, so (C is in function of δw):

$$A + B + C + D + E = \frac{R1 + R2}{2}$$
$$\left(\frac{\delta w + 0.15\delta b}{2\lambda b}\right) + \frac{3}{4\lambda a}\left(\sqrt{4\delta a^2 - \delta b^2}\right) + \frac{C(\delta w)}{\lambda b} = \frac{R1 + R2}{2} \tag{10}$$

After an interactive process, the value of C is defined as:

$$C = 1.787\delta w - 0.0016 \tag{11}$$

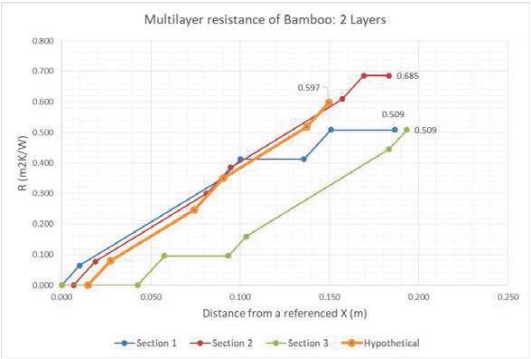

Figure 7. Thermal resistance in the axis 1, 2 and 3 and an equivalent wall, from a referenced x

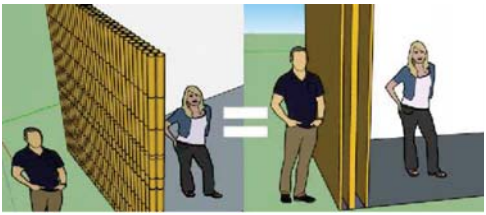

Figure 8. View of the hypothetical equivalent wall (right) and the bamboo wall (left)

The U-Value, which is a measure of the rate at which a building transmit heat [22, 23], is expressed in terms of thermal resistance. Therefore, it is given by (12).

$$U = \frac{1}{R}, \tag{12}$$

U – thermal transmittance (W/ m² K);

Consequently, the maximum value for the thermal transmittance for Guayaquil, referenced by the Argentina standard is 1.8 W/ m² K (IRAM 11.605).

According to World Meteorological Organization, Guayaquil has the following climate characteristics:

- Dew Point: 20.4 ºC;
- Hottest Month of the year: January 37.2 ºC.

For the simulations developed in this paper, the design temperature adopted will be 22.0 ºC.

The software simulation performed had the objective of analysing how the addition of more layers of Bamboo can improve the thermal characteristics of a wall and analyse the heat flux when using it as a single, double and triple insulation layer, as illustrated in Figure 8.

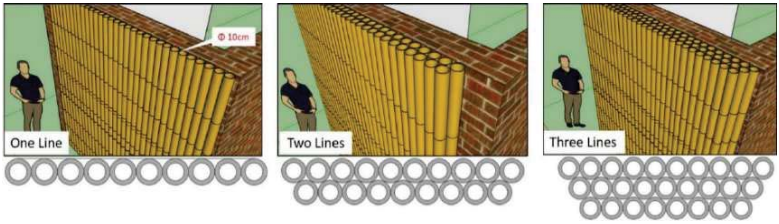

Figure 9. Proposed multi-layered bamboo façade: One layer, two layers and three layers, respectively. The first and second line for all cases are fixed at 10 cm

The specimen of Bamboo to use for calculation is Guadua - Angustifolia-Kunth. The diameter of the first line of bamboo is 10 cm, in accordance to the chapter E.7.6 of NSR 10 [24]. The elements of the second line was set at 10 cm also. According to [4] the thickness of the Guadua culms varies from 1,00 cm to 1.50 cm and regarding to the physical - thermal properties, it is adopted in accordance to the work of [10, 14, 16]. However, for this work the thickness adopted will be 10 cm.

For the simulation, it is used the software THERM 7.5, and whose initial parameters are similar to the previous numerical analysis, and the parameters expected are the heat flux, isotherms and temperature. Every extreme of the wall analysed corresponds to adiabatic sections. The air entrapped inside the every stick is considered as a Frame Cavity – CEN Simplified.

3. *Results and Discussions*

The results obtained in the software simulation are presented below (Figures 10–12). For all three simulations (single-layer, double-layer and triple-layer) it is displayed the temperature gradient through the bamboo and its heat flux.

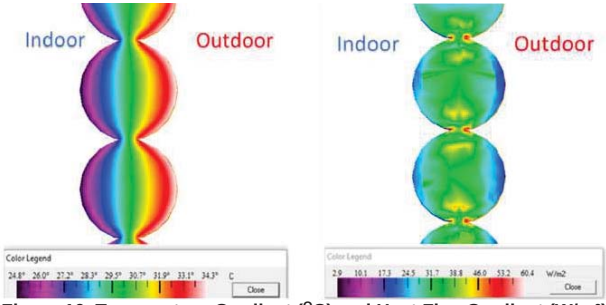

Figure 10. Temperature Gradient (^{O}C) and Heat Flux Gradient (W/m²) for Single Layer Bamboo Wall

Figure 11. Temperature Gradient (OC) and Heat Flux Gradient (W/m²) for Double-Layer Bamboo Wall

Бонивенто Брюгес Х., Виейра Г.Б., Ревело Орельяна Д., Того И. Показатели теплотехнического сопротивления бамбуковой стены // Инженерно-строительный журнал. 2018. № 7(83). С. 92–101.

Figure 12. Temperature Gradient (OC) and Heat Flux Gradient (W/m²) for Triple-Layer Bamboo Wall

When analysing the Temperature Gradient above, for all three simulations, a linear isotherm is obtained in the middle of the 2 and 3-layer wall, while the 1-layer wall illustrates a nonlinear patron. This is a result due to the rounded shape of the bamboo and as long as the walls with more layers get more stable, this variation tends to reduce. Furthermore, the heat flow gradient shows that adding a second and further a third layer of bamboo interspersed, the thermal bridges effect get reduced.

The Table 3 shows the values obtained after the Thermal Simulation. As expected, the U-Value decreased as the number of layers increased. In comparison with the standards (IRAM 11.605), both double and triple layer have a U-Value lower than the maximum recommended (1.8 W/m²K). Moreover, the amount of heat flow through the bamboos' layer decreased drastically when adding one layer as insulation material. It is important to point out that the thermal resistance shown in the Table 3 for a double layer bamboo converge with the value obtained by the hypothetical wall numerically calculated in the Figure 5.

Table 3. Results obtained for U-Value and Heat Flow

Layers	U-Value (W/m².K)	R (m².K/W)	Heat Flow (W) *
Single-Layer	2.07	0.48	34.20
Double-Layer	1.40	0.71	16.09
Triple-Layer	0.66	1.52	9.66

*Per meter

The values obtained in the Table above for simulated U-value for double layer have a close similarity with the theoretical calculated, oscillating between 1.34 and 1.67 W/m²K. Thus, the obtained result can be comparable with the research of [25], who investigated the thermal performance of many specimens of wood, for the structural softwood lumber (commonly used in construction) found a thermal conductivity between 0.1–0.4 W/mK (12 % of humidity); if a typical wood wall made of two panels of 13 cm thick from this wood and cavity air of 5 cm, have an approximate thermal resistance of 0.533 m²K/W (U = 1.87 W/m²K), it can be inferred that a bamboo wall layer, assuming complete contact between sticks, have similar thermal transmittance to a common system of wood panel with air cavity in-between.

Due to the non-homogeneity of bamboo and scarcity of literature about the thermal performance of bamboo walls, the values of thermal-resistance obtained is object of comparison with further studies.

4. Conclusion

A wall made of the renewable woody vegetal, bamboo, represents suitable values of thermal resistance for construction in regions with analogous climate characteristics, and energy-efficient regulations as the studied in this paper. Therefore, this paper concludes that:

- The results for U-Value obtained from the numerical evaluation and software simulation for double layer bamboo wall differ nearly 20 %, with values of 1.67 and 1.34 W/m²K respectively. Under the boundaries conditioned, it proofs a feasible use as construction material in building envelopments in hot regions;
- The more layers, the better the mitigation of heat leaking; it is proved that the use of three layers of bamboo, U=0.67 W/m².K, leads to an energy saving in the building;
- Therefore, it is important to mention that this investigation was carried out through computational simulation and numerical analysis and, as long as the bamboo is a heterogeneous material, it can lead to diverse results and additional measures of sealing.

Finally yet importantly, according to norms, it is necessary to submit the bamboo through some treatments in order to increase its waterproof, fire resistance and to avoid the presence of animals that can damage it. Future experimental studies will evaluate the influence of the orientation of the layers (horizontal and inclined – 45 %) and type of joins on the thermal behaviour of the bamboo. Furthermore, the analysis of relevant thermal parameters, as the thermal stability and the influence of the humidity in the conductivity, as the density changes radially.

References

1. Bakaeva, N., Klimenko, M. Technique for Reduction of Environmental Pollution from Construction Wastes. Material Science and Engineering. 2017. No. 262. 6 p.
2. Van der Lugt, P., Vogtlander, J. The Environmental Impact of Industrial Bamboo Products – Life-Cycle Assessment and Carbon Sequestration. Inbar International Network for Bamboo and Rattan. 2015. Report No. 35. Second Edition. 58p.
3. Camargo, J. Crecimiento y fijación de carbono en una plantación de guadua en la zona cafetera de Colombia. Magazine Recursos Naturales y Ambiente.2010. No. 61. Pp. 86–94. (spa)
4. Hidalgo, O. Bamboo, The Gift of the Gods. O. Hidalgo-Lopez. 2013. 221 p.
5. Archila, H. Thermo-hydro-mechanically modified cross-laminated Guadua-bamboo panels. PhD Thesis. University of Bath. 2015. 310 p.
6. Icontec. Test Methods for the Determination of Physical and Mechanical Properties of Guadua Angustifolia Kunth.NTC 5525, Norma Tecnica Colombiana (Colombian Technic Code). 2007. Pp. 22. (spa).
7. Gato´o, A., Sharma, B., Bock, M., Mulligan, H., Ramage, M. Sustainable structures: Bamboo standards and building codes. Engineering Sustainability. 2014. No. 167. Pp. 189–196.
8. NSR 10. Reglamento Colombiano de Construcción Sismo Resistente (Colombian Standard for Seismic Resistance Construction). Chapter G- 12 Guadua Structures. Colombian Association of Seismic Engineering. 2010.132p.
9. Takeuchi, C. Caracterización Mecánica del Bambú Guadua Laminado para Uso Estructural. PhD Thesis, Universidad Nacional de Colombia. 2014. 247 p. (spa)
10. Huang, P., Chang, W., Shea, A. Non-homogeneous Thermal Properties of Bamboo. Materials and Joints in Timber Structures. 2013. No. 9. Pp. 657–664.
11. Osorio, J., Vélez, J., Ciro, H. Internal Structure of the Guadua and Its Incidence in the Mechanical Properties. Dyna. 2007. Vol. 74. No. 153. Pp. 81–94.
12. López, L., Correal, J. Exploratory Study of the Glued Laminated Bamboo Guadua Angustifolia as a Structural Material. Maderas. Ciencia y tecnología. 2009. Vol. 11 No. 3. Pp. 171–182.
13. Luna, P., Takeuchi, C., Cordón, E. Mechanical Behavior of Glued Laminated Pressed Bamboo Guadua using Different Adhesives and Environmental Conditions. Engineering Materials. 2014. Vol. 600. Pp. 57–68.
14. Mata, M., Esparza, C., Ojeda, J. Modular Rural Housing of Low Cost, Low Environmental Impact and Self-Buildable Made of Bamboo Wattle & Daub & Daub in Colima, Mexico. International Journal of Thermodynamics. 2010. Pp. 174–184.
15. Lawton, M. Roppel P. Design Guide: Solutions to Prevent Thermal Bridging. Schöck Isokorb. 2014. 35 p.
16. Gordillo, F., Cortés, D., Mejia, C., Ariza, H. Behavior of Guadua angustifolia – Kunth Thermophysical Parameters Measured by Photoacoustic Technique. RCF. Revista Colombiana de Física. 2012. Vol. 44. No.1.
17. Icropera, F. Fundamentals of Heat and mass transfer. Sixth Edition. 2007.

Литература

1. Bakaeva, N., Klimenko, M. Technique for Reduction of Environmental Pollution from Construction Wastes // Material Science and Engineering. 2017. № 262. Pp. 6.
2. Van der Lugt P., Vogtlander J. The Environmental Impact of Industrial Bamboo Products - Life-Cycle Assessment and Carbon Sequestration. Inbar International Network for Bamboo and Rattan. 2015. Report No 35. Second Edition. 58 p.
3. Camargo J. Crecimiento y fijación de carbono en una plantación de guadua en la zona cafetera de Colombia // Magazine Recursos Naturales y Ambiente.2010. № 61. Pp. 86–94. (spa)
4. Hidalgo O. Bamboo, The Gift of the Gods. O. Hidalgo-Lopez. 2013. 221 p.
5. Archila H. Thermo-hydro-mechanically modified cross-laminated Guadua-bamboo panels. PhD Thesis. University of Bath. 2015. 310p.
6. Icontec. Test Methods for the Determination of Physical and Mechanical Properties of Guadua Angustifolia Kunth.NTC 5525, Norma Tecnica Colombiana (Colombian Technic Code). 2007. Pp. 22. (spa).
7. Gato´o A., Sharma B., Bock M., Mulligan H., Ramage M. Sustainable structures: Bamboo standards and building codes // Engineering Sustainability. 2014. № 167. Pp. 189–196.
8. NSR 10. Reglamento Colombiano de Construcción Sismo Resistente (Colombian Standard for Seismic Resistance Construction). Chapter G- 12 Guadua Structures. Colombian Association of Seismic Engineering. 2010. 132 p.
9. Takeuchi C. Caracterización Mecánica del Bambú Guadua Laminado para Uso Estructural. PhD Thesis, Universidad Nacional de Colombia. 2014. 247 p. (spa)
10. Huang P., Chang W., Shea A. Non-homogeneous Thermal Properties of Bamboo // Materials and Joints in Timber Structures. 2013. № 9. Pp. 657–664.
11. Osorio J., Vélez J., Ciro H. Internal Structure of the Guadua and Its Incidence in the Mechanical Properties // Dyna. 2007. Vol. 74. № 153. Pp. 81–94.
12. López L., Correal J. Exploratory Study of the Glued Laminated Bamboo Guadua Angustifolia as a Structural Material. Maderas // Ciencia y tecnología. 2009. Vol. 11. № 3. Pp. 171–182.
13. Luna P., Takeuchi C., Cordón E. Mechanical Behavior of Glued Laminated Pressed Bamboo Guadua using Different Adhesives and Environmental Conditions // Engineering Materials. 2014. Vol. 600. Pp. 57–68.
14. Mata M., Esparza C., Ojeda J. Modular Rural Housing of Low Cost, Low Environmental Impact and Self-Buildable Made of Bamboo Wattle & Daub & Daub in Colima, Mexico // International Journal of Thermodynamics. 2010. Pp. 174–184.
15. Lawton M. Roppel P. Design Guide: Solutions to Prevent Thermal Bridging. Schöck Isokorb. 2014. 35 p.
16. Gordillo F., Cortés D., Mejia C., Ariza H. Behavior of Guadua angustifolia – Kunth Thermophysical Parameters Measured by Photoacoustic Technique. RCF // Revista Colombiana de Física. 2012. Vol. 44. No.1.
17. Icropera F. Fundamentals of Heat and mass transfer. Sixth Edition. 2007.

Бонивенто Брюгес Х., Виейра Г.Б., Ревело Орельяна Д., Того И. Показатели теплотехнического сопротивления бамбуковой стены // Инженерно-строительный журнал. 2018. № 7(83). С. 92–101.

18. Liehnhard IV, J., Lienhard V, J. A heat transfer textbook. 3rd Edition. 2001. 696 p.
19. Statsenko, E.A., Ostrovaia, A.F., Musorina, TA, Kukolev, M.I., Petritchenko, M.R. The elementary mathematical model of the enclosing structure. Magazine of Civil Engineering. 2016. 68(8), Pp. 86–91.
20. Kostenko, V., Gafiyatullina, N., Zulkarneev, G., Gorshkov, A., Petrichenko, M, Movafagh, S. Solutions for Improvement of the Thermal Protection of the Administrative Building. MATEC Web of Conferences. 2016. Vol. 73. 02011.
21. Korniyenko, S.V. Multifactorial forecast of thermal behavior in building envelope elements. Magazine of Civil Engineering. 2014. 52(8), Pp. 25–37.
22. Emmit, S., Gorse C. Introduction to Construction of Buildings. 2010. 2nd Edition. 808 p
23. Zaborova, D. Temperature regimes of a flat multilayer building envelope. Master's Thesis. Peter the Great St. Petersburg Polytechnic University. 2016. 57 p.
24. NSR 10. Reglamento Colombiano de Construcción Sismo Resistente (Colombian Standard for Seismic Resistance Construction). Chapter E-7-6 Bahareque Encementado. Colombian Association of Seismic Engineering. 2010. 28 p.
25. Simpson, W., TenWolde, A. Physical Properties and Moisture Relations of Wood, Chapter 3. In Wood Handbook. Forest Product Laboratory, first edition. 1999. 463 p.

18. Liehnhard IV, J., Lienhard V, J. A heat transfer textbook. 3rd Edition. 2001. 696p.
19. Стаценко Е.А., Островая А.Ф., Мусорина Т.А., Куколев М.И., Петриченко М.Р. Простая модель теплоустойчивой ограждающей конструкции // Инженерно-строительный журнал. 2016. № 8(68). С. 86–91
20. Kostenko V., Gafiyatullina N., Zulkarneev, G., Gorshkov A., Petrichenko M, Movafagh S. Solutions for Improvement of the Thermal Protection of the Administrative Building // MATEC Web of Conferences. 2016. Vol. 73. 02011.
21. Корниенко С.В. Многофакторная оценка теплового режима в элементах оболочки здания // Инженерно-строительный журнал. 2014. №8(52). С. 25–37
22. Emmit S., Gorse C. Introduction to Construction of Buildings. 2010. 2nd Edition. 808 p
23. Zaborova D. Temperature regimes of a flat multilayer building envelope. Master's Thesis. Peter the Great St. Petersburg Polytechnic University. 2016. 57p.
24. NSR 10. Reglamento Colombiano de Construcción Sismo Resistente (Colombian Standard for Seismic Resistance Construction). Chapter E-7-6 Bahareque Encementado. Colombian Association of Seismic Engineering. 2010. 28p.
25. Simpson W., TenWolde A. Physical Properties and Moisture Relations of Wood, Chapter 3 // Wood Handbook. Forest Product Laboratory, first edition. 1999. 463 p.

Jose del Carmen Bonivento Bruges,*
+7(931)313-60-98;
ing.joseboniventob@gmail.com

Gabriel Vieira,
+7(911)177-32-31; gabriel.vieira@poli.ufrj.br

Diana Paola Revelo Orellana,
+7(951)687-34-76; diana91pao@gmail.com

Issa Togo,
+7(921)337-37-30; issatogo@mail.ru

Хосе дель Кармен Бонивенто Брюгес,*
+7(931)313-60-98;
эл. почта: ing.joseboniventob@gmail.com

Габриэль Беренгуер Виейра,
+7(911)177-32-31;
эл. почта: gabriel.vieira@poli.ufrj.br

Диана Паола Ревело Орельяна,
+7(951)687-34-76;
эл. почта: diana91pao@gmail.com

Исса Того,
+7(921)337-37-30; эл. почта: issatogo@mail.ru

Bonivento Bruges, J.C., Vieira, G., Revelo Orellana, D.P., Togo, I. Parameter of thermal resistance of bamboo multilayer wall. Magazine of Civil Engineering. 2018. 83(7). Pp. 92–101. doi: 10.18720/MCE.83.9.

doi: 10.18720/MCE.83.10

Distribution of temperature, moisture, stress and strain in the highway

Распределение температуры, влажности, напряжений и деформаций в автомобильной дороге

B.B. Teltayev*,
Kazakhstan Highway Research Institute, Almaty city, Republic of Kazakhstan
J. Liu,
School of Civil Engineering, Beijing Jiaotong University, China
E.A. Suppes,
Kazakhstan Highway Research Institute, Almaty city, Republic of Kazakhstan

Д-р техн. наук, президент Б.Б. Телтаев*,
Казахстанский дорожный научно-исследовательский институт, Алматы, Казахстан
PhD, профессор Дж. Лиу,
Пекинский транспортный университет, Пекин, Китай
научный сотрудник Е.А. Суппес,
Казахстанский дорожный научно-исследовательский институт, Алматы, Казахстан

Keywords:pavement; subgrade; temperature; moisture; cold season; freezing; unfrozen water; stress; strain

Ключевыеслова:дорожная одежда; земляное полотно; температура; влажность; холодный период; промерзание; незамерзшая вода; напряжение; деформация

Abstract. The paper analyzes regularities for the distribution of temperature, moisture, stresses and strains in pavement and subgrade of the highway, located in northern part of Kazakhstan, within one year, especially during cold season. Distribution of temperature and moisture has been determined experimentally with the use of special sensors. Stresses and strains have been calculated with the use of elastic multilayer semi-space model. It has been shown that the stiffness (elasticity modulus) of asphalt concrete layers and upper part of subgrade soil increases considerably during cold winter season: up to 18000 MPa and 10000 MPa respectively. All the components of stresses and strains vary considerably in points of pavement and subgrade during the annual cycle. Variations of pavement surface deflection and horizontal stress in the bottom asphalt concrete layer are of quasi harmonic nature, and horizontal strain in this point varies under the quasi bicyclic law. Horizontal stress during the cold season is a tensile one and has the biggest value, and during hot season it changes its sign and becomes the compressive one. Horizontal strain during the whole annual cycle remains only a tensile one. The biggest variations of stresses and strains occur in the upper part of subgrade. During cold season the vertical compressive stresses and strains are the minimal ones, and in the beginning of spring they are the maximal ones.

Аннотация: В работе анализируются закономерности распределения температуры, влажности, напряжений и деформаций в дорожной одежде и земляном полотне автомобильной дороги, расположенной в северной части Казахстана, в течение одного года, в частности в холодный период. Экспериментальным путем с помощью специальных датчиков исследуется распределение температуры и влажности. Расчеты напряжений и деформаций выполняются с использованием математической модели упругого многослойного полупространства. Показано, что жесткость (модуль упругости) асфальтобетонных слоев и верхней части земляного полотна значительно увеличивается в зимний период: до 18000 МПа и 10000 МПа, соответственно. Все компоненты напряжений и деформаций значительно изменяются в точках дорожной одежды и земляного полотна в течение годового цикла. Изменения деформации и горизонтального напряжения в нижнем асфальтобетонном слое дорожной одежды квази-гармонического характера, а горизонтальная деформация в этой точке изменяется по квазибициклическому закону. Горизонтальное напряжение в нижнем асфальтобетонном слое в зимний период является растягивающим и имеет наибольшее значение, а в летний период меняет свой знак, т.е. становится сжимающим. Горизонтальная деформация в этом асфальтобетонном слое в годовом цикле изменяется по сложной зависимости, но остается только растягивающей. Наибольшие изменения напряжений и деформаций возникают в верхней части земляного полотна. В холодный период

Телтаев Б.Б., Лиу Дж., Суппес Е.А. Распределение температуры, влажности, напряжений и деформаций в автомобильной дороге // Инженерно-строительный журнал. 2018. № 7(83). С. 102–113.

вертикальные напряжения и деформации являются минимальными, а в начале весеннего сезона они максимальные.

1. Introduction

Pavement and subgrade are the main constructive elements, on which the strength and operational life of the highway depend. Mechanical loads of moving vehicles, climatic and hydrological factors affect the highway. The temperature can be considered as one of the most important from climatic factors. For example, depending on temperature, the mechanical and physical characteristics of the asphalt concrete pavement layers vary within the wide range. The more the small-size clay particles in the subgrade soil, the more its mechanical and physical properties depend on moisture. Phase transition of the first order occurs in wet soil at the temperature of approximately 0°C, resulting in the fact that the part of moisture from liquid condition (water) transforms into solid (ice) condition, and in liquid condition remains only the so-called unfrozen water. During winter season with the decrease of negative temperature the amount of unfrozen water in soil gradually decreases, the stiffness of soil in subgrade increases, and it is expected that the increase of the stiffnes for the asphalt concrete layers and soil in winter season should impact greatly on the distribution of stresses and strains in pavement and subgrade.

As it is known, deformability, strength, thermal and physical characteristics of frozen soils differ greatly from unfrozen soils [1–4].

1. Highway specialists of the beginning of the last century understood the importance of temperature impact in subgrade on pavement state. Thus, as the short message of Wiley read [5] they believed in the Illinois University, that concrete highway cracking phenomenon can be explained by limits and rates of temperature variation in pavement and subgrade, and investigations were started. Preliminary results showed that extreme temperatures delay greatly in comparison with the air.

2. Temperature gradient shows the direction of heat flow and causes the effect of thermal diffusion (moisture transfer with availability of temperature difference). For example, it was obtained experimentally in the work Xu et al [6] that formation of water concentration gradient in subgrade soil was based, mainly, on temperature gradient.

3. Tan and Hu [7] obtained experimentally that water transfer in soil under impact of temperature gradient takes a long time. There was no obvious water transfer in the tested samples during first days. It became obvious only after expiring of five days.

4. Essential role of temperature gradient in water transfer in the frozen soil was evaluated experimentally in the work of Mao et al. [8].

5. The paper [9] mentions the practical importance of zero isotherm during construction of subgrade for railway and it is investigated experimentally by testing stand and numerical simulation.

6. They calculated temperature values in New Hampshire State [10] for the surface of highway subgrade under computer program in each month of the year and they obtained resilient modulus values for subgrade soils at those temperatures in the laboratory.

7. The works [11, 12] show existence of reliable correlation relationship between temperature and subgrade modulus.

8. The works [13, 14], mainly, analyze the impact of temperature of the asphalt concrete layers on the mechanical behavior of pavement. The first paper, measures the deflection of pavement surface, using falling weight deflectometer experimentally at different temperatures, and it is found out that the temperature and the thickness of the asphalt concrete layers impact greatly on dynamic properties of the asphalt concretes. The second paper develops the mathematical model, and with the help of it the distribution of temperature, stresses and strains in pavement has been analyzed in different time of 24 hours in the hot season of the year. It has been shown how greatly the temperature of the asphalt concrete layers impacts on the distribution of stresses and strains in pavement.

9. Some results of theoretical and experimental research for temperature variation in pavement and subgrade of the highways in sharp continental climatic conditions during various seasons of the year have been published in the works [15–18].

This paper experimentally analyzes the distribution of temperature and moisture in pavement and subgrade of the highway, located in the northern part of Kazakhstan, within one year. Using the results obtained, by calculation, the stress and strains in pavement and subgrade have been determined, their variation has been shown during the annual cycle, impact of freezing for the subgrade soil on the values of stresses and strains has been evaluated.

2. Methods

2.1. Experimental section

The section with asphalt concrete (km 76+30) pavement of “Astana-Burabai” highway was selected for performance of long-term monitoring for temperature and moisture variation in pavement structure layers and points of subgrade of the highway in climatic conditions of northern region of Kazakhstan in November 2010. Highway has 6 lanes with the width of 3.75 m each. It is allowable for car to move with the speed of 140 kph, and for trucks with the speed of 110 kph along this highway. Reconstruction of the highway was completed in November of 2009.

Pavement structure of the section with asphalt concrete (Figure 1) consists of the following layers: 1 – stone mastic asphalt concrete, 6 cm; 2 – dense asphalt concrete, 9 cm; 3 – crushed stone treated with bitumen, 12 cm; 4 – crushed stone and sand mix treated with cement (7%), 18 cm; 5 – crushed stone and sand mix, 15 cm;6 – sand, 20 cm. Subgrade is constructed from heavy sandy clay loam: moisture in the plastic limit WP = 18.7 %; moisture in the liquid limit WT =34.8 %. Underground water is deep (lower than 3.0 m).

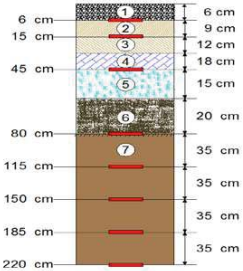

Figure 1. Scheme for location of sensors in pavement structure and subgrade for section with asphalt concrete pavement of “Astana-Burabai” highway: 1…6 – numbers of pavement layers; 7 – subgrade; – temperature and moisture sensors

2.2. Temperature and moisture sensors

Company “Interpribor” (Chelyabinsk, Russia) produced temperature and moisture sensors on the order of Kazakhstan Highway Research Institute (KazdorNII). Each sensor, produced in the form of metal capsule, contains element for measurement of temperature based on the effect of thermal resistance and element for measurement of moisture through diamagnetic permeability. Such design concept allows performing simultaneously the measurement of temperature and moisture in points of pavement and subgrade.

Figure 2 shows general view of one set of sensors visually. Temperature element of sensors was calibrated by the producer and moisture element was calibrated in the laboratory of KazdorNII. Calibration of sensors was performed with the use of soils, selected from the areas of their installation. Measurement ends of the sensors were put on the surface of the highway and fixed in measurement chamber of land system of the set (Figure 3).

Figure 2. One set of temperature and moisture sensors

Figure 3. Measurement (land) system for setof temperature and moisture sensors

Телтаев Б.Б., Лиу Дж., Суппес Е.А. Распределение температуры, влажности, напряжений и деформаций в автомобильной дороге // Инженерно-строительный журнал. 2018. № 7(83). С. 102–113.

Each set had 8 temperature and moisture sensors, 3 of which were installed in pavement layers, and 5 of them were installed into subgrade of the highway. The depth for their installation, calculated from pavement surface, were equal to: 6, 15, 45, 80, 115, 150, 185 and 220 cm.

2.3. Deformation behavior of asphalt concretes

Asphalt concrete is a visco-elastic material [19–21] and its deformation behavior depends on temperature and load duration. At present the experimental, as well as calculation methods are known for determination of elasticity modulus of the asphalt concretes. For example, the so-called model of M.W. Witczak [22], which has been used in the work [23]. In this paper the elasticity modulus of stone-mastic and porous asphalt concretes was calculated under the modified formula of Hirsh, suggested in the paper [24]:

$$E_{ac}(t) = P_c(t) \cdot \left[E_{ag} \cdot (1 - VMA) + E_b(t) \cdot VFA \cdot VMA \right], \quad (1)$$

$$P_c(t) = 0.006 + \frac{0.994}{1 + \exp\left[-\left(0.6628 + 0.5861 \cdot \ell n\left(VFA \cdot \frac{E_b(t)}{3} \right) \right) - 12.87 \cdot VMA - 0.1706 \cdot \ell n(\varepsilon \cdot 10^6) \right]}, \quad (2)$$

where $E_{ac}(t)$ is an elasticity modulus of asphalt concrete at the time moment t, $E_b(t)$ is an elasticity modulus of bitumen at the time moment t, E_{ag} is an elasticity modulus of stone aggregate, set as equal to 26 540 MPa, *VMA* are the air voids of mineral aggregate (as a decimal fraction), *VFA* are the voids, filled with binder (as a decimal fraction, ε is a level of strain, set as equal to $100 \cdot 10^{-6}$ for low and mean temperatures.

Elasticity modulus of bitumen $E_{ac}(t)$ is calculated under formula [25]:

$$E_b(t) = Eg \left[1 + \left(\frac{Eg \cdot t}{3 \cdot \eta} \right)^b \right]^{-\left(1 + \frac{1}{b}\right)} \quad (3)$$

where $E_g$is an instantaneous elasticity modulus, set as equal to 2 460 MPa, η is a coefficient of the viscosity for bitumen, MPa·s.

Coefficient of viscosity η is obtained under the expressions:

$$\begin{cases} \eta = a_{TrAhr}(T) \cdot \eta(T_r) & \mathrm{T} \le \mathrm{T}_{rb} - 10; \\ \eta = a_{Tr\,\mathrm{WLF}}(T) \cdot \eta(T_r) & \mathrm{T} > \mathrm{T}_{rb} - 10, \end{cases} \quad (4)$$

$$\eta(T_r) = 0.00124 \left[1 + 71 \cdot \exp\left[-\frac{12(20 - PI)}{5(10 + PI)} \right] \right] \cdot \exp\left(\frac{0.2011}{0.11 + 0.0077 PI} \right), \quad (5)$$

$$a_{TrAhr}(T) = \exp\left[11720 \cdot \frac{3(30 + PI)}{5(10 + PI)} \left[\frac{1}{(T + 273)} - \frac{1}{(T_{rb} + 263)} \right] \right], \quad (6)$$

$$a_{TrWLF}(T) = \exp\left[-\frac{2.303\,(T - T_{rb} + 10)}{(0.11 + 0.0077 PI)\,(114.5 + T - T_{rb})} \right]. \quad (7)$$

where *PI*and $T_{rb}$are penetration index and softening point of bitumen.

Parameter b is calculated under the expressions:

$$b = \frac{1}{\frac{1}{\beta} + \frac{\ell n(\pi)}{\ell n(2)} - 2}, \quad (8)$$

$$\beta = \frac{0.1794}{1 + 0.2084\ PI\ - 0.00524\ PI^2}. \quad (9)$$

In calculations of the values for elasticity modulus of the asphalt concretes the load duration was set as equal to 0.1 of a second. The values of Poisson's coefficient for asphalt concretes at various temperatures were obtained under formula, recommended by the Guide [26]:

$$\nu = 0.15 + \frac{0.35}{1 + \exp\left(-1.63 + 3.84 \cdot 10^{-6} \cdot E_{ac}(t)\right)}, \quad (10)$$

where ν is a Poisson's coefficient of asphalt concrete, $E_{ac}(t)$ is an elasticity modulus of asphalt concrete.

2.4. Deformation behavior of soil

The values of elasticity modulus for the soil of subgrade (heavy sandy clay loam) at the positive temperatures are set under the standard document [27] depending on soil moisture, and at negative temperatures they are obtained according to the data of the Professor N.A. Tsytovich [28] depending on the value of negative temperature and the amount of unfrozen water. The upper part of the subgrade for the highway with thickness of 140 cm (from 80 cm to 220 cm from the asphalt concrete pavement surface) was divided into 7 layers, each of them had the thickness of 20 cm. It was set that for each of those soil layers the temperature and moisture had constant values.

2.5. Deformation behavior of pavement interlayers

Values of elasticity modulus and Poisson's coefficient of the materials of pavement interlayers (crushed stone, treated with bitumen; crushed stone and sand mix, treated with cement (7 %); crushed stone and sand mix; sand) are fixed under the standard document [27] and shown in the Table 1.

Table 1. Values of elasticity modulus and Poisson's coefficient of the materials of pavement interlayers

Material	Elasticity modulus E, MPa	Poisson's coefficient v
Crushed stone treated with bitumen	600	0.25
Crushed stone and sand mix, treated with cement (7%)	500	0.25
Crushed stone and sand mix	230	0.30
Sand	120	0.30

2.6. Calculation scheme for stresses and strains in pavement and subgrade

Calculation scheme of pavement structure and subgrade is shown in Figure 4. As it is seen, the scheme shows 13 layers, out of which the first 6 simulate the pavement layers, and the other 7 layers correspond to the layers of subgrade. The materials of all the layers and soil are considered as elastic one. The lowest soil layer (the 13th layer) is considered as elastic semi-space, which has infinite thickness. Stresses and strains in such multilayer elastic system are determined with the use of the solution of Prof. A.K. Privarnikov [16]. On the surface of the upper layer there is a load q = 0.6 MPa, uniformly distributed within the circle with diameter of D = 42 cm. It corresponds to the axial load of 13 tons.

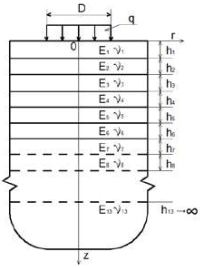

Figure4.Calculation scheme

Телтаев Б.Б., Лиу Дж., Суппес Е.А. Распределение температуры, влажности, напряжений и деформаций в автомобильной дороге // Инженерно-строительный журнал. 2018. № 7(83). С. 102–113.

3. Results and Discussion

3.1. Temperature and moisture in subgrade and pavement

Figure 5 shows the graphs of temperature distribution in the depth of highway during various seasons of the year, constructed under experimental data, which were obtained through the use of sensors. As it is seen, temperature distributions differ greatly from each other during various seasons of the year.

Figures 6 and 7 show the graphs of temperature variation in points of pavement and subgrade in summer and winter 24 hours. As it is seen daily temperature variation occurs only in asphalt concrete layers and up to the depth of 45 cm. Temperature variation does not occur below this depth, therefore, in points of subgrade in daily cycle. Temperature variation in this field is of seasonal character and it is observed in the annual cycle.

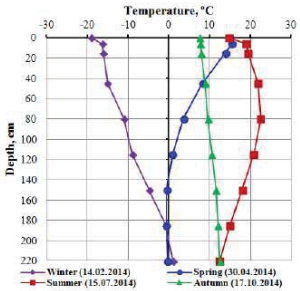

Figure 5. Temperature distribution in the depth of highway during various seasons of the year

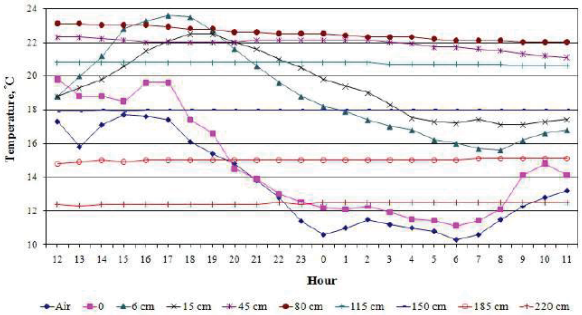

Figure 6. Temperature variation in points of pavement and subgrade in summer (14-15.07. 2014)

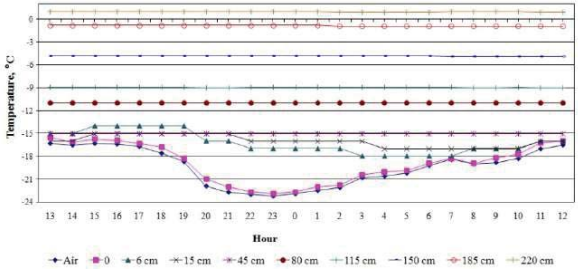

Figure 7.Temperature variation in points of pavement and subgrade in winter (13-14.02. 2014)

As expected, the biggest temperature values occur in summer and with temperature decrease in autumn temperature reduction occurs also in subgrade. Subgrade (1.50 cm) and ground foundation in

winter are in frozen condition. Temperature of subgrade surface reduces to -12 °C. Pavement and subgrade start melting in the beginning of spring from top to bottom.

Figures 8–10 show the graphs for moisture distribution in the depth of subgrade during various seasons of the year, where it can be seen that moisture values in points of subgrade are almost the same in summer and autumn seasons of the year. Part of water, contained in points of subgrade, is transferred to ice in winter with negative temperatures occurrence. Continuous line in Figures 9 and 10 shows moisture content in liquid condition (unfrozen water), and dashed line corresponds to initial moisture (before winter). It can be seen that frozen water content (ice) in subgrade decreases during winter period with the depth increase (Figure9). Defrosting of subgrade in spring occurs from top to bottom. It is clearly seen from Figure10 that upper part of subgrade defrosted to 130 cm in the end of April 2014 and the rest part of subgrade is in frozen condition.

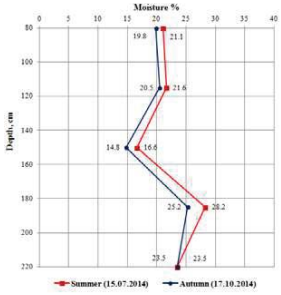

Figure 8. Moisture distribution in the depth of subgrade in summer and autumn periods of the year

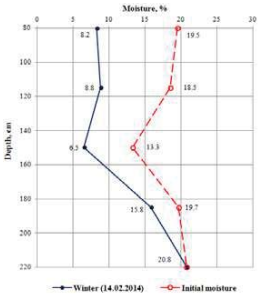

Figure 9. Moisture distribution in the depth of subgrade in winter period of the year

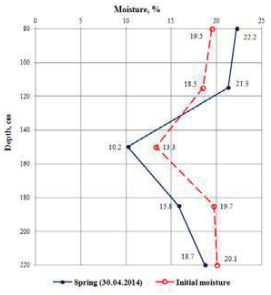

Figure 10. Moisture distribution in the depth of subgrade in spring period of the year

It is clear from the graphs of temperature and moisture variation (Figures 11, 12) on subgrade surface (80 cm) and in the depth of 115 cm, that sharp decrease of moisture occurs in winter approximately at the moment of temperature transition to negative area, and moisture is also decreases with further temperature reduction. And in spring there is intermittent increase of moisture during temperature transition from negative area to positive area. Certainly, these phenomena show phase transitions, which occur at temperature, approximately equal to 0°C.

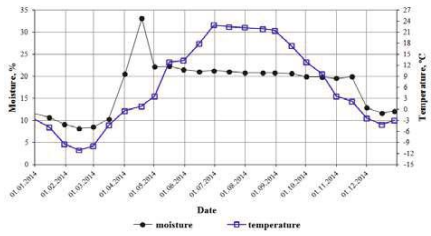

Figure 11.Temperature and moisture variation on subgrade surface (80 cm)

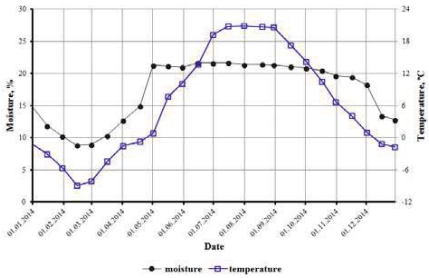

Figure 12. Temperature and moisture variation in subgrade (115 cm)

3.2. Deformation behavior of asphalt concretes

Figure 13 shows the graphs of the mean half-monthly values of temperature for asphalt concrete layers of “Astana-Burabai” highway in the course of the year (December 2013 – December 2014). Figures 14 and 15 show the values of elasticity modulus and Poisson’s coefficient of the asphalt concretes, obtained under the above expressions. It should be noted that the mean half-monthly values of the top and bottom layers for the asphalt concrete of the highway are practically the same.

Телтаев Б.Б., Лиу Дж., Суппес Е.А. Распределение температуры, влажности, напряжений и деформаций в автомобильной дороге // Инженерно-строительный журнал. 2018. № 7(83). С. 102–113.

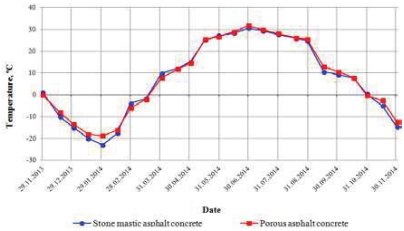

Figure 13. Mean half-monthly values of temperature for asphalt concrete layers

As one should expect, the character of variation for elasticity modulus of the asphalt concretes is fundamentally opposite to the temperature: the higher the temperature, the lower the elasticity modulus, and vice versa, the lower the temperature, the higher the elasticity modulus. And qualitative character of variation of the Poisson's coefficient coincides with the temperature: the higher the temperature, the higher the Poisson's coefficient, and vice versa, the lower the temperature, the lower Poisson's coefficient. At high temperatures (in summer) the values of elasticity modulus for both asphalt concretes are practically the same, but at low temperatures (in winter) they are essentially higher for stone mastic asphalt concrete, than for porous asphalt concrete. At high (in summer) and low (in winter) temperatures the values of Poisson's coefficient for both asphalt concretes are practically the same, but at intermediate temperatures (in spring and autumn) they are somewhat higher for the porous asphalt concrete than for stone mastic asphalt concrete.

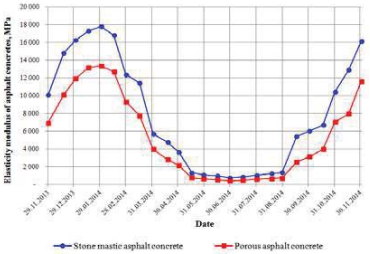

Figure 14. Values of elasticity modulus of asphalt concretes

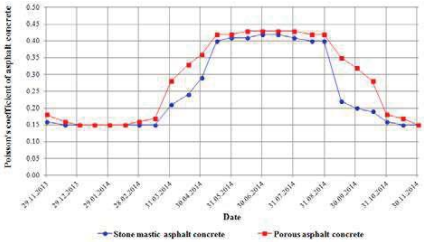

Figure 15. Values of Poisson's coefficient for asphalt concretes

3.3. Deformation behavior of soil

The values of elasticity modulus for the subgrade of the highway, obtained according to the above methods, are shown graphically in Figure 16. As it is seen, freezing in winter season increases essentially the elasticity modulus of the soil. The uppermost layer of the subgrade has the biggest value of elasticity modulus, as the minimum values of negative temperature and the lowest values of unfrozen water occur in the subgrade in winter.

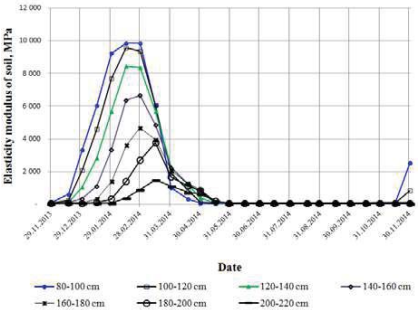

Figure 16. Values of elasticity modulus in subgrade layers of a highway

Teltayev, B.B., Liu, J., Suppes, E.A. Distribution of temperature, moisture, stress and strain in the highway. Magazine of Civil Engineering. 2018. 83(7). Pp. 102–113. doi: 10.18720/MCE.83.10.

The values of elasticity modulus decrease with the depth increase. It is explained by the fact that the temperature increase with the depth increase and, therefore, the amount of unfrozen water increases. It should be specially noted that elasticity modulus of upper layers of the soil of the subgrade reaches 8 000-10 000 MPa in winter season, which is 140-180 times more compared with spring and summer seasons. Therefore, we expect that the impact of winter freezing of the soil in the subgrade on stresses and strains in pavement and subgrade layers will be significant. Due to the absence of reliable data, the value of Poisson's coefficient for the soil of the subgrade is set as constant and it is equal to 0.35.

3.4. Stresses and strains in asphalt concrete layers

Figure 17 represents the graph, showing deflection variation for the surface of the first layer of pavement from stone mastic asphalt concrete. As it is seen, variation of mechanical characteristics for asphalt concrete layers and soil impacts greatly on the deflection value of the pavement surface. Qualitative change of the deflection is of quasi-cyclic nature. It is found that the least deflection values occur from the middle of February to the middle of March, and the biggest ones occur in the beginning of July. The biggest deflection is approximately 5 times more than the least one. Deflection of pavement surface is the only characteristics, which can be measured by non-destructive method. Therefore it is currently used in many countries, including Kazakhstan, for evaluation of strength for the pavement structure [27]. It is considered that during spring defreezing of subgrade the pavement structure has the lease strength and the biggest deflection value of the pavement surface. But the graph of deflection shows that the biggest deflection of the pavement surface occurs in the beginning of July, i.e. in summer, but not in spring. It is seen from the Figure 12 that in the beginning of July the asphalt concrete layers have the highest temperature. Therefore, it becomes clear that the biggest pavement deflection in summer season is specified by essential decrease of stiffness (moduli of stiffness) of the asphalt concrete layers due to the highest temperatures.

The next important characteristics for mechanical behavior of pavement are horizontal stress σ_r^2 and strain ε_r^2 in the bottom surface of the second asphalt concrete layer. Stress σ_r^2 and strain ε_r^2 are considered during evaluation of fatigue strength of the asphalt concrete layers. The USA [26] and many other countries include strain ε_r^2 into relevant calculations, but in the countries of the former USSR – the stress σ_r^2. It is found out (Figure 18), the qualitative character of variation for these factors is different. Graph for variation of stress σ_r^2 is identical to the graph for variation of the mean half-monthly temperature of the asphalt concrete layers (Figure 12): the lower the temperature the higher the stress. In hot period (in summer), when the stiffness (elasticity moduli) of the asphalt concretes becomes low, the stress changes its sign, i.e. transforms from tension into compression.

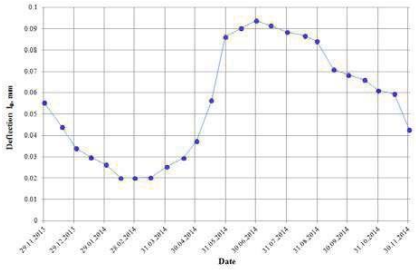

Figure 17. Deflection of the surface for the first pavement layer from stone mastic asphalt concrete

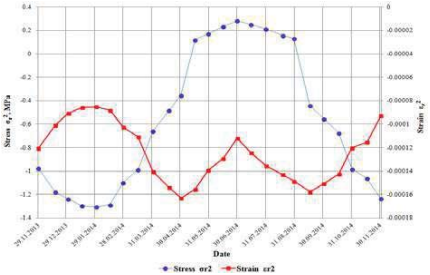

Figure 18. Horizontal stress and strain in the bottom surface of the second asphalt concrete layer

The biggest value of the tensile strength σ_r^2 occurs in the end of January and it is equal to 1.32 MPa, and the biggest value of the compressive strength occurs in the beginning of July and it is equal to 0.28 MPa. The strain ε_r^2 is changed in a more complicated way during annual cycle, but, contrary to the stress σ_r^2, it remains only tensile. Its lowest value, equal to 0.000085 occurs in the end of January, and the biggest values, equal to 0.00016 approximately, occur in the beginning of May and in the middle of September.

Телтаев Б.Б., Лиу Дж., Суппес Е.А. Распределение температуры, влажности, напряжений и деформаций в автомобильной дороге // Инженерно-строительный журнал. 2018. № 7(83). С. 102–113.

3.5. Stresses and strains in subgrade

The graphs of variation for vertical stress σ_z^{sg} and strain ε_z^{sg} in points of subgrade, located in three different depths (0, 60, 120 cm), are shown in the Figures 19 and 20. It is seen that freezing of soil of the subgrade impacts greatly on stress and strain in subgrade. The largest variation of stress and strain during annual cycle occurs on the surface of subgrade and with the increase of the depth the impact of freezing decreases. For example, on the surface of subgrade the biggest vertical stress σ_z^{sg} in the end of winter season (in the beginning of April) reaches 0.045 MPa, and in the beginning of winter season (in the middle of November) it decreases to 0.018 MPa. As it could be expected, during freezing the soil becomes stiff and the strain decreases sharply. And with the beginning of defreezing the stiffness of soil decreases sharply, which causes sharp increase of the strain. In the case considered the biggest vertical strain, equal to 0.00043, was registered on the surface of subgrade in the middle of May and it decreases gradually in time before freezing starts.

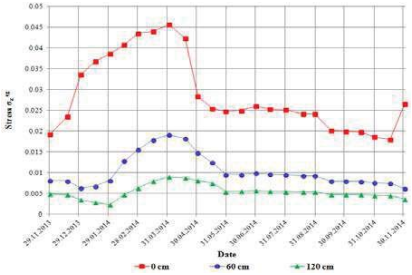

Figure 19. Vertical stress in subgrade

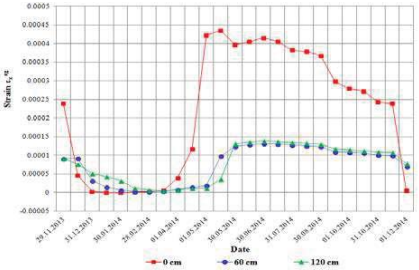

Figure 20. Vertical strain in subgrade

4. Conclusions

The results of experimental analysis for temperature and moisture variations and calculation of stresses and strains in points of pavement and subgrade in this paper allow drawing the following conclusions:

1. Daily temperature variation causes similar daily temperature variation in upper (asphalt concrete) pavement layers. Amplitude of daily temperature variations is decreased with the depth increase and in the depth, equal approximately to 45–50 cm, it is practically equal to zero. Temperature and moisture in points of subgrade do not vary within 24 hours, as the time, required for their sensible variation, is much more than the duration of 24 hours. Their variation is of seasonal nature, and it is clearly seen during annual cycle. Temperature and moisture are distributed in different ways in the depth of subgrade during various year seasons. In winter the temperature of the subgrade surface decreases to -12°C and it increases in the depth. Maximum freezing depth can reach 254 cm.

2. Deformation characteristics of the asphalt concrete pavement layers vary greatly depending on temperature. Elasticity modulus of stone mastic and porous asphalt concretes during cold winter season reaches 17 800 MPa and 13 400 MPA respectively, whereas during hot summer season they can decrease to 740 MPa and 400 MPa respectively. Transition of the part of water, contained in the subgrade soil, from liquid condition into solid one (ice) at the temperatures, which are lower than 0 ºC, also increases the stiffness (elasticity modulus) of soil. During winter season the elasticity modulus of soil for top layers of the subgrade reaches 8 000–10 000 MPa, which 140–180 times more than in spring and summer.

3. Substantial variation of mechanical characteristics of the asphalt concrete layers for pavement and the subgrade soil, caused by temperature and moisture variations during annual cycle, determines the substantial variation of stresses and strains in points of pavement and subgrade as well. For example, the deflection of the pavement surface and horizontal strain in the bottom asphalt concrete layer vary during annual cycle under quasi harmonic law. Together with it, the deflection varies in 5 times.

4. Horizontal stress in the bottom asphalt concrete layer during winter season is a tensile one and it has the biggest value, and in summer season it changes its sign, i.e. it becomes the compressive one. Horizontal strain in this asphalt concrete layer during annual cycle varies under the more complicated quasi bicyclic dependence, but remains only tensile one.

Teltayev, B.B., Liu, J., Suppes, E.A. Distribution of temperature, moisture, stress and strain in the highway. Magazine of Civil Engineering. 2018. 83(7). Pp. 102–113. doi: 10.18720/MCE.83.10.

5. The most considerable variations of stresses and strains during annual cycle occur in the top part of the subgrade. For example, the least value of vertical compressive stress was recorded on the surface of subgrade in the beginning of winter season (in the middle of November), and in the end of winter season (in the beginning of April) it increases up to the maximal one.

6. The least vertical compressive strain, close to zero, as it has been expected, occurs in winter, when the top part of subgrade is in frozen condition. When defreezing starts, the stiffness of the soil decreases and, therefore, vertical compressive strain increases, and its biggest value on the subgrade surface occurs in the middle of May.

References

1. Liu, J.K. Review of the influence of freeze-thaw cycles on the physical and mechanical properties of soil. Sciences in cold and arid regions. 2013. Vol. 5(4). Pp. 457–460.
2. Kang, M.G., Kim, J.S., Park, J.H., Lee, J.S. Freezing and thawing effects of sand-silt mixtures on elastie waves. Sciences in Cold and Arid Regions. 2013. No. 4. Pp. 418–424.
3. Kim, S.Y, Lee, J.S. Strength and stiffness variation of frozen soils according to confinement during freezing. Sciences in Cold and Arid Regions. 2015. No. 4. Pp. 335–339.
4. Petriaev, A. Stress states of thawed soil subgrade. Sciences in Cold and Arid Regions. 2015. No. 4. Pp. 348–353.
5. Wiley, C.C., Comparison of road-subgrade and air temperatures. Monthly weather review. American Meteorological Society, November, 1919. 802 p.
6. Xu, J., Niu, F., Niu, Y., Hou, Z. Analysis on the moisture migration of subgrade soil under effect of temperature gradient. Journal of Chongqing University. 2013. No. 4.
7. Tan, Y., Hu, X. Experimental study on moisture transmission of compacted laterite soil under temperature effect. Proceeding of the International Symposium on Multi-field Coupling Theory of Rock and Soil Media and Its Applications. Chengdu, China. 2010.
8. Mao, X., Miller, C., Xou, Z., Khandker, A., Xiao, X. Experimental study of soil water migration in freezing process. Geotechnical Testing Journal. 2014. Vol. 37(3). Pp. 1–11.
9. Izvolt, L., Hodas, S. Software support for Temperature regime modeling of railway track construction. Logistics. 2014. No. 4. Pp. 2861–2871.
10. Vincent, C.J., John, J.B.Jr., Glen, D.D., Charles, E.S.Jr. Resilient modulus for New Hampshire subgrade soils for use in mechanistic AASHTO design. Special ReportNo. 19991004 257. US Army Corps of Engineers Cold Regions Research and Engineering Laboratory. Hanover, New Hampshire, USA. 1999.
11. Hossian, M., Romanoschi, S., Gisi, A. Seasonal and spatial variation of subgrade response. Proceedings of Sessions of Geo-Denver 2000 "Pavement Subgrade, Unbound Materials and Nondestructive Testing". Denver, Colorado, USA, August. 2000.
12. Long, B.,Hossian, M., Gisi, A. Seasonal variation ofbackcalculated subgrade moduli. Transportation Research Record. 1997. Vol. 1577. Pp. 70–80.
13. Zheng, Y., Kang, H., Cai, Y., Zhang, Y. Effects of temperature on the dynamic properties of asphalt mixtures. Journal of Wuhan University of Technology. Material Sciences. 2010. Pp. 534–537.
14. Xue, Q., Liu, L., Zhao, Y., Chen, Y., Li, J. Dynamic behavior of asphalt pavement structure under temperature-stress coupled loading. Applied Thermal Engineering. 2013. Vol. 53. Pp. 1–7.
15. Teltayev, B. Road subgrade temperature and moisture variations. Proceedings of the 5th International Geotechnical Symposium "Geotechnical Engineering for

Литература

1. Liu J.K. Review of the influence of freeze-thaw cycles on the physical and mechanical properties of soil // Sciences in cold and arid regions. 2013.Vol. 5(4). Pp. 457–460.
2. Kang M.G., Kim J.S., Park J.H., Lee J.S. Freezing and thawing effects of sand-silt mixtures on elastic waves // Sciences in Cold and Arid Regions. 2013.№ 4. Pp. 418–424.
3. Kim S.Y, Lee J.S. Strength and stiffness variation of frozen soils according to confinement during freezing // Sciences in Cold and Arid Regions. 2015.№ 4. Pp. 335–339.
4. Petriaev A. Stress states of thawed soil subgrade // Sciences in Cold and Arid Regions. 2015.№ 4.Pp. 348-353.
5. Wiley C.C. Comparison of road-subgrade and air temperatures. Monthly weather review, American Meteorological Society, November, 1919. 802 p.
6. Xu J., Niu F., Niu Y., Hou Z. Analysis on the moisture migration of subgrade soil under effect of temperature gradient // Journal of Chongqing University. 2013.№ 4.
7. Tan Y., Hu X. Experimental study on moisture transmission of compacted laterite soil under temperature effect // Proceeding of the International Symposium on Multi-field Coupling Theory of Rock and Soil Media and Its Applications. Chengdu, China, 2010.
8. Mao X., Miller C., Xou Z., Khandker A., Xiao X. Experimental study of soil water migration in freezing process // Geotechnical Testing Journal. 2014.Vol. 37(3). Pp. 1–11.
9. Izvolt L., Hodas S. Software support for Temperature regime modeling of railway track construction // Logistics. 2014.№ 4. Pp. 2861–2871.
10. Vincent C.J., John J.B.Jr., Glen D.D., Charles E.S.Jr. Resilient modulus for New Hampshire subgrade soils for use in mechanistic AASHTO design. Special ReportNo. 19991004 257. US Army Corps of Engineers Cold Regions Research and Engineering Laboratory, Hanover, New Hampshire, USA. 1999.
11. Hossian M., Romanoschi S., Gisi A. Seasonal and spatial variation of subgrade response // Proceedings of Sessions of Geo-Denver 2000 "Pavement Subgrade, Unbound Materials and Nondestructive Testing". Denver, Colorado, USA, 2000.
12. Long B., Hossian M., Gisi A. Seasonal variation ofbackcalculated subgrade moduli // Transportation Research Record. 1997. Vol. 1577.Pp. 70–80.
13. Zheng Y., Kang H., Cai Y., Zhang Y. Effects of temperature on the dynamic properties of asphalt mixtures // Journal of Wuhan University of Technology. Material Sciences. 2010. Pp. 534–537.
14. Xue Q., Liu L., Zhao Y., Chen Y., Li, J. Dynamic behavior of asphalt pavement structure under temperature-stress coupled loading // Applied Thermal Engineering. 2013.№ 53. Pp. 1–7.
15. Teltayev B. Road subgrade temperature and moisture variations // Proceedings of the 5th International Geotechnical Symposium "Geotechnical Engineering for

Телтаев Б.Б., Лиу Дж., Суппес Е.А. Распределение температуры, влажности, напряжений и деформаций в автомобильной дороге // Инженерно-строительный журнал. 2018. № 7(83). С. 102–113.

Disaster Preventions and Redaction, Environmentally Sustainable Development. Incheon, Korea, 2013.

16. Teltayev, B., Aitbayev, K. Modeling of temperature field in flexible pavement. Indian Geotechnical Journal. 2015. Vol. 45(4). Pp. 371–377.
17. Teltayev, B., Aitbayev, K. Modeling of transient temperature distribution in multilayer asphalt pavement Geomechanics and Engeneering. 2015. Vol. 8(2). Pp. 133–152.
18. Teltayev, B.B.,Suppes, E.A., Baibatyrov, A.I. Characteristics of highway subgrade frost penetration in regions of the Kazakhstan. JapaneseGeotechnical Society Special Publication "The 15th Asian Regional Conference on Soil Mechanics and Geotechnical engineering". Fukuoka, Japan. November. 2015.
19. Huang, Y.H. Pavement Analysis and Design. Second Edition. Pearson Education, Inc. Upper Saddle River, New Jersey. 2004.
20. Papagiannakis, A.T., Masad, E.A. Pavement design and materials. John Wiley & Sons, Inc. New Jersey, NJ, USA, 2008.
21. Yoder, E.J., Witczak, M.W. Principles of pavement design. John Wiley & Sons, Inc. New Jersey. 1975. 736 p.
22. Witczak, M.W., Andrei, D., Mirza, W. Development of revised predictive model for the dynamic (complex) modulus of asphalt mixtures. Inter-team Technical Report. NCHRP Project No. 1-37A. 1999. 40 p.
23. Kondrashov, N.A., Shestopalov, A.A. Dynamic modulus application in the asphalt compaction rheological model for pavement construction. Magazine of Civil Engineering. 2014.51(7). Pp. 103–113.
24. Christensen, D.W., Bonaquist, R.F. Impoved Hirch model for estimating the modulus of hot mix asphalt. Journal of the Association of Asphalt Paving Technologists. 2015. Vol. 84. Pp. 527–562.
25. Teltayev, B., Radovskiy, B. Low temperature crackingproblem for asphalt pavements in Kazakhstan. 8th RILEM International Conference on Mechanics of Cracking and Debonding in Pavements. 2016. No.1. Pp. 139–145.
26. ARA, Inc, ERES Concultans Division. Guide for Mechanistic-Empirical Design of New and Rehabilitated Pavement Structures. Final Report. NCHRP, Project 1-37 A, Transportation Research Board of the National Academies, Washington. 2004.
27. SN RK 3.03-04-2014 Proektirovanie dorozhnyh odezhd nezhestkogo tipa. [Design of flexible pavements], Astana. 2014. 39 p. (rus.)
28. Citovich N.A. Mekhanika merzlyh gruntov. [Mechanics of frozen soils]. Moscow, 1973. 448 p. (rus.).

Disaster Preventions and Redaction, Environmentally Sustainable Development". Incheon, Korea, 2013

16. Teltayev B., Aitbayev K. Modeling of temperature field in flexible pavement // Indian Geotechnical Journal. 2015.Vol. 45(4). Pp. 371–377.
17. Teltayev B., Aitbayev K. Modeling of transient temperature distribution in multilayer asphalt pavement // Geomechanics and Engineering. 2015.Vol. 8(2). Pp. 133–152.
18. Teltayev B.B., Suppes E. A., Baibatyrov A.I. Characteristics of highway subgrade frost penetration in regions of the Kazakhstan // Japanese Geotechnical Society Special Publication "The 15th Asian Regional Conference on Soil Mechanics and Geotechnical engineering". Fukuoka, Japan, 2015.
19. Huang Y.H. Pavement Analysis and Design, Second Edition, Pearson Education, Inc., Upper Saddle River, New Jersey. 2004.
20. Papagiannakis A.T., Masad E.A. Pavement Design and Materials". John Wiley & Sons. Inc., New Jersey.2008.
21. Yoder E.J., Witczak M.W. Principles of Pavement Design. John Wiley & Sons, Inc., New Jersey. 1975.
22. Witczak M.W., Andrei D., Mirza W. Development of revised predictive model for the dynamic (complex) modulus of asphalt mixtures. Inter-team Technical Report. NCHRP Project № 1-37A. 1999. 40 p.
23. Кондрашов Н.А., Шестопалов А.А. Использование модуля деформации в реологической модели уплотнения асфальтобетонной смеси при строительстве дорожных покрытий // Инженерно-строительный журнал. 2014. №7(51). С. 55–65
24. Christensen D.W., Bonaquist R.F. Impoved Hirch model for estimating the modulus of hot mix asphalt // Journal of the Association of Asphalt Paving Technologists. 2015.Vol. 84. Pp. 527–562.
25. Teltayev B., Radovskiy B. Low temperature crackingproblem for asphalt pavements in Kazakhstan // 8th RILEM International Conference on Mechanics of Cracking and Debonding in Pavements. 2016.№ 1. Pp. 139–145.
26. ARA, Inc, ERES Concultans Division. Guide for Mechanistic-Empirical Design of New andRehabilitated Pavement Structures. Final Report. NCHRP, Project 1-37 A, Transportation Research Board of the National Academies, Washington. 2004.
27. СН РК 3.03-04-2014 Проектирование дорожных одежд нежесткого типа. Астана, 2014. 39 с.
28. Цитович Н.А. Механика мерзлых грунтов. Москва, 1973. 448 с.

Bagdat Teltayev,*
+7(701)760-67-01; bagdatbt@yahoo.com

Jiankun Liu,
+8613581986007; liujiank@mail.sysu.edu.cn

Suppes Elena,
+7(701)570-40-23; suppes08@mail.ru

Багдат Бурханбайулы Телтаев,*
+7(701)760-67-01;
эл. почта: bagdatbt@yahoo.com

Джианкун Лиу,
+8613581986007;
эл. почта:liujiank@mail.sysu.edu.cn

Елена Александровна Суппес,
+7(701)570-40-23;
эл.почта: suppes08@mail.ru

Teltayev, B.B., Liu, J., Suppes, E.A. Distribution of temperature, moisture, stress and strain in the highway. Magazine of Civil Engineering. 2018. 83(7). Pp. 102–113. doi: 10.18720/MCE.83.10.

doi: 10.18720/MCE.83.11

Implementation of pulse heat supply for dependent connection of customers

Обеспечение импульсного теплоснабжения для зависимого присоединения абонентов

A.N. Makeev,
Ogarev Mordovia State University, Saransk, Russia

Канд. техн. наук, докторант, доцент
А.Н. Макеев,
Мордовский государственный университет им. Н.П. Огарёва, г. Саранск, Россия

Key words: heat supply system; heat supply network; heat consumption system; heat supply station; shock unit; fluctuating circulation of heat-carrying agent; pulsing circulation of heat-carrying agent; available head transformation

Ключевые слова: система теплоснабжения; тепловая сеть; система теплопотребления; тепловой пункт; ударный узел; импульсная циркуляция теплоносителя; пульсирующая циркуляция теплоносителя; трансформация располагаемого напора

Abstract. This article deals with organization of pulsed and fluctuating circulation of heat-carrying agent in separate sections of heat supply system with dependent connection of customers. These types of oscillatory motion of the heat-carrying agent are proposed to be carried out in a self-sustained operation on the basis of the hydraulic ram operation principle. The relevance of the subject-matter is determined by the influence of oscillating flows on the intensity of heat exchange processes and by the possibility of using the circuit design of hydraulic ram in order to improve energy efficiency of heat supply systems. Analysis of the technical solution of a single-fluid hydraulic ram is carried out and conditions for ensuring its possible operation in a closed hydraulic circuit are determined. A sequential transition is shown for the use of this water-lifting device in the heat supply system with dependent connection of customers for organization of pulsed and fluctuating circulation of the heat-carrying agent in its separate sections. The research results form a unified view of technical realization method of the vibrational circulation of the heat-carrying agent in a self-sustained operation in separate sections of the heat supply system with dependent connection of heat consumption systems. Taking into account the achievement of intensification of heat exchange processes in these conditions, self-cleaning of heat exchange surfaces and possible strengthening of pressure in the heat consumption system only at the expense of the available pressure of the heat network, it is concluded that application of the circuit design of the hydraulic ram in the heat supply system can be used to increase its energy efficiency.

Аннотация. В статье рассматривается организация импульсной и пульсирующей циркуляции теплоносителя на отдельных участках системы теплоснабжения с зависимым присоединением абонентов. Указанные виды колебательного движения теплоносителя предлагается осуществлять в самоподдерживающемся режиме на основе принципа действия гидравлического тарана. Актуальность тематики обусловлена влиянием колеблющихся потоков на интенсивность теплообменных процессов, а также возможностью использования схемного решения гидравлического тарана применительно к повышению энергетической эффективности систем теплоснабжения. Выполнен анализ технического решения одножидкостного гидравлического тарана, определены условия для обеспечения его возможной работы в замкнутом гидравлическом контуре. Показан последовательный переход к использованию данного водоподъемного устройства в системе теплоснабжения с зависимым присоединением абонентов для организации импульсной и пульсирующей циркуляции теплоносителя на ее отдельных участках. Результаты исследования формируют единое представление о способе технической реализации колебательной циркуляции теплоносителя в самоподдерживающемся режиме на отдельных участках системы теплоснабжения с зависимым присоединением систем теплопотребления. С учетом достигаемых в этих условиях интенсификации теплообменных процессов, самоочищения теплопередающих поверхностей и возможного усиления напора в системе теплопотребления только за счет располагаемого напора тепловой сети, делается вывод о том, что применение схемного решения гидравлического тарана

Макеев А.Н. Обеспечение импульсного теплоснабжения для зависимого присоединения абонентов // Инженерно-строительный журнал. 2018. № 7(83). С. 114–125.

в системе теплоснабжения может быть использовано к повышению ее энергетической эффективности.

1. Introduction

Intensification of heat exchange is one of the priority directions of development and optimization of the design of any heat exchange equipment [1, 2]. Passive and active methods for improving heat exchange process are widely used and they were discovered and studied in various fields of science and technology [3, 4].

Taking into account this tendency research works in the study of the influence of oscillating flows on the intensity of the course of heat exchange processes [5, 6], both in individual heat and power devices [7, 8], and in entire systems based on them are actualized [9, 10].

Among such systems there is a heat supply system where along with the heat exchange intensification, the potential of the oscillating circulation of the heat-carrying agent can be used to redistribute the available head from one hydraulic circuit to another and also realize the self-cleaning effect of heat exchange surfaces from scale and sludge (slum) [11].

In the context of this article it is proposed to provide the oscillatory circulation of the heat-carrying agent in the heat supply system in a self-sustained operation according to the principle of single-fluid hydraulic ram action – with generation of pulsed and fluctuating circulation of liquids. Heat supply system with dependent connection of customers was chosen as the object for the indicated possibility realization.

The purpose of the scientific work is to realize the essence of organization of pulsed and fluctuating circulation of the heat-carrying agent in self-sustained operation in separate sections of heat supply system with dependent connection of customers due to the principle of single-fluid hydraulic ram operation.

Within the objectives to be achieved the following problems have been solved:

- analysis of peculiarities of single-fluid hydraulic ram operation in order to determine the conditions under which its operation in a closed hydraulic system is possible;
- finding a circuit solution for integrating the scheme of single-fluid hydraulic ram into a heat supply system with dependent connection of heat consumption systems;
- installation of a laboratory setup and conducting experimental studies to assess the stability of the proposed technical solution;
- protection of intellectual activity results obtained by solving above mentioned tasks by the patents of the Russian Federation for inventions and utility models;
- summing up the results of the scientific research.

2. Methods

The present work has its own scientific research containing explanation of theoretical data on the topic of effective use of technologies and tools for organizing pulsed motion of the heat-carrying agent in heat and water supply systems regarding to increase their energy conservation.

While carrying out this work the following scientific methods are used.

1. Analysis of a self-sustaining water-lifting device work based on a single-loop hydraulic ram (Figure 1), which made it possible to establish the pulse and fluctuating nature of the working medium flow in its individual sections. As a result of this analysis the conditions are also determined for ensuring the possible operation of a hydram water-lifting device in a closed hydraulic circuit with a pumping supply of working medium through its feed supply pipeline.

2. Synthesis of a technical solution that will ensure the operation of a water-lifting device based on a single-loop hydraulic ram in a closed hydraulic circuit with a pumped supply of working medium for creating pulsed and fluctuating circulation of liquid in certain sections of this circuit. The synthesized technical solution is presented in Figure 2. According to that scheme the development (Figure 3) and the installation (Figure 4) of the experimental setup for testing the adequacy of the theoretical positions obtained at the analysis and synthesis stage were made on the basis of a shock unit of an opposing construction [12].

3. A scientific experiment that ensures the reproduction of the hydraulic ram work in a closed hydraulic circuit with a pumping supply of the working medium in created and controlled conditions. The present work was carried out on the basis of the educational and scientific laboratory" Pulse heat and water

supply systems "of the Federal State Budgetary Educational Institution of Higher Education “Ogarev Mordovia State University" (Figure 4).

4. The measurement including a set of actions which are performed with the help of certain means to find the numerical value of the measured values. The volume consumption of the working medium by the shock unit was determined by the electromagnetic converter "Master Flow MF-5.2.2-B-15" which is installed at the output of the shock unit through the system of back-flow valves and rectifying hydraulic accumulators "Wester premium WAV-12" [13]. The pointing error of the flow converter is 0.05 %.

The volume consumption of the injected medium was determined by the method of draining the liquid into the measuring container at the outlet of the pressure regulator "Danfoss 003H6616 AVA" included in the injected line after the hydraulic accumulator "Dzhileks 24G " (Figure 3). The pointing error in this case is $\pm$ 0.05 %.

Pressure converters "OVEN PD100–DI1.6–171–0.5" with the output current of 4–20 mA were used to estimate the pressure changing quantity at individual points of the hydraulic circuit. These pressure transmitters are designed for a maximum pressure of 1.6 MPa and are made with a connecting male thread G1 / 2. The error in measuring this measuring equipment is $\pm$ 0.5 %.

The output signal from the converters was processed через блок токовых шунтов "Reallab! NL-8CS" with the help of the "L-Card" software and hardware complex on the basis of the analogous-digital module converter "E14-440". The limit of permissible error of measuring the dc (direct current) while using the analog-digital converter "E14-440" is $\pm$ 0.05 % in the range from 2.5 V to 10 V. The pointing error of the current shunt block (current signal converter to a voltage) "Reallab! NL-8CS" is $\pm$ 0.02 %.

Graphs of pressure pulsations in individual sections of the hydraulic circuit are shown in Figure 5 and obtained by exporting data from the hardware and software complex L-Card in Excel.

5. Statistical processing of the experimental data was carried out in the following sequence. The average value of the measured quantity was determined by the formula:

$$\overline{x} = \frac{\sum_{i=1}^{N} x_i}{N}, \quad (1)$$

where x_i – parameter value which was determined with a period of time 300 sec.

N – quantity of parameter changing, $N \geq 10$.

The mean square deviation was determined:

$$\sigma = \sqrt{\frac{\sum_{i=1}^{N} (\overline{x} - x_i)^2}{N}}. \quad (2)$$

Then the lower x_{low} upper x_{hight} of interval boundary 3σ were calculated:

$$x_{low} = \overline{x} - 3\sigma, \; x_{hight} = \overline{x} + 3\sigma. \quad (3)$$

The value of the measured parameter that overreach x_{low} or x_{hight} was dropped and the changes were repeated. The obtained numerical values of the results of the experiment are given in the text of this work below the Figure 5 when describing the obtained pressure pulsation graphs at individual points of the hydraulic circuit.

6. The analogy of the principle propagation of the action of the technical solution presented in Figure 2 and made it possible to obtain a fundamentally new scheme of the heat supply system with pulsed and fluctuating circulation of the heat-carrying agent at its separate sections (Figure 6), which can be used to increase the efficiency of heat supply systems taking into account the analysis of information sources reflected in the list of literature. According to the technical solution presented in Figure 6, from 28.05.2018 the application # 2018119526 "Heat supply system" for the invention of the Russian Federation was registered.

3. Results and Discussion

3.1. Analyses of peculiarities of the self-sustained water-lifting device on the basis of the single-liquid hydraulic ram

The use of hydraulic ram for the purposes of water supply to various customers is widely known in the world practice [14, 15]. Mass distribution of the water-lifting device is caused by simplicity and reliability of its design, as well as possibility of working in self-sustained operation over the years in the condition of automatic generation of periodic pressure shocks and subsequent use of their energy [16, 17].

Currently there is a number of technical solutions of this water-lifting device but all of them can be classified into two groups: for working with one liquid or with two unmixed liquids [18]. Within the topic of the article, the most interesting is the hydraulic ram, which works only with one liquid. According to Figure 1 let us consider the principle of its operation in details and analyze the character of the liquid circulation in its individual structural elements.

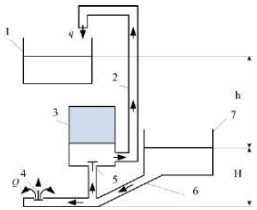

Figure 1. Hydraulic ram for working with one liquid: 1 – upper tank; 2 – discharge pipeline; 3 – air case; 4 – shock valve; 5 – discharge valve; 6 – feeding pipeline; 7 – feeding reservoir; h – water lifting height; H – water lifting height

First of all, there is selection of the weight of the impact valve 4 so that the static pressure in the feeding pipe 6 keeps it in the closed state and when the liquid flows through it so then it automatically closes. Then the shock valve 4 is put into operation by a single forced opening (manually or mechanically) and in the feed pipe 6, under the pressure action H, m a movement of water with an average consumption Q, m^3/s is generated and discharged through this valve. When the force of the flowing water balances the weight of the shock valve 4 it will close and a hydraulic shock will occur in the feed pipeline 6 [19, 20].

The positive wave of this hydraulic shock will open the back-flow valve 5, through which some water with average consumption q, m^3/s will flow into the air case 3. The liquid injection into the air case 3 will continue until the energy of the positive wave of hydraulic shock is sufficient to overcome the resistance of the compressed air which is located in it. Then, the injected medium will flow from the air case 3 into the upper tank 1 through the injection pipeline 2 overcoming the water head $h > H$.

After the positive wave of the hydraulic shock is reflected from the input to the feeding pipeline 6 it will be replaced by a negative wave. As a result of this, the pressure in the feeding pipeline 6 below the shock valve 4 becomes less than the static pressure. At this moment the back-flow valve 5 closes and the shock valve 4 opens under its own weight. Later on it will ensure the renovation of water supply through the feeding pipeline 6 and repetition of the operation cycle in the sequence which is described above.

According to the theory of hydraulic ram which is practically confirmed by the results of experimental studies, the work stability of a shock unit in a self-supported regime is ensured by stable parameters of maintained hydraulic system. The most important of these parameters are the stable damping properties of the air cap, the feed supply head and the feed rate of the working medium for the operation of the shock unit and also the height of the liquid injection. At the same time, the influence of the shock unit and pressure increase amplitude at the moment of hydraulic shock is determined by the length and diameter of the feeding pipeline. The diameter and length of the discharge pipeline and also its resistance determines the productivity of the water-lifting device [18].

With periodic complete stoppage of moving water flow in the feeding pipeline 6 and the subsequent renovation of its movement fluctuating circulation of liquid is provided. It is characterized by the change in the velocity of water from 0 to a certain maximum at which the shock valve automatically closes.

Fluctuating circulation of liquid is observed in the discharge pipeline 2. It is characterized by the change in the rate of its outflow from minimum to maximum relating to a certain average value which is the result of smoothing the pulses of pressure increase and accumulation of their energy in the air case 3.

Productivity of the hydraulic ram q, m³/s (see Figure 1) can be determined by the formula [18]

$$q = \eta Q \frac{H}{h}, \quad (4)$$

where η – coefficient of water-lifting installation performance [18];

Q – liquid consumption through the shock valve, m³/s;

H – feeding head, m;

h – injected head, m.

The lower value of the heads ratio is associated with the threshold of the hydraulic ram stability. According to the condition of ensuring of automatic work it is assumed to be equal $h/H = 1$. In this case the coefficient of performance can reach the value $\eta = 0.45$–0.5, and the discharge flow will be up to $q = 0.5Q$

The upper value of the heads ratio is associated with decrease in the coefficient of performance of the water-lifting device. For example, with the heads ratio $h/H = 30$, the efficiency is varied in the range of $\eta = 0.15 \div 0.20$. It means that the discharge flow will be only $q = 0.005 \div 0.006Q$ [18].

The change in the ratio of the hydraulic ram performance q to the consumption of liquid Q which is thrown through the shock valve depending on the ratio of the injected h and feeding H head, with the average value of the coefficient performance of the water-lifting device is given in Table 1.

Table 1. Hydrotended water-lifting installation productivity

q/Q	0.225	0.1125	0.075	0.0563	0.045	0.0375	0.0321	0.0281	0.025	0.0225
h/H	2	4	6	8	10	12	14	16	18	20

3.2. Technical solution for ensuring operation of a single-fluid hydraulic ram in a hydraulic system with pumping water supply

The scheme of the hydraulic ram which is discussed above assumes its use only in open water storages and it is not entirely suitable for the use in the heat supply system where the heat-carrying agent is supplied by an electric pump. It is explained by the following circumstances. Firstly, for operation of the shock valve it is necessary to have a drain of the working medium (liquid) from the hydraulic ram's feeding pipeline into the environment medium below the geometric level of its entry. For the heat-carrying agent in a closed heat supply system the fulfillment of this condition is not rational. Secondly, to ensure the automatic operation of the shock unit, the open feeding basin and / or equalizing tower needs to be available [18], by which the required length of the feeding pipeline is ensured. Otherwise, the stable operation of the shock valve is not guaranteed as duration and alternation of the phases of the hydraulic shock can be disrupted. Thirdly, it is necessary to periodically inflate air to the air case which dissolves in liquid as the water-lifting unit is in operation [18]. The latter circumstance will only promote corrosion of pipelines and heat-and-power devices of the heat supply system.

Taking into account the revealed features of the self-support water-lifting installation based on the hydraulic ram, we replace the shock valve by a special shock unit, the design of which is adapted to working with pumping water supply. We also limit the working length of the supply pipeline by one hydraulic accumulator, and we will use an additional hydraulic accumulator as an air case (to eliminate air dissolving). As a result, we obtain the scheme of a hydrodynamic water-lifting device based on a single-fluid hydraulic ram for its joint operation with an electric pump in a closed hydraulic system (Figure 2).

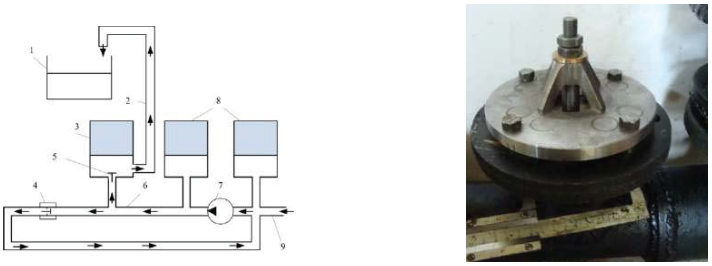

a b

Figure 2. Hydrodynamic water-lifting device on the basis of a single-fluid hydraulic ram for working in conditions of pumping water supply: a – schematic diagram; b – version of the shock valve with possibility of its installation in the inter-flange connection of a pipeline: 1 – upper tank; 2 – discharged pipeline; 3 – hydraulic accumulator; 4 – shock unit; 5 – discharged valve; 6 – feeding pipeline; 7 – circulating pump; 8 – additional hydraulic accumulators; 9 – makeup (intake) pipeline

The scheme of the presented technical solution works in the following way. Firstly, the feeding pipeline 6 which is made in the form of a closed hydraulic circuit is filled with the working medium until the air is completely removed from it. Then the pump 7 installed on the feeding pipeline 6 is put into operation. Thus, the working medium moves in the feeding pipeline 6 in a closed contour.

In case of gained velocity of the working medium loss through the shock unit 4, which is installed on the feed pipeline 6 after the pump 7 it will close. In front of the shock unit 4, a positive wave of hydraulic shock will arise that will spread to the pump output 7 while supplying the working medium through the discharge valve 5 to the hydraulic accumulator 3 and from there to the discharge pipeline 2 and the upper tank 1.

Considering that additional hydraulic accumulators 8 are installed at the input and output of the pump 7, its operation with a closed contour of the feeding pipeline 6 will be closed and will remain practically unchanged during the time of this closure, and a positive wave of hydraulic shock which is reflected from the hydraulic accumulator 8, at the output of the pump, will change the sign to negative and will head to the shock unit 4. As the result of the pressure drop before the shock unit 4, the valve will open under its own weight. The movement of the working medium in the feeding pipeline 6 in a closed contour will be renovated under the influence of the displaced air of the volume of liquid which is stored in the hydraulic accumulator 8 which is installed at the output of the pump 7, and also under the action of the pressure being created by the pump 7. Moreover, a new portion of the working fluid (liquid) equivalent to the volume displaced into the hydraulic accumulator 3 will flow through the make-up (suction) pipeline 9 to the feeding line 6. With the subsequent closure of the shock valve 4, the operation of the water-lifting device using the energy of the hydraulic shock will be repeated in the sequence which is described above and will be cyclically repeated until the circulation of the working medium due to the pump is present 7.

It should be noted that in the feeding pipeline with the installed shock unit 4 the heat-carrying agent will move impulsively with generation of pulses of the amount of its movement, and the fluctuating character of its movement will dominate in the discharge pipeline 2 due to the smoothing of the pulses by the hydraulic accumulator 3. Thus, organization of pulse circulation of the working medium is primary in relation to its fluctuating circulation.

The scheme of the experimental setup was developed for practical confirmation of the above operation theory of a water-lifting device based on a hydraulic ram with pumping supply of working medium through its supply pipeline which is shown in Figure 3. The experimental installation is a hydraulic circuit on the basis of a single-fluid hydraulic ram with pumping supply of working medium (water) through its supply pipeline and made of metal pipes with a diameter of 45 mm and wall thickness 2 mm with polypropylene "PP-R" pipes G 1/2, G 3/4 , G 1 and G 2. The length of the pipes L is indicated in mm. The length of each undefined area is less than 50 mm. Such short sections of pipes are used for connection of the separate elements of the hydraulic circuit to each other.

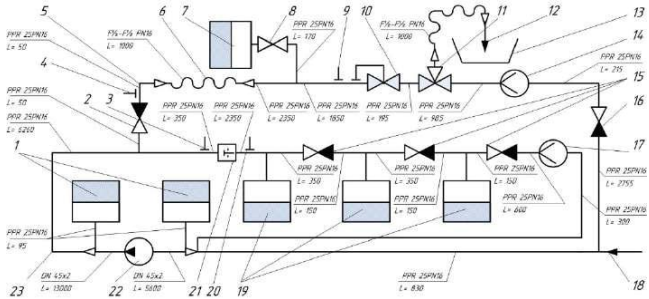

Figure 3. The scheme (schematic drawing) of the experimental setup: 1 – hydraulic accumulators for stabilizing the work of the pump; 2 – a non-return valve of the injected medium in the hydraulic accumulator of the injected medium; 3 – pressure transducer at the entrance of the shock unit; 4 – pressure transducer at the inlet of the hydraulic accumulator of the injected medium; 5 – section PP-R of the pipeline with fluctuating circulation of the injected medium; 6 – flexible pipeline of fluctuating circulation of the working medium; 7 – hydraulic accumulator of the injected medium; 8 – tap for disconnecting the hydraulic accumulator of the injected medium; 9 – pressure transducer at the outlet of the injected medium from the hydraulic accumulator; 10 – pressure regulator; 11 – a tap of a switching of a flow direction of the injected medium; 12 – discharge of the injected medium through a flexible pipeline; 13 – metering capacity; 14 – mechanical water meter; 15 – check valves of the rectifying system of an oscillations of the working medium flow consumption; 16 – a non-return valve at the inlet of the injected medium to the suction pipeline of the pump; 17 – electromagnetic flow transducer; 18 – feeding pipeline of the hydraulic circuit; 19 – hydraulic accumulators of the rectifying system of an oscillations of the working medium flow consumption; 20 – pressure transducer at the output of the shock unit; 21 – shock unit; 22 – the pump; 23 – feeding pipeline of a shock unit

This experimental setup works as follows. The pump 22 circulates the working medium along the closed hydraulic circuit through the feed pipeline 23, the shock unit 21, check valves 15 which are connected in series through the rectifying hydraulic accumulators 19 and the electromagnetic flow transducer 17. From there the pump 22 supplies the working medium through the feed pipeline 23 to the shock unit 21, which automatically closes at a certain flowrate of the working medium through it, and then it opens after generation of a hydraulic shock. A hydraulic shock occurs at the moment of the shock unit 21, the positive propagation wave which ensures that the injected medium is supplied through the inlet check valve 2 to the PP-R section of the pipeline with the pressure transducer 4, and then by the flexible line 6 through the tap 8 into the hydraulic accumulator 7. Then the injected medium is discharged through the pressure regulator 10 through the flexible pipeline 12 to the metering tank 13 for measurement the pumping amount of liquid or through the PP-R pipeline section to the pump inlet 22 through the indicating mechanical water meter 14 and the non-return valve 16. The direction of flow of the pumped medium is established by the flow switching tap 11. The hydraulic accumulators 1 which are installed at the pump inlet and outlet serve to protect the pump 22 against the hydraulic shock, the residual wave of that pump can propagate to it within an incomplete use of the hydraulic shock energy. The pressure pulsations at the individual points of the hydraulic circuit are measured with the help of flow converters 3, 4, 9, 20.

The volume consumption of the working medium was provided by the pump "K 80-50-200A" with the asynchronous motor " AIR 132M2Y2" with the power of 11 kWt. The change in pump capacity as well as frequency and amplitude of generation of local hydraulic hammers in the shock unit was carried out by the frequency converter "OVEN PCHV-2".

According to the scheme presented in Figure 3, in the educational and research laboratory "Pulse heat and water supply systems" of the Federal State Financed Academic Institution of Higher Education "Ogarev Mordovia State University" the experimental setup was assembled. Its fragment with a shock valve, back flow valve and a hydraulic accumulator connected to the discharge line is shown in Figure 4.

Evaluation of the operational capacity of this experimental setup is shown in Figure 5, where the graphs of the pressure variation in its individual sections are given.

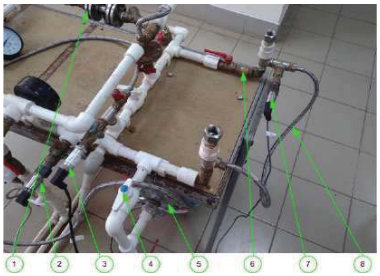

Figure 4. Appearance of a part of the experimental setup: 1 – shock unit; 2 – pressure transformer at the output of the hydraulic accumulator; 3 – pressure transformer at the input of the shock unit; 4 – handle for disconnecting the hydraulic accumulator; 5 – hydraulic accumulator; 6 – back-flow valve for injecting the medium into the hydraulic accumulator; 7 – pressure transformer at the input of the hydraulic accumulator; 8 – the line of fluctuating circulation of the injected medium

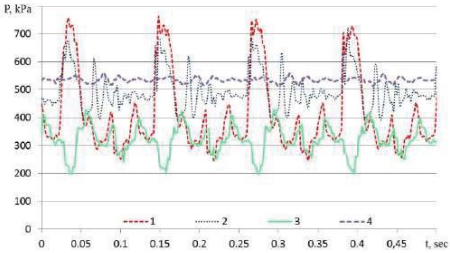

Figure 5. Graphs of pressure fluctuations: 1 – at the input of the shock unit; 2 – input of the injected medium into the hydraulic accumulator; 3 – behind the shock unit; 4 – output of the injected medium from the hydraulic accumulator

As it is seen from presented figure, the system works steadily in automatic mode with the shock valve's flow frequency of 8.74 Hz. Conditions under which these dependences are obtained are the following: the available head at the shock unit 118 kPa; discharge height provided by the pressure regulator, 512 kPa; volume consumption of the working medium through the shock valve 3.475 litter/minute; discharge consumption is 0.517 litter/minute.

Thus, with the ratio of injection and feeding heads h / H = 4.340, the ratio of injection and feeding discharges is $q / Q = 0.149$. These indicators are complying with the theoretical data of Table 1 with the coefficient of performance of the water-lifting installation $\eta = 0.65$.

We can see from Figure 5 that when the shock valve closes on the pipeline section a positive wave of hydraulic shock of the working medium appears in the front of it (the pressure increases above the value 750 kPa) and behind the shock valve there is a negative wave (the pressure drops below the value 200 kPa). A positive wave of propagation of the hydraulic shock ensures that the working medium is displaced into the hydraulic accumulator at the maximum pressure in the pulse about 670 kPa. The magnitude of this pressure cutoff is provided by damping the pulse by compressed air in the hydraulic accumulator (Figure 3). From the hydraulic accumulator, the liquid enters the discharge line and leaves it, overcoming the resistance in 512 kPa, created by the pressure regulator.

The results of the experiment which presented in Figure 5 allows to visually ascertain that the oscillatory processes occurring on separate sections of the hydraulic circuit are characterized by relatively good repeatability while maintaining a constant oscillation frequency generated by the shock unit in a self-sustaining mode. This fact shows the restoration of the initial parameters of the hydraulic system every time after a local hydraulic shock created by the shock unit. In this case the stability of the system in a self-sustaining pulse mode is determined by the stability of the inlet parameters (feeding head and the feed flowrate of the working medium) and outlet parameters (lift height and consumption of the injected medium).

The generation of pressure oscillations and their propagation in the hydraulic circuit raises the question of possible resonance. An investigation of this effect is possible with a change in the frequency of generation of the pulses of the momentum (movement quantity) of the working medium, which in the conditions of using a self-supported shock unit depends on the working medium consumption. However, the flow rate of the working medium also determines the amount of pressure increase at the hydraulic shock moment. The higher the flowrate of the working medium, the higher the frequency of generation of the pulses of pressure increase and their amplitude and also the other way around. For instance, for the water, a change in its speed per each 1 m/sec leads to an increase in pressure by 100 m [18]. Under the

conditions of such proportional dependence of the pulse generation frequency, the flow rate of the working medium and the magnitude of the resonance pressure increase are not observed in practice.

As for the beats, the occurrence is possible in a result of superposition of oscillations; theoretically they occur at the point of the hydraulic circuit where the pulsating and fluctuating flows are merging (Figure 3). However, taking into account the fact that the impulse component and the fluctuating component of the vibrational motion are smoothed and scattered as they move away from the source of the disturbance (shock unit) on the way to the point of confluence, including hydraulic accumulators which are installed in the system, then directly at the point of combining these flows the beating effect does not occur. For eliminating this effect, when connecting two oscillating streams an additional hydraulic accumulator should be used at the point of their merging.

The graphs of the pressure pulsations shown in Figure 5 make it possible to visually establish the characteristics difference between pulsed and fluctuating liquids flow in pipelines. Fluctuating circulation (graphs 1 and 3) is characterized by an instant increase of the working medium pressure before the closed shock unit and the creation of conditions for its cavitation behind it (graph 2). Fluctuating circulation (graph 4) of the injected fluid by the character of the pressure pulsations is more smoothed and, with some assumptions, closer to the shape of a sinusoid.

Taking into account the practical evaluation of the efficiency of the above scheme, it can be confirmed that application of the circuit solution of a single-fluid hydraulic ram in a heat supply system with dependent connection of customers will allow possibility of pulsed and fluctuating circulation of the liquid in certain areas.

3.3. Heat supply system for independent connection of customers with pulsed and fluctuating circulation of the heat-carrying agent

Based on the scheme of a single-fluid hydraulic ram operation in a pumping water supply system we obtain a schematic diagram of the heat supply system for dependent connection of customers with pulse and fluctuating moving of the heat-carrying agent in its separate elements. For doing this operation, we use the example of the scheme shown in Figure 2, the discharge pipeline 2 is connected to the make-up pipeline 9 and we install heating devices on the sections of the supply and discharge pipelines. As a result, the hydraulic system will be completely closed and can be successfully used for the purposes of heat supply with connection of customers according to the dependent scheme (Figure 6).

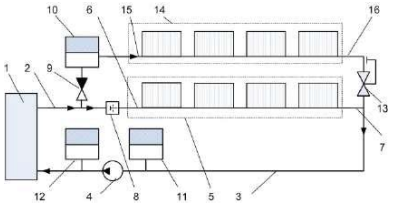

Figure 6. Heat supply system with pulsed and fluctuating circulation of the heat-carrying agent for the dependent scheme of heat consumption systems connection: 1 – heat source; 2 and 3 – supply and back-flow pipelines of the heating network; 4 – the network pump; 5 – heat consumption system with supply 6 and back-flow 7 pipelines for organization of fluctuating circulation of the heat-carrying agent; 8 – shock unit; 9 – back-flow valve; 10, 11, 12 – hydraulic accumulators; 13 – pressure regulator; 14 – thermal load with supply 15 and back-flow 16 pipelines for organization of fluctuating circulation of heat-carrying agent

The circuit which is shown in Figure 5 works in the following way. At first it is filled with a heat-carrying agent until the air is completely removed from it. The pressure regulator 13 is configured to maintain a larger pressure in the zone of the additional heat load 14 than the available head in the heat network generated by the network pump 4. Then, the heat-carrying agent is heated in the heat source 1 and its circulation through the supply pipeline 2 and return 3 pipelines of the heat network with the help of the network pump 4 is carried out. Under the conditions of different hydraulic resistance of the heat-carrying agent escaping in the heat consumption system 5 and the additional zone of heat load 14, heated the heat-carrying agent in the source 1 with the open cross-section of the shock unit 8 will flow only to the heat consumption system 5 through its supply line 6. So after giving the stored heat the heat-carrying agent leaves the heat consumption system 5 through the return line 7 and rushes into the return pipeline of the heat network 3 to the input of the network pump 4, and from there will again arrive to the source of heat.

Макеев А.Н. Обеспечение импульсного теплоснабжения для зависимого присоединения абонентов // Инженерно-строительный журнал. 2018. № 7(83). С. 114–125.

At some point in time the shock valve 8 which is tuned to a certain flow velocity of the heat-carrying agent will automatically close, so in such case it provokes appearance of a hydraulic shock in the pipeline of the heat network. The positive wave of this hydraulic shock will begin to supply the heated heat-carrying agent through the back-flow valve 9, the first hydraulic accumulator 10 to the additional zone of the heat load 14 along its supply line 15. So after giving the stored heat the heat-carrying agent leaves the heat load zone 14 through the return pipeline 16 and passing through the pressure regulator 13 will enter the return pipeline of the heat network 3.

At the same time a positive wave of hydraulic shock, reflected from the second 11 and the third 12 hydraulic accumulators will be replaced by a negative one. In such case the passage section of the shock unit 8 opens to expire the heated heat-carrying agent into the supply pipeline 6 of the heat consumption system 5, and the back-flow valve 9 closes, as a result the flow of the heated heat-carrying agent from the heat source 1 to the first hydraulic accumulator 10 will be stopped. The proportional distribution of the heat-carrying agent flow in the main 5 and additional 14 zones of the heat load will be determined on the basis of the calculated equation (1) for determining the productivity of a single-fluid hydraulic ram.

With the subsequent closing of the flow section of the shock unit 8 the operation of the heat supply system will be repeated in the sequence which is described above. At the same time the fluctuating circulation of the heat-carrying agent will be observed in the heat consumption system 5 which is characterized by a change in the velocity of the heat-carrying agent from zero to the set maximum. In the additional heat load zone 14 circulation of the heat-carrying agent will be fluctuating, which is characterized by a change in the circulation speed from minimum to maximum while saving its average value of more than zero by smoothing the pulse speed by the first hydraulic accumulator 10.

Pulse and fluctuating circulation of the heat-carrying agent can be used for the purpose of heat exchange intensifying [21] and realization of self-cleaning effect of scale [22] in various elements of the heat supply system.

In order to optimize the structural elements and links of the heat supply system, organization of pulsed and fluctuating circulation of the heat-carrying agent can be realized only within the heat point for connecting of customers according to the dependent scheme [23]. At the same time it is recommended to use technical solutions of heat exchanging devices with an oscillating heat exchange surface [24] from the usage of the pulse movement quantity of the heat-carrying agent for reducing the metal consumption and mass-dimension parameters of heat-consumption systems. When designing such systems, it is also necessary to take into account the increase in standard losses of thermal energy in heat networks [25] and heat consumption systems [26].

4. Conclusion

Investigating the principle of a single-fluid hydraulic ram operation we can conclude that its action is accompanied by differentiation of the steady flow movement into pulsed and fluctuating. In such case, the pulsed circulation of the liquid is primary in relation to the fluctuating circulation, which is provided by the air case due to smoothing of the pressure peaks of the hydraulic shock.

This self-sustaining water-lifting device initially used only for water supply purposes can be used with a closed-countour hydraulic system with a pumping supply of the working medium to organize its pulsed and fluctuating circulation in certain sections of the system. For that operation it is necessary to use special designs of shock units and hydraulic accumulators instead of the air case and the equalizing tower.

In the conditions of integration of the single-fluid hydraulic ram circuit solution into the heat supply system for dependent connection of customers the following become available:

– possibility of creating a pulsed circulation of the heat-carrying agent on the source of heat and in the heat network in a self-sustained regime;

– possibility of using the impulse movement quantity of the heat-carrying agent in the heat network in relation to the increase the available pressure of the heat consumption systems which are connected to it by the dependent scheme;

– possibility of organizing the fluctuating circulation of the heat-carrying agent in a heat consumption system.

5. Acknowledgement

The present article is prepared within the President of the Russian Federation Grant for the purpose of government support of Young Russian Researches, the Candidates of Science MK-1408.2018.8. Agreement on the provision of subsidies # 075-02-2018-408.

References

1. Butun, H., Kantor, I., Marechal, F. A heat integration method with multiple heat exchange interfaces. ENERGY: 30th International Conference on Efficiency, Cost, Optimisation, Simulation and Environmental Impact of Energy Systems (ECOS). 2018. Vol. 152. Pp. 476–488.
2. Zhang, Y., Zhang, YP., Wang, X. Thermodynamic optimization of coupled heat work conversion and heat transfer energy systems by applying inverse problem and variation method. Heat transfer research. 2017. Vol. 48. No. 18. Pp. 1637–1649.
3. Laukkanen, T., Seppala, A. Interplant heat exchanger network synthesis using nanofluids for interplant heat exchange. Applied thermal engineering. 2018. Vol. 135. Pp. 133–144.
4. Mohammadshahi, S., Nili-Ahmadabadi, M., Samsam-Khayani, H., Salimpour, M.R. Numerical study of a vortex-induced vibration technique for passive heat transfer enhancement in internal turbulent flow. European Journal of Mechanics, B/Fluids. 2018. Vol. 72. Pp. 103–113.
5. Abdel-Aziz, M.H., Nirdosh, I., Sedahmed, G.H. Mass and heat transfer behavior of oscillating helical coils in relation to heterogeneous reactor design. Aiche journal. 2017. Vol. 63. No. 7. Pp. 3141–3149.
6. Valueva, E.P., Purdin, M.S. Heat exchange at laminar flow in rectangular channels // Thermo-physics and aeromechanics. 2016. Vol. 23. No. 6. Pp. 857–867.
7. Olayiwola, B.O., Schaldach, G., Walzel, P. CFD simulations of flow and heat transfer in a zigzag channel with flow pulsation. ASME 2010 International Mechanical Engineering Congress and Exposition, IMECE 2010. Vancouver, Canada. 2010. Vol. 7. No. PARTS A and B. Pp. 1531–1541.
8. Sultan, Q., Lalizel, G., Fenot, M., Dorignac, E. Influence of coolant jet pulsation on the convective film cooling of an adiabatic wall. Journal of Heat Transfer. 2017. Vol. 139. No. 2. UNSP 2556160.
9. Levtzev, A.P., Makeev, A.N., Kudashev, S.F Pulsating heat transfer enhancement in the liquid cooling system of power semiconductor converter. Indian Journal of Science and Technology. 2016. Vol. 9(11). Pp. 1–5.
10. Sedighi, E., Amarloo, A., Shafii, B. Numerical and experimental investigation of flat-plate pulsating heat pipes with extra branches in the evaporator section. International Journal of Heat and Mass Transfer. 2018. Vol. 126. Pp. 431–441.
11. Makeyev, A.N. Vybor skhemy tekhnologicheskogo prisoyedineniya abonentov k teplovoy seti v usloviyakh perekhoda k impulsnoy tsirkulyatsii teplonositelya v oborudovanii teplovykh punktov [The choice of the technological connection of subscribers to the heat network in the transition to a pulsed circulation of the coolant in the equipment of heat points]. Vestnik Dagestanskogo gosudarstvennogo tekhnicheskogo universiteta. Tekhnicheskiye nauki. 2017. № 3(44). Pp. 72–82. (rus)
12. Levtsev, A.P., Makeev, A.N., Makeyev, S.N., Khramov, S.I., Kudashev, S.F., Zyuzin, A.M., Narvatov, Ya.A. Udarnyy uzel [Shock knot]: pat. 2558740, № 2014107201/06 ; zayavl. 25.02.2014 ; opubl. 10.08.2015. Byul. No. 22. 6 p. (rus)
13. Makeev, A.N. K voprosu lokalnoy organizatsii impulsno-koleblyushcheysya tsirkulyatsii teplonositelya v sisteme teplosnabzheniya [To the question of the local organization of the pulse-vibration circulation of the heat-supplyer in the heat supply system]. Byulleten nauki i praktiki. 2018. Vol. 4(5). Pp. 254-262. (rus)
14. Harith, M.N., Bakar, R.A., Ramasamy, D., Quanjin, M. A significant effect on flow analysis & simu-lation study of improve design hydraulic pump. IOP Conference Series:

Литература

1. Butun H., Kantor I., Marechal F. A heat integration method with multiple heat exchange interfaces // ENERGY: 30th International Conference on Efficiency, Cost, Optimisation, Simulation and Environmental Impact of Energy Systems (ECOS). 2018. Vol. 152. Pp. 476–488.
2. Zhang Y., Zhang Y.P., Wang X. Thermodynamic optimization of coupled heat work conversion and heat transfer energy systems by applying inverse problem and variation method // Heat transfer research. 2017. Vol. 48. № 18. Pp. 1637–1649.
3. Laukkanen T., Seppala A. Interplant heat exchanger network synthesis using nanofluids for interplant heat exchange // Applied thermal engineering. 2018. Vol. 135. Pp. 133–144.
4. Mohammadshahi S., Nili-Ahmadabadi M., Samsam-Khayani H., Salimpour M.R. Numerical study of a vortex-induced vibration technique for passive heat transfer enhancement in internal turbulent flow // European Journal of Mechanics, B/Fluids. 2018. Vol. 72. Pp. 103–113.
5. Abdel-Aziz M.H., Nirdosh I., Sedahmed G.H. Mass and heat transfer behavior of oscillating heli-cal coils in relation to heterogeneous reactor design // Aiche journal. 2017. Vol. 63. № 7. Pp. 3141–3149.
6. Valueva E.P., Purdin M.S. Heat exchange at laminar flow in rectangular channels // Thermo-physics and aeromechanics. 2016. Vol. 23. № 6. Pp. 857–867.
7. Olayiwola B.O., Schaldach G., Walzel P. CFD simulations of flow and heat transfer in a zigzag channel with flow pulsation // ASME 2010 International Mechanical Engineering Congress and Exposition, IMECE 2010. Vancouver, Canada. 2010. Vol. 7. № PARTS A and B. Pp. 1531–1541.
8. Sultan Q., Lalizel G., Fenot M., Dorignac E. Influence of coolant jet pulsation on the convective film cooling of an adiabatic wall // Journal of Heat Transfer. 2017. Vol. 139. № 2. UNSP 2556160.
9. Levtzev A. P., Makeev A. N., Kudashev S. F Pulsating heat transfer enhancement in the liquid cooling system of power semiconductor converter // Indian Journal of Science and Technology. 2016. Vol. 9(11). Pp. 1–5.
10. Sedighi E., Amarloo A., Shafii B. Numerical and experimental investigation of flat-plate pulsating heat pipes with extra branches in the evaporator section // International Journal of Heat and Mass Transfer. 2018. Vol. 126. Pp. 431–441.
11. Макеев А.Н. Выбор схемы технологического присоединения абонентов к тепловой сети в условиях перехода к импульсной циркуляции теплоносителя в оборудовании тепловых пунктов // Вестник Дагестанского государственного технического университета. Технические науки. 2017. № 3(44). С. 72–82.
12. Левцев А.П., Макеев А.Н., Макеев С.Н., Храмов С.И., Кудашев С.Ф., Зюзин А.М., Нарватов Я.А. Ударный узел: пат. 2558740 Российская Федерация, № 2014107201/06 ; заявл. 25.02.2014 ; опубл. 10.08.2015, Бюл. № 22. 6 с.
13. Макеев А.Н. К вопросу локальной организации импульсно-колеблющейся циркуляции теплоносителя в системе теплоснабжения // Бюллетень науки и практики. 2018. Т. 4. № 5. С. 254–262.
14. Harith M.N., Bakar R.A., Ramasamy D., Quanjin M. A significant effect on flow analysis & simu-lation study of improve design hydraulic pump // IOP Conference Series: Materials Science and Engineering. 2017. Vol. 257. № 1. UNSP 012076.
15. Hussin N.S.M., Gamil S.A., Amin N.A.M., Safar M.J.A., Majid M.S.A., Kazim M.N.F.M., Nasir N.F.M. Design and analysis of hydraulic ram water pumping system //

Макеев А.Н. Обеспечение импульсного теплоснабжения для зависимого присоединения абонентов // Инженерно-строительный журнал. 2018. № 7(83). С. 114–125.

Materials Science and Engineering. 2017. Vol. 257. No. 1. UNSP 012076.

15. Hussin, N.S.M., Gamil, S.A., Amin, N.A.M., Safar, M.J.A., Majid, M.S.A., Kazim, M.N.F.M., Nasir, N.F.M. Design and analysis of hydraulic ram water pumping system. International conference on appli-cations and design in mechanical engineering (ICADME 2017). Journal of Physics Conference Series. 2017. Vol. 908. UNSP 012052.
16. Inthachot, M., Saehaeng, S., Max, J.F.J., Muller, J., Spreer, W. Hydraulic ram pumps for irrigation in Northern Thailand. 1st international conference on Asian highland natural resources management (asiahi-land) and 2nd idrc-searca upland fellowship and conference. 2015. Vol. 5. Pp. 107–114.
17. Lee, S.H., Yoon, H., Kim, D.H., Shin, E., Kim, Y., Ko, K.S., Ha, K. Evaluation of Field Feasibility and Efficiency of Hydraulic Ram Pump. Economic and environmental geology. 2016. Vol. 49. No. 3. Pp. 243–248.
18. Ovsepyan, V.M. Gidravlicheskiy taran i tarannyye ustanovki [The hydraulic RAM and RAM setup]. Moscow: Mashinostroyeniye, 1968. 124 p. (rus)
19. Ahn, B., Ismailov, M., Heister, S. Experimental Study Swirl Injector Dynamic Response Using a Hydromechanical Pulsator. Journal of Propulsion and Power. 2012. Vol. 28, No. 3. Pp. 585–595.
20. Xie, H.B., Chen, J., Liu, F., Liu, Z.B., Yang, H.Y., Lin, S.Y., Zhang, J. Analysis and Optimization of Pressure Shock and Cylinder Stroke Deviation in Open Circuit Hydraulic System of Concrete Pump. Journal of the Chinese society of mechanical engineers. 2018. Vol. 39. No. 2. Pp. 153–161.
21. del Rio, J. A., Lopez de Haro, M., Castillo-Romero, E.S. A plausible approach to heat transfer enhancement: non-Fourier heat transfer in fluids under oscillating conditions. Journal of physics communica-tions. 2018. Vol. 2. No. 5. UNSP 055006.
22. Nussupbekov, B.R, Khassenov, A.K., Karabekova, D.Z., Stoev, M., Beysenbek, A.Z., Kazankap, B.I. New technology for the recovery of heat exchangers. Bulletin of the university of karaganda-physics. 2017. Vol. 1. No. 85. Pp. 67–72.
23. Makeev, A.N. Teplovyye punkty sistem teplosnabzheniya s impulsnoy tsirkulyatsiyey teplonositelya [Substations of district heating systems with pulse coolant circulation]. Vestnik Dagestanskogo gosudarstvennogo tekhnicheskogo universiteta. Tekhnicheskiye nauki. 2017. No. 1(44). Pp. 26–47. (rus)
24. Samana, T., Kiatsiriroat, T., Nuntaphan, A. Air-side performance analysis of a wire-on-tube heat exchanger with an oscillating heat pipe as an extended surface under natural convection conditions. Heat transfer engineering. 2012. Vol. 33. No. 12. Pp. 1033–1039.
25. Akhmetova, I., Chichirova, N., Derevianko, O. Revisiting heat losses calculation at district heating network. International Journal of Civil Engineering and Technology. 2017. Vol. 8. No. 12. Pp. 694–702.
26. Gorshkov, A., Murgul, V. Calculation of Heat Energy Consumption by a Typical Historical Building with a Courtyard. Advances in Intelligent Systems and Computing: 9th International scientific conference Energy Management of Municipal Transportation Facilities and Transport, EMMFT 2017. Khabarovsk; Russian Federation. 2018. Vol. 692. Pp. 577–591.

International conference on appli-cations and design in mechanical engineering (ICADME 2017). Journal of Physics Conference Series. 2017. Vol. 908. UNSP 012052.

16. Inthachot M., Saehaeng S., Max J.F.J., Muller J., Spreer W. Hydraulic ram pumps for irrigation in Northern Thailand // 1st international conference on Asian highland natural resources management (asiahi-land) and 2nd idrc-searca upland fellowship and conference. 2015. Vol. 5. Pp. 107–114.
17. Lee S.H., Yoon H., Kim D.H., Shin E., Kim Y., Ko K.S., Ha K. Evaluation of Field Feasibility and Efficiency of Hydraulic Ram Pump // Economic and environmental geology. 2016 JUN. Vol. 49. № 3. Pp. 243–248.
18. Овсепян В.М. Гидравлический таран и таранные установки. М.: Машиностроение, 1968. 124 с.
19. Ahn B., Ismailov M., Heister S. Experimental Study Swirl Injector Dynamic Response Using a Hydromechanical Pulsator // Journal of Propulsion and Power. 2012. Vol. 28. № 3. Pp. 585–595.
20. Xie H.B., Chen J., Liu F., Liu Z.B., Yang H.Y., Lin S.Y., Zhang J. Analysis and Optimization of Pressure Shock and Cylinder Stroke Deviation in Open Circuit Hydraulic System of Concrete Pump // Journal of the Chinese society of mechanical engineers. 2018. Vol. 39. № 2. Pp. 153–161.
21. del Rio J. A., Lopez de Haro M., Castillo-Romero E.S.A plausible approach to heat transfer enhancement: non-Fourier heat transfer in fluids under oscillating conditions // Journal of physics communica-tions. 2018. Vol. 2. № 5. UNSP 055006.
22. Nussupbekov B.R, Khassenov A.K., Karabekova D.Z., Stoev M., Beysenbek A.Z., Kazankap B.I. New technology for the recovery of heat exchangers // Bulletin of the university of karaganda-physics. 2017. Vol. 1. № 85. Pp. 67–72.
23. Макеев А.Н. Тепловые пункты систем теплоснабжения с импульсной циркуляцией теплоносителя // Вестник Дагестанского государственного технического университета. Технические науки. 2017. № 1(44). С. 26–47.
24. Samana T., Kiatsiriroat T., Nuntaphan A. Air-side performance analysis of a wire-on-tube heat exchanger with an oscillating heat pipe as an extended surface under natural convection conditions // Heat transfer engineering. 2012. Vol. 33. № 12. Pp. 1033–1039.
25. Akhmetova I., Chichirova N., Derevianko O. Revisiting heat losses calculation at district heating network // International Journal of Civil Engineering and Technology. 2017. Vol. 8. № 12. Pp. 694–702.
26. Gorshkov A., Murgul V. Calculation of Heat Energy Consumption by a Typical Historical Building with a Courtyard // Advances in Intelligent Systems and Computing: 9th International scientific conference Energy Management of Municipal Transportation Facilities and Transport, EMMFT 2017. Khabarovsk, 2018. Vol. 692. Pp. 577–591.

Andrey Makeev,
+7(917)991-62-04; tggi@rambler.ru

Андрей Николаевич Макеев,
+7(917)991-62-04; эл. почта: tggi@rambler.ru

Makeev A.N. Implementation of pulse heat supply for dependent connection of customers. Magazine of Civil Engineering. 2018. 83(7). Pp. 114–125. doi: 10.18720/MCE.83.11.

doi: 10.18720/MCE.83.12

Suspension structure with cross-laminated timber deck panels

Подвесная конструкция с настилом из поперечно ламинированных деревянных панелей

K. Buka-Vaivade,
D. Serdjuks*,
V. Goremikins,
L. Pakrastins,
Riga Technical University, Riga, Latvia
N.I. Vatin,
Peter the Great St. Petersburg Polytechnic University, St. Petersburg, Russia

M.Sc., научный сотрудник
К. Бука-Вайваде,
д-р техн. наук, профессор Д.О. Сердюк*,
д-р техн. наук, ведущий научный сотрудник В.В. Горемыкин,
д-р техн. наук, руководитель кафедры Л. Пакрастиньш,
Рижский технический университет, Рига, Латвия,
д-р техн. наук, профессор Н.И. Ватин,
Санкт-Петербургский политехнический университет Петра Великого, г. Санкт-Петербург, Россия

Key words: prestressed cable truss; cross-laminated timber deck panels; experimental verification; transformed section method; suspension bridge

Ключевые слова: предварительно напряженная вантовая ферма; поперечно ламинированные деревянные панели; экспериментальная проверка; метод трансформированного сечения; подвесной мост

Abstract. Innovative suspension structure with prestressed cable trusses as the main load-bearing members was developed. Cross-laminated timber panels of the deck are placed to the bottom chords of the prestressed cable trusses. The structure with the deck panels placed to the bottom chord with the clearances and behaves in bending in the transversal direction only, and the structure with the deck placed without clearances and behaves in bending in the transversal direction and in compression in longitudinal directions, are considered. The suspended pedestrian-bicycle bridge with the span and width equal to 60 and 5 m correspondingly and loaded by the imposed load 5 kN/m^2, was considered as an object of investigation. The optimization algorithm of the innovative suspension structure with cross-laminated timber deck panels was developed using the program ANSYS v12 optimization tools. Rational values of cross-section areas of suspenders, main load-bearing and stabilization cables were evaluated. It was shown, that placement of the deck panels without clearances, when the panels behave in compression in the longitudinal direction and in bending in transversal direction enables to decrease materials consumption by 25% in comparison with the case when the panels are placed with clearances and behave in bending in transversal direction only.

Аннотация. Предложена инновационная висячая конструкция с главными несущими элементами в виде предварительно напряженных вантовых ферм. Панели настила из склееных в двух перпендикулярных направлениях слоев досок размещены по нижнему поясу предварительно напряженных вантовых ферм. При этом рассмотрены варианты, когда панели настила размещены с зазорами и работают на изгиб только в поперечном направлении, а также вариант, когда панели размещены без зазоров и работают на сжатие в продольном направлении и на изгиб в поперечном. Подвесной пешеходно-велосипедный мост пролетом в 60 м и шириной в 5 м рассмотрен в качестве объекта исследования. Интенсивность полезной нагрузки принята равной 5 кН/м^2. Для рассмотренной конструкции разработан алгоритм оптимизации с использованием програмного комплекса ANSYS v12. С помощью разработанного алгоритма определены рациональные с точки зрения расхода материала вант сечения верхнего и нижнего поясов, а также подвесок. Показано, что размещение панелей настила по нижнему поясу без зазоров, когда панели работают на сжатие в продольном направлении и на изгиб в поперечном, позволяет уменьшить на 25 % расход

Бука-Вайваде К., Сердюк Д.О., Горемыкин В.В., Пакрастиньш Л., Ватин Н.И. Подвесная конструкция с настилом из поперечно ламинированных деревянных панелей // Инженерно-строительный журнал. 2018. № 7(83). С. 126–135.

материала вант по сравнению с вариантом, когда панели настила размещены с зазорами и работают на изгиб только в поперечном направлении.

1. Introduction

Replacement of non-renewable structural materials by the renewable ones and development of structures with rational from the point of view of materials consumption geometrical parameters, with decreased structural dead weight so as increased spans and durability are some of the modern tendencies, which enables to solve the problem of limited raw material and energy resources [1–3]. The structural efficiency can be increased by the using of renewable timber based structural materials for prestressed tensioned structures [4], which are characterized by the decreased materials consumption due to close to the uniform distribution of stresses by the area of cross-section [5, 6].

Possibilities of development of innovative suspension structure with timber deck panels were mentioned in the previous investigations [1, 5]. The prestressed cable trusses, consisting of the main load-carrying cables, stabilization cables and suspenders, were considered as the main load-carrying members of innovative suspension structure. The using of prestressed cable trusses is considered as an efficient way to decrease kinematic displacements of the innovative suspension structure [7–9]. Structural solutions of the prestressed cable trusses that are differed by the lattice configuration were considered [4, 10]. The cable truss with the vertical suspenders and chords joined in the middle of the span was considered as the most rational from the point of view of material consumption and maximum vertical displacements (Figure 1).

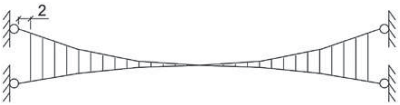

Figure 1. The cable truss with the vertical suspenders and chords joined in the middle of the span [4]

The determination of rational values of cross-sections of suspenders, main load-carrying and stabilization cables so as level of prestressing of stabilization cables probably enables to decrease materials consumption and increase the structural effectiveness of the prestressed cable truss. The rational values can be determined by the solution of optimization task.

Cross-laminated timber panels are considered as the deck material for the suspension structure. The cross-laminated timber panels are placed to the bottom chord of the cable truss without clearances and behave in the longitudinal direction in compression and in the transversal direction in bending. Such cross-laminated timber panel's placement enables to decrease cables materials consumption in comparison with the structure, when cross-laminated timber panels are placed with clearances and behaves in bending in transversal direction only [4, 11]. The optimization of the proposed cable structure with cross-laminated timber panel deck probably enables increasing structural effectiveness of the structure [1, 12].

Transformed section method was mentioned as a simple and enough precise one, which enables analysing load-carrying members from cross-laminated timber, subjected to flexure. This conclusion was obtained analytically and by the experiments conducted for the freely supported cross-laminated timber panels subjected to uniformly distributed load [13]. Other design schemes can take place for the cross-laminated timber panels subjected to flexure when the panel is suspended in four points. This case can take place in case of emergency when the deck can be disintegrated and stabilization cable excluded from the work. Therefore, the transformed section method application for the case should be also treated.

The optimization of the proposed suspension structure with prestressed cable trusses as the main load-bearing members and cross-laminated timber deck behaving in both directions is the target of the current investigation.

Possibility to decrease material consumption by the placing of CLT panels of the deck without clearances when they behave in both directions, and by evaluation of rational parameters of innovative suspension structure, should be checked.

Information regarding design procedure for analyse of timber deck panels from cross-laminated timber must be generalized and completed by the additional cases when the panel was suspended in four points.

Rational parameters of the developed structures are evaluated by the solution of optimization task. The optimization algorithm for innovative suspension structure was developed for the purpose.

2. Methods

2.1. Design methods for elements from cross-laminated timber

The most precise design method for elements from cross-laminated timber is an experimental once, but it is characterized by increased workability. Therefore, analytical methods, which are the most general and economical, are used. Nowadays, there are several analytical design procedures for elements from cross-laminated timber (CLT), including mechanically jointed beams theory (gamma method), composite theory (k-method), shear analogy method and transformed section method. No one from the above mentioned analytical design procedures has been universally accepted yet. The most widely used in practice design procedures for CLT elements and their major peculiarities are shown on Figure 2 [13–15].

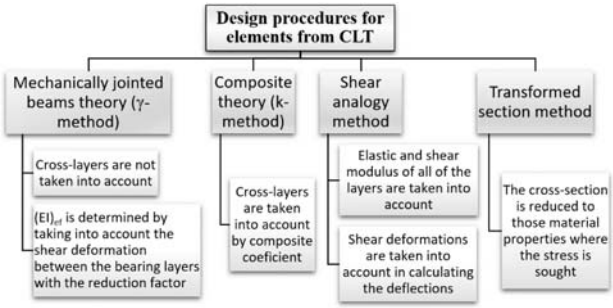

Figure 2. Design procedures for elements from cross-laminated timber

All mentioned above design procedures for CLT load-bearing members can be used for the design of out of plane loading panels subjected to flexure with span-to-depth ratio bigger or equal to 30, where shear deformation can be neglected.

The gamma method is based on Annex B of Eurocode EN 1995-1-1:2004. According to gamma method, transverse to the main load-bearing direction layers of CLT is not taken into account in the bending stiffness calculations. Shear deformation of the longitudinal layers is neglected, but the rolling shear stiffness of the transverse layers is taken into account by the reduction factor.

The composite method is based on theory used for plywood load-bearing members. All of the layers are taken into account in the bending stiffness calculations. The modulus of elasticity of the transverse layers is taken as a modulus of elasticity of external layers divided by thirty. The effective values of strength and stiffness are determined using a composition factor, which depends on loading scheme [13].

The modulus of elasticity and shear modulus of all layers in both directions are taken into account in the bending and shear stiffness calculations according to shear analogy method. The effect of shear deformation is considered in the calculations of deflection [14, 15].

The transformed section method is based on replacement of real cross-section by the equivalent transformed cross-section using the ratio of modulus of elasticity of the longitudinal and transverse layers.

$$n = \frac{E_{CR}}{E_t} \quad (1)$$

where E_{CR} – modulus of elasticity of timber in transversal direction; E_L – modulus of elasticity of timber in longitudinal direction.

Material properties of the transformed cross-section depend on the determined ratio. For example, the cross-section of the 3-layer panel must be transformed to the outer layers properties, if maximal normal stresses are calculated and to the middle layer properties if maximal shear stresses are calculated. Transformed homogenous I-shape cross-section is obtained as a result. Further calculation is carried out

according to the recommendations of the Eurocode 5. Serviceability limit state (SLS) is usually determinant check for CLT.

The CLT design procedures were verified by experiment and finite element method for options of the panels, which were differed by the schemes of loads applications and support conditions. Three-layer cross-laminated panels with the length, width and thickness equal to 2, 0.35 and 0.06 m, correspondingly, were experimentally tested in three-point and four-point bending [13, 16]. The additional experiments were done by suspending the panels in four points near it corners horizontally and under the angle equal to 16.8°. The distance between the points of suspensions was equal to 1.8 m. Suspended panels were loaded by the distributed in two zones vertical load (Figure3). The vertical load with total intensity till 9 kN was applied by pieces of steel with the approximate weight of 20 kg by the six stages with approximate intensity in 1.6 kN each to the horizontally suspended panel. The vertical load with total intensity till 5 kN was applied to the inclined panel.

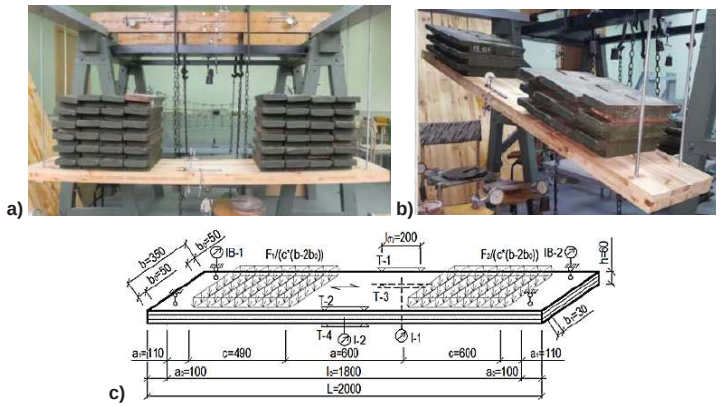

Figure 3. Design scheme and measuring devices placement for suspended CLT panel with four fixing points: a) CLT panel, which was suspended horizontally; b) CLT panel, which was suspended under the angle equal 16.8°; c) scheme of loading and measuring devices placement

Results of the three-point and four-point bending tests were summarized in [13] and show, that transformed section method enables to predict maximum vertical displacements and maximum normal stresses, acting in the edge fibres of the panels with precision from 3.3 to 20 %. Maximum vertical displacements in the middle of the span of the suspended panel with four fixing points (Figure 3), obtained by gamma method, composite method, shear analogy method and transformed section method, physical test and FEM as a function of the vertical load are shown in Figure 4. The differences between the maximum vertical displacements in the middle of the span of suspended in the four points CLT panel obtained by the gamma method, composite method, shear analogy method, transformed section method, FEM software and experimental displacement was equal to 12.5, 4.5, 7.2, 4.5 and 4.4 %, correspondingly.

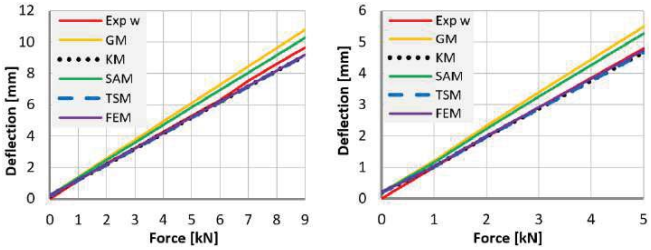

Figure 4. Maximal vertical displacements in the middle of the span as a function from the vertical load`s intensity: a) for CLT panel, which was suspended horizontally; b) for CLT panel, which was suspended under the angle equal 16.8°

Buka-Vaivade, K., Serdjuks, D., Goremikins, V., Pakrastins, L., Vatin, N.I. Suspension structure with cross-laminated timber deck panels. Magazine of Civil Engineering. 2018. 83(7). Pp. 126–135. doi: 10.18720/MCE.83.12.

Based on the obtained results it can be concluded that the transformed section method enables to predict the behaviour of CLT panels in bending with span-to-depth ratio bigger or equal to 30 with the better accuracy than gamma method and shear analogy method. The results obtained by the transformed section method and composite method are the same, but design procedure of transformed section method is simpler. The transformed section method is chosen for analyse of cross-laminated timber deck panels in frames of the current investigation.

2.2. Structural solution for innovative suspension structure

2.2.1. Structural solution of suspension truss

The bicycle-pedestrian bridge with the prestressed main load-carrying members and a deck from CLT panels was considered as an example of the proposed suspension structure. Considered bicycle-pedestrian bridge has a span and width equal to 60 and 5m, correspondingly. Cambers of the main load-carrying and stabilization cables are equal to 6 and 3m, correspondingly. The sag to span and rise to span ratios were assumed as 1:20 and 1:10, for main load-carrying and stabilization cables. The characteristic value of imposed load was equal to 5 kN/m^2 [17]. According to Eurocodes, fire load is irrelevant for the bridge structure. The quasi-permanent representative value of the variable action is recommended by the Codes for the fire situation. The combination factor for the quasi-permanent value of the variable action on footbridge ψ_2 is equal to 0. This means that only dead load of the bridge and prestressing should be considered under fire. In case of fire, the external fire curve with the maximum gas temperature equal to 680°C should be applied. The residual strength of steel for this temperature is equal to 28%. The prestressing forces will disappear under thermal elongations caused by increased temperature reserving additional capacity of cables [18]. In addition, thermal expansions will cause an increase of the camber and decrease of internal forces. This means the cable structure will not collapse under fire. The 180 mm thick bridge deck ensure R180 fire resistance under fire design situation in case of one side burning. The dynamic approach is one of the regulated bridge design parts for this type of structure. According to the codes, the natural vibration frequency of the structure should not be within the limit of 1 to 3 Hz [17]. Different method could be used for determination of natural vibration frequencies of prestressed cable structures [19], like numerical methods or the simplified analytical method, proposed by Goremikins et al. [20]. The determination of the natural vibration frequencies of the structure is not within the scope of this research.

The prestressed cable truss with joined in the middle of the span load-carrying and stressing cables and vertical suspenders, which is characterized by the minimum structural materials consumption, was considered as the main load-carrying structure of the proposed structure. The distances between the vertical suspenders were equal to 2 m (Figure 1.). The steel cables with the design resistance in tension equal to 840 MPa were considered for load-bearing and stressing cables so as for elements of the lattice. Modulus of elasticity and poisons ratio for the considered cables were equal to 150000 MPa and 0.3, correspondingly [21].

Materials consumption of the structural solutions of prestressed cable trusses, which are differed by the system of the lattice and connection of the top and bottom chords, changes within the limits from 5.31 to 11.96 t for considered bicycle-pedestrian bridge [4]. Chosen option with joined in the middle of the span stressing cables and vertical suspenders is characterized by the materials consumption 4.59 t, maximum normal stresses acting in the members 692 MPa and maximum vertical displacements 0.2 m [4]. The values were obtained for the case when cross-laminated timber panels are placed with clearances and behave in bending in transversal direction only.

2.3. Structural solution of the deck

Cross-laminated timber panels were considered as the load-bearing elements of the deck for the proposed suspension structure [22, 23].

The transformed section method discussed in the second chapter was used for evaluation of the effective dimensions of the CLT panels for the deck of the bridge. The panel with length and span equal to 5 and 2 meters was analysed. The linear supports were assumed for the panel under consideration. Based on the calculation by the transformed section method the effective depth of the panel equal to 180 mm and thicknesses of the layers were obtained (Figure 5). Thicknesses of the layers with the fibers oriented in the longitudinal direction are equal to 40 mm. Thicknesses of the layers with the fibers oriented in the transversal direction are equal to 30 mm. The serviceability limit state was decisive for selection of the effective dimensions.

Бука-Вайваде К., Сердюк Д.О., Горемыкин В.В., Пакрастиньш Л., Ватин Н.И. Подвесная конструкция с настилом из поперечно ламинированных деревянных панелей // Инженерно-строительный журнал. 2018. № 7(83). С. 126–135.

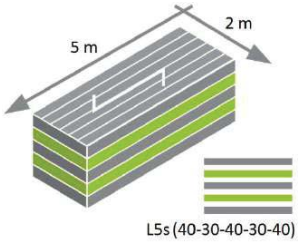

Figure 5. CLT panels for the deck of the innovative structure

The rational solution of the deck was chosen on the base of comparison of two probable options of decking panel's placement: by the top or the bottom chords of the prestressed cable trusses. Two prestressed cable trusses with joined load-bearing and stressing cables and vertical suspenders were considered as the main load-bearing structures of the pedestrian suspension bridge. Material consumption of the cable trusses was considered as a criterion for the options comparison. 2D model of the prestressed cable trusses for decking panel's placement by the top and bottom chords is shown in Figure 6.

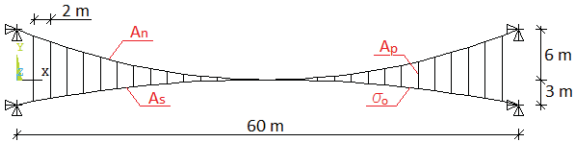

Figure 6. Numerical model of prestressed cable trusses of pedestrian suspension bridge

It was shown, that placement of the cross-laminated timber elements of the deck to the bottom chord enables decreasing by 16.7 % materials consumption of the cable trusses in comparison with the option when the elements of the deck are placed to the top chord of the cable truss. Therefore, placement of the cross-laminated timber panels to the bottom chord of prestressed cable truss is considered as the rational solution for the deck of the proposed cable structure [4]. The option of the structure with the CLT panels placed without mutual clearances enables developing the provisional longitudinal arch resisting part of the longitudinal internal forces. The combined behaviour of the prestressed cable trusses and cross-laminated timber panels in the longitudinal direction enables decreasing the materials consumption [1].

3. Results and Discussions

The optimization algorithm of the proposed cable structure with the cross-laminated timber deck was developed. The aim of the optimization is the obtaining of structural parameters which ensure minimum material consumption and maximum allowed stresses and displacements in the elements [24]. The optimization was performed using program ANSYS v12 optimization tool [25]. The 2D and 3D parametric numerical models of the prestressed bridge were developed. The first one (2D) was developed for the option of the structure with the CLT deck panels placed with mutual clearances and behaving in the transversal direction in bending only. The second one (3D) was developed for the option of the structure with CLT panels placed without clearances and behaving in both directions (figure 8).

The numerical models were developed in FEM software ANSYS 12. The 3D spar element LINK10 with tension only function was used for modelling the cable elements. The 3D layered shell element SHELL181 was used for modelling the deck. The deck and the cables were coupled in vertical and transversal direction, while in the longitudinal direction the cables and the deck were uncoupled. KILL/ALIVE commands were used for the modelling of the process of assembling the deck after prestressing. The prestressing was introduced into the stabilization cables. The prestressing of the cables was modelled by the temperature difference and thermal extension option.

The developed models with sufficient accuracy describe the behaviour of physical structures, which were experimentally tested with physical loading of prototypes of suspension bridges with a span of 2.17 m [4]. The developed optimization algorithm is shown in Figure 7.

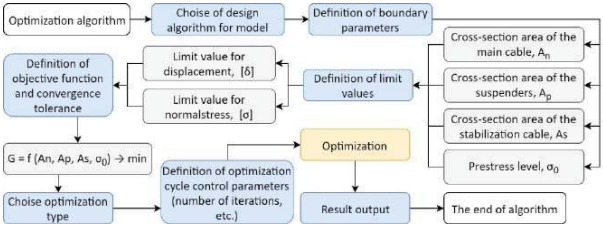

Figure 7. Optimization algorithm

The optimization of dimensions was used to get the rational parameters of the proposed structure. The size optimization is a type of structural optimization that found the optimal solution by changing the size of variables while maintaining topology. The optimization is carried out with the aim of identifying the values of the structural parameters that give the lowest consumption of the material maintaining the displacement and stress within the relevant limits.

The consumption of the material $G = f(A_n, A_p, A_s, \sigma_o)$ was taken as an objective function of the optimization task. In the equation above the variables are A_n, A_p, A_s – respectively, the cross-sectional areas of the bearing cable, the suspension and stabilization cables and σ_o – the prestressing level in the stabilization cable.

The first-order method based on the determination of the vector in each subiteration that points the direction of the greatest increase of function vectors, was used for the structural optimization.

This determines the direction of the search, and the search strategy is applied to the definition of the minimum of the objective function. The iterative process continues until convergence is achieved or the maximum number of iterations is reached.

It is assumed that the task is solved if by comparing the current iteration scheme (j) with the previous one (j-1) and the best (b) one the following conditions are fulfilled:

i) The change of the objective function in comparison with the best variant $f^{(b)}$ and the current $f^{(j)}$ is less than the accepted assumption τ:

$$f^{(j)} - f^{(b)} \leq \tau \quad (2)$$

ii) The change of the objective function in comparison with the previous variant $f^{(j-1)}$ and the current $f^{(j)}$ is less than the accepted tolerance τ:

$$f^{(j)} - f^{(j-1)} \leq \tau \quad (3)$$

The task estimation can be stopped before the approach if the maximum number of iterations is reached.

Consumption of steel material for both options of the bridge – with the CLT deck resisting and does not resisting the longitudinal direction forces of the bridge was compared by optimization of the numerical models of the suspension structure. 3D model of optimum suspension structure with CLT timber deck is shown in Figure 8.

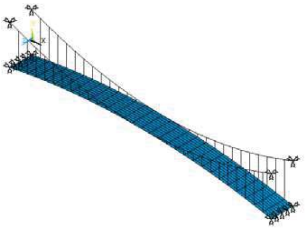

Figure 8. 3D model of optimum suspension structure with CLT timber deck which behaves in both directions

Бука-Вайваде К., Сердюк Д.О., Горемыкин В.В., Пакрастиньш Л., Ватин Н.И. Подвесная конструкция с настилом из поперечно ламинированных деревянных панелей // Инженерно-строительный журнал. 2018. № 7(83). С. 126–135.

Results of optimization show that the option of the structure with the CLT deck panels placed without clearances and behaving in both directions is characterized by the decreased materials consumption and maximum vertical displacements in comparison with the option when cross-laminated timber panels are placed with clearances and behave in bending in the transversal direction only. Results of suspended bridge optimization are given in Table 1.

Table 1. Results of suspended bridge optimization

Rational parameters of the proposed suspension structure	Option of deck	
	Deck behaves in the transversal direction only	Deck behaves in two directions
Max displacements (load on span), m	-0.20174	-0.16029
Max displacements (load on ½ of span), m	-0.19946	-0.19940
Max stresses (load on span), MPa	824	743
Max stresses (load on ½ of span), MPa	768	692
Prestress level, MPa	651	532
Cross-sectional areas of the bearing cable, mm^2	5.75E+03	2.48E+03
Cross-sectional areas of the suspension cables, mm^2	71.5	89.2
Cross-sectional areas of the stabilization cable, mm^2	2.05E+03	3.35E+03
Material consumption, m^3	0.48366	0.36263
Material consumption, t	3.77	2.83

The material consumption of the cables of the structure with the span of 60 m loaded by 5 kN/m^2, when cross-laminated timber panels are placed with clearances and behave in bending in transversal direction only, is equal to 3.77 t. The material consumption for the cables of the structure when the CLT deck panels are placed without clearances and behave in both directions (Figure 8) is equal to 2.83 t. The evaluated rational parameters of the innovative suspension structure enable to decrease material consumption by 25 % by placing of CLT panels of the deck without clearances when they behave in both directions.

4. Conclusions

Innovative suspension structure with prestressed cable trusses as the main load-bearing members and cross-laminated timber panels which is characterized by the decreased materials consumption and improved behavior was proposed.

It was stated, that the transformed section method can be used to analyse of the cross-laminated timber deck panels due to its simplicity and reasonable precision for members subjected to flexure and compression with bending.

The developed optimization algorithm for the proposed prestressed suspension structure using program ANSYS v12 optimization tools enables computation of rational parameters of the structure. The optimized proposed suspension structure with CLT panels of the deck placed to the bottom cable without mutual clearances and behaving in both directions enables decreasing the material consumption by 25 % comparing to the option of the structure with the CLT deck behaving in transversal direction only.

5. Acknowledgement

The authors staff reflect gratitude to Sconto enterprise, Ltd, Elgava, Latvia which provide CLT specimens for laboratorian experiments.

References

1. Goremikins, V., Serdjuks, D., Buka-Vaivade, K., Pakrastins, L, Vatin N. Prediction of Behaviour of Prestressed Suspension Bridge with Timber deck Panels. Baltic Journal of Road and Bridge Engineering. 2017. Vol. 12. No. 4. Pp. 234–240.
2. Walther, R., Houriet, B., Isler, W., Moia, P., Klein, J.F. Cable Stayed Bridges. 2nd edition. London: Thomas Telford, 1999. 236 p.
3. Sandovič, G., Juozapaitis, A., Gribniak, V. Experimental and Analytical Investigation of Deformations and Stress

Литература

1. Goremikins V., Serdjuks D., Buka-Vaivade K., Pakrastins L, Vatin N. Prediction of Behaviour of Prestressed Suspension Bridge with Timber deck Panels // Baltic Journal of Road and Bridge Engineering. 2017. Vol. 12. № 4. Pp. 234–240.
2. Walther R., Houriet B., Isler W., Moia P., Klein J. F. Cable Stayed Bridges. 2nd edition. London: Thomas Telford, 1999. 236 p.
3. Sandovič G., Juozapaitis A., Gribniak V. Experimental and Analytical Investigation of Deformations and Stress

Distribution in Steel Bands of a Two-Span Stress-Ribbon Pedestrian Bridge. Mathematical Problems in Engineering. 2017. Vol. 2017. Pp. 1−11.

4. Goremikins, V., Serdjuks, D., Buka-Vaivade, K., Pakrastins, L. Choice of Rational Structural Solution for Smart Innovative Suspension Structure. Procedia Engineering. 2017. Vol.172. Pp. 1212–1219.
5. Yanaka, Y., Kitagawa, M. Maintenance of steel bridges on HonshuShikoku crossing. Journal of Constructional Steel Research. 2002. Vol. 58. Pp. 131–150.
6. Gusevs, J., Serdjuks, D., Artebjakina, G.I, Afanasjeva, E.A, Goremikins, V. Behaviour of load-carrying members of velodromes' long-span steel roof. Magazine of Civil Engineering. 2016. No. 5. Pp. 3–16.
7. Goremikins, V., Rocens, K., Serdjuks, D. Decreasing Displacements of Prestressed Suspension Bridge. Journal of Civil Engineering and Management. 2012. Vol. 18(6). Pp. 858–866.
8. Serdjuks, D., Rocens, K. Decrease the Displacements of a Composite Saddle-Shaped Cable Roof. Mechanics of Composite Materials. 2004. Vol. 40(5). Pp. 437–442.
9. Goremikins, V., Rocens, K., Serdjuks, D., Pakrastins, L., Vatin, N. Cable Truss Topology Ooptimization for Prestressed Long-span Structure. Advances in Civil Engineering and Building Materials. 2015. No. IV. Pp. 363–368.
10. Chen, W.F., Duan, L. Bridge Engineering Handbook: Substructure Design. 2nd edition. Vol. 3. New York: CRC Press LLC, 2014. 722 p.
11. EN 16351: 2016 Timber structures – Cross laminated timber – Requirements.
12. Priadko, I.N., Mushcanov, V.P., Bartolo, H., Vatin, N.I., Rudnieva, I.N. Improved numerical methods ir reliability analysis of suspension roof joints Magazine of Civil Engineering. 2016. 65(5). Pp. 27–41.
13. Buka-Vaivade, K., Serdjuks, D., Goremikins, V., Vilguts, A., Pakrastins, L. Experimental Verification of Design Procedure for Elements from Cross-laminated Timber. Proceedings of 12 th International Conference Modern Building Materials Structures and Techniques, MBMST 2016, Vilnius, Lithuania, 2016. Vol. 172. Pp. 1212–1219.
14. Rayan, E.S. Interlocking Cross-laminated Timber: Alternative use of Waste Wood in Design and Construction. University of Utah, 2011. 22 p.
15. Reinhard, B. Production and Technology of Cross Laminated Timber: A State-of-the-art Report. Graz University of technology, 2012. 33 p.
16. Kovacič, B., Kamnik, R., Štrukelj, A., Vatin, N. Processing of Signals Produced by Strain Guages in Testing Measurements of the Bridges. Procedia Engineering. 2015. Vol. 117. Pp. 795–801.
17. LVS EN 1991-2: 2004 Eurocode 1: Actions on structures – Part 2: Traffic loads on bridges
18. Gravit, M.V., Nedryshkin, O.V., Ogidan, O.T. Transformable fire barriers in buildings and structures. Magazine of Civil Engineering. 2018. No. 1. Pp. 38–46.
19. Wiig Petersen, Ø., Øiseth, O., Lourens, E. Estimation of the dynamic response of a slender suspension bridge using measured acceleration data. Procedia Engineering 2017. Vol. 199. Pp. 3047–3052.
20. Goremikins, V., Rocens, K., Serdjuks, D., Sliseris, J. Simplified Method of Determination of Natural-Vibration Frequencies of Prestressed Suspension Bridge. Procedia Engineering. 2013. Vol. 57. Pp. 343–352.
21. LVS EN 1993-1-11: 2007 Eurocode 3: Design of steel structures – Part 1-11: Design of structures with tension components.

Distribution in Steel Bands of a Two-Span Stress-Ribbon Pedestrian Bridge // Mathematical Problems in Engineering. 2017. Vol. 2017. Pp. 1−11.

4. Goremikins V., Serdjuks D., Buka-Vaivade K., Pakrastins L. Choice of Rational Structural Solution for Smart Innovative Suspension Structure // Procedia Engineering. 2017. Vol. 172. Pp. 1212–1219.
5. Yanaka Y., Kitagawa M. Maintenance of steel bridges on HonshuShikoku crossing // Journal of Constructional Steel Research. 2002. Vol. 58. Pp. 131–150.
6. Гусев Е., Сердюк Д.О., Артебякина Г.И., Афанасьева Е.А., Горемыкин В.В. Работа несущих элементов большепролетного стального покрытия велодрома // Инженерно-строительный журнал. 2016. № 5(65). С. 3–16.
7. Goremikins V., Rocens K., Serdjuks D. 2012. Decreasing Displacements of Prestressed Suspension Bridge // Journal of Civil Engineering and Management. 2012. Vol. 18(6). Pp. 858–866.
8. Serdjuks D., Rocens K. Decrease the Displacements of a Composite Saddle-Shaped Cable Roof // Mechanics of Composite Materials. 2004. Vol. 40(5). Pp. 437–442.
9. Goremikins V., Rocens K., Serdjuks D., Pakrastins L., Vatin N. Cable Truss Topology Optimization for Prestressed Long-span Structure // Advances in Civil Engineering and Building Materials. 2015. № IV. Pp. 363–368.
10. Chen W.F., Duan L. Bridge Engineering Handbook: Substructure Design. 2nd edition. Vol. 3. New York: CRC Press LLC, 2014. 722 p.
11. EN 16351: 2016 Timber structures – Cross laminated timber – Requirements.
12. Прядко Ю.Н., Мущанов В.Ф., Бартоло Х., Ватин Н.И., Руднева И.Н. Усовершенствование численных методов расчета надежности узлов висячих покрытий // Инженерно-строительный журнал. 2016. № 5(65). С. 27–41.
13. Buka-Vaivade K., Serdjuks D., Goremikins V., Vilguts A., Pakrastins L. Experimental Verification of Design Procedure for Elements from Cross-laminated Timber // Proceedings of 12 th International Conference Modern Building Materials Structures and Techniques, MBMST 2016. Vilnius, Lithuania, 2016. Vol. 172. Pp. 1212–1219.
14. Rayan E.S. Interlocking Cross-laminated Timber: Alternative use of Waste Wood in Design and Construction. University of Utah, 2011. 22 p.
15. Reinhard B. Production and Technology of Cross Laminated Timber: A State-of-the-art Report. Graz University of technology, 2012. 33 p.
16. Kovacič B., Kamnik R., Štrukelj A., Vatin N. Processing of Signals Produced by Strain Guages in Testing Measurements of the Bridges // Procedia Engineering. 2015. Vol. 117. Pp. 795–801.
17. LVS EN 1991-2: 2004 Eurocode 1: Actions on structures – Part 2: Traffic loads on bridges
18. Гравит М.В., Недрышкин О.В., Огидан О.Т. Трансформируемые противопожарные преграды в сооружениях и строениях // Инженерно-строительный журнал. 2018. № 1(77). С. 38–46.
19. Wiig Petersen Ø., Øiseth O., Lourens E. Estimation of the dynamic response of a slender suspension bridge using measured acceleration data // Procedia Engineering 2017. Vol. 199. Pp. 3047–3052.
20. Goremikins V., Rocens K., Serdjuks D., Sliseris J. Simplified Method of Determination of Natural-Vibration Frequencies of Prestressed Suspension Bridge // Procedia Engineering. 2013. Vol. 57. Pp. 343–352.

Бука-Вайваде К., Сердюк Д.О., Горемыкин В.В., Пакрастиньш Л., Ватин Н.И. Подвесная конструкция с настилом из поперечно ламинированных деревянных панелей // Инженерно-строительный журнал. 2018. № 7(83). С. 126–135.

22. Green, M, Taggart, J. Tall Wood Buildings, Design, Construction and Performance. 1 st edition. Basel: Birkhauser, 2017. 176 p.
23. Hambly, E.C. Bridge Deck Behaviour. 2nd edition. New York: E & FN Spon, 1998. 308 p.
24. Belevičius, R., Juozapaitis, A., Rusakevičius, D., Šešok, D. Topology, Shape and Sizing Optimization of Under-deck Stayed Bridges. Proceedings of the Fourth International Conference on Soft Computing Technology in Civil, Structural and Environmental Engineering. 2015. Pp. 1–16.
25. ANSYS 12.1 Mechanical APDL Manual. Ansys Inc., 2009.zeolites. Material research bulletin. 2002. Vol. 37. No. 6. Pp. 1025.

21. LVS EN 1993-1-11: 2007 Eurocode 3: Design of steel structures – Part 1-11: Design of structures with tension components.
22. Green M, Taggart J. Tall Wood Buildings, Design, Construction and Performance. 1 st edition. Basel: Birkhauser, 2017. 176 p.
23. Hambly E.C. Bridge Deck Behaviour. 2nd edition. New York: E & FN Spon, 1998. 308 p.
24. Belevičius R., Juozapaitis A., Rusakevičius D., Šešok D. Topology, Shape and Sizing Optimization of Under-deck Stayed Bridges // Proceedings of the Fourth International Conference on Soft Computing Technology in Civil, Structural and Environmental Engineering. 2015. Pp. 1–16.
25. ANSYS 12.1 Mechanical APDL Manual. Ansys Inc., 2009.

Karina Buka-Vaivade,
+37126353082; karina.buka.vaivade@gmail.com

Dmitrijs Serdjuks,*
+37126353082; Dmitrijs.Serdjuks@rtu.lv

Vadims Goremikins,
+37129231772; goremikins@gmail.com

Leonids Pakrastins,
+37129452138; leonids.pakrastins@rtu.lv

Nikolai Vatin,
+79219643762; vatin@mail.ru

Карина Бука-Вайваде,
+37126353082;
эл. почта: karina.buka.vaivade@gmail.com

Дмитрий Олегович Сердюк,*
+37126353082;
эл. почта: Dmitrijs.Serdjuks@rtu.lv

Вадим Валерьевич Горемыкин,
+37129231772;
эл. почта: goremikins@gmail.com

Леонид Пакрастиньш,
+37129452138;
эл. почта: leonids.pakrastins@rtu.lv

Николай Иванович Ватин,
+79219643762; эл. почта: vatin@mail.ru

Buka-Vaivade, K., Serdjuks, D., Goremikins, V., Pakrastins, L., Vatin, N.I. Suspension structure with cross-laminated timber deck panels. Magazine of Civil Engineering. 2018. 83(7). Pp. 126–135. doi: 10.18720/MCE.83.12.

doi: 10.18720/MCE.83.13

Thermal-insulation boards from fibrous plant wastes and urea-formaldehyde binder

Теплоизоляционные плиты из волокнистых растительных отходов и карбамидоформальдегидного связующего

T.N. Vahnina,
I.V. Susoeva*,
A.A. Titunin,
Kostroma State University, Kostroma, Russia

Канд. техн. наук, доцент Т.Н. Вахнина,
канд. техн. наук, доцент И.В. Сусоева*,
д-р техн. наук, профессор А.А. Титунин,
Костромской государственный университет, г. Кострома, Россия

Key words: thermal-insulation boards; durability; static bend; thermal conductivity coefficient; water absorption; swelling; plant waste; urea-formaldehyde binder; hardener; extent of hardening

Ключевые слова: теплоизоляционные плиты; прочность; статический изгиб; коэффициент теплопроводности; водопоглощение; разбухание; растительные отходы; карбамидоформальдегидное связующее; отвердитель; степень отверждения

Abstract. Irreversible waste spinning flax and cotton are sent to landfill or incinerated, it adversely affects the environment, although it is desirable to use plant waste for production, which would be a very positive approach in terms of natural environment. Composite boards of irrecoverable waste from the processing of flax and cotton and urea-formaldehyde binder (UF) can be used as a thermal-insulation material, the development of this composite material is the purpose of this research.

The paper presents the results of laboratory research of indicators of composite thermal-insulation boards filled with irretrievable spinning flax and cotton. As the matrix of the composite used UF binder with various additives. UF binder has advantages and disadvantages: is cheaper but less waterproof than other synthetic binders. The work assessed the properties of the binder and the influence of the composition of the binder on the physical and mechanical properties of the thermal-insulating material. The IR spectrum of the binder, the dependence of the degree of curing of the UF binder on the type and proportion of the hardener additive are given. The results were obtained that the degree of curing and water resistance of the UF binder depends on the type and proportion of the hardener additive and the curing temperature.

The physical and mechanical properties and the coefficient of thermal conductivity of the boards on the UF binder were determined. It is shown that the type of additive in the UF binder affects the physical and mechanical properties of thermal-insulation composite boards from spinning flax and cotton. The paper summarizes the results of the determination of the physical and mechanical parameters of boards from plant waste, and proposed a rational combination of factors for the production of composites.

The type of additive in the binder does not have a significant effect on the thermal conductivity of the material. Composites have a coefficient of thermal conductivity required for thermal-insulation materials.

Аннотация. Невозвратные отходы прядения льна и хлопка отправляются на свалку или сжигаются, это негативно влияет на экологию, хотя растительные отходы желательно использовать для производства продукции, это было бы очень позитивным подходом с точки зрения естественной окружающей среды. Композиционные плиты из невозвратных отходов переработки льна и хлопка и карбамидоформальдегидного связующего (КФС) могут использоваться в качестве теплоизоляционного материала, разработка этого композиционного материала является целью данного исследования.

В работе представлены результаты лабораторных исследований показателей композиционных теплоизоляционных плит с наполнителем из невозвратных отходов прядения льна и хлопка. В качестве матрицы композита использовано КФС связующее с различными добавками. КФС связующее имеет достоинства и недостатки: оно является более дешевым, но менее водостойким, чем другие синтетические связующие. В работе дана оценка свойств связующего и влияния состава связующего на физико-механические свойства теплоизоляционного материала. Приведены ИК-спектр связующего, зависимости степени отверждения КФС связующего от вида и

Вахнина Т.Н., Сусоева И.В., Титунин А.А. Теплоизоляционные плиты из волокнистых растительных отходов и карбамидоформальдегидного связующего // Инженерно-строительный журнал. 2018. № 7(83). С. 136–147.

доли добавки отвердителя. Получены результаты, что степень отверждения и водостойкость КФС связующего зависит от вида и доли добавки отвердителя и температуры отверждения.

Определены физико-механические свойства и коэффициент теплопроводности плит на КФС связующем. Показано, что вид добавки в КФС связующее влияет на физико-механические показатели теплоизоляционных композиционных плит из отходов прядения льна и хлопка. В работе обобщены результаты определения физико-механических показателей плит из растительных отходов, предложено рациональное сочетание факторов производства композитов.

Вид добавки в связующее не оказывает значимого влияния на коэффициент теплопроводности материала. Композиты имеют коэффициент теплопроводности, необходимый для теплоизоляционных материалов.

1. Introduction

Development of effective materials with use of local raw materials and waste of the industry is an important task for the construction industry. The purpose of this work is justification of structure and properties of thermal-insulation board materials of construction appointment on urea-formaldehyde binder of irretrievable waste of spinning of linen and cotton fibers.

Secondary plant raw materials, along with primary waste of annual plant (such as flax shive, straw), it can be used for production of thermal-insulation elements of building constructions [1], especially in relation to wooden housing construction. A problem in development of material is creation of steady structure from plant filler and a matrix – binding.

The properties of the binder have a significant impact on the performance of composite materials, including the thermal-insulation boards [2, 3]. For thermal-insulation materials traditionally use phenol formaldehyde binder (PF) [4, 5]. Thermal-insulation boards most often make of plant fillers on the basis of inorganic binder or knitting [6–8].There are also developments of thermal-insulation board materials from cellulose hydrolysis lignin and lignocellulosic discrete wood particles, also developed, however, the complexity of the structure of the material, 90 % consisting of sawdust, is costly to manufacture [9].

The most large-capacity thermoreactive polymer in domestic and world practice is urea-formaldehyde, cost her is lower, than phenolic binder. According to G. Mantanis with colleagues, in the European industry for production of board materials are used (as use volumes) urea-formaldehyde binder (UF), melamine-urea-formaldehyde (MUF), phenol formaldehyde (PF) and polyisocyanates of PMDI (for OSB). A share of use of binder board materials in production (according to European federation of the particleboard): UF – 90 … 92 %, MUF– 6 … 7 % and PMDI – 1 … 2 %. More than 30 % of board materials are used in construction: about 20 % when finishing doors and laying floors, about 12 % – for production of panels [10].

The main lack of binder UF – adhesives occasionally exhibit some problems with long-term hydrolytic instability [11–12].

Are traditionally used for the production of insulating board materials. A significant advantage of the PF is the ability to combine with different fillers [13]. Materials based on the PF, in comparison with the composites of the urea-formaldehyde binders have higher water resistance, strength, elasticity and durability [14, 15].

In work the task of increase in water resistance of thermal-insulation composites from plant filler on UF by deepening of extent of polycondensation binding and increases in hydrolytic stability at the operating influence of technology factors of process of production of board materials is set.

Zaimatul Aqmar Abdullah used in the work a way of increase in hydrolytic stability of UF by additives of compounds of sulfur, acrylamide and PMDI, and the best results were yielded by additive of acrylamide [16]. The results in the improvement of the water resistance of thermal-insulation materials obtained by using for their production combined urea-phenol-formaldehyde binders are also known [5]. UF is generally used for production of the made foam plastic. Both the Russian, and foreign researchers note that use urea-formaldehyde binder for production of the construction materials operated under variable temperature and moist conditions is limited owing to their low water resistance [17, 11].

The gluing ability of UF glues depends on number of metilolny groups $-CH_2OH$, however a part them remains not connected in cured binder. Low hydrolytic stability of UF is due to the presence in the cured polymer of free methylolgroups – CH_2OH. Scientists of the whole world deal with problems of assessment of hydrolytic stability of UF glues for construction [16]. According to L.F. Mubarakshina, operational technical characteristics of polymeric construction materials on the basis of UF binders can be improved by their modification [8].

The lower the degree of polycondensation of the binder, the more it contains free methylol− CH_2OH groups. In additionto gidroliticheski unstablemethylol − CH_2OH groups, the polymer matrix contains UF resistant to hydrolysis methylene groups − CH_2 − and partially hydrolysable methylene-ether groups− CH_2−O−CH_2−, which can degrade under the influence of moisture and temperature.

According to M. Dunky, extent of hardening of UF glues depends on a formaldehyde share at synthesis of binder [11]. According to O. F. Shishlov with colleagues, extent of hardening binder depends on the speed of heating and a type of plant filler [18]. However except a molar ratio of UF and above the listed factors, on stitching degree and consequently and hydrolytic stability of UF glues is influenced by both a look and amount of hardener.

As UF hardeners of glues in Europe persulphate of ammonium $(NH_4)_2SO_4$ and nitrate of ammonium NH_4NO_3, NH_4Cl are used have been forbidden for the ecological reasons [10, 11], however in many countries about 20 years ago (Russia, Indonesia, etc.) chloride ammonium is still used for hardening of UF glues [19].

2. Methods

In this paper, we studied the indicators of UF resin and thermal-insulation composite boards of plant filler and UF binder.

Fiber boards by wet way of production were used as an analogue (EN 13986:2004 Wood-based panels for use in construction, Russian Standard 4598-2018).

The samples of composite thermal-insulation boards from wastes of spinning of flax and cotton fibers and binding of urea-formaldehyde binder and hardeners – the ammoniynykh salt shave been made in the work. Composite board materials were made with an average density of 370 … 410 kg/m^3, the expense of binding made 10 – 30% of the mass of plant filler. Boards were made by wet way of production. Plant wastes were mixed with water, a binder (UF resin and hardener), and molded, extra water was squeezed out. Composites were dried at a temperature of T = 100 °C and T = 170 °C to a humidity of 8 ± 0.5 %. After exposure, the physical and mechanical characteristics of the samples of the boards were determined.

Composite samples were tested for strength under static bending to EN 310. To determine the strength of the samples, a testing machine 2166 R-5 was used (division price 0.1 N). Samples were installed on the supports of the testing machine. The load was applied at a constant rate until the test specimen was destroyed. The destruction of the sample occurred within (60 ± 30) s. The maximum load was recorded with an accuracy of 0.1 N, the tensile strength of the samples during static bending was determined, MPa.

The swelling of the boards in thickness after 24 hours in water was determined. The thickness of the samples was measured before and after their stay in the water, and the thickness swelling was determined, %. The water absorption of the boards, % after 24 hours in water was determined by the weight method.

The value of the coefficient of heat conductivity of material was determined with on the help of the measuring instrument of heat conductivity of ITP-MG4. The IR spectra of the binder and composites were taken on a NETZSCH STA 449 F3 Jupiter synchronous thermal analysis unit, combined with an IR Fourier transform. For the manufacture of composites used polycondensation UF resin of the brand UFN-66-P (urea-formadehyde, non-vacuumed, for board production) was used. The manufacturer's normalized resin indicators:

- specific gravity 1.19 … 1.22 g/m^3;
- mass fraction of free formaldehyde no more than 0.1 %;
- level pH 6.5 … 7.5.

To determine the degree of curing of the binder used the following method. Samples of polymeric materials were cured, dried up in a drying cabinet at T = 105 °C, weighed with an accuracy of 0.0002 g and were located on a steam bath. Steaming was carried out during 3 h, at the same time not cured part of the binder absorbed water, samples of polymeric materials were washed out by steam. After steaming samples were dried up to the constant weight. The extent of hardening of polymeric samples of Q was determined by the formula:

$$Q = 100 – [(G_1 – G_0)]100\ \%,$$

where G_1 – the mass of a sample of polymer before extraction, g;

G_0 – the mass of a sample after extraction, g.

A physical and chemical analysis of particles from spinning flax and cotton was performed. The content of cellulose, lignin, ash content and the proportion of water-soluble substances were determined using classical methods [23].

3. Results and Discussion

Figure 1 presents the IR spectrum of the urea-formaldehyde resin, hardened at 100 °C. The spectrum is filmed at the setting of the simultaneous thermal analysis NETZSCH STA 449 F3 Jupiter, combined with the prefix FT-IR. The position and the reference of bandwidths are given in Table 1. The results showed that the transmission in the frequency domain 1002 cm^{-1} and 1128 cm^{-1}, characterizing metrolinie and methyleneimine group, has a broad intense band of complex shape and the shoulder, due, apparently, to the in-phase vibrations of the group – OH [20]. The high content of methynol groups - CH_2OH in the cured resin (transmission intensity 0.35 %) causes low hydrolytic stability of UF resin.

To increase hydrolytic stability of UF, i.e. to reduce the quantity of free metilolnykh groups in the hardened binder, is possible by deepening the extent of polycondensation of the binder. It will allow to increase the water resistance of composites. The completeness of hardening of the binder depends on the initial indicators of the pitch [21], the temperature of hardening, the type of the catalyst of reaction of polycondensation (hardener) [22].

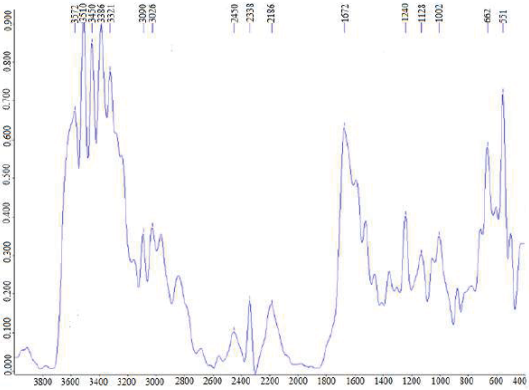

Figure 1. IR spectrum of the urea-formaldehyde resin

Table 1. Bandwidth of the urea-formaldehyde resin

Position band, cm^{-1}	Intensity transmittance, %	Allocation of band width*
3572	0.68	Intra - and intermolecular H-bonds
3510	0.9	Intra - and intermolecular H-bonds
3450	0.85	Intra - and intermolecular H-bonds
3386	0.9	Intra - and intermolecular H-bonds
3321	0.78	Intra - and intermolecular H-bonds
3090	0.37	SVcommunications in groups-C-OH and -C-H
3026	0.38	SVcommunications in groups-C-OH and -C-H
2450	0.11	SVcommunications in groups-C-OH and-C-H
2338	0.19	SVcommunicationsN-H
2186	0.18	SVcommunicationsN-C
1672	0.65	SVcommunicationsC-O andC-N
1240	0.4	DVcommunications N-HandC=O
1128	0.3	SVcommunicationsC-Oin-H_2C-O-CH_2-and -C-OH
1002	0.35	SVcommunicationsC-Oin groups-CH_2OH
662	0.58	DVcommunicationsC-H in groupsCH_2
551	0.74	DVcommunicationsC-H in groupsCH_2

* Notatio conventions: SV – stretching vibrations, DV – deformation vibrations

The extent of hardening of UF[1] cured at temperatures 100 °C and 170 °C has been investigated in the work. Ammoniyny salts: NH_4Cl ammonium chloride; urea-ammoniyny NH_4NO_3–$(NH_2)_2CO$–H_2O nitrate; nadsernokisly ammonium $(NH_4)_2S_2O_8$; hydrophosphate of ammonium $(NH_4)_2HPO_4$ were used as hardeners.

The minimum and maximum values of the degree of curing of the UF binder with NH_4Cl cured at 100 °C are given in Table 2. Dependences of the degree of UF hardening on the proportion of additives of hardeners, constructed from the average values, are shown in the Figure 2 (curing at a temperature T = 100 °C) and in the Figure 3 (T = 170 °C).

Table 2. Curing degree of UF binder with NH_4Cl, cured at 100 °C

NH_4Cl,%	0.8		1.0		1.2		1.4		1.6		2.0	
Q,%	91.57	92.1	94.74	95.27	94.61	93.87	92.68	93.24	92.16	92.39	90.32	91.60

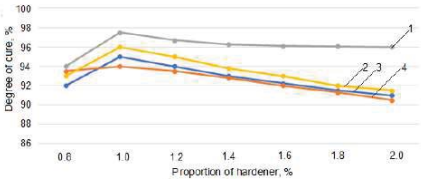

Figure 2. Dependence of the degree of curing of the urea-formaldehyde binder on the proportion of additive curing agents (the curing temperature T = 100 °C): 1 – $(NH_4)_2S_2O_8$; 2 – $(NH_4)_2HPO_4$; 3 – NH_4Cl;4 – NH_4NO_3–$(NH_2)_2CO$–H_2O

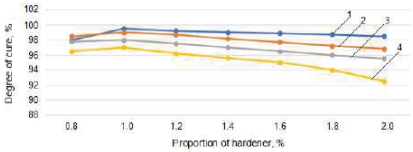

Figure 3. Dependence of the degree of curing of the urea-formaldehyde binder on the proportion of additive curing agents (the curing temperature T = 170 °C): 1– NH_4Cl; 2 – NH_4NO_3–$(NH_2)_2CO$–H_2O; 3 – $(NH_4)_2S_2O_8$; 4 – $(NH_4)_2HPO_4$

At the curing temperature of the UF binder at 100 °C, the best cure rate is provided by the use of an ammonium nitrate $(NH_4)_2S_2O_8$ additive in the amount of 1 % by the resin weight. At a curing temperature of 170 °C, the maximum cure is given by the addition of ammonium chloride in the amount of 1 %. These experimental results make it possible to choose the composition of the adhesive composition for the production of composite boards, but it is necessary to take into consideration the effect of the plant filler on the board indicators. The fractional composition of the filler from waste spinning was determined by sieving in a sieve analyzer and weighing a part of the fraction. The determination results of the fractional composition of the filler are shown in Table 3.

Table 3. Results of determination of fractional composition of filler

Fraction	Share of fraction for cotton waste i_{fr}, %	Share of fraction for flax waste i_{fr}, %
–/10	0.059	0.339
10/7	0.285	0.020
7/5	0.339	0.045
5/2	0.229	0.106
2/0.5	0.042	0.266
Pallet	0.043	0.216

Non-returnable waste of spinning and cotton has an average length:

- for cotton 4.76 mm;
- for flax 4.12 mm.

[1] The research was carried out by magister Mochalov A.N.

Вахнина Т.Н., Сусоева И.В., Титунин А.А. Теплоизоляционные плиты из волокнистых растительных отходов и карбамидоформальдегидного связующего // Инженерно-строительный журнал. 2018. № 7(83). С. 136–147.

The average length of the waste products of flax and cotton spinning is longer than the length of the wood fiber used in the production of fiberboards (2 mm for coniferous fibers, about 1.2 mm for hardwood fibers). So we have come to the conclusion that it is possible to use non-returnable waste of spinning of flax and cotton as a filler of soft boards produced by the technology of heat-insulating fiberboard. At comparable average lengths, flax spinning waste contains about 34 % of long fiber-like particles (fraction - / 10), capable of participating in creating a composite structure by felting.

Photographs of flax fiber spinning waste and a composite of flax waste made by the authors using the Quanta 3D FEG FEI Company microscope are shown in Figure 4.

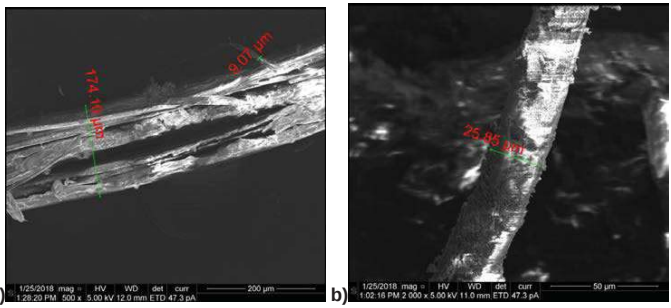

Figure 4. Photo of waste of spinning of linen fiber and composite: a – waste of spinning of linen fiber; b – composite

Filler particles from waste spinning have significant damage and a large specific surface, so the binder covers only part of the filler surface (Figure 4 b).

In Table 4 presents the results of the determination of the physical and chemical analysis of the composition of waste from the processing of plant fibers.

Table 4. Composition of plant materials, %

Irretrievable waste of spinning	Cellulose	Lignin	Ash	Water-soluble substance *
cotton	44.0	22.7	17.0	0.01
flax	54.0	24.9	5.0	0.02

* soluble in hot water

The lignin content in the irretrievable plant waste of flax and cotton is comparable to that for wood raw materials. The pulp content in cotton waste is the same as in wood. Cellulose content in flax production wastes is significantly higher than for wood raw materials. Water-soluble substances waste flax and cotton contain less than wood raw materials. Plant waste from flax and cotton has significant ash, the reason for this is contaminated waste.

Despite the increased ash content, irretrievable waste of flax and cotton can be used for the production of insulation boards. The high content of cellulose in plant waste allows you to create a composite structure due to hydrogen bonds between the particles and chemical bonds with the binder.

Glue from UF resin and hardeners used for the production of composites from flax and cotton waste.

The content of lignin in the irretrievable plant waste of flax and cotton is comparable to the indicator of wood raw materials; the same can be noted for the cellulose content in cotton waste, for flax waste, the cellulose content is much higher than for wood raw materials. Water-soluble substances waste of flax and cotton contain less than wood raw materials. It should be noted the significant ash content of the filler particles from the irretrievable waste, the reason for this is the contamination of the waste. In general, we can say that the use of technology for the production of fiberboards for plant fiber-like particles with a high content of cellulose makes it possible to create a structure of a soft thermal-insulation composite due to hydrogen bonds between particles, chemical bonds with a binder, and a felting effect.

Glutinous compositions of UF binder and hardeners, the degree of curing of which has been researched, was used for the production of thermal-insulation boards from the waste products of flax and cotton. The mass fraction of the hardener for each composition was taken in the amount that provides the maximum degree of cure at the drying temperature of the composite.

In Tables 5–7 the results of definitions of the strength of boards at a static bend, the swelling in thickness and the water absorptions of composites are given. In Table 8 the results of definitions of the coefficient of heat conductivity of board materials are given.

Table 5. Strength of composites at a static bend, MPa

Filler	Type of hardener, share of UF additive, %											
	Ammonium chloride NH_4Cl			Nadsernokisly ammonium $(NH_4)_2S_2O_8$			Karbamido-ammoniyny nitrate NH_4NO_3–$(NH_2)_2CO$–H_2O			Hydrophosphate of ammonium $(NH_4)_2HPO_4$		
	10	20	30	10	20	30	10	20	30	10	20	30
	- temperature of drying of samples T = 100 °C											
Cotton waste	0.27	0.32	0.4	0.41	0.56	0.81	0.23	0.3	0.36	0.29	0.35	0.42
Flax waste	0.4	0.55	0.67	0.54	0.71	0.88	0.38	0.5	0.58	0.41	0.65	0.76
	- temperature of drying of samples T = 170 °C											
Cotton waste	0.44	0.58	0.84	0.29	0.35	0.42	0.31	0.39	0.44	0.23	0.3	0.36
Flax waste	0.57	0.75	0.9	0.44	0.59	0.7	0.43	0.68	0.79	0.38	0.5	0.58

Table 6. Swelling on thickness for 24 h composites, %

Filler	Type of hardener, share of UF additive, %											
	Ammonium chloride NH_4Cl			Nadsernokisly ammonium $(NH_4)_2S_2O_8$			Karbamido-ammoniyny nitrate NH_4NO_3–$(NH_2)_2CO$–H_2O			Hydrophosphate of ammonium $(NH_4)_2HPO_4$		
	10	20	30	10	20	30	10	20	30	10	20	30
	- temperature of drying of samples T = 100 °C											
Cotton waste	6.2	5.4	4.3	5.6	4.8	4.1	7.5	6.8	5.6	6.5	5.9	5.1
Flax waste	5.5	5.3	4.4	5.2	4.5	3.8	6.1	5.3	4.2	5.8	5.6	4.8
	- temperature of drying of samples T = 170 °C											
Cotton waste	5.3	4.4	3.8	6.0	5.1	4.2	6.2	5.6	4.7	7.2	6.4	5.3
Flax waste	5.0	4.1	3.3	5.2	5.0	3.8	5.5	5.3	4.4	6.0	5.2	3.9

Table 7. Water absorption of composites, %

Filler	Type of hardener, share of UF additive, %											
	Ammonium chloride NH_4Cl			Nadsernokisly ammonium $(NH_4)_2S_2O_8$			Karbamido-ammoniyny nitrate NH_4NO_3–$(NH_2)_2CO$–H_2O			Hydrophosphate of ammonium $(NH_4)_2HPO_4$		
	10	20	30	10	20	30	10	20	30	10	20	30
	- temperature of drying of samples T = 100 °C											
Cotton waste	180	168	142	171	159	134	193	185	176	187	181	163
Flax waste	91	79	68	87	73	60	101	89	81	98	85	76
	- temperature of drying of samples T = 170 °C											
Cotton waste	168	155	132	178	164	139	185	179	160	190	182	173
Flax waste	85	71	58	88	77	65	96	83	72	97	86	78

Table 8. Coefficient of heat conductivity of composites, W/(m·K)

Filler	Type of hardener, share of UF additive, %											
	Ammonium chloride NH_4Cl			Nadsernokisly ammonium $(NH_4)_2S_2O_8$			Karbamido-ammoniyny nitrate NH_4NO_3–$(NH_2)_2CO$–H_2O			Hydrophosphate of ammonium $(NH_4)_2HPO_4$		
	10	20	30	10	20	30	10	20	30	10	20	30
	- temperature of drying of samples T = 100 °C											
Cotton waste	0.090	0.091	0.091	0.086	0.086	0.087	0.092	0.092	0.093	0.088	0.088	0.089
Flax waste	0.064	0.064	0.065	0.060	0.061	0.062	0.066	0.067	0.068	0.062	0.062	0.064
	- temperature of drying of samples T = 170 °C											
Cotton waste	0.085	0.086	0.088	0.089	0.090	0.091	0.087	0.088	0.089	0.091	0.093	0.095
Flax waste	0.058	0.060	0.060	0.062	0.063	0.065	0.060	0.062	0.063	0.064	0.065	0.067

Вахнина Т.Н., Сусоева И.В., Титунин А.А. Теплоизоляционные плиты из волокнистых растительных отходов и карбамидоформальдегидного связующего // Инженерно-строительный журнал. 2018. № 7(83). С. 136–147.

The strength of the boards during static bending is influenced by the drying temperature and the type of additive in the binder. For each drying temperature, a hardener is recommended, which provides the maximum degree of curing of the binder.

At a board drying temperature of 100 °C, it is recommended that the additive as a hardener of UF ammonium binder is used. If the boards are produced at a temperature of 170 °C, it is necessary to use ammonium chloride. This provides the best physical and mechanical properties of boards from plant waste.

The results of physical and mechanical tests of the boards are in good agreement with the results of determining the degree of curing of the binder at these temperatures. In the Figures 5 and 6 you can see the IR spectra of composites from flax and cotton waste on a UF binder made at a drying temperature of T = 100 °C.

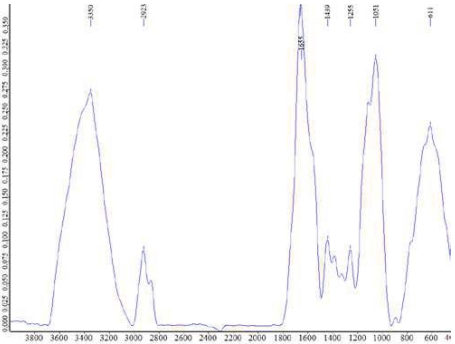

Figure 5. Composite IR spectrum from waste of cotton and UF binding with hardener $(NH_4)_2S_2O_8$ (temperature of drying of samples of T = 100 °C)

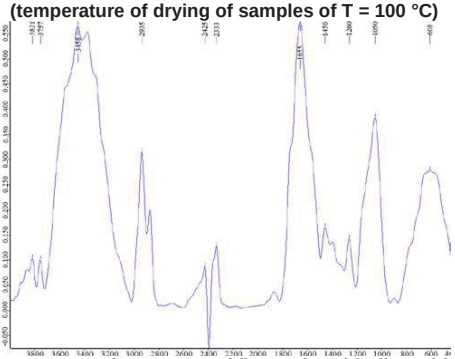

Figure 6. Composite IR spectrum from waste of flax and UF binding with hardener $(NH_4)_2S_2O_8$ (temperature of drying of samples of T = 100 °C)

While manufacturing the composites, according to the chosen values of the factors, a large number of hydrogen bonds is provided, as it is can be seen by a broad absorption band (3350 cm^{-1} for a composite of cotton waste, 3458 cm^{-1} for a composite of flax waste). The water presented in the composites is strongly bound, which can be indicated by an absorption band of 1655 cm^{-1}. Methyl groups (absorption band (1002 cm^{-1}) in composites are absent.

To create a hydrolytically board composite structure from plant waste flax and cotton and a UF binder, it is necessary to increase the degree of curing of the binder.

There are rather labor-consuming ways of assessment of extent of hardening binding. So D. Brown and G. Sherdron with colleagues estimated extent of polycondensation of a low-molecular product, binding on allocation, – waters [24]. Z. Virpsha and Ya. Brzezinski determined extent of hardening of binders by change of level pH [25]. A. A. Leonovich and A. V. Sheloumov also estimated hardening of urea-formaldehyde binding on a share of allocation of by-products and also on change pH systems [21]. Authors in general note that "… because of existence of collateral chemical reactions it is difficult to interpret

characteristics of hardening of UF" [21]. Z. Virpsha and Ya. Brzezinski have also developed a definition method "… sufficiency of hardening" on resistance of aminoplastics to effect of the boiling water [25]. However, this method is difficult to apply to composites with plant filler. After boiling the board on the UF binder is completely destroyed.

In this work dependences of extent of hardening of UF with additive the ammoniynykh of salts are experimentally received from temperature of hardening and a share of additive of hardeners. Zh.-Zh. Vilnav notes that it is in fact rather difficult to receive "the correct stitching" [26]. He offers for increase in extent of hardening of a message reaction at high temperature under pressure. However and here he notes a problem: if to use temperature above 100 °C, the "foamy" seam with a low mechanical durability [26].

Z. Akmer used in the work a way of increase in hydrolytic stability by additives of compounds of sulfur, acrylamide and PMDI, and the best results were yielded by acrylamide additive. The scientist used a similar method of assessment of depth of polycondensation and hydrolytic stability of UF. The cured binder was not steam flushed, but in water. This, in his opinion, changes the structure of the UF [16]. Binding it is possible to refer neurotoxicity of acrylamide to shortcomings of this method of increase in hydrolytic stability.

It has already been mentioned in this work, the best physical and mechanical properties of composite fibrous insulating boards from plant wastes at a drying temperature of 100 °C were obtained by adding ammonium sulfate as a curing agent, at a temperature of 170 °C, using ammonium chloride. This is consistent with the results of determining the degree of curing of the binder at the given temperatures. The coefficient of thermal conductivity of the boards 0.05 – 0.07 W/(m·K).

Ammonium sulfate (ammonium peroxodisulfate) is a highly active hardener. In the processes of board production, it allows a third to reduce the duration of pressing. This is due to the acceleration of the UF polycondensation reaction.

It is necessary to consider the features of persulphate of ammonium at temperature influence – when heated to 120 °C it decays with release of oxygen, forming pyrosulphate:

$$2(NH_4)_2S_2O_8 \rightarrow 2(NH_4)_2S_2O_7 + O_2.$$

This process is well illustrated by the curve of the extent of gelatinization of peroxodisulphate of ammonium at the temperature of 170 °C. The degree of curing of UF with the addition of persulphate does not exceed 96–98% due to the release of oxygen. When this begins the process of oxidative destruction of the binder. For these reasons, the physical and mechanical characteristics of boards made with the addition of ammonium persulfate with a drying mode of 170 ° C have low values.

Ammonium chloride has a thermal stability above 250 ° C, when it interacts with the formaldehyde of the binder, hemethylenetetramine and hydrogen chloride are formed:

$$4NH_4Cl + 6CH_2O \rightarrow 4HCl + (CH_2)_6N_4 + 6H_2O.$$

Due to the release of HCl, the pH of the binder decreases. In this case, cross-links are formed between the chains of the macromolecules of the UF oligomer. This is due to the binding of free methyl groups (bandwidth in the IR spectrum of 3090, 3026 and 2450 cm^{-1}) between themselves and with amide groups.

Urea ammonium nitrate provides the lowest values of the extent of hardening at the temperature of 100 °C and high values at the temperature of 170 °C. The temperatures of phase transition of nitrate of ammonium are 32-33 °C; 84.2 °C; 125.2 °C. Mechanism of decomposition of nitrate of ammonium can change depending on the temperature and structure of the composition. At the temperature above 110 °C nitrate of ammonium dissociates on NH_3 ammonia and HNO_3 nitric acid. Nitric acid interacts with free CH_2O formaldehyde of the binding, accelerating the hardening process.

Some part of nitric acid interacts with formaldehyde with the release of N_2 nitrogen and oxide of CO_2 carbon fabrics (IV). The urea of urea ammonium. NH_4NO_3–$(NH_2)_2CO$–H_2O nitrate is the weak basis. For this reason, in his presence, the curing rate of the binder slows down. Theoretically the urea of urea ammonium nitrate can react with free formaldehyde. However in acidic environment at small time of interaction only mono-connections will be formed of possible mono-metilol urea. It should also be borne in mind that in a strongly acidic environment (pH<3) the formed metilol urea at once are exposed to dehydration, giving the methyleneurea having amorphous structure and not participating in the process of hardening of the binder. All this is the reason that when urea ammonium nitrate is used as hardener at temperature of 170 °C less durable boards turn out, than when chloride ammonium is added.

The research showed that the type of additive in the urea-formaldehyde binder affects the physical and mechanical properties of composites made from flax and cotton waste. This is achieved by choosing an additive in a binder that ensures the maximum degree of curing of the polymer at a given temperature.

The coefficient of thermal conductivity of the material depends on the factors of production of the composite – the drying temperature, the proportion of the binder additive and the type of plant filler – flax/cotton.

The coefficient of thermal conductivity of composite boards is more affected by the mass fraction of the binder than the type of plant filler. The value of thermal conductivity for UF – 0.1–0.12 W/(m·K), for cotton – 0.05 W/(m·K), for flax – 0.04 W/(m·K). The difference in thermal conductivity of the filler is explained by the structure of discrete plant particles. In the elementary cotton fiber there is a large internal cavity (as opposed to flax fiber). Also, as noted by the authors, part of the flax particles has closed ends [27], and the presence of closed pores significantly affects the thermal conductivity of the material.

4. Conclusions

1. Thus, it is possible to increase the water resistance of a thermal-insulation board composite from waste of spinning of plant fibers and urea-formaldehyde binder due to increase in extent of hardening binding by the operating influence of technology factors of process of production of material.

2. For increase in hydrolytic stability at the choice of structure binding on the basis of the urea-formaldehyde binder for production of thermal-insulation board material from waste of spinning of plant fibers it is necessary to be guided by value of temperature parameter of process of drying of a composite.

3. The type of additive in urea-formaldehyde binder exerts impact on physical and mechanical indicators of heat-insulating composite boards from waste of spinning of a flax and cotton. This factor doesn't exert significant impact on coefficient of heat conductivity of material.

4. The best physical and mechanical indicators of composite fibrous thermal-insulation boards from the plant waste made at a temperature of drying of 100 °C are provided by additive as hardener of ammonium dust, and at a temperature of drying of 170 °C – additive of chloride ammonium.

References

1. Soldatov, D.A., Hozin, V.G. Teploizolyacionnye materialy na osnove solomy [Heat-insulating materials on the basis of straw]. News of the KSUAE. 2013. No. 1(23). Pp. 197–201. (rus)
2. Alentiev, A.Y., Yablokov, M.Yu. Svyazuyushchie dlya polimernyh kompozicionnyh materialov [Binders for polymeric composite materials]. Moscow, 2010. 69 p. (rus)
3. Askadsky, A.A., Popova, M.N., Kondrashenko, V.I. Fiziko-himiya polimernyh materialov i metody ih issledovaniya [Physical chemistry of polymeric materials and methods of their research]. Moscow, 2015. 408 p. (rus).
4. Makarov, V.P., Nedzelsky, I.A. Kompleksnoe svyazuyushchee dlya izgotovleniya plit iz bazal'tovoj vaty na osnove biopolimerov [Complex binder for the production of slabs of basalt wool on the basis of biopolymers]. Vestnik KRSU. 2012. Vol. 12. No. 6. Pp. 102–105.
5. Kanashov, S.S. Svyazuyushchie dlya proizvodstva teploizolyacionnyh materialov i izdelij [Binder for manufacturing heat-insulating materials and products] [Electronic resource] URL:http://center-science.ru/files/adhesive.pdf (date of reference: 10.11.2017). (rus)
6. Uglova, T.K., Novoselova, S.N., Khodakova, N.N., Tatarintseva, O.S. Svyazuyushchie dlya teploizolyacionnyh voloknistyh plit [Binders for insulating fiber board]. Polzunovskij vestnik. 2010. No. 4–1. Pp. 258–261. (rus).
7. Safin, R.G., Petrov, V.I., Ignat'eva, G.I., Stepanov, V.V. Halitov, R.A. Ispol'zovanie othodov lesozagotovok i derevoobrabotki dlya proizvodstva teploizolyacionnyh materialov [Use of waste timber and wood for production of heat-insulating materials]. News of higher educational institutions. Energy problems (KGEU). Kazan. 2012. No. 3–4. Pp. 94–100. (rus).

Литература

1. Солдатов Д.А., Хозин В.Г. Теплоизоляционные материалы на основе соломы // Известия КГАСУ. 2013. № 1(23). С. 197–201.
2. Алентьев А.Ю., Яблокова М.Ю. Связующие для полимерных композиционных материалов. М., 2010. 69 с.
3. Аскадский А.А., Попова М.Н., Кондращенко В.И. Физико-химия полимерных материалов и методы их исследования. М., 2015. 408 с.
4. Макаров В.П., Недзельский И.А. Комплексное связующее для изготовления плит из базальтовой ваты на основе биополимеров // Вестник КРСУ. 2012. Т. 12. № 6. С.102–105.
5. Канашов С.С. Связующие для производства теплоизоляционных материалов и изделий. [Электронный ресурс] URL:http://center-science.ru/files/adhesive.pdf (дата обращения 12.04.2018)
6. Углова Т.К., Новоселова С.Н., Ходакова Н.Н., Татаринцева О.С.. Связующие для теплоизоляционных волокнистых плит // Ползуновский вестник. 2010. № 4–1. С. 258–261.
7. Сафин Р.Г., Петров В.И., Игнатьева Г.И., Степанов В.В., Халитов Р.А. Использование отходов лесозаготовок и деревообработки для производства теплоизоляционных материалов // Известия высших учебных заведений. Проблемы энергетики (КГЭУ). Казань. 2012. № 3–4. С. 94–100.
8. Мубаракшина Л.Ф., Абдрахманова Л.А., Крадинова А.Е. Суперконцентраты для усиления строительных материалов на основе карбамидоформальдегидных смол // Известия КГАСУ. 2013. № 4. С. 240–245.
9. Halahmi I., Gross M., Iacobs L., Kadosh G. Strong durable low cost composite materials made from treated cellulose and plastic. Patent № 6863971. US6066680 B

8. Mubarakshina, L.F., Abdrahmanova, L.A., Kradinova, A.E. Masterbatches for strengthening building materials based on urea-formaldehyde resins. News of the KSUAE. 2013. No. 4. Pp. 240–245. (rus).
9. Halahmi, I., Gross, M., Iacobs, L., Kadosh, G. Strong durable low cost composite materials made from treated cellulose and plastic. Patent № 6863971. US6066680 B [Electronic resource] URL :http://www.google.tm/patents/US6066680 (date of reference: 10.11.2017).
10. Mantanis, G.I., Athanassiadou, E.Th., Barbu, M.C., Wijnendaele, K. Adhesive systems used in the European particleboard, MDF and OSB industries. Wood material science & engineering. 2017. No. 9. Pp. 1–13.
11. Dunky, M. Urea-formaldehyde (UF) adhesive resins for wood // International Journal of Adhesion & Adhesives. 1998. No. 18. Pp. 95–107.
12. Pizzi, A., Mittal, K.L. Handbook of Adhesive Technology. 2 edition Second. — Revised and Expanded. Marcel Dekker, Inc. 2003. 999 p.
13. Burdonov, A.E. Kineticheskie osobennosti vspenivaniya termoreaktivnyh polimerov pri poluchenii teploizolyacionnyh materialov v prisutstvii mineral'nogo napolnitelya [Kinetic features of foaming thermosetting polymers in the preparation of thermal insulation materials in the presence of mineral filler]. Magazine of Civil Engineering. 2014. No. 3(47). Pp. 9–16. (rus)
14. Varankina, G.S., Chubinsky, A.N. Formirovanie nizkotoksichnyh kleenyh drevesnyh materialov [The formation of low-toxic laminated wood materials]. SPb.:Spbgltu, 2014. 148 p. (rus).
15. Mamza, P.A.P., Ezeh, E.C., Gimba, E.C., Arthur, D.E. Comparative study of phenol formaldehyde and urea formaldehyde particleboards from wood waste for sustainable environment. International journal of scientific & technology research. 2014. Vol. 3. No. 9. Pp. 51–63.
16. Abdullah, Z.A., Park, B.-D. Hydrolytic stability of cured urea-formaldehyde resins modified by additives. Journal of Applied Polymer Science. 2009. No. 14. Pp. 1011–1017.
17. Sergienko, A.V., Yatsun, V.I. Vybor tipa svyazuyushchego dlya innovacionnogo teploizoliruyushchego drevesnogo materiala [Select the type of binders for thermal insulation innovative wood material]. Bulletin of science and education. 2015. No. 10(12). Pp.14–16. (rus)
18. Shishlov, O.F., Dozhdikov, S.A., Gluhih, V.V. Izuchenie vliyaniya vida napolnitelya na kinetiku otverzhdeniya kompozicionnyh materialov na osnove fenolkardanolformal'degidnyh novolachnyh smol [The influence of extender type on cure kinetics in composite materials based on fenol-kardanol-formaldegidtnovolac resins] Chemistry of vegetable raw materials. 2014. No. 4. Pp. 219–227. (rus)
19. Nuryawan, A., Risnasari, I., Sucipto, T., Herilswanto, A., Rosmala Dewi, R. Urea-formaldehyde resins: production, application, and testing // Innovation in polymer science and technology. 2016. Pp. 1–10.
20. Bell, R.J. Vvedenie v Fur'e-spektroskopiyu [Introduction to Fourier spectroscopy]. M: Mir, 1975. 380 p. (rus).
21. Leonovich, A.A., Sheloumov, A.V. Issledovanie prevrashchenij komponentov drevesnyh plit. 1. Termogravimetricheskoe izuchenie prevrashchenij karbamidoformal'degidnogo oligomera [The study of the transformations of the components of wood panels. 1. Thermogravimetric study of the transformations of urea-formaldehyde oligomer]. Khimiyarastitelnogosyrya. 2010. No. 2. Pp. 169–176. (rus).
22. Azarov, V.I., Burov, A.V., Obolenskaya, A.V. Himiya drevesiny i sinteticheskih polimerov [Chemistry of wood and synthetic polymers]. SPb.:Lan', 2010. 624 p. (rus).

[Электронный ресурс] URL: http://www.google.tm/patents/US6066680 (дата обращения: 12.04.2018).

10. Mantanis G.I., Athanassiadou E.Th., Barbu M.C., Wijnendaele K. Adhesive systems used in the European particleboard, MDF and OSB industries // Wood material science & engineering. 2017. № 9. Pp. 1–13.
11. Dunky M. Urea-formaldehyde (UF) adhesive resins for wood // International Journal of Adhesion & Adhesives. 1998. № 18. Pp. 95–107.
12. Pizzi A., Mittal K.L. Handbook of adhesive technology. 2 edition Second. Revised and Expanded. MarcelDekker, Inc. 2003. 999 p.
13. Бурдонов А.Е. Кинетические особенности вспенивания термореактивных полимеров при получении теплоизоляционных материалов в присутствии минерального наполнителя // Инженерно-строительный журнал. 2014. №3(47). С. 9–16.
14. Варанкина Г.С., Чубинский А.Н. Формирование низкотоксичных клееных древесных материалов. СПб.: СПбГЛТУ, 2014. 148 с.
15. Mamza P.A.P., Ezeh E.C., Gimba E.C., Arthur D.E. Comparative study of phenol formaldehyde and urea formaldehyde particleboards from wood waste for sustainable environment // International journal of scientific & technology research. 2014. Vol. 3. № 9. Pp. 51–63.
16. Abdullah Z.A., Park B.-D. Hydrolytic stability of cured urea-formaldehyde resins modified by additives // Journal of Applied Polymer Science. 2009. № 14. Pp. 1011–1017.
17. Сергиенко А.В., Яцун И.В. Выбор типа связующего для инновационного теплоизолирующего древесного материала // Вестник науки и образования. 2015. № 10(12). С. 14–16.
18. Шишлов О.Ф., Дождиков С.А., Глухих В.В. Изучение влияния вида наполнителя на кинетику отверждения композиционных материалов на основе фенолкарданолформальдегидных новолачных смол // Химия растительного сырья. 2014. № 4. С. 219–227.
19. Nuryawan A., Risnasari I., Sucipto T., Herilswanto A., Rosmala Dewi R. Urea-formaldehyde resins: production, application, and testing // Innovation in polymer science and technology. 2016. Pp. 1–10.
20. Белл Р.Дж. Введение в Фурье-спектроскопию. М: Мир, 1975. 380 с.
21. Леонович А.А., Шелоумов А.В. Исследование превращений компонентов древесных плит. Термогравиметрическое изучение превращений карбамидоформальдегидного олигомера // Химия растительного сырья. 2010. № 2. С. 169–176.
22. Азаров В.И., Буров А.В., Оболенская А.В. Химия древесины и синтетических полимеров. СПб.: Лань, 2010. 624 с.
23. Сусоева И.В., Вахнина Т.Н., Свиридов А.В. Химический состав и способ утилизации отходов производства хлопковых и льняных волокон // Химия растительного сырья. 2017. № 3. С. 211–220.
24. Браун Д., Шердрон Г., Керн В. Практическое руководство по синтезу и исследованию свойств полимеров. Пер. снемец. М: Химия, 1978. 256 с.
25. Вирпша З., Бжезиньский Я. Аминопласты. Пер. с пол. М: Химия, 1973. 345 с.
26. Вильнав Ж.-Ж. Клеевые соединения. Пер. с франц. М: Техносфера, 2007. 384 с.
27. Сусоева И.В., Вахнина Т.Н., Титунин А.А., Асаткина Я.А. Показатели композитов из растительного сырья при изменениях температуры и влажности // Инженерно-строительный журнал. 2017. № 3(71). С. 39–50.

Вахнина Т.Н., Сусоева И.В., Титунин А.А. Теплоизоляционные плиты из волокнистых растительных отходов и карбамидоформальдегидного связующего // Инженерно-строительный журнал. 2018. № 7(83). С. 136–147.

23. Susoeva, I.V. Vakhnina, T.N., Sviridov, A.V. Himicheskij sostav i sposob utilizacii othodov proizvodstva hlopkovyh i l'nyanyh volokon [Chemical composition and way of recycling productions of cotton and linen fibers] Khimiyarastitelnogosyrya. 2017. No. 3. P. 211–220. (rus).
24. Braun, D., Sherdron, G., Kern, V. Prakticheskoe rukovodstvo po sintezu i issledovaniyu svojstv polimerov [Practical guidance on synthesis and a research of properties of polymers]. Moscow: Himiya, 1978. 256 p. (rus)
25. Virpsha, Z., Bzhezin'skij, Y.A. Aminoplasty [Aminoplastics]. Moscow: Himiya, 1973. 345 p. (rus).
26. Vil'nav, Zh.-Zh. Kleevye soedineniya [Gluejoint]. Moscow: Tekhnosfera, 2007. 384 p. (rus).
27. Susoeva, I.V. Vakhnina, T.N., Titunin, A.A., Asatkina, J.A. The performance of composites from vegetable raw materials with changes in temperature and humidity. Magazine of Civil Engineering. 2017. No. 3(71). Pp. 39–50.

Tatiana Vahnina,
+7(960)748-64-71; t_vachnina@mail.ru

Irina Susoeva,*
+7(915)903-86-70; i.susoeva@yandex.ru

Andrey Titunin,
+7(910)804-55-75; titunin62@mail.ru

Татьяна Николаевна Вахнина,
+7(960)748-64-71;
эл. почта: t_vachnina@mail.ru

Ирина Вячеславовна Сусоева,*
+7(915)903-86-70;
эл. почта: i.susoeva@yandex.ru

Андрей Александрович Титунин,
+7(910)804-55-75; эл. почта: titunin62@mail.ru

Vahnina, T.N., Susoeva, I.V., Titunin, A.A. Thermal-insulation boards from fibrous plant wastes and urea-formaldehyde binder. Magazine of Civil Engineering. 2018. 83(7). Pp. 136–147. doi: 10.18720/MCE.83.13.

doi: 10.18720/MCE.83.14

Water permeability of the polymer screen with a system of slits of hydraulic structures

Водопроницаемость полимерного экрана с системой щелей гидротехнических сооружений

Yu.M. Kosichenko,
O.A. Baev*,
Russian Scientific Research Institute of Land Improvement Problems, Novocherkassk, Rostov region, Russian Federation

Д-р техн. наук, главный научный сотрудник Ю.М. Косиченко,
канд. техн. наук, старший научный сотрудник О.А. Баев*,
Российский научно-исследовательский институт проблем мелиорации, г. Новочеркасск, Ростовская область, Россия

Key words: water permeability; polymer screen; filtration theory; conformal mapping; velocity hodograph; irrigation

Ключевые слова: водопроницаемость; полимерный экран; теория фильтрации; конформные отображения; годограф скорости, ирригация

Abstract. The calculation of water permeability through a system of defects (long narrow slits in the junctions) in the screen is considered based on the filtration model. Its structural layout and description of the model main elements are given. The solution is carried out for the plane formulation of the problem by the methods of the filtration theory using the method of conformal mappings and the velocity hodograph method. A distinctive feature is the study of free filtration through a system of screen slits (the isolated standard fragment with a single defect), characterized by a pressure movement of the filtration flow in the protective layer and pressure/pressure-free movement at the bottom of the screen, taking into account the mutual influence of the slits on each other. We obtained the calculated dependences for the determination of the specific filtration flow through the screen slit, as well as the total flow through the system of slits and the averaged screen filtration factor, the results of the calculations are compared to the known formulas for the defect system. For practical use, a table of averaged screen filtration factors and a graph of the change in the reduced flow rate through the screen, considering and not considering the influence of the underlying base are made.

Аннотация. Рассматривается расчет водопроницаемости через систему дефектов (узких протяженных щелей в местах стыков) в экране на основе фильтрационной модели. Приводится ее структурная схема и описание основных элементов модели. Решение осуществляется для плоской постановки задачи методами теории фильтрации с использованием метода конформных отображений и способа годографа скорости. Отличительной особенностью является изучение свободной фильтрации через систему щелей экрана (выделенный стандартный фрагмент с единичным дефектом), характеризующиеся напорным движением фильтрационного потока в защитном слое и напорно-безнапорным движением в основании экрана с учетом взаимовлияния щелей друг на друга. Получены расчетные зависимости для определения удельного фильтрационного расхода через щель экрана, а также суммарного расхода через систему щелей и осредненного коэффициента фильтрации экрана, результаты расчетов сопоставлены с известными формулами для системы дефектов. Для практического использования составлена таблица осредненных коэффициентов фильтрации экрана и график изменения приведенного расхода через экран с учетом влияния подстилающего основания и без его учета.

1. Introduction

In hydraulic engineering construction, impervious screens of polymeric materials, geomembranes, and geocomposites are becoming increasingly used as more efficient and durable [1]. Their averaged filtration factor is 10^{-8}–10^{-10} cm/s, which is two to four orders of magnitude lower than for film screens, and the predicted service life is 50–100 years, which is 2–3 times longer than one of film screens.

The relevance of the use of geosynthetic materials in hydraulic engineering is also confirmed by B. E. Vedeneev Institute of VNIIG [2–4], SpbSTU [5, 6] and other authors [7, 9].

Косиченко Ю.М., Баев О.А. Водопроницаемость полимерного экрана с системой щелей гидротехнических сооружений // Инженерно-строительный журнал. 2018. № 7(83). С. 148–164.

The normative document [10] regulates the use of polymeric materials for anti-filtration devices of hydraulic structures. According to paragraph 5.50 [10], they can be used for dams of III and IV classes, and with proper justification for I and II class dams up to 60 m high.

European experience in the use of geosynthetic materials for anti-filtration screens of waste storage facilities is considered in the work of A.V. Pryamitsky and Yu. Shlee [11]. Here, the requirements of the American Environmental Protection Agency, the European Directive and the German Geotechnical Society for the construction of waste storage facilities are analyzed.

According to the authoritative experts on polymer screens [12], polymeric (film and sheet) geomembrane coatings can not be considered as waterproof, because through various defects and damages, filtration leaks occur that are formed during construction and operation.

At first, the problems of water permeability of polymer screens in the hydromechanical installation were raised and solved by V.P. Nedriga [13], and then by Yu.M. Kosichenko and O.A. Baev [13–16], A.V. Ishchenko [17]. Similar problems were considered by P.Ya. Polubarinova-Kochina and N.E. Zhukovsky [18] for a single drain, by V.V. Vedernikov [18, 19] for a system of drains, by S.F. Averyanov [20] for a channel with a finite depth of occurrence of a watertight stratum. In [15, 16] the main special functions are presented, which are used in the theory of filtration. In [21] methods of calculating the theory of analytic functions are given, and in [22] the main special functions used in the theory of filtration are presented.

The authors of [13] give the well-known approximate formula of V.P. Nedrigi (1976), which he obtained as a result of the solution of the problem of permeability for sheet pile walls, and used in connection with film screens with continuous gaps. However, the formula obtained is approximate, since the solution of such a problem is obtained in a simplified formulation, where the filtration region is an infinite half-strip. It was shown in [13] that V.P. Nedrigi's formula gives a significant discrepancy (from 30 to 50 %) with more exact dependencies.

The authors of this article considered the solution of the problem of axisymmetric filtration through small holes [14–16], and work [13] analyzes the main methods for calculating water permeability of polymer impervious screens for the first time. At the same time, special attention is paid to theoretical methods based on rigorous analytical solutions by methods of the theory of functions of a complex variable, as giving more accurate computational formulas with physically correct results. A hydraulic model to calculate water permeability of large channel liners is presented in [16].

Among the close problems of the theory of filtration, we consider the solution V.V. Vedernikov [18, 19] obtained for the drain system and it can be applied to the problems of water permeability of screens. The solution of this problem is carried out in a pressure installation on the basis of the application of Schwarz-Christoffel integral and elliptic integrals. However, the calculated formulas are rather cumbersome and do not allow us to calculate the filtration features with small parameters. Therefore, for their application in calculating the water permeability of the screen slits, it is necessary to reduce such dependences to an approximate form with the possibility of calculation with small parameters.

Methods for calculating the permeability of geomembrane screens with defects are widespread abroad, see works by J.P. Giroud, R. Bonaparte, K. Badu-Tweneboah [22–28], they are based on experimental and theoretical dependences of degree type, using empirical factors based on field research data reflecting the quality of the contact between geomembrane and base soil. The works by R.K. Rowe, N. Touze-Foltz and C. Duquennoi [29–31] present rather cumbersome theoretical dependences for computations of heads and flow rates through round and rectangular defects in geomembranes using special Bessel functions, which significantly complicates their calculations.

As shown below, when comparing the calculation results for the various formulas in Table 1, it was found that the dependences of J.P. Giroud on filtration through defects in geomembrane are considerably overestimated. In the last works of authors [32, 33] the review of efficiency of geosynthetics for environmental protection and methods of numerical modeling of geosynthetic systems is presented. The works [34–38] is devoted to the evaluation of the performance of underground dams and self-healing cracks of the polymer screen, as well as to the study of other anti-filtration devices.

As the main types of damage in the geomembrane, defects in joints in the form of narrow, long slits and round holes in the form of punctures are usually considered [8, 14, 23].

In present practice, we have to see not only individual defects in polymeric impervious screens, but also several damages in the form of long narrow slits that are formed at the joints of the cloths due to their poor connection. Such damage, located at an equal distance from each other, is called a system of slits.

They are especially common where the jointing of geomembranes or films is performed by welding with extruders. Due to poor quality welding, defects such as low current welding or burned welding of joints with the formation of the through slits can be observed.

The aim of the study is to develop a filtration model of water permeability for a polymer screen of broken continuity with a system of targets.

Objectives of the study:

- to obtain an analytical solution of a polymer screen water permeability with a system of slits by the methods of filtration theory, based on the methods of the theory of functions of a complex variable;
- to find the calculated dependencies to determine the main features of water permeability;
- to compare the obtained dependencies with ones of other authors and evaluate their applicability for practical calculations;
- for the purpose of practical use of the results of calculations based on the developed filtration model, to build a graph of the change in the reduced filtration flow through the slit of a polymer screen and make a table of the average screen filtration factor, depending on the parameters of the slits system.

Thus, the subject of the study is a filtration model of water permeability of a polymer screen of external continuity with a system of slits.

2. Methods

2.1. The filtration model description

To study the water permeability of a polymer screen with a slit system, an analytical method was chosen on the filtration model, which is most often used in the theory of filtration in the steady motion of the filtration flow [18]. In cases of unsteady, as well as spatial (three-dimensional and axisymmetric) motion of the filtration flow, it is advisable to use numerical calculation models, as, for example, in [33, 39].

Figure 1 shows a block diagram of the filtration model of the water permeability of a polymer screen with broken continuity, developed by the authors of this paper, in the form of a system of extended slits.

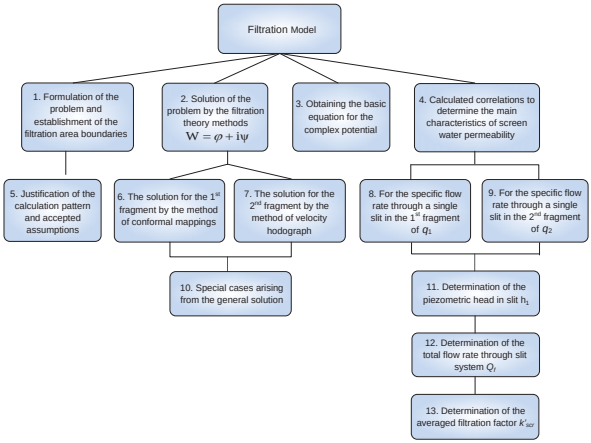

Figure 1. Structural diagram of the filtration model of a polymer screen water permeability through a system of slits

This model includes the following main structural blocks: block 1 – formulation of the problem of water permeability through the system of screen slits and the establishment of boundary conditions in the physical filtering area, which consists of sub-block 5 to justify the calculation pattern and accepted assumptions; block 2 – the solution of the problem with the methods of the filtration theory, which is divided into sub-blocks 6 and 7 in accordance with the solution of the general problem for I and II fragments with

the method of conformal mappings and velocity hodograph; block 3 – obtaining the basic equation for the complex potential; block 4 – calculated dependences for determining the main characteristics of water permeability of the screen slits, consisting of sub-blocks 8, 9, 11–13, where specific flow rates are first determined per a single gap in I and II fragment (q_1) and (q_2), and then the piezometric head in the slit (h_1) is determined, the total flow through the slits system (Q_f) and the averaged filtration factor (k'_{scr}). Piezometric head (h_1) can be calculated by the iteration method (successive approximation) or can be determined directly with the formulas. In sub-block 10 there are particular cases arising from the general solution. Thus, for example, when the underlying base is composed of more permeable soils at $k_2 > 10k_1$, then it is neglected in the calculations.

More details of building the filtration model are considered further.

2.2. Research Methodology

The methodology for studying the water permeability of polymer screen slits system in the filtration model is based on the hydromechanical approach to the solution of the problem widely used in the theory of filtration [12, 13]. The method of conformal mappings and the velocity hodograph method are used.

The calculation pattern of the filtration model (Figure 2) includes a system of screen slits of small dimensions located at a distance of (l), protective layer with a thickness of (δ_0) and the underlying base of unlimited depth, in which sets of filtering areas in the protective layer are formed – when the filtration flow moves from the channel or a reservoir to each slit, in the underlying base - when the filtration flow moves from each slit to the ground base to infinity with their interaction.

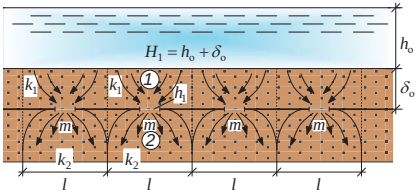

Figure 2. Calculation scheme of the polymer screen slit system

A feature of water permeability here is filtration through each slit with the formation of an independent filtration flow. Therefore, to solve this problem, it is advisable to consider a separate fragment of the filtration region, with its conventional release along the boundary line of the current in the protective layer on the right and on the left (fragment 1), and in the underlying base (where the flow movement will be forced/unforced) considering the interaction with the adjacent area in the general line of current (fragment 2), the velocity of the filtration flow is assumed to be infinite.

In solving this problem, we will make the following assumptions:

- the movement of the filtration flow through the slit is considered to be steady and according to the Darcy's law (with laminar conditions);
- the soil of the protective layer and the base of the screen is assumed to be homogeneous with the filtration factors, respectively, k_1 and k_2;
- the thickness of the polymer screen is neglected in view of its smallness in comparison with the thickness of the protective layer;
- the screen has a certain flexibility, in connection with which it fits snugly to the underlying base;
- capillary flow spreading in the base is accounted by the height of the soil capillary vacuum (H_c, m).

To solve the task in hydromechanical formulation, we shall separately consider the 1st fragment in the protective layer of the soil, and then the 2nd fragment in the underlying soil layer, while establishing a connection between the fragments at the slit boundary with the help of an unknown parameter (h_1), representing the piezometric head in the slit (Figure 1).

Figure 3 shows the pattern of conformal mappings for the 1st fragment of the filtration area.

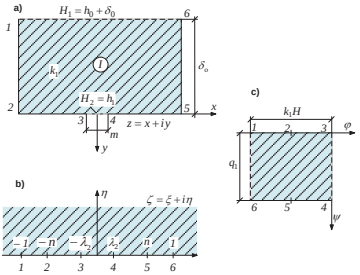

Figure 3. A pattern of conformal mappings for the 1st fragment of the filtration area: a) the filtration area *z*; b) an auxiliary semiplane ζ ; c) the region of the complex potential *W*

The physical area (Figure 3, a) is a rectangle with permeable boundaries 1-6 and 3-4, where the heads, respectively, are set as $H_1 = h_0 + \delta_0$ and $H_2 = h_1$. The impenetrable boundaries are lines 1-2-3 and 6-5-4, which are boundary lines of the current. Within the filtration range of 1-2-3-4-5-6, the flow will be purely forced, which occurs under the action of pressure $H = H_1 - H_2 = h_0 + \delta_0 - h_1$, with h_0 being water depth, m; δ_0 – the thickness of the protective layer, m; h_1 – piezometric head in the screen slit, m.

2.3. A solution by the method of conformal mappings

Now we will consider the solution for fragment I by means of conformal mappings [18, 19, 21].

We will map the polygon of the real filtration region to the upper semiplane (Figure 3, a, b) using the Schwartz-Christoffel integral:

$$z = A\int_0^{\zeta} (\zeta^2 - 1)^{-1/2} \cdot (\zeta^2 - n^2)^{-1/2} \cdot d\zeta + B = A\int_0^{\zeta} \frac{d\zeta}{\sqrt{(\zeta^2 - 1)\cdot(\zeta^2 - n^2)}} + B = \\ = A\lambda\int_0^{\zeta} \frac{d\zeta}{\sqrt{(1-\zeta^2)\cdot(1-\lambda^2\zeta^2)}} + B, \quad (1)$$

where $\lambda = \frac{1}{n} > 1$.

The resulting formula (1) is an elliptic integral of the first kind with λ modulus. Since in equation (1) $\lambda_1 > 1$, we make a change of variables, assuming:

$$\zeta = \frac{t}{\lambda},\ d\zeta = \frac{1}{\lambda} dt.$$

Then equation (1) can be written in the following form:

$$z = A\int_0^{t} \frac{dt}{\sqrt{\left(1 - \frac{t^2}{\lambda^2}\right)\cdot\left(1 - t^2\right)}} + B = AF\left(t, \lambda_1\right) + B, \quad (2)$$

where $\lambda_1 = \frac{1}{\lambda} < 1$ – being the elliptic integral modulus; $F\left(t, \lambda_1\right)$ is an elliptic integral of the first kind with λ_1 modulus.

From the correspondence of points 2 and 5 in the equation (2), we will find the constants A and B:

$$A = \frac{l}{2K(\lambda_1)};\ B = 0.$$

From the correspondence of point 1 we will have:

$$A = \frac{\delta_o}{K'(\lambda_1)} = \frac{l}{2K(\lambda_1)},$$

or:

$$\frac{l}{\delta_o} = \frac{K(\lambda_1)}{K'(\lambda_1)}, \quad (3)$$

where $K(\lambda_1)$, $K'(\lambda_1)$ are full elliptic integral of the fist kind, respectively, with modulus λ_1 and additional modulus $\lambda_1'\sqrt{1-\lambda_1^2}$.

The elliptic integral modulus in equation (2) is determined from correlation (3). Putting the identified constants (*A* and *B*) to equation (2), we will have:

$$z = \frac{l}{2K(\lambda_1)} F(t, \lambda_1), \quad (4)$$

or, replacing $t = \lambda\zeta$:

$$z = \frac{l}{2K(\lambda_1)} F(\lambda\zeta, \lambda_1). \quad (5)$$

Hence, from (5) the inverse function is expressed through elliptic sine:

$$z = \lambda_1 sn\left(\frac{mK(\lambda_1)}{l}; \lambda_1\right). \quad (6)$$

From the correlation of point 4 ($z = m/2$, $\zeta = \lambda_2$) and formula (6) we will determine the unknown parameter (λ_2):

$$\lambda_2 = \lambda_1 sn\left(\frac{mK(\lambda_1)}{l}; \lambda_1\right). \quad (7)$$

Mapping semiplane ζ to the region of complex potential W (see Figure 2.3, b, c) we will find:

$$W = C\int_0^{\zeta} (\zeta^2 - 1)^{-1/2} \cdot (\zeta^2 - \lambda_2^2)^{-1/2} d\zeta + D = \frac{C}{\lambda_2}\int_0^{\zeta} \frac{d\zeta}{\sqrt{(1-\zeta^2)\cdot(1-\lambda_3^2\zeta^2)}} + D, \quad (8)$$

where $\lambda_3 = \frac{1}{\lambda_2} > 1$.

As $\lambda_3 > 1$ we will perform the replacement $\zeta = \frac{\tau}{\lambda_3} = \tau\lambda_2$, $d\zeta = \lambda_2 d\tau$, then equation (8) will look as follows:

$$W = C\int_0^{\tau} \frac{d\tau}{\sqrt{(1-\tau^2)\cdot(1-\lambda_2^2\tau^2)}} + D = CF(\tau, \lambda_2) + D = CF\left(\frac{1}{\lambda_2}\tau, \lambda_2\right) + D. \quad (9)$$

From the correlation of points 4, 6 and equation (9) we will find the constants of Schwarz-Christoffel integral:

$$C = -i\frac{k_1 H}{K'(\lambda_2)};\ D = i\frac{k_1 H}{K'(\lambda_2)} K(\lambda_2) - k_1 H. \quad (10)$$

Putting correlations (2.10) into equation (2.9), we will obtain a complex potential that looks as follows:

$$W = -i\frac{k_1 H}{K'(\lambda_2)} \cdot F\left(\tau, \lambda_2\right) + i\frac{k_1 H}{K'(\lambda_2)} K(\lambda_2) - k_1 H . \quad (11)$$

From formula (11) we will find specific filtration rate at section 1–6:

$$W = -k_1 H + i\psi ,\ \psi = q_{1-6},\ \zeta = \xi ,\ z = x .$$

Then:

$$q_{1-6} = \frac{k_1 H}{K'(\lambda_2)} \left\{ K(\lambda_2) - F\left(\tau, \lambda_2\right) \right\}, \quad (12)$$

where $\tau = \frac{1}{\lambda_2}\xi$,. $\zeta = \lambda_1 sn(U_1,\ \lambda_1)$.

We will determine the specific rate through a screen slit by putting $\xi = \lambda_2$, $q = q_1$, $F\left(\tau, \lambda_2\right) = F\left(-1, \lambda_2\right) = -K\left(\lambda_2\right)$ into formula (12):

$$q_1 = \frac{2k_1 H}{K'(\lambda_2)} K(\lambda_2), \quad (13)$$

or:

$$q_1 = \frac{2k_1 H}{K(\lambda_2')} K(\lambda_2), \quad (14)$$

where $\lambda_2 = \lambda_1 sn\left(\frac{mK(\lambda_1)}{l}, \lambda_1\right)$; $\frac{K(\lambda_1)}{K'(\lambda_1)} = \frac{l}{2\delta_o} \to \lambda_1$ [13]; $H = h_o + \delta_o - h_1$ – being head at the screen; $\lambda_2' = \sqrt{1-\lambda_2^2}$ – being a complementary elliptic integral modulus.

At a small value of the screen slit width (m) from a geomembrane, close to zero $(m \to 0)$, which is often the case in practice, the formula for the specific flow rate through the screen slit (14) (considering approximations [22, 40] $K\left(\lambda_2\right) \approx \frac{\pi}{2}$, $K\left(\lambda_2'\right) \approx \ln\frac{4}{\lambda_2}$) will look as follows:

$$q_1 = \frac{\pi k_1 \left(h_o + \delta_o - h_1\right)}{\ln\left(4/\lambda_2\right)}, \quad (15)$$

where $\lambda_2 = \lambda_1 K\left(\lambda_1\right)\frac{m}{l}$.

With $\delta_0 / l < 1$, when the elliptic integral modulus $\lambda_1 \to 1.0$, the equation can be written in the following way: $K\left(\lambda_2\right) \approx \ln\left(4/\lambda_1'\right)$, $K\left(\lambda_1'\right) \approx \frac{\pi}{2}$.

Then the dependence for modulus λ_2 (7), considering the correlations (3) and the degeneracy of elliptic functions into hyperbolic functions [40], takes the following form:

$$\lambda_2 = th\left(\pi m / 4\delta_o\right). \quad (16)$$

Substituting (16) in (15), we will find the approximate formula for flow rate through the screen slit:

$$q_1 = \frac{\pi k_1 \left(h_o + \delta_o - h_1\right)}{\ln[4cth\left(\pi m / 4\delta_o\right)]}. \quad (17)$$

This formula is applicable at $m / l \le 0.01$.

Косиченко Ю.М., Баев О.А. Водопроницаемость полимерного экрана с системой щелей гидротехнических сооружений // Инженерно-строительный журнал. 2018. № 7(83). С. 148–164.

Under condition that $m/\delta_0 < 0.25$ formula (17) is simplified and expressed in terms of elementary logarithmic functions:

$$q_1 = \frac{\pi k_1 (h_o + \delta_o - h_1)}{\ln(16\delta_o / \pi m)}. \quad (18)$$

In the extreme event, when $m = l$, from equations (3) and (7) we have:

$$\lambda_2 = \lambda_1 \lim_{m \to l} sn\left\{\frac{mK(\lambda_1)}{l}, \lambda_1\right\} = \lambda_1 sn\{K(\lambda_1), \lambda_1\} = \lambda_1.$$

Then the specific filtration flow rate through the protective layer of soil (with no screen) from (2.14) can be written as:

$$q_1 = 2K_1 H \frac{K(\lambda_1)}{K(\lambda_1')}.$$

From this, according to (3), we will find $q_1 = k_1 l \frac{H}{\delta_o}$, which completely corresponds to Darcy's formula [12], if we take (l) as flow area, and $I = H/\delta_o$ as pressure gradient.

Thus, we can assume that the resulting formula of the specific filtration rate through the screen slit (14) gives correct results, and therefore it has a physically correct structure, which is confirmed by the classical Darcy's law in the limiting case, which is fundamental for filtration problems.

With $\delta_0 / l > 1.0$, when the elliptic integral modulus $\lambda_1 \to 0$:

$$K(\lambda_1) \approx \frac{\pi}{2};\ K(\lambda_1) \approx \ln(4/\lambda_1).$$

Taking into account the last correlations and the degeneracy of the elliptic sine into the trigonometric sine (with $\lambda_1 = 0$), formula (7) gives us this:

$$\lambda_2 = \lambda_1 \sin(\pi m / 2l). \quad (19)$$

Modulus (λ_1) from (2.3) can also be expressed by an exponential function:

$$\lambda_1 = 4\exp(-\pi\delta_o / l). \quad (20)$$

Then the screen slit filtration flow formula from (15) looks like:

$$q_1 = \frac{\pi k_1 (h_o + \delta_o - h_1)}{\ln\left(\exp\frac{\pi\delta_o}{l} \Big/ \sin\frac{\pi m}{2l}\right)}. \quad (21)$$

Using the reciprocal representations of the exponential and logarithmic functions for large values of the arguments [22, 40], we will write the correspondence (21) as follows:

$$q_1 = \frac{\pi k_1 (h_o + \delta_o - h_1)}{Arsh\left(ch\frac{\pi\delta_o}{l} \Big/ \sin\frac{\pi m}{2l}\right)}. \quad (22)$$

Now let us find the main indicator of the screen water permeability – the averaged filtration factor with a protective layer, using the formula [13]:

$$k'_{scr} = \frac{Q_f \cdot \delta_o}{(h_o + \delta_o) \cdot F_o}, \quad (23)$$

where $Q_f = \sum_{i=1}^{n} (q_1 \cdot \bar{l}_s)$ – being total flow through a sealed screen with a slits system in the area F_o.

Putting formula (14) in (23), we obtain the most general and exact correspondence to determine the averaged screen filtration factor with a slits system:

$$k'_{scr} = \frac{2k_1 \cdot \delta_o \cdot K(\lambda_2) \cdot \bar{l}_s \cdot n}{F_o \cdot K(\lambda'_2)}, \quad (24)$$

where k_1 – being the filtration factor of the screen protective layer, m/day; $\bar{l}_s$ – the average statistical length of the screen slit, m; δ_o – protective layer thickness, m; n – the number of geomembrane screen slits, pcs.; F_o – screen area, m².

From correlation (24) and taking into account the approximated formula (18), we find the averaged screen filtration factor with a slits system without taking into account the underlying base:

$$k'_{scr} = \pi k_1 \frac{\delta_o \cdot \bar{l}_s \cdot n}{F_o \cdot \ln(16\delta_o / \pi m)}. \quad (25)$$

The obtained dependence (25) to determine screen water permeability index (k'_{scr}) is a simplified and approximated one, which can be used under condition $m/\delta_0 < 0.25$.

The averaged filtration screen factor, taking into account the influence of the underlying substrate permeability will be found from (22) as follows:

$$k'_{scr} = \frac{\pi k_1 \delta_0 (h_0 + \delta_0 - h_1) \cdot \bar{l}_s \cdot n}{F_o Arsh(ch\frac{\pi\delta_0}{l} / \sin\frac{\pi m}{2l} \cdot (h_0 + \delta_0)}. \quad (26)$$

2.4. The solution by the velocity hodograph method

Now let us consider the solution for fragment II in the screen underlying base, where forced/unforced filtration is observed, and when the slits are located closely to one another their mutual influence will occur (Figure 2).

Figure 4 shows the calculated pattern of half the filtration region fragment (a) and the sequence of conformal mappings onto the region of the complex potential (b-e). The surface curve (Figure 4, a) is characterized by a point of inflection (a).

The solution of this problem is carried out by the velocity hodograph method and the conformal mapping method [18]. The presence of a point of inflection on the surface curve is reflected in the velocity hodograph region by a double pass of a part of the circumference (Figure 4, b). Accordingly, the inversion of the complex velocity hodograph has the form shown in Figure 4, d.

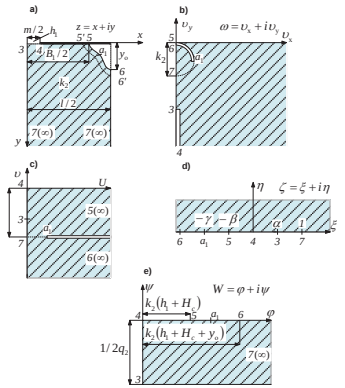

Figure 4. A pattern of conformal mappings for the 2nd fragment of the filtration area: a) a half of the filtration area *z*; b) velocity hodograph ω; c) velocity inversion region $\bar{\omega}$; d) an auxiliary semi-plane ζ; e) the region of the complex potential *W*

Косиченко Ю.М., Баев О.А. Водопроницаемость полимерного экрана с системой щелей гидротехнических сооружений // Инженерно-строительный журнал. 2018. № 7(83). С. 148–164.

The mapping of the inversion region of velocity hodograph ($\overline{\omega}$) on a semi-plane (Figure 4, c, d) is performed by Schwarz-Christoffel formula [18, 21, 22]:

$$\overline{\omega} = C\int_0^{\zeta} \frac{\zeta+\gamma}{(\zeta+\beta)\cdot\sqrt{\zeta}}\cdot d\zeta + D. \quad (27)$$

From there, after *C* and *D* constants are determined from equation (27) in section 4-3-7(∞) we obtain this:

$$\overline{\omega} = -\frac{2i}{\pi k_2}\cdot\left[\frac{\sqrt{\zeta\beta}}{\gamma-\beta} + arctg\sqrt{\frac{\zeta}{\beta}}\right]. \quad (28)$$

Mapping the region of the complex potential *W* on the semi-plane ζ (Figure 4, d, e), we will have:

- in section 4-5-6:

$$W = \frac{q_2}{2\pi} Arch\frac{\alpha-\zeta(2-\alpha)}{\alpha(1-\zeta)}; \quad (29)$$

- in section 3-4:

$$W = -\frac{q_2}{2\pi} i\arccos\frac{\alpha-\zeta(2-\alpha)}{\alpha(1-\zeta)}; \quad (30)$$

where q_2 – being specific filtration rate through fragment 2 slit.

Applying the obtained correlations (29) and (30) to formula (31):

$$\overline{\omega} = \frac{dz}{dW} = \frac{1}{\upsilon_x - i\upsilon_y}, \quad (31)$$

we will find:

- in section 4-5:

$$z = \frac{iq_2}{\pi^2 k_2}\int_0^{\zeta}\left[\frac{\sqrt{-\beta\zeta}}{\gamma-\beta} + Arth\sqrt{\frac{-\zeta}{\beta}}\right]\cdot\frac{(1-\alpha)d\zeta}{\sqrt{\zeta(1-\alpha)\cdot(d-\zeta)}(1-\zeta)} + \frac{m}{2}; \quad (32)$$

- in section 5-6:

$$z = \frac{iq_2}{\pi^2 k_2}\int_{-\beta}^{\zeta}\left[\frac{\sqrt{\beta\zeta}}{\gamma-\beta} + Arcrc\sqrt{\frac{-\zeta}{\beta}} - \frac{\pi}{2}i\right]\cdot\frac{(1-\alpha)d\zeta}{\sqrt{\zeta(1-\alpha)\cdot(d-\zeta)}(1-\zeta)} + \frac{B_1}{2}, \quad (33)$$

where B_1 – being the width of the filtration flow rate spreading under the screen; k_2 – the base soil filtration factor.

From (32) and (33), omitting the intermediate transformations, we define the unknown coordinates of points 5 and 6:

$$B_1 = \frac{4q_2}{\pi^2 k_2}\left[\frac{\sqrt{\beta}}{\gamma-\beta}\left(arctg\sqrt{\frac{\alpha-\beta}{1-\alpha}} - arctg\sqrt{\frac{\alpha}{1-\alpha}}\right) + \frac{1}{\sqrt{1-\alpha}}\int_0^{\sqrt{\beta}}\frac{Arth\frac{t}{\sqrt{\beta}}dt}{(1+t^2)\sqrt{\beta+t^2}}\right] + m; \quad (34)$$

$$y_o = \frac{q_2\sqrt{1-\alpha}}{\pi k_2}\left[Arch\frac{1}{\sqrt{\alpha}} - Arch\sqrt{\frac{\beta}{\alpha(1-\beta)}}\right]. \quad (35)$$

The specific filtration rate through fragment 2 slit will be found, putting the coordinates of point 5 [$\zeta = -\beta; W = k_2(h_1 + H_c)$] into equation (29):

$$q_2 = \frac{2\pi k_2 (h_1 + H_c)}{Arch\left[\frac{\alpha + \beta(2-\alpha)}{\alpha(1+\beta)}\right]}, \quad (36)$$

where h_1 – being piezometric head in the slit; H_c – base soil capillary vacuum.

Parameters α and β are determined from the simultaneous equations:

$$\frac{\pi_2 m k_2}{4q_2} = arctg\sqrt{\beta}\arcsin\sqrt{\alpha} + \frac{1}{\sqrt{1-\alpha}}\int\limits_{arctg\sqrt{\beta}}^{\pi/2} \frac{arctg\left(\sqrt{\alpha/\beta}\sin\varphi\right)d\varphi}{1-\alpha^2\sin^2\varphi}; \quad (37)$$

$$\frac{\pi_2 (l-m) k_2}{4q_2} - arctg\sqrt{\beta}\arccos\sqrt{\alpha} + \frac{1}{\sqrt{1-\alpha}}\left[\int\limits_0^{\sqrt{\beta}} \frac{Arth\left(t/\sqrt{\beta}\right)dt}{(1+t^2)\sqrt{\alpha+t^2}} + \int\limits_{arctg\sqrt{\beta}}^{\pi/2} \frac{Arctg\left(tg\varphi/\sqrt{\beta}\right)d\varphi}{\sqrt{\alpha+tg^2\varphi}}\right]. \quad (38)$$

In a special case, when the forced/unforced flow mode of motion changes into forced flow and the point 5 coincides with the point 6, we will have $\beta \to \gamma \to \infty$. Putting coordinates of point 7 ($\overline{\omega} = -i/k_2$; $\zeta = 1$), into equation (2.28) after simple transformations, we obtain $arctg\sqrt{\beta} = \pi/2$.

Then the simultaneous equations (37) and (38) will look as follows:

$$\frac{\pi_2 m k_2}{4q_2} = \frac{\pi}{2}\arcsin\sqrt{\alpha}; \quad (39)$$

$$\frac{\pi_2 (l-m) k_2}{4q_2} = \frac{\pi}{2}\arccos\sqrt{\alpha}. \quad (40)$$

Solving equations (39) and (40) jointly, we will find the filtration flow rate from the screen slit to infinity:

$$q_2 = k_2 l, \quad (41)$$

where l – being the width of the considered fragment of the filtration area.

A similar expression (41) is given by P.Ya. Polubarinova-Kochina in her work [18] for filtration from a channel of shallow depth to infinity, which confirms the validity of the theoretical solution obtained by the authors.

Thus, the authors obtained exact solutions of the problems of water permeability through a slits system for one of the filtration area fragments, including the problem of water permeability through a slit in the screen with a protective layer of soil and the problem of water permeability through a slit of the screen with underlying soil base.

To determine the piezometric head in the slit of the polymer screen, from the condition of continuity of the flow, we equate the rates through fragments 1 and 2 ($q_1 = q_2$) according to the approximate formulas (17) and (36), from which we will obtain:

$$h_1 = \frac{\sigma(h_o + \delta_o) Arch\left[\frac{\alpha + \beta(2-\alpha)}{\alpha(1+\beta)}\right] - 2H_c \cdot \ln\left[4cth\left(\pi m/4\delta_o\right)\right]}{\sigma Arch\left[\frac{\alpha + \beta(2-\alpha)}{\alpha(1+\beta)}\right] + 2\ln\left[4cth\left(\pi m/4\delta_o\right)\right]}, \quad (42)$$

where $\sigma = k_1/k_2$, α and β – being parameters determined from simultaneous equations (37) and (38).

To calculate the piezometric head in the slit of a polymer screen with a protective layer of soil (h_1), a correlation similar to that obtained earlier in [14] can also be used:

$$h_1 = \frac{\sigma(h_0 + \delta_0)Arch(1/\sqrt{\alpha_1 - 1}) - H_c \ln(16\delta_0 / \pi m)}{\sigma Arch(1/\sqrt{\alpha_1 - 1}) + \ln(16\delta_0 / \pi m)}, \quad (43)$$

where α_1 – being a calculated parameter, defined in tabulated form by function $F_1(\alpha_1)$ [14].

On the basis of the above theoretical conclusions, the following simplified formulas can be used for practical application to determine the total flow rate through a polymer screen with a slit system:

- with the use of correlation (17):

$$Q_f = \frac{\pi k_1 (h_o + \delta_o - h_l) \cdot \bar{l}_s \cdot n}{\ln\left(4cth\left(\pi m / 4\delta_o\right)\right)}; \quad (44)$$

- with the use of correlation (18):

$$Q_f = \frac{\pi k_1 (h_o + \delta_o - h_1) \cdot \bar{l}_s \cdot n}{\ln(16\delta_o / \pi m)}; \quad (45)$$

- with the use of correlation (23):

$$Q_f = k'_{scr} \frac{h_o + \delta_o - h_l}{\delta_o} \cdot F_o. \quad (46)$$

where h_1 – being piezometric head in the slit of the polymer screen, determined by correlation (42) or (43);

k'_{scr} – being the averaged screen filtration factor, calculated by formulas (24) or (25);

$\bar{l}_s$ – being the average statistical length of the screen slit;

n – the number of geomembrane screen slits;

F_o being the screen area.

3. Results and Discussion

For the purpose of the results reconciliation, we perform calculations of the water permeability of a polymer screen of a broken continuity with a slit system using the known formulas by V.P. Nedriga and V.V. Vedernikov, also obtained in the first case for a slits system in a film screen, and in the second case – for a drain system on watertight stratum as well as J.P. Giroud – for geomembranes with defects in the form of extended slits [17].

In the calculation, we use solutions for the general case, when we take into account the influence of the underlying base with slit head h_1 at $k_2 < k_1$, and for a special case without considering the influence of the base at $h_1 = 0$ and $k_2 \le 10k_1$.

Inputs for calculation: $h_1 = 3.0$ m, $\delta_0 = 0.5$ m, $k_1 = 1.0$ m/day, $k_2 = 0.3$ m/day, $l = 3.0$ m, $H_c = 0.5 \cdot h_0 = 0.5 \cdot 1.0 = 0.5$ m, $m = 0.001 - 0.1$ m, $\bar{l}_s = 1.0$ m, $n = 10$, $h_1 = 0$, $C_{q_0} = 0.21$, $C_{q_\infty} = 0.52$ (with C_{q_0} and $C_{q\infty}$ – being the factors of quality of a contact between the geomembrane and the base soil with a good contact by J.P. Giroud) [23].

The total filtration rate through the slit system according to the authors' formula is calculated from the correlations (44) and (45), and the piezometric head in the slit h_1 – by formula (43).

Analysis of calculation results shows that in case of considering the permeability of the underlying base, the total filtration rate according to the formulas by the authors of the work is reduced 2.7–3.3 times.

Table 1. The comparison of the results of calculating the total filtration flow rate through the system of screen slits according to the known formulas

m, m	h_1, m	By the authors' formulas						
		Authors (43), (44)	V.P. Nedriga		V.V. Vedernikov		J.P. Giroud	
		Q_f, m³/ day	Q_f, m³/ day	ε, %	Q_f, m³/ day	ε, %	$Q_{f\,(min)}$, m³/ day	ε, %
0.001	2.21	5.17/14.02	4.53/12.28	-12.4	5.87/15.90	13.4	8.66	67.5
0.005	2.24	6.35/17.64	5.89/17.01	-7.2	7.02/19.85	10.5	12.10	90.5
0.01	2.28	6.92/19.84	6.57/18.84	-5.0	7.59/21.83	10.0	14.13	106.9
0.05	2.35	9.19/27.96	8.54/27.03	-7.1	11.35/36.12	23.5	20.00	117.6
0.1	2.43	10.37/33.92	9.53/31.13	-8.0	13.24/43.26	27.5	23.73	128.8

Note: The numerator shows the values of the total filtration rates through the slits system considering the head in the slit h_1, and in the denominator – without considering h_1 ($h_1 = 0$).

The reconciliation of the obtained flow values (Q_f) by the authors' formulas with ones by V.P. Nedriga, gives a variance from 5.0 to 12.4 %, and by V.V. Vedernikov's – from 10.0 to 27.5 %, which can be considered a satisfactory match. However, when comparing the results with the formula by J.P. Giroud, the discrepancy with the minimum flow rate at factor $C_{q_0} = 0.21$, $Q_{f\min}$ reaches from 67.5 % to 128.8 % in the whole range of possible defects (slits) in practice within $m = 0.001 \div 0.1$ m. At the same time, with the maximum value of factor $C_{q_0} = 0.15$ the rate will already increase 5 times. Such significantly overestimated values of rates by J.P. Giroud are explained by the fact that his formula differs fundamentally from other authors' ones in structure that can be considered experimental and theoretical, taking into account empirical factors C_{q_0} and $C_{q\infty}$ according to field study data and various degrees at the main design parameters m, h_1, and k_2. In this regard, its dependence does not comply with Darcy's law, which is fundamental in filtration problems. In addition, different degrees in the main variables indicate a violation of the principle of compliance with the dimension.

In contrast, in the three dependencies by the following authors: V.P. Nedriga and V.V. Vedernikov, who give close values of rates, which are based on strict filtration theory using the Darcy's law, the results are unquestionable and confirm each other.

Nevertheless, we believe that the assumed calculated correlations by J.P. Giroud also have their value and can be used for they are based on a large number of field and in-situ experiments and apparently have already been undergone extensive testing at US facilities.

Apparently, these formulas require their specification for Russian conditions according to field research data.

To calculate the piezometric head in the slit of a polymer screen with a protective layer of soil, the dependence obtained earlier in [14] can also be tested:

$$h_1 = \frac{\sigma(h_0 + \delta_0)Arsh(1/\sqrt{\alpha_1 - 1}) - H_c \ln(16\delta_0 / \pi m)}{\sigma \cdot Arsh(1/\sqrt{\alpha_1 - 1}) + \ln(16\delta_0 / \pi m)}, \qquad (47)$$

where d_1 – being calculated parameter, defined in tabulated form by function $F_1(d_1)$ [14].

For practical application, a graph was built to show the dependence of the reduced filtration flow through the slit of the polymer screen on its width and on the thickness of the protective layer $q_r = f(m, \delta_0)$ (Figure 5), where the reduced flow rate is understood as the correlation of the real filtration flow, the base soil filtration factor and the screen head factor: $q_r = q/(k \cdot H)$, with q_r – being the reduced filtration rate; k – soil filtration factor of protective layer or protective cover; H – the on-screen head.

The analysis of the obtained graphical dependencies shows that in the case of considering the permeability of the underlying base, the resulted rates q_r are reduced in comparison with the curves,

without consideration of the base, both in the thickness of the protective layer at $\delta_0 = 0.5$ m and at $\delta_0 = 1.0$ m approximately by 12.5 %.

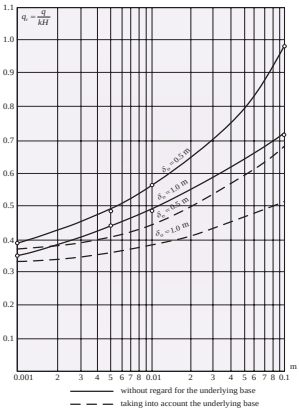

Figure 5. The graph of the dependence of the reduced filtration flow through the slit of the polymer screen on its width and the thickness of the protective layer

The averaged filtration factor of the polymer screen has also been calculated by formulas (25) and (26), with its values over a wide range of slit widths $m = 0.001 \div 0.1$ m and their numbers $n = 1.0 \div 20.0$ presented in Table 2.

Table 2. The values of the averaged filtration factor of a polymer screen with a slits system k_{scr}, m/s

Number of slits, *n*	The width of the slit in the screen, *m*						
	0.001	0.003	0.005	0.01	0.03	0.05	0.1
At $k_2 \geq 10k_1$ (without considering head h_1)							
1	5.8×10^{-10}	6.7×10^{-10}	7.3×10^{-10}	8.2×10^{-10}	1.0×10^{-9}	1.2×10^{-9}	1.4×10^{-9}
5	2.9×10^{-9}	3.3×10^{-9}	3.6×10^{-9}	4.1×10^{-9}	5.0×10^{-9}	6.0×10^{-9}	7.0×10^{-9}
10	5.8×10^{-9}	6.7×10^{-9}	7.3×10^{-9}	8.2×10^{-9}	1.0×10^{-8}	1.2×10^{-8}	1.4×10^{-8}
15	8.7×10^{-9}	1.0×10^{-8}	1.1×10^{-8}	1.2×10^{-8}	1.5×10^{-8}	1.8×10^{-8}	2.1×10^{-8}
20	1.2×10^{-8}	1.3×10^{-8}	1.5×10^{-8}	1.6×10^{-8}	2.0×10^{-8}	2.4×10^{-8}	2.8×10^{-8}
At $k_2 \leq 10k_1$ (considering head h_1)							
1	2.0×10^{-10}	2.3×10^{-10}	2.4×10^{-10}	2.6×10^{-10}	3.1×10^{-10}	3.3×10^{-10}	3.7×10^{-10}
5	1.0×10^{-9}	1.1×10^{-9}	1.2×10^{-9}	1.3×10^{-9}	1.5×10^{-9}	1.6×10^{-9}	1.8×10^{-9}
10	2.0×10^{-9}	2.3×10^{-9}	2.4×10^{-9}	2.6×10^{-9}	3.1×10^{-9}	3.3×10^{-9}	3.7×10^{-9}
15	3.0×10^{-9}	3.4×10^{-9}	3.6×10^{-9}	3.9×10^{-9}	4.6×10^{-9}	4.9×10^{-9}	5.5×10^{-9}
20	4.0×10^{-9}	4.6×10^{-9}	4.8×10^{-9}	5.2×10^{-9}	6.2×10^{-9}	6.6×10^{-9}	7.4×10^{-9}

The following data were taken into account: $\delta_0 = 0.5$ m, $h_0 = 3.0$ m, $k_1 = 1.0$ m/day, $k_2 = 0.3$ m/day, $\bar{l}_s = 1.0$ m, $F_0 = 400$ м², $l = 3.0$ m.

The comparison of the values of factor k_{scr} at $k_2 \geq 10k_1$ (without considering head h_1) and $k_2 \leq 10k_1$ (considering head h_1) shows that in the latter case the filtration factors are almost 3 times reduced. Obviously, this is due to the lower permeability of the underlying soil base compared to the protective layer ($k_2 < k_1$; 0.3 m/day < 1.0 m/day).

The reconciliation of calculated values k_{scr} for a slits system by J.P. Giroud [23] for round holes in the geomembrane at the same depths $h = 3.0$ m indicates a close order of the numbers, although here we also see that their values are overestimated as compared to our data, especially for large holes sizes.

4. Conclusions

1. A filtration model of water permeability for a polymer screen through a slits system has been developed, it includes an analytical solution of the problem by isolating standard fragments of the local filtration area including head filtration area to the screen slit with a soil protective layer and an unforced filtration area from the screen slit at its base.

2. As a result of the solution, the calculated correlations were obtained to determine the specific filtration flow rate through a system of slits with their small dimensions and averaged screen filter factors. The calculation results were compared to the formulas by V.P. Nedriga, V.V. Vedernikov, and J.P. Giroud.

3. For practical use, a graph of the change in the reduced filtration flow rate was made in its dependence of $q_r = f(m, \delta_0)$ as well as a table of changing the values of the averaged filtration factor.

5. Acknowledgement

This work was supported by a grant from the President of the Russian Federation for national support of young scientists and candidates of science (MK-33.04.2018.8).

References

1. Kosichenko, Yu.M., Baev, O.A. Vysokonadezhnyye konstruktsii protivofil'tratsionnykh pokrytiy kanalov i vodoyomov, kriterii ikh effektivnosti i nadezhnosti [Highly reliable structures of anti-filtration coatings of canals and reservoirs, criteria of their efficiency and reliability]. Power technology and engineering. 2014. No. 8. Pp. 18–25. (rus)
2. Glagovskiy, V.B., Solskiy, S.V., Lopatina, M.G., Dubrovskaya, N.V., Orlova, N.L. Geosinteticheskiye materialy v gidrotekhnicheskom stroitelstve [Geosynthetics in hydraulic engineering]. Gidrotekhnicheskoye stroitelstvo. 2014. No. 9. Pp. 23–27. (rus)
3. Solskiy, S.V., Orlova, N.L. Perspektivy i problemy primeneniya v gruntovykh gidrotekhnicheskikh sooruzheniyakh sovremennykh geosinteticheskikh materialov [Prospects and problems of application in groundwater hydraulic structures of modern geosynthetic materials]. Izvestiya VNIIG im. B.Ye. Vedeneyeva. 2010. Vol. 260. Pp. 61–68. (rus)
4. Solskiy, S.V., Lopatina, M.G., Orlova, N.L. Laboratornyye issledovaniy geosinteticheskikh materialov dlya obosnovaniya ikh primeneniya v konstruktsiyakh gruntovykh gidrotekhnicheskikh sooruzheniy [Laboratory studies of geosynthetic materials to justify their use in the construction of groundwater structures]. Izvestiya VNIIG. im. B.Ye. Vedeneyeva. 2015. Vol. 276. Pp. 84–91. (rus)
5. Lupachev O.Yu., Teleshev V.I. The watertight geomembrane elements. Use experience in the hydraulic engineering. Magazine of Civil Engineering. 2009. No. 6. Pp. 35–43. (rus)
6. Lupachev, O.Yu., Teleshev, V.I. Primeneniye geosinteticheskikh materialov v gidrotekhnicheskom stroitelstve v kachestve protivofiltratsionnykh elementov plotin i damb [Application of geosynthetic materials in hydraulic engineering construction as anti-filtration elements of dams and dams]. Gidrotekhnika. 2009. No. 1. Pp. 71–75. (rus)
7. Koerner, R.M., Hsuan, Y.G., Koerner, G.R. Lifetime predictions of eposed geotextiles and geomembranes. Geosynthetics International. 2017. No. 24(2). Pp. 198–212.
8. Tian, K., Benson, C.H., Tinjum, Y.M., Edil, T.B. Antioxidant depletion and service life prediction for HDPE geomembranes exposed to low-level radioactive waste leachate. Journal of Geotechnical and Geoenvironmental Engineering, 2017. No. 143(6). Pp. 22–29.
9. Gallagher, E.M., Tonks, D.M., Shevelan, J., Belton, A.R., Blackmore, R.E. Investigations of geomembrane integrity within a 25-2017 old landfill capping. Geotextiles and Geomembranes. 2016. No. 4(5). Pp. 770–780.
10. Russian Construction Norms SP 39.13330.2012. (rus)

Литература

1. Косиченко Ю.М., Баев О.А. Высоконадежные конструкции противофильтрационных покрытий каналов и водоёмов, критерии их эффективности и надежности // Гидротехническое строительство. 2014. № 8. С. 18–25.
2. Глаговский В.Б., Сольский С.В., Лопатина М.Г., Дубровская Н.В., Орлова Н.Л. Геосинтетические материалы в гидротехническом строительстве // Гидротехническое строительство. 2014. № 9. С. 23–27.
3. Сольский С.В., Орлова Н.Л. Перспективы и проблемы применения в грунтовых гидротехнических сооружениях современных геосинтетических материалов // Известия ВНИИГ им. Б.Е. Веденеева. 2010. Т. 260. С. 61–68.
4. Сольский С.В., Лопатина М.Г., Орлова Н.Л. Лабораторные исследований геосинтетических материалов для обоснования их применения в конструкциях грунтовых гидротехнических сооружений // Известия ВНИИГ. им. Б.Е. Веденеева. 2015. Т. 276. С. 84–91.
5. Лупачев О.Ю., Телешев В.И. Противофильтрационные элементы из геомембран. Опыт применения в гидротехническом строительстве // Инженерно-строительный журнал. 2009. № 6. С. 35–43.
6. Лупачев О.Ю., Телешев В.И. Применение геосинтетических материалов в гидротехническом строительстве в качестве противофильтрационных элементов плотин и дамб // Гидротехника. 2009. № 1. С. 71–75.
7. Koerner R.M., Hsuan Y.G., Koerner G.R. Lifetime predictions of eposed geotextiles and geomembranes // Geosynthetics International. 2017. № 24(2). Pp. 198–212.
8. Tian K., Benson C.H., Tinjum Y.M., Edil T.B. Antioxidant depletion and service life prediction for HDPE geomembranes exposed to low-level radioactive waste leachate // Journal of Geotechnical and Geoenvironmental Engineering. 2017. № 143(6). Pp. 22–29.
9. Gallagher E.M., Tonks D.M., Shevelan J., Belton A.R., Blackmore R.E. Investigations of geomembrane integrity within a 25-2017 old landfill capping // Geotextiles and Geomembranes. 2016. № 4(5). Pp. 770–780.
10. СП 39.13330.2012. Актуализированная редакция СНиП 2.06.05-84. Плотины из грунтовых материалов.
11. Прямицкий А.В., Шлее Ю. Европейский опыт использования геосинтетических материалов в строительстве хранилищ отходов // Гидротехника XXI век. 2010. № 1(21). С. 52–56.
12. Чумаганов А.П. Сирота Ю.Я. За порогом надежности эксплуатации гидротехнических сооружений, входящих в промышленные комплексы различных

Косиченко Ю.М., Баев О.А. Водопроницаемость полимерного экрана с системой щелей гидротехнических сооружений // Инженерно-строительный журнал. 2018. № 7(83). С. 148–164.

11. Pryamitskiy, A.V., Shleye, Yu. Yevropeyskiy opyt ispolzovaniya geosinteticheskikh materialov v stroitelstve khranilishch otkhodov [European experience of using geosynthetic materials in the construction of waste storages]. Gidrotekhnika XXI vek. 2010. No. 1(21). Pp. 52–56. (rus)
12. Chumaganov, A.P. Sirota, Yu.Ya. Za porogom nadezhnosti ekspluatatsii gidrotekhnicheskikh sooruzheniy, vkhodyashchikh v promyshlennyye kompleksy razlichnykh predpriyatiy [Beyond the threshold of reliability of operation of hydraulic structures within the industrial complexes of various enterprises]. Gidrotekhnika XXI vek. 2010. No. 1. Pp. 46–51. (rus)
13. Kosichenko, Yu.M., Bayev, O.A. Metody rascheta vodopronitsayemosti polimernykh protivofiltratsionnykh ekranov gidrotekhnicheskikh sooruzheniy [Methods for calculating the permeability of polymer anti-filtration screens of hydraulic structures]. Izvestiya VNIIG im. B.Ye. Vedeneyeva. 2017. Vol. 286. Pp. 10–21. (rus)
14. Kosichenko, Yu.M., Bayev, O.A. Teoreticheskaya otsenka vodopronitsayemosti protivofiltratsionnoy oblitsovki narushennoy sploshnosti [Theoretical assessment of the permeability of the impervious lining of the broken continuity]. Izvestiya vysshikh uchebnykh zavedeniy. Severo-Kavkazskiy region. Seriya: Tekhnicheskiye nauki. 2014. No. 3(178). Pp. 68–74. (rus)
15. Kosichenko, Yu.M., Bayev, O.A. Matematicheskoye i fizicheskoye modelirovaniye filtratsii cherez malyye povrezhdeniya protivofiltratsionnykh ustroystv iz polimernykh geomembran [Mathematical and physical modeling of filtering through small damages of impervious devices from polymeric geomembranes]. Izvestiya VNIIG im. B.Ye. Vedeneyeva. 2014. Vol. 274. Pp. 60–74. (rus)
16. Kosichenko, Yu.M., Baev, O.A. Design of impervious coatings with enhanced reliability made from innovative materials. Procedia Engineering. 2016. Vol. 150. Pp. 1503–1509.
17. Ishchenko, A.V. Gidravlicheskaya model vodopronitsayemosti i effektivnosti protivofiltratsionnykh oblitsovok krupnykh kanalov [Hydraulic model of permeability and efficiency of anti-filtration facing of large canals]. Izvestiya VNIIG im. B.Ye. Vedeneyeva. 2010. Vol. 258. Pp. 51–64. (rus)
18. Polubarinova-Kochina, P.Ya. Teoriya dvizheniya gruntovykh vod [Theory of groundwater movement]. Moscow: Nauka. 1977. 664 p. (rus)
19. Lavrik, V.I., Filchakova, S.P., Yashin, A.A. Konformnyye otobrazheniya fiziko-topologicheskikh modeley [Conformal mappings of physico-topological models]. Kiyev: Naukova Dumka. 1990. 376 p. (rus)
20. Averyanov, S.F. Filtratsiya iz kanalov i yeye vliyaniye na rezhim gruntovykh vod [Filtration from canals and its effect on groundwater regime]. Moscow: «Kolos». 1982. 237 p. (rus)
21. Hurwitz, A., Courant, R. Theory of functions. Springer-varlag. Berlin. 1964. 648 p.
22. Handbook of mathematical functions, with formulas, graphs and mathematical tables. Edited by Abramowitz M., Stegun A. National bureau standards applied mathematics series 55. 1964. 230 p.
23. Giroud, J.P. Equations for calculating the rate of liquid migration through composite lines due to geomembrane defects. Geosynthetics International. 1997. Vol. 4. No. 3-4. Pp. 335–348.
24. Bonaparte, R., Giroud, J.P., Gross, B.A. Rates of Leakage through Landfill Liners. Proceedings of Geosynthetics. 1989. Vol. 1. Pp. 18–29.
25. Giroud, J.P., Khatami, A., Badu-Tweneboah, K. Evaluation of the Rate of Leakage through Composite Liners. Geotextiles and Geomembranes. 1989. Vol. 8. No. 4. Pp. 337–340.
26. Giroud, J.P., Badu-Tweneboah, K., Bonaparte, R. Rate of Leakage Through a Composite Liner due to Geomembrane Defects. Geotextiles and Geomembranes. 1992. Vol. 11. No. 1. Pp. 1–28.

предприятий // Гидротехника XXI век. 2010. № 1. С. 46–51.

13. Косиченко Ю.М., Баев О.А. Методы расчета водопроницаемости полимерных противофильтрационных экранов гидротехнических сооружений // Известия ВНИИГ им. Б.Е. Веденеева. 2017. Т. 286. С. 10–21.
14. Косиченко Ю.М., Баев О.А. Теоретическая оценка водопроницаемости противофильтрационной облицовки нарушенной сплошности // Известия высших учебных заведений. Северо-Кавказский регион. Серия: Технические науки. 2014. № 3(178). С. 68–74.
15. Косиченко Ю.М., Баев О.А. Математическое и физическое моделирование фильтрации через малые повреждения противофильтрационных устройств из полимерных геомембран // Известия ВНИИГ им. Б.Е. Веденеева. 2014. Т. 274. С. 60–74.
16. Kosichenko Yu.M., Baev O.A. Design of Impervious Coatings with Enhanced Reliability Made from Innovative Materials // Procedia Engineering. 2016. Vol. 150. Pp. 1503–1509.
17. Ищенко А.В. Гидравлическая модель водопроницаемости и эффективности противофильтрационных облицовок крупных каналов // Известия ВНИИГ им. Б.Е. Веденеева. 2010. Т. 258. С. 51–64.
18. Полубаринова-Кочина П.Я. Теория движения грунтовых вод. М.: «Наука». 1977. 664 с.
19. Лаврик В.И., Фильчакова С.П., Яшин А.А. Конформные отображения физико-топологических моделей / Акад. наук АН УССР. Киев: Наукова Думка. 1990. 376 с.
20. Аверьянов С.Ф. Фильтрация из каналов и ее влияние на режим грунтовых вод. М.: «Колос». 1982. 237 с.
21. Hurwitz A., Courant R. Theory of functions. Springer-varlag. Berlin. 1964. 648 p.
22. Handbook of mathematical functions, with formulas, graphs and mathematical tables. Edited by Abramowitz M., Stegun A. National bureau standards applied mathematics series 55. 1964. 230 p.
23. Giroud J.P. Equations for calculating the rate of liquid migration through composite lines due to geomembrane defects // Geosynthetics International. 1997. Vol. 4. № 3-4. Pp. 335–348.
24. Bonaparte R., Giroud J.P., Gross B.A. Rates of Leakage through Landfill Liners. Proceedings of Geosynthetics. 1989. Vol. 1. Pp. 18–29.
25. Giroud J.P., Khatami A., Badu-Tweneboah K. Evaluation of the Rate of Leakage through Composite Liners // Geotextiles and Geomembranes. 1989. Vol. 8. № 4. Pp. 337–340.
26. Giroud J.P., Badu-Tweneboah K., Bonaparte R. Rate of Leakage Through a Composite Liner due to Geomembrane Defects // Geotextiles and Geomembranes. 1992. Vol. 11. № 1. Pp. 1–28.
27. Giroud J.P., Badu-Tweneboah K., Soderman K.L. Evaluation of Landfill Liners. Proceedings of the Filth International Conference on Geotextiles, Geomembranes and Related Products. Singapore, September 1994. Vol. 3. Pp. 981–986.
28. Giroud J.P., Touze-Foltz N. Equations for calculating the rate of liquid flow through geomembrane defects of uniform width and finite or infinite length // Geosynthetics International. 2005. Vol. 12. Pp. 191–204.
29. Touze-Foltz N., Rowe R.K., Duquennoi, C. Liquid flow through composite liners due to geomembrane defects: analytical solutions for axi-symmetric and two-dimensional problems // Geosynthetics International. 2000. Vol. 6. № 6. Pp. 455–479.
30. Rowe R.K. Geosynthetics and the Minimization of Contaminant Migration Through Barrier Systems Beneath Solid Waste. Keynote paper, Proceedings of the Sixth International Conference on Geosynthetics. Vol. 1. Atlanta, Georgia, USA, March 1998. Pp. 27–103.

Kosichenko, Yu.M., Baev, O.A. Water permeability of the polymer screen with a system of slits of hydraulic structures. Magazine of Civil Engineering. 2018. 83(7). Pp. 148–164. doi: 10.18720/MCE.83.14.

27. Giroud, J.P., Badu-Tweneboah, K., Soderman, K.L. Evaluation of Landfill Lines. Proceedings of the Filth International Conference on Geotextiles, Geomembranes and Related Products. Singapore, September 1994. Vol. 3. Pp. 981–986.
28. Giroud, J.P., Touze-Foltz, N. Equations for calculating the rate of liquid flow through geomembrane defects of uniform width and finite or infinite length. Geosynthetics International. 2005. Vol. 12. Pp. 191–204.
29. Touze-Foltz, N., Rowe, R.K., Duquennoi, C. Liquid Flow Through Composite Liners due to Geomembrane Defects: Analytical Solutions for Axi-Symmetric and Two-Dimensional Problems. Geosynthetics International. 2000. Vol. 6. No. 6. Pp. 455–479.
30. Rowe, R.K. Geosynthetics and the Minimization of Contaminant Migration Through Barrier Systems Beneath Solid Waste. Keynote paper, Proceedings of the Sixth International Conference on Geosynthetics. Atlanta, Georgia, USA, March 1998. Vol. 1. Pp. 27–103.
31. Touze-Foltz, N. Large scale tests for the evaluation of composite liners hydraulic performance: a preliminary study. Proceedings of the Seventh International Waste Management and Landfill Symposium. S. Margherita di Pula, Italy. October 1999. Vol. 3. Pp. 157–164.
32. Touze-Foltz, N., Bannour, H., Barral, C., Stoltz, G. A review of the performance of geosynthetics for environmental protection. Geotextiles and Geomembrane. 2016. Vol. 44(5). Pp. 656–672.
33. Tano, B.F.G., Stoltz, G., Touze-Foltz, N., Dias, D., Olivier, F. A numerical modelling technique for geosynthetics validated on a cavity model test. Geotextiles and Geomembranes. 2017. Vol. 45. Pp 339–349.
34. Sainov, M.P., Zverev, A.O. Workability of high rockfill dam with a polymer face. Magazine of Civil Engineering. 2017. 75(7). Pp. 76–83.
35. Solsky, S.V., Orlova, N.L., Velichko, A.S. Crack self-healing in clay-sement concrete diaphragm of embankment dam. Magazine of Civil Engineering. 2018. 77(1). Pp. 3–12.
36. Sainov, M.P. Analysis of normal operation of a rockfill dam with combination of seepage-control elements: reinforced concrete face and a clay-cement-concrete wall. Magazine of Civil Engineering. 2016. 64(4). Pp. 3–9.
37. Anakhaev, K.N., Aniskin, N.A., Amshokov, B.Kh., Anakhaeva, Kh.K. Calculation of filtration in earth-fill dams with impervious diaphragms. Power technology and Engineering. 51(5). 2018. Pp.42–47.
38. Rasskazov, L.N., Yadgorov, E.Kh., Nikolaev, V.B. Fild observations of soil settlements, displacements, and pore pressure in dams. Power technology and Engineering. No. 51(2). Pp. 1–10.
39. Golovanov, A.I., Sukharev, Yu.I., Solskiy, S.V. Metod rascheta filtratsionnykh kupolov pod dnishchem basseynov sutochnogo regulirovaniya GES [The method of calculating the filtration domes under the bottom of the basins for daily regulation of hydropower]. Prirodoobustroystvo. 2014. Vol. 5. Pp. 37–42. (rus)
40. Yanke, Ye., Emde, F., Lesh, F. Spetsialnyye funktsii [Special Functions]. Moscow: «Nauka». 1977. 342 p. (rus)
31. Touze-Foltz N. Large Scale Tests for the Evaluation of Composite Liners Hydraulic Performance: a Preliminary Study. Proceedings of the Seventh International Waste Management and Landfill Symposium. S. Margherita di Pula, Cagliari, Sardinia, Italy. October 1999. Vol. 3. Pp. 157–164.
32. Touze-Foltz N., Bannour H., Barral C., Stoltz G. A review of the performance of geosynthetics for environmental protection // Geotextiles and Geomembrane. 2016. Vol. 44(5). Pp. 656–672.
33. Tano B.F.G., Stoltz G., Touze-Foltz N., Dias D., Olivier F. A numerical modelling technique for geosynthetics validated on a cavity model test // Geotextiles and Geomembranes. 2017. Vol. 45. Pp. 339–349.
34. Саинов М.П., Зверев А.О. Работоспособность высокой каменно-набросной плотины с полимерным экраном // Инженерно-строительный журнал. 2017. № 7(75). С. 76–83.
35. Сольский С.В., Орлова Н.Л., Величко А.С. Самозалечивания трещин в глиноцементобетонной диафрагме грунтовой плотины // Инженерно-строительный журнал. 2018. № 1(77). С. 3–12.
36. Саинов М.П. Анализ работоспособности каменной плотины с комбинацией противофильтрационных элементов – железобетонного экрана и глиноцементобетонной стены // Инженерно-строительный журнал. 2016. №4 (64). С. 3–9.
37. Anakhaev K.N., Aniskin N.A., Amshokov B.Kh., Anakhaeva Kh.K. Calculation of filtration in earth-fill dams with impervious diaphragms // Power technology and Engineering. № 51(5). 2018. Pp.42–47.
38. Rasskazov L.N., Yadgorov E.Kh., Nikolaev V.B. Fild observations of soil settlements, displacements, and pore pressure in dams // Power technology and Engineering. № 51(2). Pp.1–10.
39. Голованов А.И., Сухарев Ю.И., Сольский С.В. Метод расчета фильтрационных куполов под днищем бассейнов суточного регулирования ГЭС // Природообустройство. 2014. № 5. С. 37–42.
40. Янке Е., Эмде Ф., Леш Ф. Специальные функции. М.: «Наука». 1977. 342 с.

Yuri Kosichenko,
+7(909)404-92-88; kosichenko-11@mail.ru

Oleg Baev,*
+7(961)282-96-79; Oleg-Baev1@yandex.ru

Юрий Михайлович Косиченко,
+7(909)404-92-88;
эл. почта: kosichenko-11@mail.ru

Олег Андреевич Баев,*
+7(961)282-96-79;
эл. почта: Oleg-Baev1@yandex.ru

Косиченко Ю.М., Баев О.А. Водопроницаемость полимерного экрана с системой щелей гидротехнических сооружений // Инженерно-строительный журнал. 2018. № 7(83). С. 148–164.

doi: 10.18720/MCE.83.15

Ultimate state of the support zone of reinforced concrete beams

Предельное состояние приопорной зоны железобетонных балок

V.I. Travush,
GORPROJECT, Moscow, Russia
S.B. Krylov*,
D.V. Konin,
A.S. Krylov,
JSC Research Center of Construction, Moscow, Russia

Д-р техн. наук, главный конструктор, заместитель генерального директора по научной работе В.И. Травуш,
ЗАО «ГОРПРОЕКТ», Москва, Россия
д-р техн. наук, заведующий лабораторией С.Б. Крылов*,
канд. техн. наук, заведующий сектором Д.В. Конин,
научный сотрудник А.С. Крылов,
АО «Научно-исследовательский центр «Строительство», Москва, Россия

Key words: concrete; reinforced concrete; reinforcement; inclined cross-section; shear force; strength; numerical simulation

Ключевые слова: бетон; железобетон; арматура; наклонное сечение; поперечная сила; прочность; численное моделирование

Abstract. A brief review of actual methods of calculation of the shear forces is performed; the calculated dependences are analyzed and their estimation is given. The shortcomings of the methods are noted, the main one is the empirical approach to the solution of the problem. The features of destruction of reinforced concrete elements along an inclined section are considered; the mechanism of destruction, on which the actual normative documents are based, is analyzed. A method of design of reinforced concrete elements under the action of shear forces is proposed. The method is developed on the basis of analysis of the stress-strain state of the support zone of a reinforced concrete beam of rectangular cross-section. In the design work, two stages are distinguished. This made it possible to avoid empirical coefficients in the equations. A numerical model was created. Stress distribution in the beam was obtained and analyzed. Conclusions about the actual stress distribution in the compressed zone of concrete above the top of the inclined crack and the actual compressive strength of concrete are made. The proposed design method made it possible to describe the process of destruction of the inclined section in strict accordance with the experimental data. The proposed approach allows to obtain accurate results not only for reinforced concrete elements of simple cross-section (rectangular, T-section), but also for other shapes of sections of a more complex configuration.

Аннотация. Выполнен краткий обзор современных методов расчета на действие поперечных сил; проанализированы расчетные зависимости, дана их оценка. Отмечены недостатки современных методов, главным из которых является эмпирический подход к решению задачи. Рассмотрены особенности разрушения железобетонных элементов по наклонному сечению; проанализирован механизм разрушения, заложенный в основу современных нормативных документов. Предложен метод расчета железобетонных элементов при действии поперечных сил. Метод разработан на основе анализа напряженно-деформированного состояния приопорной зоны железобетонной балки прямоугольного сечения. В работе конструкции было выделены два этапа, что позволило избежать эмпирических коэффициентов в расчетных зависимостях. Создана численная модель, получена и проанализирована картина распределения напряжений в балке. Сделаны выводы о фактическом распределении напряжений в сжатой зоне бетона над вершиной наклонной трещины и о фактической прочности бетона при сжатии. Предложенный метод расчёта позволил описать процесс разрушения по наклонному сечению в строгом соответствии с опытными данными. Предложенный подход позволяет получить точные результаты не только для железобетонных элементов простого поперечного сечения (прямоугольного, таврового), но и для других форм сечений, имеющих более сложную конфигурацию.

Травуш В.И., Крылов С.Б., Конин Д.В., Крылов А.С. Предельное состояние приопорной зоны железобетонных балок // Инженерно-строительный журнал. 2018. № 7(83). С. 165–174.

1. Introduction

The issue of calculation of structures under the action of shear forces is still actual, since an exact analytical solution of the problem is not found. The methodologies underlying the major domestic and foreign regulations have similar approaches to addressing this issue. However, the calculation introduces various factors, and this leads to different results. Moreover, all design formulas without exception are based on empirical and semi-empirical dependences [1], which allows to obtain the final result only with a certain degree of accuracy and with a number of limitations. The purpose of this study is to develop a method that does not have empirical dependencies at its core; the method should have an area of application not only for reinforced concrete elements of simple cross-section (rectangular, T- section), but also for other shapes of sections of a more complex configuration.

In the works of various authors, the issues of a general nature, such as the stress-strain state of reinforced concrete elements in the area of shear forces, are considered, as well as a narrower range of issues concerning one of the force factors acting in the inclined section [2, 3] or, for example, the loading conditions [4], type of shear reinforcement [5]. There are works in which analysis of cracking is made [6]. In connection with the development of technological processes in the manufacture, creation and research [7, 8, 9] of new types of concrete, many publications are devoted to the review of high-performance concretes (HPC and UHPC) behavior [10–13] and fiber concrete [11, 13–16] under the action of shear forces. A significant part of the publications includes experimental studies of the elements behavior along an inclined section [17–20]. In addition to these, we can note the work on the study of reinforced concrete elements in various environments, including under the influence of water [21]. There are publications in which biaxial stress state is considered [22]. Special attention is paid to the behavior of composite steel and concrete structures [10, 23]. Let us also mention the publications devoted to improving the methods of computer modeling when considering the features of the calculation of structures under the action of shear forces [24, 25]. Much of the work is aimed at developing theoretical bases of calculation under the action of shear forces [26–28], most publications note the shortcomings of the empirical approach and suggest new ways to resolve this issue [1, 29, 30].

2. Methods

In general, there are three possible variants of destruction of elements along an inclined section – along a concrete strip between inclined cracks, along a compressed zone of concrete above the top of an inclined crack, and along a stretched zone in case of violation of the anchoring or the yield strength in the longitudinal reinforcement is reached (Figure 1).

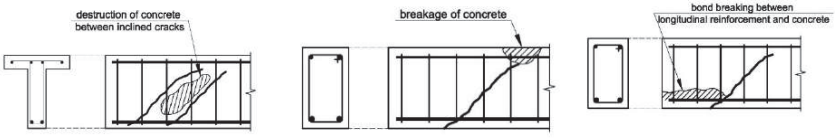

a) along a concrete strip between inclined cracks

b) along a compressed zone of concrete

c) along a stretched zone of concrete (bond breaking between longitudinal reinforcement and concrete)

Figure1. Schemes of a reinforced concrete element destruction along an inclined section

Let us consider in more detail the approach implemented in the Russian Standard SP 63.13330 "Concrete and won concrete construction. Design requirements" and consider the main design case – the calculation along the inclined section for the action of the shear force. It corresponds to the case of destruction in the compressed zone as a result of the concrete fragmentation over the crack (or its cutoff in the direction of the inclined crack).

The main difficulty in the design is caused by determination of the magnitude of the transverse force received by the concrete part of the cross section of the element. The main parameters, which determine the magnitude of the shear force received by the concrete in an inclined section in accordance with Russian Standard SP 63.13330, are the cross section width of the element b and the working section height h_0, as well as the concrete tensile strength R_{bt}:

$$Q_b = \frac{\varphi_{b2} R_{bt} b h_0^2}{c} \quad (1)$$

Thus, in the design formula there is only the value of R_{bt}, and the concrete compression strength R_b is not used. This indicates that the inclined section reaches the limit state only due to the formation and opening of the inclined crack. In fact, even after the formation of inclined cracks, reinforced concrete element continues to receive the applied loads and does not immediately lose the load-bearing capacity. In formula (1) this is taken into account by introducing the coefficient φ_{b2}. As a result, the destruction occurs due to the destruction (fragmentation) of compressed concrete over the crack, where the deformation and stress of the material exceed its compression limits. That is, the physical essence of the phenomenon differs from the approach taken in regulatory documents.

It is also worth mentioning the significant similarity in the approaches to solving problems related to the action of shear forces and the punching. The difference is the coefficient equal to 1.5.

Let us mention that the calculation dependences in the problems on the action of shear forces in both domestic and foreign regulations are based on a similar principle – the behavior of a concrete tensile area equal to the projection of the inclined section on the longitudinal axis of the element is considered. The area of concrete that is entered into the design is represented as a product of the working height of the section by its width, with the former being equal to the projection of the inclined crack with an angle of its inclination 45º. In addition, the design formulas in Russian Standard and Eurocode 2 "Design of concrete structures" include empirical coefficients that "transform" the basis of the formula (the product $R_{bt}bh_0$ – for formula (1)) in the final result, which is confirmed by numerous experiments. Additionally, Standard SP 63.13330 takes into account the influence of the distance from the support to the top of the crack on the result of the calculation. In Eurocode 2, this effect is not taken into account, which makes the result less accurate.

In the formulas of Eurocode 2, the value of the concrete tensile strength does not appear explicitly. The value of the shear force received by the concrete section is determined by the formula:

$$V_{Rd,c} = \left[C_{Rd,c}k(100\rho_1 f_{ck})^{\frac{1}{3}} + k_1\sigma_{cp}\right]b_w d, \quad (2)$$

where $C_{Rd,c}$, k, k_1 – coefficients;

ρ_1 – percentage of the cross-section reinforcement;

σ_{cp} – stresses in the cross section caused by prestressing;

b_w, d – the element cross-section dimensions;

f_{ck} – the cylindrical compression strength of concrete.

Cube root of the value f_{ck} means transition from concrete compression strength to tensile strength that is somewhat different from the table values. It looks close to the Feray formula. It can be directly verified that the expression $f_{ck}^{1/3}$ is an averaged transition function from the normalized cylindrical compression strength to the average tensile strength. For low-strength concretes, the tensile strength is somewhat overestimated, and for high-performance concrete it is underestimated, with an error of up to 12 %.

Let us mention that the formulas for design of limit shear force received by the concrete section and for determination of the load-bearing capacity in the punching calculation in Eurocode 2 coincide completely, unlike Russian Standard.

A significant advantage of the domestic dependencies for determining the limit shear force received by the concrete is the taking into account the value of the projection of the inclined section on the longitudinal axis of the element, which greatly affects the final result (1).

The reason for the simplifications and empirical approach in the calculation dependencies in the regulation documents is a consequence of the main problem in the calculation of the strength of the concrete elements with respect to the action of transverse forces – the number of equations is insufficient for determining all the unknowns. In the general case, the following forces act in the inclined section (Figure 2):

- in the concrete - the longitudinal N_b and the transverse Q_b components;
- in the shear reinforcement – Q_{sw};
- in the tension bars of longitudinal reinforcement – the longitudinal N_s and the transverse Q_s components;

- the forces of bonding on the sides of the inclined crack F_{crc} – the longitudinal N_{crc} and the transverse Q_{crc} components.

In addition, in order to determine the entire complex of forces, it is also necessary to know the height of the compressed section area.

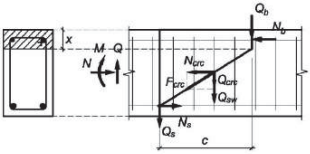

Figure 2. Forces acting in the inclined section

The modern approach in regulatory documents does not take into account the bonding forces along the sides of the inclined crack ($F_{crc}, Q_{crc}, N_{crc}$) and the transverse component in the longitudinal reinforcement (Q_s). In the proposed method, these values, in the strength margin, also will not be taken into account. Therefore, the following unknowns remain:

- in the concrete - the longitudinal N_b and the transverse Q_b components;
- in the shear reinforcement – Q_{sw};
- in the stretched bars of longitudinal reinforcement – the longitudinal component N_s;
- the reactive force at support Q.

In the general case, in order to determine all the unknowns, the design should be based on the joint solution of the system of three equilibrium equations – the sum of the projections on the longitudinal and transverse axes and the sum of the moments of all forces relative to the selected axis. Moreover, the equations will still include the height of the compressed zone as an unknown value. Even in this simplified form, the equilibrium equations alone are not sufficient to fully solve the problem.

3. Results and Discussion

Let us consider the most common case of destruction of the reinforced concrete element from the action of shear forces - as a result of exhaustion of the bearing capacity of the compressed concrete over the crack. We will consider an element that does not have shear reinforcement.

In order for the problem to have a mathematically correct solution, one more additional condition to the existing system of equilibrium equations is necessary. To obtain the missing condition, we single out two stages:

Stage 1. Inclined crack formation. Development and formation of cracks takes place. In the compressed zone of the concrete above the crack, the main force factor is the longitudinal force; the state of the compressed concrete can be considered as conditionally unidirectional and, accordingly, the strength characteristics of the material will accurately correspond to the standard strength values. At this stage, we determine the shear force at which the crack is initiated.

We introduce the assumption that the inclined crack is formed as a result of the separation of the lower part of the concrete (located below the crack) from the upper part of the concrete (located above the crack) – Figure 3.

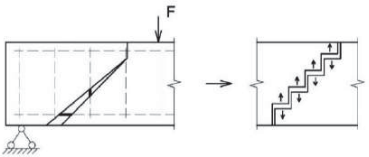

Figure 3. Scheme of the inclined crack development

The presented mechanism of destruction is similar to the destruction at punching. Therefore, the value of the shear force corresponding to the moment of crack development can be determined by a similar formula for design the limit force received by the concrete during punching.

$$Q_1 = R_{bt} A_b, \quad (3)$$

where A_b – is the calculated cross-sectional area defined as:

$$A_b = bc, \quad (4)$$

where c – is the length of the inclined section projection onto the longitudinal axis of the element,

b – is the width of the cross section.

Let us direct our attention to the following features of the structure behavior: after the initiation of an inclined crack and with a further increase in the load, its length varies slightly. In addition, the crack is not strictly inclined. Its upper part, following the trajectory of the main stresses (Figure 4), smoothly approaches the horizontal. This gives a ground to believe that the height of the compressed zone of the concrete after the initiation of an inclined crack remains constant until the loss of the bearing capacity of the element. Such assumption allows to determine the height of the compressed zone of the cross section from the equilibrium conditions at the initial stage of the crack development (in fact, considering the reinforced concrete element at the time before formation of the crack), when the strength characteristics of the concrete have not changed much due to the complex stress state arising in the future as a result of the biaxial compression over the top of the inclined crack.

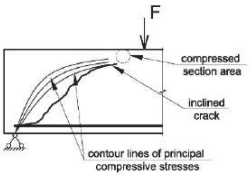

Figure 4. Schematics of the inclined crack propagation along the trajectory of the main compression stresses

The schematics of forces, when considering the equilibrium of the reinforced concrete beam section, are shown in Figure 5. From the equation of equilibrium of moments with respect to C (5), the height of the compressed zone x is determined.

$$\sum M_C = 0; \; -Qc + N_b(h_0 - 0.5x) = 0, \quad (5)$$

from which we obtain:

$$N_b = \frac{Qc}{h_0 - 0.5x} \quad (6)$$

On the other hand, the force in the compressed concrete is represented as

$$N_b = \sigma_b bx = R_b bx \quad (7)$$

We equate expressions (6) and (7):

$$\frac{Qc}{h_0 - 0.5x} = R_b bx \quad (8)$$

$$0.5x^2 - h_0 x + \frac{Qc}{R_b b} = 0 \quad (9)$$

The value of *x* is determined from the solution of the square equation (9).

Knowing the value of the compressed section area, it is possible to determine from the available equilibrium equations the value of the shear force. When it is reached, the loss of the load-bearing capacity of the element occurs. But before that, we will analyze the stress-strain state of the concrete of the compressed zone above the top of the inclined crack.

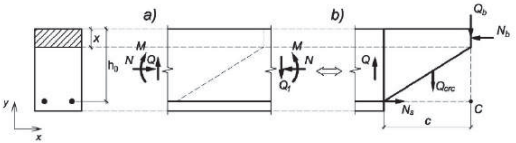

a) the beginning of the development of the inclined crack
b) the inclined crack had some propagation
Figure 5. Equilibrium of a section of the reinforced concrete beam with an inclined crack

Stage 2. Inclined crack propagation. In connection with the opening of the inclined crack, the contribution of the bonding forces to the load-bearing capacity of the element decreases, the tangential and normal stresses in the concrete of the element are mainly concentrated within the compressed section zone. Here, a horizontal compression force is observed not only along the axis of the element, but also across it (from the bending plane) – due to the arising expansion of the material (characterized by the Poisson's ratio), which is resisted by the adjacent layers of concrete. Therefore, in the compressed section area above the crack, the stress state of the concrete can be characterized as three-axial (Figure 6).

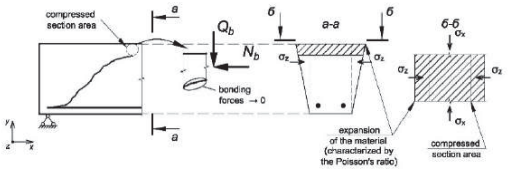

Figure 6. Forces in the compressed concrete area above the crack before the loss of the load-bearing ability of the element

Changing the stress-strain state of the material leads to a significant change in its strength and deformation characteristics. The strength of the concrete will depend on the ratio of the existing forces in the compressed zone (for different directions). To clarify this value, a numerical model is made in the ANSYS software package. The modeling of a reinforced concrete hinged beam with a crack in the support zone was performed. Solid 185-type volumetric finite elements were used in the creation of the model. The reinforced concrete beam of rectangular cross-section having only longitudinal reinforcement in the stretched zone is considered. A general view of the calculation scheme is shown in Figure 7. The inclined crack is modeled by FE (finite elements) of small rigidity. To prevent unintended destruction, nonlinear FE are introduced only in the study zone – around the top of the inclined crack. The nonlinear FE in Figure 8 are marked by red.

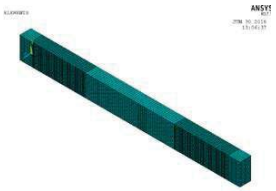

a) general view

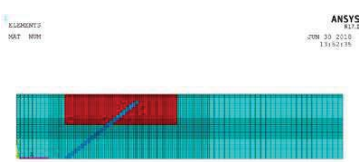

b) color representation of different types of elements (turquoise – concrete with linear characteristics, red – concrete with non-linear characteristics)

Figure 7. Computational model of a reinforced concrete beam with an inclined crack

The results of calculations are given for the supporting beam fragment with nonlinear elements at the top of the critical crack in Figures 8-10.

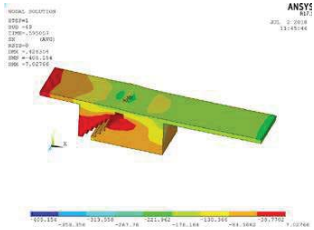

Figure 8. Longitudinal stresses σ_x, MPa×10^{-1}

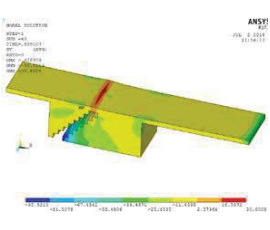

Figure 9. Vertical stresses σ_y, MPa×10^{-1}

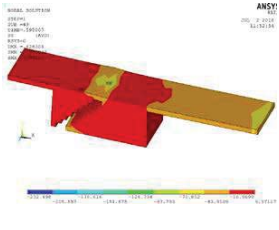

Figure 10. Horizontal stresses (from bending plane) σ_z, MPa×10^{-1}

Having obtained a stress distribution at triaxial stress state and referring to the data of [31], it is possible to determine the actual value of the concrete strength in case of compression from the surface limiting the area of strong resistance (Figure 11). A more detailed analysis of the stress-strain state shows that the vertical stresses concentrated within the height of the compressed zone above the crack quickly changes along the length of the beam and rapidly decreases along the height of the section. In addition, their value is much lower (up to ten times) compared to the horizontal longitudinal stress. At the same time, the horizontal stresses across the beam make up almost half of the longitudinal compression stresses. This allows us to neglect the vertical stresses and to classify the condition of the concrete above the crack as conditionally biaxial. This assumption simplifies the problem, allowing you to refer to the results of the study of concrete in a biaxial stress state. According to data of [31], the strength limit with obtained the ratio between principal stresses σ_1 and σ_2 rises up to 1.5 times (Figure12). This means that the maximum permissible transverse load will be 1.5 times higher than the one for the first stage of the element operation – the case of crack formation. These data correspond to experimental studies and materials of Russian Standard. Now, knowing the actual compression strength of the concrete and having the height of the compressed zone, calculated at the first stage, it is possible to determine from the equation of equilibrium of moments (5) the limiting shear force received by the concrete element.

$$Q_{b,ult} = \frac{N_b(h_0 - 0.5x)}{c}, \tag{10}$$

where

$$N_b = \sigma_b bx = 1.5R_b bx \tag{11}$$

The value *x* in formulas (10) and (11) should be taken equal to the value determined at the first stage of operation of the reinforced concrete element from equation (9).

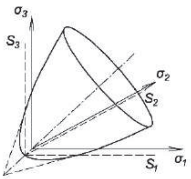

Figure 11. Surface limiting the area of strong resistance at triaxial stress state according to [31]

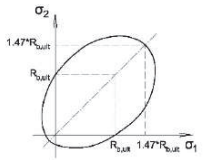

Figure 12. Curve limiting the area of strong resistance at biaxial stress state according to [31]

The proposed method of calculation allows to describe the process of destruction of the inclined section in strict accordance with the experimental data, in contrast to the methods adopted in the current regulatory documents. For rectangular sections, the proposed approach does not provide any significant advantages, except for the correct description of the physics of the phenomenon. But for cross-sections, different from rectangular ones (T-shaped, I-beam, round and generally arbitrary symmetric sections), the proposed approach allows to obtain much more accurate results compared to the known methods.

Травуш В.И., Крылов С.Б., Конин Д.В., Крылов А.С. Предельное состояние приопорной зоны железобетонных балок // Инженерно-строительный журнал. 2018. № 7(83). С. 165–174.

In contrast to the classical approach of the stress-strain state of concrete over the top of an inclined crack, realized in the calculated dependences in [1, 30], in this paper, a revision of the material RSS is made, which became a prerequisite for the implementation of this method. Of course, the proposed method needs some refinement and it is not the only alternative to modern normative documents. For a long time both semi-empirical methods, such as the modified theory of compression fields [29], and methods approaching the complete rejection of empirical dependences [1, 30] have been proposed. However, most of the proposed methods have some scope of applicability, or have excessively complex dependencies in relation to manual calculation. These methods are based on approaches different from those proposed in this paper.

4. Conclusions

1. The existing methods for design structures under the action of shear forces are analyzed. The shortcomings are noted, the main one being the approach based on empirical dependencies and the inability to use them to determine the ultimate shear force in concrete for an arbitrary cross section.

2. A method of design of reinforced concrete elements under the action of shear forces is proposed. It is based on the strict principles of mechanics. There are no empirical coefficients in the calculated dependencies. The method is applicable not only to reinforced concrete elements of simple cross-section (rectangular, T- section), but also for other shapes of sections of a more complex configuration.

3. A numerical model of a reinforced concrete element of a rectangular cross-section with an inclined crack under the action of shear forces is created. The analysis of the stress-strain state of the support zone of the beam is performed. A numerical substantiation of the accepted hypotheses and assumptions is given.

4. A good agreement between the results of numerical calculations and the results of regulatory documents for rectangular cross sections is obtained. The discrepancy is 5 %.

References

1. Zalesov, A.S. Kratkiye zametki o raschete zhelezobetonnykh konstruktsiy na deystviye poperechnykh sil [Brief notes on the calculation of reinforced concrete structures for the action of shear forces]. Moscow: 2008. 22 p. (rus).
2. Silantiev, A.S. Prochnost' izgibayemykh zhelezobetonnykh elementov bez khomutov po naklonnym secheniyam s uchetom parametrov prodol'nogo armirovaniya [Shear strength of bended reinforced concrete elements without stirrups according to longitude reinforcement]. Vestnik MGSU. 2001. No. 2. Pp. 163–169. (rus).
3. Filatov, V.B. Raschet zhestkikh naklonnykh secheniy iz gibkikh zhelezobetonnykh elementov s uchetom silovykh zatsepleniy v naklonnoy treshchine [Calculation of the strength of inclined sections of bent reinforced concrete elements taking into account the bonding forces in an inclined crack]. Concrete Technologies. 2014. No. 10. Pp. 46–49. (rus).
4. Huber, P., Huber, T., Kollegger, J. Influence of loading conditions on the shear capacity of post–tensioned beams with low shear reinforcement ratios. Engineering Structures. 2018. Vol. 170. Pp. 91–102.
5. Shatarat, N., Katkhuda, H., Abdel-Jaber, M., Alqam, M. Experimental investigation of reinforced concrete beams with spiral reinforcement in shear. Construction and Building Materials. 2016. Vol. 125. Pp. 585–594.
6. Huber, P., Huber, T., Kollegger, J. Investigation of the shear behavior of RC beams on the basis of measured crack kinematics. Engineering Structures. Vol. 113. Pp. 41–58.
7. Travush, V.I., Konin, D.V., Krylov, A.S., Kapriyelov, S.S., Chilin, I.A. Experimental study of composite structures for bending elements. Building and Reconstruction. 2017. No. 4(72). Pp. 63–71. (rus).
8. Travush, V.I., Konin, D.V., Krylov, A.S. Strength of reinforced concrete beams of high–performance concrete and fiber reinforced concrete. Magazine of Civil Engineering. 2018. 77(1). Pp. 90–100.

Литература

1. Залесов А.С. Краткие заметки о расчете железобетонных конструкций на действие поперечных сил. М.: 2008.
2. Силантьев А.С. Прочность изгибаемых железобетонных элементов без хомутов по наклонным сечениям с учетом параметров продольного армирования // Вестник МГСУ. 2001. № 2. С. 163–169.
3. Филатов В.Б. Расчет прочности наклонных сечений изгибаемых железобетонных элементов с учетом сил зацепления в наклонной трещине // Технологии бетонов. 2014. № 10. С. 46–49.
4. Huber P., Huber T., Kollegger J. Influence of loading conditions on the shear capacity of post-tensioned beams with low shear reinforcement ratios // Engineering Structures. 2018. Vol. 170. Pp. 91–102.
5. Shatarat N., Katkhuda H., Abdel-Jaber M., Alqam M. Experimental investigation of reinforced concrete beams with spiral reinforcement in shear // Construction and Building Materials. 2016. Vol. 125. Pp. 585–594.
6. Huber P., Huber T., Kollegger J. Investigation of the shear behavior of RC beams on the basis of measured crack kinematics // Engineering Structures. Vol. 113. Pp. 41–58.
7. Травуш В.И., Конин Д.В., Крылов А.С., Каприелов С.С., Чилин И.А. Экспериментальные исследования сталежелезобетонных конструкций, работающих на изгиб // Строительство и реконструкция. 2017. № 4(72). С. 63–71.
8. Травуш В.И., Конин Д.В., Крылов А.С. Прочность железобетонных балок из высокопрочных бетонов и фибробетонов // Инженерно-строительный журнал. 2018. № 1(77). С. 90–100.
9. Травуш В.И., Конин Д.В., Крылов А.С. Прочность железобетонных балок с жесткой арматурой из высокопрочного бетона // Инженерно-строительный журнал. 2018. № 3(79). С. 36–44.
10. Zhou J., Fang X., Yao Z. Mechanical behavior o f a steel tube-confined high-strength concrete shear wall under combined tensile and shear loading // Engineering Structures. 2018. Vol. 171. Pp. 673–685.

Travush, V.I., Krylov, S.B., Konin, D.V., Krylov, A.S. Ultimate state of the support zone of reinforced concrete beams. Magazine of Civil Engineering. 2018. 83(7). Pp. 165–174. doi: 10.18720/MCE.83.15.

9. Travush, V.I., Konin, D.V., Krylov, A.S. Strength of composite steel and concrete beams of high-performance concrete. Magazine of Civil Engineering. 2018. 79(3). Pp. 36–44.
10. Zhou J., Fang X., Yao Z. Mechanical behavior of a steel tube–confined high–strength concrete shear wall under combined tensile and shear loading. Engineering Structures. 2018. Vol. 171. Pp. 673–685.
11. Mészöly, T., Randl, N. Shear behavior of fiber–reinforced ultra–high performance concrete beams. Engineering Structures. 2018. Vol. 168. Pp. 119–127.
12. Yang, K.-H., Chung, H.-S., Lee, E.-T., Eun, H.-C. Shear characteristics of high–strength concrete deep beams without shear reinforcements. Engineering Structures. 2003. Vol. 25. No. 10. Pp. 1343–1352.
13. Zagon, R., Matthys, S., Kissa, Z. Shear behaviour of SFR-UHPC I-shaped beams. Construction and Building Materials. 2016. Vol. 124. Pp. 258–268.
14. Tung, N.D., Tue, N.V. Shear resistance of steel fiber–reinforced concrete beams without conventional shear reinforcement on the basis of the critical shear band concept. Engineering Structures. 2018. Vol. 168. Pp. 698–707.
15. Pansuk, W., Nguyen, T.N., Sato, Y., Den Uijl, J.A., Walravenc, J.C. Shear capacity of high performance fiber reinforced concrete I-beams. Construction and Building Materials. 2017. Vol. 157. Pp. 182–193.
16. Amin, A., Foster, S.J. Shear strength of steel fibre reinforced concrete beams with stirrups. Engineering Structures. 2016. Vol. 111. Pp. 323–332.
17. Hu B., Wu Y.-F. Effect of shear span–to–depth ratio on shear strength components of RC beams. Engineering Structures. 2018. Vol. 168. 1 August. Pp. 770–783.
18. Joergensen, H.B., Hansen, S.G. Experimental investigation on the shear capacity of RC beams with curtailed reinforcement. Engineering Structures. 2018. Vol. 169. Pp. 81–93.
19. Kim, G., Sim, J., Oh, H. Shear strength of strengthened RC beams with FRPs in shear. Construction and Building Materials. 2008. Vol. 22. No. 6. Pp. 1261–1270.
20. Morozov, A.N. K teorii zhestkikh zhelezobetonnykh elementov po naklonnym secheniyam [To the theory of strength of reinforced concrete elements in inclined sections]. Industrial and civil engineering. 2018. No. 2. Pp. 53–59. (rus).
21. Erlend Bognøy, Tor Magne Sølverød Mo, Vegard Vee. Fatigue Capacity of partially loaded Areas in Concrete Structures submerged in Water. Norwegian University of Science and Technology. 2014. 107 p.
22. Tinini, A., Minelli, F., Belletti, B., Scolari, M. Biaxial shear in RC square beams: Experimental, numerical and analytical program. Engineering Structures. 2016. Vol. 126. Pp. 469–480.
23. Filatov, V.B., Zhiltsov, Yu.V. Osobennosti raboty i effektivnoye ispol'zovaniye zhestkoy poperechnoy armatury zhelezobetonnykh balok [Features of work and effective use of the rigid cross fittings in ferroconcrete beams]. Izvestia of Samara Scientific Center of the Russian Academy of Sciences. 2012. P. 14. No. 4–5. Pp. 1325–1328. (rus).
24. Slobbe, T., Hendriks, M.A.N., Rots, J.G. Sequentially linear analysis of shear critical reinforced concrete beams without shear reinforcement. Finite Elements in Analysis and Design. 2012. Vol. 50. Pp. 108–124.
25. Breveglieri, M., Barros, J.A.O., Aprile, A., Ventura-Gouveia, A. Strategies for numerical modeling the behavior of RC beams strengthened in shear using the ETS technique. Engineering Structures. 2016. Vol. 128. Pp. 296–315.
11. Mészöly T., Randl N. Shear behavior of fiber-reinforced ultra-high performance concrete beams // Engineering Structures. 2018. Vol. 168. Pp. 119–127.
12. Yang K.-H., Chung H.-S., Lee E.-T., Eun H.-C. Shear characteristics of high-strength concrete deep beams without shear reinforcements // Engineering Structures. 2003. Vol. 25. № 10. Pp. 1343–1352.
13. Zagon R., Matthys S., Kissa Z. Shear behaviour of SFR–UHPC I–shaped beams // Construction and Building Materials. 2016. Vol. 124. Pp. 258–268.
14. Tung N.D., Tue N.V. Shear resistance of steel fiber–reinforced concrete beams without conventional shear reinforcement on the basis of the critical shear band concept // Engineering Structures. 2018. Vol. 168. Pp. 698–707.
15. Pansuk W., Nguyen T.N., Sato Y., Den Uijl J.A., Walravenc J.C. Shear capacity of high performance fiber reinforced concrete I–beams // Construction and Building Materials. 2017. Vol. 157. Pp. 182–193.
16. Amin A., Foster S.J. Shear strength of steel fibre reinforced concrete beams with stirrups // Engineering Structures. 2016. Vol. 111. Pp. 323–332.
17. Hu B., Wu Y.-F. Effect of shear span–to–depth ratio on shear strength components of RC beams // Engineering Structures. 2018. Vol. 168. Pp. 770–783.
18. Joergensen H.B., Hansen S.G. Experimental investigation on the shear capacity of RC beams with curtailed reinforcement // Engineering Structures. 2018. Vol. 169. Pp. 81–93.
19. Kim G., Sim J., Oh H. Shear strength of strengthened RC beams with FRPs in shear // Construction and Building Materials. 2008. Vol. 22. № 6. Pp. 1261–1270.
20. Морозов А.Н. К теории прочности железобетонных элементов по наклонным сечениям // Промышленное и гражданское строительство. 2018. № 2. С. 53–59.
21. Erlend Bognøy, Tor Magne Sølverød Mo, Vegard Vee. Fatigue Capacity of partially loaded Areas in Concrete Structures submerged in Water. Norwegian University of Science and Technology. 2014. 107 p.
22. Tinini A., Minelli F., Belletti B., Scolari M. Biaxial shear in RC square beams: Experimental, numerical and analytical program // Engineering Structures. 2016. Vol. 126. Pp. 469–480.
23. Филатов В.Б., Жильцов Ю.В. Особенности работы и эффективное использование жесткой поперечной арматуры железобетонных балок // Известия самарского научного центра российской академии наук. 2012. Т. 14. № 4–5. С. 1325–1328.
24. Slobbe T., Hendriks M. A. N., Rots J. G. Sequentially linear analysis of shear critical reinforced concrete beams without shear reinforcement // Finite Elements in Analysis and Design. 2012. Vol. 50. Pp. 108–124.
25. Breveglieri M., Barros J.A.O., Aprile A., Ventura-Gouveia A. Strategies for numerical modeling the behavior of RC beams strengthened in shear using the ETS technique. Engineering Structures. 2016. Vol. 128. Pp. 296–315.
26. Limam S., Nana W.S.A., Bui T.T., Limam A., Abouri S. Experimental investigation and analytical calculations on shear strength of full–scale RC slabs with shear reinforcement for nuclear power plants // Nuclear Engineering and Design. 2017. Vol. 324. Pp. 143–157.
27. Nagrodzka-Godycka K., Wiśniowska M. Verification of Selected Calculation Methods Regarding Shear Strength in Reinforced and Prestressed Concrete Beams // Procedia Engineering. 2017. Vol. 193. Pp. 136–143.
28. Ribeiro A.B., Calixto J.M.F., Diniz S.M.C. Assessment of epistemic uncertainties in the shear strength of slender reinforced concrete beams // Engineering Structures. 2016. Vol. 116. Pp. 140–147.

Травуш В.И., Крылов С.Б., Конин Д.В., Крылов А.С. Предельное состояние приопорной зоны железобетонных балок // Инженерно-строительный журнал. 2018. № 7(83). С. 165–174.

26. Limam, S., Nana, W.S.A., Bui, T.T., Limam, A., Abouri, S Experimental investigation and analytical calculations on shear strength of full–scale RC slabs with shear reinforcement for nuclear power plants. Nuclear Engineering and Design. 2017. Vol. 324. Pp. 143–157.
27. Nagrodzka-Godycka, K., Wiśniowska, M. Verification of Selected Calculation Methods Regarding Shear Strength in Reinforced and Prestressed Concrete Beams. Procedia Engineering. 2017. Vol. 193. Pp. 136–143.
28. Ribeiro, A.B., Calixto, J.M.F., Diniz, S.M.C. Assessment of epistemic uncertainties in the shear strength of slender reinforced concrete beams. Engineering Structures. 2016. Vol. 116. Pp. 140–147.
29. Vecchio, F.J., Collins, M.P. The Modified Compression Field Theory for Reinforced Concrete Elements Subjected to Shear. ACI Journal, Proceedings. 1986. Vol. 83. No. 2. Pp. 219–231.
30. Karpenko N.I. Obshchiye modeli mekhaniki zhelezobetona [Models of reinforced concrete mechanics]. Moscow: Stroyizdat, 1996. 416 p. (rus).
31. Geniyev, G.A., Kissyuk, V.N., Tyupin, G.A. Teoriya plastichnosti betona i zhelezobetona [Theory of plasticity of concrete and reinforced concrete]. Moscow: Stroyizdat, 1974. 316 p. (rus).

29. Vecchio F.J., Collins M.P. The Modified Compression Field Theory for Reinforced Concrete Elements Subjected to Shear // ACI Journal, Proceedings. 1986. Vol. 83. № 2. Pp. 219–231.
30. Карпенко Н.И Общие Модели Механики Железобетона. М.: Стройиздат, 1996. 416 с.
31. Гениев Г.А., Киссюк В.Н., Тюпин Г.А. Теория пластичности бетона и железобетона. М.: Стройиздат, 1974. 316 с.

Vladimir Travush,
+7(495)775-75-65; travush@mail.ru

Sergey Krylov,*
+7(965)322-21-47; krylov_s_b@mail.ru

Denis Konin,
+7(926)853-99-73; konden@inbox.ru

Alexey Krylov,
+7(919)723-05-71; kryl07@mail.ru

Владимир Ильич Травуш,
+7(495)775-75-65; эл. почта: travush@mail.ru

Сергей Борисович Крылов,*
+7(965)322-21-47;
эл. почта: krylov_s_b@mail.ru

Денис Владимирович Конин,
+7(926)853-99-73; эл. почта: konden@inbox.ru

Алексей Сергеевич Крылов,
+7(919)723-05-71; эл. почта: kryl07@mail.ru

Travush, V.I., Krylov, S.B., Konin, D.V., Krylov, A.S. Ultimate state of the support zone of reinforced concrete beams. Magazine of Civil Engineering. 2018. 83(7). Pp. 165–174. doi: 10.18720/MCE.83.15.

doi: 10.18720/MCE.83.16

Optimization of hybrid I-beams using modified particle swarm method

Оптимизация бистальных балок на основе модификации метода роя частиц

A.V. Alekseytsev*,
National Research Moscow State Civil Engineering University, Moscow, Russia
M. Al Ali,
Technical University in Košice, Košice, Slovak Republic

Канд. техн. наук, доцент
А.В. Алексейцев*,
Национальный исследовательский Московский государственный строительный университет, Москва, Россия
канд. техн. наук, заведующий кафедрой
М. Ал Али,
Технический университет г. Кошице, Кошице, Словакия

Key words: particle swarm optimization; I-beam; hybrid beam; stiffeners; flange; web; finite element method; plastic deformations; local stability; overall stability

Ключевые слова: рой частиц; оптимизация; бистальная балка; ребра жесткости; пояса; стенка; метод конечных элементов; пластические деформации; местная устойчивость; общая устойчивость

Abstract. An approach for the optimization of hybrid welded I-beams based on the modification of the particle swarm method is proposed. A solution search is performed on discrete sets of variable parameters, which are taken as the size of sheets of rolled steel and steel grades. Depending on the values of the variables, a design of the support and ordinary stiffeners and their location along the length of the beam is performed. When varying the thickness of the sheets, the change in the design resistance is taken into account. As a mathematical model for calculating the stress-strain state, analytical expressions are used. To save the best solutions, the method of copying particles and their storage strategy in the database are used. This database is generated in accordance with the elitist principle, known in the evolutionary modeling theory. This makes it possible to obtain a high-performance optimization algorithm for structures of this type. The verification of the solution is performed using the finite element analysis.

Аннотация. Предложен подход к оптимизации бистальных сварных балок, базирующийся на модификации метода роя частиц. Поиск решений выполняется на дискретных множествах варьируемых параметров, в качестве которых принимаются размеры листов стального проката и марки стали. В зависимости от значений варьируемых параметров выполняется проектирование опорных и рядовых ребер жесткости, рациональная их расстановка по длине балки. При варьировании толщин листов учитывается изменение расчетного сопротивления. В качестве математической модели для оценки напряженно-деформируемого состояния используются аналитические выражения, что позволяет получить высокопроизводительный алгоритм оптимизации для конструкций такого типа. Для сохранения лучших решений используется прием копирования лучших частиц и стратегия их хранения в базе данных. Эта база формируется в соответствии с известным в теории эволюционного моделирования принципом элитизма. Расчет полученного решения в программном комплексе конечно-элементного анализа NX Nastran показал работоспособность предлагаемой поисковой методики.

1. Introduction

In the process of steel-frame structures construction, welded I-beams made of hot-rolled steel sheets are frequently used. The subject matter of study of such structures, related to the topology and parameter optimization, bears relevance. Thus, special attention is paid to the formation of the web topology [1, 3, 13, 20], search for the rational shape of a cross-section [2, 8] and the adjustment of the section sizes [6, 9, 12, 15]. The tasks of the optimization of compound and inhomogeneous bars were addressed in [7, 9, 10, 11, 23]. When optimizing thin-walled beams the single-purpose approach with regard to the production and transportation costs, expenditures on the painting of beams [5], on the emission of green-house gases into

Алексейцев А.В., Ал Али М. Оптимизация бистальных балок на основе модификации метода роя частиц // Инженерно-строительный журнал. 2018. № 7(83). С. 175–185.

the atmosphere [16], as well as multi-purpose approaches [12] were used. To search for solutions, PSO [2, 24], SGA [6], ACO [8] methods, simulated annealing [9], quadratic programming [19], modified genetic algorithms [19, 20, 21, 28], mixed metaheuristic approaches [17, 27, 29] were used. In the research process [14] a thin-walled beam was optimized with regard to the fault stability in the emergency conditions [18, 22]. Along with the optimization algorithms, the complex issues of assessing the stress-strain state of I-beams [4, 15] are being studied, taking into account the contact with a solid body, bending with relation to two central axes of inertia, free and constrained torsion.

One of the effective types of thin-walled I-section structures is a hybrid (consisting of various steels types and grades) beam, which can be used in constructions of a normal level of reliability without permanent human presence. For example, these include beam grillages, girders (Figure 1,a) and supporting structures of auxiliary facilities of treatment plants, meat packing plants, shops specializing in cooling and processing of semi-finished products, etc. With a rational approach to the design of hybrid I-beams, it is possible to significantly reduce the steel consumption, as compared to structures made from homogeneous steel. However, the process of optimal design with regard to the sufficiently wide range of steel grades and sheet sizes is very time-consuming.

The goal of this research is the development of a computational algorithm for obtaining rational design solutions on the basis of a system of numerous steel grades and sheet steel dimensions associated with the characteristics of a particular steel. To achieve the stated goal, the approach based on the modification of the particle swarm method [2] is used.

2. Methods

2.1. Formulation of the problem

For a hybrid beam structure of an I-section, the problem of the search for minimum of the objective function on discrete sets $\{V\}$ of variables is formed

$$C(\{V\}_i)+C(D)\to \min,\ i\in[1;in], \tag{1}$$

where in is the quantity of variables. As independent variables, the width and height of the sheets constituting the I- beam, as well as the steel grades, from which these sheets are made, are taken. Thicknesses of flanges and the web are supposed to be dependent variables determined by values, acceptable for a particular steel grade. The value of the objective function are the costs that are required to manufacture a beam. These costs include both the cost of the flat steel $C(\{V\}_i)$, as well as associated works $C(D)$, where $D=\{D_1,..,D_y\}$, $q\in[1;y]$ y is the number of associated works. The costs of the following works is considered: welding with ultrasonic quality control D_1, end milling D_2, marking and cutting of stiffeners D_3, anti-corrosion treatment D_4, expendable materials D_5. All these costs are calculated in accordance with the formulas of research [5]. The result is:

$$C(D)=\sum_{q=1}^{5} C(D_q). \tag{2}$$

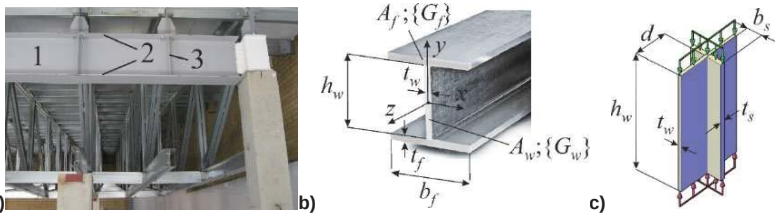

a) b) c)

Figure 1. For the calculation of stress-strain state of the hybrid I-beam: a – field appearance of one structure variant, 1 – web, 2 – flanges, 3 – stiffeners; b – sectional parameters, A_w, A_f – web and flanges areas, $\{G_f\}$ $\{G_w\}$ – discrete sets of steel grades for flanges and web; c – computational model for the assessment of vertical stiffeners stability

In the course of solving the problem, the volume of rolled steel sheets is directly calculated, the steel grade for webs and flanges of the beam is selected, and the rest of the costs can be approximately assessed based on the data of the manufacturing plants, depending on the volume received. According to commercial proposals of enterprises, it was established that the cost of beams manufacturing $C(D)$ is about 0.3–0.4 of the value $C(\{V\}_i)$.

It is assumed, that the beam bends in the plane of its maximum stiffness. Beam flanges operate under conditions of elastic deformations, and the web operates under limited elastoplastic deformations. These deformations continue, until the stresses in the flanges reach the yield point. In this case, to ensure local stability of the web, it is possible to set vertical stiffeners. These elements are manufactured of the same steel as the web. The load is applied to the upper flange of the beam. To calculate the stress state of the structures under consideration, a mathematical model from regulatory standards [25] is used. For each of the design load cases the following active constraints are taken into account [25]:

1. Structural strength with regard to the development of plastic deformations in the web

$$\frac{\sigma_z}{c_{xr}\beta R_w} \le 1,$$

$$\beta = 1 - \frac{0,2}{(R_f A_f)/(R_w A_w) + 0.25}\left(\frac{\tau_x}{R_{sw}}\right)^4;\ \tau_x = \frac{Q_x}{A_w}; \qquad (3)$$

$$c_{xr} = \frac{(R_f A_f)/(R_w A_w) + 0.2 - 0.0833(R_f / R_w)^2}{A_f / A_w + 0.167}.$$

Here, σ_z, τ_x are the maximum axial and shear stresses in the cross-section of the beam with the bending relatively to the x axis (Figure 1, b), Q_x is the maximum shear force, A_f, A_w are the flange and web areas respectively, R_f, R_w are the design resistances to the bend (allowable bending stresses) for the flange and web respectively.

2. Overall stability of the I-beam [25]

$$\frac{\sigma_x}{\varphi_b R_f} \le 1, \qquad (4)$$

where φ_b is the stability coefficient, determined in accordance with the Supplement in [25].

It should be noted, that the buckling out of the vertical plane of the beam, due to loss of the flat shape bending stability, do not allow in the following ways:

- the I-beam cross-sectional dimensions at varying geometry are assigned so that the values J_x and J_y moments of inertia (Figure 1,b) differ slightly. That is, it is adopted wide-sectional form;
- restriction of the displacements for the beams upper belt out the plane of their bending.
- the following condition for the stability of a flat bend for an I-section is verified [30]:

$$M_{\max} \le M_{cr} = k\frac{\sqrt{EJ_y C}}{l},\ k^2 = \pi^2\left(1 + \pi^2\frac{D_y h^2}{2Cl^2}\right), C = G(J_x + J_y), \qquad (5)$$

where M_{cr} is conditional bending moment, corresponding to loss of stability, h, l, C, G, D_y are the section height, beam span, torsional stiffness of the section, shear modulus and shelves stiffness respectively.

3. Local stability of the flange compression [25]:

$$\overline{\lambda} \le \lambda_{ub},\ \overline{\lambda} = \frac{l_f}{b_f}\sqrt{\frac{R_f}{E}};$$

$$\lambda_{ub} = \delta_x(0.35 + 0.0032\frac{b_f}{t_f} + (0.76 - 0.02\ \frac{b_f}{t_f})\ \times$$
$$\times\frac{b_f}{h_w}\sqrt{\frac{R_f}{\sigma_z}};\ \ \delta_x = 1 - 0.6(c_{x1} - 1)/(c_{xr} - 1); \quad (6)$$

$$c_{x1} = \max\left\{\sigma_x / R_f;\ \beta c_{xr}\right\}\ .$$

Here l_f is the effective length of the flange between the restraining points from the main loading plane of the beam, E is the elastic modulus of the steel, b_f, t_f, h_w are the dimensions of the section shown in Figure 1, a.

Local stability of stiffeners. The computational model for paired stiffeners is shown in Figure 1, c. The stability condition is presented in the following form [25]:

$$\frac{\sigma}{\varphi_e R} \le 1, \varphi_e = 0.5(\delta - \sqrt{\delta^2 - 39.48\overline{\lambda}^2}/\overline{\lambda}^2;$$
$$\delta = 9.87(0.96 + 0.09\overline{\lambda}) + \overline{\lambda}^2;\ \overline{\lambda} = (h_w / i)\sqrt{\frac{R_w}{E}}\ . \quad (7)$$

The radius of inertia i is calculated for the conditional section, including the web with the length of $2d$ and the stiffeners adjacent to it in this area (see Figure 1, b). The value d is found as $d = 0.65t_w\sqrt{E / R_w}$

The structural stiffness $\left|\delta_{\max}\right| \le \left[\delta\right]$, where $\left[\delta\right]$ is the allowable value of displacement. The displacements of the system to accelerate calculations are calculated on the basis of formulas obtained using Mohr's integrals. For the final solution, a verifying calculation of the shift is performed on the basis of the finite element method.

The welding condition of sheets of the web and flanges is verified as a passive constraint. The sheet thicknesses obtained in the process of search for the solution are verified according to Table 1 with regard to the condition of $k_f \le 1,2t_{\max}$, k_f is the weld leg, $t_{\max}$ is the maximum thickness of welded elements.

Table 1. Selection of the weld leg, joining the flange with the web

Joint type	Welding type	Steel yield stress, N/mm²	Minimal weld leg k_f, mm, with the thickness of thicker welded element t, mm						
			4-5	6-10	11-16	17-22	23-32	33-40	41-80
T-joint with double-sided fillet welds	Automatic and machine welding	< 285	3	4	4	5	5	6	6
		285…390	3	4	5	6	7	8	9
		390…590	4	5	6	7	8	9	10

2.2. Method of solving the problem

The principle stages is performed.

1. *Initialization of parameters and ranges of their acceptable values.* Each variant of the structure, formed on the basis of variables, is interpreted as a "particle" (Figure 2). For each variable parameter *i* the range of acceptable values is formed in the type of discrete sets $\{V_k\}_i$, $k \in [1; m]$, m is the quantity of

these values. Elements of these sets should be put in descending order of values. It is assumed that at the maximum values of parameters all the formulated constraints are satisfied. Then the relation for the object cost can be represented as follows: $C(\{V_k\}_i) = f(v_1^{(\max)},...,v_i^{(\max)},...,v_{in}^{(\max)})$. The value $C(\{V_k\}_i)$ should not be more than an order of magnitude greater than the average cost of similar objects introduced on the market.

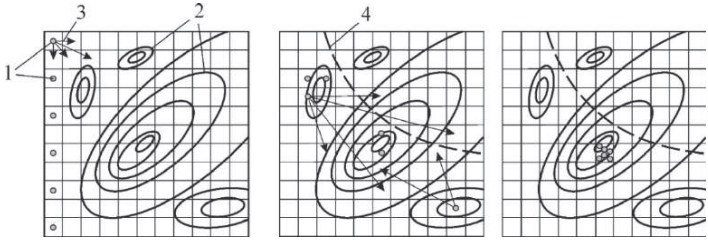

1. Initialization of parameters and ranges of their acceptable values

2. Identification of the permissible solutions range and particle motion

3. Maintenance of motion. Passing of the local optima

Figure 2. Illustration of the extremum seeking through the example of six particles: 1 – formed particles, 2 – contour lines of values of the function $C(\{V\}_i)$, 3 – directions Pos_i of the particle motion, 4 – boundary between the area of permissible solutions (on the bottom) and the area of infeasible solutions

The decomposition of the parameters by dividing them into independent and dependent variables is performed. The individual particle is presented in the form: $P: \left\{ V_1,...,V_{i_0},V_{i_0+1}(V_j),...,V_{in}(V_j) \right\}$, $j \in [1; i_0]$. Parameters $V_1 - V_i$ for the I-section is the independently variable width of the flange b_f and the height of the web h_w, resistance to bending of flanges R_f and the web R_w, determined by the respective steel grades; i_0 is the number of independent variables. Dependent variables $V_{i_0+1}(V_j) - V_{in}(V_j)$ are thicknesses of flanges $t_f(R_f)$ and of the web $t_w(R_w)$.

The search for the parameters of sheets of flanges and a web for all possible combinations of steel grades of web and flanges is presented. For each of these combinations initial, the sets of particles $P^{(\tilde{c})}$, where $\tilde{c}$ is the number of the combination, is created. For each particle in the set, we a group of positions is formed. The maximum size of such a group is determined by the minimum number m defined in the analysis of all variable parameters. Then the positions of the particles can be represented in the form of the following notation.

$$\begin{array}{c|cccc} Pos_1: & V_{1,1}^{(\max)} & ... & V_{1,in-1}^{(\max)} & V_{1,in}^{(\max)} \\ \hline ... & ... & ... & ... & ... \\ \hline Pos_{n_0}: & V_{m,1}^{(\min)} & ... & V_{m,in-1}^{(\min)} & V_{m,in}^{(\min)} \end{array}. \quad (8)$$

2. Identification of the permissible solutions range and particle motion. Each particle of the set $P^{(\tilde{c})}$ is tested for the constraint satisfaction. At the same time, an automated design of the stiffeners is performed. To do so, the following steps are implemented:

2.1. For bearing support stiffeners the thickness t_{sr} and width b_{sr} are calculated [25]:

$$b_{sr} = 0.5\left(b_f - t_w\right) - 0.015,\ (m);\ t_{sr} = 1.5\sqrt{R_w / E}\,. \quad (9)$$

2.2. The need to install stiffeners in the compartments is determined. The compartments are formed by dividing the beam by the boundary stiffeners, which are affixed in a mandatory manner in the places where the concentrated loads are applied. If a uniformly distributed load is applied, the boundary stiffeners are placed on the area of the beam where the bending moment is $M \geq 0.7M_{\max}$. Spacing l_s of stiffeners inside the compartments is determined depending on the value of the specified flexibility of the web $\bar{\lambda}_w = (h_w / t_w)\sqrt{R_{wy} / E}$.

Further the following condition [25] is checked

$$\begin{cases} \bar{\lambda}_w \geq 3.2 \rightarrow l_s = 2h_w \\ \bar{\lambda}_w < 3.2 \rightarrow l_s = 2.5h_w \end{cases}. \quad (10)$$

The thickness of these stiffeners t_s and the width b_s is determined by equations:

$$t_s = \sqrt{R_{wy} / E}\ ,\ b_s = 0.1h_w - 0.025,\ (m). \quad (11)$$

2.3. The stability of the transversal stiffeners located under the concentrated forces is verified. The calculation is performed for the most stressed sector of the beam, which is a cross-shaped segment, shown in Figure 1, c.

2.3.1. Material cost calculation. For those particles, that satisfy all constraints, the value $C(\{V\}_i)$ is calculated. If the constraints are satisfied for the initial particle with the minimum values of all variables, then this implies that all solutions are in the permissible range and further reduction of the values of variables is needed. That is, we must return to the stage of the formation of discrete sets. After that we obtain a number of particles for which one or more constraints will be violated. Thus, we separate the range of permissible solutions from the range of infeasible solutions.

2.3.2. Sorting and saving solutions. Particles in the range of permissible solutions are stored in a database, implemented in the form of structured arrays. At this stage, the positions of all the reserved particles are considered to be initial.

2.3.3. Initiation of motion. The modeling of the particle motion is starting. For each of the particles in the initial position, the current set of positions is formed, according to the following principle. In the set only those positions is included, in which the number of the value of one of the variable is reduced by one. Thus, we somewhat imitate the movement of the particle to the optimum, which is assumed by us as a minimum. Further, for each of the particles obtained, constraint satisfaction is verified and the objective function is calculated. If for different positions of the particle the best value of the objective function is the same, then in the next stage all such positions are considered, that is, the particle multiplies.

3. Maintenance of motion. Passing of the local optima. All new particle positions corresponding to the state of variables providing the best value of the objective function when all constraints are satisfied are stored in the database. Further, for these positions the stage of particle motion is performed. That is, the current position is adopted as the initial one and the procedure described above is performed. The process of particle motion continues, until the improvement of the objective function with a change of the position occurs for at least one of the particles.

In order to pass local optima for all particles in their best positions, the formation of possible positions in the range of infeasible solutions is conducted. For these positions, constraints are verified. If constraints are satisfied for any of the positions, this testifies to the fact that the particle falls into the local optimum in its previous position. If the new position of the particle, while satisfying the constraints, exists, then it is memorized and the procedures of motion and motion maintenance are performed for this particle.

4. *Selection of best particles.* For each of the combinations of steel grades of flanges and the web of the beam, the calculation of the value $C(D)$ is performed, the verification of the passive constraint (welding conditions) is conducted. For the selected solutions, the checking calculation through a finite element analysis is performed. As a result, one best option can be selected, which corresponds to the territorial possibilities of manufacture and minimization of costs

3. Results and Discussion

The main beam with support of secondary structures on the upper flange is considered, the analogue is shown in Figure 1,a. We assume that the secondary structures divide the span of the main beam into 4

compartments equal in length and transmit concentrated forces to its upper flange. The computational model is shown in Figure 3.

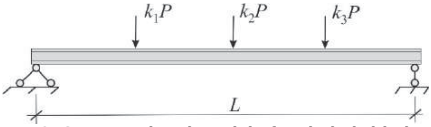

Figure 3. Computational model of main hybrid I-beam

The value $L = 12$ m is set. The following sets of steel grades [26] were accepted for the flanges: $\{G_f\} = \{\text{C345, C375, C390}\}$, for the web, bearing support stiffeners and stiffeners: $\{G_w\} = \{\text{C245, C255, C285}\}$ (Figure 1,b). Concentrated force is $P = 40$ kH. Two loads were taken into account: in the first case $k_1 = k_3 = 1$, $k_2 = 4$ were taken, in the second case $k_1 = 3$, $k_2 = 2$, $k_3 = 1$ were taken. There was a restriction on the movements $[\delta] = 6$ *cm*. The limitation of displacements from the plane of the beam bending are assigned to the supports and points of the load application. For each of the possible combinations of steels formed from the sets $\{G_f\}$ $\{G_w\}$, the choice of flat steel thicknesses was allowed in accordance with Table. 2. Independent variables values are presented in Table 3. To account for the difference in the cost of steel grades, cost factors k_c were introduced. The minimum cost has steel C245, for which the factor is $k_c = 1$. The permissible stresses and values k_c for the steel grades under consideration are given in Table 4.

As a result, for these load-bearing and kinematic constraints, 9 solutions were found with a different conditional cost, presented in Table 5.

Table 2. Ranges of thicknesses allowable for the selection

Thickness of sheets t, mm for a steel grade [26]					
C245	C255	C285	C345	C375	C390
6, 7, 8	7, 8, 9, 10, 12, 14, 16, 18 ,20, 22, 24, 26, 28, 30, 32, 34, 36, 40	7, 8, 9, 10, 12, 14, 16, 18, 20	7, 8, 9, 10, 12, 14, 16, 18 ,20, 22, 24, 26, 28, 30, 32, 34, 36, 40, 42, 44, 46 48, 50	7, 8, 9, 10, 12, 14, 16, 18 ,20, 22, 24, 26, 28, 30, 32, 34, 36, 40	7, 8, 9, 10, 12, 14, 16, 18 ,20, 22, 24, 26, 28, 30, 32, 34, 36, 40, 42, 44, 46 48, 50

Table 3 Ranges of plates allowable for the choice of dimensions

Dimensions of beam sheets [26], mm	
h_w	b_f
200, 220, 240, 260, 280, 300, 320, 340, 360, 380, 400, 420, 440, 460, 480, 500 530, 560, 600, 630, 670, 700, 750, 800, 1000, 1200	200, 220, 240, 260, 280, 300, 320, 340, 360, 380, 400, 420, 440, 460, 480, 500 530, 560, 600, 630, 670, 700, 750, 800

Table 4. Ranges of permissible values of design resistances

Yield stress, MPa for steel grades					
C245	C255	C285	C345	C375	C390
225	235 $\forall t \in [7;20)$, 225 $\forall t \in [20;40]$.	260 $\forall t \in [7;12)$, 250 $\forall t \in [12;20]$.	290 $\forall t \in [7;40)$, 270 $\forall t \in [40;50]$.	340 $\forall t \in [7;24)$, 320 $\forall t \in [24;40]$.	370
Coefficients k_c cost of steel grades					
1.0	1.05	1.08	1.11	1.16	1.22

Table 5. Results of beam costs calculation

Cost of materials $C(\{V\}_i)$ for the solution number:								
1	2	3	4	5	6	7	8	9
98152	89046	87801	75606	90592	98950	95361	92020	72345
Manufacturing costs $C(D)$								
29445.6	28494.72	31608.36	26462.1	29895.36	29685	28608.3	28526.2	24597.3
Total costs $C(\{V\}_i)+C(D)$								
127597.6	117540.7	119409.4	102068.1	120487.4	128635	123969.3	120546.2	100559.6

The presented algorithm was implemented within the I-BEAM software developed by the authors of this article. The user interface is presented in Figure 4. Table 5 summarizes the obtained solutions for nine parallel running threads in an iterative process. Each thread corresponds to a combination of steel grades for the wall and shelves, all combinations are given in Table 6. The data on the convergence of these iterative processes are shown in Figure 5,a. Parameters of the nine best solutions are represented in Table 6. Spacing of stiffeners in all options equals to 1 m.

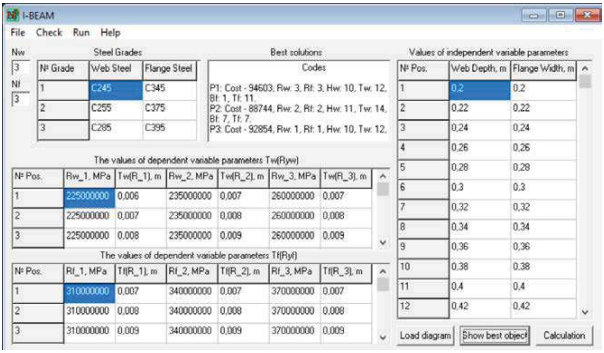

Figure 4. Initial data and calculation results in the I-BEAM software

Table 6. Parameters of a beam, obtained in the result of the problem solution

No.	Steel grade of a web	Steel grade of a flange	h_w, cm	t_w, mm	b_f, cm	t_f, mm	b_{sr}, mm	t_{sr}, mm	b_s, mm	t_s, mm
1	C285	C390	38	7	42	24	191	22	63	15
2	C255	C375	40	16	48	16	217	24	65	16
3	C245	C345	38	6	42	24	192	21	63	14
4	C285	C375	42	7	48	16	221	26	67	17
5	C285	C345	38	7	42	24	191	22	63	15
6	C255	C390	38	12	42	22	189	21	63	14
7	C245	C390	38	6	42	24	192	21	63	14
8	C255	C345	38	12	42	22	189	21	63	14
9	C245	C375	42	6	48	16	222	24	67	16

Table 6 shows that the best solution number 9 on the condition of a minimum of total costs was found. This girder structure is better, if the manufacturer has available steel grades C245 and C375 to produce. If, for example, steel grades C255 and C375 are available for production, then the best solution is beam number 2. For the purpose of verification of the obtained solution, a finite element analysis of beam number 9 was performed. This beam is divided in accordance with clauses 2.1, 2.2 of the proposed algorithm into four compartments I-IV (Figure 5, b). The boundaries of these compartments are determined by the location of the bearing support stiffeners s_1 and stiffeners under load s_2. Ordinary stiffeners s_3 are installed inside the compartments, which provide local stability of the flanges and the web of the beam.

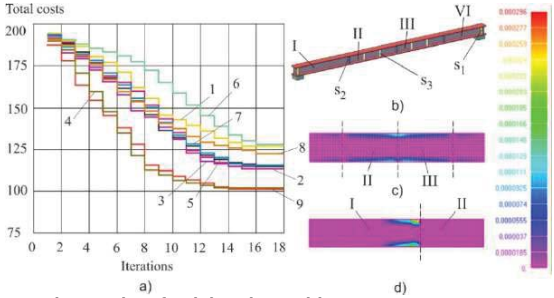

Figure 5. Data on the results of solving the problem: a – convergence graph of iterative processes, 1-9 number of solution on Table 6; b – I-beam stiffeners design topology; c, d – plastic strains on top fiber of the web for load cases 1 and 2 respectively

The FE-analysis of the overall stability of structure No. 9 from Table 5 in the NX Nastran software package (buckling mode) was performed. A shell model with “Plate” type of finite elements was used. As a result, a safety factor of 1.3257 was obtained. Local stability of the I-beam walls and shelves is also provided. Also an analysis under a static loading considering physical nonlinearity (nonlinear static mode) for this object has been performed. In the process the ideal elastoplastic Prandtl model was used to describe the material behavior. This calculation showed, that plastic deformations are present in the wall of the beam. This circumstance confirms the optimality of the obtained solution. The result is shown in Table 7 and Figure 5, c-d.

As a result of the calculation of the beam according to the method [25], the following values of the maximum deflections were obtained. The deflections, determined using the Mohr integrals, from the action of load case 1 and load case 2 were 5.81 mm and 5.94 mm, respectively. From Table 7 it can be seen that the allowable stresses correspond to the set limits. There are differences in displacement by 16.4% and 19.4%. These discrepancies are due to the physical nonlinearity in the finite element analysis.

The presented algorithm can be used effectively for statically definable beams and beam structures. When there is a large number of combinations of steel grades of a web and flanges, as well as when repeatedly statically indeterminate systems for the particle motion modelling are considered, it seems reasonable to introduce genetic algorithms with the finite element method to calculate the displacements [6, 20, 21].

According to the results of calculations for the specified hybrid beams, the displacement values, calculated on the basis of the control finite element analysis under a static loading considering physical nonlinearity, can surpass the deflection calculated on the basis of Mohr's integrals. If such excesses are impermissible according to manufacturing process or aesthetic requirements, the allowable movements should be reduced by 10-25% and the optimal search should be repeated.

Table 7. Components of the stress-strain state of the best solution (No. 9 in Table 5)

Load case	Compartment	Maximum equivalent stresses in the upper flange, MPa	Maximum equivalent stresses in the web, MPa	Maximum plastic strain in the web	Maximum deflection, cm
1	I II III IV	157 164 182 332	134 143 225 225	0.0 0.0 0.00000 0.00007	6.95
2	I II III IV	313 218 229 307	225 146 154 225	0.00024 0.0 0.0 0.00007	7.37

4. Conclusion

A method of search for rational solutions for hybrid I-beams on the basis of the particle swarm method modification was developed. It allows to design a hybrid I-beams, the web and flanges of which are made of different steels. The search is performed on discrete sets of the web and flanges dimensions’

values, as well as on the steel grades from which they are made. Optimization efficiency is achieved by parallel reproduction of the calculation procedure for each of the possible combinations of steel grades for flanges and web. In this case, the analytical dependencies used take into account the strength, stiffness, local and overall stability of the structure. The considered method has high convergence and allows to search for several solutions, based on the possibility of manufacturing the structure. The presented approach can be adapted to optimize other bearing structures, such as trusses and arches.

5. Acknowledgement

The reported study was funded by Russian Foundation for Basic Research (RFBR) according to the research project № 19-08-00103.

References

1. Tsavdaridis, K.D., D'Mello, C. Optimization of novel elliptically-based web opening shapes of perforated steel beams. Journal of Constructional Steel Re-search. 2012. No. 76. Pp. 39–53.
2. Ye, J., Hajirasouliha, I., Becque, J. Optimum design of cold-formed steel beams using Particle Swarm Optimisation method. Journal of Constructional Steel Research. 2016. No. 122. Pp. 80–93.
3. Tsavdaridis, K.D., Kingman, J.J., Toropov, V.V. Application of structural topology optimisation to perforated steel beams. Computers & structures. 2015. No. 158. Pp. 108–123.
4. Gąska, D., Haniszewski, T., Margielewicz, J. I-beam girders dimensioning with numerical modelling of local stresses in wheel-supporting flanges. Mechanika. 2017. Vol. 23(3). Pp. 347–352.
5. Mela, K., Heinisuo, M. Weight and cost optimization of welded high strength steel beams. Engineering Structures. 2014. No. 79. Pp. 354–364.
6. Pedro, R.L., Demarche, J., Miguel, L.F.F. An efficient approach for the optimization of simply supported steel-concrete composite I-girder bridges. Advances in Engineering Software. 2017. No. 112. Pp. 31–45.
7. Andreev, V., Barmenkova, E. Optimization of the thin-walled rod with an open profile. 5th International Scientific Conference on Integration, Partnership and Innovation in Construction Science and Education, 2016 (IPICSE): MATEC Web of Conferences. 2016. No. 86. 01033.
8. Sharafi, P., The, L.H., Hadi, M.N.S. Shape optimization of thin-walled steel sections using graph theory and ACO algorithm. Journal of Constructional Steel Re-search. 2014. No. 101. Pp. 331–341.
9. Reguera, F., Cortinez, H.V. Optimal design of compo-site thin-walled beams using simulated annealing. Thin-walled Structures. 2016. No. 104. Pp. 71–81.
10. Xuan-Hoang, N., Kim, N.-I., Lee, J. Optimum design of thin-walled composite beams for flexural-torsional buckling problem. Composite Structures. 2015. No. 132. Pp. 1065–1074.
11. Tan-Tien, N., Lee, J. Optimal design of thin-walled functionally graded beams for buckling problems. Composite Structures. 2017. No. 179. Pp. 459–467.
12. Ostwald, M., Rodak, M. Multicriteria optimization of cold-formed thin-walled beams with generalized open shape under different loads. Thin-walled Structures. 2013. No. 65. Pp. 26–33.
13. Kim, D.-M., Kim, S.I., Choi, S. Topology optimization of thin-walled box beam structures based on the higher-order beam theory. International Journal for Numerical Methods in Engineering. 2016. Vol. 106(7). Pp. 576–590.
14. Zeng, D., Duddeck, F. Improved hybrid cellular au-tomata for crashworthiness optimization of thin-walled structures. Structural and Multidisciplinary Optimization. 2017. No. 56. Pp. 101–115.
15. Andjelic, N., Milosevic-Mitic, V. Optimum design of thin-walled i-beam subjected to stress constraint. Journal of

Литература

1. Tsavdaridis K.D., D'Mello C. Optimization of novel elliptically-based web opening shapes of perforated steel beams // Journal of Constructional Steel Research. 2012. № 76. Pp. 39–53.
2. Ye J., Hajirasouliha I., Becque J. Optimum design of cold-formed steel beams using Particle Swarm Optimisation method // Journal of Constructional Steel Research. 2016. № 122. Pp. 80–93.
3. Tsavdaridis K.D., Kingman J.J., Toropov V.V. Application of structural topology optimisation to perforated steel beams // Computers & structures. 2015. № 158. Pp. 108–123.
4. Gąska D., Haniszewski T., Margielewicz J. I-beam girders dimensioning with numerical modelling of local stresses in wheel-supporting flanges // Mechanika. 2017. Vol. 23(3). Pp. 347–352.
5. Mela K., Heinisuo M. Weight and cost optimization of welded high strength steel beams // Engineering Structures. 2014. № 79. Pp. 354–364.
6. Pedro R.L., Demarche J., Miguel L.F.F. An efficient approach for the optimization of simply supported steel-concrete composite I-girder bridges // Advances in Engineering Software. 2017. № 112. Pp. 31–45.
7. Andreev V., Barmenkova E. Optimization of the thin-walled rod with an open profile // 5th International Scientific Conference on Integration, Partnership and Innovation in Construction Science and Education, 2016 (IPICSE): MATEC Web of Conferences. 2016. № 86. 01033.
8. Sharafi P., Teh L.H., Hadi M.N.S. Shape optimization of thin-walled steel sections using graph theory and ACO algorithm // Journal of Constructional Steel Research. 2014. № 101. Pp. 331–341.
9. Reguera F., Cortinez H.V. Optimal design of composite thin-walled beams using simulated annealing // Thin-walled Structures. 2016. № 104. Pp. 71–81.
10. Xuan-Hoang N., Kim N.-I., Lee J. Optimum design of thin-walled composite beams for flexural-torsional buckling problem // Composite Structures. 2015. № 132. Pp. 1065-1074.
11. Tan-Tien N., Lee J. Optimal design of thin-walled functionally graded beams for buckling problems // Composite Structures. 2017. № 179. Pp. 459–467.
12. Ostwald M., Rodak M. Multicriteria optimization of cold-formed thin-walled beams with generalized open shape under different loads // Thin-walled Structures. 2013. № 65. Pp. 26–33.
13. Kim D.-M., Kim S.I., Choi S. Topology optimization of thin-walled box beam structures based on the higher-order beam theory // International Journal for Numerical Methods in Engineering. 2016. Vol. 106(7). Pp. 576–590.
14. Zeng D., Duddeck F. Improved hybrid cellular automata for crashworthiness optimization of thin-walled structures // Structural and Multidisciplinary Optimization. 2017. № 56. Pp. 101–115.
15. Andjelic N., Milosevic-Mitic V. Optimum design of thin-walled i-beam subjected to stress constraint // Journal of Theoretical and Applied mechanics. 2012. № 50(4). Pp. 987–999.

Alekseytsev, A.V., Al Ali, M. Optimization of hybrid I-beams using modified particle swarm method. Magazine of Civil Engineering. 2018. 83(7). Pp. 175–185. doi: 10.18720/MCE.83.16.

Theoretical and Applied mechanics. 2012. Vol. 50(4). Pp. 987–999.
16. Li, B., Hong, J., Liu, Z. A novel topology optimization method of welded box-beam structures motivated by low-carbon manufacturing concerns. Journal of Cleaner Production. 2017. No. 142. Pp. 2792–2803.
17. Zhang, H., Liu, T., Liu, H. Optimization design for beam and column of steel structure residence, (ICICTA) 2015: International Conference on Intelligent Computation Technology and Automation. 2015. Pp. 609–612.
18. Alekseytsev, A.V., Kurchenko, N.S. Deformations of steel roof trusses under shock emergency action. Magazine of Civil Engineering. 2017. 73(5). Pp. 3–13.
19. Serpik, I.N., Alekseytsev, A.V. Optimization of flat steel frame and foundation posts system. Magazine of Civil Engineering. 2016. 61(1). Pp. 14–24.
20. Suharjanto, S. Design Optimization Shape Web Opening of Cellular Steel Beams, (ISTIE) 3rd Interna-tional Conference on Internet Services Technology and Information Engineering, Kuta, Indonesia, Advanced science letters. 2015. Vol. 21(10). Pp. 3175–3179.
21. Wolf, C. Stadler, A.T., Baumgartner, W. Cross-section optimisation for cold-rolled steel beams using a ge-netic algorithm. Metal 2016: 25th anniversary inter-national conference on metallurgy and materials. 2016. Pp. 507–512.
22. Shifferaw, Y., Schafer, B.W. Inelastic bending capacity of cold-formed steel members. Journal of Structural Engineering ASCE. 2012. No. 138. Pp. 468–480.
23. Cardoso, J.B., Valido, A.J. Cross-section optimal de-sign of composite laminated thin-walled beams. Composite Structures. 2011. No. 89. Pp. 1069–1076.
24. Poli, R., Kennedy, J., Blackwell, T. Particle swarm op-timization – an overview. Swarm Intell. 2007. No. 1. Pp. 33–57.
25. Russian Construction Norms. SP 16.13330.2017 Steel structures. (rus)
26. Russian State Standard GOST 19903-2015 Hot-rolled steel sheets.
27. Serpik, I.N., Alekseytsev, A.V., Balabin, P.Y. Mixed approaches to handle limitations and execute mutation in the genetic algorithm for truss size, shape and topology optimization. Periodica Polytechnica Civil Engineering. 2017. Vol. 61(3). Pp. 471–482.
28. Alekseytsev, A.V. Evolutionary optimization of steel trusses with the nodal joints of rods. Magazine of Civil Engineering. 2013. 40(5). Pp. 28–37.
29. Serpik, I.N., Alekseytsev, A.V., Balabin, P.Yu., Kurchenko, N.S. Flat rod systems: optimization with overall stability control. Magazine of Civil Engineering. 2017. 76(8). Pp. 181–192.
30. Feppl, A., Feppl, L. Sila i deformaciya. Prikladnaya teoriya uprugosti [The force and deformation. Applied theory of elasticity]. Vol. 2, Moscow, 1936. 408 p. (rus)

Anatoly Alekseytsev,*
+7(960)564-33-58; aalexw@mail.ru

Mohamad Al Ali,
00421905359228; mohamad.alali@tuke.sk

16. Li B., Hong J., Liu Z. A novel topology optimization method of welded box-beam structures motivated by low-carbon manufacturing concerns // Journal of Cleaner Production. 2017. № 142. Pp. 2792–2803.
17. Zhang H., Liu T., Liu H. Optimization design for beam and column of steel structure residence // (ICICTA) 2015: International Conference on Intelligent Computation Technology and Automation. 2015. Pp. 609–612.
18. Алексейцев А.В., Курченко Н.С. Деформации стальных стропильных ферм при ударных аварийных воздействиях // Инженерно-строительный журнал. 2017. № 5(73). С. 3–13.
19. Серпик И.Н., Алексейцев А.В. Оптимизация системы стальной плоской рамы и столбчатых фундаментов // Инженерно-строительный журнал. 2016. № 1(61). С. 14–24.
20. Suharjanto S. Design Optimization Shape Web Opening of Cellular Steel Beams // (ISTIE) 3rd International Conference on Internet Services Technology and Information Engineering, Kuta, Indonesia, Advanced science letters. 2015. Vol. 21(10). Pp. 3175–3179.
21. Wolf C. Stadler A.T., Baumgartner W. Cross-section optimisation for cold-rolled steel beams using a genetic algorithm // Metal 2016: 25th anniversary international conference on metallurgy and materials: 2016. Pp. 507–512.
22. Shifferaw Y., Schafer B.W. Inelastic bending capacity of cold-formed steel members // Journal of Structural Engineering ASCE. 2012. № 138. Pp. 468–480.
23. Cardoso J.B., Valido A.J. Cross-section optimal design of composite laminated thin-walled beams // Composite Structures. 2011. № 89. Pp. 1069–1076.
24. Poli R., Kennedy J., Blackwell T. Particle swarm optimization – an overview // Swarm Intell. 2007. № 1. Pp. 33–57.
25. СП 16.13330.2017 «СНиП II-23-81* Стальные конструкции» (Приказ Минстроя России от 27 февраля 2017 г. № 126/пр.
26. ГОСТ 19903-2015 Прокат листовой горячекатаный. Сортамент.
27. Serpik I. N., Alekseytsev A.V., Balabin P.Y. Mixed Approaches to Handle Limitations and Execute Mutation in the Genetic Algorithm for Truss Size, Shape and Topology Optimization // Periodica Polytechnica Civil Engineering. № 61(3). 2017. Pp. 471–482.
28. Алексейцев А.В. Эволюционная оптимизация стальных ферм с учетом узловых соединений стержней // Инженерно-строительный журнал. 2013. №5(40). С. 28–37.
29. Серпик И.Н., Алексейцев А.В., Балабин П.Ю., Курченко Н.С. Плоские стержневые системы: оптимизация с контролем общей устойчивости // Инженерно-строительный журнал. 2017. № 8(76). С. 181–192.
30. Фепплъ А., Фепплъ Л. Сила и деформация. Прикладная теория упругости. Т.2. Москва, 1936. 408 с.

Анатолий Викторович Алексейцев,*
+7(960)564-33-58; эл. почта: aalexw@mail.ru

Мохамад Ал Али,
00421905359228;
эл. почта: mohamad.alali@tuke.sk

Алексейцев А.В., Ал Али М. Оптимизация бистальных балок на основе модификации метода роя частиц // Инженерно-строительный журнал. 2018. № 7(83). С. 175–185.

doi: 10.18720/MCE.83.17

Method of calculating the optimal sand content in normal-weight concrete

Метод расчета оптимального содержания песка в тяжелом бетоне

L.I. Dvorkin,
National University of Water Environmental Engineering, Rivne, Ukraine

Д-р техн. наук, заведующий кафедрой Л.И. Дворкин,
Национальный университет водного хозяйства и природопользования, Ровно, Украина

Key words: concrete mixture; optimal sand content; viscosity; water demand; water separation; the volume of the entrained air; calculation

Ключевые слова: бетонная смесь; оптимальное содержание песка; вязкость; водопотребность; водоотделение; объем вовлеченного воздуха; расчет

Abstract. In the practice of proportioning concrete compositions, the optimum sand content in a mixture of aggregates is usually found empirically. The disadvantage of this approach is the considerable complexity and duration of the required tests. The aim of the work is to develop a calculation methodology for finding the content of sand in the normal-weight concrete, taking into account the optimality criteria given. Based on the well-known theoretical concepts, the design equations are substantiated for finding the content of sand in a mixture of concrete aggregates, which ensures the lowest viscosity of the concrete mixture and prevent water separation. Using the experimental-statistical model, a method is also proposed for finding the sand content in concrete that provides the required volume of entrained air. The proposed calculation methods are confirmed experimentally.

Аннотация. В практике подбора составов бетона оптимальное содержание песка в смеси заполнителей находят обычно эмпирически. Недостатком такого подхода является значительная трудоемкость и продолжительность необходимых испытаний. Целью работы является разработка расчетной методики определения содержания песка в тяжелом бетоне с учетом заданных критериев оптимальности. На основе известных теоретических представлений обосновываются расчетные уравнения для нахождения содержания песка в смеси заполнителей бетона, обеспечивающего наименьшую вязкость бетонной смеси и предотвращение водоотделения. С помощью экспериментально-статистической модели предлагается также метод нахождения содержания песка в бетоне, обеспечивающего требуемый объем вовлеченного воздуха. Предлагаемые расчетные методики подтверждаются экспериментально.

1. Introduction

One of the primary goals of concrete composition optimization is obtaining the aggregates ratio, providing the minimal cement consumption at normalized concrete properties. Selection of fine and coarse aggregates ratio in concrete based on taking into account its influence on the properties of the concrete mixture and concrete on the one hand and cement consumption on the other. In concrete proportioning practice empirical recommendations are usually used for finding a portion of sand in a mixture of aggregates (r) or unequivocally related to this portion coefficient K_s, considering moving apart of a coarse aggregate grains by cement – sand mortar.

One of the first attempts to receive an analytical dependence for finding the grading of aggregates in view of concrete mixtures workability was made by Bolomey [1]. Unlike other known dependencies, proposed for finding the grading of dry mixtures with maximum density, characterizing the so-called 'ideal' sifting curves [1–3], Bolomey proposed to divide concrete mixtures into two types – stiff (semi-dry or dry) and plastic by applying a special coefficient in the formula he offered.

A general form of Bolomey's formula is given below:

$$y = A + (100 - A)\sqrt{\frac{d}{D}}, \quad (1)$$

where y – the content of aggregates passing through a sieve, %; d – the diameter of sieve openings, mm; D – ultimate aggregates grains size, mm; A – a coefficient that at the use of gravel and sand equals 8 and 10 for stiff and plastic concrete mixtures correspondingly, and at the use of crushed stone and sand – 10 and 12, respectively.

Later equations for design of concrete mixtures grains size distribution with a more narrow workability gradation were proposed [4–6]. However empirical dependences of this type are excessively general, do not consider the cement paste consumption and specific materials features [7–13].

Further attempts to calculate the optimum sand content in concrete mixtures were made at different time and based on various theoretical preconditions [14–16].

The optimum sand content rule can be considered as consequence of concrete mixtures water demand constancy rule. The water demand constancy rule (WDCR) has been found in the beginning of 30th of the last century by Soroker in the USSR and McMillan in the USA [1–3]. It was reported that at constant water content cement consumption within the limits of 200…400 kg/m^3 does not essentially affect the concrete mixtures workability. Initially WDCR was applied only to low-slump mixtures. Later it was experimentally confirmed for no-slump and high-slump concrete mixtures.

Based on WDCR, graphs and tables for rough estimation of concrete mixtures water content, depending on cone slump and Vebe time were proposed [1, 17, 18]. Empirical recommendations for finding the concrete mixtures water content considering WDCR are presently used in normal weight concrete proportioning methods, recommended in many countries.

Essential stabilization of the upper limit of WDCR area and considering the features of cements, is achieved by expressing it by critical water-cement ratio ($(W/C)_{cr}$), equal to 1.68 N.C (average), where N.C, is a W/C, corresponding to the cement paste normal consistency [19, 20].

The water demand constancy rule proceed from a simplified picture of concrete mixture rheological properties changes depending on W/C. It was shown [1, 20] that the logarithm of concrete mixture viscosity changes linearly practically in the entire W/C range. However, if W/C varies from 0.8 to 0.5, viscosity changes from 10 to 100 poises, than at W/C change from 0.5 to 0.2 viscosity increases from 100 to 10000 poises i.e. an order above.

Different equations were proposed for dispersion systems viscosity (ηsm). These equations are modifications of Einstein's formula [1].

Powers has proposed an exponential equation for concrete mixtures viscosity [21]:

$$\eta / \eta_0 = e^{K\varphi}, \quad (2)$$

where η and η_0 are viscosity of mixture and initial dispersion medium; K is a coefficient; φ is the dispersion phase volumetric concentration.

Experimental data [1] allow presenting Eg (2) as:

$$\eta_{c.m} = K_o e^{\eta_{cem.p}.\varphi_{agg}}, \quad (3)$$

where $\eta_{c.m}$ – viscosity of concrete mixture, $\eta_{cem.p}$ – cement paste viscosity, K_O – proportionality coefficient ($K_O \approx 20$), φ_{agg} – aggregate volumetric concentration.

In turn the cement paste viscosity:

$$\eta_{cem.p.} = be^{a\varphi_{cem}}, \quad (4)$$

where a and b – average empirical coefficients (a = 19, b = 5.3·10^{-4}); φ_{cem} – volumetric concentration of cement in the cement paste.

The volumetric concentration of cement in the cement paste is unequivocally characterized by the cement – water ratio (V_{cem}/V_w):

$$\varphi_{cem} = \frac{V_{cem}/V_w}{1+V_{cem}/V_w}. \quad (5)$$

where V_{cem} is the volume of cement, V_w is the water volume.

The aggregate volumetric concentration:

$$\varphi_{agg} = \frac{K_1-1}{K_1+\delta K_2}, \quad (6)$$

where δ – average thickness of the cement paste film; $K_1 = \left(P_{agg}+1\right)/P_{agg}$ is a coefficient, considering the aggregates voidage; $K_2 = U_{agg}/P_{agg}$ is a coefficient, considering complexly the aggregates voidage and specific surface.

Taking into account the above mentioned expressions, the equation for concrete mixture viscosity (3) takes the following form [1]:

$$\eta_{c.m} = K_o \exp\left(\frac{b(K_1-1)}{K_1+\delta K_2}\exp\frac{a(V_{cem}/V_w}{1+V_{cem}/V_w}\right) \quad (7)$$

As shown by a number of researchers, the sand content in the mixture of aggregates affects not only on its water content but water-holding and air-entraining ability [1, 22] also, which is important to consider when designing concrete compositions.

In our study, the results of which are presented this article proposes the calculated dependencies that allow to select the optimal sand content in the design determination of the composition of the concrete mixture with the subsequent experimental refinement.

The aim of the work was to theoretically substantiate and develop a method for calculating the optimal sand content in a mixture of aggregates of concrete mixtures (r_0). Three characteristic options for optimization of the conditions are considered:

minimizing viscosity ($\eta_{c.m}$) or water content (W) of concrete mixture:

$$r \rightarrow r_{opt} \text{ at } \eta_{c.m} \rightarrow min \ (W \rightarrow min)$$

1. minimization of water separation (W_s) concrete mixture:

$$r \rightarrow r'_{opt} \text{ at } W_s \rightarrow min$$

2. ensure the required content of entrained air (A^r)

$$r \rightarrow r''_{opt} \text{ at } A^0 \rightarrow A^r$$

To achieve this goal it was necessary to justify:

- the design equation for the viscosity of a concrete mixture, taking into account the impact of a certain cement-water ratio of aggregates with regard to their voidness and specific surface, as well as the volume of cement paste;
- the equation that allows to determine the amount of water kept in the concrete mixture, taking into account the content and water demand of cement, the water demand and the ratio of aggregates;
- the equation that allows to calculate the volume of entrained air for concrete mixtures of different workability depending on the main factors characterizing their composition.

2. Methods and materials

The experiments were carried out using a typical mid-aluminate Portland cement that does not contain mineral additives.

Quartz sands with a modulus of fineness M_f = 1.7 and M_f = 2.4 and a water demand of respectively 7 and 9.5 % were used as fine aggregate of concrete.

The water demand of sand (W_s) was found by the method [23], which consists in determining the amount of water in% of the mass of sand, which must be added to the mortar mixture of 1:2, so that its mobility on the shaking table was identical the mobility of the cement paste of normal consistency.

$$W_s = \frac{(W/C)_m - (W/C)_{c.p}}{2} \cdot 100\%, \quad (8)$$

where $(W/C)_m$ – the water-cement ratio of the mortar mixture with the spreading of the cone equal to the spreading of the cement paste; $(W/C)_{c.p}$ – (W/C) of the normal consistency cement paste.

Granite crushed stone of fraction 5...20 mm was used as a coarse aggregate.

Determination of the properties of the concrete mixture was performed in accordance with EN 206-1: 2000. Water separation (W_s) was characterized by the volume of water separated from the concrete mixture after 1.5 h, to its volume by the formula:

$$W_s = \frac{m_{w.s}}{\rho_w V_{c.m}}, \quad (9)$$

where $m_{w.s}$ – the mass of separated water, g; ρ_w – the density of water (ρ_w = g/cm³); $V_{c.m}$ – is the volume of compacted concrete mixture, cm³.

For a certain volume of entrained air, a compression method based on the Boyle-Mariotte law was used, which establishes the relationship between the air volume and the applied pressure.

For receiving a polynomial model of the entrained air volume experiments were carried out according to factorial plan Ha_5 [14]. As initial materials for a concrete mixture were Portland cement (28 day compressive strength is 50 MPa) without mineral admixtures, crushed granite stone 5…20 mm, quartz sand (clay, silt and dust content is 0.8 %). The sand was divided into two fractions: 0.63...2.5 mm and less than 0.63 mm which were mixed in a required proportion. Air-entrained admixture was used.

3. Results and Discussion

As it follows from Eq. (7), viscosity and consequently workability of concrete mixtures with constant initial materials is defined in a common case by the cement paste cement-water ratio and by the thickness of the cement paste film (δ) on the aggregates grains.

Calculating δ is possible at known values of cement paste volume ($V_{c.p}$), aggregates voidage (P_{agg}) relative to their absolute volume (P_{agg}) and coarse and fine aggregates' total specific surface (U_{agg} V_{agg}):

$$\delta = \frac{V_{c.p} - P_{agg}(1 - V_{c.p})}{U_{agg} V_{agg}}, \quad (10)$$

where U_{agg} – the specific surface of the aggregates mixture, m²/m³; V_{agg} – the volume of the aggregates mixture, m³.

The aggregates' surface monotonically increases with sand content growth and can be calculated at known values of fine and coarse aggregates specific surfaces (U_s) and ($U_{cr.s}$) using the condition:

$$U_{agg} V_{agg} = U_s r + U_{cr.s}(1 - r) = U_{cr.s} + (U_s - U_{cr.s}) r. \quad (11)$$

It is practically impossible to carry out an exact theoretical calculation of aggregates' voidage depending on their volumetric ratio, because the integral value P_{agg} of aggregates' mixture depends on their location in a space, which is in turn defined by form, grains' surface features, etc. Rough calculation of fine and coarse aggregates dry mixture's voidage is possible by assuming a parabolic type approximating curve (Figure 1) and writing equations for its three points:

$$\begin{cases} P_{cr.s} = ar_1^2 + br_1 + c \\ P_s = ar_2^2 + br_2 + c \\ P_x = ar_x^2 + br_x + c \end{cases}, \quad (12)$$

where $P_{cr.s}$, P_s are the values of voidage (by absolute volume) of coarse and fine aggregates, accordingly in compacted (by vibrating) condition; r_1 and r_2- are the border values of r on the curve (Figure 1); $P_{a.x}$ is the experimental value of aggregates mixture voidage in compacted condition at some intermediate value of r_x.

Solving the equations system (12) yields the coefficients values:

$$a = \frac{P_{cr.s}r_x - P_{cr.s} + P_x - P_s r_x}{r_x^2 - r_x},$$

$$b = \frac{P_{cr.s} - P_{cr.s}r_x^2 - P_s r_x^2 + P_x}{r_x^2 - r_x}, \quad (13)$$

$$c = P_{cr.s}.$$

Nomograms for obtaining coefficients *A* and *b* in Eqs. 12 are given in Figure 2.

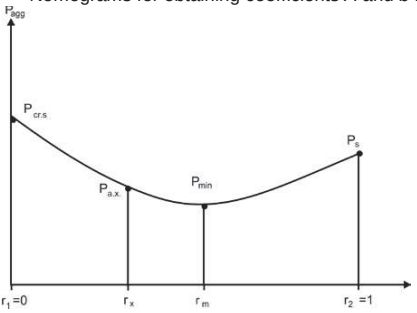

Figure1. Dependence between dry aggregates mixture voidage and the portion of sand in the sand – crushed stone mixture

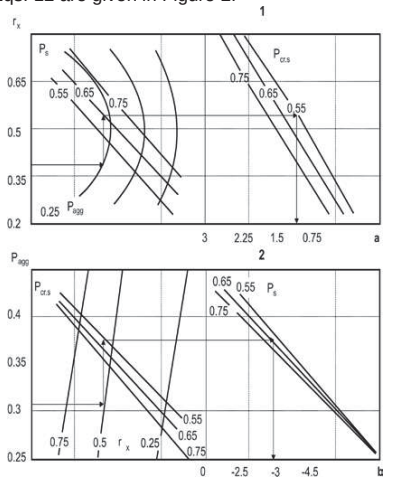

Figure 2. Nomograms for obtaining

Experimental voidage value for coarse and fine aggregates and their mixture can be easy found, knowing the real (ρ) and bulk (ρ_b) densities values: ($P_{agg} = 1 - \frac{\rho}{\rho_в}$).

Дворкин Л.И. Метод расчета оптимального содержания песка в тяжелом бетоне // Инженерно-строительный журнал. 2018. № 7(83). С. 186–197.

Voidage of a dry concrete aggregates mixture can be calculated using a quadratic equation:

$$P_{agg} = ar^2 + br + P_{cr.s}\,. \tag{14}$$

Eq. (10) for calculating δ considering Eqs. (11) and (14) as well as taking into account the cement paste consumption for filling the aggregates pores (K_p) and the entrained air volume (V_{air}) can be presented as:

$$\delta = \frac{K_p V_{c.p} - \left(ar^2 + br + P_{cr.s}\right)\ \left(1 - K_p V_{c.p} - V_{air}\right)}{U_{cr.s} + (U_s - U_{cr.s})r}. \tag{15}$$

From $\partial\delta / \partial r = 0$ condition the corresponding nomogram for obtaining the optimal portion of sand in the aggregates' mixture r_{opt}^{δ}, providing the maximum thickness value (δ) at cement paste volume $V_{c.p}$ = const can be created (Figure 3).

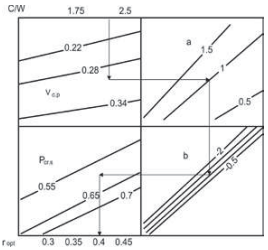

Figure 3. Nomogram for obtaining r_{opt}^{δ}

Note: The nomogram is prepared for crushed stone with specific surface of 6 cm²/cm³ and sand with specific surface of 160 cm²/cm³. If fine aggregate with lower specific surface is used, the values of r_{opt} should be increased by 0.01 per 20 cm²/cm³.

From Figures 4 follows that as $V_{c.p}$ increases, the design value of r_{opt}^{δ} decreases more sharply than the empirical optimal ones r. It can be explained by the fact that with an increase of $V_{c.p}$ due to higher C/W the growth of concrete mixture viscosity is not compensated in full by growth of δ (Figure 5).

Water demand constancy within some C/W range at given workability can be achieved just at corresponding correction of r.

Experimental values of r_{opt} are presented in Table 1 and Figure 5 were obtained for concrete mixtures with best workability for given compositions.

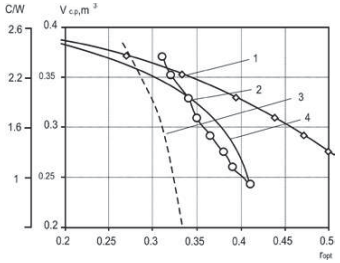

Figure 4. Dependence between optimal portion of sand in the aggregates mixture and the cement paste volume. 1 – ropt according to maximum δ condition (Figure 3). 2 – experimental values of ropt following [24]. 3 – experimental values of ropt following [23]. 4 – ropt values, considering $K_{C/W}$ coefficient

Dvorkin, L.I. Method of calculating the optimal sand content in normal-weight concrete. Magazine of Civil Engineering. 2018. 83(7). Pp. 186–197. doi: 10.18720/MCE.83.17.

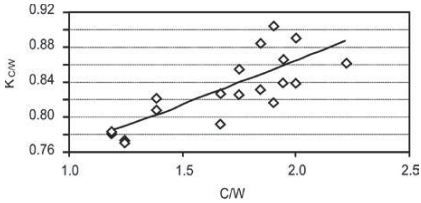

Figure 5. Regression dependence $K_{C/W}$ = f(C/W)

Following the data, given in Table 1, the optimal value of r_{opt} should be calculated according to the following equation:

$$r_{opt} = K_{C/W} r_{opt}^{\delta} \quad (16)$$

where $K_{C/W}$ – a coefficient, considering variations in concrete mixture's viscosity depending on C/W at δ = const.

Coefficient $K_{C/W}$ can be approximated by the following function:

$$K_{C/W} = K_1 e^{K_2 C/W} \quad (17)$$

where K_1 and K_2 are coefficients, depending on the initial materials features.

Table 1. Coefficient $K_{C/W}$ for calculating r_{opt}

No.	Consumptions of cement (C) and water (W), kg/m³		C/W	Values of r_{opt}^{δ}	Exp. values of r_{opt}	$K_{C/W}$= r_{opt}/r_{opt}^{δ}	$K_{C/W}$ (Eq. 17)	$\Delta K_{C/W}$, %
	C	W						
Water demand of sand W_s = 7.5%								
1	250	180	1.39	0.460	0.37	0.804	0.803	0.14
2	250	200	1.25	0.429	0.34	0.768	0.790	2.82
3	250	210	1.19	0.413	0.32	0.775	0.784	1.20
4	350	180	1.94	0.409	0.35	0.856	0.859	0.33
5	350	190	1.84	0.391	0.33	0.870	0.848	2.47
6	350	200	1.75	0.372	0.31	0.807	0.839	3.92
7	350	210	1.67	0.351	0.29	0.770	0.831	7.91
8	400	180	2.22	0.379	0.34	0.870	0.888	2.03
9	400	200	2.00	0.337	0.29	0.860	0.864	0.51
10	400	210	1.90	0.313	0.27	0.862	0.855	0.83
Water demand of sand W_s = 9.5%								
11	250	180	1.39	0.455	0.37	0.835	0.800	4.21
12	250	200	1.25	0.422	0.33	0.783	0.787	0.53
13	250	210	1.19	0.403	0.32	0.794	0.778	1.95
14	350	180	1.94	0.399	0.34	0.853	0.833	2.35
15	350	190	1.84	0.379	0.32	0.845	0.854	1.04
16	350	200	1.75	0.357	0.30	0.869	0.822	5.46
17	350	210	1.67	0.333	0.28	0.842	0.836	0.75
18	400	180	2.22	0.365	0.32	0.876	0.892	1.80
19	400	200	2.00	0.317	0.27	0.853	0.844	0.95
20	400	210	1.90	0.288	0.25	0.832	0.850	2.07

For present experimental conditions K_1 = 0.68 , K_2 = 0.12.

Knowing r_{opt}, it is easy to calculate the coefficient, considering moving apart of coarse aggregate grains by cement-sand mortar K_s:

$$K_s = \frac{(V_{c.p} + rV_{agg})}{(1-r)P_{cr.s}V_{agg}}. \quad (18)$$

Characteristic design values of r_{opt} and K_s are given in Table 2.

Table 2. Optimal calculated values of sand portion in the aggregates mixture (r_{opt}) and moving apart coefficient (K_s).

Sl, cm	*W*, l/m³	*C*, kg/m³	$V_{c.p}$, m³	r_{opt}	K_s	$\delta\mu m$
15	232	400	0.36	0.26	1.41	33
	228	350	0.34	0.30	1.40	23
	225	300	0.32	0.33	1.38	17
	225	250	0.31	0.35	1.35	12
	225	200	0.29	0.36	1.31	8
10	221	450	0.37	0.25	1.43	40
	216	400	0.35	0.30	1.42	25
	210	350	0.32	0.34	1.41	18
	210	300	0.31	0.36	1.38	13
	210	250	0.29	0.37	1.34	8
	210	200	0.27	0.38	1.30	5
6	207	450	0.35	0.29	1.45	28
	200	400	0.33	0.34	1.44	20
	196	350	0.31	0.37	1.41	15
	195	300	0.29	0.39	1.38	10
	195	250	0.28	0.40	1.33	5
	196	200	0.26	0.40	1.29	2

Note: The data in this table is obtained for crushed stone with specific surface $U_{cr.s}$ = 6 cm²/cm³, $P_{cr.s}$ = 0.65, sand with U_s = 160 cm²/cm³, P_s = 0.65.

For high-slump concrete mixtures, applied for thin-walled, densely reinforced structures, underwater concreting, etc. the portion of sand in the aggregates' mixture is appointed considering water separation prevention (W_{sep}). With this aim known empirical recommendations are used [20, 22, 25].

Equating for calculating the maximum possible water quantity (W_k) kept by concrete mixture, can be presented as:

$$W_k = 1.65 \cdot N.C \cdot C + W_s r\left(1-V_{c.p}\right)\rho_s + W_{cr.s}\left(1-r\right)\left(1-V_{c.p}\right)\rho_{cr.s}. \quad (19)$$

where $N.C$ – cement paste normal consistency; C – specific consumption of cement; W_s and $W_{cr.s}$ – water demand of sand and crush stone; $V_{c.p}$ – the cement paste volume; ρ_s and $\rho_{cr.s}$ are the densities of sand and crush stone respectively.

Than assuming that $W = W_k$, it is possible to get a design equation for finding the required portion of sand r'_{opt} for preventing water separation in high-slump concrete mixtures:

$$r'_{opt} = \frac{W - 1.65 \cdot N.C \cdot C - W_{cr.s}\left(1-V_{c.p}\right)\rho_{cr.s}}{\left(W_s\rho_s - W_{cr.s}\rho_{cr.s}\right)\left(1-V_{c.p}\right)}. \quad (20)$$

At compositions proportioning it is expediently to find first r_{opt} from the best concrete mixture workability condition (minimal viscosity) and then if necessary to check the water separation possibility and to obtain the required value of r'_{opt} [1, 22].

Table 3 presents the values of r_{opt} and r'_{opt} for different concrete mixture compositions and experimental results for water separation, obtained following [24]. This data confirms the efficiency of providing of concrete mixtures water keeping capacity obtained by correcting the optimum sand content value.

Table 3. The optimal sand portion values for concrete mixtures ($N.C = 0.24$, $W_s = 7$ %, $W_{cr.s} = 2$ %)

No.	Consumptions of cement (C) and water (W), kg/m³		C/W	W_k, kg/m³	Values of r_{opt} following [24]	Optimal calculated values of r_{opt} and r'_{opt}	Water separation in concrete mixture, %
	C	W					
1	350	200	1.75	196	0.39	0.36 / -	-
2	350	210	1.67	188	0.4	0.34 / 0.37	2.6 / -
3	350	220	1.59	187	0.41	0.32 / 0.49	2.9 / -
4	400	200	2.00	204	0.37	0.34 / -	-
5	400	210	1.90	203	0.39	0.32 / -	-
6	400	220	1.82	202	0.4	0.29 / 0.3	0.6 / -
7	400	240	1.67	201	-	0.27 / 0.54	3.2 / -
8	450	210	2.14	218	0.37	0.32 / -	-
9	450	220	2.05	217	0.38	0.29 / -	-

Notes: 1. Numerator presents the values of *r* and water separation, calculated from the viewpoint of minimum viscosity (r_{opt}), denominator shows the (r'_{opt}) values according to Eq. (20). 2. "-" indicates that there is practically no water separation.

The air pores, involved at increasing the sand content in a concrete mixture, yield an essential increase of frost resistance, as at adding air-entrained admixtures. The main composition factor, affecting air entrainment in concrete without admixtures is the sand to cement ratio [20, 25]. Thus essential influence is contributed by W/C and grading of sand. It is known that the most active air-entraining sand fraction is 0.15…0.6 mm. Less than 0.07 mm in the size particles decrease air entrainment in the same measure, like cement [1]. At the same time 0.07…0.15 mm grains have little effect on air entrainment.

Complexity of the air- entraining mechanism and variety of influencing factors do not enable to develop general enough dependences [1, 18]. At the same time for specific initial conditions appropriate regression equations can be used for optimum concrete compositions design [14].

At the planning conditions given in Table 4 and experimental results (Table 5) the following square polynomial model of entrained air volume in coded variables was obtained by statistical processing [14] of the experimental data:

$$Y = 2.78 - 0.725X_1 - 0.313X_2 + 0.35X_3 + 0.45X_4 + 0.8X_5 + 0.275X_1^2 - \\ -0.09X_2^2 + 0.11X_3^2 + 0.05X_4^2 - 0.244X_5^2 - 0.07X_1X_3 - 0.1X_1X_4 + \\ +0.15X_1X_5 - 0.09X_3X_5 - 0.16X_4X_5 \quad (21)$$

Table 4. Conditions of experiments planning for investigating the effect of concrete mixtures compositions on entrained air content

Factors	Variation levels			Variation interval
	-1	0	+1	
Concrete mixture water demand (X_1), l//m³	160	195	230	35
Cement consumption (X_2), kgr/m³	250	375	500	125
Content of sand fraction less than 0.63 mm (X_3), %	30	55	80	25
Portion of sand in aggregates mixture (X_4)	0.3	0.4	0.5	0.1
Air-entrained admixture (X_5), %	0.0	0.015	0.03	0.015

The analysis of this model shows that in the chosen factorial space area the entrained air volume varies from 0.5 to 5.5 %, i.e. in a range being typical for concrete mixtures. In stiff mixtures of the entrained air volume increases 2…2.5 times without air-entrained admixture. Using air-entrained admixture additionally increases the entrained air volume by 40...60 %. Varying the sand content and its fractional composition at the same water content without air-entrained admixture enables to change the entrained air volume more than 2 times both in stiff and high-slump mixtures, increasing it up to 4.5 and 1.8 % accordingly.

Table 5. Planning matrix and air entrainment testing results

No.	Coded factors values					Entrained air volume (V_{air}), %		Slump Sl, cm	Vebe time Vb, s
	X_1	X_2	X_3	X_4	X_5	Exper.	Calc.		
1	+	+	+	+	+	2.61	2.72	18	—
2	-	-	+	+	+	4.92	5.13	—	13
3	-	+	-	-	-	2.7	2.57	—	5
4	+	-	-	-	-	1.98	2.08	22	—
5	-	+	-	+	+	3.81	3.67	—	7
6	+	-	-	+	+	2.52	2.78	20	—
7	+	+	+	-	-	2.10	2.02	21	—
8	-	-	+	-	-	3.91	4.03	—	10
9	-	+	+	+	-	4.46	4.51	—	9
10	+	-	+	+	-	3.41	3.34	17	—
11	+	+	-	-	+	1.54	1.46	18	—
12	-	-	-	-	+	3.11	3.19	—	9
13	-	+	+	-	+	3.58	3.41	—	7
14	+	-	+	-	+	2.49	2.64	19	—
15	+	+	-	+	-	2.26	2.16	17	—
16	-	-	-	+	-	4.18	4.29	—	11
17	+	0	0	0	0	2.19	2.33	22	—
18	-	0	0	0	0	3.63	3.78	—	8
19	0	+	0	0	0	2.41	2.38	5	—
20	0	-	0	0	0	2.88	3.00	7	—
21	0	0	+	0	0	3.19	3.24	6	—
22	0	0	-	0	0	2.60	2.54	8	—
23	0	0	0	+	0	3.14	3.28	5	—
24	0	0	0	-	0	2.29	2.38	8	—
25	0	0	0	0	+	3.41	3.34	8	—
26	0	0	0	0	-	1.77	1.74	7	—
27	0	0	0	0	0	2.76	2.78	7	—

The air-entrained admixture content, necessary for achieving the required entrained air volume can essentially change depending on the sand content in the concrete mixture and its grading. Interpolation calculations corresponding to Eq. (21) can be carried out using a nomogramm given in (Figure 7).

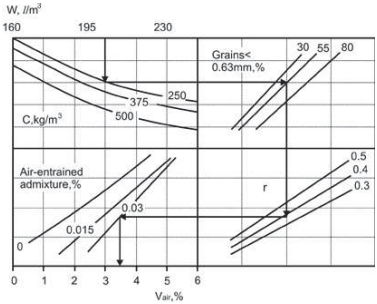

Figure 7. Nomogram for calculations the entrained air volume Vair depending on the concrete mixture composition factors

Usually, $r_{opt} \le r'_{opt} \le r''_{opt}$. At compositions proportioning, when it is expediently to obtain r'_{opt} and r''_{opt} corresponding water and cement contents correction, considering possible increase of the sand portion in the aggregates mixture, is required.

Thus, for multi parametric concrete compositions design problems the optimum sand content rule is that the optimal sand content in a concrete mixture provides in the best way the complex of given properties, and not just the mixture workability and concrete strength.

4. Conclusions

1. Based on the modified equation of viscosity of the concrete mixture, taking into account the effect of the cement-water ratio, voidness of the aggregate mixture and their specific surface, as well as the thickness of the cement paste layer on the aggregate grains, a method is proposed for calculating the optimal sand content that ensures the minimum water demand of the concrete mix.

2. The equations characterizing the amount of water kept by the concrete mixture, the calculated formula for the proportion of sand in the aggregate mixture, which prevents water separation, are substantiated.

3. A polynomial experimental-statistical model was obtained that allows calculating the required sand content for concrete mixtures of a particular workability depending on the required volume of entrained air, taking into account the water demand of the concrete mixture, cement consumption, sand fraction less than 0.63 mm and air entraining agent.

References

1. Dvorkin, L., Dvorkin, O. Basics of concrete science:optimum design of concrete mixtures. Amazon (Kindle edition) / e-book, Stroi-Beton, S- Peterburg, 2006, 382 p.
2. ACI Manual of Concrete Practice. American Concrete Institute, Detroit, 20121980, 150 p.
3. Dvorkin, L., Nwaubani, S., Dvorkin, O. Construction materials, Nova Science Publishers. New York, 2010. 410 p.
4. Design and Control of Concrete Mixtures. 15th edition, Portland Cement Association.2011. 460 p.
5. Li, N., Shi, C., Zhang, Z., Zhi, D. A mixture proportioning method for the development of performance – based alkaliactivated slag-based concrete. Cement and Concrete Composites. 2018. Vol. 23. Pp. 163–174.
6. Neville, A.M. Properties of concrete. 4-th edition, Wiley, 1996. 844 p.
7. Cepuritis, R., Sacobsen, S., Smeplass, S., Mortsell, E. Influence of crushed aggregate fines with micro-proportioned particle size distributions on rheology of cement paste. Cement and Concrete Composites. 2017. Vol. 80. Pp. 64-79.
8. Yeh, C. Computer – aided design for optimum concrete mixtures. Cement and Concrete Composites, 2007.
9. Husken, C., Brouwers, H. A new mix design concept for earth-moist concrete: A theoretical and experimental study. Cement and Concrete Research. 2008.
10. Wu, J., Feng, M., Meo, X., Xu, J. Particle size distribution of aggregate effects on mechanical and structural properties of cemented rockfill: Experiments and modeling. J. Construction and Building Materials. 2018. Vol. 193. Pp. 295–311.
11. Sitton, J., Zeinali, Y., Heidarian, W., Story, B. Effect of mix design on compressed earth block strength. Construction and Building Materials. 2018. Vol. 158. Pp. 124–131.
12. Miller, S., Monteiro, P., Ostertlag, C., Horvath, A. Concrete mixture proportioning for desired strength and reduced global warming potential. Construction and Building Materials. 2016. Vol. 128. Pp. 410–421.
13. Nguen, D., Sebaibi, N., Boutouil, M., Leleyter, L., Baraud, F. A modified method for the design of pervious concrete mix Construction and Building Materials. 2014. Vol. 73. Pp. 271–282.
14. Dvorkin, L., Dvorkin, O., Ribakov, Y. Mathematical experiments planning in concrete technology. Nova Science Publishers, New York, 2012. 173 p.

Литература

1. Dvorkin L., Dvorkin O. Basics of concrete science: optimum design of concrete mixtures. Amazon (Kindle edition) / e-book, Stroi-Beton, S- Peterburg, 2006, 382 p.
2. ACI Manual of Concrete Practice. American Concrete Institute, Detroit, 20121980, 150 p.
3. Dvorkin L., Nwaubani S., Dvorkin O. Construction materials, Nova Science Publishers. New York 2010. 410 p
4. Design and Control of Concrete Mixtures. 15th edition, Portland Cement Association.2011, 460 p.
5. Li N., Shi C., Zhang Z., Zhi D. A mixture proportioning method for the development of performance – based alkaliactivated slag-based concrete // Cement and Concrete Composites. 2018. Vol. 23. Pp. 163–174.
6. Neville A.M. Properties of concrete. 4-th edition, Wiley, 1996, 844 p.
7. Cepuritis R., Sacobsen S., Smeplass S., Mortsell E. Influence of crushed aggregate fines with micro-proportioned particle size distributions on rheology of cement paste // Cement and Concrete Composites. 2017. Vol. 80. Pp. 64–79.
8. Yeh C. Computer – aided design for optimum concrete mixtures // Cement and Concrete Composites. 2007.
9. Husken C., Brouwers H. A new mix design concept for earth-moist concrete: A theoretical and experimental study // Cement and Concrete Research. 2008.
10. Wu J., Feng M., Meo X., Xu J. Particle size distribution of aggregate effects on mechanical and structural properties of cemented rockfill: Experiments and modeling // J. Construction and Building Materials. 2018. Vol. 193. Pp. 295–311.
11. Sitton J., Zeinali Y., Heidarian W., Story B. Effect of mix design on compressed earth block strength // Construction and Building Materials. 2018. Vol. 158. Pp. 124–131.
12. Miller S., Monteiro P., Ostertlag C., Horvath A. Concrete mixture proportioning for desired strength and reduced global warming potential // Construction and Building Materials. 2016. Vol. 128. Pp. 410–421.
13. Nguen D., Sebaibi N., Boutouil M., Leleyter L., Baraud F. A modified method for the design of pervious concrete mix // Construction and Building Materials. 2014. Vol. 73. Pp. 271–282.
14. Dvorkin L., Dvorkin O., Ribakov Y. Mathematical experiments planning in concrete technology. Nova Science Publishers, New York, 2012, 173 p.

Дворкин Л.И. Метод расчета оптимального содержания песка в тяжелом бетоне // Инженерно-строительный журнал. 2018. № 7(83). С. 186–197.

15. Dvorkin, L., Dvorkin, O., Ribakov, Y. Construction Materials Based on Industrial Waste Products. Nova Science Publishers, New York, 2016. 242 p.
16. Dvorkin, L., Zhitkovsky, V., Ribakov, Y. Concrete and Mortar Production Using Stone Siftings. CRC Press, Taylor and Francis Group, Boca Raton, London, New York, 2018. 158 p.
17. Cheng Yeh, I. Modeling slump flow of concrete using second-order regressions and artificial neural networks. Cement and Concrete Composites. 2007. Vol. 29. Pp. 474–480.
18. Vatin, N.I., Barabanshchikov, Yu.G., Komarinskiy, M.V., Smirnov, S.I. Modification of the cast concrete mixture by air-entraining agents. *Magazine of Civil Engineering*. 2015. 56(4). Pp. 3–10. (rus)
19. Akhverdov, I.N. Osnovy fiziki betona [Basics of concrete physic]. Moscow: Stroyizdat, 1981. 464 p. (rus)
20. Lea's Chemistry of cement and concrete. Ed. by Peter C. Hewlett, 4-th edition, Butterworth-Heinemann, 2004. 1092 p.
21. Powers, T. Structures and physical properties of hardened Portlandcement paste. J. Amer. Ceram. Soc. 1958. Vol. 41. Pp. 18–26.
22. Neville, A.M. Properties of concrete. 4-th edition, Wiley, 1996. 844 p.
23. Skramtayev, B.G., Shubenkin, P.F., Bazhenov, Yu.M. Sposoby opredeleniya sostava betona razlichnykh vidov [Methods of concrete design composition]. Moscow: Stroyizdat, 1966. 159 p. (rus)
24. Sizov V.P. Proyektirovaniye sostavov tyazhelogo betona [Design of concrete normal-weight concrete compositions]. Moscow: Stroyizdat, 1980. 144 p. (rus)
25. Taylor, H.F.W. Cement Chemistry. London, Academic Press, 1990. 475 p.

Leonid Dvorkin,
+38(068)3533338; dvorkin.leonid@gmail.com

15. Dvorkin L., Dvorkin O., Ribakov Y. Construction Materials Based on Industrial Waste Products. Nova Science Publishers, New York, 2016, 242 p.
16. Dvorkin L., Zhitkovsky V., Ribakov Y. Concrete and Mortar Production Using Stone Siftings. CRC Press, Taylor and Francis Group, Boca Raton, London, New York, 2018. 158 p.
17. Cheng Yeh I. Modeling slump flow of concrete using second-order regressions and artificial neural networks // Cement and Concrete Composites. 2007. Vol. 29. Pp. 474–480.
18. Ватин Н.И., Барабанщиков Ю.Г., Комаринский М.В., Смирнов С.И. Модификация литой бетонной смеси воздухововлекающей добавкой // Инженерно-строительный журнал. 2015. № 4(56). С. 3–10.
19. Ахвердов И.Н. Основы физики бетона. М.: Стройиздат, 1981. 464 с.
20. Lea's Chemistry of cement and concrete. Ed. by Peter C. Hewlett, 4-th edition, Butterworth-Heinemann, 2004, 1092 p.
21. Powers T. Structures and physical properties of hardened Portlandcement paste // J. Amer. Ceram. Soc. 1958. Vol. 41. Pp. 18–26.
22. Neville A.M. Properties of concrete. 4-th edition, Wiley, 1996, 844 p.
23. Скрамтаев Б.Г., Шубенкин П.Ф., Баженов Ю.М. Способы определения состава бетона различных видов. М.: Стройиздат, 1966. 159 с.
24. Сизов В.П. Проектирование составов тяжелого бетона. М.: Стройиздат, 1980. 144 с.
25. Taylor H.F.W. Cement Chemistry. London, Academic Press, 1990, 475 p.

Леонид Иосифович Дворкин,
+38(068)3533338;
эл. почта: dvorkin.leonid@gmail.com

Dvorkin, L.I. Method of calculating the optimal sand content in normal-weight concrete. Magazine of Civil Engineering. 2018. 83(7). Pp. 186–197. doi: 10.18720/MCE.83.17.

doi: 10.18720/MCE.83.18

Mathematical modeling of the colmatation of concrete pores during corrosion

Математическое моделирование кольматации пор бетона при коррозии

S.V. Fedosov,
V.E. Rumyantseva,
I.V. Krasilnikov,
V.S. Konovalova*,
A.S. Evsyakov,
Ivanovo State Polytechnic University, Ivanovo, Russia

Д-р техн. наук, акад. РААСН, заведующий кафедрой, профессор С.В. Федосов,
д-р техн. наук, директор института, заведующий кафедрой, профессор В.Е. Румянцева,
канд. техн. наук, руководитель центра научно-исследовательских работ и технической экспертизы И.В. Красильников,
канд. техн. наук, старший преподаватель В.С. Коновалова*,
аспирант А.С. Евсяков,
Ивановский государственный политехнический университет, г. Иваново, Россия

Key words: colmatation; colmatation of pores; corrosion of concrete; mathematical modeling; colmatation model

Ключевые слова: кольматация; кольматирование пор; коррозия бетона; математическое моделирование; модель кольматации

Abstract. Pore colmatation plays a positive role, since the decrease in the permeability of cement concrete due to the deposition of insoluble corrosion products in the pores leads to a slowdown in corrosion processes. The mathematical model of concrete pore colmatation based on the mass transfer equations is given, which allows to estimate the depth of corrosion damage of concretes in media of various degrees of aggressiveness. The presented model describes the rate of advance of the deposition zone of corrosion products depending on the conditions of the corrosion process. Mathematical models of the kinetics and dynamics of mass transfer accompanied by a decrease in permeability during chemical corrosion of cement stone are presented. Equations are obtained for determining the rate of advancement of the colmatation zone and the thickness of the colmatant layer during concrete corrosion. The dependence of the rate of clogging of pores and capillaries and the thickness of the sediment layer on the change in mass transfer characteristics, taking into account the porosity of the bedding layer, is shown. Graphic dependences of the rate of advancement of the colmatage zone and the thickness of the layer of corrosion products are obtained at the established porosity of the layer for cases of linear and exponential changes in the mass diffusivity coefficient over time. The obtained graphic dependences show that the intensity of the colmatation process decreases, and also illustrate a significant decrease in the intensity of the process with a slight decrease in the porosity of the sediment layer.

Аннотация. Кольматация пор играет положительную роль, поскольку снижение проницаемости цементного бетона вследствие осаждения в порах нерастворимых продуктов коррозии приводит к замедлению коррозионных процессов. Приведена математическая модель кольматации пор бетона, основанная на уравнениях массопереноса, которая позволяет оценивать глубину коррозионных повреждений бетонов в средах различной степени агрессивности. Представленная модель описывает скорость продвижения зоны осаждения продуктов коррозии в зависимости от условий протекания процесса коррозии. Приведены математические модели кинетики и динамики массопереноса, сопровождаемого снижением проницаемости, при химической коррозии цементного камня. Получены уравнения для определения скорости продвижения зоны кольматации и толщины слоя кольматанта при коррозии бетона. Показана зависимость скорости закупоривания пор и капилляров и толщины слоя осадка от изменения характеристик

Федосов С.В., Румянцева В.Е., Красильников И.В., Коновалова В.С., Евсяков А.С. Математическое моделирование кольматации пор бетона при коррозии // Инженерно-строительный журнал. 2018. № 7(83). С. 198–207.

массопереноса с учетом порозности слоя кольматанта. Получены графические зависимости скорости продвижения зоны кольматации и толщины слоя продуктов коррозии при установленной порозности слоя для случаев линейного и экспоненциального изменения коэффициента массопроводности во времени. Полученные графические зависимости показывают, что интенсивность процесса кольматации уменьшается, а также иллюстрируют значительное снижение интенсивности процесса при незначительном уменьшении пористости слоя осадка.

1. Intoduction

At corrosion of concrete and reinforced concrete products mudding is the process of penetration of particles (disperce and dissolved) in the pores, cracks and voids of concrete and is physical and chemical deposition in it, contributing to the grouting, reduction the water permeability of concrete, and as a result increase the frost resistance and corrosion resistance [1, 2].

Usually, the term "colmatation" is used to refer to the process of mechanical deposition of particles in the pore space [3].

Concrete is a capillary-porous material, as if permeated with a thin mesh of pores and capillaries of various sizes [4]. When the concrete is moistened, the smallest pores and capillaries are filled with an aggressive environment which interacts with calcium hydroxide to form insoluble reaction products, which clog these capillaries. Coming, as they say, "colmatation" of the pores and capillaries that leads to reduction of permeability of concrete [4].

At the interaction of components of the cement matrix of the concrete with the aggressive environment two types of colmatant are formed [5]: the first consists of a gel of silicic acid, which is formed as a result of the interaction of the silicate component of the cement stone with an aggressive environment; the second is formed as a result of the chemical reaction of the components of the aggressive environment with the main parts of the cement stone containing calcium ions: $CaCO_3$, $Mg(OH)_2$, etc.

With the increase in the age of concrete, the nature of its porosity changes, the volume of macropores which overgrown with cement hydration products gradually decreases, and as a result the permeability of concrete decreases [4].

In artificial conditions (at the construction and operation of engineering structures) colmation plays a dual role – positive and negative.

The positive impact is, for example, clogging of the pores of the asphalt- and concrete when exposed to de-icing compositions [6], improvement of the strength characteristics of ceramic bricks after treatment by water-repellent and clogging compounds [7], clogging the internal structure of capillaries and pores of the wood and the formation of more strong ties of wood with cement stone in the production of arbolite [8], increasing of water-tightness of concrete structures due to colmatation of capillary pores of concrete with the introduction of special additives [9, 10], increasing the strength and density of concrete when applying waterproofing coating [11].

The negative impact of colmatation is manifested in drilling, development and operation of water wells in mechanical, chemical and biological colmatage [12]; in loss of water permeability of geotextiles and reduction of filtration properties due to colmatation of the material during water filtration [13]; in violation of the operation mode of ore-bearing wells due to deposition of solid phases formed by dissolution of metal ore-containing rocks [14].

The use of the colmatation effect for practical purposes allows to increase the degree of self-inhibition of corrosion processes and to make a choice of cement type for concrete which are operated in various aggressive environments [5].

It is necessary to make a model of collation and determine the parameters of mass transfer to have an opportunity to effectively use the process of collation in preventing the spread of corrosion front deep into the concrete.

All corrosion processes of the second type are accompanied by the release of the solid phase as a result of the chemical interaction of the concrete components and the aggressive liquid medium. The chemical interaction of the components of the aggressive environment in the liquid phase with dissolved in the pore fluid calcium hydroxide leading to the appearance of a colmatant layer flows through the reaction of the species (Figure 1):

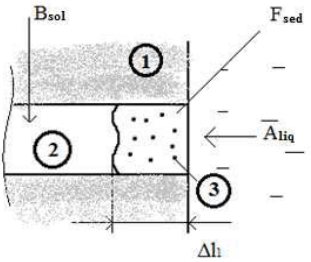

Figure 1. Pore: 1) concrete matrix; 2) pore; 3) sediment

A typical example of this type of reaction is [15]:

$$Ca(OH)_2 + MgCl_2 = CaCl_2 + Mg(OH)_2\downarrow. \quad (1)$$

Calcium hydroxide (B_{sol}) interacts with an aggressive component ($A_{liq} \rightarrow MgCl_2$); because of this interaction, calcium ions Ca^{2+} (R_{liq}) pass into the liquid phase and a solid phase (F_{sed}) is formed. The process is supposed to proceed through a complex mechanism that takes place in two stages. The first stage proceeds on the external diffusion-kinetic mechanism on the interface of phases "solid-liquid" and therefore insoluble reaction product is deposited on the surface of concrete. The second stage takes place in the diffusion-kinetic mechanism [15].

The mechanism and kinetics of mass transfer at the first stage are described in detail in [15]. The second stage is discussed below.

2. Methods

To describe the nature of corrosion processes occurring during liquid corrosion of concretes, methods of mathematical modeling based on the mass transfer equations are used. Methods of mathematical physics for solving boundary problems of mass transfer are applied as a mathematical apparatus. To establish the longevity of concretes exposed to aggressive chloride-containing media, mathematical models of corrosion of concrete have been obtained, which take into account the pore colmatation. For the experimental study of the properties, structure and composition of the materials studied in the work (solid and liquid phase), methods of chemical and physicochemical analysis are used, such as: quantitative analysis of calcium cations in a liquid medium by the method of complexometric titration; electrometric method for measuring the pH of the medium; method for determining the density, water absorption and porosity of cement stone; X-ray diffraction analysis of cement stone before and after exposure to corrosive liquids.

3. Results and Discussion

To estimate the depth of corrosion damage, various equations are proposed to predict the resistance of concrete in an aggressive environment [16–20]. These equations take into account the rate of corrosion of concrete in the initial period, the rate of heterogeneous reactions and the nature of the control (kinetic or diffusion), the kinetics of the internal diffusion process with a constant diffusion coefficient in time, the porosity of the cement stone, the dependence of the mass transfer coefficients on the structure and composition of the concretes, as well as the composition and concentration of aggressive media, relative humidity (degree of saturation) and concentration of calcium ions in pore solution, formation of calcite and dissolution of of hydration products, simultaneous influence of power loading and negative effects of aggressive media on concrete and reinforced concrete structures. On the basis of the theory of mass transfer processes the equations for the mathematical description of kinetic dependences of corrosion process most often occurring in practice are offered. These equations describe extensive and intensive processes of concrete corrosion inhibition [5, 21]. However, these models do not fully take into account the process of colmatation of pores and capillaries of concrete, which remains not fully understood.

We believe that at the initial moment, when only the aggressive environment interacts with the concrete at the thickness of the structure, there is a uniform distribution of the main component:

$$C_B(x,\tau) = C_{B.o.}, \quad (2)$$

where: x – coordinate, m; τ – time, s; $C(x,\tau)$ – concentration of «free $Ca(OH)_2$» in concrete at the moment of time τ at an arbitrary point with a coordinate x, in terms of CaO (kg CaO/kg of concrete); C_0 – concentration of «free $Ca(OH)_2$» in concrete in the initial time to an arbitrary point with coordinate x, in terms of CaO (kg CaO/kg of concrete).

By the time τ_1 the concentration of calcium ions at the interface will be zero. From that moment the aggressive component starts to flow inside the pores of the concrete and the reaction product, sediment, promotes the formation of a porous structure of the sediment inside the pores of the concrete.

During the time $\Delta\tau_1$ in the pore of concrete (open or through) the sediment layer determined by a formula is formed:

$$\Delta V_{m1} = (1 - \varepsilon_{sed})\pi R^2 \cdot \Delta l_1. \quad (3)$$

Here: ε_{sed} – porosity layer of sediment, which characterizes the volume of voids in the layer of sediment; R is the radius of the pore, m.

The mass of the sediment will be:

$$\Delta M_{sed1} = (1 - \varepsilon_{sed})\pi R^2 \cdot \Delta l_1 \cdot \rho_{sed}. \quad (4)$$

Dividing both parts on $\Delta\tau_1$ for which there was a mass accumulation write:

$$\frac{\Delta M_{sed1}}{\Delta\tau_1} = \frac{\Delta l_1}{\Delta\tau_1}(1 - \varepsilon_{sed})\pi R^2 \cdot \rho_m, \quad (5)$$

or in differential form:

$$\frac{dM_{\text{sed}}}{d\tau} = \frac{dl}{d\tau}(1 - \varepsilon_{\text{sed}})\pi \text{R}^2 \cdot \rho_{\text{sed}}. \quad (6)$$

Using the concept of mass flow rate, we can write:

$$\frac{dM_{sed}}{\pi R^2 \cdot d\tau} = \frac{dl}{d\tau}(1 - \varepsilon_{sed}) \cdot \rho_{sed} \rightarrow \frac{dl}{d\tau} = \frac{dM_{sed}}{\pi R^2}(1 - \varepsilon_{sed}) \cdot \rho_{sed}, \quad (7)$$

At the moment when the period of mass transfer controlled by external diffusion is completed, on the thickness of a wall of a design (product) concentration field of "free calcium hydroxide", is formed, determined by the function $C_B(x,\tau)|_{\tau=\tau_1}$– dimension of the function: kg of the component / kg of concrete.

The mass flow density of the reagent at the interface of the phase will be determined by a known ratio similar to the first Fick`s law [22]:

$$q_R(\tau)|_{\tau=\tau_1} = -k_B \frac{\partial C_B(x,\tau)}{\partial x}\Big|_{\substack{x=R_s \\ \tau=\tau_1}} \cdot \rho_{con}. \quad (8)$$

Here: R_s – designation of the surface of the structure (the interface), through which the mass of the target component is transferred from the solid phase to the liquid; k_B – coefficient of mass conductivity of the component B_{sol} (calcium hydroxide in concrete), m^2/s; ρ_{con} - density of concrete, kg/m^3.

In accordance with the methodology of experimental studies of mass transfer processes, the numerical values of the mass conductivity coefficient are determined in relation to the geometric surface of the body involved in the mass transfer process. At the same time, the substance (reagent) from the liquid phase comes only through the surface of the open pores.

In the time $\Delta\tau_1$ the amount of the substance will approach from the inside of the solid phase to the surface:

$$\Delta M_{B.1} = q_R(\tau)|_{\tau=\tau_1} \cdot \pi R^2 \cdot \Delta\tau_1 = -k_B \cdot \rho_{con} \cdot \frac{\partial C_B(x,\tau)}{\partial x}\Big|_{\substack{x=R_s \\ \tau=\tau_1}} \cdot \pi R^2 \cdot \Delta\tau_1. \quad (9)$$

This amount of substance reacts with the reagent A, the corresponding amount of the substance F_{sed} which is dropping out in a deposit as a result is formed.

During the period $\Delta\tau_1$ the single pore will be clogged with substance F_{sed}, the mass of which will be:

$$\Delta M_{FI} = V_{lim} \cdot \rho_{sed} \cdot (1 - \varepsilon_{sed}) = \pi R^2 \cdot \Delta l_1 \cdot \rho_{sed} \cdot (1 - \varepsilon_{sed}). \quad (10)$$

The total amount of substance deposited in the pores of the concrete will be determined as:

$$\Delta M_{totalI} = \Sigma \Delta M_{FI} = \pi R^2_{mid} \cdot \Delta l_1 \cdot \rho_{sed} \cdot (1 - \varepsilon_{sed}) \cdot \hat{n}. \quad (11)$$

Here: $\hat{n} = \frac{S_{surface}}{\pi R^2}$ – the number of pores per given surface.

On the other hand, this amount of substance can be defined as:

$$\sum \Delta M_{FI} = -k_B \cdot \rho_{con} \cdot \frac{\partial C_B(x,\tau)}{\partial x}\Big|_{\substack{x=R_s \\ \tau=\tau_I}} \cdot \pi R^2 \cdot \Delta\tau_I \cdot \nu_{AD}, \quad (12)$$

where: ν_{AD} – stoichiometric coefficient.

It follows from the balance:

$$\pi R^2_{mid} \cdot \Delta l_1 \cdot \rho_{sed} \cdot (1 - \varepsilon_{sed}) \cdot \hat{n} = -k_B \cdot \rho_{con} \cdot \frac{\partial C_B(x,\tau)}{\partial x}\Big|_{\substack{x=R_s \\ \tau=\tau_I}} \cdot \pi R^2 \cdot \Delta\tau_I \cdot \nu_{AD} \quad (13)$$

Hence, for the rate of advance of the size of the colmation zone (divided on $\Delta\tau_I$):

$$\frac{dl(\tau)}{d\tau} = -k_B \cdot \frac{\rho_{con}}{\rho_{sed}} \cdot \frac{\partial C_B(x,\tau)}{\partial x}\Big|_{x=R_s} \cdot \frac{\nu_{AD}}{(1-\varepsilon_{sed})}. \quad (14)$$

We receive:

$$\frac{d[l(\tau)/\delta_{con}]}{d[\tau \cdot k_B/\delta^2_{con}]} = K_\rho \cdot \frac{\partial[C_{B.o.} - C_B(x,\tau)]}{\partial(x/\delta_{con}) \cdot C_{B.o.}}\Big|_{x=R_s} \cdot \frac{\nu_{AD} \cdot C_{B.o.}}{(1-\varepsilon_{sed})}. \quad (15)$$

Let us introduce dimensionless variables of the form:

$$\bar{x} = \frac{x}{\delta_{con}};\ \theta_B = \frac{C_{B.o.} - C_B(x,\tau)}{C_{B.o.}};\ Fo_m = \frac{k_B \cdot \tau}{\delta^2_{con}};\ L(Fo_m) = \frac{l(\tau)}{\delta_{con}}. \quad (16)$$

We present equation (18) to a dimensionless form. For this:

a) we multiply both parts of the equation on $\delta^2_{con}/\delta_{con}$;
b) we divide both parts by k_B;
c) we enter the value of the density coefficient: $K_\rho = \frac{\rho_{con}}{\rho_{sed}}$.

And finally:

$$\frac{dL(Fo_m)}{dFo_m} = K_\rho \cdot C_{B.o.} \cdot \frac{\partial \theta_B(\bar{x},Fo_m)}{\partial \bar{x}}\Big|_{\bar{x}=\bar{R}_s} \cdot \frac{\nu_{AD}}{(1-\varepsilon_{sed})}. \quad (17)$$

Or another recording:

$$\frac{dL(Fo_m)}{dFo_m} = K_{\rho c} \cdot \frac{\partial \theta_B(\bar{R}_x,Fo_m)}{\partial \bar{x}} \cdot \frac{\nu_{AD}}{(1-\varepsilon_{sed})}. \quad (18)$$

Here: $K_{\rho c} = K_\rho \cdot C_{B.o.}$

We consider and graphically illustrate some special cases.

1. Physical-mechanical and mass-conducting characteristics of the material remain unchanged during the process: the main such characteristics in this case are the coefficients of porosity and density of concrete and sediment materials, as well as the coefficient of mass conductivity k_B (straight 1 of Figure 2).

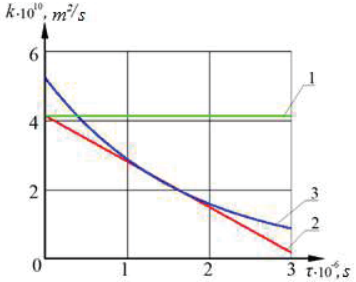

Figure 2. Particular cases of changes in the mass conductivity coefficient k_B in the process of colmatation: 1 – no change in time; 2 – change by linear dependence; 3 – change by exponential dependence

Федосов С.В., Румянцева В.Е., Красильников И.В., Коновалова В.С., Евсяков А.С. Математическое моделирование кольматации пор бетона при коррозии // Инженерно-строительный журнал. 2018. № 7(83). С. 198–207.

The integration of equation (18) in the processes from zero to the current value Fo_m and from zero to $L(Fo_m)$ gives the law of promotion of the colmatant layer in the pores of the concrete at constant values of the coefficient of mass conductivity:

$$L(Fo_m) = K_{\rho c} \cdot \frac{\partial \theta_B(\bar{R}_x, Fo_m)}{\partial \bar{x}} \cdot \frac{\nu_{AD}}{(1-\varepsilon_{sed})} \cdot Fo_m \quad (19)$$

2. It is experimentally established that the coefficient of mass conductivity of the material in the solid phase decreases sharply during the process [23]. These data can be approximated by linear or exponential dependencies of the form:

$$k_B(\tau) = k_{B0} \cdot (1 - A_0\tau), \quad (20)$$

$$k_B(\tau) = k_{B0} \cdot A_1 \cdot exp(-B_1\tau). \quad (21)$$

– For linear dependence expressions (18) and (19) are converted to view:

$$\frac{dL(Fo_m)}{dFo_m} = (1 - \hat{A}_0 Fo_m) \cdot \frac{\partial \theta(\bar{R}_k, Fo_m)}{\partial \bar{x}} \cdot \frac{\nu_{AD} \cdot K_{\rho c}}{(1-\varepsilon_{sed})}, \quad (22)$$

$$L(Fo_m) = \frac{\partial \theta(\bar{R}_k, Fo_m)}{\partial \bar{x}} \cdot \frac{\nu_{AD} \cdot K_{\rho c} \cdot Fo_m}{(1-\varepsilon_{sed})} \cdot (1 - 0.5\hat{A}_0 Fo_m), \quad (23)$$

Here:

$$\hat{A}_0 = \frac{A_0 \cdot \delta_{con}^2}{k_{B0}}. \quad (24)$$

– For exponential dependence expressions (18) and (19) take the form of:

$$\frac{dL(Fo_m)}{dFo_m} = A_1 \cdot exp(-\hat{B}_1 Fo_m) \cdot \frac{\partial \theta_B(\bar{R}_k, Fo_m)}{\partial \bar{x}} \cdot \frac{\nu_{AD} \cdot K_{\rho c}}{(1-\varepsilon_{sed})}, \quad (25)$$

$$L(Fo_m) = \frac{\partial \theta_B(\bar{R}_k, Fo_m)}{\partial \bar{x}} \cdot \frac{A_1 \cdot K_{\rho c} \cdot \nu_{AD}}{\hat{B}_1 \cdot (1-\varepsilon_{sed})} \cdot \left[1 - exp\left(-\hat{B}_1 Fo_m\right)\right]. \quad (26)$$

Here: $\hat{B}_1 = \frac{B_1 \cdot \delta_{con}^2}{k_{B0}}$.

As an example, some results of calculations on the obtained expressions are shown in Figures 3-6.

Figure 3 shows how the collation rate, $\frac{dL(Fo_m)}{dFo_m}$, and the thickness of the colmatant layer, $L(Fo_m)$, change from the mass transfer Fourier criterion, Fo_m, and the porosity of the sediment layer, ε_{sed}, while the mass conductivity coefficient is assumed to be constant (k_{B0} = 4.11·10^{-10} m^2/s), and the calculations were carried out in terms of (15) and (17).

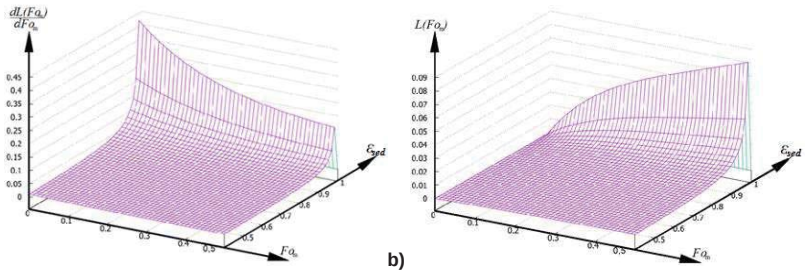

a) b)

Figure 3. The dependence of the colmatation rate, $\frac{dL(Fo_m)}{dFo_m}$, (a) and the thickness of the colmatant layer, $L(Fo_m)$, (b) from the mass transfer Fourier criterion, Fo_m, and the porosity of the sediment layer, ε_{sed}, at a constant value of the mass conductivity coefficient (k_{B0} = 4.11·10^{-10} m^2/s)

Figure 4 illustrates how the speed of colmatation, $\frac{dL(Fo_m)}{dFo_m}$, and the thickness of the colmatant layer, $L(Fo_m)$, change from the mass transfer Fourier criterion, Fo_m, and the porosity of the sediment layer, ε_{sed}, but unlike Figure 3, the mass conductivity coefficient changes linearly (inclined line 2 of Figure 2).

But Figure 5 presents the graphical results of calculations of the colmatation rate, $\frac{dL(Fo_m)}{dFo_m}$, and the thickness of the colmatant layer, $L(Fo_m)$, from the mass transfer Fourier criterion, Fo_m, and porosity of the sediment layer, ε_{sed}, at the coefficient of mass conductivity of the material in the solid phase sharply decreasing in time of the process, for calculations its values are approximated by exponential (curve 3 Figure 2) dependence.

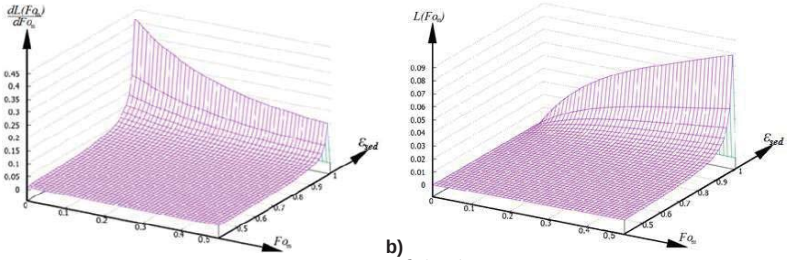

a) b)

Figure 4. The dependence of the colmatation rate, $\frac{dL(Fo_m)}{dFo_m}$, (a) and the thickness of the colmatant layer, $L(Fo_m)$, (b) from the mass transfer Fourier criterion, Fo_m, and the porosity of the sediment layer, ε_{sed}, when the mass conductivity coefficient changes according to the linear law

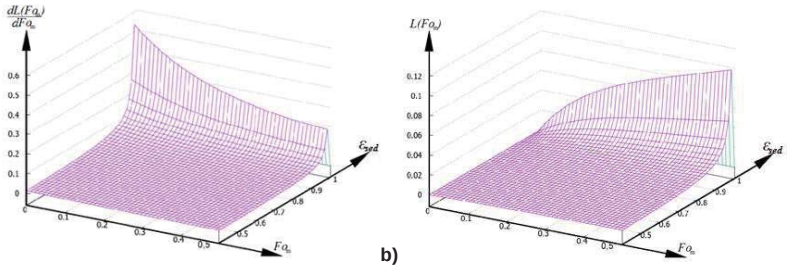

a) b)

Figure 5. The dependence of the colmatation rate, $\frac{dL(Fo_m)}{dFo_m}$, (a) and the thickness of the colmatant layer, $L(Fo_m)$, (b) from the mass transfer Fourier criterion, Fo_m, and the porosity of the sediment layer, ε_{sed}, when the mass conductivity coefficient changes according to the exponential dependence

The obtained graphic dependences show that the intensity of the colmatation process decreases, and also illustrate a significant decrease in the intensity of the process with a slight decrease in the porosity of the sediment layer (from 1 to 0.9).

To demonstrate the influence of the coefficient of mass conductivity we will present the profiles of the colmatation rate, $\frac{dL(Fo_m)}{dFo_m}$, and the thickness of the colmatant layer, $L(Fo_m)$, from the mass transfer Fourier criterion, Fo_m, at the same value of the porosity of the layer of sediment, ε_{sed} = 0.5, for each particular case (Figure 6). Here, curve 1 shows the results of calculations for a time-constant mass conductivity coefficient; curve 2 shows the change in linear slope dependence; and curve 3 shows the change in exponential dependence.

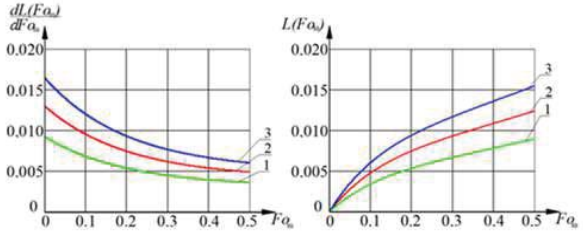

a) b)

Figure 6. The dependence of the colmatation rate, $\frac{dL(Fo_m)}{dFo_m}$, (a) and the thickness of the colmatant layer, $L(Fo_m)$, (b) from the mass transfer Fourier criterion, Fo_m, when the porosity of the layer of sediment ε_{sed} = 0.5, when the mass conductivity coefficient: 1 – constant (k_{B0} = 4.11·10^{-10} m^2/s); 2 – changes according to the incline linear dependence; 3 – changes according to the exponential dependence

Figure 7 shows the profiles of the dependence of the colmatation rate, $\frac{dL(Fo_m)}{dFo_m}$, and the thickness of the colmatant layer, $L(Fo_m)$, from the mass transfer Fourier criterion, Fo_m, when the porosity of the layer of sediment ε_{sed} = 0.5, at a variable mass flow value, $\frac{\partial\theta(\bar{R}_k,Fo_m)}{\partial\bar{x}}$. Profiles show that over time there is a weakening of the mass flow which obviously is connected with an increase in the colmatant layer. The speed of colmatation is also reduced due to the fact that the layer of colmatant partially or completely clogged pores and prevents the further penetration of the aggressive environment deep into the concrete.

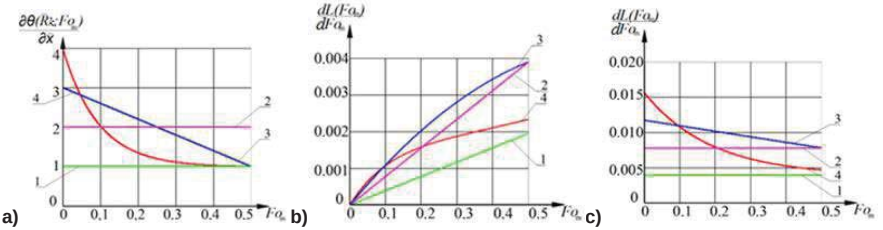

a) b) c)

Figure 7. The dependence of the colmatation rate, $\frac{dL(Fo_m)}{dFo_m}$, (b) and the thickness of the colmatant layer, $L(Fo_m)$, (c) from the mass transfer Fourier criterion, Fo_m, when the porosity of the layer of sediment ε_{sed} = 0.5, when the value of the mass flow (a), $\frac{\partial\theta(\bar{R}_k,Fo_m)}{\partial\bar{x}}$: 1,2 – constant; 3 – changes according to the incline linear dependence; 4 – changes according to the exponential dependence

4. Conclusions

1. The presented model of colmatation allows to predict the corrosion rate of cement concrete considering the movement of the front of colmatation and the thickness of the colmatant layer.

2. Mathematical modeling gives the chance to use the phenomenon of a colmatation of concrete pores to prevent the development of corrosion processes in further experimental studies.

3. Graphic dependencies show that the rate of colmatation of concrete pores during corrosion is slowed down over time, which is associated with an increase in the thickness of the colmatant layer. Due to the pore colmatation, the corrosion of concrete is inhibited, since penetration of the aggressive medium is difficult.

References

1. Mukhametshin, V.V., Kadyrov, R.R. Vliyaniye nanodobavok na mekhanicheskiye i vodoizoliruyushchiye svoystva sostavov na osnove tsementa [Influence of nanoadditives on mechanical and isolating properties of cement-based compositions]. Nanotechnologies in

Литература

1. Мухаметшин В.В., Кадыров Р.Р. Влияние нанодобавок на механические и водоизолирующие свойства составов на основе цемента // Нанотехнологии в строительстве: научный интернет-журнал. 2017. Т. 9. № 6. С. 18–36.

Fedosov, S.V., Rumyantseva, V.E., Krasilnikov, I.V., Konovalova, V.S., Evsyakov, A.S. Mathematical modeling of the colmatation of concrete pores during corrosion. Magazine of Civil Engineering. 2018. 83(7). Pp. 198–207. doi: 10.18720/MCE.83.18.

construction-a scientific internet-journal. 2017. Vol. 9. No. 6. Pp. 18–36. (rus)

2. Barabanshchikov, Yu.G., Belyaeva, S.V., Arkhipov, I.E., Antonova, M.V., Shkol'nikova, A.A., Lebedeva, K.S. Influence of superplasticizers on the concrete mix properties. Magazine of Civil Engineering. 2017. No. 6. Pp. 140–146.
3. Bertolini, L., Elsener, B., Pedeferri, P., Redaelli, E., Polder, R.B. Corrosion of Steel in Concrete: Prevention, Diagnosis, Repair. John Wiley & Sons, 2013. 434 p.
4. Yanakhmetov, M.R., Chuykin, A.E., Massalimov, I.A. Modifitsirovaniye porovoy struktury tsementnykh betonov propitkoy serosoderzhashchimi rastvorami [Pore structure modification of cement concretes by impregnation with sulfur-containing compounds]. Nanotechnologies in construction: a scientific internet-journal. 2015. Vol. 7. No. 1. Pp. 63–72. (rus)
5. Patel, R.A., Perko, J., Jacques, D., De Schutter, G., Ye, G., Van Bruegel, K. Effective diffusivity of cement pastes from virtual microstructures: Role of gel Porosity and capillary pore percolation. Construction and Building Materials. 2018. Vol. 165. Pp. 833–845.
6. Podolsky, V.P., Long, N.V., Hao, N.K., Sy, N.D. The study of operating capacity of asphalt concrete modified with an additive Wetfix Be. Scientific herald of the Voronesh state university of architecture and civil engineering. Construction and architecture. 2016. No. 1(29). Pp. 75–83.
7. Urkhanova, L.A., Savelyeva, M.A. Vliyaniye zoley razlichnogo sostava na izmeneniye struktury i svoystv tsementnogo kamnya [The effect of different composition sols on change of structure and properties of cement stone]. Nanotechnologies in construction-a scientific internet-journal. 2016. Vol. 8. No. 6. Pp. 20–42. (rus)
8. Jaya, H., Omar, M.F., Akil, H.M., Ahmad, Z.A., Zulkepli, N.N. Effect of particle size on mechanical properties of sawdust-high density polyethylene composites under various strain rates. Bioresources. 2016. Vol. 11. No. 3. Pp. 6489-6504.
9. Leonovich, S.N., Sviridov, D.V., Shchukin, G.L., Belanovich, A.L., Savenko, V.P., Karpushenkov, S.A. Vliyanie citrata natriya na process formirovaniya cementnogo kamnya v glinozemistom vyazhushchem [Sodium citrate influence on formation of cement stone in the aluminous binder]. Science & Technique. 2016. Vol. 15. No. 4. Pp. 281–286. (rus)
10. Massalimov, I.A., Yanakhmetov, M.R., Chuykin, A.E., Massalimov, B.I., Urakaev, F.H., Uralbekov, B.M., Burkitbaev, M.M. Gidrofobizatsiya plotnogo i melkozernistogo betonov polisulfidnymi rastvorami [Hydrophobization of dense and fine concrete by polysulfide solutions]. Nanotechnologies in construction-a scientific internet-journal. 2016. Vol. 8. No. 5. Pp. 85–99. (rus)
11. Kudryavtsev, P.G., Figovskii, O.L. Organic water-soluble-silicates for protective coatings. Russian journal of building construction and architecture. 2017. No. 3(35). Pp. 17–31.
12. Artamonova, O.V., Sclavcheva, G.S. Structure of cement systems as object of nanomodification. Scientific herald of the Voronesh state university of architecture and civil engineering. Construction and architecture. 2016. No. 1(29). Pp. 13–26.
13. Cetin, D., Sengul, T., Bhatia, S.K., Khachan, M.M. Effect of polymer and fiber usage on dewatering and compressibility behavior of fly ash slurries. Marine georesources and geotechnology. 2017. Vol. 35. No. 5. Pp. 678–687.
14. Gilligan, R., Nikoloski, A.N. Leaching of brannerite in the ferric sulphate system – Part 1: Kinetics and reaction mechanisms. Hydrometallurgy. 2015. Vol. 156. Pp. 71–80.

2. Барабанщиков Ю.Г., Беляева С.В., Архипов И.Е., Антонова М.В., Школьникова А.А., Лебедева К.С. Влияние суперпластификаторов на свойства бетонной смеси // Инженерно-строительный журнал. 2017. № 6(74). С. 140–146.
3. Bertolini L., Elsener B., Pedeferri P., Redaelli E., Polder R.B. Corrosion of Steel in Concrete: Prevention, Diagnosis, Repair. John Wiley & Sons, 2013. 434 p.
4. Янахметов М.Р., Чуйкин А.Е., Массалимов И.А. Модифицирование поровой структуры цементных бетонов пропиткой серосодержащими растворами // Нанотехнологии в строительстве: научный интернет-журнал. 2015. Т. 7. № 1. С. 63–72.
5. Patel R.A., Perko J., Jacques D., De Schutter G., Ye G., Van Bruegel K. Effective diffusivity of cement pastes from virtual microstructures: Role of gel Porosity and capillary pore percolation // Construction and Building Materials. 2018. Vol. 165. Pp. 833–845.
6. Podolsky V.P., Long N.V., Hao N.K., Sy N.D. The study of operating capacity of asphalt concrete modified with an additive Wetfix Be // Scientific herald of the Voronesh state university of architecture and civil engineering. Construction and architecture. 2016. № 1(29). Pp. 75–83.
7. Урханова Л.А., Савельева М.А. Влияние золей различного состава на изменение структуры и свойств цементного камня // Нанотехнологии в строительстве: научный интернет-журнал. 2016. Т. 8. № 6. С. 20–42.
8. Jaya H., Omar M.F., Akil H.M., Ahmad Z.A., Zulkepli N.N. Effect of particle size on mechanical properties of sawdust-high density polyethylene composites under various strain rates // Bioresources. 2016. Vol. 11. № 3. Pp. 6489–6504.
9. Леонович С.Н., Свиридов Д.В., Щукин Г.Л., Беланович А.Л., Савенко В.П., Карпушенков С.А. Влияние цитрата натрия на процесс формирования цементного камня в глиноземистом вяжущем // Наука и техника. 2016. Т. 15. № 4. С. 281–286.
10. Массалимов И.А., Янахметов М.Р., Чуйкин А.Е., Массалимов Б.И., Уракаев Ф.Х., Уралбеков Б.М., Буркитбаев М.М. Гидрофобизация плотного и мелкозернистого бетонов полисульфидными растворами // Нанотехнологии в строительстве: научный интернет-журнал. 2016. Т. 8. № 5. С. 85–99.
11. Kudryavtsev P.G., Figovskii O.L. Organic water-soluble-silicates for protective coatings // Russian journal of building construction and architecture. 2017. № 3(35). Pp. 17–31.
12. Artamonova O.V., Sclavcheva G.S. Structure of cement systems as object of nanomodification // Scientific herald of the Voronesh state university of architecture and civil engineering. Construction and architecture. 2016. № 1(29). Pp. 13–26.
13. Cetin D., Sengul T., Bhatia S.K., Khachan M.M. Effect of polymer and fiber usage on dewatering and compressibility behavior of fly ash slurries // Marine georesources and geotechnology. 2017. Vol. 35. № 5. Pp. 678–687.
14. Gilligan R., Nikoloski A.N. Leaching of brannerite in the ferric sulphate system – Part 1: Kinetics and reaction mechanisms // Hydrometallurgy. 2015. Vol. 156. Pp. 71–80.
15. Koksharov S.A., Bazanov A.V., Fedosov S.V., Akulova M.V., Slizneva T.E. Condition of the mechanoactivated calcium chloride solution and its influence on structural and mechanical characteristics of cement stone // Eurasian Chemico-Technological Journal. 2015. Vol. 17. № 4. Pp. 327–333.
16. Левандовский А.Н., Мельников Б.Е., Шамкин А.А. Моделирование разрушения пористого материала // Инженерно-строительный журнал. 2017. № 1(69). С. 3–22.

Федосов С.В., Румянцева В.Е., Красильников И.В., Коновалова В.С., Евсяков А.С. Математическое моделирование кольматации пор бетона при коррозии // Инженерно-строительный журнал. 2018. № 7(83). С. 198–207.

15. Koksharov, S.A., Bazanov, A.V., Fedosov, S.V., Akulova, M.V., Slizneva, T.E. Condition of the mechanoactivated calcium chloride solution and its influence on structural and mechanical characteristics of cement stone. Eurasian Chemico-Technological Journal. 2015. Vol. 17. No. 4. Pp. 327–333.
16. Levandovskiy, A.N., Melnikov, B.E., Shamkin, A.A. Modeling of porous material fracture. Magazine of Civil Engineering. 2017. 69(1). Pp. 3–22. (rus)
17. Cherniakevich, O.Y., Leonovich, S.N. Raschet sostava betona zhelezobetonnykh konstruktsiy, ekspluatiruyushchikhsya v usloviyakh klassa KhS1, v zavisimosti ot tolshchiny zashchitnogo sloya [Concrete mix design for structures subjected to exposure class XC1 depending on concrete cover]. Science & Technique. 2016. Vol. 15. No. 6. Pp. 460-468. (rus)
18. Nikolskiy, S.G., Pertseva, O.N., Ivanova, V.I. Substantiation of an express-method for determining the freeze-thaw resistance of cellular materials. Magazine of Civil Engineering. 2015. 60(8). Pp. 7–19. (rus)
19. Sugiyama, T., Ritthichauy, W., Tsuji, Y. Experimental investigation and numerical modeling of chloride penetration and calcium dissolution in saturated concrete. Cement and Concrete Research. 2008. No. 38. Pp. 49–67.
20. Terenchuk, S., Pashko, A., Yeremenko, B., Kartavykh, S., Ershova, N. Modeling an intelligent system for the estimation of technical state of construction. EasternEuropean Journal of Enterprise Technologies. 2018. Vol. 3. No. 2(93). Pp. 47–53.
21. Gilmutdinov, T.Z., Fedorov, P.A., Latypov, V.M., Lutsyk, E.V., Latypova, T.V. Carbonation of concrete taking into account the cracks in the protective concrete layer. ARPN Journal of Engineering and Applied Sciences. 2017. Vol. 12. No. 15. Pp. 4406–4413.
22. Selyaev, V.P., Neverov, V.A., Selyaev, P.V., Sorokin, E.V., Yudina, O.A. Predicting the durability of concrete structures, including sulfate corrosion of concrete. Magazine of Civil Engineering. 2014. 45(1). Pp. 41–52. (rus)
23. Fedosov, S.V., Roumyantseva, V.E., Krasilnikov, I.V., Narmania, B.E. Formulation of mathematical problem describing physical and chemical processes at concrete corrosion. International journal for computational civil and structural engineering. 2017. Vol. 13. No. 2. Pp. 45–49. https://doi.org/10.22337/2587-9618-2017-13-2-45-49

17. Чернякевич О.Ю., Леонович С.Н. Расчет состава бетона железобетонных конструкций, эксплуатирующихся в условиях класса XC1, в зависимости от толщины защитного слоя // Наука и техника. 2016. Т. 15. № 6. С. 460–468.
18. Никольский С.Г., Перцева О.Н., Иванова В.И. Обоснование экспресс-метода определения морозостойкости пористых материалов // Инженерно-строительный журнал. 2015. № 8. С. 7–19.
19. Sugiyama T., Ritthichauy W., Tsuji Y. Experimental investigation and numerical modeling of chloride penetration and calcium dissolution in saturated concrete // Cement and Concrete Research. 2008. № 38. Pp. 49–67.
20. Terenchuk S., Pashko A., Yeremenko B., Kartavykh S., Ershova N. Modeling an intelligent system for the estimation of technical state of construction // EasternEuropean Journal of Enterprise Technologies. 2018. Vol. 3. № 2(93). Pp. 47–53.
21. Gilmutdinov T.Z., Fedorov P.A., Latypov V.M., Lutsyk E.V., Latypova T.V. Carbonation of concrete taking into account the cracks in the protective concrete layer // ARPN Journal of Engineering and Applied Sciences. 2017. Vol. 12. № 15. Pp. 4406–4413.
22. Селяев В.П., Неверов В.А., Селяев П.В., Сорокин Е.В., Юдина О.А. Прогнозирование долговечности железобетонных конструкций с учетом сульфатной коррозии бетона // Инженерно-строительный журнал. 2014. № 1(45). С. 41–52.
23. Fedosov S.V., Roumyantseva V.E., Krasilnikov I.V., Narmania B.E. Formulation of mathematical problem describing physical and chemical processes at concrete corrosion // International journal for computational civil and structural engineering. 2017. Vol. 13. № 2. Pp. 45–49. https://doi.org/10.22337/2587-9618-2017-13-2-45-49

Sergey Fedosov,
+7(980)694-81-41; fedosov-academic53@mail.ru

Varvara Rumyantseva,
+7(906)617-17-84; varrym@gmail.com

Igor Krasilnikov,
+7(910)691-64-22; korasb@mail.ru

Viktoriya Konovalova,*
+7(910)997-02-68; kotprotiv@yandex.ru

Artem Evsyakov,
+7(920)121-43-30; smart47@rambler.ru

Сергей Викторович Федосов,
+7(980)694-81-41;
эл. почта: fedosov-academic53@mail.ru

Варвара Евгеньевна Румянцева,
+7(906)617-17-84;
эл. почта: varrym@gmail.com

Игорь Викторович Красильников,
+7(910)691-64-22; эл. почта: korasb@mail.ru

Виктория Сергеевна Коновалова,*
+7(910)997-02-68;
эл. почта: kotprotiv@yandex.ru

Артем Сергеевич Евсяков,
+7(920)121-43-30;
эл. почта: smart47@rambler.ru

Fedosov, S.V., Rumyantseva, V.E., Krasilnikov, I.V., Konovalova, V.S., Evsyakov, A.S. Mathematical modeling of the colmatation of concrete pores during corrosion. Magazine of Civil Engineering. 2018. 83(7). Pp. 198–207. doi: 10.18720/MCE.83.18.

doi: 10.18720/MCE.83.19

Experimental justification of strainer meshes of NPP sump

Экспериментальное обоснование сеток фильтров баков-приямков АЭС

V.B. Shtilman,
B.N. Pogrebnyak,
P.A. Arseniev,
Yu.V. Shevchenko*,
"B.E. Vedeneev VNIIG", JSC, Saint Petersburg, Russia,
V.O. Kukhtevich,
A.I. Kurchevsky,
L.A. Matyushev,
JSC «ATOMPROEKT», St. Petersburg, Russia

Д-р техн. наук, директор по научной деятельности В.Б. Штильман,
ст. науч. сотр. Б.Н. Погребняк,
ведущий инженер П.А. Арсеньев,
канд. техн. наук, ст. науч. сотр. Ю.В. Шевченко*,
АО "ВНИИГ им. Б.Е. Веденеева", Санкт-Петербург, Россия
канд. техн. наук, начальник отдела В.О. Кухтевич,
начальник лаборатории А.И. Курчевский,
ведущий инженер-конструктор Л.А. Матюшев,
АО "АТОМПРОЕКТ", Санкт-Петербург, Россия

Key words: nuclear power plant (NPP); hydraulic studies; debris; head loss; flow rate; insulation; filter element

Ключевые слова: гидравлические исследования; дебрис; потери напора; расход; теплоизоляция; фильтрующее устройство

Abstract. Processes of filter meshes clogging of emergency core cooling system sump intended for cleaning water incoming in recirculation system from sump are studied. Test rig for study of hydraulic characteristics of filter elements, which is a closed circulation loop are described. Basic principles of modeling of coolant recirculation through a filter element, occurring in event of an emergency depressurization of primary circuit, and experimental research methods are presented. Dependences of pressure drop on meshes on flow rate and amount of debris for several types of meshes on ordinary and borated water are obtained and analyzed. It is shown that the use of borated water leads to an increase in both time to reach steady state and pressure loss on meshes. Constructive measures to reduce pressure losses are proposed.

Аннотация. Изучены процессы засорения сеток фильтров бака-приямка системы аварийного охлаждения зоны, предназначенных для очистки от загрязнений воды, поступающей в систему рециркуляции из баков-приямков. Описана экспериментальная установка для исследования гидравлических характеристик фильтрующих элементов, представляющая собой замкнутый циркуляционный контур. Приведены основные принципы моделирования рециркуляции теплоносителя через фильтрующий элемент, происходящей в случае аварийной разгерметизации первого контура, и методика экспериментальных исследований. Получены и проанализированы зависимости перепада давления на сетках от расхода и количества дебриса для нескольких видов сеток на обычной и на борированной воде. Показано, что использование борированной воды приводит к увеличению как времени достижения установившегося режима, так и потерь давления на сетках. Предложены конструктивные мероприятия для уменьшения потерь давления.

1. Introduction

At analyzing possible accidents at nuclear power plants (NPP), special attention should be paid to sudden depressurization of reactor cooling circuit caused, for example, by rupture of primary circuit pipeline. Naturally, intensity of course of such an accident, its various hydrodynamic, thermal and force effects depend significantly on size of suddenly created hole through which coolant will flow out. In all countries, including in Russia, for a maximum design accident a sudden transverse rupture of main circulation circuit pipeline with simultaneous flow of coolant from both ends is adopted.

Штильман В.Б., Погребняк Б.Н., Арсеньев П.А., Шевченко Ю.В.. Кухтевич В.О., Курчевский А.И., Матюшев Л.А. Экспериментальное обоснование сеток фильтров баков-приямков АЭС // Инженерно-строительный журнал. 2018. № 7(83). С. 208–221.

In case of accidents involving rupture of pipelines with high parameters there are destruction of thermal insulation, structural elements and structures. Part of garbage (debris) formed during accident can get into water intake devices for recirculation systems and disable these systems.

Since system contains a coolant with a high temperature (~300 °C) and at a high pressure (~160 kg/cm^2), a sudden decrease of pressure results in boiling of water and formation of steam. Within a short interval of time, main part of coolant in volume of ~300 m^3 flows through gap. During this period pressure and temperature under containment of reactor compartment increase, heat transfer in reactor core sharply worsens, temperature of fuel elements rises and it depressurization may occur. On pressure decrease signal in primary circuit, high and low pressure of emergency core cooling system (ECCS) pumps are automatically turned on, and borated water is supplied from sump of containment. On pressure increase signal in containment sprinkler pumps are automatically turned on and water is injected into air space of containment to condense steam and remove heat from atmosphere of containment.

Function of sprinkler system is also cooling of water to provide acceptable temperature conditions during operation of emergency core cooling system pumps (high and low pressure emergency injection systems). At the stage of long-term recirculation, the water taken through sumps serves for removal of residual heat during post-accidental cooling of reactor core.

Reliability of emergency core cooling system and removal of heat from containment depends on failure-free operation of pumps, which in turn depends on degree of clogging of meshes – filter active of ECCS sump designed for cleaning from contaminations of water entering in recirculation system from sumps. Clogging of grids and filters with elements by damaged pipeline rupture thermal insulation and other debris reduces supply of pumps and can cause it increased vibration and intensive cavitation wear. Meshes used for filtering the sumps diverse in designs and parameters. Results of tests allows determine most effective mesh for clogging of debris at minimum head loss on it.

For control of impurities coolant recirculation system must be equipped with filter structures, functioning and proper operation of which by means of tests must be checked. These tests should be carried out in chemically specific conditions using insulation of appropriate excerpt and coating material.

Based on analysis of operational experience of various stations, regulatory documents have been developed that establish requirements for water intake devices for recirculation systems and a methodology for ensuring these requirements, compulsory component of which is determination of hydraulic characteristics of filter elements depending on it contamination and specific flow rate of coolant [1–6].

Therefore, researches of aspects complex of sump operation in various operating conditions and development of constructive measures based on obtained results to ensure it trouble-free operation are carried out [7-26]. Thus, the works [7–12, 14, 16] are devoted to studies of composition, properties, characteristics of debris, and its modeling. Chemical properties of coolant and debris are discussed in the works [13, 17, 20, 23]. The results of physical and mathematical modeling of the motion of a coolant with debris particles, including through filters, are given in [15, 18, 19, 21–26].

In Russia, such researches have been carried out since beginning of 21st century [27–30], while experiments become more complicated and ever closer to real conditions of hypothetical accidents. Particular attention to this was paid after the accident at the Fukushima NPP, the study of causes and effects of which to a large number of studies are devoted [31–33].

This paper describes experimental hydraulic researches of meshes and slotted gratings of filter elements, results of which can be used as input data for justified determination of required filter surface and for design of filter active of ECCS sump. The results are deliberately conservative due to horizontal arrangement of meshes, as a result of which all debris introduced into flow reached it, without possibility of sedimentation from entering in unit to test mesh of strainer.

2. Methods

Hydraulic characteristics of filter elements depending on type of debris, amount of debris and reduced flow rate of coolant (nominal flow through model – nominal flow through 1 channel, reduced to area of tested mesh) were determined. During tests:

- type and brand of insulation, included in composition of debris, corresponded to those, that will be used in reactor building of NPP;
- quality of insulation (density, humidity, fractional composition, etc.) corresponded to characteristics of insulation exposed to steam (steam-water) jet during destruction;

– as filter elements were researched a slotted filter and meshes with a cell size of 1.0 mm and 0.7 mm;

– research section (pipe) with installed filter element in its hydraulic characteristics corresponded to full-scale.

Scope of tests included:

– determination of hydraulic characteristics (dependence of pressure losses on specific flow rate) of a "clean" filter element;

– determination of hydraulic characteristics (dependence of pressure losses on specific flow rate and quantity of insulation) of element contaminated with insulation;

– determination of effect on hydraulic characteristics of additional contaminations (sand, paint coatings), chemical agents (boric acid H_3BO), etc.

Solve technical tasks, by experimenting with models, possibly, if use notion of similarity of physical phenomena: research of clogging process of a filter element fragment (grid or mesh) of ECCS sump filters is possible when there is a correspondence between characteristics of nature and its model and, knowing characteristics of nature and form of this correspondence (similarity), one can find characteristics of nature.

Created model corresponded to basic similarity conditions, since were researched filter element fragments with fragments of destroyed natural insulation and other debris of same brands, sizes and other characteristics as in nature (debris included various fractions of artificially aged insulation fragments, sand, clay, zinc, particles and paint plates). At the same time, research at same flow rate of coolant and debris in terms of 1 cm^2 of mesh, as in NPP conditions was carried out. The time modeling scale is one. Thus, geometric (scale 1:1) and kinematic similarity were provided.

The only difference from nature is use of water at temperature of 20 °C instead of 95 °C. However, this approach is conservative because of increase in water viscosity.

One of main objectives of research is research of filter device clogging in order to develop recommendations aimed at ensuring trouble-free operation of "sump–pump" system. Hydraulically, containment device is a local resistance in a system including supply pipeline, pump, discharge pipe. For stable normal operation of this system it is necessary that pressure in inlet pipe of pump is not less than cavitation margin allowed for given pump brand.

Results of numerous tests have shown that hydraulic performance of pump inlet connections is a function of Froude number Fr. Other dimensionless parameters (for example, Reynolds numbers Re and Weber We) have a secondary meaning. In our case (with respect to filter mesh) Froude numbers on model and in nature are equal:

$$\mathrm{Fr}_{\mathrm{mod}} = \mathrm{Fr}_{\mathrm{nat}} = \frac{v_{\mathrm{p}}}{\sqrt{gh}},$$

where v_p – fluid velocity in pipeline; h – static head in pipe above mesh, g – acceleration of gravity. For example, at $v_{\mathrm{p}} = 0.012$ m/s and $h = 1$ m number of Froude is $\mathrm{Fr} = 0.0038$.

Value of local resistance coefficient of filter mesh ζ_{m} reflects the loss of pressure Δh_{m} when liquid flows through it:

$$\zeta_m = \frac{2g\Delta h_m}{v_p^2}.$$

Thus, by measuring flow rate and pressure drop on contaminated mesh on model, it is possible to calculate its resistance coefficient corresponding to volume of debris that has been introduced into water per unit area of mesh.

Clear size of mesh cell d_{cell}, like velocity of flow through it V_{cell}, is the same for model and nature. Therefore, Reynolds number

$$Re = \frac{V_{cell} d_{cell}}{\nu}, \quad (1)$$

where ν – kinematic viscosity coefficient, at 20°C $\nu_{20} = 1.01 \cdot 10^{-6}$ m²/s.

In Table 1 shown the values of Reynolds numbers calculated at this temperature at a nominal flow rate of water of 0.0947 m³/h, and also at a flow rate of 0.5 m³/h.

***Table 1. Velocity V_{cell} and Reynolds numbers* Re**

Mesh	Clear size of mesh cell		Flow rate of water			
			0.0947 m³/h		0.5000 m³/h	
	m²	%	V_{cell}, m/s	Re	V_{cell}, m/s	Re
Cell 0.7 mm	0.013	47	0.0020	1	0.0107	5
Cell 1.0 mm	0.015	51	0.0018	2	0.0093	6
Slot 1.0 mm	0.010	35	0.0026	3	0.0139	9

Thus, for all tested filter devices in entire range of flow rates, the Reynolds numbers ranged from 1 to 9, indicating a laminar flow near meshes. This conclusion was confirmed experimentally (visually when particles of debris move), when turbulent flow at beginning of working section below diffuser was observed. Next, almost to confuser, flow mode remained laminar – particles moved linearly vertically downward.

Therefore, dependence of pressure drop (in other words, the head loss) on filter device of flow rate must be linear. In addition, it does not depend on pressure ahead in front of filter device with debris that has settled on it, which can be considered as a porous material. However, for obtaining each of these dependencies for a different amount of debris requires a certain amount of time, and when performing tests under influence of water flow there was compaction of debris settled on mesh, and pores of settled debris are clogged with small particles, which introduce a certain nonlinearity. These processes were especially noticeable in borated water (tests on cold water were carried out, then some of it on borated water were repeated).

The researches in test rig consisting of a closed circulation circuit (Figure 1) in which filter meshes were located horizontally on working section of rig, which introduced additional conservatism in obtained results were carried out: entire debris, with exception of smallest particles passing through mesh, settled on it, unlike actual filter modules, when particles with larger hydraulic size settle to the bottom before it enter directly to filters. Horizontal filter configuration did not assume a reflection of its real location, but served only to ensure development of a homogeneous layer with well-defined characteristics.

In Figure 2 on a larger scale fragment of working section with installed in it filter element (red color is given to sealing rings) is shown. A photo of filter element prepared with a stainless steel mesh is shown in Figure 3.

Pressure drop across filter element, as well as pressure before and after it, by differential pressure sensors MP5010 DP and piezometers mounted on rings for selection and averaging of pressure were fixed (Figure 4). Results of flow rate and pressure measurements entered to computer by data acquisition and processing software were processed.

Since total design area of filter surface of one channel is preliminary, it was necessary to carry out tests in such way that it results could be used both with decreasing and with increasing this area. Such change leads to corresponding change as well as in amount of debris per unit area and flow rate of coolant through mesh (and flow rate associated with it on model).

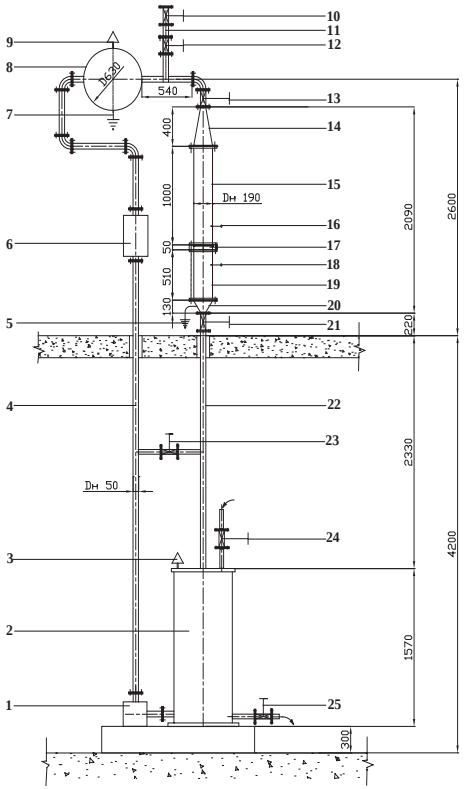

Figure 1. Scheme of test rig: 1 – pump, 2 – lower tank, 3, 9 – air bleed valve, 4 – pipeline inlet section, 5, 7 – drain outlet, 6 – flow meter, 8 – upper tank, 10 – gate valve upper, 11 – gate for debris introduction, 12 – gate valve lower, 13 – valve upper, 14 – diffuser, 15 – supply pipe of working section, 16, 18 – pressure sensor, 17 – detachable section with a filter element, 19 – outlet pipeline of working section, 20 – confuser, 21 – valve lower, 22 – outlet section of pipeline, 23 – bypass valve, 24 – water inlet valve, 25 – water drainage valve

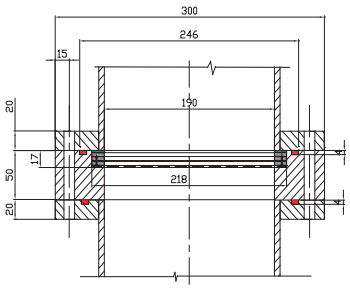

Figure 2. Fragment of working section with filter element

Figure 3. Filter element

Штильман В.Б., Погребняк Б.Н., Арсеньев П.А., Шевченко Ю.В.. Кухтевич В.О., Курчевский А.И., Матюшев Л.А. Экспериментальное обоснование сеток фильтров баков-приямков АЭС // Инженерно-строительный журнал. 2018. № 7(83). С. 208–221.

Figure 4. Rings for selection of pressure

Therefore, tests to cover entire range of possible changes in these parameters were designed. Tests with a different amount of debris, ranging from 0 to 150 % of nominal with a step of 25 % (in first tests) and 15 % were carried out. Here, for nominal amount of debris its weight per area of testing mesh on model for given area of filter surface of one channel is taken. At the same time, flow velocity at approach to filter (and hence flow rate through mesh) in first tests was up to 20 nominal (which corresponding to flow rate of model approximately 2 m^3/h), in further (after processing first obtained results) – to 5 nominal (flow rate approximately 0.5 m^3/h). This range of velocities covered and possible unevenness of velocities in lower and upper parts of future filter module, related both to nature of meshes clogging by debris, and to parameters of modules and collector.

Debris after appropriate preparation was packaged, receiving either 10 portions of debris at 15 % of nominal amount per 1 channel, or 6 portions of 25 % (Figure 5).

Figure 5. 25% of dry debris

Soaking of debris an hour before first introduction into flow of test rig was carried out, which corresponded to time interval between possible accident and beginning of debris arrival to meshes of strainers.

Tests simulated behavior of filters in first few hours after possible accident with loss of coolant. In general case, if further analysis of results of tests does not indicate otherwise, they were carried out in following sequence.

1. Soaking debris portions in approximately 800 ml of water.

2. Test rig was turned on, head loss on mesh on clean water was measured, flow rate of about 0.5 m^3/h was set.

3. One hour after soaking of debris, first portion (15 %) through gate was introduced.

4. After 10 minutes first measurement of flow rate and pressure drop was made. Within 10 minutes almost entire visually visible part of debris on mesh was settled (Figure 6), mode became steady, and measured characteristics ceased to change significantly. For borated water process, as before, remained unsteady.

5. Then flow rate by four steps to minimum level was reduced, after that it to original 0.5 m^3/h was returned. Measurement of flow rate and pressure drop in each mode 5 minutes after flow rate change was carried out. Thus, duration of one cycle was 35 minutes.

6. Next portion of debris was introduced, after which actions of two preceding paragraphs 4 and 5 were repeated. If, at a flow rate of 0.5 m^3/h, pressure loss exceeded test rig limit of 1.8 m, initial flow rate before introduction of debris was reduced and set so, that in 35 minutes, taking into account possible

growth of difference on mesh, pressure loss did not exceed 1.8 m. However, in some tests with large amounts of debris flow rate was not regulated forcefully, it decreased spontaneously during growth of resistance coefficient of clogged filter. However, time intervals between measurements were maintained as before.

7. Mesh with settled debris at the end of test was removed, dried and determined weight of debris delayed by mesh.

8. Mesh with fine cell of 0.1 mm was installed and at flow rate up to 15 m^3/h water in test rig debris particles not delayed by mesh being tested was cleaned, as long as pressure drop and flow rate did not cease to change with time.

9. At the end of cleaning fine mesh with settled particles of debris was removed, dried and determined weight of debris not delayed by test mesh of filter.

after introduction of debris portion:

after 10 seconds **after 10 minutes**

Figure 6. View of work section after introduction of debris portion

3. *Results and Discussions*

In course of research dependences of head loss on different filter meshes for various amounts of debris was obtained. At flow rate up to 0.5 m^3/h in absence of debris pressure drop for all tested meshes was zero. As an example, test results for 1.0 mm mesh are given.

Research of 1.0 mm mesh on water

In Figure 7 shown general view of debris delayed by mesh. Separate plates of paint are clearly visible.

Figure 7. Dried debris on mesh

In tests with debris a very wide dispersion of pressure drop values is observed, which is associated with a significant dependence of these values on character of the fall and packing of debris on mesh, which occurs at random. With larger meshes this spread should decrease. However, with a conservative

approach to design and calculations, it is recommended to be guided by largest (worst) values of pressure drop.

In Figure 8 shown dependence of difference on mesh on amount of introduced debris at nominal flow rate of 0.0947 m³/h. Results of tests in form of graphs of dependences of difference on mesh with debris on flow at different amounts of introduced debris are given in Figure 9.

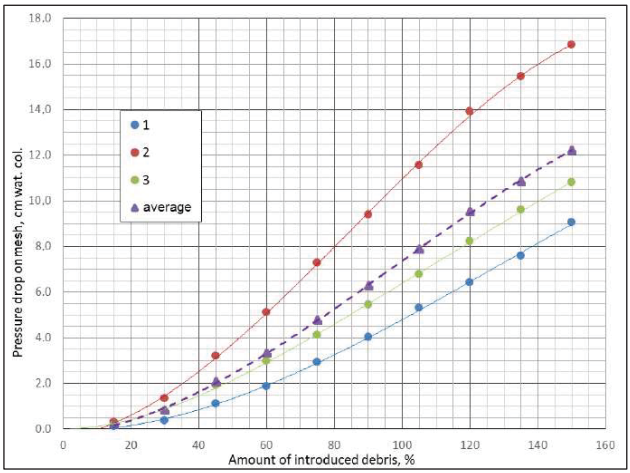

Figure 8. Dependence of pressure drop on filter with mesh of 1.0 mm on amount of debris at nominal flow rate of 0.0947 m³/h for tests 1, 2 and 3

Maximum drop at nominal flow rate of 0.0947 m³/h and 100 % of debris was about 11 cm, which is more than 3 times lower than for mesh with a cell of 0.7 mm. Pressure loss on mesh in these tests has a smaller spread and smaller average values than in tests with cell of 0.7 mm: average difference on mesh is 1.0 mm with 105 % of introduced debris and flow rate of 0.5 m³/h was about 57 cm (in tests 28, 36 and 61 cm), whereas on mesh with cell of 0.7 mm it is 99 cm (in tests 33, 79 and 184 cm).

In Table 2 shown weights of introduced and delayed debris by filter mesh with a cell of 1.0 mm for three tests. Weight of debris not delayed by filter was up to 22 %, in three tests from 78 to 95 % of debris was delayed. At the same time, relation with head loss was reversed: with maximum weight of delayed debris pressure drop was minimal, with minimum weight – maximum. This shows that greatest influence on drop when debris falls accidentally exerts nature of its distribution along mesh.

Table 2. Weights of introduced and delayed debris on filter mesh with a cell of 1.0 mm

Test number	Weight of debris		
	introduced, g	delayed	
		g	%
1	139.0	131.7	95
2	139.0	109.1	78
3	139.0	116.3	84

Long-term test on borated water of mesh with a cell of 1.0 mm

A long-term test is most indicative from point of view of measuring maximum difference on mesh, since it shows its magnitude in fully stable mode when all debris particles have already settled on filter, including those that passed through mesh initially. During a continuous test lasting more than 52 hours water performed approximately 10 turns.

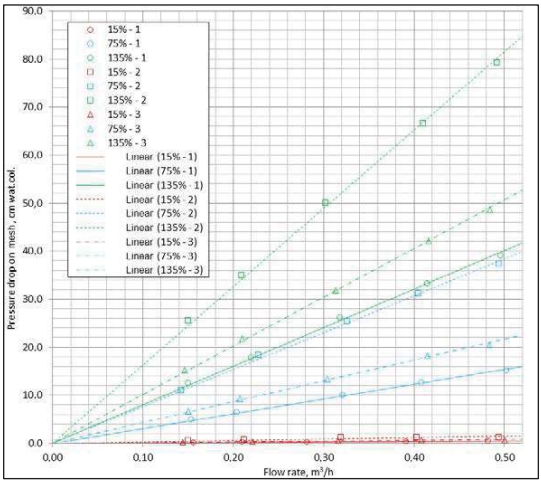

Figure 9. Dependence of drop on filter with mesh of 1.0 mm on flow rate for tests 1, 2 and 3 at various amount of introduced debris

Test without paint plates was carried out: it is heavy and drown in both conventional and borated water. Therefore, a low fence around strainers or small rise it above floor will prevent these plates getting to meshes, which will significantly reduce pressure loss on strainers.

Test at constant flow rate of 0.150 ± 0.005 m^3/h (with decrease of flow rate, by opening valve below working section was increased) was carried out. This is approximately in 1.5 times more than nominal, which is conservative solution, as it causes more pressure losses on mesh, including due to stronger compaction of debris.

In addition, debris by portions of 5 % at intervals of 20 minutes was introduced, which also leads to more uniform tightening of mesh by debris and stronger compaction. At the same time, first 60 % of debris within three hours forty minutes after beginning of test was introduced (in Figure 10 shown a photograph of filter with settled debris after 23 hours 45 minutes after beginning of test), another 40 % - within two hours twenty minutes after day after beginning of test (in Figure 11 shown a photograph of filter with settled debris after 52 hours 35 minutes after beginning of test).

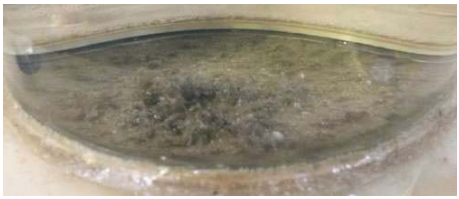

Figure 10. Mesh with a cell of 1.0 mm with 60% of debris without paint plates, borated water

Figure 11. Mesh with a cell of 1.0 mm with 100% of debris without paint plates, borated water

Штильман В.Б., Погребняк Б.Н., Арсеньев П.А., Шевченко Ю.В.. Кухтевич В.О., Курчевский А.И., Матюшев Л.А. Экспериментальное обоснование сеток фильтров баков-приямков АЭС // Инженерно-строительный журнал. 2018. № 7(83). С. 208–221.

In Figure 12 shown pressure and flow rate graphs during test. It can be seen that growth of pressure losses on mesh continued even after introduction of both 60 % and 100 % of debris, but at slightly slower rate. It ceased only 45 hours after beginning of test (18 hours after introduction of 100 % debris) and remained unchanged for more than 7 hours until end of test, amounting to only 24 cm.

Mesh with delayed debris from test rig after hysteresis test was removed. Thickness of delayed debris in wet state was about 3 mm. On mesh with cell of 1.0 mm 49.6 g of debris was delayed, which is 73 % of introduced 68.0 g of debris. This approximately corresponds to proportion of delayed debris in ordinary tests. However, in reality, weight of delayed debris was larger, since part of it was lost (passed through mesh) when water from test rig to remove filter module was drained.

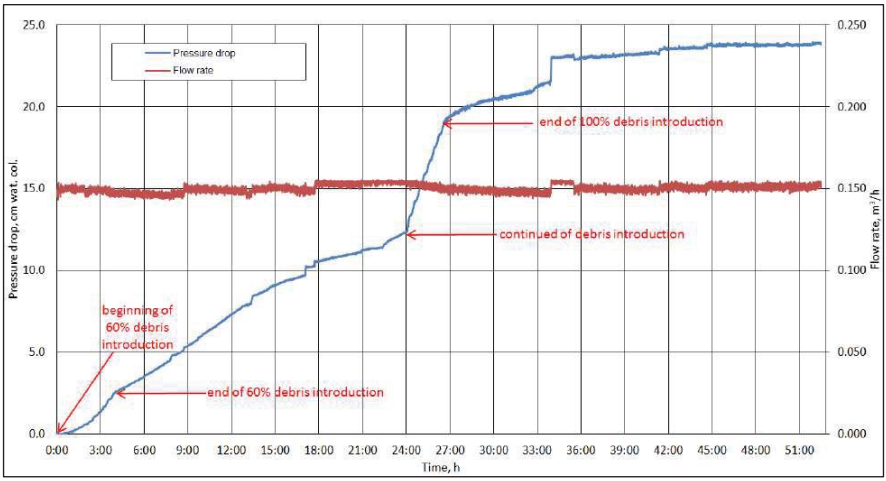

Figure 12. The change of difference on mesh with cell of 1.0 mm over time, borated water

Hysteresis test on borated water

Immediately after end of long-term test, without turning off pump, test to determine dependence of drop on debris of flow rate with determination of flow rate at which pressure loss on mesh is 150 cm of wat. col. was started, as well as to determine hysteresis, which allows determine how completely compacted debris on mesh in conditions that are as close as possible to actual ones. The results of continuous recording of this test are presented in Figures 13 and 14.

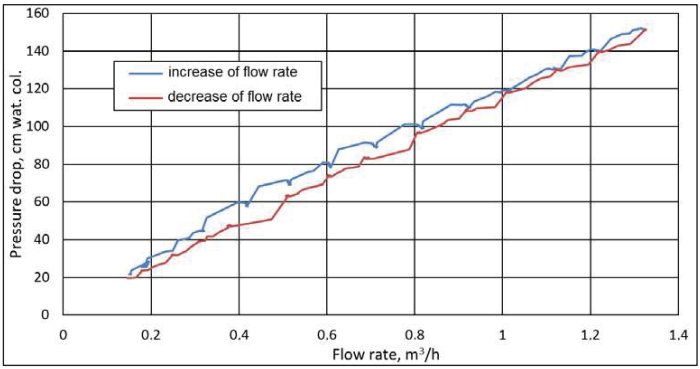

Figure 13. Dependence of drop on mesh with cell of 1.0 mm of flow rate after long-term test, borated water

Shtilman, V.B., Pogrebnyak, B.N., Arseniev, P.A., Shevchenko, Yu.V., Kukhtevich, V.O., Kurchevsky, A.I., Matyushev, L.A. Experimental justification of strainer meshes of NPP sump. Magazine of Civil Engineering. 2018. 83(7). Pp. 208–221. doi: 10.18720/MCE.83.19.

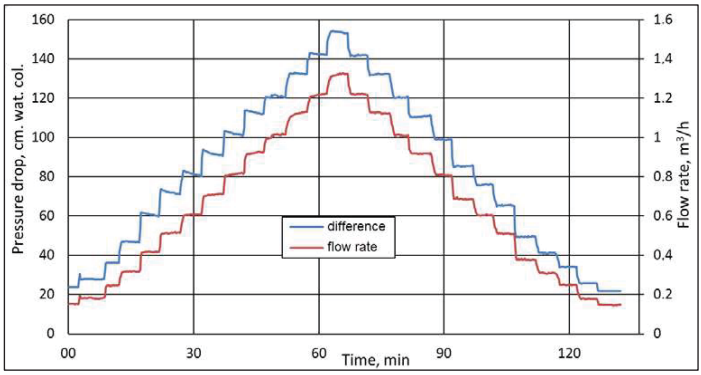

Figure 14. The change drop on mesh with cell of 1.0 mm when flow rate is changed, borated water

The difference reached 150 cm of wat. col. at flow rate of about 1.25 m³/h, and after reducing flow rate again to level of 0.15 m³/h, it even became 2 cm of wat. col. below original. Thus, there was no further compaction of debris, and at high flow rates, perhaps, there was an insignificant flushing out of individual particles from debris delayed by mesh. This confirms validity of conclusion that after 45 hours of fluid circulation during long-term test process of pressure losses growth on mesh ceased.

4. Conclusion

1. In tests with debris a very wide dispersion of pressure drop values is observed, which is associated with a significant dependence of these values on nature of fall and packing of debris on mesh, which occurs at random. With larger meshes this spread should decrease. However, with a conservative approach, it is recommended in further calculations to be guided by largest (worst) values of pressure drop.

2. Borated water, apparently, prevents fine particles of debris from sticking together in flow, so they settle longer, but it can be seen colmatage of filtration passages in layer of delayed debris by mesh, and pressure drop on mesh is approximately 10 times greater than in tests with ordinary water, with equal flow rates and amounts of insulation. Wherein, time to reach steady-state mode increases substantially, when flow rate and pressure loss on mesh stabilize. 30 minutes after introduction of debris portion (total amount reached 75%), pressure drop across with cell of 1.0 mm was about 75 cm at nominal flow rate of 0.0947 m³/h.

3. Research of filter clogging process with separation of debris into two types (paint plates and rest) showed that it joint flow to filter leads to a sharp jump-like increase in pressure drop. Thus, at nominal flow rate of 0.0947 m³/h with introduction only plates, the difference on mesh with cell of 1.0 mm was zero, with introduction of various debris without plates – from several centimeters in standard tests to thirteen after long-term test. At the same time, when it was jointly introduced in amount of already 90 %, pressure loss was not less than 75 cm.

4. Paint plates are quite heavy and quickly drown in both conventional and borated water. Therefore, a low fence around strainers or small rise it above floor will prevent these plates getting to meshes, which will significantly reduce pressure loss on filters.

5. Due to above factors, the results obtained with a long-term test are most indicative and approximate to real conditions of hypothetical accident, with exception of coolant temperature. At the same time, the difference on mesh with cell of 1.0 mm in steady-state mode (more than 51 hours after beginning of debris introduction) was: at nominal flow rate of 0.0947 m³/h – about 12 cm, at flow rate of 0.5 m³/h – about 68 cm.

6. Results of tests are used as initial data for justified choice of type of meshes and determination of necessary filtering surface at designing of filtering devices of ECCS sumps.

Штильман В.Б., Погребняк Б.Н., Арсеньев П.А., Шевченко Ю.В.. Кухтевич В.О., Курчевский А.И., Матюшев Л.А. Экспериментальное обоснование сеток фильтров баков-приямков АЭС // Инженерно-строительный журнал. 2018. № 7(83). С. 208–221.

References

1. PWR Primary Water Chemistry Guidelines. Vol. 2, Rev. 5. 1002884-V2. EPRI, Palo Alto, USA. 2003. 115 p.
2. Pressurized Water Reactor Primary Water Chemistry Guidelines. Vol. 2, Rev. 6. 1014986. EPRI, Palo Alto, USA. 2007. 117 p.
3. NEI 04-07, Revision 0. Pressurized Water Reactor Sump Performance Evaluation Methodology. December 2004. Vol. 1. 336 p.
4. NEI 04-07, Revision 0. Pressurized Water Reactor Sump Performance Evaluation Methodology. December 2004. Vol. 2. 476 p.
5. IAEA Safety Standard Series Safety Guide No. NS-G-1.9 Design of the Reactor Coolant System and Associated Systems in Nuclear Power Plants. International Atomic Energy Agency, Vienna, Austria, 2004. 89 p.
6. Regulatory guide 1.82. Water Sources for Long-Term Recirculation Cooling Following a Loss-Of-Coolant Accident, Revision 4. U.S. Nuclear Regulatory Commission, March 2012. 54 p.
7. Popovics, S. Concrete Materials – Properties, Specifications and Testing (2nd Edition). William Andrew Publishing, 1992. 674 p.
8. Bourcier William, L. Critical Review of Glass Performance Modeling. Argonne National Laboratory Report ANL-94/17, July 1994. 45 p.
9. Smallman, R.E., Bishop, R.J. Modern Physical Metallurgy and Materials Engineering - Science, Process, Applications (6th Edition). Elsevier, 1999. 448 p.
10. Biggs, C.A., Lant, P.A. On-Line Determination of Floc Size and the Effect of Shear. Water Research. 2000. Vol. 34(9). Pp. 2542–2550.
11. Revie, R.W. Uhlig's Corrosion Handbook (2nd Edition). John Wiley & Sons, 2000. 1344 p.
12. Bynum, R.T. Insulation Handbook. McGraw-Hill, 2001. 512 p.
13. Giulietti, M., et al. Industrial Crystalization and Precipitation from Solutions State of the Technique. Brazilian Journal of Chemical Engineering. 2001. Vol. 18. No. 4. Pp. 423–440.
14. Harper, C.A. Handbook of Materials for Product Design. McGraw-Hill, 2001. 1409 p.
15. Prasser, H.-M., Grunwald, G., Höhne, T., Weiss, F.-P. Coolant Mixing in a Pressurized Water Reactor: Deboration Transients, Steam-Line Breaks, and Emergency Core Cooling Injection. Nuclear Technology. 2003. Vol. 143. No. 1. Pp. 37–56.
16. Jarvis, P., Jefferson, B., Parsons, S. Measuring Floc Structural Characteristics. Reviews in Environmental Science and Biotechnology. 2005. Vol. 4. No. 1-2. Pp. 1–18.
17. Bahn, C.B. Chemical effects on PWR sump strainer blockage after a loss-of-coolant accident: Review on US research efforts. Nuclear Engineering and Technology. 2013. Vol. 45. No. 3. Pp. 295–310.
18. Höhne, T., Grahn, A., Kliem, S., Rohde, U., Weiss, F.-P. Numerical simulation of the insulation material transport to a PWR core under loss of coolant accident conditions. Nuclear Engineering and Design. 2013. Vol. 258. Pp. 241–248.
19. Jung, M.-S., Kim, K.-T. Debris filtering efficiency and its effect on long term cooling capability. Nuclear Engineering and Design. 2013. Vol. 261. Pp. 1–9.
20. Li, J., Tang, H., Zhao, Y., Luo, M., Wang, Q., Wang, Z. Chemical effect evaluation of containment sump filter of CPR1000 nuclear power plants. Hedongli Gongcheng / Nuclear Power Engineering. 2015. Vol. 36. No. 3. Pp. 125–128.
21. Jacquemain, D., Vola, D., Meignen, R., Bonnet, J.-M., Fichot, F., Raimond, E., Barrachin, M. Past and Future

Литература

1. PWR Primary Water Chemistry Guidelines. Vol. 2, Rev. 5. 1002884-V2. EPRI, Palo Alto, USA. 2003. 115 p.
2. Pressurized Water Reactor Primary Water Chemistry Guidelines. Vol. 2, Rev. 6. 1014986. EPRI, Palo Alto, USA. 2007. 117 p.
3. NEI 04-07, Revision 0. Pressurized Water Reactor Sump Performance Evaluation Methodology. December 2004. Vol. 1. 336 p.
4. NEI 04-07, Revision 0. Pressurized Water Reactor Sump Performance Evaluation Methodology. December 2004. Vol. 2. 476 p.
5. IAEA Safety Standard Series Safety Guide No. NS-G-1.9 Design of the Reactor Coolant System and Associated Systems in Nuclear Power Plants. International Atomic Energy Agency, Vienna, Austria, 2004. 89 p.
6. Regulatory guide 1.82. Water Sources for Long-Term Recirculation Cooling Following a Loss-Of-Coolant Accident, Revision 4. U.S. Nuclear Regulatory Commission, March 2012. 54 p.
7. Popovics S. Concrete Materials – Properties, Specifications and Testing (2nd Edition). William Andrew Publishing, 1992. 674 p.
8. Bourcier William L. Critical Review of Glass Performance Modeling. Argonne National Laboratory Report ANL-94/17, July 1994. 45 p.
9. Smallman R.E., Bishop R.J. Modern Physical Metallurgy and Materials Engineering - Science, Process, Applications (6th Edition). Elsevier, 1999. 448 p.
10. Biggs C.A., Lant P.A. On-Line Determination of Floc Size and the Effect of Shear // Water Research. 2000. Vol. 34(9). Pp. 2542–2550.
11. Revie R.W. Uhlig's Corrosion Handbook (2nd Edition). John Wiley & Sons, 2000. 1344 p.
12. Bynum R.T. Insulation Handbook. McGraw-Hill, 2001. 512 p.
13. Giulietti M., et al. Industrial Crystalization and Precipitation from Solutions State of the Technique // Brazilian Journal of Chemical Engineering. 2001. Vol. 18. № 4. Pp. 423–440.
14. Harper C.A. Handbook of Materials for Product Design. McGraw-Hill, 2001. 1409 p.
15. Prasser H.-M., Grunwald G., Höhne T., Weiss F.-P. Coolant Mixing in a Pressurized Water Reactor: Deboration Transients, Steam-Line Breaks, and Emergency Core Cooling Injection // Nuclear Technology. 2003. Vol. 143. № 1. Pp. 37–56.
16. Jarvis P., Jefferson B., Parsons S. Measuring Floc Structural Characteristics // Reviews in Environmental Science and Biotechnology. 2005. Vol. 4. № 1-2. Pp. 1–18.
17. Bahn C.B. Chemical effects on PWR sump strainer blockage after a loss-of-coolant accident: Review on US research efforts // Nuclear Engineering and Technology. 2013. Vol. 45. № 3. Pp. 295–310.
18. Höhne T., Grahn A., Kliem S., Rohde U., Weiss F.-P. Numerical simulation of the insulation material transport to a PWR core under loss of coolant accident conditions // Nuclear Engineering and Design. 2013. Vol. 258. Pp. 241–248.
19. Jung M.-S., Kim K.-T. Debris filtering efficiency and its effect on long term cooling capability // Nuclear Engineering and Design. 2013. Vol. 261. Pp. 1–9.
20. Li J., Tang H., Zhao Y., Luo M., Wang Q., Wang Z. Chemical effect evaluation of containment sump filter of CPR1000 nuclear power plants // Hedongli Gongcheng / Nuclear Power Engineering. 2015. Vol. 36. № 3. Pp. 125–128.
21. Jacquemain D., Vola D., Meignen R., Bonnet J.-M., Fichot F., Raimond E., Barrachin M. Past and Future Research at IRSN on Corium Progression and Related Mitigation

Shtilman, V.B., Pogrebnyak, B.N., Arseniev, P.A., Shevchenko, Yu.V., Kukhtevich, V.O., Kurchevsky, A.I., Matyushev, L.A. Experimental justification of strainer meshes of NPP sump. Magazine of Civil Engineering. 2018. 83(7). Pp. 208–221. doi: 10.18720/MCE.83.19.

Research at IRSN on Corium Progression and Related Mitigation Strategies in a Severe Accident. Nuclear Technology. 2016. Vol. 196. No. 2. Pp. 161–174.

22. Huang, X., Cheng, X., Klein-Heßling, W.Evaluation of Passive Containment Cooling with an Advanced Water Film Model in a Lumped-Parameter Code. Nuclear Technology. 2016. Vol. 196. No. 2. Pp. 248–259.
23. Ali, A., Howe, K., Blandford, D.E. Chemical Head Loss Measurements on Multi-Constituent Debris Beds in a Small-Scale Experiments. Nuclear technology. 2018. Vol. 204. No. 3. Pp. 318–329.
24. Flaspoehler, T., Petrovic, B. Contributon-Based Mesh-Reduction Methodology for Hybrid Deterministic-Stochastic Particle Transport Simulations Using Block-Structured Grids. Nuclear Science and Engineering. 2018. Vol. 192. No. 3. Pp. 254–274.
25. Park, J.-K., Lee, S.-K., Kim J.-H. Development of an evaluation method for nuclear fuel debris-filtering performance. Nuclear Engineering and Technology. 2018. Vol. 50. No. 5. Pp. 738–744.
26. Azam, M.S., Niu, F., Wang, D., Zhuo, W. Experimental and CFD analysis of the effects of debris deposition across the fuel assemblies. Nuclear Engineering and Design. 2018. Vol. 332. Pp. 238–251.
27. Bellendir, L.E., Pogrebnyak, B.N., Shtilman, V.B. Gidravlicheskiye laboratornyye issledovaniya priyamka zashchitnoy obolochki AES [Hydraulic laboratory tests of containment sump of NPP]. Gidravlika (nauka i distsiplina). Materialy Mezhdunarodnoy nauchno-teoreticheskoy konferentsii. S.-Pb.: SPbGTU. 2004. P. 4. (rus)
28. Altshuller, A.M., Antropov, G.A., Bellendir, L.E., Pogrebnyak, B.N., Shtilman, V.B. Gidravlicheskiye laboratornyye issledovaniya priyamka zashchitnoy obolochki AES [Hydraulic laboratory tests of containment sump of NPP]. Gidrotekhnicheskoye stroitelstvo. 2005. No. 5. Pp. 36–40. (rus)
29. Levina, S.M., Shtilman, V.B. Issledovaniya po obespecheniyu nadezhnosti oborudovaniya gidrotekhnicheskikh sooruzheniy GES i AES [Research on reliability of hydraulic structures equipment of HPP and NPP]. Gidrotekhnicheskoye stroitelstvo. 2011. No 5. Pp. 32–36.
30. Pogrebnyak, B.N., Korobko, N.V., Legina, E.E., Shtilman, V.B. Gidravlicheskiye issledovaniya filtruyushchikh elementov dlya proyektirovaniya filtrov bakov-priyamkov AES [Hydraulic studies of filter elements for design of sump filters of NPPs]. Desyataya nauchno-tekhnicheskaya konferentsiya: Gidroenergetika. Gidrotekhnika. Novyye razrabotki i tekhnologii. Tezisy dokladov. S.-Pb.: AO «VNIIG im. B.E. Vedeneeva». 2016. Pp. 256.
31. Sugimoto, J. Severe Accident Research in Japan After the Fukushima Daiichi Nuclear Power Station Accident. Nuclear Technology. 2016. Vol. 196. No. 2. Pp. 149–160.
32. Sonnenkalb, M., Band, S. ATHLET-CD/COCOSYS Analyses of Severe Accidents in Fukushima Daiichi Units 2 and 3: German Contribution to the OECD/NEA BSAF Project, Phase 1. Nuclear Technology. 2016. Vol. 196. No. 2. Pp. 211–222.
33. Luxat, D.L., Gabor, J.R., Wachowiak, R.M., Yang, R.L. EPRI MAAP5 Fukushima Daiichi Analysis. Nuclear Technology. 2016. Vol. 196. No. 2. Pp. 698–711.

Strategies in a Severe Accident // Nuclear Technology. 2016. Vol. 196. № 2. Pp. 161–174.

22. Huang X., Cheng X., Klein-Heßling W. Evaluation of Passive Containment Cooling with an Advanced Water Film Model in a Lumped-Parameter Code // Nuclear Technology. 2016. Vol. 196. № 2. Pp. 248–259.
23. Ali A., Howe K., Blandford D.E. Chemical Head Loss Measurements on Multi-Constituent Debris Beds in a Small-Scale Experiments // Nuclear technology. 2018. Vol. 204. № 3. Pp. 318–329.
24. Flaspoehler T., Petrovic B. Contributon-Based Mesh-Reduction Methodology for Hybrid Deterministic-Stochastic Particle Transport Simulations Using Block-Structured Grids // Nuclear Science and Engineering. 2018. Vol. 192. № 3 Pp. 254–274.
25. Park J.-K., Lee S.-K., Kim J.-H. Development of an evaluation method for nuclear fuel debris-filtering performance // Nuclear Engineering and Technology. 2018. Vol. 50. № 5. Pp. 738–744.
26. Azam M.S., Niu F., Wang D., Zhuo W. Experimental and CFD analysis of the effects of debris deposition across the fuel assemblies // Nuclear Engineering and Design. 2018. Vol. 332. Pp. 238–251.
27. Беллендир Л.Э., Погребняк Б.Н., Штильман В.Б. Гидравлические лабораторные исследования приямка защитной оболочки АЭС // Гидравлика (наука и дисциплина). Материалы Международной научно-теоретической конференции. С.-Пб.: СПбГТУ. 2004. С. 4.
28. Альтшуллер А.М., Антропов Г.А., Беллендир Л.Э., Погребняк Б.Н., Штильман В.Б. Гидравлические лабораторные исследования приямка защитной оболочки АЭС // Гидротехническое строительство. 2005. № 5. С. 36–40.
29. Левина С.М., Штильман В.Б. Исследования по обеспечению надежности оборудования гидротехнических сооружений ГЭС и АЭС // Гидротехническое строительство. 2011. № 5. С. 32–36.
30. Погребняк Б.Н., Коробко Н.В., Легина Е.Е., Штильман В.Б. Гидравлические исследования фильтрующих элементов для проектирования фильтров баков-приямков АЭС // Десятая научно-техническая конференция: Гидроэнергетика. Гидротехника. Новые разработки и технологии. Тезисы докладов. С.-Пб.: АО «ВНИИГ им. Б.Е. Веденеева». 2016. С. 256.
31. Sugimoto J. Severe Accident Research in Japan After the Fukushima Daiichi Nuclear Power Station Accident // Nuclear Technology. 2016. Vol. 196. No. 2. Pp. 149–160.
32. Sonnenkalb M., Band S. ATHLET-CD/COCOSYS Analyses of Severe Accidents in Fukushima Daiichi Units 2 and 3: German Contribution to the OECD/NEA BSAF Project, Phase 1 // Nuclear Technology. 2016. Vol. 196. № 2. Pp. 211–222.
33. Luxat D.L., Gabor J.R., Wachowiak R.M., Yang R.L. EPRI MAAP5 Fukushima Daiichi Analysis // Nuclear Technology. 2016. Vol. 196. № 2. Pp. 698–711.

Штильман В.Б., Погребняк Б.Н., Арсеньев П.А., Шевченко Ю.В.. Кухтевич В.О., Курчевский А.И., Матюшев Л.А. Экспериментальное обоснование сеток фильтров баков-приямков АЭС // Инженерно-строительный журнал. 2018. № 7(83). С. 208–221.

Vladimir Shtilman,
+7(921)936-57-43; ShtilmanVB@vniig.ru

Boris Pogrebnyak,
+7(812)493-91-36; PogrebnyakBN@vniig.ru

Pavel Arseniev,
+7(812)493-94-21; ArsenjevPA@vniig.ru

Yurii Shevchenko,*
+7(911)193-84-47; ShevchenkoYuV@gmail.com

Vladimir Kukhtevich,
+7(812)3391515(55153);
VOKukhtevich@atomproekt.com

Aleksey Kurchevsky,
+7(812)3391515(55153);
AIKurchevsky@atomproekt.com

Leonid Matyushev,
+7(812)3391515(55133);
LAMatyushev@atomproekt.com

Владимир Борисович Штильман,
+7(921)936-57-43;
эл. почта: ShtilmanVB@vniig.ru

Борис Нилович Погребняк,
+7(812)493-91-36;
эл. почта: PogrebnyakBN@vniig.ru

Павел Андреевич Арсеньев,
+7(812)493-94-21;
эл. почта: ArsenjevPA@vniig.ru

Юрий Васильевич Шевченко,*
+7(911)193-84-47;
эл. почта: ShevchenkoYuV@gmail.com

Владимир Олегович Кухтевич,
+7(812)3391515(55153);
эл. почта: VOKukhtevich@atomproekt.com

Алексей Иванович Курчевский,
+7(812)3391515(55153);
эл. почта: AIKurchevsky@atomproekt.com

Леонид Александрович Матюшев,
+7(812)3391515(55133);
эл. почта: LAMatyushev@atomproekt.com

Shtilman, V.B., Pogrebnyak, B.N., Arseniev, P.A., Shevchenko, Yu.V., Kukhtevich, V.O., Kurchevsky, A.I., Matyushev, L.A. Experimental justification of strainer meshes of NPP sump. Magazine of Civil Engineering. 2018. 83(7). Pp. 208–221. doi: 10.18720/MCE.83.19.

doi: 10.18720/MCE.83.20

Improvement of the soil deformation modulus using an expandable polyurethane resin

Улучшение модуля деформации грунта с использованием расширяющейся полиуретановой смолы

M.M. Sabri*,
Peter the Great St. Petersburg Polytechnic University, St. Petersburg, Russia
K.G. Shashkin,
OOO "PI Georekonstruktsiya", Saint Petersburg, Russia

M.Sc., аспирант М.М. Сабри*,
Санкт-Петербургский политехнический университет Петра Великого, г. Санкт-Петербург, Россия
канд. техн. наук, зам. директора, член технического комитета № 207 ISSMGE К.Г. Шашкин,
ООО "ПИ Геореконструкция", г. Санкт-Петербург, Россия

Key words: soil injection technology; soil modulus of deformation; soil stiffness; foundation lifting; soil consolidation; soil improvement; foundations settlement; soil bearing capacity; polyurethane resin

Ключевые слова: осадка фундаментов; усиление грунтов; технология инъектирования грунтов; модуль деформации грунта; жесткость грунта; подъем фундаментов; консолидация грунта; несущая способность грунтов

Abstract. Different methods are used in the field for foundations remediation and improvement of the soil properties, but every method has its advantages and limitations. Moreover, not all the existing methods are able to stabilize the soil and elevate the foundations effectively, regulating the process depending on the desired results. The settlements of the foundations of the buildings and structures lead to negative consequences and controlling the settlements is complex itself essentially in the type of soils which contains organic materials or acids where the treated materials used might react with the soil components. The soil injection technology using an expandable polyurethane resin is an innovative technique that leads to the stabilization of the soil beside lifting and remediating of the foundations. Therefore, a full-scale experiment has been implemented in-situ to investigate the effect of injecting an expandable polyurethane resin on different soil properties besides lifting a concrete foundation. The paper demonstrates the results of an experiment which has been conducted to improve the soil's modulus of deformation, lifting of a concrete foundation, settlement compensation and increase the bearing capacity of the investigated soil after the injection of an expandable polyurethane resin consists of two components. The deformation modulus (E) of the investigated soil before and after the injection of the resin at different depths are achieved and incorporated. Also, comparisons of the load-settlement graphs at different soil depths before and after the injection of the resin are presented and analyzed. The in-situ injection process and the propagation of the resin in the soil massive are obtained and described in this paper.

Аннотация. Существует множество методов, которые используются для стабилизации грунтов и подъема фундаментов, но каждый из этих методов имеет свои область применения, преимущества и недостатки. Более того, не все методы, используемые на мировом рынке, способны стабилизировать грунт и компенсировать осадку фундаментов комплексно, регулируя сам процесс в зависимости от ожидаемого результата. Осадка фундаментов зданий и сооружений приводит к негативным последствиям. Контроль осадок требует комплексного подхода, так как некоторые грунты, которые включают в себя органические материалы или кислоты, могут реагировать с обработанном материалом, использованным в том или ином методе. Технология инъектирования грунтов расширяемой полиуретановой смолой является новаторским способом, ведущим к контролируемому процессу стабилизации грунтов и подъему фундаментов. На основе проведенного анализа был выполнен натурный эксперимент для наблюдения контроля подъема фундамента и определения влияния расширяемой смолы на различные свойства грунтов. В статье показаны результаты проведенного эксперимента, а именно: улучшение модуля деформации грунта, контрольный подъем и восстановление бетонного фундамента, компенсации осадок и увеличение несущей способности исследуемого грунта после инъекции полиуретановой смолы. Модуль деформации грунта (E) и сопоставление расчетных графиков зависимости осадки от

Сабри М.М., Шашкин К.Г. Улучшение модуля деформации грунта с использованием расширяющейся полиуретановой смолы // Инженерно-строительный журнал. 2018. № 7(83). С. 222–234.

нагрузки на разных глубинах до и после инъекции смолы достигаются и проанализированы. Также в данной статье описаны результаты процесса инъектирования и распространения смолы в массиве грунта.

1. Introduction

One of the main problems which face the construction engineers is the settlement of the soil beneath foundations during the construction and exploitation processes [1]. Settlements are divided into two main types uniform and differential. In most cases, a uniform settlement causes no problems, when the whole construction is settled. Problems arise when differential settlements occur due to various reasons such as errors in construction design, non-qualitative of geological surveys before construction, poor quality of the soil compaction while construction, the variation of the groundwater level and other reasons [2–4]. Another problem is a weak soil which is not able to carry the applied or designed load of the construction because of many reasons. For instance, the type of the soil is soft and need to be stabilized, changes in the moisture content of soil which leads to changes in the physical and the mechanical properties of it and others[5, 6]. Moreover, the soil might contain organic materials or acids which can have negative influences on the soil properties leading to adverse effects on the foundations. [7]. Furthermore, differential settlements cause adverse consequences on the foundations and other construction parts. It leads to increase the stresses in foundations, walls and other construction parts which lead to cracks, fractures and even collapsing the construction in some cases [8-10]. Also, sometimes it is necessary to increase the bearing capacity of the soil to be able to carry an extra load added to the construction when required to increase the load of the construction or according to clients wishes in case of adding extra floors to the construction [11, 12].

There are many classical methods used to compensate settlements, foundations lifting and soil stabilization such as Jet-Grouting, Root piles, chemical stabilization, and other methods. However, every method has advantages and disadvantages or limitations [13, 14]. Some methods require extensive preparation and instruments, others are high in cost or necessitate huge time to implement until obtaining the desired result in addition to the restrictions of use in the limited construction area. Additionally, most of the existing methods include materials which can react with the soil contents especially if the soil contains acids or other reactive materials. [15, 16].

The density of the soil beds plays a significant role in the design of any foundation. It was proved that the high values of soil density lead to control of the operating conditions of an artificial foundation and what called plate effect can be noticed. Highly compacted soil beds and reinforced soil beds can lead to reduce the thickness of the beds and increase the bearing capacity of the soil which can decrease the designed dimensions of an artificial foundation reducing the cost and the time required [17, 18]. Moreover, the soil might be exposed to high strain conditions where the construction is built on the mountains like in Tajikistan where the mountains and hilly areas cover around 90 % of the areas or for other reasons. Consequently, using a combination of soil stabilization methods lead to ensure the stability of the slope reducing the collapse of the soil as stated in [19].

For all the issues stated above and others, actions need to be taken in order to develop a fast and controlled method for solving various settlements problems and remediation of the foundations. Soil injection technology using an expandable polyurethane resin might offer an optimum solution for most of the mentioned problems either by implementing the technology alone or in a system of methods combination in complex soil problems.

As the modulus of deformation of the soil is a significant parameter to measure the soil stiffness and to design any constructions. The deformation modulus of the soil is affected and variable according to many factors such as the type and the depth of the soil, the soil moisture content and other factors [20, 21]. Therefore, an experiment was conducted in the field to investigate the effect of soil injection technology using an expandable polyurethane resin on different soil properties at different depths and to reduce the soil settlement beside evaluating the performance of lifting a concrete foundation.

2. Methods

2.1. The aim of the experiment

The experiment was conducted for investigating the effect of injecting an expandable Polyurethane resin on different sandy soil parameters such as the soil modulus of deformation (E), settlement reduction and compensation and increasing the bearing capacity of the soil beneath a concrete plate which was exposed to a load in order to behave like a real foundation beside lifting this plate to the pre-designed level. The level of lifting is designed to exceed the value of (1 cm).

2.2. Location of the experiment and the type of the investigated soil

The conducted experiment took place in an open storage area located in the western part of the plant of the company “MC-Bauchemie-Russia” in Kirovsk, Leningradskaya region, Russian Federation as shown in Figure [1]. The type of the investigated soil is non-cohesive sandy soil according to the factory geological report.

Figure 1. The layout of the object (the red Line highlighted the boundary of the plant; red fill indicates the test area) [22]

The soil was investigated in September 2014 by a geotechnical company, and the experiment was conducted based on the geological report given to the factory. According to the geological report of the factory, the soil being investigated in this experiment consists of the following layers: the first layer is a technogenic layer represented by bulk sand of different sizes grading (from small sand to gravels, with gravel, pebbles and building debris) within a depth up to (2 m) and the sediment layer is (1.5–2 m). The Bulk sand is heterogeneous having uneven density and compressibility. The second layer is a glacial soil layer widespread under the bulk sand consist of fine sand medium density and medium degree of saturation. Sediment power is from (3.5–6 m). In the period of geological surveying in September 2014, drilling up to 8m in depth, it was found that the groundwater level located within (2.2–2.5 m). The properties of the investigated soil according to the report are given in Table 1.

Table 1. The properties of the investigated soil as given in the geotechnical report of the factory

Geological Index	Soil Name (type)	Layer No.	Density t/m^3	Porosity factor e	Strength indicators		E, MPa	Calculated resistant R0, kPa	Filtration coefficient, m/day
					C, kPa	Φ, grad			
t IV	Bulk sand different sizes	1	R0=100 kPa						
lg III	Fine sand, medium density and medium degree of saturation and fully saturated	2	1.94	0.65	4**	30**	18**	200**	4.47*

* According to laboratory investigation data, ** According to SP 22.13330.2011 [23].

2.3. Experiment Description and the test site

In the test site, two plots, each measuring 3 m per side, were chosen, covering a total surface area of (3*3 m) as shown in Figure 2. Soil stabilization using an expandable polyurethane resin was applied in one plot while the second plot considered as a reference plot (no injection was carried out in this plot) for the comparison of the results. Then, the concrete plate of the injected plot was cut, and a total load of (11 ton) approximately was placed on it to ensure that the plot acts like a real foundation as shown in Figure 3.

Figure 2. The selected experiment plots

Figure 3. The injected plot under the load during the injection process

The injection of the expandable resin was carried out at five different points along the injected area utilizing injecting tubes which inserted to different depths. The injection of the resin carried out at depths (0.5, 1, 2 m) to assess the effect of the injected resin on the properties of the investigated soil at different layers. The injected geological section with the concrete plate and injection zones are shown in Figure 4. The injected resin consists of two components (component A and component B) of the polyurethane resin (MC-MONTAN INJEKT-LE) produced by the company MC-BAUCHEIME-Russia. The components of the resin were mixed in a hydraulic system under high pressure to control the mixing of the two components of the resin and injected incrementally into the soil using the injection pistol. The pressure of the injection mix was more than 100 bars, and the temperature of the mix was varied and controlled but mostly (15 C°). Then, both plots were excavated to investigate the propagation of the polyurethane resin and to conduct plate load test (plate-bearing test).

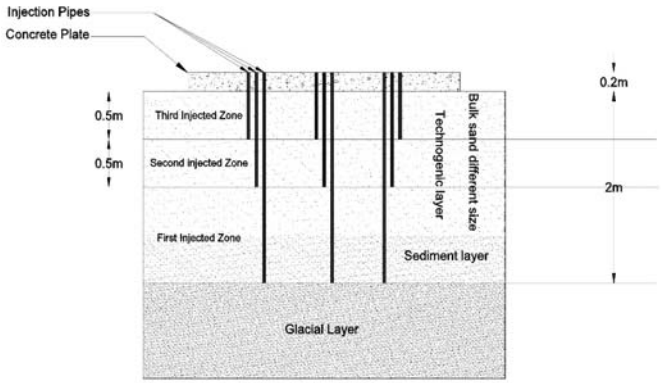

Figure 4. The geological section of the injected area and the in-situ injected zones

2.4. Excavation process and the plate load test

Different depths of excavation were chosen to investigate the effect of the resin on the modulus of deformation (E) by conducting plate load test, and to locate the propagation of the resin in the soil massive at different depths. The Depths of the excavation were selected considering different conditions which can influence the accuracy of the obtained results such as the groundwater level of the tested area. Moreover, the excavation process was carried out manually to avoid any disturbance to the soil which might affect the results of the plate load test and to be able to locate the resin accurately.

Each plot was divided into four quarters and only a quarter of each plot was selected for the investigations at this step. The pre-designed depths of the plate load test (0.5 m) which is the depth of the injection in the first layer of the investigated soil and (1.5 m) for the second layer of the soil as this depth represents the average of the injection depth in the second part of the soil layer (1–2 m). During the excavation process, it was noticed that the groundwater level located at the depth (1.4 m) as shown in

Figure 5. It is the author opinion that the reason behind the groundwater level rise is the seasonal variation of the groundwater as the excavation process was performed in autumn when the water level rises. Thus, the selected excavated points for the plate load test were replaced by another point, and the in-situ depths of the plate load test were taken as explained in Table 2. The concrete plate cutting process is shown in Figure 6.

Figure 5. The groundwater level during the excavation process at a depth of (1.9 m)

(A) The cutting process (B) A section of the injected plot after cutting

Figure 6. The cutting process of the injected plot. (A) The cutting process, (B) A section of the injected plot after cutting

Five different points were chosen for performing the plate load test, two points in the reference plot at depths (0.4,1.2 m) and two points in the injected plot at depths (0.4, 1.1 m) in addition to one point in the injected area on the (resin-soil composition) as shown in figure (7). Furthermore, dynamic cone penetration test DCPT was conducted, and the results of the test are achieved and described in a previous article [22].

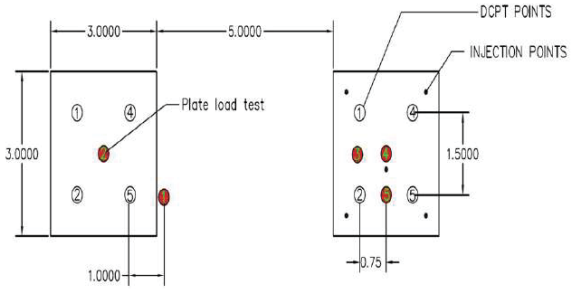

Figures 7. The in-situ location of the plate load in the reference and the injected plot

It means that two points at depth in the injected plot were compared to two other points in the reference plot at different soil depths for the comparison of the results, while, the last test was performed separately. In the last test, the center of the steel plate was placed to fit the center of the resin to investigate the modulus of deformation (E) including the resin and the soil together and not only on the soil itself as shown in Figure 8.

Table 2. The excavation zones and the actual depth of the in-situ plate load test

Zones of the test	Number of the test	The depth of the test, (m)
Without injection (Reference plot)	1	0.4
	2	1.2
With injection (Injected plot)	3	0.4
	4	1.1
With injection on the resin-soil (Injected plot)	5	1.1

(A) The location of the steel plate. (B) The soil-resin under the load.

Figure 8. The steel plate as placed in-situ in point number (5). (A) The setting up the plate on the resin-soil composition, (B) The soil-resin under the load in this point

The main aim of the test is the determination the modulus of deformation of the investigated sandy soil (E) at different soil depths and the graphs of load-settlement relationships according to specified load before and after the injection of the expandable polyurethane resin in order to precisely investigate the effect of the injected resin on different soil characteristics and on the bearing capacity of the investigated soil.

Six concrete plates with total load around 25 ton were used for applying the load on a circular steel plate. The load was chosen to ensure that the load applied to the soil area is enough to reach the failure of the soil. The diameter of the chosen steel plate is 27.6 cm, and the area of it is 600 square centimeters. So, the maximum load according to the equation below is around 416 ton/m^2.

$$6 = P/A$$

where P – the load of the concrete plates, A: The area of the steel plate.

In order to transfer and control the load of the concrete plate to the steel plate, an aluminum jack was used with a capacity of loading up to 150 ton. Also, a manual hydraulic jack was calibrated to create and control the load during the testing process. Three sensors connected to the steel plates carefully for reading the settlements of the soil during each process of loading and unloading the soil (release the load and control the settlement). Figures 9, 10 show the plate load test in-situ at different points of the experiment.

Figure 9. The plate load test under the load in point (3)

Figure 10. The plate load test under the load in point (4)

Furthermore, the diameter effect of the applied load was considered when the locations of the plate load tests were chosen. To ensure that no results are overlapping of the applied load of one tested point to another, the minimum distance between plate load tests was (75 cm) as the diameter effect of the applied load in this test is assumed to be double than the diameter of the steel plate which is (55.2 cm).

3. Results and Discussion

3.1. Results of lifting

The concrete foundation (the plate under the load) was regulated and lifted up to (12 mm) after the injection of the resin. The results were carried out Immediately at each point, then the last elevating of the whole plate was controlled through the middle point (point 3). The injection process was proceeded and monitored using a high accuracy laser level instrument during the injection process until the designed level for this experiment was obtained. The temperature of mixing the components of the resin and the pressure of injection was variated depending on the elevating required for each point. Results of lifting the concrete plate are shown in Figures 11, 12.

(A) Before **(B) After**

Figure 11. A side section of the concrete plate side of the injected plot before and after the injection of the resin. (A) Before injection, (B) After injection

(A) Before **(B) After**

Figure 12. The concrete plate of the injected plot before and after the injection of the resin. (A) Before injection, (B) After injection

3.2. Resin propagation

The resin diffused in the soil massive forming shapes similar to walls of foam plates along the injected soil depth from all sides within a distance interval around 30–50 cm and the average thickness of the resin is 2 cm approximately as measured. It was found that the resin propagated through the whole excavated depth of the soil. Moreover, the resin was continuous through the whole excavated depth of the soil and not separated. Figures 13, 14 illustrate different sections of the resin propagation.

Figure 13. Different sections of the resin injection in the injected plot at depth (0.4 m).

Figures 14. Different sections of the resin diffusion in the injected plot at depth (1.1 m)

3.3. Results of plate load test

According to the Russian standard GOST (20276-12) [24], the load must be applied within an interval of loading and unloading (steps) which depends on the type of the soil. Thus, the loading interval was taken in this experiment (0.5 kg/cm^2). Then, waiting for the stabilization of the settlement reading (the release of the load) until it becomes equal or less than (0.1 mm) within a specified time before applying the second load. This interval was used for the first ten steps (till 5 kg/cm^2), then, the interval was increased to (1 kg/cm^2) until obtaining the ultimate load where the failure of the soil occurs or reaching a specified load of (20 kg/cm^2). The cracks of the soil around the steel plate under the ultimate load is a sign of soil failure as shown in figure (15). In point number (4), the soil was very compacted after the injection of the resin, and the failure of the soil did not occur at the maximum specified load for this experiment (20 kg/cm^2). Therefore, the mentioned intervals were taken until reaching the pre-designed load for the comparison of this experiment (20 kg/cm^2), and by exceeding this value the load was increased rapidly without following the requirements of the settlement stabilization intervals (without releasing the load) until the ultimate load where the soil was failed in order to investigate the ultimate load of that point (the failure of the soil) after the injection of the resin.

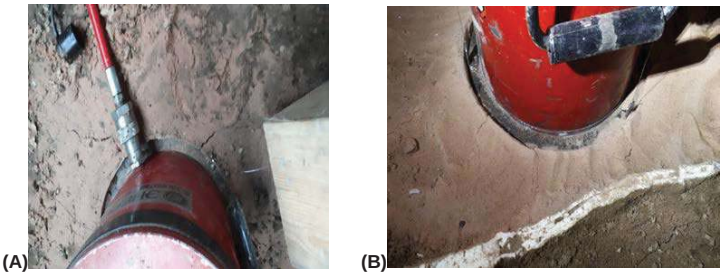

Figure 15. The soil under the ultimate load and cracks shown as a sign of the soil failure. (A) failure in the reference, (B) failure in the injected plot

Furthermore, the modulus of deformation of the soil was calculated for each step individually according to the following equation:

$$E = (1 - v2)\, Kp * K1 * D\, (\Delta P / \Delta S)$$

where E= modulus of deformation of the soil,

V = 0.3 Poisson's ratio, Kp = 1 as the test done in the pit, $K1$ = 0.79 for circular solid steel plate,

D = 27.6 cm the plate diameter, ΔP = The pressure increment, ΔS = The Settlement increment.

Table 3. The loading stages (steps) and the modulus of deformation (E) obtained from every loading stage

Number of loading stages	The range of loading, Kg/cm^2	The obtained values of the soil deformation modulus (E) at each loading stage				
		Number of the tested points				
		1	**2**	**3**	**4**	**5**
1	0.0-0.5	178.3	951.1	124.1	167.8	124.1
2	0.5-1.0	25.7	226.5	36.0	44.3	34.3
3	1.0-1.5	17.5	20.9	23.6	47.6	26.4
4	1.5-2.0	13.3	12.0	17.7	38.6	25.0
5	2.0-2.5	15.4	11.3	16.9	36.6	22.5
6	2.5-3.0	9.6	12.1	13.6	34.7	23.9
7	3.0-3.5	8.4	10.1	17.3	27.4	19.7
8	3.5-4.0	9.1	10.0	17.1	32.1	20.7
9	4.0-4.5	8.4	11.1	18.3	25.7	18.5
10	4.5-5.0	4.8	7.6	16.4	22.1	14.6
11	5.0-6.0	4.7	10.9	12.9	29.1	16.0
12	6.0-7.0	4.1	10.2	12.1	23.3	12.4
13	7.0-8.0	3.6	10.0	12.1	26.6	6.5
14	8.0-9.0	2.6	10.4	11.5	20.7	7.2
15	9.0-10.0	2.1	9.6	10.0	17.5	2.0
16	10.0-11.0	1.8	6.8	9.6	18.8	
17	11.0-12.0	1.4	3.3	9.0	16.1	
18	12.0-13.0			8.6	16.2	
19	13.0-14.0			7.4	16.7	
20	14.0-15.0			6.3	13.9	
21	15.0-16.0			7.4	13.2	
22	16.0-17.0			4.0	12.6	
23	17.0-18.0			3.0	11.5	
24	18.0-19.0			2.7	10.6	
25	19.0-20.0			1.4	9.9	

The gray color shown in table 3 is the range by which the soil deformation modulus (E) is defined as the total value of the deformation modulus is calculated by taking the average of five stable stages results. Table 4 shows the zones of plate load test and the total soil deformation modulus (E) achieved from each tested point before and after the injection of the resin.

Table 4. The zones of plate load test and the total soil deformation modulus (E) in each tested point

Zones of the test	Test number	Test depth,(m)	Deformation modulus (E), MPa	Maximum load applied, Kg/cm^2
Without injection (Reference plot)	1	0.4	10.6	12
	2	1.2	11.1	12
With injection (Injected plot)	3	0.4	16.4	20
	4	1.1	33.6	27
With injection on the resin-soil	5	1.1	22.3	10

Сабри М.М., Шашкин К.Г. Улучшение модуля деформации грунта с использованием расширяющейся полиуретановой смолы // Инженерно-строительный журнал. 2018. № 7(83). С. 222–234.

Focusing on Figure 16 which shows the results of load-settlement before and after the injection process at depth (0.4 m) in points (1, 3). Clearly, the soil failed at load (20 kg/cm^2) after the injection of the resin (injected plot), while, the failure point of the soil occurred at a load of (12 kg/cm^2) before the injection of the resin (reference plot) and the settlement of the soil was decreased too during all loading steps. The settlement was around (75 mm) before the injection when exposed to the ultimate load (12 kg/cm^2) where the failure of the soil appeared while it decreased remarkably after the injection of the resin under the same loading and the same test conditions.

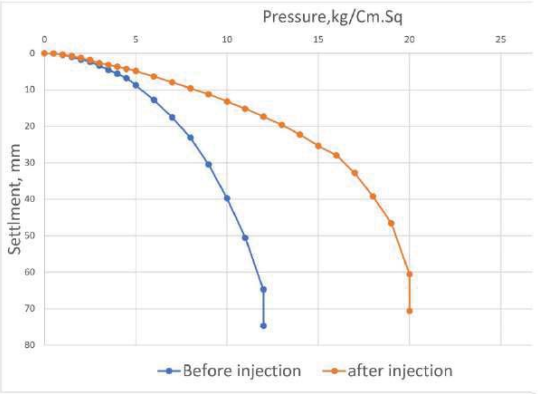

Figure 16. The graph of load-settlement in point number (1,3)) at a depth of 0.4 m before and after the injection of the resin

Furthermore, emphasizing on Figure 17 which shows the results of the load-settlement of the soil in points (2, 4) at depth (1.2, 1.1 m) respectively. Obviously, in point number (4) the soil did not fail under the designed load for this experiment as mentioned above. The soil failed under a load of (12 kg/cm^2) before the injection of the resin (reference plot), while, it exceeded the pre-designed load for the comparison of this experiment and the failure of the soil occurred at a load of (27 kg/cm^2) after the injection of the expandable resin (injected plot). Moreover, the settlement result was around (36 mm) under the failure load (12 kg/cm^2) in the reference area, while, it decreased tremendously under the same loading steps and the same test conditions in the injected area.

Results of both incorporated graphs (16, 17) prove that the soil was more compacted with a high degree of compaction and the settlement of the soil decreased at all comparison depths after the treatment of the soil using the expabdable polyurethane resin.

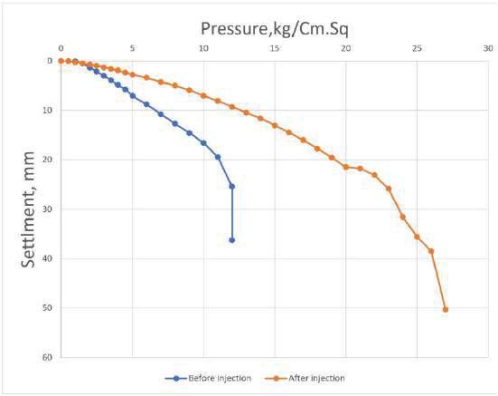

Figure 17. The results of load-settlement in points (2, 4) at a depth of (1.1,1.2 m) respectively before and after the injection of the resin

Focusing on Figure 18 which presents the results of the plate load test in point (5). The result of the soil deformation modulus was increased after the injection of the resin, and the settlement was decreased in comparison to both points (1, 2) in the reference plot, while the failure load of the soil was low (10 kg/cm^2) comparing to the failure load of the reference points. According to the author opinion, the low value of the limit pressure on this tested point (with the inclusion of the resin) is explained by the diversity of the base (soil and resin) under the steel plate. At a particular pressure, the resin which is adjacent to the steel plate is not strictly vertical, began to deform (up to rupture at bending), deforming the surrounded tested soil.

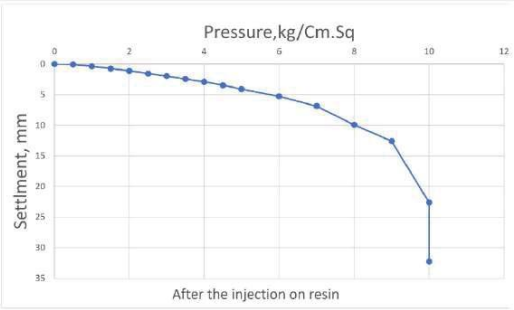

Figure 18. The results of load-settlement in point number (5) at a depth of 1.1 m

The analysis of the results of the plate load test has shown the significant influence of the injected expandable polyurethane resin on the properties of the investigated soil. Results of all graphs (16, 17, 18) improve certainly that the soil in the injected plot became more compacted comparing to the reference plot. Moreover, according to the obtained results, the settlement of the soil decreased in all tested points and at all tested depths after the injection of the resin. Furthermore, the coherent of the plate load test results in each plot at different depths and the diversity of the selected points beside the high accuracy of the selected test in this experiment prove with no doubt the improvement of the properties of the investigated soil which achieved after the injection of the expandable resin.

Moreover, the modulus of deformation of the investigated soil has been increased enormously after the injection of the resin. The effect of the resin on the density of the sandy soil is clearly noticed as the soil in the injected plot became denser in comparison to the soil in the reference plot and the bearing capacity of the investigated soil is improved as the load required for the soil failure increased within a constant area (the area of the steel plate) as illustrated in the graphs of load-settlement.

It is the author opinion that the more load applied on the soil can lead to better results because the resin propagates from the bottom moving towards the upper soil layers exerting pressure on the soil vertically and laterally facing the load of the construction from the opposite direction which leads to an outcome of the pressure applied on the soil and finally leading to strengthening the soil by increasing the cohesion. This opinion is enhanced by focusing on the results of the plate load test at depths of (1.1, 1.2 m) which show that the soil deformation modulus and the soil stabilization was improved after the injection process while less improvement noticed in the same properties at the depth (0.4 m). Moreover, the resin leads to reduce the soil void ratio and extrude the water from the soil decreasing the soil water content beside the presence of the injected resin itself (additional volume of the injected resin is added to the soil while the weight of the resin is small relatively) leading to increase the density and strengthening the soil preventing further future settlements.

4. Conclusion

The paper presents the results of full-scale experimental research carried out before and after the injection of an expandable polyurethane resin consists of two components in non-cohesive sandy soil. An outcome of the results proves the significant improvement of the investigated soil deformation modulus (E) after the injection of the resin in the injected plot while no improvement was observed in the reference plot where no soil treatment carried out. Also, the settlement of the investigated soil was decreased remarkably in the injected plot as demonstrated in the graphs of load-settlement after the injection of the resin. The failure load of the soil occurred at a load of (12 kg/cm^2) in the reference plot while the failure load was increased to be (20, 27 kg/cm^2) in the injected plot proving the increasing of the soil bearing capacity after the injection of the expandable resin. The lifting and regulating of the concrete foundation to the pre-

designed level were achieved (up to 12 mm) which proves the efficiency of the injected resin and the effect of it on both applications (foundation lifting and settlement compensation besides strengthening of the injected soil). The resin propagates in baths under high pressure leading to the soil consolidation forming like continues walls of foam plates from all excavated sides and along the whole injected depth of the soil. The obtained results are valid, actual and can be applied in all similar types of non-cohesive sandy soil as the resin increases the cohesion of the treated sand. Furthermore, the outcome of the forces exerted on the soil (load-resin forces) in opposite directions beside the lateral pressure which applies on the soil during the injection process, and the additional volume of the injected resin lead to increase the mass density of the soil (soil compaction). Thus, the soil injection technology using an expandable polyurethane resin might also be applied almost in all soil types except the rocks according to the author opinion and as explained in this article. The injection process is simple and efficient with less equipment and labor required in comparison to other techniques used in this field and with no inherent to the soil ecology and the soil groundwater level.

5. Acknowledgment

The author would like to show gratitude to the company MC-Bauchemie-Russia for funding the experiment and for the great support through the whole experiment especially to Evgenii N. Zakharin, for the significant effort in the injection process and in all the experiment.

Special thanks to Alexey Vladimirovich Ulybin, head manager of the company “OZIS-Venture” for the contribution in the field plate load test and in the whole experiment.

References

1. Favaretti, M., Germanino, G., Pasquetto, A., Vinco, G. Interventi di consolidamento dei terreni di fondazione di una torre campanaria con iniezioni di resina ad alta pressione d’espansione. Proceedings of XXII Convegno Nazionale di Geotecnica. Palermo, Associazione Geotecnica Italiana. 2004. Vol. 40(12). Pp. 1–19.
2. van Reenen, R. Uretek Deep Injection Method Lifting of settled foundations Analysis of full scale test results. M. Sc. Thesis, Civil Engineering department, delft university, Delft, Netherlands 2006.
3. Lewis, M.R., Davie, J.R., Weaver, C.L. Differential Settlement of Nuclear Power Plant Foundations. International Conference on Case Histories in Geotechnical Engineering. Vol. 24. University of Missouri, Missouri, USA, 1988.
4. Seawsirikul, S., Chantawarangul, K., Vardhanabhuti, B. Evaluation of Differential Settlement along Bridge Approach Structure on Soft Bangkok Clay. Geotechnical Safety and Risk. 2015. Vol. 614(7). Pp. 614–620.
5. Santarato, G., Ranieri, G., Occhi, M., Morelli, G., Fischanger, F., Gualerzi, D. Three-dimensional electrical resistivity tomography to control the injection of expanding resins for the treatment and stabilization of foundation soils. Engineering Geology. 2011. Vol. 119(1-2). Pp.18–30.
6. Buzzi, O., Fityus, S., Sasaki, Y., Sloan, S.W. Structures and properties of expanding polyurethane foam in the context of foundation remediation in expansive soil. Mechanics of Materials Journal. 2008. Vol. 40(12). Pp. 1012–1021.
7. Golovanov, A.M., Pashkov, V.I., Revo, G.A., Pashkov, D.V., Nerchinskiy, O.V., Turenko R.I. Case study of stabilization of structural-unstable soils using grouting. Vestnik MGSU. 2013. Vol. 624(138). Pp. 59–67. (rus)
8. Saha, M.C., Mahfuz, H., Chakravarty, U.K., Uddin, M., Kabir, M.E., Jeelani S. Effect of density microstructure and strain rate on compression behavior of polymeric foams. Materials Science and Engineering Journal. 2005. Vol. 406(1–2). Pp. 328–336.
9. Nowamooz, H. Resin injection in clays with high plasticity. Mécanique. 2016. Vol. 344(11-12). Pp. 797–806.
10. Lanka, S.T., Aswathi, T.S., Poongothai, A. Rectification of settled Foundations. Proceedings of 6th IRF International Conference. Chennai, India, 2014.
11. Apuani, T., Beretta, G.P., Pellegrini, R. Linee Guida per L’inertizzazione InSitu dei Suoli Contaminati. 2006. Vol. 12.

Литература

1. Favaretti M., Germanino G., Pasquetto A., Vinco G. Interventi di consolidamento dei terreni di fondazione di una torre campanaria con iniezioni di resina ad alta pressione d’espansione // Proceedings of XXII Convegno Nazionale di Geotecnica, Palermo, Associazione Geotecnica Italiana. 2004. Vol. 40(12). Pp. 1–19.
2. van Reenen R. Uretek Deep Injection Method Lifting of settled foundations Analysis of full scale test results. M. Sc. Thesis, Civil Engineering department, delft university, Delft, Netherlands 2006.
3. Lewis M.R., Davie J.R., Weaver C.L. Differential Settlement of Nuclear Power Plant Foundations // International Conference on Case Histories in Geotechnical Engineering. Vol. 24. University of Missouri, Missouri, USA, 1988.
4. Seawsirikul S., Chantawarangul K., Vardhanabhuti B. Evaluation of Differential Settlement along Bridge Approach Structure on Soft Bangkok Clay // Geotechnical Safety and Risk. 2015. Vol. 614(7). Pp. 614–620.
5. Santarato G., Ranieri G., Occhi M., Morelli G., Fischanger F., Gualerzi D. Three-Dimensional Electrical Resistivity Tomography to control the injection of expanding resins for the treatment and stabilization of foundation soils // Engineering Geology. 2011. Vol. 119(1-2). Pp.18–30.
6. Buzzi O, Fityus S, Sasaki Y & Sloan SW, “Structures and properties of expanding polyurethane foam in the context of foundation remediation in expansive soil // Mechanics of Materials Journal. 2008. Vol. 40(12). Pp. 1012–1021.
7. Голованов А.М., Пашков В.И., Рево Г.А., Пашков Д.В., Нерчинский О.В., Туренко Р.И. Опыт закрепления структурно-неустойчивых грунтов цементацией // Вестник МГСУ. 2013. № 8. С. 59–67.
8. Saha M.C., Mahfuz H., Chakravarty U.K., Uddin M., Kabir M.E., Jeelani S. Effect of density microstructure and strain rate on compression behavior of polymeric foams // Materials Science and Engineering Journal. 2005. Vol. 406(1–2). Pp. 328–336.
9. Nowamooz H. Resin injection in clays with high plasticity // Mécanique. 2016. Vol. 344(11-12). Pp. 797–806.
10. Lanka S.T., Aswathi T.S., Poongothai A. Rectification of settled Foundations // Proceedings of 6th IRF International Conference. Chennai, India, 2014.
11. Apuani T., Beretta G.P., Pellegrini R. Linee Guida per L’inertizzazione InSitu dei Suoli Contaminati. 2006. Vol.12.
12. Meyerhof G.G, The Ultimate Bearing Capacity of Foundations // Geotechnique. 1951. Vol. 2(4). Pp. 301–332.

Sabri, M.M., Shashkin, K.G. Improvement of the soil deformation modulus using an expandable polyurethane resin. Magazine of Civil Engineering. 2018. 83(7). Pp. 222–234. doi: 10.18720/MCE.83.20.

12. Meyerhof, G.G. The Ultimate Bearing Capacity of Foundations, Geotechnique. 1951. Vol. 2(4). Pp. 301–332.
13. Dalinchuk, V.S., Ilmenderov, M.S., Iarkin, V.V. Eliminating drawdown bases with the help of technology SLAB LIFTING. Construction of Unique Buildings and Structures. 2015. No. 11(38). Pp. 15–26. (rus)
14. Page, R.J., Ong, J.C.W., Osborn, N. Jet Grouting for Excavations in Soft Clay- design and construction issues. International Conference on Deep Excavations (ICDE). Singapore, 2006.
15. Samokhvalov, M.A. Vzaimodeystviye Buro-Inyektsionnykh Svay Imeyushchikh Kontroliruyemoye Ushireniye S Pylevato-Glinistym Gruntovym Osnovaniyem [Interaction of brown-injection piles with controlled broadening with a silty clay base]. PhD diss. 05.23.02. Tyumen, Russia, 2016. (rus)
16. Raevskiy, V.V. Runways and taxiways repairing and reconstruction with the usage of two components penopolyuretane resin. Transfer of overall runway repair into current repair. Construction of Unique Buildings and Structures. 2014. Vol. 11(26). Pp. 18–32. (rus)
17. Usmanov, R., Vatin, N., Murgul, V. Experimental research of a highly compacted soil beds. Applied Mechanics and Materials. Vol. 633-634. Pp. 1082–1085.
18. Usmanov, R., Mrdak, I., Vatin, N., Murgul, V. Reinforced soil beds on weak soils. Applied Mechanics and Materials. 2014. Vol. 633-634. Pp. 932–935.
19. Usmanov, R., Rakocevic, M., Murgul V., Vatin N. Problems of sub-mountain area development associated with collapsing loess soils (Case of Tajikistan). Applied Mechanics and Materials. Vol. 633-634. Pp. 927–931.
20. Uletskiy, V.M, Shashkin, A.G, Shashkin, K.G, Shashkin, V.A, Osnovy sovmestnykh raschetov zdaniy i osnovaniy [Basics of joint calculation of buildings and grounds]. Izdatelstvo Instituta Georekonstruktsiya. Sankt-Peterburg, 2014. (rus)
21. Pantelidis L. Determination of Soil Strength Characteristics Performing the Plate Bearing Test. 3rd International Conference of Modern Technologies in Highway Engineering. Aristotle University of Thessaloniki, Greece, 2005.
22. Sabri, M.M., Shashkin, K.G., Zakharin, E. Ulybin, A.V. Soil stabilization and foundation restoration using an expandable polyurethane resin. Magazine of Civil Engineering. 2018. 82(6). Pp. 68–80.
23. Russian Construction Norms SP 22.13330-2011.
24. Russian State Standard GOST 20276-2012.

13. Далинчук В.С., Ильмендеров М.С., Яркин В.В. Устранение просадки фундаментов с помощью технологии SLAB LIFTING // Строительство уникальных зданий и сооружений. 2015. № 11(38). С. 15–26.
14. Page R.J., Ong J.C.W., Osborn N. Jet Grouting for Excavations in Soft Clay- design and construction issues // International Conference on Deep Excavations (ICDE). Singapore, 2006.
15. Самохвалов М.А. Взаимодействие буро-инъекционных свай имеющих контролируемое уширение с пылевато-глинистым грунтовым основанием. Диссертация на соиск. уч. ст. к.т.н. 05.23.02. Тюмень, 2016.
16. Раевский В.В. Реконструкция и ремонт взлетно-посадочных полос (ВПП) и рулежных дорожек с применением двухкомпонентной пенополиуретановой смолы. Перевод капитального ремонта ВПП в текущий ремонт // Строительство уникальных зданий и сооружений. 2014. № 11(26). С. 18–32.
17. Usmanov R., Vatin N., Murgul V. Experimental research of a highly compacted soil beds // Applied Mechanics and Materials. 2014. Vol. 633-634. Pp. 1082–1085.
18. Usmanov R., Mrdak I., Vatin N., Murgul V. Reinforced soil beds on weak soils // Applied Mechanics and Materials. 2014. Vol. 633-634. Pp. 932–935.
19. Usmanov R., Rakocevic M., Murgul V., Vatin N. Problems of sub-mountain area development associated with collapsing loess soils (Case of Tajikistan) // Applied Mechanics and Materials. 2014. Vol. 633-634. Pp. 927–931.
20. Улецкий В.М, Шашкин А.Г, Шашкин К.Г, Шашкин В.А, Основы совместных расчетов зданий и оснований. Изд-во Института Геореконструкция, Санкт-Петербург, Россия, 2014.
21. Pantelidis L. Determination of Soil strength characteristics performing the plate bearing test // 3rd International Conference of Modern Technologies in Highway Engineering. Aristotle University of Thessaloniki, Greece, September 2005.
22. Сабри М.М., Шашкин К.Г., Захарьин Е., Улыбин А.В. Стабилизация грунтов и восстановление фундамента с использованием расширяющейся полиуретановой смолы // Инженерно-строительный журнал. 2018. № 6(82). С. 68–80.
23. Свод Правил Основания зданий и сооружении, СП 22.13330-2011.
24. ГОСТ 20276-2012. Грунты. “Методы полевого определения характеристик прочности и деформируемости,”2012.

Mohanad Muayad Sabri,*
+7(905)264-53-57; mohanad.m.sabri@gmail.com

Konstantin Shashkin,
+7(921)916-66-54; cshashkin@yandex.ru

Моханад Муаяд Сабри,*
+7(905)264-53-57;
эл. почта: mohanad.m.sabri@gmail.com

Константин Георгиевич Шашкин,
+7(921)916-66-54;
эл. почта: cshashkin@yandex.ru

Сабри М.М., Шашкин К.Г. Улучшение модуля деформации грунта с использованием расширяющейся полиуретановой смолы // Инженерно-строительный журнал. 2018. № 7(83). С. 222–234.

Федеральное государственное автономное образовательное учреждение высшего образования
Санкт-Петербургский политехнический университет Петра Великого

ПОЛИТЕХ
Санкт-Петербургский политехнический университет Петра Великого

Инженерно-строительный институт
Центр дополнительных профессиональных программ

195251, г. Санкт-Петербург, Политехническая ул., 29,
тел/факс: 552-94-60, www.stroikursi.spbstu.ru,
stroikursi@mail.ru

Приглашает специалистов проектных и строительных организаций, не имеющих базового профильного высшего образования на курсы профессиональной переподготовки (от 500 часов) по направлению «Строительство» по программам:

П-01 «Промышленное и гражданское строительство»

Программа включает учебные разделы:

- ***Основы строительного дела***
- ***Инженерное оборудование зданий и сооружений***
- ***Технология и контроль качества строительства***
- ***Основы проектирования зданий и сооружений***
- ***Автоматизация проектных работ с использованием AutoCAD***
- ***Автоматизация сметного дела в строительстве***
- ***Управление строительной организацией***
- ***Управление инвестиционно-строительными проектами. Выполнение функций технического заказчика***

П-02 «Экономика и управление в строительстве»

Программа включает учебные разделы:

- ***Основы строительного дела***
- ***Инженерное оборудование зданий и сооружений***
- ***Технология и контроль качества строительства***
- ***Управление инвестиционно-строительными проектами. Выполнение функций технического заказчика и генерального подрядчика***
- ***Управление строительной организацией***
- ***Экономика и ценообразование в строительстве***
- ***Управление строительной организацией***
- ***Организация, управление и планирование в строительстве***
- ***Автоматизация сметного дела в строительстве***

П-03 «Инженерные системы зданий и сооружений»

Программа включает учебные разделы:

- ***Основы механики жидкости и газа***
- ***Инженерное оборудование зданий и сооружений***
- ***Проектирование, монтаж и эксплуатация систем вентиляции и кондиционирования***
- ***Проектирование, монтаж и эксплуатация систем отопления и теплоснабжения***
- ***Проектирование, монтаж и эксплуатация систем водоснабжения и водоотведения***
- ***Автоматизация проектных работ с использованием AutoCAD***
- ***Электроснабжение и электрооборудование объектов***

П-04 «Проектирование и конструирование зданий и сооружений»

Программа включает учебные разделы:

- ***Основы сопротивления материалов и механики стержневых систем***
- ***Проектирование и расчет оснований и фундаментов зданий и сооружений***
- ***Проектирование и расчет железобетонных конструкций***
- ***Проектирование и расчет металлических конструкций***
- ***Проектирование зданий и сооружений с использованием AutoCAD***
- ***Расчет строительных конструкций с использованием SCAD Office***

П-05 «Контроль качества строительства»

Программа включает учебные разделы:

- ***Основы строительного дела***
- ***Инженерное оборудование зданий и сооружений***
- ***Технология и контроль качества строительства***
- ***Проектирование и расчет железобетонных конструкций***
- ***Проектирование и расчет металлических конструкций***
- ***Обследование строительных конструкций зданий и сооружений***
- ***Выполнение функций технического заказчика и генерального подрядчика***

По окончании курса слушателю выдается диплом о профессиональной переподготовке установленного образца, дающий право на ведение профессиональной деятельности